

Insights in biomaterials novel developments, current challenges, and future perspectives 2022 / 2023

Edited by

Hasan Uludag, Yunbing Wang, Nihal Engin Vrana,
Candan Tamerler, Chandra Kothapalli and Milana C. Vasudev

Published in

Frontiers in Bioengineering and Biotechnology



FRONTIERS EBOOK COPYRIGHT STATEMENT

The copyright in the text of individual articles in this ebook is the property of their respective authors or their respective institutions or funders. The copyright in graphics and images within each article may be subject to copyright of other parties. In both cases this is subject to a license granted to Frontiers.

The compilation of articles constituting this ebook is the property of Frontiers.

Each article within this ebook, and the ebook itself, are published under the most recent version of the Creative Commons CC-BY licence. The version current at the date of publication of this ebook is CC-BY 4.0. If the CC-BY licence is updated, the licence granted by Frontiers is automatically updated to the new version.

When exercising any right under the CC-BY licence, Frontiers must be attributed as the original publisher of the article or ebook, as applicable.

Authors have the responsibility of ensuring that any graphics or other materials which are the property of others may be included in the CC-BY licence, but this should be checked before relying on the CC-BY licence to reproduce those materials. Any copyright notices relating to those materials must be complied with.

Copyright and source acknowledgement notices may not be removed and must be displayed in any copy, derivative work or partial copy which includes the elements in question.

All copyright, and all rights therein, are protected by national and international copyright laws. The above represents a summary only. For further information please read Frontiers' Conditions for Website Use and Copyright Statement, and the applicable CC-BY licence.

ISSN 1664-8714
ISBN 978-2-8325-4414-3
DOI 10.3389/978-2-8325-4414-3

About Frontiers

Frontiers is more than just an open access publisher of scholarly articles: it is a pioneering approach to the world of academia, radically improving the way scholarly research is managed. The grand vision of Frontiers is a world where all people have an equal opportunity to seek, share and generate knowledge. Frontiers provides immediate and permanent online open access to all its publications, but this alone is not enough to realize our grand goals.

Frontiers journal series

The Frontiers journal series is a multi-tier and interdisciplinary set of open-access, online journals, promising a paradigm shift from the current review, selection and dissemination processes in academic publishing. All Frontiers journals are driven by researchers for researchers; therefore, they constitute a service to the scholarly community. At the same time, the *Frontiers journal series* operates on a revolutionary invention, the tiered publishing system, initially addressing specific communities of scholars, and gradually climbing up to broader public understanding, thus serving the interests of the lay society, too.

Dedication to quality

Each Frontiers article is a landmark of the highest quality, thanks to genuinely collaborative interactions between authors and review editors, who include some of the world's best academicians. Research must be certified by peers before entering a stream of knowledge that may eventually reach the public - and shape society; therefore, Frontiers only applies the most rigorous and unbiased reviews. Frontiers revolutionizes research publishing by freely delivering the most outstanding research, evaluated with no bias from both the academic and social point of view. By applying the most advanced information technologies, Frontiers is catapulting scholarly publishing into a new generation.

What are Frontiers Research Topics?

Frontiers Research Topics are very popular trademarks of the *Frontiers journals series*: they are collections of at least ten articles, all centered on a particular subject. With their unique mix of varied contributions from Original Research to Review Articles, Frontiers Research Topics unify the most influential researchers, the latest key findings and historical advances in a hot research area.

Find out more on how to host your own Frontiers Research Topic or contribute to one as an author by contacting the Frontiers editorial office: frontiersin.org/about/contact

Insights in biomaterials 2022 / 2023 - novel developments, current challenges, and future perspectives

Topic editors

Hasan Uludag — University of Alberta, Canada

Yunbing Wang — Sichuan University, China

Nihal Engin Vrana — Sparta Medical, France

Candan Tamerler — University of Kansas, United States

Chandra Kothapalli — Cleveland State University, United States

Milana C. Vasudev — University of Massachusetts Dartmouth, United States

Citation

Uludag, H., Wang, Y., Vrana, N. E., Tamerler, C., Kothapalli, C., Vasudev, M. C., eds. (2024). *Insights In biomaterials 2022 / 2023 - novel developments, current challenges, and future perspectives*. Lausanne: Frontiers Media SA.
doi: 10.3389/978-2-8325-4414-3

Table of contents

- 05 **Editorial: Insights in biomaterials 2022 / 2023—novel developments, current challenges and future perspectives**
Hasan Uludağ, Yunbing Wang, Nihal Engin Vrana, Candan Tamerler, Chandra Kothapalli and Milana C. Vasudev
- 08 **Hydrogels for Single-Cell Microgel Production: Recent Advances and Applications**
B. M. Tiemeijer and J. Tel
- 27 **Recent advances in engineering nanotopographic substrates for cell studies**
Ignasi Casanellas, Josep Samitier and Anna Lagunas
- 36 **Past, present, and future perspectives of biodegradable films for soil: A 30-year systematic review**
Yitao Sun, Wenlong Yang, Hongxia Shi, Sikander Khan Tanveer and Jiangbo Hai
- 56 **Modifications of cellulose-based biomaterials for biomedical applications**
Nour Fatema, Ruben Michael Ceballos and Chenguang Fan
- 64 **Protease-degradable hydrogels with multifunctional biomimetic peptides for bone tissue engineering**
Lluís Oliver-Cervelló, Helena Martín-Gómez, Cristina Gonzalez-Garcia, Manuel Salmeron-Sanchez, Maria-Pau Ginebra and Carlos Mas-Moruno
- 81 **A review of the development of interventional devices for mitral valve repair with the implantation of artificial chords**
Tingchao Zhang, Yichen Dou, Rifang Luo, Li Yang, Weiwei Zhang, Kangmu Ma, Yunbing Wang and Xingdong Zhang
- 98 **A versatile, bioengineered skin reconstruction device designed for use in austere environments**
Joachim G. S. Veit, Morgan Weidow and Monica A. Serban
- 112 **Nanoparticles and cytokine response**
Mohammad Nasrullah, Daniel Nisakar Meenakshi Sundaram, Jillian Claerhout, Khanh Ha, Erkan Demirkaya and Hasan Uludag
- 126 **Camouflaged angiogenic BMP-2 functions exposed by pico-paracrine biohybrids**
Herbert P. Jennissen
- 131 **State-of-the-art polyetheretherketone three-dimensional printing and multifunctional modification for dental implants**
Meiqing Chen, Mei Ren, Yingqi Shi, Xiuyu Liu and Hongtao Wei

- 156 **Exploring stimuli-responsive elastin-like polypeptide for biomedicine and beyond: potential application as programmable soft actuators**
Yeongjin Noh, Eunjoo Son and Chaenyung Cha
- 172 **Resorbable conductive materials for optimally interfacing medical devices with the living**
Marta Sacchi, Fabien Sauter-Starace, Pascal Mailley and Isabelle Texier



OPEN ACCESS

EDITED AND REVIEWED BY
John Forsythe,
Monash University, Australia

*CORRESPONDENCE
Hasan Uludağ,
✉ hasan.uludag@ualberta.ca

RECEIVED 02 January 2024
ACCEPTED 11 January 2024
PUBLISHED 23 January 2024

CITATION
Uludağ H, Wang Y, Vrana NE, Tamerler C,
Kothapalli C and Vasudev MC (2024), Editorial:
Insights in biomaterials 2022 / 2023—novel
developments, current challenges and
future perspectives.
Front. Bioeng. Biotechnol. 12:1364724.
doi: 10.3389/fbioe.2024.1364724

COPYRIGHT
© 2024 Uludağ, Wang, Vrana, Tamerler,
Kothapalli and Vasudev. This is an open-access
article distributed under the terms of the
[Creative Commons Attribution License \(CC BY\)](#).
The use, distribution or reproduction in other
forums is permitted, provided the original
author(s) and the copyright owner(s) are
credited and that the original publication in this
journal is cited, in accordance with accepted
academic practice. No use, distribution or
reproduction is permitted which does not
comply with these terms.

Editorial: Insights in biomaterials 2022 / 2023—novel developments, current challenges and future perspectives

Hasan Uludağ^{1*}, Yunbing Wang², Nihal Engin Vrana³,
Candan Tamerler⁴, Chandra Kothapalli⁵ and Milana C. Vasudev⁶

¹Faculty of Engineering, University of Alberta, Edmonton, AB, Canada, ²National Engineering Research Center for Biomaterials, Sichuan University, Chengdu, China, ³Spartha Medical, Strasbourg, France, ⁴Mechanical Engineering, University of Kansas, Lawrence, KS, United States, ⁵Washkewicz College of Engineering, Cleveland State University, Cleveland, OH, United States, ⁶Bioengineering, University of Massachusetts Dartmouth, North Dartmouth, MA, United States

KEYWORDS

biomaterials, scaffold, tissue engineering, therapy, diagnostics, drug delivery, biocompatibility

Editorial on the Research Topic

Insights in biomaterials 2022 / 2023—novel developments, current challenges, and future perspectives

We are now entering the third decade of the 21st century, and, especially in the last few years, the achievements made by scientists have been exceptional, leading to major advancements in the rapidly growing fields of bioengineering and biotechnology. New biomaterials designed with advanced features have been the driving force behind the applications in bioengineering and biotechnology fields. This annual Research Topic, which highlights article submissions typically from our Editorial Board members, looks to explore new insights, novel developments, current challenges, latest discoveries, recent advances, and future perspectives in the field of **Biomaterials**. This Research Topic solicited brief, forward-looking contributions that describe the state of the art, outlining recent developments and major accomplishments that have been achieved and that need to occur to move the field forward. We wanted to shed light on the progress made in the past decade in the biomaterials field, and on its future challenges, to provide a thorough overview of the field. This article Research Topic is intended to inspire, inform and provide direction and guidance to researchers in the field. Eleven articles have been finally accepted for this Research Topic which were a mixture of review papers and technical articles.

The review paper by [Tiemeijer and Tel](#) summarized the current state of affairs in utilization of **hydrogels** for single cell microgel production. Hydrogels, with their high-water content and being readily tunable for physicochemical features, offer an opportunity to create suitable microenvironments for cell cultivation at microscale so as to foster selection of individual cells (or clones) for selection for a variety of reasons. While microdrop production has been used for cell encapsulation since 1980s, using microfluidics devices that emerged in the last decade provides exquisite control over the hydrogel features at the micro scale. Common materials used for microgel production was reviewed as well as a survey of applications including sequencing, biosensing using entrapped cells and enhanced cultivation for various purposes, including therapy. The technology is bound to yield

novel diagnostic and therapeutic approaches based on cellular cultivation. The review article by [Cassenellas et al.](#) have focussed on recent advances in *engineering nanotopographic substrates* for cell studies. As in engineered microgels above, 'nano-engineered' surfaces could provide unique and improved features for cultivation of cells intended for a variety of reasons. The authors briefly summarized the mechanistic effects of nano-engineered topography on cellular processes, while providing a summary of main fabrication techniques to achieve the desired nanotopographies. Various biological applications were summarized in this context, and the authors briefly commented on the 'stimuli-responsive' nanotopographies to present fruitful opportunities in the future.

The nano-structured particles, as in surfaces, have also found widespread use in medicine. The early host response to such nanoparticles following the initial opsonization is typically the cytokine secretion, which has important implications on host physiology as well as the compatibility of the nanoparticles in the long run. [Nasrullah et al.](#) summarized the most recent literature on *cytokine responses to nanoparticulate systems* and identified the main factors of nanoparticles affecting this response. For diseases arising from the altered cytokine pathophysiology, attempts to silence the individual components of cytokine response are summarized, and the roles of nanoparticle features in this respect were presented. The authors provide their perspective on the possibility of engineering nanoparticle delivery systems with controlled cytokine responses as the basis of new therapeutic modalities.

In an original article, [Cervello et al.](#) probed the *protease-degradable hydrogels* with multifunctional biomimetic peptides for bone tissue engineering. Integrin-binding and osteogenic Bone Morphogenetic Protein-2 (BMP-2) derived peptides were used to functionalize hydrogels, leading to successful cultivation of mesenchymal stem cells (MSCs) and significantly improving their osteogenic differentiation. Such biomimetic materials can find application in tissue engineering efforts when constructing functional tissues *ex vivo* as well as in regenerative medicine to stimulate innate bone regeneration *in situ*. The design principles emanating from such exquisitely-engineered biomaterials are bound to be applicable to other scaffolds intended for other types of tissues as well. The perspective article by [Jennissen](#) on one of the first morphogens discovered, BMP-2, keeps the light shining on this enigmatic protein; the author describes experimental systems composed of BMP-2 and electrospun poly (L-lactide) nanofibers that point out new mechanisms of action for BMP-2 (pro- and anti-angiogenic functions) at picomolar range, which is substantially lower than typical doses used in clinical setting (mg/mL) and small preclinical animal models (µg/mL). Careful considerations and better understanding of physiochemical features and *in situ* levels of the protein is bound to guide better design of *devices incorporating tissue-inducing morphogens*, aiming for more physiological tissue repair.

The compiled Research Topic provided valuable perspectives on specific types of biomaterials utilized in biotechnological and medical applications. *Cellulose*, one of the most abundant materials in nature, is a versatile biomaterial that has been explored for numerous applications to improve human health. Its modification is continually attempted to finetune the

physicochemical properties for new applications. [Fatema et al.](#) summarized recent developments in modified celluloses, summarizing physical and chemical means to undertake the desired modifications. The range of applications pursued with cellulose are presented with a keen eye on possible future developments. Focus on nanoscale features are particularly emphasized as the next frontier in celluloses' use as a biomaterial. With respect to a specific biomaterial for a target application, [Chen et al.](#) highlighted the current state of three-dimensional printing of *polyetheretherketone* (PEEK) and its multifunctional modification for dental implants. PEEK is an attractive polymer that can be engineered to display an elastic modulus close to that of the mineralized tissues. That makes it suitable for implantation at such sites from a mechanical perspective but its other features pose severe barriers for full histocompatibility. The authors reviewed the recent attempts to modify the material and deploy it in 3D-printing processes to create the ideal dental implant. The experience gained by the PEEK could illuminate the path for new generation of synthetic polymers as biomedical implants. In a review article, [Noh et al.](#) explored the technology of stimuli-responsive *elastin-like polypeptides* (ELPs) for biomedicine and beyond, especially their potential application as programmable soft actuators. A summary of stimuli-response biomaterials has been presented as the foundation of biomedical actuators, driven by electrical, thermal, pH and light responsive elements. The ELPs stand out as thermoresponsive materials; the authors presented a spectrum of uses for ELPs and provided differentiated features of ELPs as compared to other thermoresponsive materials. Recent developments in the field have been summarized in detail while the critical next-steps to move ELP towards actuators has been briefly outlined.

Two articles in this described devices intended for targeted applications. [Zhang et al.](#) reviewed recent developments in interventional devices for mitral valve repair with implantation of artificial chords. The article focussed on mitral regurgitation and its repair, outlining several approaches to surgical repair and highlighting currently used devices in a clinical setting. The use of one of the first synthetic polymers in modern medicine, namely, expanded *polytetrafluoroethylene* (ePTFE), has been highlighted in this application. More importantly, factors contributing to the failure of artificial chords have been probed. This is critical to develop the next-generation materials (or surgical approaches) to improve mitral interventions. The authors highlight the expected evolution of the field in the direction of interventional transcatheter chordae repair devices. On the other hand, [Veit et al.](#) report an original study on a versatile, bioengineered skin reconstruction device designed for use in austere environments. *Silk fibroin with an antioxidant hyaluronic acid* derivative were formulated into a skin compliant device with controlled drug delivery and self-adherent features. This engineered device performed well in an *in vitro* model with good integration into the tissue by allowing cellular migration into and above the device. The prototype described in this study will illuminate the path for simple-yet-functional regenerative devices where limited medical resources are available.

Finally, a review article by [Sun et al.](#) describes the past experience with *biodegradable films* for soil by conducting a 30-year systematic review. Polymer science has increasingly provided the foundation and

the materials for biodegradable films with minimal environmental footprint. Although the focus is not biomedical use of materials, the analytical methodology on published literature described in this paper as well as the mechanistic insight into biodegradation mechanism(s) may pave ways for development of new materials in biomedical enterprise. The environmental considerations and clinical perspective both recognize the biodegradation as ideal to reduce waste and to leave a minimal footprint in the host. This philosophy could promote ecologically sustainable development, and this article may further sensitize biomedical engineers and scientists in this regard.

The Research Topic of articles provides important additions to biomedical literature where traditional, mechanically oriented and inert biomaterials as well as more recent biomimetic regenerative biomaterials are formulated for various applications. Emphasis on application-oriented contributions emphasize the need to design, manufacture and optimize the biomaterial and device features for the intended applications. Our imagination and a plethora of state-of-the-art tools drive this venture. Transdisciplinary scientific and engineering pursuits are evident in the collected papers where the traditional silos are routinely crossed to yield effective interventions for the benefit of patients.

Author contributions

HU: Conceptualization, Writing–original draft. YW: Writing–review and editing. NV: Writing–original draft,

Writing–review and editing. CT: Writing–review and editing. CK: Writing–review and editing. MV: Writing–review and editing.

Funding

The author(s) declare that no financial support was received for the research, authorship, and/or publication of this article.

Conflict of interest

The authors declare that the research was conducted in the absence of any commercial or financial relationships that could be construed as a potential conflict of interest.

The author(s) declared that they were an editorial board member of Frontiers, at the time of submission. This had no impact on the peer review process and the final decision.

Publisher's note

All claims expressed in this article are solely those of the authors and do not necessarily represent those of their affiliated organizations, or those of the publisher, the editors and the reviewers. Any product that may be evaluated in this article, or claim that may be made by its manufacturer, is not guaranteed or endorsed by the publisher.



Hydrogels for Single-Cell Microgel Production: Recent Advances and Applications

B. M. Tiemeijer^{1,2} and J. Tel^{1,2*}

¹Laboratory of Immunoengineering, Department of Biomedical Engineering, TU Eindhoven, Eindhoven, Netherlands, ²Institute of Complex Molecular Systems, TU Eindhoven, Eindhoven, Netherlands

OPEN ACCESS

Edited by:

Tiago G. Fernandes,
University of Lisbon, Portugal

Reviewed by:

Ulyana Shimanovich,
Weizmann Institute of Science, Israel
Jonghyun Oh,
Jeonbuk National University, South
Korea

*Correspondence:

J. Tel
J.Tel@tue.nl

Specialty section:

This article was submitted to
Biomaterials,
a section of the journal
Frontiers in Bioengineering and
Biotechnology

Received: 07 March 2022

Accepted: 09 May 2022

Published: 17 June 2022

Citation:

Tiemeijer BM and Tel J (2022)
Hydrogels for Single-Cell Microgel
Production: Recent Advances
and Applications.
Front. Bioeng. Biotechnol. 10:891461.
doi: 10.3389/fbioe.2022.891461

Single-cell techniques have become more and more incorporated in cell biological research over the past decades. Various approaches have been proposed to isolate, culture, sort, and analyze individual cells to understand cellular heterogeneity, which is at the foundation of every systematic cellular response in the human body. Microfluidics is undoubtedly the most suitable method of manipulating cells, due to its small scale, high degree of control, and gentle nature toward vulnerable cells. More specifically, the technique of microfluidic droplet production has proven to provide reproducible single-cell encapsulation with high throughput. Various in-droplet applications have been explored, ranging from immunoassays, cytotoxicity assays, and single-cell sequencing. All rely on the theoretically unlimited throughput that can be achieved and the monodispersity of each individual droplet. To make these platforms more suitable for adherent cells or to maintain spatial control after de-emulsification, hydrogels can be included during droplet production to obtain “microgels.” Over the past years, a multitude of research has focused on the possibilities these can provide. Also, as the technique matures, it is becoming clear that it will result in advantages over conventional droplet approaches. In this review, we provide a comprehensive overview on how various types of hydrogels can be incorporated into different droplet-based approaches and provide novel and more robust analytic and screening applications. We will further focus on a wide range of recently published applications for microgels and how these can be applied in cell biological research at the single- to multicell scale.

Keywords: single cell, hydrogel, droplet, microfluidics, microgel, immunology, pairing

INTRODUCTION

The vast complexity of the human body is gradually being unraveled. However, the more we discover about various types and sub-populations of cells, the more questions are often raised. Furthermore, the complex web of intercellular interactions they maintain makes fully understanding the depth of biological processes and regulators challenging. Over the years, research has downsized by moving from a tissue, to cell population, and to single-cell resolution, in order to grasp the most basic interactions underlying systemic responses (Altschuler and Wu, 2010; Satija and Shalek, 2014). This miniaturization has not only allowed the reduction of noise in measuring systems but also allowed more precise measurement, smaller sample sizes, and less reagent consumption. In addition, it has broadened the view on how homogenous, cellular behavior within well-defined populations of cells, really is. As technology advanced and cell behavior was studied at a smaller and smaller level, it

became clear that cell populations displayed much more heterogeneous behavior than previously thought (Woodland and Dutton, 2003a; Gordon and Taylor, 2005; Villani et al., 2017). This allowed for characterization of vast amounts of sub-populations of cells with specific specializations. By looking at individual cells instead of populations, the masking cloud of averaged measurements could be elevated, showing that some cells are more potent at specific tasks than others (Dueck et al., 2016). This way of looking at cellular heterogeneity could explain the fact that cell-therapies are often less effective *in vivo* as they are predicted to be *in vitro*, and often vary immensely between subjects (Chattopadhyay et al., 2014; Satija and Shalek, 2014). To fully dissect the complexity of cellular heterogeneity and cell-cell interactions, reliable methods of high-throughput single-cell research must be developed. The developments in the field of microsystems and microfluidics have proven to be a valuable tool in establishing such novel approaches.

Since the rise of soft lithography (Xia and Whitesides, 1998), microfluidics has been making major leaps forward with increasingly complex device designs (Murphy et al., 2017; Shinde et al., 2018; Jammes and Maerkl, 2020). Generally, these have consisted of intriguing labyrinths of channels connected to low-volume fluidic pumps. These designs allow for very low sample sizes but high precision experimental setups, which efficiently scales down but improves experimental control. More importantly, the micrometer scale is ideal for physical manipulation of cells using fluidics (Sims and Allbritton, 2007; Shinde et al., 2018; Luo et al., 2019; Yeh and Hsu, 2019). The relatively gentle nature of moving cells around with fluids puts it at a high advantage over mechanical approaches. Nevertheless, the production of these conventional microfluidic devices with various capture chambers, wells, and often multilayered channels can be tedious and generally the throughput is limited by the device dimensions.

Droplet-based microfluidics uses relatively simple device designs in which laminar flow under low Reynolds number allows for fast, reliable, and reproducible droplet production (Shang et al., 2017). These droplets, ranging from sizes in the pico- to nanoliter scale can be used as a tool to encapsulate and thus spatially control cells, similar to what capture chambers and wells aim to do in conventional microfluidic devices. In droplets however, the number of processed cells is only limited by the available amount of reagent, as samples are continuously flushed through the microfluidic device. This potential for theoretically unlimited throughput together with flexibility and a huge range of applications has allowed droplet-based microfluidics to rapidly become a discipline of its own (Shembekar et al., 2016; Sinha et al., 2018).

Even though variations exist, typical droplet-based approaches for cell encapsulation utilize two phases of fluids. The dispersed phase is a water-based cell suspension, and the continuous phase is an oil. This approach has gained much interest as the focus of cell biological research has shifted from studying cell populations to conducting experiments with single-cell resolution (Matuła et al., 2020). Droplet microfluidics has proven suitable to encapsulate these single cells, bringing them from a “bulk” cell

suspension to a “single-cell” suspension where cells are separated by water–oil interfaces. However, capturing cells in oil also makes it very difficult to further influence, manipulate, measure, or process them without breaking the emulsion and returning to the “bulk” cell suspension (Luo et al., 2019).

Over recent years, the combination of hydrogel and microfluidic droplets has been applied to maintain spatial control over cells after de-emulsification or to provide cells with a solid droplet environment (Zhu and Yang, 2017; Kamperman et al., 2018; Mohamed et al., 2020). Various hydrogels, gelation methods, droplet production techniques, and cell types gave rise to large amounts of unique research (Goy et al., 2019). This strong combination is utilized for a variety of innovative single cell techniques, which can be applied to *in vitro* analytical approaches (Figure 1). Here, we will discuss the current state-of-the-art of single- and multicell droplet techniques, and how these can be complemented with the use of hydrogel. We will start with discussing the basic principles of microfluidics and droplet formation and how commonly used hydrogels can be integrated into this approach. We will then discuss various microgel applications, starting with a single-cell analysis and single-cell pairing and how these can benefit from microgels, followed by the application of semi-permeable hydrogel shells, and finishing with microgel coculture. We believe recent advances in this field demonstrate that this multifaceted combination will allow for promising new applications, facilitate a high-throughput droplets analysis, or provide more suitable culture conditions for adherent cells.

HYDROGEL DROPLETS

Microfluidics

Microfluidic devices for droplet production are commonly produced using soft lithography of polydimethylsiloxane (PDMS) (Xia and Whitesides, 1998). The technique has persisted and remained relevant over years of research due to its ease of use, low cost, and precision, which together allow for fast prototyping of novel microfluidic designs. Such prototyping has mostly been an advantage for complex microfluidic systems, whereas for droplet production, the basics of device designs have remained mostly the same. A generic droplet device consists of two inlets for the continuous and the dispersed phase followed by an outlet for collecting the produced emulsion (Figure 2A). Inside the device, co-flow, flow-focusing, or T-junction geometries ensure the controlled mixing of the two immiscible fluids, which due to laminar flow produces highly homogenous droplet sizes. The distribution of cells in the dispersed phase follows a Poisson distribution (Collins et al., 2015), allowing droplets to be tuned to contain multiple cells or approach single-cell encapsulation. The concepts behind the fluid dynamics of droplet formation have been extensively described previously (Cubaud and Mason, 2008; Shembekar et al., 2016; Tawfik, Griffiths; Zhu and Wang, 2017), and will therefore not be discussed in detail.

When droplet volume and cell concentration are tuned correctly, this can result in a cell distribution, which closely

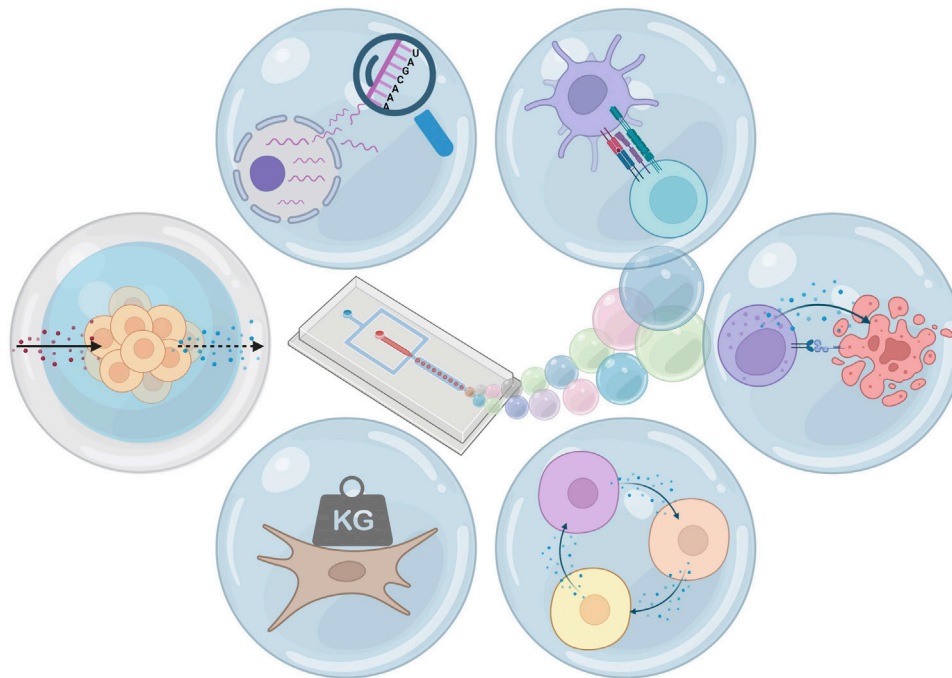


FIGURE 1 | Hydrogel microfluidic droplets: applications. From top-left clockwise: single-cell sequencing, pairing for cell interaction, pairing for cytotoxicity, coculture, changing and measurement of mechanical properties, and selectively permeable hydrogel shells. Figure created using Biorender.

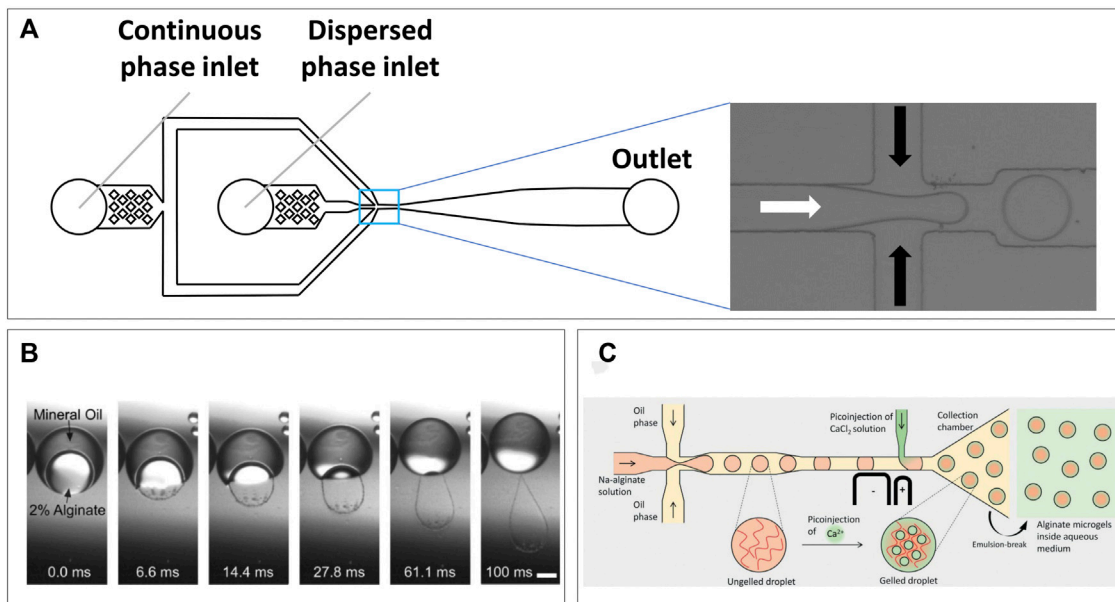


FIGURE 2 | Microfluidic droplet formation. **(A)** Generic emulsification device, two inlets for the continuous and dispersed phases which mix at the channel intersection (pop-out), droplets then continue flowing toward collection from outlet. **(B)** Transfer of alginate solution from a double-emulsion toward a CaCl_2 solution causes gelation within 100 ms (Martinez et al., 2012). **(C)** Microfluidic design utilizing pico-injection of CaCl_2 after droplet formation point to prevent premature gelation of alginate solution (Ahmed et al., 2021).

approaches single-cell encapsulation. Deviation from this optimized point will result in either more empty droplets, or more multicell droplets, as in compliance with Poisson

distribution (Collins et al., 2015). Single-cell research is commonly used to deprive cells from cell-cell interactions and discover their innate capabilities and potential for responding to

specific stimuli. When comparing droplet-based approaches to well- or trap-based applications, the main advantage is the potential for high-throughput, which is indispensable when screening for rare cell behavior or sub-populations. In addition, the oil–water interface ensures complete isolation between cells, while in some well/trap-based microfluidic approaches paracrine signaling cannot be ruled out (Guldevall et al., 2016; Zhou et al., 2020). However, the absence of cellular adhesion and the difficulty to manipulate cells when in oil–water emulsion are inherent challenges of single-cell droplet encapsulation. The addition of hydrogel in droplets to produce microgels proves a double-edged sword, providing solutions to both problems. Cellular adherence and mechanical cues can be provided *via* biocompatible hydrogels providing a semi-solid extracellular matrix-like environment (Dumbleton et al., 2016; Hasturk and Kaplan, 2019; Tiemeijer et al., 2021). On the other hand, the hydrogel can maintain spatial control over cells after de-emulsification while allowing for diffusion and downstream processing using analytes or other reagents (Leonaviciene et al., 2020; di Girolamo et al., 2020; Yanakieva et al., 2020; Chokkalingam et al., 2013).

Some variations of the basic droplet production approach are needed when hydrogel is added to the dispersed water phase. The implementation strongly depends on the type of hydrogel and method of cross-linking. Droplet breakoff is dictated by the ratio of viscosity between the continuous and dispersed phases (Günther and Jensen, 2006). Thus, premature hydrogel gelation, resulting in increased viscosity of the dispersed phase, is detrimental for a consistent droplet size. Therefore, the type of crosslinking dictates droplet formation and adjustments that need to be made to device design. Commonly used types are ionic cross-linking (Choi et al., 2007; Workman et al., 2007; Utech et al., 2015; Ahmed and Stokke, 2021), photo-cross-linking (Zhao et al., 2016; Mohamed et al., 2019; Nan et al., 2019), and thermo-responsive cross-linking (Dolega et al., 2015; Yanakieva et al., 2020; Tiemeijer et al., 2021; Zhang et al., 2021). By design, the latter two do not require on-chip mixing of different aqueous phases and can still be used in conventional device designs. However, the first might require gelators to be mixed in, which means an extra dispersed phase inlet is required for on-chip mixing, just prior to or right after, droplet formation (figure of various designs). Various types of hydrogels have been used in droplet microfluidics, which can roughly be divided into natural polymers and synthetic polymers (Table 1).

Hydrogels and Cross Linking

Natural Hydrogels

Natural polymers have the advantage of being natively biocompatible and are generally cross-linked *via* relatively mild gelation processes increasing cell survival. They form structures that are very comparable to mammalian extracellular matrix and thus ideal for harboring cells (Gasperini et al., 2014).

Alginate is potentially the most used natural polymer to produce microfluidic hydrogel droplets with. The brown algae-derived polysaccharide has been favored due to its biocompatibility (Lee and Mooney, 2012) and various

strategies for cross-linking. The polymer forms a hydrogel either due to lowering of pH or in the presence of divalent cations due to ionic interactions (Gurikov and Smirnova, 2018). These ionic interactions allow the alginate fibers to form a supramolecular “Egg-box” structure (Braccini and Pérez, 2001). In droplet applications, the latter is by far more commonly used and often calcium is used for this as released in a CaCl_2 solution. This will result in extremely fast gelation, and although it has been demonstrated that droplets can be produced by on-chip mixing (Choi et al., 2007), this will generally result in instant and uncontrolled gelation. Illustrative for this instant gelation was the formation of “rain-droplet” shaped hydrogels when alginate was retrieved from double-emulsions into a CaCl_2 solution (Figure 2B) (Martinez et al., 2012). Therefore, other strategies can be needed for on-chip droplet formation to ensure constant low viscosity during droplet production. Recently, Ahmed et al. demonstrated a unique device design which produced alginate droplets following a conventional approach but used on-chip pico-injection of CaCl_2 solution to prevent problems with premature gelation and obtain monodisperse hydrogel droplets (Figure 2C) (Ahmed and Stokke, 2021). Alternatives to CaCl_2 are partially soluble or insoluble calcium salts such as calcium sulfate (Kong et al., 2003) and calcium carbonate (Tan and Takeuchi, 2007; Workman et al., 2007), respectively. As these have lower solubility in water compared to calcium chloride, gelation occurs slower, although this still proves challenging to control (Kuo and Ma, 2001). A promising approach comes in the triggered release of Ca ions from strong chelators such as EDTA. Calcium–chelator complexes are mixed with alginate solutions where the high chelator affinity prevents direct gelation. By decreasing pH, calcium is released which allows cross-linking. This approach proved suitable to maintain stability of droplet formation while triggering gelation directly on-chip (Shao et al., 2020), or at a later time point by acidifying the continuous oil phase off-chip (Utech et al., 2015). Adaptations of this approach utilize competitive chelator kinetics (Bassett et al., 2016), aiming to have more control over gelation dynamics and improved cell viability (Häti et al., 2016). Alginate has a large pore-size of 5–150 nm (Martinsen et al., 1989), which is dictated by the calcium concentration used for cross linking. Although small molecules can diffuse in, large protein diffusion can be limited (Tanaka et al., 1984), which is most likely due to a combination of a non-homogenous pore size on gelation surface, and protein charge at neutral pH (Smidsrød and Skjåk-Bræk, 1990). This should be considered when designing cell studies in alginate droplets. Although perfectly biocompatible, alginate does not provide cells with adherence and will, thus, have to be functionalized with, for example, Arg-Gly-Asp (RGD) motifs (Yu et al., 2009), or be used in a composite with adherent polymers (Xu et al., 2007; Dixon et al., 2014).

Another commonly used natural polymer is agarose, which is like alginate derived from specific types of algae. Unlike alginate it cross-links due to temperature changes and exhibits hysteresis (Indovina et al., 1979). The polysaccharide dissolves at temperatures around 90°C and cross-links due to hydrogen bonds when cooled to around 35–50°C depending on which type of algae was the source. The polymer chains form helical

fibers which aggregate into a 3D supramolecular structure (Xiong et al., 2005). Although these transition temperatures are not suitable for cell applications, agarose can be methylated to lower gelling temperature (Gu et al., 2017). Therefore, ultralow gelling point agarose has proven very suitable for hydrogel droplet encapsulation of cells (Chokkalingam et al., 2013; Sinha et al., 2019; Yanakieva et al., 2020). With a gelling temperature of 8°–17°C, it can be dissolved at high temperatures but used to encapsulate cells safely at much lower biological compatible temperatures, without premature gelation. Gelation can easily be triggered by cooling down anywhere between droplet production and droplet-demulsification. Agarose droplets are especially useful for cell processing after de-emulsification due to their stability and relatively large pore-size, which is partially dependent on polymer concentration (Narayanan et al., 2006). Their pore size within the range of 100–600 nm facilitates diffusion of virtually any soluble molecule including antibodies (~10 nm (Reth, 2013)), which allows inflow of nutrients or fluorescent markers for analysis. This property combined with their stability at lower temperatures has facilitated a whole-droplet flow cytometric analysis (Chokkalingam et al., 2013), and even sorting (Fang et al., 2017; Yanakieva et al., 2020). Agarose is inherently non-adherent to cells, and thus needs functionalization with extracellular matrix molecules to obtain cellular attachment in droplets (Karoubi et al., 2009). Furthermore, agarose is non-degradable by mammalian cells, and thus bacteria-derived agarose (Fu and Kim, 2010), or production of degradable composite hydrogels (Zhang et al., 2012), is needed to retrieve cells. This can be a limiting factor when downstream cell recovery is required as reheating to above the melting point will kill cells and destroy proteins of interest.

Although alginate and agarose are frequently used and offer several desirable characteristics, they are not inherently cell-adherent. Therefore, an alternative can be connective tissue-derived hydrogels which contain peptide motifs facilitating cell attachment. Collagen (Antoine et al., 2014) and its derivative gelatin (Jaipen et al., 2017) are arguably the most commonly used. Gelatin is obtained by breaking collagen down to single-strain molecules (Kuijpers et al., 1999). Both yield thermo-reversible hydrogels with transition temperatures within biocompatible ranges. Uniquely, collagen will cross-link when heated to physiological temperature (Xu et al., 2009), whereas gelatin will cross-link when it is cooled below 35°C (Hellio and Djabourov, 2006). As collagen is the main component of extracellular matrix, these hydrogels are highly biomimetic and often used in tissue engineering approach due to their biodegradability (Antoine et al., 2014; Tondera et al., 2016). In droplet microfluidics, Matrigel® is a commonly used commercially available collagen-based hydrogel (Dolega et al., 2015; Zhang et al., 2021). Below room temperature allows droplet formation, and by simply bringing droplets to culturing temperature, cross-linking occurs. This process is fully reversible, allowing for cell retrieval. As gelatin-based hydrogels will return to the liquid phase at culture temperatures, these have routinely been chemically modified. A commercially available gelatin-based hydrogel is GelMA,

which is enriched with methacrylate groups to facilitate UV-triggered cross-linking (van den Bulcke et al., 2000; Sun et al., 2018). These have allowed for both on-chip (Mohamed et al., 2019; Nan et al., 2019) and off-chip (Zhao et al., 2016) gelation and production of microfluidic droplets. A major downside of collagen and gelatin-based hydrogel droplets is their tendency to merge and aggregate after de-emulsification, as was observed for both Matrigel® and GelMA. This makes downstream processing after removal of the continuous phase very challenging.

Synthetic Hydrogels

Examples of synthetic polymers used in production of hydrogel droplet microfluidics are poly(ethylene glycol) (PEG), poly(acrylic acid), poly(vinyl alcohol) (PVA), poly(acrylamide), and their derivatives (Wan, 2012). The main advantages of synthetic over natural polymers are their reproducibility of synthesis and the possibility for chemical modification (Hern and Hubbell, 1998). They are inherently non-adhesive to cells and unless modified they are non-biodegradable. Functionalization with molecules such as Arg-Gly-Asp (RGD) motifs (Sionkowska, 2011; Kim et al., 2019), or mixing of natural and synthetic polymers (Krutkramelis et al., 2016), is therefore required for many cellular applications. Alterations of these polymers can be used to provide useful cross-linking approaches such as photopolymerization as demonstrated in PEG (Young et al., 2013; Xia et al., 2017) and PVA (Zhao et al., 2010). Similarly, combinations of natural and synthetic polymers can be combined with temperature responsive moieties to obtain hydrogels with unique swelling and gelling properties (Jiang et al., 2019a). Such composite hydrogels can also allow for fine-tuning of hydrogel degradation (Benavente Babace et al., 2019; Neubauer et al., 2019), which offers lots of potential for *in vivo* applications. In addition, alterations can facilitate complex techniques that would be extremely difficult or impossible with natural hydrogels. Some examples are detection of cell forces (Allazetta et al., 2017), tuning hydrogel stiffness (Rahimian et al., 2019), and controlling diffusion (Zhu, 2010; Leonaviciene et al., 2020). The possibilities for adaptations to synthetic hydrogels are too wide to be covered in this review, but its applications for tissue engineering purposes are very adequately discussed in a review by Jummin Zhu (White et al., 2021).

Recovery of Microgels

A hydrogel in oil emulsification using microfluidics is praised for its production of highly monodisperse microgels in a high-throughput fashion. To recover the microgels for downstream applications, the emulsion must be broken to separate the water and oil phases. Generally, this separation can be achieved using chemical breaking, electrostatic displacement, or washing. All three can be performed either on-chip or in bulk after droplet collection. For off-chip chemical breaking, destabilizing of droplet surface tension using 1H,1H,2H,2H-perfluoro-1-octanol (PFO) is very common practice for fluorinated oils (Karbasschi et al., 2017). This chemical displaces the surfactants in the oil forcing the droplets to coalesce, with the advantages of being quick and easy. As a downside, the

TABLE 1 | List of recently published research using various types of natural and synthetic hydrogels for innovative single-cell microgel techniques.

Type	Hydrogel	Cross linking	Application	Reference
Natural	Alginate	Calcium release from EDTA complex	Controlled gelation of microgels for cell encapsulation	Utech et al. (2015)
		On-chip picoinjection of CaCl ₂	Picoinjection of CaCl ₂ for controlled gelation of microgels for cell encapsulation	Ahmed and Stokke, (2021)
		On-chip mixing of alginate with Ca chelators	Testing of different chelators for cell encapsulation in microgels	Shao et al. (2020)
		Competitive ligand exchange crosslinking	Cell encapsulation with increased gelation control and improved cell viability	Håti et al. (2016)
		Alginate + CaCl ₂ in oil phase	Monodisperse microgels for cell aggregate encapsulation	Wang et al. (2021)
	Agarose	Cooling below 18°C	Pairing of secreting cell with reporter cell and flow cytometric sorting	Yanakieva et al. (2020)
			Pairing of secreting cell with detection beads for flow cytometric measurement	Chokkalingam et al. (2013)
			Encapsulation of cells to monitor cell egress	Neubauer et al. (2019)
	Gelatin based	Cooling on ice and genipin addition	Monitoring single tumor-cell response to adherence on gelatin microgels	Nan et al. (2019)
		Off-chip UV exposure (GelMA)	Rapid generation of injectable stem cell-laden microgels for tissue engineering	Zhao et al. (2016)
Synthetic	PEG based	On-Chip UV exposure (GelMA)	On-chip gelation and retrieval from oil phase for cell encapsulation	Mohamed et al. (2019)
			On-chip gelation and sorting into aqueous medium	Hong et al. (2012)
		Collagen based	On-chip gelation for cell encapsulation	Bavli et al. (2021)
			Production of large monodisperse organoids for drug testing	Zhang et al. (2021)
		Emulsification in the 37°C oil phase	Production of endothelial cell organoids	Dolega et al. (2015)
		Heating to 37°C (Matrigel®)		
	Polyisocyanide	Mixing acrylated PEG with dextran	Production of semi-permeable shell capsules for multistep processing of large biomolecules	Leonaviciene et al. (2020)
		Mixing thiolated PEG with PEG-dimaleimide	Production of hydrogel beads with force-responsive fluorescence	Allazetta et al. (2017)
		Mixing vinylsulfone-PEG with thiol-PEG	Production of hydrogel beads with tunable stiffness and tunable RGD functionalization	Rahimian et al. (2019)
		Mixing maleimide-PEG with dithiotriol	Production of semi-permeable hydrogel shells for immunoassays	Zhu, (2010)
		Mixing of PEGDT with MALDEX	Single-cell encapsulation for culture of clones and subsequent mRNA sequencing	Zhao et al. (2021)
		Mixing of thiol-hyaluronic acid with PEGDA	Monodisperse microgels for cell encapsulation with semi-permeable silica coating	Mazutis et al. (2013)
		Heating to above 15°C	Prolonged encapsulation of adherent cells for culture with cell retrieval afterward due to thermoreversibility	Tiemeijer et al. (2021)

approach is generally regarded to affect viability of vulnerable cells. Therefore, a chemical-free alternative can be washing (Chokkalingam et al., 2013) or the use of electrostatics to be gentler on cells (Chokkalingam et al., 2014). On-chip recovery of microgels can also be achieved using PFO (Shao et al., 2020) and electrostatic manipulation to allow direct recovery of microgels in water. The electrostatic approach can either be used to force droplets to coalesce (Huang et al., 2015) or the charge difference can be used to push/pull hydrogels across an oil–water interface (Huang and He, 2014). The latter technique has recently been demonstrated by White et al. as an automated method to selectively sort cell-containing microgels from empty microgels (Wang et al., 2021), thus increasing downstream efficiency and avoiding empty droplets. For washing, on-chip designs have been proposed to get microgels from the oil phase into the water phase. Passive methods use the interfacial tension of the water–oil droplets to allow microgels to merge into a parallel flowing extraction aqueous phase (Wong et al., 2009; Deng et al., 2011). More active approaches use filtering (Bavli et al., 2021) or slow infusion of the aqueous phase (Tang et al., 2009).

HYDROGEL DROPLET SINGLE-CELL APPLICATIONS AND ANALYSIS

The interest in single-cell analysis has spiked over the past years because of highly heterogenous cell populations being discovered and proving their importance (Altschuler and Wu, 2010; Satija and Shalek, 2014). Droplet microfluidics allow for a high-throughput approach for single-cell encapsulation and thus isolation, creating reproductive nano-bioreactors facilitating, for example, single-cell sequencing. Furthermore, incorporation of hydrogels allowed control over mechanical properties at single-cell resolution.

Single-Cell Sequencing

Being able to discern which RNA molecules originate from which cell, while maintaining high throughput, has likely been the biggest challenge in performing single-cell RNA (scRNA) sequencing. Lysis of cell suspensions will result in an indiscernible mixture of nucleic acids. Therefore, the first published case of scRNA sequencing performed lysis of just 1 cell within just one tube (Islam et al., 2011). To increase throughput, this was followed up by parallel processing in well

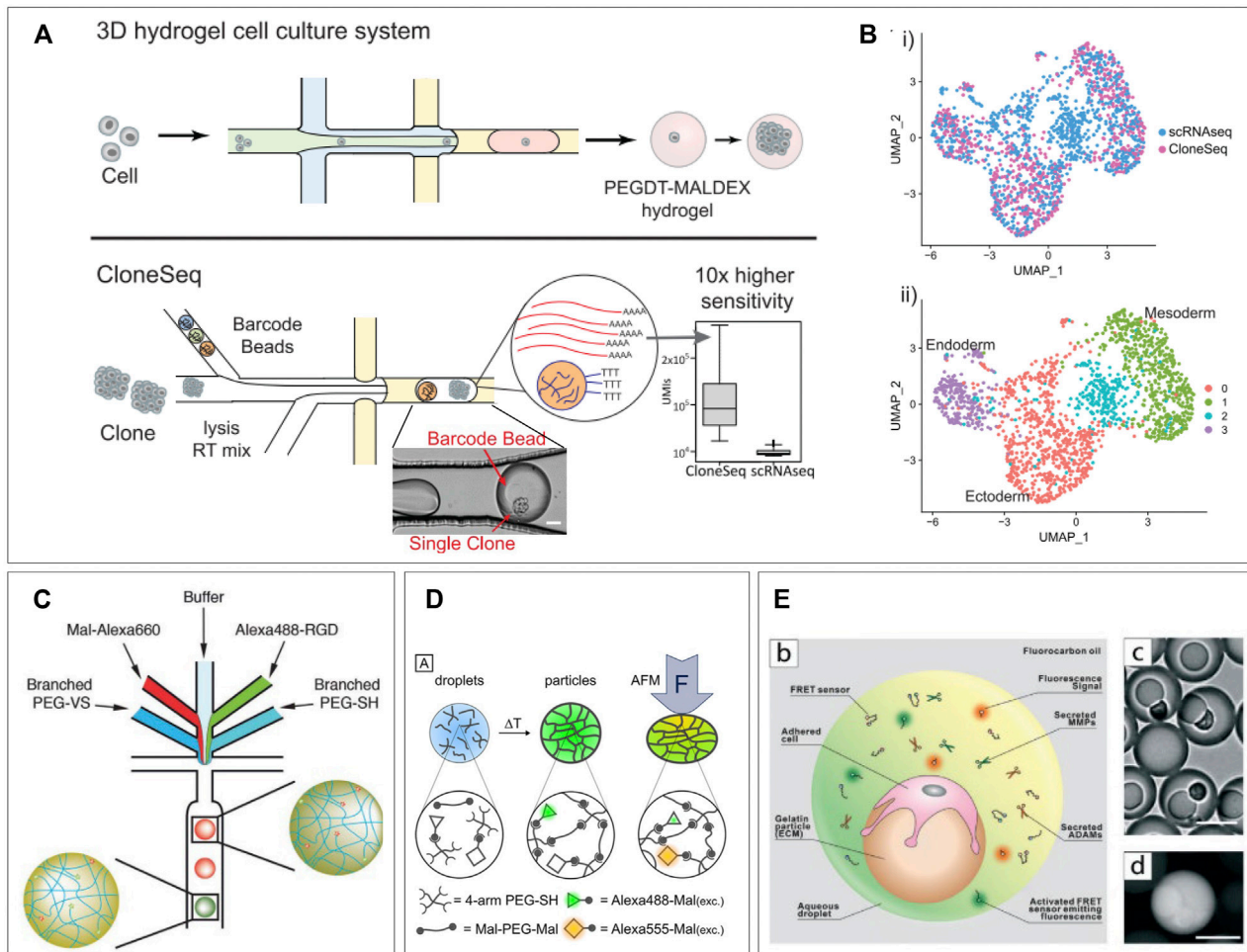


FIGURE 3 | Single-cell applications. **(A)** CloneSeq platform: single-cells are encapsulated in a hydrogel droplet and cultured to form a population of clones. This population is sequenced using an adapted sequencing protocol. **(B)** CloneSeq protocol exhibits improved separation of different stem cell differentiation states compared to conventional single-cell RNA sequencing (Bavli et al., 2021). **(C)** Microfluidic device for production of a library of droplets with unique mechanical and functionalization properties, which can be detected based on fluorescent signature. Adjusting the ratios of branched PEGs and the fluorophore channels allows tuning of droplet properties during production (Allazetta et al., 2017). **(D)** PEG-based hydrogel droplets incorporated with FRET pairs display fluorescence as a result of deformation, creating the potential to measure cell-exerted forces in-droplet (Neubauer et al., 2019). **(E)** Hydrogel droplets with attached cells are re-encapsulated in droplets along with FRET sensors which become fluorescent when bound by various proteases. This platform allows the single-cell measurement of proteases on different types of tumor cells to probe their metastatic behavior (Wang et al., 2021).

plates (Klein et al., 2015). Labeling of RNA strands in wells allowed for bulk polymerase chain reaction (PCR) and retracing cell identity after sequencing. However, this approach was still physically limited by wells' plate size. In 2015, two separate publications described the application of microfluidics droplet encapsulation to process single-cells with high throughput (Leng et al., 2010; Macosko et al., 2015). Co-encapsulation of cells and functional beads allowed for cell lysis, labeling of strands, and reverse transcription inside the droplets, before amplifying the transcripts with PCR in bulk. These applications used droplets for labeling purposes only and performed PCR afterward. To perform PCR in droplets, agarose droplets have been proposed to entrap large molecules of nucleic acid. Such techniques were reported for applications like single-cell molecule amplification (Novak et al., 2011), single-cell DNA trapping (Zhu et al., 2012),

or rare pathogen detection (Zilionis et al., 2016). A more recent application of RNA sequencing using hydrogel presented "CloneSeq", which utilizes in-droplet labeling but with hydrogel droplet pre-cultured single-cell clones to improve sequencing sensitivity (Zhao et al., 2021). Bavli et al. performed a first round of single-cell encapsulation of barcoded cells in PEGDT-Maldex hydrogel droplets, followed by a period of expansion to obtain a clump of clone cells from a single mother cell. The clone-cell clump is then re-encapsulated along with a barcoded bead as in the InDrops protocol (Kumachev et al., 2011) (Figure 3A). Their approach exploits the fact that clonal daughter cells maintain transcriptional similarities, to obtain a 10-fold larger library of unique RNA transcripts allowing for an increased sensitivity. This allowed them to prove that 3D culturing in these microgels maintains

more cellular stemness compared to bulk 2D culturing. In addition, they showed that in a mouse model of embryonic stem cells, CloneSeq was much more capable of discerning endo-, ecto-, and mesoderm differentiation states compared to conventional scRNA sequencing (**Figure 3B**). Also, in the detected differentiation states much more significantly enriched early differentiation genes were measured. In this approach, the implementation of hydrogel facilitates the expansion and spatial control of single-cell clones while allowing re-encapsulation with barcoded beads for sequencing with improved sensitivity. It underlines the potential for hydrogel droplets to improve similar novel techniques while providing suitable culture conditions for cells.

Tuning Hydrogel Mechanical Properties for Screening of Cellular Responses

Incorporation of hydrogels in microfluidic droplets has allowed for control over an extra parameter: mechanical properties. Tuning of hydrogel stiffness and elasticity is achieved by varying polymeric components and has been previously performed in droplets (Rahimian et al., 2019; Dagogo-Jack and Shaw, 2017). This allows for several directions of analytic tools, from testing individual cell forces (Allazetta et al., 2017), to screening gradients of hydrogel stiffness (Zhao et al., 2016), and the resulting cell responses (Nan et al., 2019). Apart from creating separate batches of hydrogels with varying properties, within a batch gradients of hydrogel stiffness can be screened. By including an extra dispersed phase inlet for different polymeric components and adjusting ratios, hydrogels can be obtained within a wide spectrum of mechanical properties. Kumachev et al. demonstrated this technique in 2011 by combining two streams of different agarose concentrations to create microgels with varying stiffness, suitable for cell encapsulation (Dagogo-Jack and Shaw, 2017). Allazetta et al. adapted the approach by using separate inlets for 4-armed PEG macromers and 8-armed PEG macromers plus a third inlet for red fluorescent maleimide groups (Rahimian et al., 2019). By changing the flow speed ratio between the PEG channels and the fluorescent channel, hydrogels with varying Young's moduli and reversely correlated fluorescent intensity could be created. These values were shown to correlate linearly allowing for a direct readout of the stiffnesses per individual microgel. Furthermore, by adding two extra dispersed phase inlets, one for buffer and one for green-fluorescent RGD molecules, microgels with tunable and detectable amounts of RGD, covalently build into the polymer structure, could be produced. In a final more complex microfluidic design, this allowed for independent programming of microgel stiffness and RGD-bioactivity along with direct fluorescent readout of exact microgel properties (**Figure 3C**). In addition, they demonstrated the potency of their platform by producing 100 unique microgel compositions with different functionalization and stiffness. Such tunable libraries of droplets with unique mechanical and chemical characteristics are a potential asset for screening of cell responses to different materials. Other recent research shows potential for in-droplet measurement of such cellular behavior. Neubauer et al. developed an interesting approach to a construct in which direct measurement of exerted forces by single cells can be possible

(Allazetta et al., 2017). Their PEG-based hydrogel droplets were incorporated with Alexa488 and Alexa555 as Förster resonance energy transfer (FRET) pairs. These molecules will undergo a fluorescence shift when they are moved into closer proximity. Therefore, deformation of the hydrogel droplets will result in a fluorescent readout (**Figure 3D**). Although only tested with atomic force microscopy indentation, the technique holds promise for real-time visualization of cell forces as the polymers are easily functionalized with cell-binding sites. A recent work by Wang et al. also utilizes FRET signals to detect single-cell responses to differences in mechanical properties of droplets. They produced gelatin beads onto which single cells were allowed to adhere. After adherence, the beads are re-encapsulated in microfluidic droplets along with FRET sensors. These sensors consist of a FRET pair which can be cleaved by specific cell-secreted proteases causing a fluorescent shift. They report on the effects ECM stiffness has on single tumor cells and their production of metastasis-related proteases (Nan et al., 2019). They created gelatin microgels with tunable stiffness onto which three types of human breast cells could adhere: non-tumorigenic cells, non-metastatic cancer cells, and metastatic cancer cells. By re-encapsulating these along with the FRET sensors, the single-cell expression of MMP2, MMP3, MMP9, and ADAM8 could be measured based on droplet fluorescence (**Figure 3E**). This gave insight into heterogeneous cell responses to substrate stiffness correlating to metastatic or non-metastatic behavior. Such research is of high value as therapy resistance is generally attributed to tumor heterogeneity (Meacham and Morrison, 2013; Xi et al., 2017).

HYDROGEL DROPLETS FOR CELL PAIRING APPLICATIONS AND ANALYSIS

Just like with trap- or well-based microfluidics, droplet-based microfluidics can be utilized to pair cells in close confinement. This relatively untapped category of applications is specifically promising in combination with hydrogels as it allows permanent spatial control, independent of emulsion integrity. This enables delivery of cell nutrients, allows for downstream processing, or co-analysis, all at a high throughput.

Co-Encapsulation Efficiency and Deterministic Encapsulation

When co-encapsulating a pair of heterotypic particles, the Poisson distribution proves a difficult hurdle (Collins et al., 2015), forcing a trade-off between either too few heterotypic pairs or too many droplets containing homotypic particles. In random encapsulation with a mixture of particles only a small fraction of droplets will contain exactly one particle of each type, which can only be optimized to a certain extent based on concentration and droplet size. Droplets containing the desired number of particles can be sorted on-chip (Hu et al., 2015; Segre and Silberg, 1961), but this will only improve purity and not increase production rate. Therefore, advances have been made in deterministic encapsulation of particles in droplets to skew the Poisson distribution into a desired direction. To achieve this,

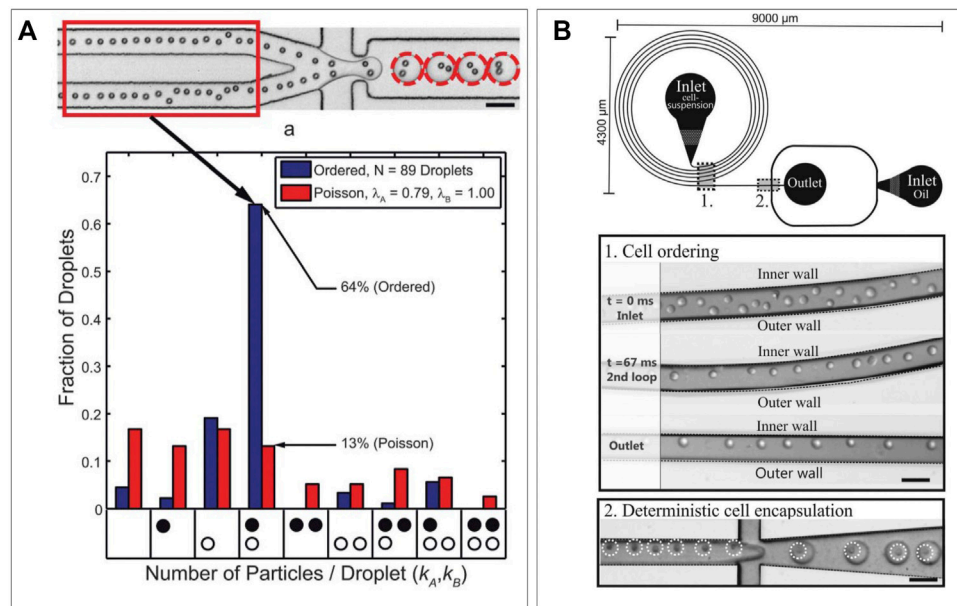


FIGURE 4 | Deterministic encapsulation. **(A)** Radial displacement leading to a particle train which can be synced with frequency of production rate to obtain increased cell-pairing efficiency (Lagus et al., 2013). **(B)** Deans flow in spiral shaped channels can form particle trains on the inner wall, which can be used to obtain deterministic encapsulation (Kemna et al., 2012).

spatial control of particles inside microfluidic channels is required, which can be achieved *via* inertial focusing through radial particle displacement in long channels (Dean, 2009) (Figure 4A), or Deans flow in spiral-shaped channels (Russom et al., 2009; Kemna et al., 2012) (Figure 4B). Both will result in ordering in an equally spaced train of particles, and when spacing is matched with frequency of droplet production, this can double the efficiency of single particle encapsulation compared to random Poisson encapsulation (Lagus and Edd, 2012; Lagus and Edd, 2013). When ordering is performed on particles in two different inlets, the encapsulation efficiency of two unique particles can be increased to around five times the efficiency of random Poisson encapsulation (Yaghoobi et al., 2020; Duchamp et al., 2021). Performing such inertial ordering requires relatively simple device designs while maintaining the high-throughput nature characteristic to droplet microfluidics. Other more complex approaches utilize droplet merging to obtain cell pairs more efficiently. These can be performed either using traps (Schoeman et al., 2014; Chung et al., 2017) or by merging droplets inside the device channels (Wimmers et al., 2018). However, results from these efforts have been limited by on-chip capacity or efficiency and, thus, fall short compared to deterministic encapsulation.

Pairing for Single-Cell Immune Assays

Cell-Cell Pairing

The ability of microfluidic droplets to bring two heterotypic cells in confined proximity finds an ideal application in fundamental immunological research. Many immune responses are heavily dependent on cells being adjacent for paracrine signaling or even connecting for juxtacrine signaling. High-throughput droplet encapsulation was readily proven an ideal method to screen

immune cell heterogeneity in response to paracrine cues, as modeled by co-encapsulation of various stimuli (Tiemeijer et al., 2021; Konry et al., 2011; van Eyndhoven et al., 2021; Konry et al., 2013). Co-encapsulation allows similar setups for investigating contact-dependent juxtacrine interactions referred to as immune synapses. These have been readily investigated at single-cell level in context of contact-dependent activation (Sarkar et al., 2015; Antona et al., 2020b), and contact-dependent cytotoxicity (Subedi et al., 2021; Sarkar et al., 2017; Dik et al., 2005). The first of the two arises primarily between antigen-presenting cells and lymphoid cells to initiate the adaptive immune response. When dendritic cells (DCs) use the immune synapse to present T cells with antigens, T cells are activated, start proliferating, and become potent killers of virus-infected cells or tumor cells. Not only due to the immense T-cell receptor variation (stPaul and Ohashi, 2020) but also because of the high degree of T-cell heterogeneity (Woodland and Dutton, 2003b; Dura et al., 2015; Ma et al., 2021), this can be a very heterogenous process, in which droplet-based single-cell approaches could improve fundamental research greatly and pave the way for high-throughput screening for therapeutic applications (Hondowicz et al., 2012; Shahi et al., 2017; Sarkar et al., 2016). Konry et al. co-encapsulated mouse DCs and T cells and visualized them in droplets, where they could observe formation of immune synapses based on tubulin localization (Sarkar et al., 2015) (Figure 5A), demonstrating that these cellular interactions can be monitored real-time using microscopy in droplet confinement. Later, in-droplet research included detection of synapse-based activation *via* dynamic calcium signals (Antona et al., 2020b) and demonstrated that synapse duration is dependent on antigen presence

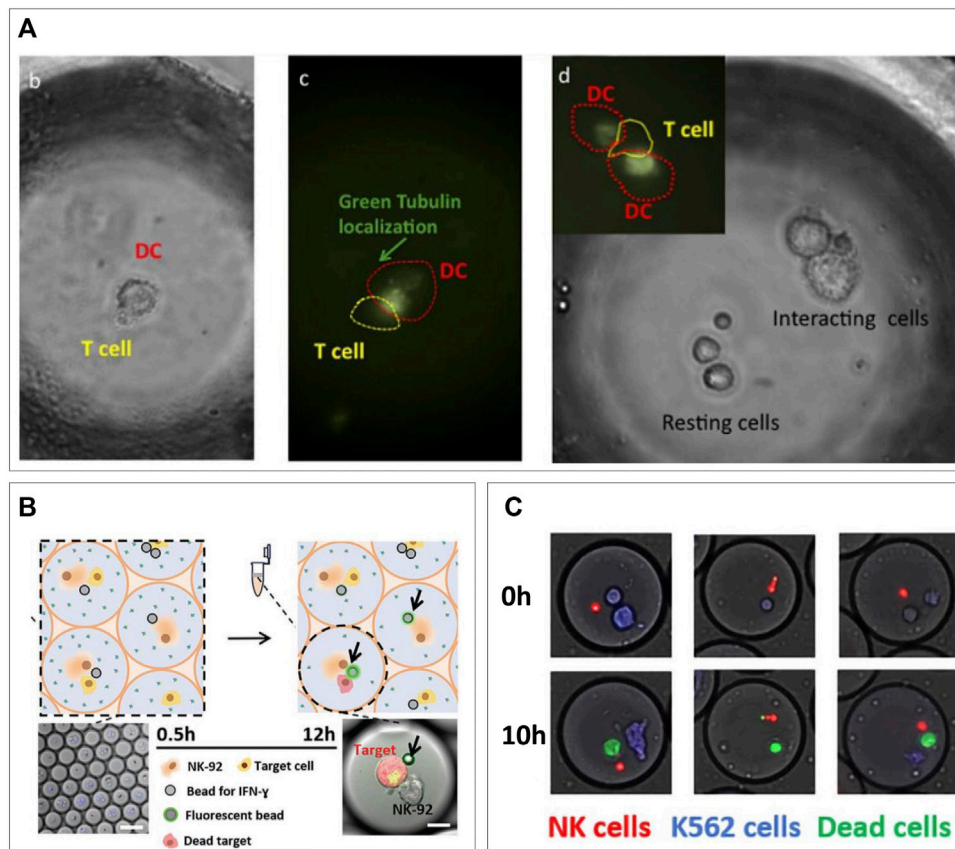


FIGURE 5 | Cell-cell pairing for single-cell immune interactions. **(A)** Microscopic visualization of DC/T-cell interactions. Tubulin localization indicates presence of immune synapses present at different ratios of cells (Konry et al., 2013). **(B)** Monitoring of IFN- γ secretion during NK/tumor cells killing interaction (Antona et al., 2020). **(C)** Primary NK cells killing tumor cells in droplets (Subedi et al., 2021).

(Vanherberghen et al., 2013). In addition, they showed contact-dependent T cell-mediated tumor cell cytotoxicity in droplets, which they were able to boost or inhibit *via* added stimuli or cytokine inhibition, respectively (Vanherberghen et al., 2013). In addition to T cells, natural killer (NK) cells are very potent cytotoxic cells, which on contact with a target cell exhibit antigen-independent killing demonstrate serial killing and have been shown to behave with a highly heterogeneous nature (Guldevall et al., 2016; Antona et al., 2020b). The immune synapses *via* which their cytotoxicity is elicited are varying in duration and can occur several times for a single target cell or several target cells resulting in serial killing. These repeated killing synapses were studied in droplets between NK cells and different types of tumor cells by Antona et al. (2020a). They encapsulated varying numbers or target cells in droplets of different sizes and showed that serial killing was controlled by both variables. In a different application, they complemented the cytotoxicity assay with monitoring of IFN- γ secretion by NK cells (Sarkar et al., 2020) (Figure 5B), which allowed them to show that only about half of the NK cells killing K562 tumor cells produces IFN- γ in the process, underlining their heterogeneous nature. As these assays are all monitored using microscopy over time, manual analysis is tedious and can potentially be biased. Subedi et al.

developed an automated real-time analysis script which allows for these killing assays to be performed in an unbiased manner (Sarkar et al., 2017). In addition, they showed the suitability for this platform for killing by primary isolated human NK cells (Figure 5C). These droplet techniques for analysis of immune synapses have proven valuable in progressing of basic knowledge of immune cell interaction. They have underlined its potential for elucidating heterogeneity and proven their usefulness in finding sub-populations of therapeutic interest. Nevertheless, in terms of the high-throughput potential droplet-microfluidics natively has, there is still much progress to be made. These techniques rely on microscopic visualization in observation wells and chambers for the analysis of pairs which allows measurement of several hundred (Scanlon et al., 2014; Antona et al., 2020a) to few thousand events (Sarkar et al., 2017), respectively, but are thereby inherently limited in its throughput to the size of the microfluidic device. This is where application of hydrogel in droplets can allow for upscaling to achieve not only very high throughput but also recovery of droplets from the experimental setup and maintaining the spatial bond between cell pairs after de-emulsification of droplets. This has been previously performed in screening of bacterial colonies. Scanlon et al. co-encapsulated antibiotic expressing *E. coli* in agarose droplets along with *S.*

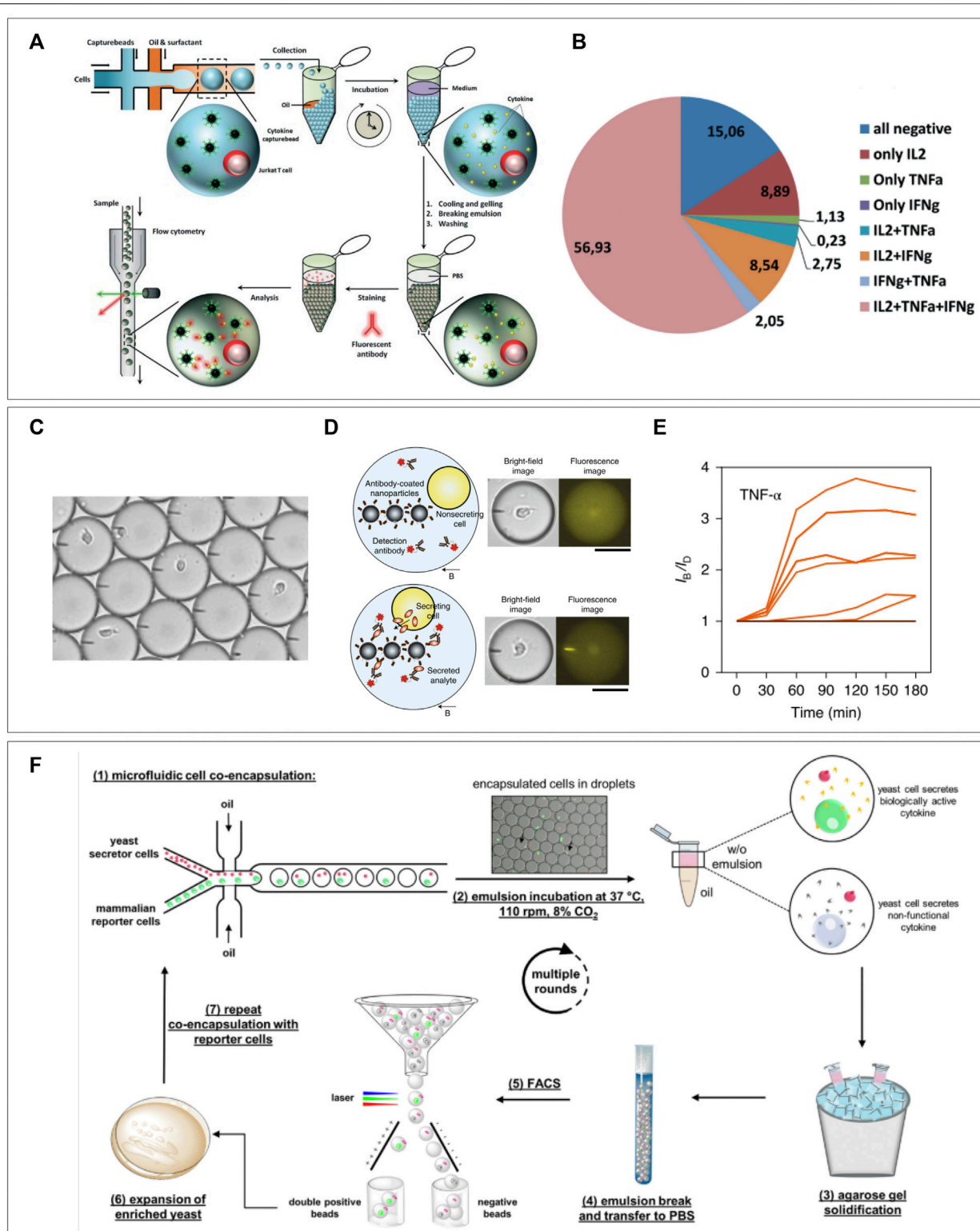


FIGURE 6 | Cell-reporter pairing for immune assays. **(A)** Capture beads specific for three different cytokines are co-encapsulated in hydrogel droplets, after gelation and emulsion breaking the whole droplet can be stained for captured cytokines and measured using flow cytometry. **(B)** Secretional heterogeneity of Jurkat T cells can be detected using this method of multiparameter single-cell cytokine detection (Chokkalingam et al., 2013). **(C)** Bead-line encapsulation evades the Poisson distribution as every droplet will contain around 1,000 nm-sized capture beads. **(D)** Cellular cytokine secretion can be observed and **(E)** quantified over time by measuring translocation of co-encapsulated fluorescent antibodies (Bounab et al., 2020). **(F)** Yeast cells are co-encapsulated with murine IL-3 reporter cells. Gelation of droplets and de-emulsification allows flow cytometric sorting of IL-3 producing yeast cells. Expansion and repeating of procedure allows enrichment of secreting yeast cells (Yanakieva et al., 2020).

aureus and a fluorescent viability marker (Kitaeva et al., 2020). The combination of production rates up to 3,000 drops/s and off-chip collection in centrifuge tubes allowed theoretical unlimited flow through. An analysis was performed by gelation of the agarose droplet, de-emulsification, and whole droplets measurement of *S. aureus* viability using flow cytometry. This ultrahigh-throughput allowed for the detection and sorting of up to five million clones/day to screen for potential novel antibiotics. Such upscaling is expected to greatly benefit the field of immune therapy by allowing ultrahigh-throughput of cell pairs and their immune synapses, which will improve drug testing (Jiang et al., 2019b) and help in the discovery of tumor neoantigens (Heo et al., 2020) and specialized cell populations (Altschuler and Wu, 2010).

Cell-Reporter Pairing

In addition to using pairing of heterotypic cells in droplets to measure their interactions, a cell of interest can also be encapsulated alongside a “reporter” particle or cell. After periods of culture/stimulation fluorescent signal can be measured on the reporter cell either due to translocation of co-encapsulated markers (Fang et al., 2017; Sarkar et al., 2020; Bounab et al., 2020; Gérard et al., 2020; Garti and Bisperink, 1998) or by direct staining after de-emulsification (Yanakieva et al., 2020; Chokkalingam et al., 2013). The main advantage of co-encapsulation of fluorescent markers is that microscopic imaging allows continuous measurement to obtain temporal information. For staining after de-emulsification, a hydrogel is indispensable as it maintains the spatial coupling of the interrogated cell and reporter particle. This latter approach was demonstrated in research by Chokkalingam et al. where Jurkat T cells were co-encapsulated with functionalized cytokine capture beads (Chokkalingam et al., 2013) (**Figure 6A**). Beads contained antibodies specific for IL-2, TNF- α , and IFN- γ so that cytokines secreted by co-encapsulated cells would be captured on the beads during incubation in the droplets. As they co-encapsulated a solution of low melting-point agarose, simple cooling of the droplets after culturing allowed spatial linking of the Jurkat T cells with the capture beads allowing for flow cytometric detection of cytokines for each individual cell. This revealed heterogeneous secretion behavior and distinct secretion profiles (**Figure 6B**). Since analysis for such experiments is performed using flow cytometry, it has the potential to immediately sort cells of interest, as was demonstrated for bacteria by Scanlon et al. Another recently published protocol by Bounab et al. cleverly utilizes fluorescent translocation to monitor timing of cytokine secretion by monocytes and T cells or IgG production by B cells, at a single-cell level (Gérard et al., 2020). In addition, they were able to cheat the Poisson distribution hurdle by co-encapsulating with a high concentration of nanometer-sized magnetic particles. After droplet capture these form a “beadline” in response to a magnetic field, and they will be present in every droplet due to the high concentration of particles (**Figure 6C**). The magnetic particles are functionalized with cytokine-specific capture antibodies and fluorescent detection antibodies are co-encapsulated in the droplets. Cytokine secretion by encapsulated cells will therefore result in a real-time

observable antibody-cytokine sandwich which can be visualized by fluorescent translocation to the beadline (**Figures 6D,E**). Although the throughput is limited by the size of their observation chamber, the approach still allows for analysis of up to 300,000 single cells per experiment. The versatility of this technique was demonstrated by immobilization of heat killed bacteria on the beadline (Bounab et al., 2020). This “Bactoline” allowed screening of IgG and IgM production by mice B cells before and after immunization, which provided valuable insights into single-cell heterogeneity of antibody specificity, affinity, and cross-reactivity. Apart from beadline measurement in observation chambers, translocation of fluorophores can also be measured in droplets flow on-chip (Garti and Bisperink, 1998). This allowed for direct sorting of B cells producing antibodies to co-encapsulated antigens and sequencing of their IgG sequences. The method was further shown to be suitable for screening of *ex vivo* stimulated human peripheral memory B cells, indicating the potential for these types of techniques to contribute to development of immune techniques.

In addition to reporter particles, several applications have been demonstrated using reporter cells (Garti and Bisperink, 1998; Fang et al., 2017; Yanakieva et al., 2020). Fang et al. used hydrogel droplet sorting to enrich rare antibody clones as produced by transfected yeast cells. They co-encapsulated antibody producing yeast cells with A431 tumor cells expressing the relative antigen. Gelation of the agarose droplets before de-emulsification spatially bound the producer and reporter cell. After de-emulsification pairs of yeast and A431 cells in hydrogel droplet were washed to get rid of non-specific IgG's and stained using fluorescent anti-human IgG to visualize A431 bound antibodies. During flow cytometric sorting these A431 could be detected based on fluorescence and sorted out. As they were spatially confined to the corresponding yeast cells, these were collected as well, thus increasing purity of yeast cells of interest. More recently, a similar approach using agarose droplets was demonstrated for enrichment of cytokine secreting yeast by Yanakieva et al. (2020) (**Figure 6D**). Here, however, no additional fluorescent staining was required as they used mCherry positive murine IL-3 secreting yeast cells in combination with murine reporter cells, which expressed green fluorescent protein (GFP) upon stimulation with IL-3. Co-encapsulation of both cells would therefore result in a double positive signal for mCherry and GFP. By flow cytometric sorting of double positive droplets, IL-3 producers could be enriched and expanded before additional rounds of encapsulation with reporter cells. This allowed them to enrich yeast that produced functional IL-3 from yeast producing inactive IL-3 from a 1:10,000 mixture by 70-fold with only two rounds of sorting. This technique of repeated enrichment combined with unlimited throughput proves suitable for efficient selection of yeast clones secreting biorelevant proteins.

SEMI-PERMEABLE HYDROGEL SHELLS

The production of double emulsions of water and oil has been investigated for a few decades (Chong et al., 2015), but the rise of

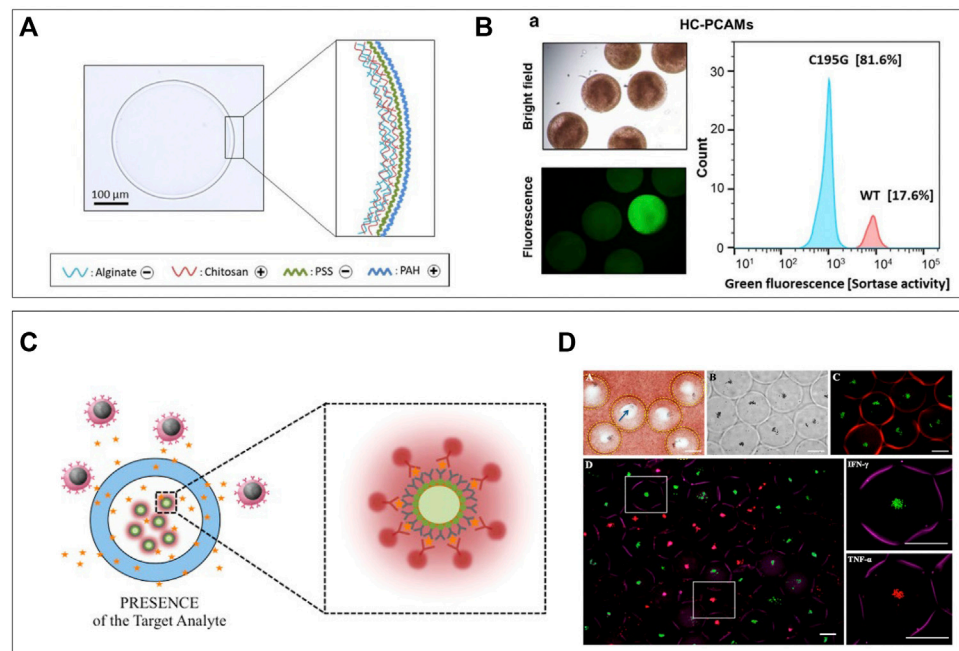


FIGURE 7 | Semi-permeable hydrogel shells. **(A)** Hydrogel shell droplets are coated with polyelectrolytes to decrease permeability. This successfully allows the diffusion of nutrients and lysis buffer, but keeps DNA inside after lysis. **(B)** Particles can be analyzed and sorted based on fluorescence in a large particle sorter (di Girolamo et al., 2020). **(C)** Selectively permeable hydrogel shell particles used as sensors preventing cells to reach the microbeads but letting cytokine and detection antibodies diffuse in. **(D)** Sensor particles submerged in whole blood and after washing and incubation with detection antibodies. IFN- γ specific particles are green, and TNF- α specific particles are red (Rahimian et al., 2019).

droplet microfluidics has enabled stable and high-throughput production (Huang et al., 2017). Adding hydrogel into the “shell” has resulted in the facile production of semi-permeable particles suitable for cell analytical procedures (Choi et al., 2016). Shells can be obtained by direct on-chip formation of hydrogel layers (Cai et al., 2019; Mak et al., 2008), deposition of silica (Mazutis et al., 2013), or polyelectrolytes (Fischlechner et al., 2014; Ferreira et al., 2013) after droplet production. The latter is used to drastically decrease permeability to selectively retain macromolecules but allow diffusion of small molecules. di Girolamo et al. (2020) utilized the technique to further increase the selectivity of their chitosan-shell alginate-core droplets, which allowed for retention of ~ 30 kDa molecules and diffusion of ~ 1 kDa molecules. First, they produced alginate beads using common microfluidic techniques that allowed for cell encapsulation. These microgels could then be coated with chitosan, after which the alginate core was dissolved using sodium citrate. These hollow core chitosan–alginate capsules could then be coated with subsequent layers of poly(styrene sulfonate) and poly(allylamine hydro-chloride) to control permeability (Figure 7A). Their particles were suitable for encapsulation and cultivation of *E. Coli* and by culturing these from single-cells to over two million per capsule, they demonstrated the shell did not prevent diffusion of nutrients and oxygen. Subsequently lysis buffer could be washed in to digest the cells, after which cellular large proteins and DNA were retained by the coating. Fluorescent probes specific for enzymes of interest could be washed in to detect which

droplets contained cells producing these enzymes. Such an approach can be combined with fluorescence-based sorting techniques to facilitate directed evolution (Figure 7B). Hydrogel shells without polyelectrolyte generally have larger pore size and are thus selective to a different range of molecular sizes. A dextran-core PEGDA-shell particle was designed by Leonaviciene et al. which they approximated to have a pore size of around 30 nm, thus successfully retaining DNA fragments of around 340 kDa and higher (Leonaviciene et al., 2020). This allowed them to wash lysis buffer and genome amplification reagents in and out of the particles in a multistep process. As the amount of reagent was not dependent on the droplet volume, this resulted in a 2-fold higher yield of DNA macromolecules compared to conventional water-in-oil droplets, in which supply of reagent is limited by what is initially encapsulated. By using their approach to cultivate biodegradable plastic producing bacteria, they demonstrated detection of functional products as a readout, in addition to amplification of genomic contents. An opposite approach of such semi-permeable shells is to prohibit cells from entering the core but allowing specific analytes in. Rahimian et al. applied this concept in an immunoassay for the *ex vivo* analysis of whole blood for specific secreted factors (Zhu, 2010). A thin PEG shell was produced surrounding a 400- μ m size particle containing antibody-coated beads specific for both TNF α and IFN γ , which are important pro-inflammatory markers. The coating prevented leukocyte interactions with the detection beads while secreted cytokines could enter and bind the beads (Figure 7C). Retrieval of

beads by simple filtering, followed by addition of fluorescent detection antibodies allowed for cytokine analysis without preceding cell-separation steps. They demonstrated the feasibility of the platform by detection of IFN γ in blood of patients with a latent tuberculosis infection (Figure 7D). Comparison to the current gold standard method resulted in 11 out of 14 patients getting the correct diagnosis, and the three incorrect diagnoses were false-negatives. Although most of the aforementioned methods are executed with bacteria, these can easily be translated to mammalian cells. Such approaches would yield unique opportunities for prolonged single-cell cultures or single-cell cloning due to unlimited inflow of cell nutrients. In addition, hydrogel-shell particles can be utilized as miniaturized bioreactors for chemical reactions such as PCR.

HYDROGEL DROPLETS FOR COCULTURES

Although exact cell pairing efficiency remains a challenging hurdle, various efforts have been made to utilize hydrogel droplets for cellular coculture with multiple cells. As cellular interactions are fundamental in biology, downscaling can help understand them at the most basic level. Hydrogel droplets facilitate this type of research by bringing few-cells in tight proximity and keeping them there after de-emulsification. As this allows inflow of nutrients these cocultures can be maintained over a much longer period (Tumarkin et al., 2011) to study cell–cell effects (Kmiec, 2001). A great example is the effect of cocultures of liver cells on activity and viability of hepatocytes, as such interactions have proven complex (Kmiec, 2001) and hepatocytes alone display very little liver specific functions (van Poll et al., 2006; Cho et al., 2010). These cocultures were demonstrated in organoids previously (Darakhshan et al., 2020), but for further downscaling and increased throughput, droplet microfluidics was applied. Cocultures of hepatocytes were produced as spheroids (Chan et al., 2016) or in a core-shell orientation (Lu et al., 2015; Chen et al., 2016). Chan et al. used a coculture of endothelial progenitor cells and hepatocytes in hydrogel droplets with a mix of alginate and collagen type I⁷². They utilized alginate-in-oil-in-water double emulsions to produce droplets and eliminated the oil phase in the presence of calcium ions to gelate the droplets. They showed that even at these miniature scales of only several cells, coculture effect was observed in increased production of several functional liver metabolites. Furthermore, tuning composition of alginate and collagen hydrogel in droplets proved to outperform the golden standard for 2D hepatocyte culture in terms of metabolite production (Dunn et al., 1991; Chan et al., 2016). In research by Chen et al., it was shown that in shell-core hydrogel droplets coculture different types of cells could be confined to either encapsulation in the core or shell part of the droplets (Chen et al., 2016). They were able to achieve this distribution by quick on-chip gelation of the alginate shell by acidification of calcium–EDTA complexes using a 4-inlet microfluidic device. In addition, they showed that cell viability was unaffected, and that coculture resulted in increased secretion of liver specific metabolites albumin and urea. Such miniaturized *in vitro* coculture models

prove a valuable tool for understanding basic biology, high-throughput drug screening (Darakhshan et al., 2020) or potentially therapeutic applications.

CONCLUDING REMARKS

Single-cell technologies are increasingly more integrated into modern cell biological research. As this leads to discovery of more heterogeneity and rare subpopulations the need for robust high-throughput platforms becomes clearer. The role of microfluidics in achieving single-cell resolution has been cut out for almost 2 decades due to its possibilities to physically manipulate single cells using fluids. Droplet-based microfluidics has obtained its own prominent seat within this field due to the high-throughput and reproducible nature of the resulting micro-scale emulsions. An impressive resume of single-cell applications (Klein et al., 2015; Macosko et al., 2015; Wimmers et al., 2018; Antona et al., 2020b; Bounab et al., 2020; Gérard et al., 2020; Subedi et al., 2021; van Eyndhoven et al., 2021) predicts that droplet encapsulation will continue to play an important role in isolation of individual cells over years to come. A promising addition to the field is the application of hydrogel to produce microgels for single-cell encapsulation. This allows the development of various novel techniques, has the potential to greatly increase throughput, provides improved spatial control, and gives encapsulated cells a mechanically active environment.

Encapsulation of cells in aqueous droplets will result in cells being in forced suspension. This is fine for non-adherent cells but might affect the viability and phenotype of adherent cells that require mechanical stimuli and attachment molecules (Gilmore, 2005; Taddei et al., 2012; Tiemeijer et al., 2021). As hydrogels often mimic the stiffness of extracellular matrix and can be functionalized to facilitate adherence, production of microgels can open the technology to a broader range of cell applications. Current research is still based on proof-of-principle experiments to explore possibilities for adherent cells. But future work can include more complex experimental setups including tunable mechanical properties (Allazetta et al., 2017) and screening of resulting cellular responses (Neubauer et al., 2019; Wang et al., 2021). Such experiments can gain invaluable insights in the fundamentals of cell interactions with their environment and their responses to stiffness, which will be especially useful for development of tissue engineering approaches (Liebschner et al., 2005; Kurazumi et al., 2011; Wissing et al., 2017).

Although still limited by the Poisson distribution, cell pairing in droplets has been applied previously to bring two types of cells in isolated proximity (Hondroulis et al., 2017; Antona et al., 2020b; Gérard et al., 2020; Subedi et al., 2021). In conventional aqueous droplets, this pairing can only be maintained if droplets are kept in emulsion; however, this will limit downstream processing and prohibits diffusion of nutrients and additional reagents. Pairing of cells in microgels will result in maintained spatial control after de-emulsification. Continuing the culture of cells in microgels after emulsion breaking allows for paracrine cell communication between droplets and should, therefore, be used with caution. However, the most promising microgel pairing application will

be the downstream analysis of cell pairs. Especially in the field of immunology, this will create many new experimental opportunities, as immune synapses are the key to the onset and progression of immune responses. Performing single-cell pairing experiments at a high-throughput scale is therefore indispensable to obtain fundamental knowledge required for designing immune therapeutic techniques.

In conclusion, the field of single-cell droplet-based microfluidics will greatly benefit from incorporation of various types of hydrogels. The addition of these “solids” in microfluidics will improve control and robustness, thereby paving the way for standardized high-throughput screening techniques and immune assays. Although until now most applications have been proof-of-principles and focused on finding possibilities, once matured, these technologies will be highly compatible with the future of cell biological research and immunotherapy.

REFERENCES

- Ahmed, H., and Stokke, B. T. (2021). Fabrication of Monodisperse Alginate Microgel Beads by Microfluidic Pico-injection: a Chelate Free Approach. *Lab. Chip* 21 (11), 2232–2243. doi:10.1039/D1LC00111F
- Allazetta, S., Negro, A., and Lutolf, M. P. (2017). Microfluidic Programming of Compositional Hydrogel Landscapes. *Macromol. Rapid Commun.* 38 (15), 1–10. doi:10.1002/marc.201700255
- Altschuler, S. J., and Wu, L. F. (2010). Cellular Heterogeneity: Do Differences Make a Difference? *Cell* 141 (4), 559–563. doi:10.1016/j.cell.2010.04.033
- Antoine, E. E., Vlachos, P. P., and Rylander, M. N. (2014). Review of Collagen I Hydrogels for Bioengineered Tissue Microenvironments: Characterization of Mechanics, Structure, and Transport. *Tissue Eng. Part B Rev.* 20 (6), 683–696. doi:10.1089/TEN.TEB.2014.0086
- Antona, S., Abele, T., Jahnke, K., Yannik, D., Kerstin, G., and Ilia, P. (2020a). Droplet-Based Combinatorial Assay for Cell Cytotoxicity and Cytokine Release Evaluation. *Adv. Funct. Mater.* 30 (46). doi:10.1002/adfm.202003479
- Antona, S., Platzman, I., and Spatz, J. P. (2020b). Droplet-Based Cytotoxicity Assay: Implementation of Time-Efficient Screening of Antitumor Activity of Natural Killer Cells. *ACS Omega* 5 (38), 24674–24683. doi:10.1021/acsomega.0c03264
- Antona, S., Abele, T., Jahnke, K., Yannik, D., Kerstin, G., and Ilia, P. (2020b). Droplet-Based Combinatorial Assay for Cell Cytotoxicity and Cytokine Release Evaluation. *Adv. Funct. Mater.* 30 (46). doi:10.1002/adfm.202003479
- Bassett, D. C., Håti, A. G., Melø, T. B., Stokke, B. T., and Sikorski, P. (2016). Competitive Ligand Exchange of Crosslinking Ions for Ionotropic Hydrogel Formation. *J. Mat. Chem. B* 4 (37), 6175–6182. doi:10.1039/c6tb01812b
- Bavli, D., Sun, X., Kozulin, C., Ennis, D., Motzik, A., Biran, A., et al. (2021). CloneSeq: A Highly Sensitive Analysis Platform for the Characterization of 3D-Cultured Single-Cell-Derived Clones. *Dev. Cell* 56 (12), 1804–1817. e7. doi:10.1016/J.DEVCEL.2021.04.026
- Benavente Babace, A., Haase, K., Stewart, D. J., and Godin, M. (2019). Strategies for Controlling Egress of Therapeutic Cells from Hydrogel Microcapsules. *J. Tissue Eng. Regen. Med.* 13 (4), 612–624. doi:10.1002/term.2818
- Bounab, Y., Eyer, K., Dixneuf, S., Magda, R., Cécile, C., Maxime, M., et al. (2020). Dynamic Single-Cell Phenotyping of Immune Cells Using the Microfluidic Platform DropMap. *Nat. Protoc.* 15 (9), 2920–2955. doi:10.1038/s41596-020-0354-0
- Braccini, I., and Pérez, S. (2001). Molecular Basis of Ca²⁺-Induced Gelation in Alginates and Pectins: The Egg-Box Model Revisited. *Biomacromolecules* 2 (4), 1089–1096. doi:10.1021/BM010008G
- Cai, B., Ji, T. T., Wang, N., Xin-Bo, L., Rong-Xiang, H., Wei, L., et al. (2019). A Microfluidic Platform Utilizing Anchored Water-In-Oil-In-Water Double Emulsions to Create a Niche for Analyzing Single Non-adherent Cells. *Lab a Chip* 19 (3), 422–431. doi:10.1039/c8lc01130c

AUTHOR CONTRIBUTIONS

This publication was conceptualized by BT and JT, written by BT, and revised and approved by JT.

FUNDING

This work was supported by the European Research Council (ERC) under the European Union's Horizon 2020 Research and Innovation Program (Grant agreement No. 802791).

ACKNOWLEDGMENTS

The authors would like to acknowledge the generous support by the Eindhoven University of Technology.

- Chan, H. F., Zhang, Y., and Leong, K. W. (2016). Efficient One-step Production of Microencapsulated Hepatocyte Spheroids with Enhanced Functions. *Small* 12 (20), 2720. doi:10.1002/SMLL.201502932
- Chattopadhyay, P. K., Gierahn, T. M., Roederer, M., and Love, J. C. (2014). Single-cell Technologies for Monitoring Immune Systems. *Nat. Immunol.* 15 (2), 128–135. doi:10.1038/ni.2796
- Chen, Q., Utech, S., Chen, D., Prodanovic, R., Lin, J. M., and Weitz, D. A. (2016). Controlled Assembly of Heterotypic Cells in a Core-Shell Scaffold: Organ in a Droplet. *Lab. Chip* 16 (8), 1346. doi:10.1039/C6LC00231E
- Cho, C. H., Park, J., Tilles, A. W., Berthiaume, F., Toner, M., and Yarmush, M. L. (2010). Layered Patterning of Hepatocytes in Co-culture Systems Using Microfabricated Stencils. *Biotechniques* 48 (1), 47–52. doi:10.2144/000113317/ASSET/IMAGES/LARGE/FIGURE4.JPG
- Choi, C.-H., Jung, J.-H., Rhee, Y. W., Kim, D.-P., Shim, S.-E., and Lee, C.-S. (2007). Generation of Monodisperse Alginate Microbeads and *In Situ* Encapsulation of Cell in Microfluidic Device. *Biomed. Microdevices* 9 (6), 855–862. doi:10.1007/S10544-007-9098-7/FIGURES/6
- Choi, C. H., Wang, H., Lee, H., June Hwan, K., Liyuan, Z., Angelo, M., et al. (2016). One-step Generation of Cell-Laden Microgels Using Double Emulsion Drops with a Sacrificial Ultra-thin Oil Shell. *Lab. Chip* 16 (9), 1549. doi:10.1039/C6LC00261G
- Chokkalingam, V., Ma, Y., Thiele, J., Schalk, W., Tel, J., and Huck, W. T. S. (2014). An Electro-Coalescence Chip for Effective Emulsion Breaking in Droplet Microfluidics. *Lab. Chip* 14 (14), 2398–2402. doi:10.1039/C4LC00365A
- Chokkalingam, V., Tel, J., Wimmers, F., Liu, X., Semenov, S., Thiele, J., et al. (2013). Probing Cellular Heterogeneity in Cytokine-Secreting Immune Cells Using Droplet-Based Microfluidics. *Lab. Chip* 13 (24), 4740–4744. doi:10.1039/c3lc50945a
- Chong, D. T., Liu, X. S., Ma, H. J., GuoYou, H., Yu, L. H., XingYe, C., et al. (2015). Advances in Fabricating Double-Emulsion Droplets and Their Biomedical Applications. *Microfluid. Nanofluidics* 19 (5), 1071–1090. doi:10.1007/S10404-015-1635-8
- Chung, M. T., Núñez, D., Cai, D., and Kurabayashi, K. (2017). Deterministic Droplet-Based Co-encapsulation and Pairing of Microparticles via Active Sorting and Downstream Merging. *Lab a Chip* 17 (21), 3664–3671. doi:10.1039/C7LC00745K
- Collins, D. J., Neild, A., DeMello, A., Liu, A.-Q., and Ai, Y. (2015). The Poisson Distribution and beyond: Methods for Microfluidic Droplet Production and Single Cell Encapsulation. *Lab. Chip* 15 (17), 3439–3459. doi:10.1039/c5lc00614g
- Cubaud, T., and Mason, T. G. (2008). Capillary Threads and Viscous Droplets in Square Microchannels. *Phys. Fluids* 20 (5), 053302. doi:10.1063/1.2911716
- Dagogo-Jack, I., and Shaw, A. T. (2017). Tumour Heterogeneity and Resistance to Cancer Therapies. *Nat. Rev. Clin. Oncol.* 15 (2), 81–94. doi:10.1038/nrclinonc.2017.166

- Darakshshan, S., Bidmeshki Pour, A., Kowsari-Esfahan, R., Massoud, V., Leila, M., Mohammad, H. G., et al. (2020). Generation of Scalable Hepatic Micro-tissues as a Platform for Toxicological Studies. *Tissue Eng. Regen. Med.* 17 (4), 459. doi:10.1007/S13770-020-00272-6
- Dean, W. R. (2009). LXXII. The Stream-Line Motion of Fluid in a Curved Pipe (Second Paper). *Lond. Edinb. Dublin Philosophical Mag. J. Sci.* 5 (30), 673–695. doi:10.1080/14786440408564513
- Deng, Y., Zhang, N., Zhao, L., Yu, X., Ji, X., Liu, W., et al. (2011). Rapid Purification of Cell Encapsulated Hydrogel Beads from Oil Phase to Aqueous Phase in a Microfluidic Device. *Lab. Chip* 11 (23), 4117–4121. doi:10.1039/C1LC20494G
- di Girolamo, S., Puorger, C., and Lipps, G. (2020). Stable and Selective Permeable Hydrogel Microcapsules for High-Throughput Cell Cultivation and Enzymatic Analysis. *Microb. Cell Fact.* 19 (1). doi:10.1186/s12934-020-01427-9
- Dik, W. A., Pike-Overzet, K., and Weerkamp, F. (2005). New Insights on Human T Cell Development by Quantitative T Cell Receptor Gene Rearrangement Studies and Gene Expression Profiling. *J. Exp. Med.* 201 (11), 1715. doi:10.1084/JEM.20042524
- Dixon, J. E., Shah, D. A., Rogers, C., Hall, S., Weston, N., Parmenter, C. D. J., et al. (2014). Combined Hydrogels that Switch Human Pluripotent Stem Cells from Self-Renewal to Differentiation. *Proc. Natl. Acad. Sci. U.S.A.* 111 (15), 5580–5585. doi:10.1073/PNAS.1319685111
- Dolega, M. E., Abeille, F., Picollet-D'hahan, N., and Gidrol, X. (2015). Controlled 3D Culture in Matrigel Microbeads to Analyze Clonal Acinar Development. *Biomaterials* 52 (1), 347–357. doi:10.1016/j.biomaterials.2015.02.042
- Duchamp, M., Arnaud, M., Bobisse, S., Coukos, G., Harari, A., and Renaud, P. (2021). Microfluidic Device for Droplet Pairing by Combining Droplet Railing and Floating Trap Arrays. *Micromachines (Basel)*. 12 (9). doi:10.3390/M12091076/S1
- Dueck, H., Eberwine, J., and Kim, J. (2016). Variation Is Function: Are Single Cell Differences Functionally Important? *BioEssays* 38 (2), 172–180. doi:10.1002/bies.201500124
- Dumbleton, J., Agarwal, P., Huang, H., Hogrebe, N., Han, R., Gooch, K. J., et al. (2016). The Effect of RGD Peptide on 2D and Miniaturized 3D Culture of HEPM Cells, MSCs, and ADSCs with Alginate Hydrogel. *Cel. Mol. Bioeng.* 9 (2), 277–288. doi:10.1007/s12195-016-0428-9
- Dunn, J. C. Y., Tompkins, R. G., and Yarmush, M. L. (1991). Long-Term *In Vitro* Function of Adult Hepatocytes in a Collagen Sandwich Configuration. *Biotechnol. Prog.* 7 (3), 237–245. doi:10.1021/BP00009A007
- Dura, B., Dougan, S. K., Barisa, M., Melanie, M. H., Lo, C. T., Hidde, L. P., et al. (2015). Profiling Lymphocyte Interactions at the Single-Cell Level by Microfluidic Cell Pairing. *Nat. Commun.* 6 (1), 1–13. doi:10.1038/ncomms6940
- Fang, Y., Chu, T. H., Ackerman, M. E., and Griswold, K. E. (2017). Going Native: Direct High Throughput Screening of Secreted Full-Length IgG Antibodies against Cell Membrane Proteins. *MAbs* 9 (8), 1253–1261. doi:10.1080/19420862.2017.1381812
- Ferreira, D. S., Reis, R. L., and Azevedo, H. S. (2013). Peptide-based Microcapsules Obtained by Self-Assembly and Microfluidics as Controlled Environments for Cell Culture. *Soft Matter* 9 (38), 9237–9248. doi:10.1039/c3sm51189h
- Fischlechner, M., Schaerli, Y., Mohamed, M. F., Patil, S., Abell, C., and Hollfelder, F. (2014). Evolution of Enzyme Catalysts Caged in Biomimetic Gel-Shell Beads. *Nat. Chem.* 6 (9), 791–796. doi:10.1038/nchem.1996
- Fu, X. T., and Kim, S. M. (2010). Agarase: Review of Major Sources, Categories, Purification Method, Enzyme Characteristics and Applications. *Mar. Drugs* 8 (1), 200–218. doi:10.3390/MD8010200
- Garti, N., and Bisperink, C. (1998). Double Emulsions: Progress and Applications. *Curr. Opin. Colloid & Interface Sci.* 3 (6), 657–667. doi:10.1016/S1359-0294(98)80096-4
- Gasparini, L., Mano, J. F., and Reis, R. L. (2014). Natural Polymers for the Microencapsulation of Cells. *J. R. Soc. Interface*. 11 (100), 20140817. doi:10.1098/RSIF.2014.0817
- Gérard, A., Woolfe, A., Mottet, G., Marcel, R., Carlos, C., Vera, M., et al. (2020). High-throughput Single-Cell Activity-Based Screening and Sequencing of Antibodies Using Droplet Microfluidics. *Nat. Biotechnol.* 38 (6), 715–721. doi:10.1038/s41587-020-0466-7
- Gilmore, A. P. (2005). Anoikis. *Cell Death Differ.* 12, 1473–1477. doi:10.1038/sj.cdd.4401723
- Gordon, S., and Taylor, P. R. (2005). Monocyte and Macrophage Heterogeneity. *Nat. Rev. Immunol.* 5 (12), 953–964. doi:10.1038/nri1733
- Goy, C. B., Chaile, R. E., and Madrid, R. E. (2019). Microfluidics and Hydrogel: A Powerful Combination. *React. Funct. Polym.* 145, 104314. doi:10.1016/j.reactfunctpolym.2019.104314
- Gu, Y., Cheong, K. L., and Du, H. (2017). Modification and Comparison of Three Gracilaria Spp. Agarose with Methylation for Promotion of its Gelling Properties. *Chem. Cent. J.* 11 (1), 104–110. doi:10.1186/S13065-017-0334-9/TABLES/3
- Guldevall, K., Brandt, L., Forslund, E., Olofsson, K., Frisk, T. W., Olofsson, P. E., et al. (2016). Microchip Screening Platform for Single Cell Assessment of NK Cell Cytotoxicity. *Front. Immunol.* 7 (APR). doi:10.3389/FIMMU.2016.00119
- Günther, A., and Jensen, K. F. (2006). Multiphase Microfluidics: from Flow Characteristics to Chemical and Materials Synthesis. *Lab. Chip* 6 (12), 1487–1503. doi:10.1039/B609851G
- Gurikov, P., and Smirnova, I. (2018). Non-conventional Methods for Gelation of Alginate. *Gels* 4 (1), 14. doi:10.3390/GELS4010014
- Hasturk, O., and Kaplan, D. L. (2019). Cell Armor for Protection against Environmental Stress: Advances, Challenges and Applications in Micro- and Nanoencapsulation of Mammalian Cells. *Acta Biomater.* 95, 3–31. doi:10.1016/j.actbio.2018.11.040
- Hâti, A. G., Bassett, D. C., Ribe, J. M., Sikorski, P., Weitz, D. A., and Stokke, B. T. (2016). Versatile, Cell and Chip Friendly Method to Gel Alginate in Microfluidic Devices. *Lab. Chip* 16 (19), 3718–3727. doi:10.1039/C6LC00769D
- Hellio, D., and Djabourov, M. (2006). Physically and Chemically Crosslinked Gelatin Gels. *Macromol. Symp.* 241, 23–27. doi:10.1002/masy.200650904
- Heo, M., Chenon, G., Castrillon, C., Jérôme, B., Pierre, B., Andrew, D. G., et al. (2020). Deep Phenotypic Characterization of Immunization-Induced Antibacterial IgG Repertoires in Mice Using a Single-Antibody Bioassay. *Commun. Biol.* 3 (1), 1–11. doi:10.1038/s42003-020-01296-3
- Hern, D. L., and Hubbell, J. A. (1998). Incorporation of Adhesion Peptides into Nonadhesive Hydrogels Useful for Tissue Resurfacing. *J. Biomed. Mat. Res.* 39, 266–276. doi:10.1002/(SICI)1097-4636(199802)39:2<266::AID-JBM14>3.0.CO;2-B
- Hondowicz, B. D., Schwedhelm, K. v., and Kas, A. (2012). Discovery of T Cell Antigens by High-Throughput Screening of Synthetic Minigene Libraries. *PLoS ONE* 7 (1). doi:10.1371/JOURNAL.PONE.0029949
- Hondroulis, E., Movila, A., Sabhachandani, P., Saheli, S., Noa, C., Toshihisa, K., et al. (2017). A Droplet-Merging Platform for Comparative Functional Analysis of M1 and M2 Macrophages in Response to E. Coli-Induced Stimuli. *Biotechnol. Bioeng.* 114, 705–709. doi:10.1002/bit.26196/abstract
- Hong, S., Hsu, H.-J., Kaunas, R., and Kameoka, J. (2012). Collagen Microsphere Production on a Chip. *Lab. Chip* 12 (18), 3277–3280. doi:10.1039/C2LC40558J
- Hu, H., Eustace, D., and Merten, C. A. (2015). Efficient Cell Pairing in Droplets Using Dual-Color Sorting. *Lab a Chip* 15 (20), 3989–3993. doi:10.1039/C5LC00686D
- Huang, H., Yu, Y., Hu, Y., He, X., Berk Usta, O., and Yarmush, M. L. (2017). Generation and Manipulation of Hydrogel Microcapsules by Droplet-Based Microfluidics for Mammalian Cell Culture. *Lab a Chip* 17 (11), 1913–1932. doi:10.1039/c7lc00262a
- Huang, H., and He, X. (2014). Interfacial Tension Based On-Chip Extraction of Microparticles Confined in Microfluidic Stokes Flows. *Appl. Phys. Lett.* 105 (14), 143704. doi:10.1063/1.4898040
- Huang, H., Sun, M., Heisler-Taylor, T., Kiourti, A., Volakis, J., Lafyatis, G., et al. (2015). Stiffness-Independent Highly Efficient On-Chip Extraction of Cell-Laden Hydrogel Microcapsules from Oil Emulsion into Aqueous Solution by Dielectrophoresis. *Small* 11 (40), 5369–5374. doi:10.1002/smll.201501388
- Indovina, P. L., TettamantiMicciancio-Giammarinaro, E., Micciancio-Giammarinaro, M. S., and Palma, M. U. (1979). Thermal Hysteresis and Reversibility of Gel-Sol Transition in Agarose-Water Systems. *J. Chem. Phys.* 70 (6), 2841–2847. doi:10.1063/1.437817
- Islam, S. K., Una, K., Annalena, M., Pawel, Z., Jian-Bing, F., Peter, L., et al. (2011). Characterization of the Single-Cell Transcriptional Landscape by Highly Multiplex RNA-Seq. *Genome Res.* 21 (7), 1160–1167. doi:10.1101/GR.110882.110
- Jaipán, P., Nguyen, A., and Narayan, R. J. (2017). Gelatin-based Hydrogels for Biomedical Applications. *MRS Commun.* 7 (3), 416–426. doi:10.1557/mrc.2017.92
- Jammes, F. C., and Maerkl, S. J. (2020). How Single-Cell Immunology Is Benefiting from Microfluidic Technologies. *Microsyst. Nanoeng.* 6 (1), 1–14. doi:10.1038/s41378-020-0140-8

- Jiang, T., Shi, T., Zhang, H., Jie, H., Yuanlin, S., Jia, W., et al. (2019). Tumor Neoantigens: from Basic Research to Clinical Applications. *J. Hematol. Oncol.* 12 (1), 1–13. doi:10.1186/S13045-019-0787-5
- Jiang, Z., Shaha, R., Jiang, K., McBride, R., Frick, C., and Oakey, J. (2019). Composite Hydrogels with Controlled Degradation in 3D Printed Scaffolds. *IEEE Trans. on Nanobioscience* 18 (2), 261–264. doi:10.1109/TNB.2019.2905510
- Kamperman, T., Karperien, M., le Gac, S., and Leijten, J. (2018). Single-Cell Microgels: Technology, Challenges, and Applications. *Trends Biotechnol.* 36, 850–865. doi:10.1016/j.tibtech.2018.03.001
- Karbaschi, M., Shahi, P., and Abate, A. R. (2017). Rapid, Chemical-free Breaking of Microfluidic Emulsions with a Hand-Held Antistatic Gun. *Biomicrofluidics* 11 (4), 044107. doi:10.1063/1.4995479
- Karoubi, G., Ormiston, M. L., Stewart, D. J., and Courtman, D. W. (2009). Single-cell Hydrogel Encapsulation for Enhanced Survival of Human Marrow Stromal Cells. *Biomaterials* 30 (29), 5445–5455. doi:10.1016/j.biomaterials.2009.06.035
- Kemna, E. W. M., Schoeman, R. M., Wolbers, F., Vermes, I., Weitz, D. A., and van den Berg, A. (2012). High-yield Cell Ordering and Deterministic Cell-In-Droplet Encapsulation Using Dean Flow in a Curved Microchannel. *Lab a Chip* 12 (16), 2881–2887. doi:10.1039/C2LC00013J
- Kim, S., Lee, S. M., Lee, S. S., and Shin, D. S. (2019). Microfluidic Generation of Amino-Functionalized Hydrogel Microbeads Capable of On-Bead Bioassay. *Micromachines* 10 (8), 527–529. doi:10.3390/mi10080527
- Kitaeva, K. V., Rutland, C. S., Rizvanov, A. A., and Solovyeva, V. V. (2020). Cell Culture Based *In Vitro* Test Systems for Anticancer Drug Screening. *Front. Bioeng. Biotechnol.* 8, 322. doi:10.3389/FBIOE.2020.00322/BIBTEX
- Klein, A. M., Mazutis, L., and Akartuna, I. (2015). Droplet Barcoding for Single Cell Transcriptomics Applied to Embryonic Stem Cells. *Cell* 161 (5), 1187. doi:10.1016/J.CELL.2015.04.044
- Kmiec, Z. (2001). Cooperation of Liver Cells in Health and Disease. *Adv. Anat. Embryol. Cell Biol.* 161. doi:10.1007/978-3-642-56553-3
- Kong, H., Smith, M. K., and Mooney, D. J. (2003). Designing Alginate Hydrogels to Maintain Viability of Immobilized Cells. *Biomaterials* 24 (22), 4023–4029. doi:10.1016/S0142-9612(03)00295-3
- Konry, T., Dominguez-Villar, M., Baecher-Allan, C., Hafler, D. A., and Yarmush, M. L. (2011). Droplet-based Microfluidic Platforms for Single T Cell Secretion Analysis of IL-10 Cytokine. *Biosens. Bioelectron.* 26 (5), 2707. doi:10.1016/J.BIOS.2010.09.006
- Konry, T., Golberg, A., and Yarmush, M. (2013). Live Single Cell Functional Phenotyping in Droplet Nano-Liter Reactors. *Sci. Rep.* 3 (1), 1–5. doi:10.1038/srep03179
- Krutkramelis, K., Xia, B., and Oakey, J. (2016). Monodisperse Polyethylene Glycol Diacrylate Hydrogel Microsphere Formation by Oxygen-Controlled Photopolymerization in a Microfluidic Device. *Lab. Chip* 16 (8), 1457–1465. doi:10.1039/c6lc00254d
- Kuijpers, A. J., Engbers, G. H. M., Feijen, J., De Smedt, S. C., Meyvis, T. K. L., Demeester, J., et al. (1999). Characterization of the Network Structure of Carbodiimide Cross-Linked Gelatin Gels. *Macromolecules* 32 (10), 3325–3333. doi:10.1021/MA981929V
- Kumachev, A., Greener, J., Tumarkin, E., Eiser, E., Zandstra, P. W., and Kumacheva, E. (2011). High-throughput Generation of Hydrogel Microbeads with Varying Elasticity for Cell Encapsulation. *Biomaterials* 32 (6), 1477–1483. doi:10.1016/J.BIOMATERIALS.2010.10.033
- Kuo, C. K., and Ma, P. X. (2001). Ionically Crosslinked Alginate Hydrogels as Scaffolds for Tissue Engineering: Part I. Structure, Gelation Rate and Mechanical Properties. *Biomaterials* 22 (6), 511–521. doi:10.1016/S0142-9612(00)00201-5
- Kurazumi, H., Kubo, M., Ohshima, M., Yumi, Y., Yoshihiro, T., Ryo, S., et al. (2011). The Effects of Mechanical Stress on the Growth, Differentiation, and Paracrine Factor Production of Cardiac Stem Cells. *PLOS ONE* 6 (12), e28890. doi:10.1371/JOURNAL.PONE.0028890
- Lagus, T. P., and Edd, J. F. (2012). High Throughput Single-Cell and Multiple-Cell Micro-encapsulation. *J. Vis. Exp. JoVE*. 64, 4096. doi:10.3791/4096
- Lagus, T. P., and Edd, J. F. (2013). High-throughput Co-encapsulation of Self-Ordered Cell Trains: Cell Pair Interactions in Microdroplets. *RSC Adv.* 3 (43), 20512–20522. doi:10.1039/C3RA43624A
- Lee, K. Y., and Mooney, D. J. (2012). Alginate: Properties and Biomedical Applications. *Prog. Polym. Sci.* 37 (1), 106–126. doi:10.1016/J.PROGPOLYMSCI.2011.06.003
- Leng, X., Zhang, W., Wang, C., Cui, L., and Yang, C. J. (2010). Agarose Droplet Microfluidics for Highly Parallel and Efficient Single Molecule Emulsion PCR. *Lab a Chip* 10 (21), 2841–2843. doi:10.1039/c0lc00145g
- Leonaviciene, G., Leonavicius, K., Meskys, R., and Mazutis, L. (2020). Multi-step Processing of Single Cells Using Semi-permeable Capsules. *Lab. Chip* 20 (21), 4052–4062. doi:10.1039/D0LC00660B
- Liebschner, M., Bucklen, B., and Wettergreen, M. (2005). Mechanical Aspects of Tissue Engineering. *Seminars Plastic Surg.* 19 (3), 217. doi:10.1055/S-2005-919717
- Lu, Y. C., Song, W., An, D., Beum Jun, K., Robert, S., Mingming, W., et al. (2015). Designing Compartmentalized Hydrogel Microparticles for Cell Encapsulation and Scalable 3D Cell Culture. *J. Mater. Chem. B* 3 (3), 353–360. doi:10.1039/c4tb01735h
- Luo, T., Fan, L., Zhu, R., and Sun, D. (2019). Microfluidic Single-Cell Manipulation and Analysis: Methods and Applications. *Micromachines* 10 (2), 104. doi:10.3390/mi10020104
- Ma, K. Y., Schonnesen, A. A., and He, C. (2021). High-throughput and High-Dimensional Single-Cell Analysis of Antigen-specific CD8+ T Cells. *Nat. Immunol.* 22 (12), 1590–1598. doi:10.1038/s41590-021-01073-2
- Macosko, E. Z., Basu, A., and Satija, R. (2015). Highly Parallel Genome-wide Expression Profiling of Individual Cells Using Nanoliter Droplets. *Cell* 161 (5), 1202. doi:10.1016/J.CELL.2015.05.002
- Mak, W. C., Cheung, K. Y., and Trau, D. (2008). Diffusion Controlled and Temperature Stable Microcapsule Reaction Compartments for High-Throughput Microcapsule-PCR. *Adv. Funct. Mater.* 18 (19), 2930–2937. doi:10.1002/adfm.200800388
- Martinez, C. J., Kim, J. W., Ye, C., Ortiz, I., Rowat, A. C., Marquez, M., et al. (2012). A Microfluidic Approach to Encapsulate Living Cells in Uniform Alginate Hydrogel Microparticles. *Macromol. Biosci.* 12 (7), 946–951. doi:10.1002/MABI.201100351
- Martinsen, A., Skjåk-Braek, G., and Smidsrod, O. (1989). Alginate as Immobilization Material: I. Correlation between Chemical and Physical Properties of Alginate Gel Beads. *Biotechnol. Bioeng.* 33 (1), 79–89. doi:10.1002/bit.260330111
- Mason, T. O., and Shimanovich, U. (2018). Fibrous Protein Self-Assembly in Biomimetic Materials. *Adv. Mat.* 30 (41), 1706462. doi:10.1002/ADMA.201706462
- Matuła, K., Rivello, F., and Huck, W. T. S. (2020). Single-Cell Analysis Using Droplet Microfluidics. *Adv. Biosys.* 4 (1), 1900188. doi:10.1002/adbi.201900188
- Mazutis, L., Gilbert, J., Ung, W. L., Weitz, D. A., Griffiths, A. D., and Heyman, J. A. (2013). Single-cell Analysis and Sorting Using Droplet-Based Microfluidics. *Nat. Protoc.* 8 (5), 870–891. doi:10.1038/nprot.2013.046
- Meacham, C. E., and Morrison, S. J. (2013). Tumor Heterogeneity and Cancer Cell Plasticity. *Nature* 501 (7467), 328. doi:10.1038/NATURE12624
- Mohamed, M. G. A., Ambhorkar, P., Samanipour, R., Yang, A., Ghafoor, A., and Kim, K. (2020). Microfluidics-based Fabrication of Cell-Laden Microgels. *Biomicrofluidics* 14 (2), 021501. doi:10.1063/1.5134060
- Mohamed, M. G. A., Kheiri, S., Islam, S., Kumar, H., Yang, A., and Kim, K. (2019). An Integrated Microfluidic Flow-Focusing Platform for On-Chip Fabrication and Filtration of Cell-Laden Microgels. *Lab. Chip* 19 (9), 1621–1632. doi:10.1039/c9lc00073a
- Murphy, T. W., Zhang, Q., Naler, L. B., Ma, S., and Lu, C. (2017). Recent Advances in the Use of Microfluidic Technologies for Single Cell Analysis. *Analyst* 143 (1), 60–80. doi:10.1039/C7AN01346A
- Nan, L., Yang, Z., Lyu, H., Lau, K. Y. Y., and Shum, H. C. (2019). A Microfluidic System for One-Chip Harvesting of Single-Cell-Laden Hydrogels in Culture Medium. *Adv. Biosys.* 3 (11), 1900076. doi:10.1002/adbi.201900076
- Narayanan, J., Xiong, J.-Y., and Liu, X.-Y. (2006). Determination of Agarose Gel Pore Size: Absorbance Measurements Vis a Vis Other Techniques. *J. Phys. Conf. Ser.* 28, 83–86. doi:10.1088/1742-6596/28/1/017
- Neubauer, J. W., Hauck, N., Männel, M. J., Seuss, M., Fery, A., and Thiele, J. (2019). Mechanoresponsive Hydrogel Particles as a Platform for Three-Dimensional Force Sensing. *ACS Appl. Mat. Interfaces* 11 (29), 26307–26313. doi:10.1021/acsami.9b04312
- Novak, R., Zeng, Y., Shuga, J., Gautham, V., Daniel, A. F., Martyn, T. S., et al. (2011). Single-Cell Multiplex Gene Detection and Sequencing with

- Microfluidically Generated Agarose Emulsions. *Angew. Chem. Int. Ed.* 50 (2), 390–395. doi:10.1002/ANIE.201006089
- Rahimian, A., Siltanen, C., Feyzizarnagh, H., Escalante, P., and Revzin, A. (2019). Microencapsulated Immunoassays for Detection of Cytokines in Human Blood. *ACS Sens.* 4 (3), 578–585. doi:10.1021/acssensors.8b01033
- Reth, M. (2013). Matching Cellular Dimensions with Molecular Sizes. *Nat. Immunol.* 14 (8), 765–767. doi:10.1038/ni.2621
- Russom, A., Gupta, A. K., Nagrath, S., Carlo, D. D., Edd, J. F., and Toner, M. (2009). Differential Inertial Focusing of Particles in Curved Low-Aspect-Ratio Microchannels. *New J. Phys.* 11, 075025. doi:10.1088/1367-2630/11/7/075025
- Sarkar, S., Kang, W., Jiang, S., Kunpeng, L., Somak, R., Ed, L., et al. (2020). Machine Learning-Aided Quantification of Antibody-Based Cancer Immunotherapy by Natural Killer Cells in Microfluidic Droplets. *Lab a Chip* 20, 2317. doi:10.1039/d0lc00158a
- Sarkar, S., Motwani, V., Sabhachandani, P., Cohen, N., and Konry, T. (2015). T Cell Dynamic Activation and Functional Analysis in Nanoliter Droplet Microarray. *J. Clin. Cell Immunol.* 6 (3). doi:10.4172/2155-9899.1000334
- Sarkar, S., Sabhachandani, P., and Ravi, D. (2017). Dynamic Analysis of Human Natural Killer Cell Response at Single-Cell Resolution in B-Cell Non-hodgkin Lymphoma. *Front. Immunol.* 8 (DEC), 1736. doi:10.3389/FIMMU.2017.01736/FULL
- Sarkar, S., Sabhachandani, P., Stroopinsky, D., Palmer, K., Cohen, N., Rosenblatt, J., et al. (2016). Dynamic Analysis of Immune and Cancer Cell Interactions at Single Cell Level in Microfluidic Droplets. *Biomicrofluidics* 10, 054115. doi:10.1063/1.4964716
- Satija, R., and Shalek, A. K. (2014). Heterogeneity in Immune Responses: From Populations to Single Cells. *Trends Immunol.* 35 (5), 219–229. doi:10.1016/j.it.2014.03.004
- Scanlon, T. C., Dostal, S. M., and Griswold, K. E. (2014). A High-Throughput Screen for Antibiotic Drug Discovery. *Biotechnol. Bioeng.* 111 (2), 232. doi:10.1002/BIT.25019
- Schoeman, R. M., Kemna, E. W. M., Wolbers, F., and van den Berg, A. (2014). High-throughput Deterministic Single-Cell Encapsulation and Droplet Pairing, Fusion, and Shrinkage in a Single Microfluidic Device. *Electrophoresis* 35 (2–3), 385–392. doi:10.1002/elps.201300179
- Segre, G., and Silber, A. (1961). Radial Particle Displacements in Poiseuille Flow of Suspensions. *Nature* 189 (4760), 209–210. doi:10.1038/189209a0
- Shahi, P., Kim, S. C., Haliburton, J. R., Gartner, Z. J., and Abate, A. R. (2017). Abseq: Ultrahigh-Throughput Single Cell Protein Profiling with Droplet Microfluidic Barcoding. *Sci. Rep.* 7 (1), 1–12. doi:10.1038/srep44447
- Shang, L., Cheng, Y., and Zhao, Y. (2017). Emerging Droplet Microfluidics. *Chem. Rev.* 117 (12), 7964–8040. doi:10.1021/ACS.CHEMREV.6B00848
- Shao, F., Yu, L., Zhang, Y., An, C., Zhang, H., Zhang, Y., et al. (2020). Microfluidic Encapsulation of Single Cells by Alginate Microgels Using a Trigger-Gellified Strategy. *Front. Bioeng. Biotechnol.* 8. doi:10.3389/fbioe.2020.583065
- Shembekar, N., Chaipan, C., Utharala, R., and Merten, C. A. (2016). Droplet-based Microfluidics in Drug Discovery, Transcriptomics and High-Throughput Molecular Genetics. *Lab. Chip* 16 (8), 1314–1331. doi:10.1039/C6LC00249H
- Shinde, P., Mohan, L., Kumar, A., Dey, K., Maddi, A., Patananan, A., et al. (2018). Current Trends of Microfluidic Single-Cell Technologies. *Ijms* 19 (10), 3143. doi:10.3390/ijms19103143
- Sims, C. E., and Allbritton, N. L. (2007). Analysis of Single Mammalian Cells On-Chip. *Lab. Chip* 7 (4), 423–440. doi:10.1039/b615235j
- Sinha, N., Subedi, N., and Tel, J. (2018). Integrating Immunology and Microfluidics for Single Immune Cell Analysis. *Front. Immunol.* 9 (OCT), 2373. doi:10.3389/fimmu.2018.02373
- Sinha, N., Subedi, N., Wimmers, F., Soennichsen, M., and Tel, J. (2019). A Pipette-Tip Based Method for Seeding Cells to Droplet Microfluidic Platforms. *JoVE* 144, e57848. doi:10.3791/57848
- Sionkowska, A. (2011). Current Research on the Blends of Natural and Synthetic Polymers as New Biomaterials: Review. *Prog. Polym. Sci.* 36 (9), 1254–1276. doi:10.1016/j.PROGPOLYMSCI.2011.05.003
- Smidsrød, O., and Skjåk-Bræk, G. (1990). Alginate as Immobilization Matrix for Cells. *Trends Biotechnol.* 8 (3), 71–78. doi:10.1016/0167-7799(90)90139-O
- stPaul, M., and Ohashi, P. S. (2020). The Roles of CD8+ T Cell Subsets in Antitumor Immunity. *Trends Cell Biol.* 30 (9), 695–704. doi:10.1016/j.tcb.2020.06.003
- Subedi, N., van Eyndhoven, L. C., and Hokke, A. M. (2021). An Automated Real-Time Microfluidic Platform to Probe Single NK Cell Heterogeneity and Cytotoxicity On-Chip. *Sci. Rep.* 11 (1), 1–11. doi:10.1038/s41598-021-96609-9
- Sun, M., Sun, X., Wang, Z., Guo, S., Yu, G., and Yang, H. (2018). Synthesis and Properties of Gelatin Methacryloyl (GelMA) Hydrogels and Their Recent Applications in Load-Bearing Tissue. *Polymers* 10 (11), 1290. doi:10.3390/POLYM10111290
- Taddei, M., Giannoni, E., Fiaschi, T., and Chiarugi, P. (2012). Anoikis: an Emerging Hallmark in Health and Diseases. *J. Pathology* 226 (2), 380–393. doi:10.1002/path.3000
- Tan, W.-H., and Takeuchi, S. (2007). Monodisperse Alginate Hydrogel Microbeads for Cell Encapsulation. *Adv. Mat.* 19 (18), 2696–2701. doi:10.1002/ADMA.200700433
- Tanaka, H., Matsumura, M., and Veliky, I. A. (1984). Diffusion Characteristics of Substrates in Ca-Alginate Gel Beads. *Biotechnol. Bioeng.* 26 (1), 53–58. doi:10.1002/bit.260260111
- Tang, F., Barbacioru, C., Wang, Y., Nordman, E., Lee, C., Xu, N., et al. (2009). mRNA-Seq Whole-Transcriptome Analysis of a Single Cell. *Nat. Methods* 6 (5), 377–382. doi:10.1038/nmeth.1315
- Tawfik, D. S., and Griffiths, A. D. (). Man-made Cell-like Compartments for Molecular Evolution. *Nat. Biotechnol.* 16 (7), 652–656. doi:10.1038/nbt0798-652
- Tiemeijer, B. M., Sweep, M. W. D., Sleetboom, J. J. F., Steps, K. J., van Sprang, J. F., De Almeida, P., et al. (2021). Probing Single-Cell Macrophage Polarization and Heterogeneity Using Thermo-Reversible Hydrogels in Droplet-Based Microfluidics. *Front. Bioeng. Biotechnol.* 9 (October), 1–14. doi:10.3389/fbioe.2021.715408
- Tondera, C., Hauser, S., Krüger-Genge, A., Jung, F., Neffe, A. T., Lendlein, A., et al. (2016). Gelatin-based Hydrogel Degradation and Tissue Interaction *In Vivo*: Insights from Multimodal Preclinical Imaging in Immunocompetent Nude Mice. *Theranostics* 6 (12), 2114–2128. doi:10.7150/THNO.16614
- Tumarkin, E., Tzadu, L., Csaszar, E., Minseok, S., Hong, Z., Anna, L., et al. (2011). High-throughput Combinatorial Cell Co-culture Using Microfluidics. *Integr. Biol.* 3 (6), 653–662. doi:10.1039/c1ib00002k
- Utech, S., Prodanovic, R., Mao, A. S., Ostafe, R., Mooney, D. J., and Weitz, D. A. (2015). Microfluidic Generation of Monodisperse, Structurally Homogeneous Alginate Microgels for Cell Encapsulation and 3D Cell Culture. *Adv. Healthc. Mat.* 4 (11), 1628–1633. doi:10.1002/adhm.201500021
- van den Bulcke, A. I., Bogdanov, B., de Rooze, N., Schacht, E. H., Cornelissen, M., and Berghmans, H. (2000). Structural and Rheological Properties of Methacrylamide Modified Gelatin Hydrogels. *Biomacromolecules* 1 (1), 31–38. doi:10.1021/bm990017d
- van Eyndhoven, L. C., Chouri, E., Subedi, N., and Tel, J. (2021). Phenotypical Diversification of Early IFN α -Producing Human Plasmacytoid Dendritic Cells Using Droplet-Based Microfluidics. *Front. Immunol.* 12, 1592. doi:10.3389/fimmu.2021.672729/BIBTEX
- van Poll, D., Sokmensuer, C., Ahmad, N., Arno, W. T., François, B., Mehmet, T., et al. (2006). Elevated Hepatocyte-specific Functions in Fetal Rat Hepatocytes Co-cultured with Adult Rat Hepatocytes. *Tissue Eng.* 12 (10), 2965–2973. doi:10.1089/TEN.2006.12.2965
- Vanherberghen, B., Olofsson, P. E., Forslund, E., Sternberg-Simon, Mohammad Ali, M. K., Simon, P., et al. (2013). Classification of Human Natural Killer Cells Based on Migration Behavior and Cytotoxic Response. *Blood* 121 (8), 1326–1334. doi:10.1182/BLOOD-2012-06-439851
- Villani, A. C., Satija, R., Reynolds, G., Sarkizova, S., Shekhar, K., Fletcher, J., et al. (2017). Single-cell RNA-Seq Reveals New Types of Human Blood Dendritic Cells, Monocytes, and Progenitors. *Science* 356 (6335). doi:10.1126/SCIENCE.AAH4573
- Wan, J. (2012). Microfluidic-Based Synthesis of Hydrogel Particles for Cell Microencapsulation and Cell-Based Drug Delivery. *Polymers* 4 (2), 1084–1108. doi:10.3390/POLYM4021084
- Wang, M., Nai, M. H., Huang, R. Y.-J., Leo, H. L., Lim, C. T., and Chen, C.-H. (2021). High-throughput Functional Profiling of Single Adherent Cells via Hydrogel Drop-Screen. *Lab. Chip* 21 (4), 764–774. doi:10.1039/D0LC01294G
- White, A. M., Zhang, Y., Shamul, J. G., Xu, J., Kwizera, E. A., Jiang, B., et al. (2021). Deep Learning-Enabled Label-Free On-Chip Detection and Selective

- Extraction of Cell Aggregate-Laden Hydrogel Microcapsules. *Small* 17 (23), 2100491. doi:10.1002/SMLL.202100491
- Wimmers, F., Subedi, N., van Buuringen, N., Daan, H., Judith, V., Beeren-Reinieren, I., et al. (2018). Single-cell Analysis Reveals that Stochasticity and Paracrine Signaling Control Interferon-Alpha Production by Plasmacytoid Dendritic Cells. *Nat. Commun.* 9 (1). doi:10.1038/s41467-018-05784-3
- Wissing, T. B., Bonito, V., Bouten, C. V. C., and Smits, A. I. P. M. (2017). Biomaterial-driven *In Situ* Cardiovascular Tissue Engineering—A Multi-Disciplinary Perspective. *npj Regen. Med.* 2 (1), 1–20. doi:10.1038/s41536-017-0023-2
- Wong, E. H.-m., Rondeau, E., Schuetz, P., and Cooper-White, J. (2009). A Microfluidic-Based Method for the Transfer of Biopolymer Particles from an Oil Phase to an Aqueous Phase. *Lab. Chip* 9 (17), 2582–2590. doi:10.1039/B903774H
- Woodland, D. L., and Dutton, R. W. (2003). Heterogeneity of CD4+ and CD8+ T Cells. *Curr. Opin. Immunol.* 15 (3), 336–342. doi:10.1016/S0952-7915(03)00037-2
- Woodland, D. L., and Dutton, R. W. (2003). Heterogeneity of CD4+ and CD8+ T Cells. *Curr. Opin. Immunol.* 15 (3), 336–342. doi:10.1016/S0952-7915(03)00037-2
- Workman, V. L., Dunnett, S. B., Kille, P., and Palmer, D. D. (2007). Microfluidic Chip-Based Synthesis of Alginate Microspheres for Encapsulation of Immortalized Human Cells. *Biomicrofluidics* 1 (1), 014105. doi:10.1063/1.2431860
- Xi, H. D., Zheng, H., Guo, W., Gañán-Calvo, A. M., Ye, A., Chia-Wen, T., et al. (2017). Active Droplet Sorting in Microfluidics: a Review. *Lab a Chip* 17 (5), 751–771. doi:10.1039/c6lc01435f
- Xia, B., Jiang, Z., Debroy, D., Li, D., and Oakey, J. (2017). Cytocompatible Cell Encapsulation via Hydrogel Photopolymerization in Microfluidic Emulsion Droplets. *Biomicrofluidics* 11 (4), 044102. doi:10.1063/1.4993122
- Xia, Y., and Whitesides, G. M. (1998). Soft Lithography. *Annu. Rev. Mater. Sci.* 28, 153–184. doi:10.1146/annurev.matsci.28.1.153
- Xiong, J.-Y., Narayanan, J., Liu, X.-Y., Chong, T. K., Chen, S. B., and Chung, T.-S. (2005). Topology Evolution and Gelation Mechanism of Agarose Gel. *J. Phys. Chem. B* 109 (12), 5638–5643. doi:10.1021/JP044473U
- Xu, T., Molnar, P., Gregory, C., Das, M., Boland, T., and Hickman, J. J. (2009). Electrophysiological Characterization of Embryonic Hippocampal Neurons Cultured in a 3D Collagen Hydrogel. *Biomaterials* 30 (26), 4377–4383. doi:10.1016/J.BIOMATERIALS.2009.04.047
- Xu, Y., Zhan, C., Fan, L., Wang, L., and Zheng, H. (2007). Preparation of Dual Crosslinked Alginate-Chitosan Blend Gel Beads and *In Vitro* Controlled Release in Oral Site-specific Drug Delivery System. *Int. J. Pharm.* 336, 329–337. doi:10.1016/j.ijpharm.2006.12.019
- Yaghoobi, M., Saidi, M. S., Ghadami, S., and Kashaninejad, N. (2020). An Interface-Particle Interaction Approach for Evaluation of the Co-encapsulation Efficiency of Cells in a Flow-Focusing Droplet Generator. *Sensors* 2020 (13), 37743774. doi:10.3390/S20133774
- Yanakiya, D., Elter, A., Bratsch, J., Friedrich, K., Becker, S., and Kolmar, H. (2020). FACS-based Functional Protein Screening via Microfluidic Co-encapsulation of Yeast Secretor and Mammalian Reporter Cells. *Sci. Rep.* 10 (1), 1–13. doi:10.1038/s41598-020-66927-5
- Yeh, C.-F., and Hsu, C.-H. (2019). “Microfluidic Techniques for Single-Cell Culture,” in *Single-Cell Omics: Volume 1: Technological Advances and Applications* (Elsevier), 137–151. doi:10.1016/B978-0-12-814919-5.00007-5
- Young, C., Rozario, K., Serra, C., Poole-Warren, L., and Martens, P. (2013). Poly(vinyl Alcohol)-Heparin Biosynthetic Microspheres Produced by Microfluidics and Ultraviolet Photopolymerisation. *Biomicrofluidics* 7 (4), 044109. doi:10.1063/1.4816714
- Yu, J., Gu, Y., Du, K. T., Mihardja, S., Sievers, R. E., and Lee, R. J. (2009). The Effect of Injected RGD Modified Alginate on Angiogenesis and Left Ventricular Function in a Chronic Rat Infarct Model. *Biomaterials* 30 (5), 751–756. doi:10.1016/J.BIOMATERIALS.2008.09.059
- Zhang, L.-M., Wu, C.-X., Huang, J.-Y., Peng, X.-H., Chen, P., and Tang, S.-Q. (2012). Synthesis and Characterization of a Degradable Composite Agarose/HA Hydrogel. *Carbohydr. Polym.* 88 (4), 1445–1452. doi:10.1016/J.CARBOL.2012.02.050
- Zhang, W., Li, D., Jiang, S., Galan, E. A., Zhang, Z., Huang, L., et al. (2021). Microfluidic Droplets as Structural Templates for Matrigel to Enable 1-week Large Organoid Modeling. *Chem. Eng. Sci.* 238, 116632. doi:10.1016/J.CES.2021.116632
- Zhao, S., Cao, M., Li, H., Li, L., and Xu, W. (2010). Synthesis and Characterization of Thermo-Sensitive Semi-IPN Hydrogels Based on Poly(ethylene Glycol)-Co-Poly(ϵ -Caprolactone) Macromer, N-Isopropylacrylamide, and Sodium Alginate. *Carbohydr. Res.* 345 (3), 425–431. doi:10.1016/J.CARRES.2009.11.014
- Zhao, S., Wen, H., Ou, Y., Li, M., Wang, L., Zhou, H., et al. (2021). A New Design for Living Cell-Based Biosensors: Microgels with a Selectively Permeable Shell that Can Harbor Bacterial Species. *Sensors Actuators B Chem.* 334, 129648. doi:10.1016/J.SNB.2021.129648
- Zhao, X., Liu, S., Yildirimer, L., Zhao, H., Ding, R., Wang, H., et al. (2016). Injectable Stem Cell-Laden Photocrosslinkable Microspheres Fabricated Using Microfluidics for Rapid Generation of Osteogenic Tissue Constructs. *Adv. Funct. Mat.* 26 (17), 2809–2819. doi:10.1002/ADFM.201504943
- Zhou, Y., Shao, N., Bessa de Castro, R., Zhang, P., Ma, Y., Liu, X., et al. (2020). Evaluation of Single-Cell Cytokine Secretion and Cell-Cell Interactions with a Hierarchical Loading Microwell Chip. *Cell Rep.* 31 (4), 107574. doi:10.1016/j.celrep.2020.107574
- Zhu, J. (2010). Bioactive Modification of Poly(ethylene Glycol) Hydrogels for Tissue Engineering. *Biomaterials* 31 (17), 4639–4656. doi:10.1016/J.BIOMATERIALS.2010.02.044
- Zhu, P., and Wang, L. (2017). Passive and Active Droplet Generation with Microfluidics: a Review. *Lab. Chip* 17, 34–75. doi:10.1039/C6LC01018K
- Zhu, Z., Zhang, W., Leng, X., Mingxia, Z., Zhichao, G., Jiangquan, L., et al. (2012). Highly Sensitive and Quantitative Detection of Rare Pathogens through Agarose Droplet Microfluidic Emulsion PCR at the Single-Cell Level. *Lab a Chip* 12 (20), 3907–3913. doi:10.1039/C2LC40461C
- Zhu, Z., and Yang, C. J. (2017). Hydrogel Droplet Microfluidics for High-Throughput Single Molecule/cell Analysis. *Acc. Chem. Res.* 50 (1), 22–31. doi:10.1021/acs.accounts.6b00370
- Zilionis, R., Nainys, J., Veres, A., Virginia, S., David, Z., Allon, M. K., et al. (2016). Single-cell Barcoding and Sequencing Using Droplet Microfluidics. *Nat. Protoc.* 12 (1), 44–73. doi:10.1038/nprot.2016.154

Conflict of Interest: The authors declare that the research was conducted in the absence of any commercial or financial relationships that could be construed as a potential conflict of interest.

Publisher's Note: All claims expressed in this article are solely those of the authors and do not necessarily represent those of their affiliated organizations, or those of the publisher, the editors, and the reviewers. Any product that may be evaluated in this article, or claim that may be made by its manufacturer, is not guaranteed or endorsed by the publisher.

Copyright © 2022 Tiemeijer and Tel. This is an open-access article distributed under the terms of the Creative Commons Attribution License (CC BY). The use, distribution or reproduction in other forums is permitted, provided the original author(s) and the copyright owner(s) are credited and that the original publication in this journal is cited, in accordance with accepted academic practice. No use, distribution or reproduction is permitted which does not comply with these terms.



OPEN ACCESS

EDITED BY
Nihal Engin Vrana,
Sparta Medical, France

REVIEWED BY
Pietro Parisse,
National Research Council (CNR), Italy

*CORRESPONDENCE
Anna Lagunas,
alagunas@ibecbarcelona.eu

SPECIALTY SECTION
This article was submitted to
Biomaterials,
a section of the journal
Frontiers in Bioengineering and
Biotechnology

RECEIVED 25 July 2022
ACCEPTED 16 August 2022
PUBLISHED 06 September 2022

CITATION
Casanelas I, Samitier J and Lagunas A
(2022), Recent advances in engineering
nanotopographic substrates for
cell studies.
Front. Bioeng. Biotechnol. 10:1002967.
doi: 10.3389/fbioe.2022.1002967

COPYRIGHT
© 2022 Casanelas, Samitier and
Lagunas. This is an open-access article
distributed under the terms of the
[Creative Commons Attribution License](#)
(CC BY). The use, distribution or
reproduction in other forums is
permitted, provided the original
author(s) and the copyright owner(s) are
credited and that the original
publication in this journal is cited, in
accordance with accepted academic
practice. No use, distribution or
reproduction is permitted which does
not comply with these terms.

Recent advances in engineering nanotopographic substrates for cell studies

Ignasi Casanelas^{1,2,3}, Josep Samitier^{1,2,3} and Anna Lagunas^{1,3*}

¹Nanobioengineering Group, Institute for Bioengineering of Catalonia (IBEC), Barcelona Institute of Science and Technology (BIST), Barcelona, Spain, ²Department of Electronics and Biomedical Engineering, Faculty of Physics, University of Barcelona (UB), Barcelona, Spain, ³Biomedical Research Networking Center in Bioengineering, Biomaterials, and Nanomedicine (CIBER-BBN), Madrid, Spain

Cells sense their environment through the cell membrane receptors. Interaction with extracellular ligands induces receptor clustering at the nanoscale, assembly of the signaling complexes in the cytosol and activation of downstream signaling pathways, regulating cell response. Nanoclusters of receptors can be further organized hierarchically in the cell membrane at the meso- and micro-levels to exert different biological functions. To study and guide cell response, cell culture substrates have been engineered with features that can interact with the cells at different scales, eliciting controlled cell responses. In particular, nanoscale features of 1–100 nm in size allow direct interaction between the material and single cell receptors and their nanoclusters. Since the first “contact guidance” experiments on parallel microstructures, many other studies followed with increasing feature resolution and biological complexity. Here we present an overview of the advances in the field summarizing the biological scenario, substrate fabrication techniques and applications, highlighting the most recent developments.

KEYWORDS

receptor nanoclustering, nanofabrication, nanotopography, nanopatterning, cell response

1 Introduction

The compartmentalization of cellular functions is a ubiquitous strategy to increase efficiency, providing spatio-temporally discrete domains for dynamic processes to take place simultaneously, in close vicinity, and without interfering with each other. The plasma membrane is generally accepted as being compartmentalized (Garcia-Parajo et al., 2014; Nicolson, 2014). This characteristic emerges from the temporary limitation of lateral diffusion, promoting confinement and allowing lipids and proteins to be organized in specific locations of variable size and composition (Kusumi et al., 1993; Jacobson et al., 2019). Restrictions in lateral diffusion of membrane components have been mainly attributed to their association to the underlying cytoskeleton as described by the “membrane skeleton fence model”, in which fences or corrals are defined by transmembrane proteins acting as posts

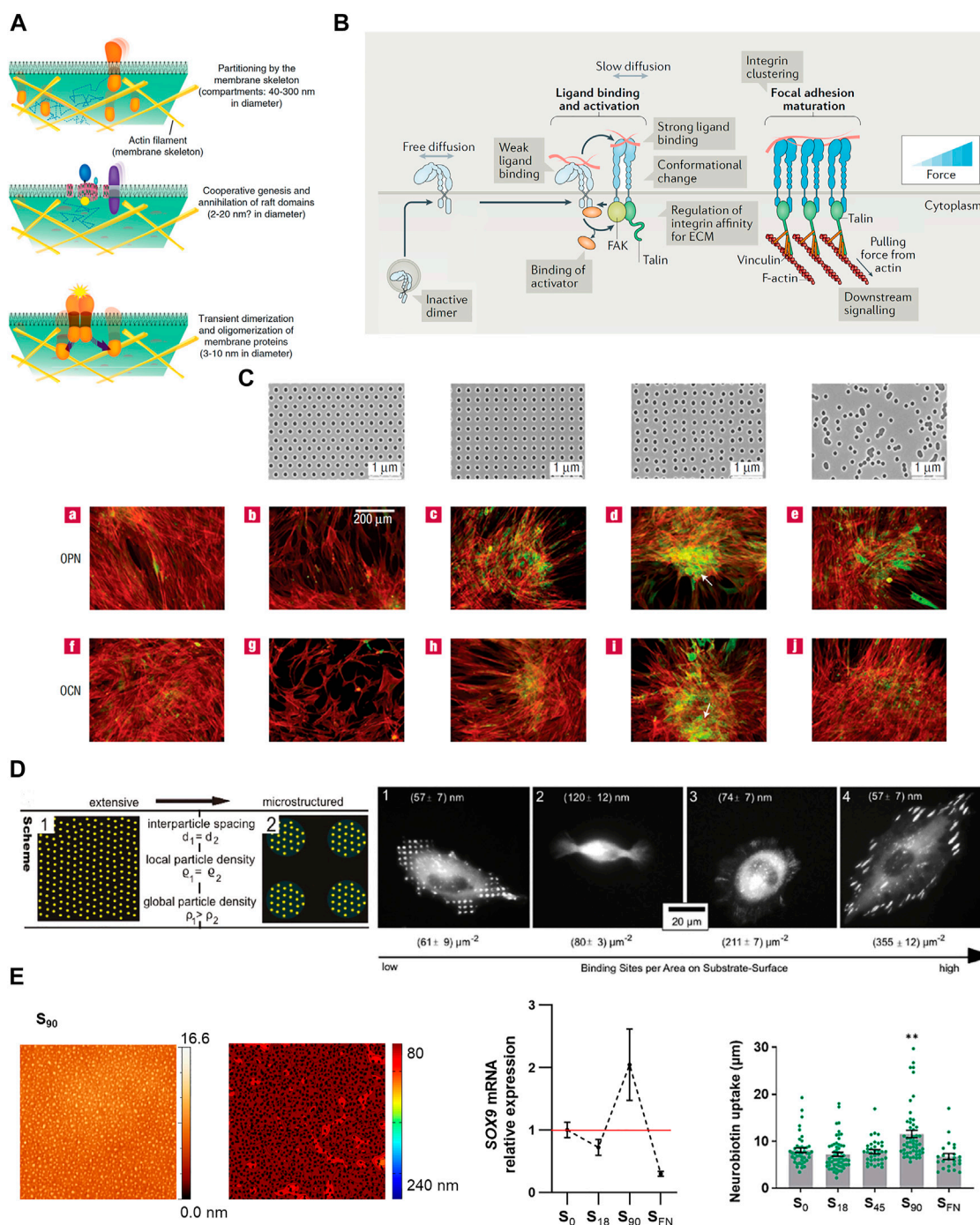


FIGURE 1

(A) Hierarchical organization of cell membrane compartments. Reprinted with permission from Kusumi et al., 2011. Copyright 2011 Elsevier. (B) Receptor nanoclustering: Ligand-mediated integrin clustering initiates the recruitment of adaptor proteins at FAs, leading to cytoskeleton engagement, force transmission and downstream signaling activation. Adapted with permission from Kechagia et al., 2019. Copyright 2019 Springer Nature. (C) Osteoprogenitor differentiation (osteopontin (OCP) and osteocalcin (OCN) expression, and bone nodule formation (white arrows)) on nanotopographies with different levels of disorder, fabricated by EBL. Reprinted with permission from Dalby et al., 2007b. Copyright 2007 Springer Nature. (D) BCML combined with photolithography were used to create micro- and nanopatterned surfaces of the cell adhesive ligand cyclic-(RGDfK). The development of stable FAs, number, size and adhesion strength is more influenced by local than global ligand density. Adapted with permission from Deeg et al., 2011. Copyright 2011 American Chemical Society. (E) The nanopatterning of RGD functionalized dendrimers revealed a threshold nanopattern configuration to induce cell response promoting chondrogenic differentiation and enhancing GJIC. Adapted from Casanellas et al., 2020 and Reprinted with permission Casanellas et al., 2022. Copyright 2022 Future Medicine Ltd.

linked to the cytoskeletal structures (Kusumi and Sako, 1996; Kusumi et al., 2012). Also, the presence of extracellular lattices (Lajoie et al., 2009), or specific lipid domains or “lipid rafts” (van Meer et al., 1987) can create regions of restricted lateral diffusion in the plasma membrane. This compartmentalization is hierarchically organized from small nanoclusters of dynamic small protein oligomers (of 3–10 nm diameter) and lipid rafts (2–20 nm) to actin-cytoskeletal fence domains (40–300 nm) up to bigger domains of several micrometers, thereby allowing the multiscale regulation of the membrane protein function (Kusumi et al., 2011) (Figure 1A).

The cellular microenvironment is also organized at the nanoscale, as seen for collagen, the main structural protein in the extracellular matrix (ECM). Collagen I is assembled by three peptide chains of collagen that conform a helical structure of around 1.5 nm diameter and 300 nm length, which then organize into microfibrils with a cross-section of around 3×5 nm (Jiang et al., 2004). The ECM protein fibronectin forms bundles of fibrils, in which the average span of a fibronectin molecule (a dimer of two polynucleotides) in each fibronectin fibril is ~92 nm (Früh et al., 2015). This favors ligand interaction with the receptors at the cell membrane in a particular configuration that is confined to the nanometer scale.

Therefore, nanotopography represents an effective physical approach for studies on cell behavior mediated by cell-cell environment interactions. Nanotopographies (1–100 nm) lie in the same scale range as many ECM proteins, allowing the direct interaction of the material with single cell receptors and their nanoclusters. Nanoscale surface topography affects cellular and tissue responses, including adhesion, migration, growth, morphogenesis, and differentiation (Martínez et al., 2009; Luo et al., 2022).

2 Receptor nanoclustering

Specific protein-protein and protein-lipid interactions promote oligomerization, aiding the formation of signaling complexes at the cell membrane. Glycosylphosphatidyl-anchored proteins (GPI-APs) are a class of soluble proteins attached to the external side of the plasma membrane. They form small clusters of up to four molecules (<5 nm) stabilized in sphingolipid- and cholesterol-dependent domains or rafts. These lipid rafts act as sorting platforms for the GPI-APs selective delivery to the apical membrane in polarized epithelial cells, where they exert specialized functions (Zurzolo and Simons, 2016). Besides lipid-linked proteins, many transmembrane proteins also cluster to exert their functions.

The clustering of transmembrane receptors is common among different types of immune cells (Dustin and Groves, 2012; Li and Yu, 2021). T cell receptors (TCRs) on resting T cells can be found as monomers and as cholesterol- and

sphingomyelin-stabilized nanoclusters (<10%) containing 2–30 TCRs each (Molnár et al., 2012). Upon activation of TCRs, they assemble into larger clusters of ten up to hundreds of receptors, which recruit kinases and adaptor proteins including Lck, ZAP-70, Lat, and SLP76. These microclusters initiate and sustain TCR signaling at the immunological synapse. Moreover, TCR microclusters associate and are transported by cortical F-actin flows over micrometer distances along the synapse (Dustin and Groves, 2012; Yi et al., 2019; Balagopalan et al., 2021). The enrichment of oligomeric TCRs has been reported to increase the sensitivity of memory T cells compared to naïve T cells (Kumar et al., 2011). A similar hierarchical organization has been described for integrin receptors. Integrins are transmembrane receptors that mediate cell-cell and cell-extracellular matrix (ECM) adhesion (Kechagia et al., 2019). However, integrin binding alone is insufficient to elicit full adhesion. Instead, upon ligand binding, integrin receptors arrange into nanoclusters that build tension through the recruitment of adaptor proteins such as paxillin, vinculin, talin, FAK or SRC, cytoskeletal engagement into focal adhesions (FAs) and downstream signaling activation (Hu et al., 2015; Kechagia et al., 2019) (Figure 1B). Remarkably, within FAs, active and inactive $\beta 1$ integrins segregate into different nanoclusters, thus suggesting integrin activity is not only regulated at the monomeric level but is subjected to collective or coordinate regulation at the level of the nanoclusters (Spiess et al., 2018). As integrins, Eph tyrosine kinase receptors cluster upon the interaction with their ligand, ephrin, which is presented on the surface of neighboring cell membranes. During development, Eph receptors act as positional cues in tissue patterning by regulating cell adhesion and repulsion. Ephrin ligands presented as concentration gradients guide axonal patterning in retinotectal mapping and stem cell migration in the developing intestines (Klein, 2012). Activation of Eph receptors occurs immediately after ligand interaction, inducing receptor polymerization. Maximum receptor activation is reached on clusters of five to eight receptors, after which oligomers cannot grow further by recruiting more monomers and instead, they grow through the condensation of oligomers into larger complexes that dampen the signaling. These polymerization–condensation dynamics provide a framework for the mechanism by which cells properly respond to variable concentrations and gradients of the ephrin ligand (Ojosnegros et al., 2017).

3 Nanofabrication

From the first contact guidance experiments (Curtis and Varde, 1964), microfabrication techniques first developed for the electronics industry came into use to produce micro- and nanopatterned surfaces for cell studies, with high feature resolution and increased biological complexity. Fabrication

methods to produce controlled nanotopographies on cell culture substrates mainly rely on the use of lithographic techniques, which in general require specialized equipment and skilled personnel, thus limiting their widespread application. The later introduction of the directed self-assembly techniques to produce nanostructured surfaces greatly facilitated the implementation of nanotopography production in general wet labs. Here we summarize the main fabrication techniques used to generate nanotopographical substrates, and their characteristics.

3.1 Photolithography

Photolithography or optical lithography is a patterning technique in which a light-sensitive chemical (photoresist) coated on the substrate is selectively exposed to light through a mask. The photoresist either collapses or hardens in the regions exposed to light and the pattern emerges on the substrate by dissolving the softer parts of the coating, which can subsequently be transferred to the substrate material. The wavelength of the light used determines the minimum feature size that can be impressed on the photoresist: The use of incoherent, vacuum ultraviolet (VUV) radiation of 172 nm allowed the production of nanoscale features with a minimum lateral feature size of 350 nm (Mironov et al., 2020). To overcome the resolution limitations, surface plasmon polaritons (SPPs), able to surpass the diffraction-limits, have been used for the fabrication of nanopatterns with a half-pitch resolution of less than 15 nm (Luo and Ishihara, 2004; Dong et al., 2014).

3.2 Electron beam lithography and ion beam lithography

In electron beam lithography or e-beam lithography (EBL), a focused beam of electrons is applied (direct-writing) on an electron sensitive coating on a substrate (Lercel et al., 1994). This is a maskless lithography technique in which custom nanopatterns can be transferred to a substrate with up to 3–5 nm resolution (Ermiş et al., 2018). Like photolithography, the coating is degraded or crosslinked upon exposure and after a development process, patterns are revealed. While conventional lithography mostly relies on flat wafer-base processing, EBL can be applied on curved surfaces (Lee et al., 2019). However, compared to photolithography, only small areas can be patterned at a time and the equipment manipulation is tough, which makes the whole process significantly slower. Ion beam lithography (IBL) or focused ion beam lithography (FIBL) uses a narrow scanning ion beam source (typically of gallium ions) instead of a focused beam of electrons to pattern a resist. Compared to EBL, IBL offers higher resolution due to ions have much heavier mass than electrons and more momentum, thus leading to smaller wavelengths and

reducing diffraction, but also minimizing the back scattering and radiation towards sensitive resists (Joshi-Imre and Bauerdick, 2014; Li et al., 2021).

3.3 Scanning probe lithography approaches

SPL approaches are a set of maskless nanolithographic techniques based on the ability of scanning probe microscopy to create variable surface patterns either by adsorption, nanoshaving and/or nanografting (Rosa and Liang, 2009). They include dip-pen nanolithography (DPN), fluidic force microscopy (FluidFM), and polymer pen lithography (PPL), among others. DPN was pioneered by the group of Prof. Mirkin (Piner et al., 1999; Salaita et al., 2007), where an AFM tip is used to create patterns of 15–100 nm by direct writing on the substrate. A molecular ink is transferred from the atomic force microscope (AFM) tip to the substrate by the spontaneous formation of a water meniscus, which is facilitated by the ambient conditions. DPN can work in sequential or parallel modes (multiplexed DPN), where parallel DPN tip arrays are scanned on the substrate simultaneously, thus significantly improving the throughput limitations of the technique (Ma et al., 2018). FluidFM introduces microfluidic channels (300 nm–8 µm) into the AFM probes allowing to dispense volumes of fluid that can be below the femtoliter range. The patterns are created when the nanopipette contacts the surface and the ink is released from the probe with a short pressure pulse (few hPa) (Zambelli et al., 2018). Alternatively, a cantilever-free scanning probe molecular printing technology referred as polymer pen nanolithography (PPL) was introduced to overcome the throughput issues and the use of complicated pen arrays (Huo et al., 2008). Since the SPL techniques work under mild conditions, they allow patterning sensitive compounds such as DNA, proteins, lipids, viruses and even polymers for 3D additive manufacturing (Liu et al., 2022).

3.4 Nanoimprint lithography

Nanoimprint lithography (NIL) is a simple and low-cost lithography technique in which a pattern is transferred by mechanical deformation of a polymer resist from a previously nanostructured mold (created by photolithography or EBL). The transfer of the nanopattern can be conducted in several ways: by thermocompression using high temperatures to soften the polymer resist while pressing it with the stamp, also known as hot embossing lithography, or by using UV light to cross-link and harden a soft polymer resist during the imprint (UV-NIL). UV-NIL requires the substrate and/or stamp to be transparent to UV wavelengths (Modaresialam et al., 2021).

TABLE 1 Influence of nanotopographies on cell response.

Technique	Cell type	Cell response	Ref
NIL (Hot embossing)	SMC	Nanopatterned gratings with 350 nm line width, 700 nm pitch, and 350 nm depth in PMMA, produced cell alignment towards the gratings both of nuclei and cell body, elongation, polarization of MTOC towards the axis of cell alignment, and reduced cell proliferation	Yim et al. (2005)
EBL	Human fibroblasts	The nanopits (of 100 nm diameter and 100 nm depth on PMMA) reduced adhesion, spreading and stress fiber formation. Also reduced the nuclear area and there was a closer spacing of centrosomes within the nucleus	Dalby et al. (2007a)
EBL, Hot embossing	Osteoprogenitors from bone marrow samples, hMSCs	120 nm diameter, 100 nm depth, 300 nm mean spacing nanopits in PMMA with different levels of disorder. Highly ordered nanotopographies produce low to negligible cellular adhesion and osteoblastic differentiation	Dalby et al. (2007b)
Soft lithography, Hot embossing	hMSCs	The nanopatterned gratings (350 nm line width, 700 nm pitch and 350 nm in depth in PDMS and TCPS) decreased the expression of integrins and promote an aligned actin cytoskeleton towards the gratings. On the rigid TCPs, gratings (500 nm line width, 1 μ m pitch and 350 nm in depth) affect the mechanical properties of the cells	Yim et al. (2010)
DPN	hMSCs	Nanodots with 70 nm diameter, separated by defined spacings of 140–1,000 nm with different terminal groups (carboxyl, amino, methyl and hydroxyl). Spacing and chemistry have different effects on adhesion and stemness maintenance	Curran et al. (2010)
EBL, Hot embossing	MSCs from bone marrow, SaOS2 osteoblasts	Pits of 120 nm diameter, 100 nm depth and a random displacement of ± 50 nm, with mean 300 nm pitch in PCL increase cell adhesion in both cell lines and promote osteogenic differentiation through adhesion in MSCs	Allan et al. (2018)
BCML with poly-styrene (PS) homopolymer as an ordering interference reagent	MC3T3-E1 osteoblasts	Integrin clustering depends on the local order of RGD ligands when the global average ligand spacing is larger than 70 nm	Huang et al. (2009)
BCML, photolithography	REF	Cell adhesion more influenced by local (<60 nm ligand spacing) than global ligand density	Deeg et al. (2011)
BCML	HSCs	32 nm maximum ligand spacing for cell adhesion, and lipid raft clustering	Altrock et al. (2012)
BCML	hMSCs	Maintenance of undifferentiated state favored on nanopatterns of 68 nm spacing	Medda et al. (2014)
BCML, transfer lithography	rMSCs	Large (161 nm) nanospacings favor chondrogenic differentiation	Li et al. (2015)
BCML, photolithography, and transfer lithography	hMSCs	Adipogenic and osteogenic differentiation favored on large (95 nm) nanospacings	Wang et al. (2015)
BCML, with poly-styrene (PS) homopolymer as an ordering interference reagent, transfer lithography	Human breast myoepithelial cell line, HUVECs, MEFs, MCF 10A	Integrin clustering and the formation of FAs integrate the effects of ligand spacing and substrate force loading	Oria et al. (2017)
Self-assembled diblock copolymers	HEK293T expressing the EphB2 receptor fused to the fluorescent protein mRuby	Nanopatterns of surface-bound ephrinB1/Fc ligands accelerate receptor oligomerization (receptor monomer polymerization was accelerated by 25–30%)	Hortigüela et al. (2018)
Dendrimer nanopatterning	hASCs	Chondrogenesis and GJIC are enhanced by a nanopattern configuration in which 90% of the surface area presents adhesion sites separated <70 nm, providing an onset for cell signaling	(Lagunas et al., 2017; Casanellas et al., 2022)

SMC: bovine pulmonary artery smooth muscle cells; PMMA: polymethylmethacrylate; MTOC: microtubule organizing centers; hMSCs: human mesenchymal stem cells; PDMS: polydimethylsiloxane; TCPS: tissue culture polystyrene; PCL: polycaprolactone; REF: rat embryonic fibroblasts; HSCs: hematopoietic stem cells; rMSCs: rat mesenchymal stem cells; HUVECs: human umbilical vein endothelial cells; MEFs: mouse embryonic fibroblasts; MCF, 10A: mammary epithelial cells; HEK293T: human epithelial kidney 293 cells; hASCs: human adipose-derived mesenchymal stem cells.

3.5 Soft lithography

First introduced by Bain and Whitesides in 1989 (Bain and Whitesides, 1989), soft lithography refers to a number of techniques that use elastomeric stamps (typically of polydimethylsiloxane (PDMS)) previously cast on a master, to transfer micro- or nanopatterns to a substrate. It includes replica molding, microcontact printing, micromolding in microcapillaries, microtransfer molding, and solvent-assisted micromolding. Soft lithography is a low-cost technique that does not require stringent control over the environment (such as a clean-room facilities), thus being accessible to general wet labs (Qin et al., 2010).

3.6 Directed self-assembly of nanostructures

Supramolecular chemistry can be used as a bottom-up approach to achieve nanopatterned surfaces based on the self-organization of molecular scale architectures, allowing precision on the nanofeature position. Compared to the self-assembly of small molecules, polymers offer higher stability and durability due to their mechanical and physical properties. Self-assembly of block copolymers (BCPs) has attracted considerable attention in nanoscience due to its ability to self-assemble both in bulk and in solution into different types of nanostructures through the repulsion of their immiscible blocks (Mai and Eisenberg, 2012). BCP micelle nanolithography (BCML) has been extensively used to generate ordered and disordered nanopatterns of gold nanoclusters on surfaces with well-controlled interparticle distances (Glass et al., 2003). Dendrimers, presenting a highly branched and easily tunable size and chemical structure, have been used to create nanopatterns with a liquid-like order on low charged surfaces (Lagunas et al., 2014), and DNA and peptides have been used to build nanostructures presenting multiple epitopes with nanoscale spatial control (Stephanopoulos et al., 2015; Wang et al., 2021).

4 Biological applications

The first visible phenomena of nanostructures-cell interaction are the changes in cell adhesion, spreading and morphology, which provide cues to predict cellular functions. Studies have explored the influence of different nanotopographies on the adhesive/spreading behavior of various cell types, some of them summarized in Table 1. Nanotopography has been vastly employed to control cell differentiation with especial emphasis on enhancing tissue integration in bone implants (Chen et al., 2018). Due to the easy manufacturing, first attempts were conducted by using the surface roughness strategy. However, the lack of control in the

produced structures, and poor reproducibility, prompted the use of lithographic techniques to fabricate nanostructured biocompatible materials that promote osteointegration (Figure 1C and Table 1).

In many cases, the assembly of membrane receptors into fully functional microcomplexes requires of both ligand occupancy and receptor clustering. Spatz and coworkers used BCML to create ordered gold nanopatterns coated with the integrin receptor ligand arginine-glycine-aspartic acid (RGD), present in many ECM proteins. The gold nanodots, of less than 8 nm in diameter, allowed the binding of one integrin per dot and were positioned at different interdot spacings on a non-fouling substrate. Authors observed that a ligand spacing of more than 73 nm impairs integrin clustering, cell adhesion and spreading, and dramatically reduces the formation of FAs and actin stress fibers (Arnold et al., 2004). Since this seminal work, BCML has been used in a number of cell studies, showing the prevalence of local over global ligand density (Deeg et al., 2011) (Figure 1D and Table 1), and that integrin clustering influences many aspects of cell behavior, including cell differentiation (Table 1). More recently, Roca-Cusachs and coworkers used BCML to create cell adhesive nanopatterns on substrates of different rigidity, and they found that the optimal ligand spacing for cell adhesion increases as substrate stiffness decreases (Oria et al., 2017) (Table 1).

The multivalent interactions between ligand and receptors, in which the simultaneous binding of multiple ligands on receptor complexes takes place (Kießling et al., 2006), have been extensively used to study receptor clustering and the downstream signaling in cells. Self-assembled diblock copolymers of polystyrene-blockpoly(methyl methacrylate) (PS-*b*-PMMA) were used to produce nanopatterned substrates able to establish multivalent interactions between surface-bound ephrinB1 ligands and membrane EphB2 receptors. The preclustering of ephrinB1 ligands in the nanopatterns resulted in a more efficient and faster receptor oligomerization kinetics compared to the traditional cross-linked ligand presentation (Hortigüela et al., 2018). Also, dendrimer nanopatterning of RGD-functionalized dendrimers was used to study the effects of the local RGD ligand density on the adhesion, differentiation, and gap junction intercellular communication (GJIC) of mesenchymal stem cells (Lagunas et al., 2017; Casanellas et al., 2020; Casanellas et al., 2022) (Figure 1E).

5 Conclusions and perspectives

Nanoscale cell-environmental interactions regulate cell behavior. Nanotopography produced by lithographic techniques and/or by the self-assembly of molecular scale architectures effectively mimics those interactions, helping to direct particular cell responses and providing information about the underlying mechanisms. We expect that further advances in

the field by including stimuli-responsive materials, combined with super-resolution microscopies, will bring more detailed information on the molecular mechanisms that direct cell function, unveiling traits that are normally hidden by the ensemble average in bulk experiments. This will provide an otherwise unavailable insight on the cell interactions at the nanoscale so that they can be used to systematically drive cell responses by fabricating the appropriate nanotopographical substrates, with potential applications in translational medicine.

Author contributions

AL: defined the focus of the review, writing, reviewing, and editing. IC and JS: writing, reviewing, and editing.

Funding

This work was supported by the Biomedical Research Networking Center (CIBER), Spain. CIBER is an initiative funded by the VI National R&D&I Plan 2008–2011, Iniciativa Ingenio 2010, Consolider Program, CIBER Actions, and the Instituto de Salud Carlos III, with the support of the European Regional Development Fund (ERDF). This work

was funded by the CERCA Program and by the Commission for Universities and Research of the Department of Innovation, Universities, and Enterprise of the Generalitat de Catalunya (2017 SGR 1079). IC was supported by the Spanish Ministry of Science through the Subsidies for Predoctoral Contracts for the Training of Doctors open call, co-funded by the European Social Fund, grant number: BES-2016-076682.

Conflict of interest

The authors declare that the research was conducted in the absence of any commercial or financial relationships that could be construed as a potential conflict of interest.

Publisher's note

All claims expressed in this article are solely those of the authors and do not necessarily represent those of their affiliated organizations, or those of the publisher, the editors and the reviewers. Any product that may be evaluated in this article, or claim that may be made by its manufacturer, is not guaranteed or endorsed by the publisher.

References

- Allan, C., Ker, A., Smith, C. -A., Tsimbouri, P. M., Borsoi, J., O'Neill, S., et al. (2018). Osteoblast response to disordered nanotopography. *J. Tissue Eng.* 9, 204173141878409–7. doi:10.1177/2041731418784098
- Altrock, E., Muth, C. A., Klein, G., Spatz, J. P., and Lee-Thedieck, C. (2012). The significance of integrin ligand nanopatterning on lipid raft clustering in hematopoietic stem cells. *Biomaterials* 33 (11), 3107–3118. doi:10.1016/j.biomaterials.2012.01.002
- Bain, C. D., and Whitesides, G. M. (1989). Modeling organic surfaces with self-assembled monolayers. *Angew. Chem. Int. Ed. Engl.* 28 (4), 522–528. doi:10.1002/ange.19891010446
- Balogopalan, L., Raychaudhuri, K., and Samelson, L. E. (2021). Microclusters as T Cell signaling hubs: Structure, kinetics, and regulation. *Front. Cell Dev. Biol.* 8, 608530. doi:10.3389/fcell.2020.608530
- Casanellas, I., Lagunas, A., Vida, Y., Pérez-Inestrosa, E., Andrades, J. A., Becerra, J., et al. (2020). The janus role of adhesion in chondrogenesis. *Int. J. Mol. Sci.* 21 (15), 5269. doi:10.3390/ijms21155269
- Casanellas, I., Lagunas, A., Vida, Y., Pérez-Inestrosa, E., Rodríguez-Pereira, C., Magalhaes, J., et al. (2022). Nanoscale ligand density modulates gap junction intercellular communication of cell condensates during chondrogenesis. *Nanomedicine (Lond.)* 17 (11), 775–791. doi:10.2217/nnm-2021-0399
- Chen, S., Guo, Y., Liu, R., Wu, S., Fang, J., Huang, B., et al. (2018). Tuning surface properties of bone biomaterials to manipulate osteoblastic cell adhesion and the signaling pathways for the enhancement of early osseointegration. *Colloids Surfaces B Biointerfaces* 164, 58–69. doi:10.1016/j.colsurfb.2018.01.022
- Curran, J. M., Stokes, R., Irvine, E., Graham, D., Amro, N. A., Sanedrin, R. G., et al. (2010). Introducing dip pen nanolithography as a tool for controlling stem cell behaviour: Unlocking the potential of the next generation of smart materials in regenerative medicine. *Lab. Chip* 10 (13), 1662–1670. doi:10.1039/C004149A
- Curtis, A., and Varde, M. (1964). Control of cell behavior: Topological factors. *J. Natl. Cancer Inst.* 33 (1), 15–26. doi:10.1093/jnci/33.1.15
- Dalby, M. J., Biggs, M. J. P., Gadegaard, N., Kalna, G., Wilkinson, C. D. W., and Curtis, A. S. G. (2007a). Nanotopographical stimulation of mechanotransduction and changes in interphase centromere positioning. *J. Cell. Biochem.* 100 (2), 326–38. doi:10.1002/jcb.21058
- Dalby, M. J., Gadegaard, N., Tare, R., Andar, A., Riehle, M. O., Herzyk, P., et al. (2007b). The control of human mesenchymal cell differentiation using nanoscale symmetry and disorder. *Nat. Mat.* 6, 997–1003. doi:10.1038/nmat2013
- Deeg, J. A., Louban, I., Aydin, D., Selhuber-Unkel, C., Kessler, H., and Spatz, J. P. (2011). Impact of local versus global ligand density on cellular adhesion. *Nano Lett.* 11 (4), 1469–1476. doi:10.1021/nl104079r
- Dong, J., Liu, J., Kang, G., Xie, J., and Wang, Y. (2014). Pushing the resolution of photolithography down to 15 nm by surface plasmon interference. *Sci. Rep.* 4, 5618. doi:10.1038/srep05618
- Dustin, M. L., and Groves, J. T. (2012). Receptor signaling clusters in the immune synapse. *Annu. Rev. Biophys.* 41, 543–556. doi:10.1146/annurev-biophys-042910-155238
- Ermis, M., Antmen, E., and Hasirci, V. (2018). Micro and nanofabrication methods to control cell-substrate interactions and cell behavior: A review from the tissue engineering perspective. *Bioact. Mat.* 3 (3), 355–369. doi:10.1016/j.bioactmat.2018.05.005
- Früh, S. M., Schoen, I., Ries, J., and Vogel, V. (2015). Molecular architecture of native fibronectin fibrils. *Nat. Commun.* 6, 7275. doi:10.1038/ncomms8275
- García-Parajo, M. F., Cambi, A., Torreno-Pina, J. A., Thompson, N., and Jacobson, K. (2014). Nanoclustering as a dominant feature of plasma membrane organization. *J. Cell Sci.* 127 (23), 4995–5005. doi:10.1242/jcs.146340
- Glass, R., Möller, M., and Spatz, J. P. (2003). Block copolymer micelle nanolithography. *Nanotechnology* 14 (10), 1153–1160. doi:10.1088/0957-4484/14/10/314
- Hortiguera, V., Larranaga, E., Cutrale, F., Seriola, A., García-Díaz, M., Lagunas, A., et al. (2018). Nanopatterns of surface-bound EphrinB1 produce multivalent Ligand–Receptor interactions that tune EphB2 receptor clustering. *Nano Lett.* 18 (1), 629–637. doi:10.1021/acs.nanolett.7b04904

- Hu, S., Tee, Y. -H., Kabla, A., Zaidel-Bar, R., Bershadsky, A., and Hersen, P. (2015). Structured illumination microscopy reveals focal adhesions are composed of linear subunits. *Cytoskeleton* 72, 235–245. doi:10.1002/cm.21223
- Huang, J., Gräter, S. V., Corbellini, F., Rinck, S., Bock, E., Kemkemer, R., et al. (2009). Impact of order and disorder in RGD nanopatterns on cell adhesion. *Nano Lett.* 9 (3), 1111–1116. doi:10.1021/nl803548b
- Huo, F., Zheng, Z., Zheng, G., Giam, L. R., Zhang, H., and Mirkin, C. A. (2008). Polymer pen lithography. *Science* 321 (5896), 1658–1660. doi:10.1126/science.1162193
- Jacobson, K., Liu, P., and Lagerholm, B. C. (2019). The lateral organization and mobility of plasma membrane components. *Cell* 177 (4), 806–819. doi:10.1016/j.cell.2019.04.018
- Jiang, F., Hörber, H., Howard, J., and Müller, D. J. (2004). Assembly of collagen into microribbons: Effects of pH and electrolytes. *J. Struct. Biol.* 148 (3), 268–278. doi:10.1016/j.jsb.2004.07.001
- Joshi-Imre, A., and Bauerdick, S. (2014). Direct-write ion beam lithography. *J. Nanotechnol.* 2014, 170415. doi:10.1155/2014/170415
- Kechagia, J. Z., Ivaska, J., and Roca-Cusachs, P. (2019). Integrins as biomechanical sensors of the microenvironment. *Nat. Rev. Mol. Cell Biol.* 20 (8), 457–473. doi:10.1038/s41580-019-0134-2
- Kiessling, L. L., Gestwicki, J. E., and Strong, L. E. (2006). Synthetic multivalent ligands as probes of signal transduction. *Angew. Chem. Int. Ed.* 45 (15), 2348–2368. doi:10.1002/anie.200502794
- Klein, R. (2012). Eph/ephrin signalling during development. *Development* 139, 4105–4109. doi:10.1242/dev.074997
- Kumar, R., Ferez, M., Swamy, M., Arechaga, I., Rejas, M. T., Valpuesta, J. M., et al. (2011). Increased sensitivity of antigen-experienced T cells through the enrichment of oligomeric T cell receptor complexes. *Immunity* 35 (3), 375–387. doi:10.1016/j.immuni.2011.08.010
- Kusumi, A., Fujiwara, T. K., Chadda, R., Xie, M., Tsunoyama, T. A., Kalay, Z., et al. (2012). Dynamic organizing principles of the plasma membrane that regulate signal transduction: Commemorating the fortieth anniversary of singer and nicolson's fluid-mosaic model. *Annu. Rev. Cell Dev. Biol.* 28, 215–250. doi:10.1146/annurev-cellbio-100809-151736
- Kusumi, A., and Sako, Y. (1996). Cell surface organization by the membrane skeleton. *Curr. Opin. Cell Biol.* 8 (4), 566–574. doi:10.1016/s0955-0674(96)80036-6
- Kusumi, A., Sako, Y., and Yamamoto, M. (1993). Confined lateral diffusion of membrane receptors as studied by single particle tracking (nanovid microscopy). Effects of calcium-induced differentiation in cultured epithelial cells. *Biophys. J.* 65 (5), 2021–2040. doi:10.1016/S0006-3495(93)81253-0
- Kusumi, A., Suzuki, K. G., Kasai, R. S., Ritchie, K., and Fujiwara, T. K. (2011). Hierarchical mesoscale domain organization of the plasma membrane. *Trends biochem. Sci.* 36 (11), 604–615. doi:10.1016/j.tibs.2011.08.001
- Lagunas, A., Castaño, A. G., Artés, J. M., Vida, Y., Collado, D., Pérez-Inestrosa, E., et al. (2014). Large-scale dendrimer-based uneven nanopatterns for the study of local arginine-glycine-aspartic acid (RGD) density effects on cell adhesion. *Nano Res.* 7 (3), 399–409. doi:10.1007/s12274-014-0406-2
- Lagunas, A., Tsintzou, I., Vida, Y., Collado, D., Pérez-Inestrosa, E., Rodríguez Pereira, C., et al. (2017). Tailoring RGD local surface density at the nanoscale toward adult stem cell chondrogenic commitment. *Nano Res.* 10 (6), 1959–1971. doi:10.1007/s12274-016-1382-5
- Lajoie, P., Goetz, J. G., Dennis, J. W., and Nabi, I. R. (2009). Lattices, rafts, and scaffolds: Domain regulation of receptor signaling at the plasma membrane. *J. Cell Biol.* 185 (3), 381–385. doi:10.1083/jcb.200811059
- Lee, C. R., Ok, J. G., and Jeong, M. Y. (2019). Nanopatterning on the cylindrical surface using an E-beam pre-mapping algorithm. *J. Micromech. Microeng.* 29, 015004. doi:10.1088/1361-6439/aae448
- Lercel, M. J., Redinbo, G. F., Pardo, F. D., Rooks, M., Tiberio, R. C., Simpson, P., et al. (1994). Electron beam lithography with monolayers of alkylthiols and alkylsiloxanes. *J. Vac. Sci. Technol. B* 12, 3663–3667. doi:10.1116/1.587635
- Li, M., and Yu, Y. (2021). Innate immune receptor clustering and its role in immune regulation. *J. Cell Sci.* 134 (4), jcs249318. doi:10.1242/jcs.249318
- Li, P., Chen, S., Dai, H., Yang, Z., Chen, Z., Wang, Y., et al. (2021). Recent advances in focused ion beam nanofabrication for nanostructures and devices: Fundamentals and applications. *Nanoscale* 13, 1529–1565. doi:10.1039/d0nr07539f
- Li, Z., Cao, B., Wang, X., Ye, K., Li, S., and Ding, J. (2015). Effects of RGD nanospacing on chondrogenic differentiation of mesenchymal stem cells. *J. Mat. Chem. B* 3, 5197–5209. doi:10.1039/C5TB00455A
- Liu, G., Rong, M., Hu, H., Chen, L., Xie, Z., and Zheng, Z. (2022). 3D dip-pen nanolithography. *Adv. Mat. Technol.* 7, 2101493. doi:10.1002/admt.202101493
- Luo, J., Walker, M., Xiao, Y., Donnelly, H., Dalby, M. J., and Salmeron-Sanchez, M. (2022). The influence of nanopotography on cell behaviour through interactions with the extracellular matrix – a review. *Bioact. Mat.* 15, 145–159. doi:10.1016/j.bioactmat.2021.11.024
- Luo, X., and Ishihara, T. (2004). Subwavelength photolithography based on surface-plasmon polariton resonance. *Opt. Express* 12 (14), 3055–3065. doi:10.1364/OPEX.12.003055
- Ma, H., Jiang, Z., Xie, X., Huang, L., and Huang, W. (2018). Multiplexed biomolecular arrays generated via parallel dip-pen nanolithography. *ACS Appl. Mat. Interfaces* 10 (30), 25121–25126. doi:10.1021/acsami.8b07369
- Mai, Y., Eisenberg, A., Lin, J., Zhang, L., Cai, C., Yao, Y., et al. (2012). Self-assembly of rod-coil block copolymers on a substrate into micrometer-scale ordered stripe nanopatterns. *Polym. Chem.* 11 (47), 7487–7496. doi:10.1039/D0PY01404D
- Martínez, E., Lagunas, A., Mills, C. A., Rodríguez-Seguí, S., Estévez, M., Oberhansl, S., et al. (2009). Stem cell differentiation by functionalized micro- and nanostructured surfaces. *Nanomedicine (Lond)* 4 (1), 65–82. doi:10.2217/17435889.4.1.65
- Medda, R., Helth, A., Herre, P., Pohl, D., Rellinghaus, B., Perschmann, N., et al. (2014). Investigation of early cell-surface interactions of human mesenchymal stem cells on nanopatterned β -type titanium-niobium alloy surfaces. *Interface Focus* 4, 20130046. doi:10.1098/rsfs.2013.0046
- Mironov, A. E., Kim, J., Huang, Y., Steinförth, A. W., Sievers, D. J., and Eden, J. G. (2020). Photolithography in the vacuum ultraviolet (172 nm) with sub-400 nm resolution: Photoablative patterning of nanostructures and optical components in bulk polymers and thin films on semiconductors. *Nanoscale* 12 (32), 16796–16804. doi:10.1039/d0nr04142d
- Modaresialam, M., Chehadi, Z., Bottein, T., Abbarchi, M., and Grosso, D. (2021). Nanoimprint lithography processing of inorganic-based materials. *Chem. Mat.* 33 (14), 5464–5482. doi:10.1021/acs.chemmater.1c00693
- Molnár, E., Swamy, M., Holzer, M., Beck-García, K., Worch, R., Thiele, C., et al. (2012). Cholesterol and sphingomyelin drive ligand-independent T-cell antigen receptor nanoclustering. *J. Biol. Chem.* 287 (51), 42664–42674. doi:10.1074/jbc.M112.386045
- Nicolson, G. L. (2014). The fluid—mosaic model of membrane structure: Still relevant to understanding the structure, function and dynamics of biological membranes after more than 40 years. *Biochimica Biophysica Acta - Biomembr.* 1838 (6), 1451–1466. doi:10.1016/j.bbamem.2013.10.019
- Ojosnegros, S., Cutrale, F., Rodríguez, D., Otterstrom, J. J., Chiu, C. L., Hortigüela, V., et al. (2017). Eph-ephrin signaling modulated by polymerization and condensation of receptors. *Proc. Natl. Acad. Sci. U. S. A.* 114 (50), 13188–13193. doi:10.1073/pnas.1713564114
- Oria, R., Wiegand, T., Escribano, J., Elosegui-Artola, A., Uriarte, J. J., Moreno-Pulido, C., et al. (2017). Force loading explains spatial sensing of ligands by cells. *Nature* 552, 219–224. doi:10.1038/nature24662
- Piner, R. D., Zhu, J., Xu, F., Hong, S., and Mirkin, C. A. (1999). Dip-Pen" nanolithography. *Science* 283 (5402), 661–663. doi:10.1126/science.283.5402.661
- Qin, D., Xia, Y., and Whitesides, G. M. (2010). Soft lithography for micro- and nanoscale patterning. *Nat. Protoc.* 5, 491–502. doi:10.1038/nprot.2009.234
- Rosa, L. G., and Liang, J. (2009). Atomic force microscope nanolithography: Dip-pen, nanoshaving, nanografting, tapping mode, electrochemical and thermal nanolithography. *J. Phys. Condens. Matter* 21 (48), 483001. doi:10.1088/0953-8984/21/48/483001
- Salaita, K., Wang, Y., and Mirkin, C. A. (2007). Applications of dip-pen nanolithography. *Nat. Nanotechnol.* 2 (3), 145–55. doi:10.1038/nnano.2007.39
- Spiess, M., Hernandez-Varas, P., Oddone, A., Olofsson, H., Blom, H., Waithe, D., et al. (2018). Active and inactive β 1 integrins segregate into distinct nanoclusters in focal adhesions. *J. Cell Biol.* 217 (6), 1929–1940. doi:10.1083/jcb.201707075
- Stephanopoulos, N., Freeman, R., North, H. A., Sur, S., Jeong, S. J., Tantakitti, F., et al. (2015). Bioactive DNA-peptide nanotubes enhance the differentiation of neural stem cells into neurons. *Nano Lett.* 15 (1), 603–609. doi:10.1021/nl504079q
- van Meer, G., Stelzer, E. H., Wijnaendts-van-Resandt, R. W., and Simons, K. (1987). Sorting of sphingolipids in epithelial (Madin-Darby canine kidney) cells. *J. Cell Biol.* 105 (4), 1623–1635. doi:10.1083/jcb.105.4.1623
- Wang, K., Park, S. H., Zhu, J., Kim, J. K., Zhang, L., and Yi, G. -R. (2021). Self-assembled colloidal nanopatterns toward unnatural optical meta-materials. *Adv. Funct. Mat.* 31, 2008246. doi:10.1002/adfm.202008246

- Wang, X., Li, S., Yan, C., Liu, P., and Ding, J. (2015). Fabrication of RGD micro/nanopattern and corresponding study of stem cell differentiation. *Nano Lett.* 15 (3), 1457–1467. doi:10.1021/nl5049862
- Yi, J., Balagopalan, L., Nguyen, T., McIntire, K. M., and Samelson, L. E. (2019). TCR microclusters form spatially segregated domains and sequentially assemble in calcium-dependent kinetic steps. *Nat. Commun.* 10, 277. doi:10.1038/s41467-018-08064-2
- Yim, E. K., Darling, E. M., Kulangara, K., Guilak, F., and Leong, K. W. (2010). Nanotopography induced changes in focal adhesions, cytoskeletal organization, and mechanical properties of human mesenchymal stem cells. *Biomaterials* 31 (6), 1299–1306. doi:10.1016/j.biomaterials.2009.10.037
- Yim, E. K., Reano, R. M., Pang, S. W., Yee, A. F., Chen, C. S., and Leong, K. W. (2005). Nanopattern induced changes in morphology and motility of smooth muscle cells. *Biomaterials* 26 (26), 5405–5413. doi:10.1016/j.biomaterials.2005.01.058
- Zambelli, T., Aebersold, M. J., Behr, P., Han, H., Hirt, L., Martinez, V., et al. (2018). “FluidFM: Development of the instrument as well as its applications for 2D and 3D lithography”. in *open-space microfluidics: Concepts, implementations, applications*. Editors E. Delamarche and G. V. Kaigala (Weinheim, Germany: Wiley VCH), 295–323.
- Zurzolo, C., and Simons, K. (2016). Glycosylphosphatidylinositol-anchored proteins: Membrane organization and transport. *Biochimica Biophysica Acta - Biomembr.* 1858 (4), 632–639. doi:10.1016/j.bbamem.2015.12.018



OPEN ACCESS

EDITED BY

Nihal Engin Vrana,
Sparta Medical, France

REVIEWED BY

Ahmed Abdelhafez,
The New Valley University, Egypt
Aansa Rukya Saleem, Bahria University,
Pakistan

*CORRESPONDENCE

Jiangbo Hai,
haijiangbo@126.com

SPECIALTY SECTION

This article was submitted to
Biomaterials,
a section of the journal
Frontiers in Bioengineering and
Biotechnology

RECEIVED 29 July 2022

ACCEPTED 03 October 2022

PUBLISHED 17 October 2022

CITATION

Sun Y, Yang W, Shi H, Tanveer SK and
Hai J (2022), Past, present, and future
perspectives of biodegradable films for
soil: A 30-year systematic review.
Front. Bioeng. Biotechnol. 10:1006388.
doi: 10.3389/fbioe.2022.1006388

COPYRIGHT

© 2022 Sun, Yang, Shi, Tanveer and Hai.
This is an open-access article
distributed under the terms of the
[Creative Commons Attribution License](#)
(CC BY). The use, distribution or
reproduction in other forums is
permitted, provided the original
author(s) and the copyright owner(s) are
credited and that the original
publication in this journal is cited, in
accordance with accepted academic
practice. No use, distribution or
reproduction is permitted which does
not comply with these terms.

Past, present, and future perspectives of biodegradable films for soil: A 30-year systematic review

Yitao Sun¹, Wenlong Yang¹, Hongxia Shi¹,
Sikander Khan Tanveer² and Jiangbo Hai^{1*}

¹College of Agronomy, Northwest A&F University, Yangling, China, ²National Agriculture Research Center, Islamabad, Pakistan

Based on the Web of Science Core Collection (WOSCC) database, the academic works published in the past 30 years on biodegradable films for soil were analyzed. In order to ensure the rigor of this experiment, this paper is based on the mathematical double matrix model VOS Viewer software and CiteSpace software. This work shows that publications of biodegradable films for soil are increasing year by year; polymer science is the hottest subject in the field of biodegradable films for soil; China and the United States are the countries with the most significant number of publications in this field, has an important position; Washington State University is the most published institution. This study further identifies and reveals the essential characteristics, research strength, knowledge structure, main research fields, and research hotspots in the late stage of the field of biodegradable films for soil and introduces the Activity Index (AI) and the Attractive Index (AAI), thereby assessing trends and performance in different countries. The paper also further illustrates the importance of biodegradable films by presenting field trials using biodegradable films on different plants. The research in the field of biodegradable films for soil is divided into four categories: "The research field of degradation," "The effect of biodegradable film on soil," "Performance and mechanism of the biodegradable film," and "Effects of biodegradable film on crop growth and development.". The study can be seen as a microcosm of the development of biodegradable films for soils, which will help researchers quickly identify their general patterns. Readers can better understand the changes and development trends in this field in the past 30 years and provide references for future research.

KEYWORDS

biodegradable film, soil, quantitative analysis, hot frontiers, knowledge structure

1 Introduction

With the continuous improvement of the level of global industrialization and urbanization, the world today is undergoing tremendous changes unseen in a century, and the ensuing energy crisis and environmental problems have attracted significant attention from leaders of various countries (Titirici et al., 2015; Luo et al., 2021; Zhang et al., 2021). Soil is a fragile, non-renewable resource whose health and sustainable development are affected by human activities and natural processes (Bouma, 2014; Keesstra et al., 2016). Plastic film is a material applied to or grown on the soil surface (Liang et al., 2002). At the same time, due to the lack of biodegradability of plastic itself and the massive and inappropriate use of human beings, more and more plastic wastes are found in natural ecosystems such as soil, wetlands, rivers, and oceans, bringing a substantial environmental impact to the earth and ecological crisis (Barboza et al., 2018; Deng et al., 2019).

When the soil is covered with film, it will promote the growth and development of annual and perennial crops and increase the yield (Schonbeck and Evanylo, 1998; Weber, 2003; Liu et al., 2014). Today, the most common film for soil is plastic film. Plastic film can effectively improve the field microclimate for crop growth, increase crop yield, and enable crops to develop well in soils with limited moisture (Kader et al., 2017; Lamont, 2005; R. Li R et al., 2021). However, the residues of plastic film will seriously harm the ecological environment and have a series of adverse effects on the soil, such as reducing soil porosity, soil water content, and increasing soil bulk density (Y. L. Qi Y. L et al., 2020). Therefore, to ensure the sustainability of the ecosystem, protect the ecological environment, and alleviate the energy crisis, the development and use of new film materials have become a new trend in the research progress of soil film. To date, various films have been developed that can be degraded by microorganisms in the soil, including paper films (Siwek et al., 2019), oxidatively degradable plastic films (Nagashima et al., 2012), and biodegradable films (Hayes et al., 2017; Saglam et al., 2017; Serrano-Ruiz et al., 2018). Biodegradable materials that can be degraded by microorganisms (bacteria, fungi, or algae), either from renewable or fossil fuel resources or a mixture of both (Vroman and Tighzert, 2009). The products of this decomposition are water, carbon dioxide, or methane (only under anaerobic conditions), with no residues or new organisms (Orgiles-Calpena et al., 2014; Siwek et al., 2019). The biodegradable film is innovative biotechnology designed to maintain traditional plastic film production properties (Siwek et al., 2019). American Society for Testing and Materials (ASTM) (Gueymard et al., 2002) defines the biodegradable film as a material that can degrade from natural microorganisms such as bacteria, fungi, and algae.

Over the past three decades, numerous academic papers have been published on biodegradable films for soil. However, these substantial scientific achievements are not conducive to our

quick grasp of hot spots and insight into future directions. To more fully illustrate the importance of biodegradable films to soils, rigorous quantitative analysis and statistical justification based on mathematical models are required. A significant disadvantage of conducting retrospective studies under traditional methods is the reliance on limited publications to create personal biases that can lead to biased and flawed results. In contrast, bibliometric analysis overcomes the subjective factors in traditional reviews. It can quantitatively explore knowledge structures, research hotspots, and insights into specific scientific fields by comprehensively filming all literature in a selected period and omitting crucial literature. New Insights (Yeo et al., 2014). Bibliometric analysis is a new data-driven method that applies statistical methods to scientific results and is widely used in research trend detection, institutional cooperation analysis, national cooperation analysis, changes in subject areas, etc., with knowledge-oriented quantitative functions (Kapanen et al., 2008; Y. Q. Sun et al., 2019; Tan et al., 2021; Zhou et al., 2018). By filtering and processing a large amount of information, the correlation between various data can tap the potential value of knowledge. As mathematics, statistics, and computer science underlie its discipline, bibliometrics can provide intuitive data analysis and accurate insights into the progress of scientific research (Durieux and Gevenois, 2010; Bornmann and Mutz, 2015). The purpose of this paper is to perform bibliometric analysis using the analysis tools that come with Web of Science (WOS), VOS Viewer software, and CiteSpace software (C. M. Chen, 2006; van Eck and Waltman, 2010), and a comprehensive review and in-depth assessment of the research field of biodegradable films for soils, with unique insights into its prospects and opportunities, shed light on current research hotspots and knowledge gaps.

This study is mainly carried out from four perspectives: 1) Understanding the research strength of biodegradable films for soil (publication trends, representative countries, institutions, essential subject areas, citations, and representative journals); 2) Recognize the knowledge structure of this research field; 3) Reveal the changing trend of research topics and research hotspots; 4) Determine future research directions in this field.

2 Methodology and data

2.1 Data source and retrieval

The critical research work of this study is determined to be 30 years from 1992 to 2021, and related articles on biodegradable films for soil are carried out in the Web of Science Core Collection (ScienceCitation Index Expanded, SCIE) database, and the retrieval time is 2022 April 24. The reason why the WOSCC database is selected for search is that compared with other databases (PubMed and Scopus), it contains more than

10,000 subject fields such as environment, medical care, ecology, agriculture, etc., and has international authority, great influence, high quality and long history of research data (Harzing and Alakangas, 2016; Mongeon and Paul-Hus, 2016; Zhao, 2017). In order to avoid bias due to the daily update of the WOS database, the articles required for the search were conducted within 24 April 2022, and articles published from 1 January 2022, onwards were excluded because, from this period, Any collection from that year will include incomplete bibliometric data for that year. The retrieval parameters for biodegradable membranes for soil are set as (TI = ((“biodegradable*” OR “biological degradation*” OR “biodegradation*” OR “bio degradable*” OR “biodegradability*”) and (“film*” OR “films*” OR “film film*” OR “film films*” OR “film*” OR “films*” OR “cover*”) and (“soil*” OR “land*” OR “farmland*” OR “cropland*” OR “cultivated land*”))) OR (AB = ((“biodegradable*” OR “biological degradation*” OR “biodegradation*” OR “bio degradable*” OR “biodegradability*”) and (“film*” OR “films*” OR “film film*” OR “film films*” OR “film*” OR “films*” OR “cover*”) and (“soil*” OR “land*” OR “farmland*” OR “cropland*” OR “cultivated land*”))), Search time range: (Time = 1 January 1992–31 December 2021).

The raw data analyzed in this paper is the content of 1222 publications in the field of biodegradable films for soils obtained from the Web of Science Core Collection (ScienceCitation Index Expanded, SCIE) database. Document types include 1086 research papers, 56 proceeding papers, 62 review papers, and 18 other types (meeting abstract, early access, editorial material, and note). These papers come from 200 institutions in 87 countries, covering 90 research directions, 200 published journals, and 200 authors. Most categories belong to the literature subject categories: Polymer Science, Environmental Sciences, Engineering Environmental, Agronomy, and Biotechnology Applied Microbiology.

2.2 Scientometric analysis methods

Referring to previous studies, for example, development trends and hotspots of global forest carbon sinks and natural disaster research (Huang et al., 2020; S. Shen et al., 2018), we employed two indexes, the Activity Index (AI) and the Attractive Index (AAI), to evaluate the relative effort to a research field and the relative impact made by a country in terms of citations of its publications. The AI indicates the relative effort a country puts into a research area, while the AAI shows the relative impact a country has had in attracting citations through its publications.

Activity Index (AI):

$$AI_i^t = \frac{P_i^t / \sum P}{TP^t / \sum TP} \quad (1)$$

Attractive Index (AAI):

$$AAI_i^t = \frac{C_i^t / \sum C}{TC^t / \sum TC} \quad (2)$$

$$\text{Centrality (node } i) = \sum_{i \neq j \neq k} \frac{P_{jk}(i)}{P_{jk}} \quad (3)$$

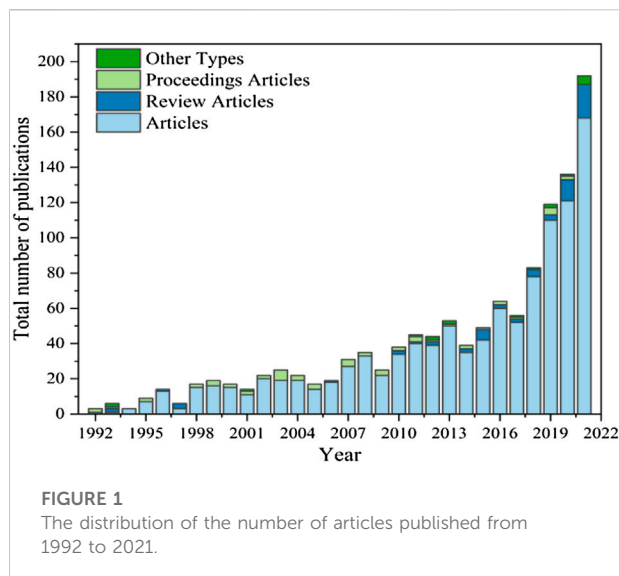
In Eqs 1, 2, AI_i^t is the Activity Index of country i in year t ; P_i^t is the number of articles about a field published by country i in year t ; $\sum P$ is the total number of a field publications in a country during the publication period; TP^t is year t of global a field publications; $\sum TP$ is the sum of global a field publications over a period of time. Similarly, AAI_i^t represents the attractiveness index of country i in year t ; C_i^t is the citations of a field publications in country i in year t ; $\sum C$ is the total number of citations of a field publications in country i over a period of time; TC^t represents year t The global a field citations $\sum TC$ in year t and t refers to the total number of a field citations in the same period as that of $\sum C$ $AI = 1$ and $AAI = 1$ represent the average level of global a field research work and academic impact, respectively. $AI > 1$ or $AI < 1$ means a country's research work is above or below the global average; $AAI > 1$ or $AAI < 1$ means a country attracts citations greater or less than the global average.

In Eq. 3, p_{jk} represents the number of shortest paths between node j and node k , and $p_{jk}(i)$ is the number of those paths that pass-through node i . In CiteSpace, nodes whose betweenness centrality exceeds 0.1 are called key nodes. At the documental level, each document's importance in a co-citing network can be partially evaluated by the indicator of betweenness centrality (Ghisi et al., 2020).

3 Results and discussion

3.1 Characteristics of publication outputs

Figure 1 shows the number of articles published on biodegradable membranes used in soil from 1992 to 2021. The period from 1992 to 2000 was the initial stage, with 94 articles and an average annual publication of about 10.4. Although the number of articles is small, there are high-quality articles, such as Drumright, RE et al. (Drumright et al., 2000) in 1992, proving that polylactic acid (a biodegradable made of renewable resources, can produce H_2O and CO_2 after decomposition and hummus) can replace the plastics of petrochemical products and are used in many fields; 2001–2016 was a period of rapid growth, with a total of 542 publications and an average annual publication volume of about 33.9. The research in the field of the biodegradable membrane is more in-depth, and people's research interest in this field is gradually increasing; 2017–2021 is an explosive growth stage, with a total of 586 papers published, with an



average annual publication volume of about 117.2 papers, and in 2021 The number of publications reached its peak at 192.

3.2 Analysis of subject categories, countries, institutions, authors, and cited journals

3.2.1 Subject categories

The top 10 subject categories in biodegradable films for soil are shown in [Table 1](#), with a 10-year cycle divided into 1992–2001, 2002–2011, and 2012–2021. The field of biodegradable films for soil includes Polymer Science (365 papers, 29.87% of the total); Environmental Sciences (287, 23.49%); Engineering Environmental (173, 14.16%); Agronomy (87, 7.12%); Biotechnology Applied Microbiology (76, 6.22%); Chemistry Applied (75, 6.14%); Engineering

Chemical (62, 5.07%); Water Resources (57, 4.66%); Soil Science (56, 4.58%) and Horticulture (53, 4.34%). It is worth noting that Polymer Science and Environmental Sciences fields accounted for more than 50% of the total number of articles, which shows that these two fields are the main research fields of biodegradable films for soil. From 2002 to 2011, publications in Agronomy, Chemistry Applied, and Horticulture increased significantly, with slow growth in other fields. It is worth noting that from 2012 to 2021, the publications in the fields of Agronomy, Chemistry Applied, and Horticulture still increased significantly, which shows that research in these three fields will still become the future research hotspots and trends.

3.2.2 Country

To date, 87 countries worldwide have contributed to the field of degradable films for soil. [Table 2](#) lists the top 10 most productive countries in this field. Visual analysis and mapping of study countries were performed using WOSCC database statistics and VOS Viewer software ([Figure 2](#)). Each node in [Figure 2](#) represents a different country, the node's size represents the scientific output of that country, and the colors and lines of the nodes represent different clusters based on the co-creation matrix of the corresponding country. The line between the two nodes represents the knowledge cooperation between countries, and the thickness of the line represents the degree of cooperation. The stronger the connection between the two nodes, the deeper the connection and cooperation between the two countries. The VOS Viewer software sets the parameter as the number of national publications greater than or equal to 1.

In the field of biodegradable films used in soil, China and the United States are the most representative countries, of which China has published 231 papers, accounting for 18.90% of the world; TC^a value is 4,592 times, TC/P^b value is 19.88, the h-index value is 32; followed by the United States (230, 18.82%, 11,782, 51.23, 46), the TC/P^b value of the United States is the highest among the top ten countries, at 51.23, and the h-index value is

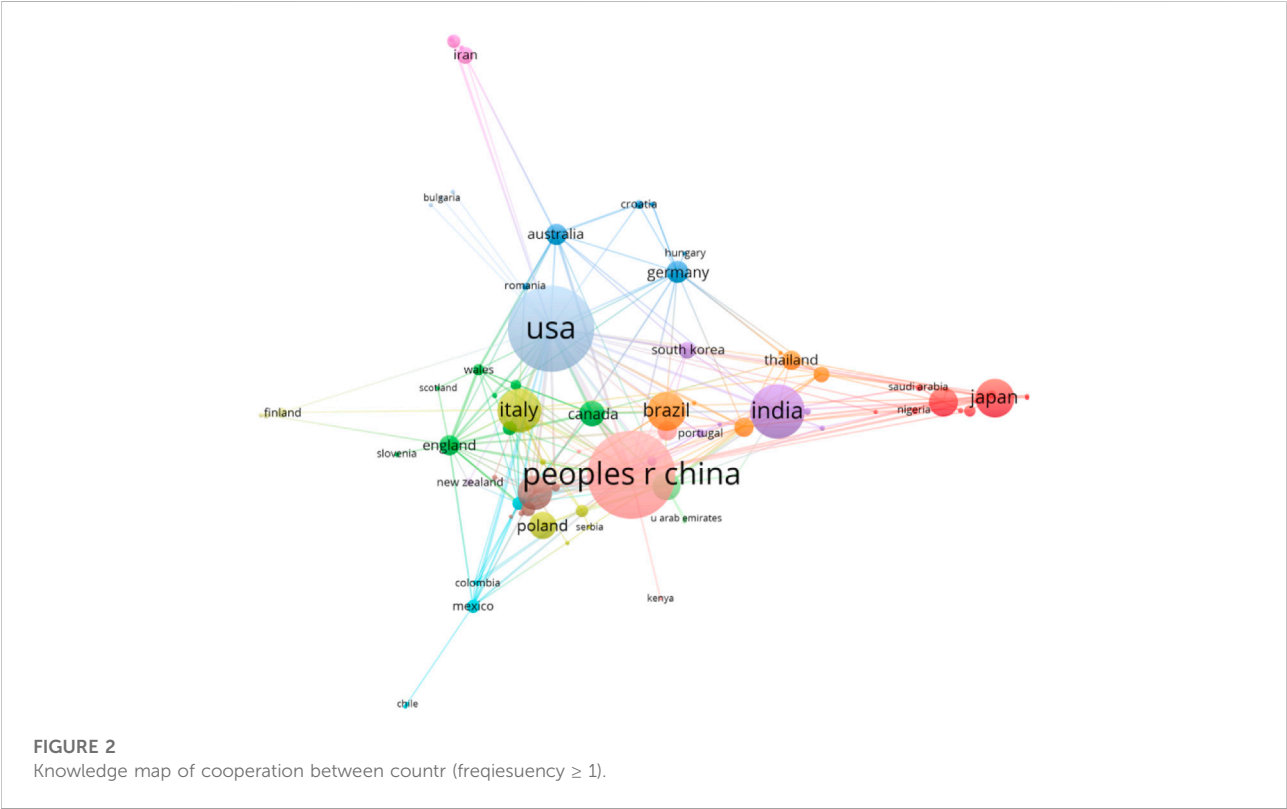
TABLE 1 Article output in ten subject categories for research on biodegradable films for soil.

Subject category (biodegradable film for soil)	1992–2001	2002–2011	2012–2021
Polymer Science	41	107	217
Environmental Sciences	24	56	207
Engineering Environmental	19	44	110
Agronomy	2	13	72
Biotechnology Applied Microbiology	15	23	38
Chemistry Applied	3	12	60
Engineering Chemical	6	14	42
Water Resources	11	12	34
Soil Science	3	11	42
Horticulture	1	10	42

TABLE 2 Top ten most productive countries in terms of relevant articles.

Country (biodegradable film for soil)	Ps	Percentage (%)	TC ^a	TC/P ^b	h-index
China	231	18.90	4,592	19.88	32
United States	230	18.82	11,782	51.23	46
India	113	9.25	2,963	26.22	29
Italy	82	6.71	2,455	29.94	29
Brazil	71	5.81	1,085	15.28	19
Japan	69	5.65	1,684	24.41	24
Spain	56	4.58	1,844	32.93	23
France	44	3.60	1,726	39.23	22
Malaysia	44	3.60	679	15.43	15
Poland	40	3.27	577	14.43	13

Note: Ps: the total number of articles published. TC^a: the total citations for a country. TC/P^b: average number of citations per paper for a country. h-index: according to Hirsch in 2005 (Hirsch, 2005): A scientist has index H if H of his/her Np papers have at least H citations each, and the other Np-H papers have no more than H citations each, in which Np is the number of articles published during n years. A higher H-index indicates greater academic impact.



also the highest, at 46. Although the number of publications in the United States is not the highest among the top ten countries, the h-index calculated by the system is the highest due to the highest number of citations. It can be seen that the United States has tremendous academic influence. As shown in Figure 2, the

United States and China have the most frequent cooperation, followed by the United States and India and China and India.

Currently, the United States uses about 450,000 tons of agricultural plastics every year, and China uses plastic films, with an estimated 12,500–140,000 tons of film applied annually,

TABLE 3 Top ten most productive institutions in terms of relevant articles.

Institutions (biodegradable film for soil)	Ps	Percentage (%)	Country	TC ^a	TC/P ^b	h-index
Washington State University	47	3.85	United States	895	19.04	17
University of Tennessee Knoxville	36	2.95	United States	806	22.39	15
University of Tennessee System	36	2.95	United States	806	22.39	15
Northwest A&F University China	31	2.54	China	1,085	35	18
Chinese Academy of Sciences	29	2.37	China	336	11.59	11
UT Institute of Agriculture	29	2.37	United States	723	24.93	14
Centre National De La Recherche Scientifique CNRS	28	2.29	France	1,136	40.57	18
Consiglio Nazionale Delle Ricerche CNR	24	1.96	Italy	669	27.88	15
United States Department of Agriculture USDA	24	1.96	United States	939	39.13	16
Russian Academy of Sciences	19	1.55	Russia	276	14.53	10

3.2.4 Cited-journal analysis

Related articles in the field of biodegradable films for soil have been published in a total of 200 journals in the Web of Science Core Collection (ScienceCitation Index Expanded, SCIE) database, and the top 10 journals with published papers (Table 3) and the number of citations Top 10 articles (Table 4). As can be seen from Table 3, JPolymer Degradation and Stability is the most published journal, with a total of 64 related articles, accounting for 5.24% of all articles, and the journal has a total of 27,899 citations; followed by Journal of Polymers and the Environment, published 62 related articles, accounting for 5.07% of all articles, and the journals were cited 6,899 times. Among the top ten journals with published articles, four journals belong to the United States, which shows that the United States has a very high research status in this field. It is worth noting that the top ten journals with published papers are all developed country journals. It can be seen that there are many types of research and articles on environmental protection, energy-saving, and consumption reduction in developed countries. In addition, the impact factor (IF) and JCI of these journals can also measure their value according to their role and status in science communication. Among them, “Carbohydrate Polymers” has the highest JCI of 1.99, which is 99% higher than the average citation impact of similar journals, and the IF value is 8.678, which indicates that the journal has significant international influence. There are seven journals whose citation impact (JCI > 1) and impact factor (IF > 4) are higher than the average citation impact of similar journals, and the remaining six journals are: “Polymer Degradation and Stability,” with a JCI value of 1.11, higher than similar journals The average value is 11%, and the IF value is 5.207; the JCI value of “Science of the Total Environment” is 1.66, which is 66% higher than the average cited the impact of similar journals, and the IF value is 7.842; the JCI value of “Agricultural Water Management” is 1.71. The

citation impact is 71% higher than the average citation impact of similar journals, with an IF value of 5.12; the JCI value of the International Journal of Biological Macromolecules is 1.38, which is 38% higher than the average citation impact of similar journals, with an IF value of 6.737; the CI value of Waste Management The JCI value of International Biodeterioration & Biodegradation is 1.02, which is 2% higher than the average citation impact of similar journals, and the IF value is 4.719.

As can be seen from Table 4, two articles in the field of biodegradable films for soil have been cited more than 1000 times, namely “Advanced oxidation processes for organic contaminant destruction based on the Fenton reaction and related chemistry” published in 2006 and “Polylactic acid technology” published in 2000. These two articles are the most representative and have particular reference values and foundations for researchers to engage in research in this field. Pignatello, JJ et al. (Pignatello et al., 2006) published “Advanced oxidation processes for organic contaminant destruction based on the Fenton reaction and related chemistry,” which mainly describes the complex mechanisms of Fenton and Fenton-like reactions and the crucial factors affecting these reactions, in water and soil Applications in processing, with sections devoted to non-classical pathways, by-products, kinetic and process modeling, experimental design methods, soil and aquifer processing, the use of Fenton in conjunction with other advanced oxidation processes or biodegradation. “Polylactic acid technology,” published by Drumright, RE, et al. (Drumright et al., 2000), mainly describes the polylactic acid technology that can replace petrochemical products. Because of its biodegradability as a renewable resource, it can be actively applied in film and packaging, increasing the need for demand for agricultural products such as corn and sugar beets and reducing plastics’ dependence on oil.

TABLE 4 Top ten journals with publication volume.

Journal	Ps	Percentage (%)	Publisher	Region	Total citations	IF	JCI
Polymer Degradation and Stability	64	5.24	Elsevier SCI Ltd.	England	27,899	5.207	1.11
Journal of Polymers and the Environment	62	5.07	Springer	United States	6,899	3.536	0.6
Journal of Applied Polymer Science	41	3.36	Wiley	United States	68,877	2.754	0.7
Science of the Total Environment	29	2.37	Elsevier	Netherlands	210,144	7.842	1.66
Carbohydrate Polymers	22	1.80	Elsevier SCI Ltd.	England	104,570	8.678	1.99
Agricultural Water Management	21	1.72	Elsevier	Netherlands	22,091	5.12	1.71
Hortscience	20	1.64	Amer Soc Horticultural Science	United States	12,336	1.617	0.59
International Journal of Biological Macromolecules	19	1.55	Elsevier	Netherlands	79,247	6.737	1.38
Waste Management	18	1.47	Pergamon-Elsevier Science Ltd.	United States	41,731	7.907	1.16
International Biodeterioration & Biodegradation	17	1.39	Elsevier SCI Ltd.	England	14,127	4.719	1.02

Note: JCI: Journal Citation Indicator; IF: 5-year impact factor, impact factor data from the 2020 edition of Journal Citation Reports® in Web of Science. The Journal Citation Indicator (JCI) is the average Category Normalized Citation Impact (CNCI) of citable items (articles and reviews) published by a journal over a recent 3 year period. The average JCI in a category is 1. Journals with a JCI of 1.5 have 50% more citation impact than the average in that category.

3.3 Field experiments with biodegradable films for soil

The difference between the plastic film and biodegradable film used for the soil on tomatoes was explored through field experiments. It was found that compared with bare soil, both of them could increase the soil temperature respectively, and the plastic film was more significant, and the plastic film increased. The soil temperature ranged from 5.9°C to 6.9°C, while the biodegradable film was 5.5°C–5.8°C. Compared with bare soil, the increase in temperature under the film will limit soil microbial activity. Compared with bare soil next to the crop, plastic film, Its soil microbial biomass carbon (SMBC) decreased from 1703 ng g⁻¹ to a minimum of 1005 ng g⁻¹, and its soil organic matter mineralization (SOMM) decreased from 558 µg OM g⁻¹ to a minimum of 451 µg OM g⁻¹ for 15 days⁻¹; while the biodegradable film decreased to a minimum value of 1183 ng g⁻¹ and 499 µg OM g⁻¹ 15 days⁻¹, respectively, showing that the negative impact of plastic film on soil microbial characteristics was more significant (Moreno and Moreno, 2008).

Due to plastic films, plastic residues may accumulate in the soil, which poses serious environmental problems for agroecosystems. As an alternative, biodegradable films are expected to reduce plastic debris accumulation and soil pollution. Yueling Qi et al. (Y. Qi Y et al., 2020) found that biodegradable plastic residues significantly affected rhizosphere bacterial communities and rhizosphere volatiles mixture. When harvested at 4 months, compared with the pH value of the blank control of 7.01, the pH values of the plastic film and the biodegradable thin film decreased, and the pH value of the plastic film decreased more significantly. The pH of Ma size and Mi size plastic films was 6.86 and 6.91, respectively, while the pH values of Ma-size and Mi-size biodegradable films were 6.91 and 6.96, respectively. Compared with the blank control

C:N of 15.84, Mi-sized plastic film and Mi-sized biodegradable film are more significant, 19.43 and 18.84, respectively.

Biodegradable films are recommended as a viable option for conventional plastic films for winter rapeseed production. Xiao-Bo Gu et al. (Gu et al., 2017), a 3-year field experiment, systematically analyzed and compared conventional plastic films (PM) and biodegradable films (BM) and no plastic film filming (CK) on each index of winter rapeseed due to the degradation of biofilm, the increase of soil temperature and soil water storage in BM at 150 days after sowing was significantly lower than that of PM; The PM depth was 1.7 cm; the mean evapotranspiration (ET) in the BM group was 10.0% higher than that in the PM group and 10.4% lower than that in the CK group. BM's average yield and water use efficiencies were 5.8% and 14.3% lower than those of PM and 38.4% and 54.5% higher than CK's. The contents of erucic acid and glucosinolates in BM were lower than those in PM, while the contents of seed oil, protein, and oleic acid in BM and PM were not significantly different.

To determine the optimal biodegradable film for summer maize, Minhua Yin et al. (Yin et al., 2019) combined three biodegradable films (one with a fast degradation rate (BM1), one with a medium degradation rate (BM2), and one with a slow degradation rate (BM3)) were compared with plastic film (PM), and no film was used as a control (CK). Soil temperature and soil water storage increased significantly under BM1 (3.6°C higher at 5 cm and 2.4°C higher at 25 cm) and BM2 (3.7°C higher at 5 cm and 2.3°C higher at 25 cm) compared with CK before the biodegradable film degraded. The soil organic carbon of the CK group was 2.85%, 5.30%, 11.72%, and 15.07% higher than that of BM1, BM2, BM3, and PM, respectively; Average grain yield, water use efficiency, and net revenue in BM2 were 18.40%, 25.10% and 32.97%, 11.90%, 6.62% and 20.46%, 11.43%, 6.82%, and 15.71%, and 32.50%, 45.64% and 41.05% higher than in

BM1, BM3, PM, and CK, respectively. The results show that, compared with BM1, BM3, and PM, the biodegradable film of BM2 can improve the soil environment, promote the growth of maize, increase the net income, and reduce the loss of soil organic carbon.

In order to verify the suitability of biodegradable films for peanuts to adjust soil temperature and moisture, improve photosynthesis and yield, Tao Sun et al. (T. Sun et al., 2018) combined four biodegradable films [0% (BM1), 10% (BM2), 15% (BM3) and 20% (BM4)], plastic film (PM), and no film (CK) were compared. The results showed that the soil temperature of the BM3 treatment was higher than that of the other three biodegradable films throughout the growing season. Compared with other treatments, BM3-covered peanuts maintained a higher leaf area index, chlorophyll content, and net photosynthetic rate in later growth stages.

Ning Chen et al. (Chen et al., 2020) investigated the effects of plastic film and biodegradable film on nitrogen absorption, distribution, and leaching in drip irrigation sandy land and found $\text{NO}_3\text{-N}$ concentration, N absorption, and $\text{NO}_3\text{-N}$ leaching under biodegradable film Unevenness increased with increasing nitrogen application rate. In the 0–20 cm soil layer, the $\text{NO}_3\text{-N}$ concentration of the biodegradable film increased by 3.9% compared with the plastic film. In arid areas, the biodegradable film can be used as a good substitute for plastic film to avoid plastic pollution, and In sandy farmland, the application of 210 kg ha^{-1} nitrogen fertilizer and the biodegradable film is the best solution.

Many scholars have compared plastic films for soil with biodegradable films in field trials, and appropriate film should be selected for different crops and geographical environments. However, the biodegradable film, with its superior characteristics and favorable factors for soil and plants, protects the ecological environment and biodiversity, maintains green and sustainable development, and the biodegradable film for soil has been obtained. More and more scholars supported and recommended and gradually entered the field of biodegradable films and carried out corresponding research.

3.4 Degradation process of biodegradable films

The biodegradation process of biodegradable films used in the soil is mainly divided into three basic steps (Figure 4): 1) Microbial colonization of the surface of biodegradable films by bacteria and fungi in the soil. 2) The biodegradable film fragments undergo enzymatic depolymerization by extracellular hydrolases. Moreover, 3) Microorganisms absorb and utilize monomers and short oligomers to release CO_2 , generate energy, and promote the activity of soil microorganisms and the cycle of nutrients (Sander, 2019).

3.5 Analysis of the activity index and the Attractive Index

In this part, we use the Activity Index (AI) and the Attractive Index (AAI) to evaluate the temporal changes in research and academic impact for selected countries. Considering there is usually a lag between when an article is published and cited, we set the time horizon for the attraction index to be 2 years later than the activity index. The starting year of the Activity Index for a given country is when the country first published an article in the field. Therefore, the activity and Attractive Index's time horizons are set as 1992 to 2019 and 1994 to 2021, respectively. The Activity Index (AI) and Attractive Index (AAI) of the top 10 countries with the most publications were calculated (Supplementary Tables S1, S2) and presented in a quadrant diagram (Figure 5). The reference line ($y = x$) reflects how a country's research efforts are balanced against the impact it cites in field research. These selected countries have undergone four types of evolution. Quadrants 1-4 in Figure 5 represent four different situations, respectively. The points in the first quadrant represent the years in which the country's Activity Index (AI) and Attractive Index (AAI) are both higher than the global average; Dots represent years in which the country's Attractive Index (AAI) is higher than the global average, and the Activity Index (AI) is lower than the global average; the dots in the third quadrant represent the country's Activity Index (AI) and Attractive Index (AAI) are both low Years in which the country's Activity Index (AI) is above the global average. The Attractive Index (AAI) is below the global average.

Comparing country performance using the Activity Index (AI) and the Attractive Index (AAI) shows that, in most years, the United States, Italy, Japan, and France have higher research effort and academic influence than the global average; China, India, Malaysia, Brazil Research effort and academic impact in, Poland and Spain are below the global average in most years. But developing countries (China, India, Malaysia, Poland, and Brazil) have surpassed the global average since 2019, which means research, technology, and economies in developing countries are starting to improve; developed countries (US, Italy, Japan, France and Spain) research effort and impact declined relatively over the same period. However, developed countries still significantly influence and status on the research of biodegradable films for soil. Furthermore, China and Poland are relatively close to the reference line in terms of the distance between the points representing a particular country and the reference line, which means that their research efforts are balanced against the impact of citations.

3.6 Keywords in different countries

This field has been extensively studied worldwide based on biodegradable films for soil. However, the subjects studied vary

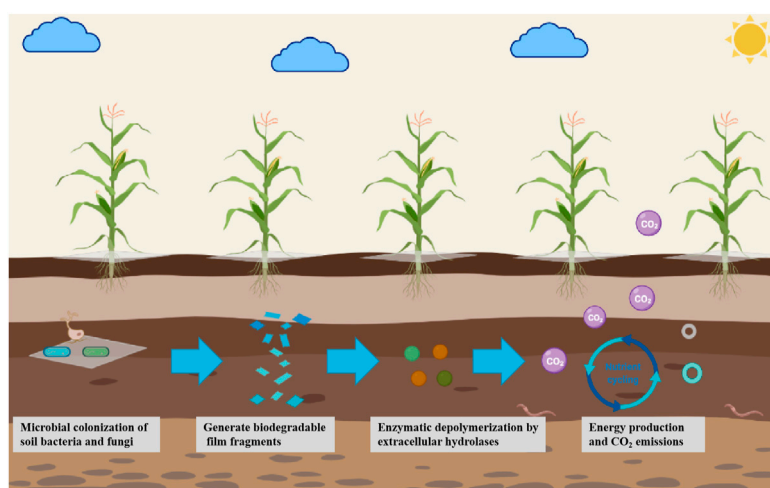


FIGURE 4
Main degradation processes of biodegradable films for soil.

from region to region due to differences in geographical features, history, and economic and climatic conditions. Figure 6 provides the five most frequently used keywords in the ten most influential countries. Keywords vary from country to country. For example, from 1992 to 2021, the most frequently used keywords in China are “degradation” (34 times, centrality is 0.62), “water use efficiency” (34 times, centrality is 0.05), “temperature” (21 times, centrality 0.06), while the most frequently used keywords in the United States are “degradation” (33 times, centrality 0.46), “film” (22 times, centrality 0.2), and “soil” (21 times, centrality 0.22). It is worth noting that, as seen from Figure 6, among the keywords of 10 countries, the betweenness centrality of the keyword “degradation” is more significant than 0.1, which shows that it is used as a critical node in different countries. Other keywords play an excellent role in mediating connections.

3.7 Knowledge structure and sub-fields

As the core of a document, keywords are words with substantive meaning condensed from the document’s leading content and have a high guiding role for academic research in a field. Keyword co-occurrence is to mine the relationship between high-frequency keywords. If a particular keyword appears in different documents with high frequency simultaneously, their correlation is very close, representing the hot research in this field. Only considering the relationship of the keyword dimension for clustering has certain limitations, ignoring the influence of cooperative relationships (such as countries, authors, institutions, and journals), and it is not easy to deeply interpret the Frontier fields in terms of classification. Therefore, this study

constructed a bimodal matrix, that is, systematic clustering analysis of high-frequency keywords. Citespace software has diversified, time-sharing, and dynamic citation visualization analysis, allowing readers to understand a topic’s knowledge domain through visualization (C. M. Chen et al., 2010; Xie, 2015). The keywords in the field of biodegradable films for soil were visualized and analyzed by VOS Viewer software (Figure 7A); Visualize the data to draw a graph of keyword co-occurrence (Figure 7B) and a graph of keyword clusters (Figure 7C). In Figure 7A, blue, red, green, and yellow represent four clusters; the color of the section in Figure 7B represents the year, the size of the node represents the number or frequency, the larger the node, the more the number or frequency; The line between them represents the strength of the association, and the color of the line represents the change in the years of cooperation. In addition, the thicker the node ring, the higher the frequency of terms, and the thicker the line between nodes, the closer the distance between them (Ping et al., 2017); Figure 7C performs a top ten systematic clustering of all related keywords.

As can be seen from Figure 7A, the keywords are clustered into 4 clusters, which are the yellow clusters represented by “biodegradation,” “polymers,” and “polyethylene”; the yellow clusters represented by “soi,” “water,” and “bacteria” Red clusters; green clusters represented by “biodegradability,” “films” and “starch”; and blue clusters represented by “growth,” “yield” and “film.” It can be seen from Figure 7B that the node with the keyword “degradation” is the most significant, indicating the highest frequency of occurrence, followed by the keywords “mechanical property,” “soil,” “biodegradation,” “film,” and “blend.” Through keyword clustering, the keywords are systematically clustered into

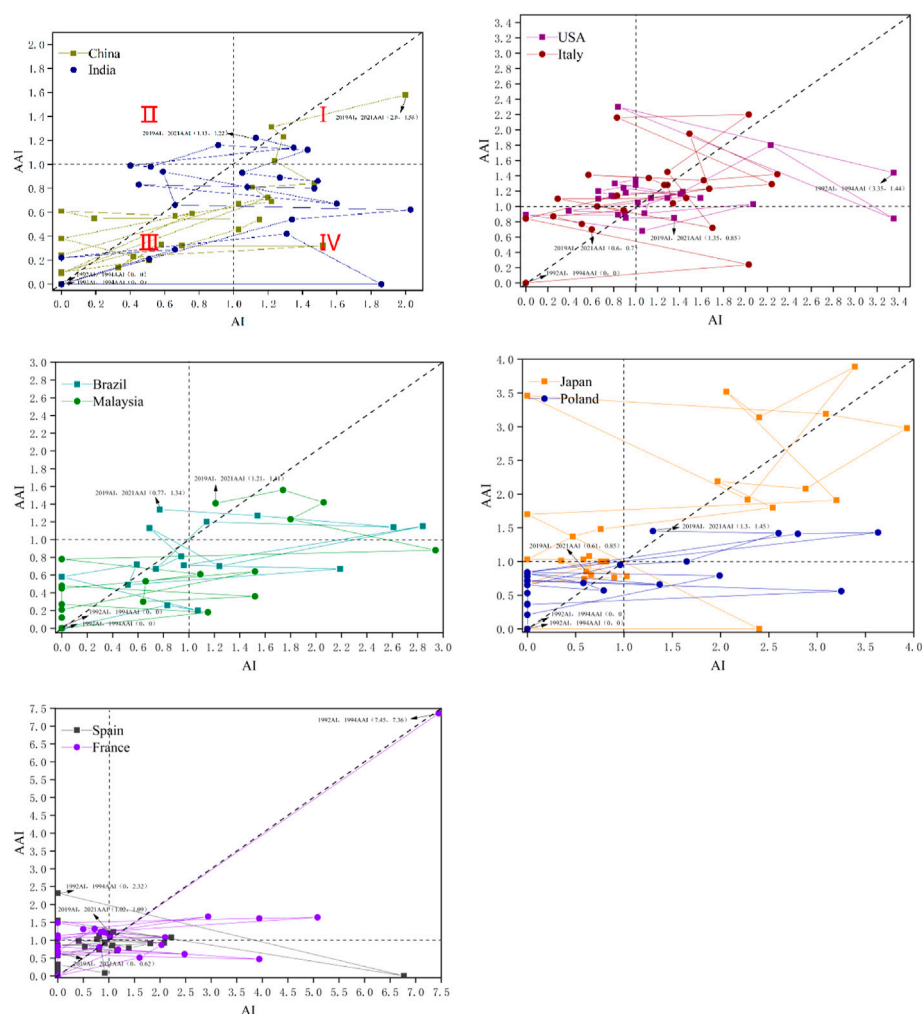


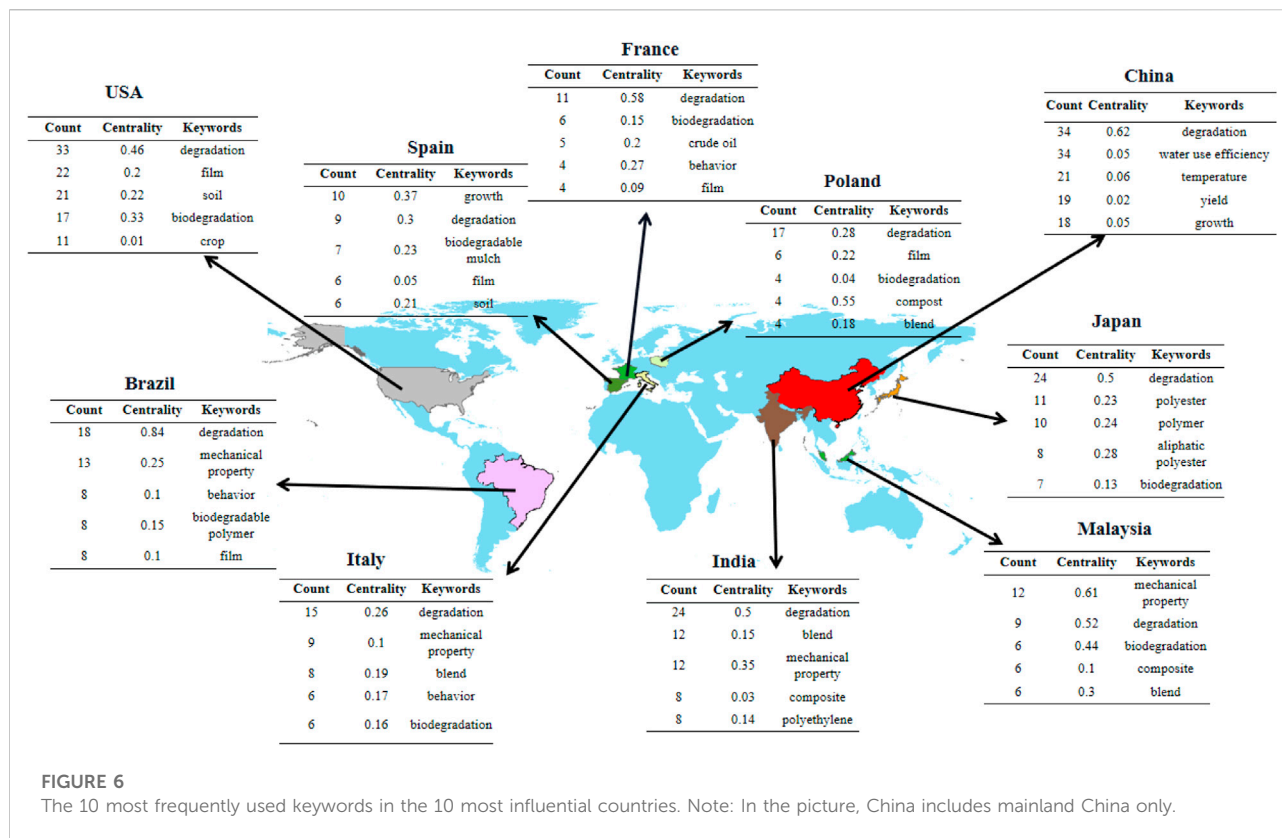
FIGURE 5
Relational chart of AI and AAI from 1992 to 2021 for 10 countries/regions.

10 clusters such as “food packaging,” “degradation,” and “aliphatic polyester.” Using CiteSpace software, 1222 articles about the field of biodegradable films for soil were analyzed by time-segment keyword, as shown in Table 5. The keyword “degradation,” the most critical node, has the most significant number and the highest betweenness centrality in the first two periods. It is worth noting that although the number of this node has been increasing in the three periods, the betweenness centrality is decreased from 0.45 in 1992–2001 to 0.18 in 2012–2021, indicating that its ability to act as a medium began to decline; at the same time, the betweenness centrality of the keyword “biodegradation” reached 2012–2021. The highest value is 0.19, which exceeds “degradation.” It can be seen that the research on biodegradation has gradually replaced the research on degradation, and biodegradation will continue to be a hot research direction for researchers in the future.

In summary, the research on biodegradable membranes for soil can be divided into four main categories of knowledge structures (Figure 8): The research field of degradation, The effect of biodegradable film on soil, The Performance and mechanism of biodegradable film, and the Effects of biodegradable film on crop growth and development.

3.7.1 The research field of degradation

Synthetic polymers are mainly derived from petrochemical raw materials (crude oil, natural gas) and have a very long period of self-degradation, which can last for decades or even hundreds of years. According to statistics, synthetic polymers account for nearly 98% of the polymer materials currently produced, of which more than 80% are produced by petrochemicals (Song et al., 2009; Galizia and Bye, 2018). Plastics are resistant to microorganisms, and due to their short existence in natural



evolution, it is impossible to design new enzymatic structures capable of degrading synthetic polymers (Mueller, 2006). The dramatic increase in production and lack of biodegradability of some polymers, such as plastic films for packaging, industry, agriculture, etc., has drawn public attention to the enormous environmental accumulation and pollution problems that may persist for decades or even centuries (Malizia and Monmany-Garzia, 2019). Biodegradable materials can degrade and have faster degradation rates in municipal and industrial biological waste treatment facilities, opening the way for the development and innovation of waste management strategies (Witt et al., 1997; Raddadi and Fava, 2019). Therefore, the research and development, promotion, and use of biodegradable materials have become the general trend in the future.

3.7.2 The effect of biodegradable film on soil

Nowadays, biodegradable materials are gradually accepted by society, and after they are used in soil, they can be decomposed by bacteria in the soil environment (Purahong et al., 2021; Tanunchai et al., 2021). However, the impact of these natural degradation processes on soil bacteria is unclear, and it is feared that the decomposition of the biodegradable film by bacteria will disrupt the soil bacterial community structure (Breza-Boruta et al., 2016). Several studies have shown that biodegradable film results in increased microbial biomass and enzymatic

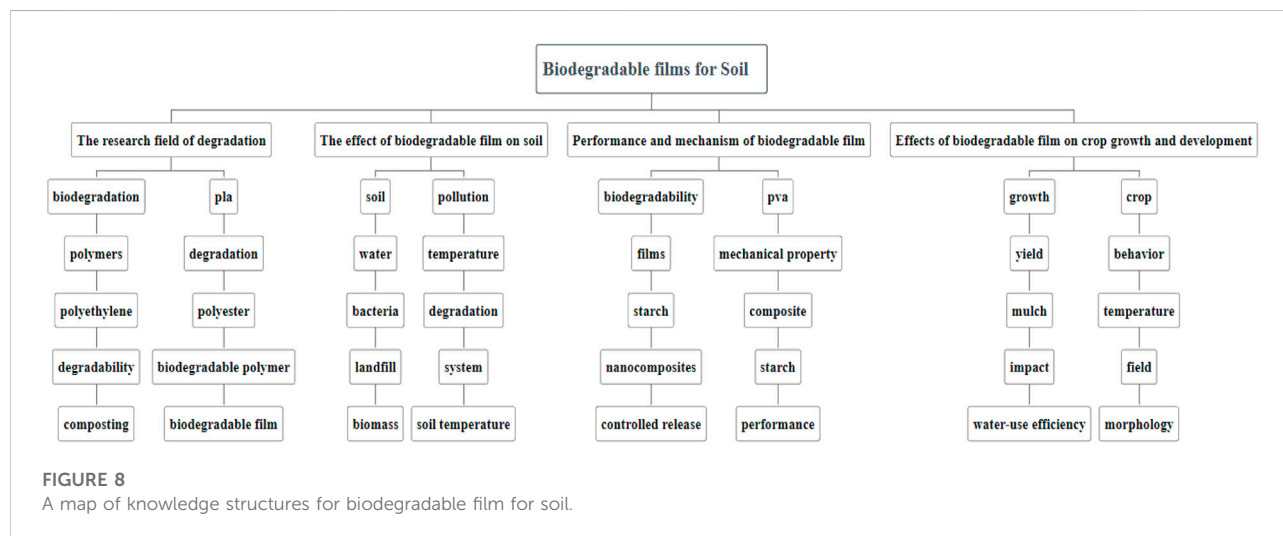
activity in soil (Bonanomi et al., 2008; Yamamoto-Tamura et al., 2015), increased soil fungal abundance (Rychter et al., 2006; Ma et al., 2016), and altered soil microbial community structure (C. H. Li et al., 2014; Muroi et al., 2016), ultimately altering carbon cycling and storage in soils. Masui A et al. (Masui et al., 2011) proved that if the biodegradable film is used in the farmland in the usual way and frequency and then plowed into the farmland, there is almost no pressure on the soil environment, but it has a significant impact on the soil environment such as the soil bacterial community. Rong Li et al. (R. Li et al., 2016) used polyethylene film (PM), biodegradable polymer film (BM), corn stover (MM), liquid film (LM), and uncovered film in a field experiment on the Loess Plateau of China over 3 years. Comparing the control (CK), five film treatments verified that the biodegradable film could significantly improve the soil moisture and temperature conditions in the semi-arid Loess Plateau and reduce soil environmental pollution compared with other treatments. Biodegradable film fragments added to soil are generally considered safe from a toxicological standpoint. For example, Sforzini S et al. (Sforzini et al., 2016) tested a starch copolyester blend, Mater-Bi R, showing no ecotoxicity effects, and Ardisson GB et al. (Ardisson et al., 2014) verified experimentally that biodegradable film fragments did not negatively affect nitrification potential effect.



et al., 2008). Although the degradation of these biodegradable films facilitates their export management, the various properties of the films (water vapor permeability, mechanical and radiation properties) also gradually decline over time (Briassoulis, 2007;

TABLE 5 Top ten cited articles and journals.

Title	Journal	Citations	Citations per year	Year	First author
Advanced oxidation processes for organic contaminant destruction based on the Fenton reaction and related chemistry	Critical Reviews in Environmental Science and Technology	2,534	158.38	2006	Pignatello, JJ (Pignatello et al., 2006)
Polylactic acid technology	Advanced Materials	1,946	88.45	2000	Drumright, RE (Drumright et al., 2000)
Polyethylene and biodegradable films for agricultural applications: a review	Agronomy for Sustainable Development	511	51.10	2012	Kasirajan, S (Kasirajan and Ngouajio, 2012)
'White revolution' to 'white pollution'-agricultural plastic film in China	Environmental Research Letters	280	35.00	2014	Liu, EK (Liu et al., 2014)
Municipal solid waste management from a systems perspective	Journal of Cleaner Production	272	16.00	2005	Eriksson, O (Eriksson et al., 2005)
Environmental stability of selected petroleum hydrocarbon source and weathering ratios	Environmental Science & Technology	265	10.19	1996	Douglas, GS (Douglas et al., 1996)
Mechanical, barrier, and biodegradability properties of bagasse cellulose whiskers reinforced natural rubber nanocomposites	Industrial Crops and Products	251	20.92	2010	Bras, J (Bras et al., 2010)
Macro- and micro- plastics in soil-plant system: Effects of plastic film residues on wheat (<i>Triticum aestivum</i>) growth	Science of the Total Environment	243	60.75	2018	Qi, YL (Qi et al., 2018)
Wood-Based Nanotechnologies toward Sustainability	Advanced Materials	226	56.50	2018	Jiang, F (Jiang et al., 2018)
Biodegradation behavior of poly (butylene adipate-co-terephthalate) (PBAT), poly (lactic acid) (PLA), and their blend under soil conditions	Polymer Testing	223	24.78	2013	Weng, YX (Weng et al., 2013)



Bilck et al., 2010). In addition to self-aging, degradable thin films undergo biodegradation mechanisms by soil bacteria (W. Wang et al., 2021), fungi (Kessler et al., 2014), microbial enzymes (Bhardwaj et al., 2013), and other factors (animals, earthworms, ants). Biodegradable films can also be blended with biodegradable polymers to improve processability and mechanical properties. Touchaleaume F et al. (Touchaleaume et al., 2018), by comparing the field experiments of biodegradable

film mixtures (PBAT/PLA, PBAT/PPC, and PBAT/starch), verified the degradation status of the biodegradable film and the location of the material, soil burial. The different aging mechanisms occurred at the site and the upper part of the soil, and although the mechanical properties decreased due to factors such as ultraviolet rays, the biodegradability of the material did not change even after 18 months of field aging (Xiang et al., 2021), verified that the inhibitory effect of heavy soil

TABLE 6 Related keywords of biodegradable films for soil in different periods from 1992 to 2021.

1992–2001			2002–2011			2012–2021		
Keywords	Ps	Centrality	Keywords	Ps	Centrality	Keywords	Ps	Centrality
degradation	16	0.45	degradation	62	0.41	degradation	158	0.18
biodegradation	7	0.17	biodegradation	27	0.28	film	72	0.07
soil	6	0.11	polymer	25	0.1	mechanical property	71	0.08
blend	5	0.1	mechanical property	23	0.14	soil	65	0.14
polymer	4	0.06	soil	22	0.23	biodegradation	54	0.19
polyvinyl alcohol	4	0.02	behavior	19	0.13	blend	54	0.08
copolymer	3	0.04	blend	18	0.13	growth	45	0.05
microorganism	3	0.09	poly (3 hydroxybutyrate)	11	0.03	polymer	40	0.07
biodegradability	3	0.02	water	9	0.02	yield	40	0.05
film	3	0.03	biodegradable polymer	9	0.05	water	39	0.13

metals on biodegradability combined with three-dimensional cross-linked superabsorbent polymers can effectively reduce the nutrient release of the biodegradable film. Javadi et al. (Javadi et al., 2010), blended the polyhydroxyalkanoate copolymer poly (3-hydroxybutyrate-co-3-hydroxy valerate) with a biodegradable film by microporous and conventional injection molding, significantly improving its toughness. Biodegradable materials can be combined with organic materials, such as food, vegetable waste, and manure, to generate carbon-rich composts (Mujtaba et al., 2021), which must maintain their physical and mechanical properties at the time of use, but also at the end of use. Composted or biodegraded by microorganisms (Abu Qdais and Hamoda, 2004). Most ecotoxicity studies have been performed after the biodegradable film has degraded in soil or compost (Kapanen et al., 2008; Ardisson et al., 2014). In contrast, the biodegradable film may be abiotically degraded in contact with the natural environment before entering soil (such as hydrolysis) (Kapanen et al., 2008). H. Serrano-Ruiz et al. (Serrano-Ruiz et al., 2020) found that BDP releases compounds in the aqueous environment before biodegradation begins. Fertilizer coating is a general controlled release method. The coating material insulates the fertilizer from the soil and slowly dissolves into the soil—the role of proportionality (Ge et al., 2002). Lu P et al. (Lu et al., 2016) studies have shown that polymer-coated urea (PCU), a new type of controlled-release fertilizer, is biodegradable in soil compared to conventional starch coatings and is more efficient in water and soil. They have a reduced nitrogen release rate. For some dry regions worldwide, superabsorbent polymers as coating materials can add moisture retention to fertilizers (Bao et al., 2015). Sarmah D et al. (Sarmah and Karak, 2020) conducted experiments on the superabsorbent hydrogel of starch-modified polyacrylic acid and found that it can be used as a controlled release carrier and water retention agent in different fields.

3.7.4 Effects of biodegradable film on crop growth and development

Covering the soil with the plastic film will promote the growth and development of annual and perennial crops and increase the yield. Film can effectively improve the field microclimate for crop growth, increase crop yield, and enable crops to develop well in soils with little water (Lamont, 2005; R. Li R et al., 2021). Experiments have shown that the application of biodegradable film in the soil can promote the growth and development of crops such as pepper (Mari et al., 2020), tomato (Cirujeda et al., 2012; Abduwaiti et al., 2021), corn (N. Chen et al., 2021), and cotton (L. X. Shen et al., 2019; Z. H. Wang et al., 2019). The utilization rate of water is conducive to increasing temperature and moisture, promoting the increase of output and bringing more excellent economic benefits. Biodegradable film can eventually be integrated directly into the soil, where soil microbes convert carbon dioxide or methane, water, and biomass for uptake by some crops (Immirzi et al., 2003). Caruso G et al. (Caruso et al., 2019) validated that the use of biodegradable film in soil resulted in a 17.4% higher Phytoanalytical Development (SPAD) index of growing leaves and a significant improvement in Perennial wall rockets' leaf quality.

3.8 Research Frontier identification

Using CiteSpace software for explosive detection of literature, Table 6 shows the top 25 explosive keywords. From the most intense keywords, we can determine the development of keywords and potential research topics (Y. N. Li Y. N et al., 2021), which can be clearly defined. See when keywords appear, when they end, keyword strength, and predict future research trends in hot areas. As shown in Table 6, the earliest and longest-lasting keyword was “bacteria” in 1998, with a burst intensity of

TABLE 7 Top 20 keywords with strongest citation bursts.

Keywords	Year	Strength	Begin	End	1992–2021
bacteria	1992	3.74	1998	2014	
polymer	1992	4.48	2001	2012	
poly (3 hydroxybutyrate)	1992	5.63	2003	2012	
behavior	1992	4.21	2006	2011	
low density polyethylene	1992	3.77	2007	2012	
morphology	1992	4.53	2009	2018	
ldpe	1992	3.67	2009	2015	
polyester	1992	4.48	2010	2014	
thermal degradation	1992	3.56	2011	2012	
wheat	1992	4.43	2012	2017	
soil	1992	3.52	2012	2014	
impact	1992	3.65	2016	2021	
food packaging	1992	3.79	2017	2019	
nanocomposite	1992	3.87	2018	2021	
quality	1992	3.74	2018	2021	
water use efficiency	1992	4.77	2019	2021	
crop	1992	4.7	2019	2021	
moisture	1992	4.01	2019	2021	
chitosan	1992	3.98	2019	2021	
carbon	1992	3.78	2019	2021	

3.74, lasting 17 years. The keyword “poly (3 hydroxybutyrate)” had the highest burst strength of 5.63. In addition, we can see that 8 explosive keywords such as “impact”, “nanocomposite”, “quality”, “water use efficiency”, “crop”, “moisture”, “chitosan” and “carbon” have been emerging in recent years. It will continue to explode in 2021, so it can be speculated that these keywords will still become the hot research direction of scholars and institutions in this field. From these eight keywords, it can be concluded that in the future, scholars and institutions in the field of biodegradable soil films will shift from single research to more diversified research, focusing on the ecological and environmental protection of biodegradable films, crop growth, and development, and research on soil traits.

Combined with the analysis results of keyword clustering analysis, the emerging research fronts of biodegradable films for soil are summarized as follows: removal and disposal of

traditional polyethylene film remain significant agronomic, economic, and environmental constraints; biodegradable plastic films transform soil carbon dioxide, water, and natural matter through microbial activity, contributing to microclimate change, soil biota, soil fertility, and crop yield. It has positive effects; biodegradable films are widely used in agriculture to increase crop yield, soil moisture, and increase soil temperature by suppressing weeds and protecting crops; microplastics may interact with soil physicochemical properties and organisms, negatively affecting plant growth. Impact, to mitigate environmental plastic pollution, biodegradable films are replacing non-biodegradable polymers; excess plastic residue soils lead to soil pollution, vegetation destruction in horticulture and agriculture. Biodegradable films are considered ideal substitutes for traditional plastics due to their biodegradable properties to reduce plastic waste and promote

ecologically sustainable development; chitosan, as new film material, can be exceptional. The biodegradability of the enhanced film, its co-use with other materials, and its contribution to the ecological soil environment system needs to be further studied. Table 7.

4 Conclusion

This paper presents a retrospective evaluation of the field of biodegradable films used in soils over the past three decades from a bibliometric perspective. Through quantitative analysis and network mapping, we identified the most influential subject categories/countries/institutions/journals, understood collaborative networks, and visualized the evolution of keyword co-occurrence networks.

Many scholars have compared the best choices of different plants for soil plastic films and biodegradable films in field experiments. The results show that biodegradable soil films are supported and recommended by more and more scholars due to their superior characteristics. Moreover, it gradually entered the field of biodegradable films and carried out corresponding research.

Comparing country performance using the Activity Index (AI) and Attractive Index (AAI) shows that developing countries (China, India, Malaysia, Poland, and Brazil) have surpassed the global average since 2019, meaning that research in developing countries, technology, and the economy began to improve; however, developed countries still have a significant influence and position in the research of biodegradable films for soil. Furthermore, China and Poland are relatively close to the reference line in terms of the distance between the points representing a particular country and the reference line, which means that their research efforts are balanced against the impact of citations.

As the concepts of environmental protection, energy saving, low carbon, emission reduction, and sustainable development are highly praised worldwide, the research on biodegradable films will continue to increase. Transforming biodegradable membranes will become a research hotspot and research trend for membranes used in soil, and future research trends in this field will be diversified in many countries. Scholars and institutions engaged in biodegradable soil film will shift from single research to diversified research, focusing on the research field of degradation, the effect of biodegradable film on soil, performance, and mechanism of biodegradable film, and the effects of biodegradable film on crop growth and development.

This study can be seen as a microcosm of the field of biodegradable soil membranes, and it will help researchers quickly identify their general patterns. Readers can gain exciting information from the rich bibliometric data. There are still some limitations of this study; the data in this paper are only from the Web of Science Core Collection

(ScienceCitation Index Expanded, SCIE) database and may not include other citation information. Despite the above limitations, this paper can provide suggestions for scholars interested in identity recognition to help them understand development trajectories and statistical models more quickly.

Data availability statement

The original contributions presented in the study are included in the article/Supplementary Material, further inquiries can be directed to the corresponding author.

Author contributions

YS: Conceptualization, Writing an original draft. Methodology; WY: Visualization; HS: Conceptualization; ST: Visualization; JH: Resources, Project administration, Validation.

Funding

This study was supported by the Ecological Security and Bioremediation Mechanism of Saline-alkali Soil Improvement in the Middle Yellow River (No. DL2021172002L). The research was financially supported by the Ecological Security and Bioremediation Mechanism of Saline-alkali Soil Improvement in the Middle Yellow River (No. DL2021172002L).

Conflict of interest

The authors declare that the research was conducted in the absence of any commercial or financial relationships that could be construed as a potential conflict of interest.

Publisher's note

All claims expressed in this article are solely those of the authors and do not necessarily represent those of their affiliated organizations, or those of the publisher, the editors and the reviewers. Any product that may be evaluated in this article, or claim that may be made by its manufacturer, is not guaranteed or endorsed by the publisher.

Supplementary material

The Supplementary Material for this article can be found online at: <https://www.frontiersin.org/articles/10.3389/fbioe.2022.1006388/full#supplementary-material>

References

- Abduwaiti, A., Liu, X. W., Yan, C. R., Xue, Y. H., Jin, T., Wu, H. Q., et al. (2021). Testing biodegradable films as alternatives to plastic-film mulching for enhancing the yield and economic benefits of processed tomato in Xinjiang region. *Sustainability* 13 (6), 13. doi:10.3390/su13063093
- Abu Qdais, H. A., and Hamoda, M. F. (2004). Enhancement of carbon and nitrogen transformations during composting of municipal solid waste. *J. Environ. Sci. Health Part A-Toxic/Hazardous Subst. Environ. Eng.* 39 (2), 409–420. doi:10.1081/ese-120027532
- Amirbagheri, K., Nunez-Carballosa, A., Guitart-Tarres, L., and Merigo, J. M. (2019). Research on green supply chain: A bibliometric analysis. *Clean. Technol. Environ. Policy* 21 (1), 3–22. doi:10.1007/s10098-018-1624-1
- Ardisson, G. B., Tosin, M., Barbale, M., and Degli-Innocenti, F. (2014). Biodegradation of plastics in soil and effects on nitrification activity. A laboratory approach. *Front. Microbiol.* 5, 710. doi:10.3389/fmicb.2014.00710
- Bao, X. Y., Ali, A., Qiao, D. L., Liu, H. S., Chen, L., and Yu, L. (2015). Application of polymer materials in developing slow/control release fertilizer. *Acta Polym. Sin.* (9), 1010–1019. doi:10.1177/j.issn1000-3304.2015.15091
- Barboza, L. G. A., Vethaak, A. D., Lavarante, B., Lundebye, A. K., and Guilhermino, L. (2018). Marine microplastic debris: An emerging issue for food security, food safety and human health. *Mar. Pollut. Bull.* 133, 336–348. doi:10.1016/j.marpolbul.2018.05.047
- Bhardwaj, H., Gupta, R., and Tiwari, A. (2013). Communities of microbial enzymes associated with biodegradation of plastics. *J. Polym. Environ.* 21 (2), 575–579. doi:10.1007/s10924-012-0456-z
- Bilck, A. P., Grossmann, M. V. E., and Yamashita, F. (2010). Biodegradable mulch films for strawberry production. *Polym. Test.* 29 (4), 471–476. doi:10.1016/j.polymertesting.2010.02.007
- Bonanomi, G., Chiuazzini, M., Caporaso, S., Del Sorbo, G., Moschetti, G., and Felice, S. (2008). Soil solarization with biodegradable materials and its impact on soil microbial communities. *Soil Biol. Biochem.* 40 (8), 1989–1998. doi:10.1016/j.soilbio.2008.02.009
- Bornmann, L., and Mutz, R. (2015). Growth rates of modern science: A bibliometric analysis based on the number of publications and cited references. *J. Assoc. Inf. Sci. Technol.* 66 (11), 2215–2222. doi:10.1002/asi.23329
- Bouma, J. (2014). Soil science contributions towards sustainable development Goals and their implementation: Linking soil functions with ecosystem services. *Z. Pflanzenernähr. Boden.* 177 (2), 111–120. doi:10.1002/jpln.201300646
- Boyack, K. W., and Klavans, R. (2010). Co-citation analysis, bibliographic coupling, and Direct citation: Which citation approach represents the research front most accurately? *J. Am. Soc. Inf. Sci. Technol.* 61 (12), 2389–2404. doi:10.1002/asi.21419
- Bras, J., Hassan, M. L., Bruzesse, C., Hassan, E. A., El-Wakil, N. A., and Dufresne, A. (2010). Mechanical, barrier, and biodegradability properties of bagasse cellulose whiskers reinforced natural rubber nanocomposites. *Industrial Crops Prod.* 32 (3), 627–633. doi:10.1016/j.indcrop.2010.07.018
- Breza-Boruta, B., Lemanowicz, J., and Bartkowiak, A. (2016). Variation in biological and physicochemical parameters of the soil affected by uncontrolled landfill sites. *Environ. Earth Sci.* 75 (3), 201. doi:10.1007/s12665-015-4955-9
- Briassoulis, D. (2007). Analysis of the mechanical and degradation performances of optimised agricultural biodegradable films. *Polym. Degrad. Stab.* 92 (6), 1115–1132. doi:10.1016/j.polymdegradstab.2007.01.024
- Caruso, G., Stoleru, V., De Pascale, S., Cozzolino, E., Pannico, A., Giordano, M., et al. (2019). Production, leaf quality and Antioxidants of perennial wall rocket as affected by crop cycle and mulching type. *Agron. (Basel)*. 9 (4), 194. doi:10.3390/agronomy9040194
- Chen, C. M. (2006). CiteSpace II: Detecting and visualizing emerging trends and transient patterns in scientific literature. *J. Am. Soc. Inf. Sci. Technol.* 57 (3), 359–377. doi:10.1002/asi.20317
- Chen, C. M., Ibekwe-SanJuan, F., and Hou, J. H. (2010). The structure and dynamics of Cocitation clusters: A Multiple-perspective Cocitation analysis. *J. Am. Soc. Inf. Sci. Technol.* 61 (7), 1386–1409. doi:10.1002/asi.21309
- Chen, N., Li, X., Simunek, J., Shi, H., Ding, Z., and Zhang, Y. (2020). The effects of biodegradable and plastic film mulching on nitrogen uptake, distribution, and leaching in a drip-irrigated sandy field. *Agric. Ecosyst. Environ.* 292. doi:10.1016/j.agee.2020.106817
- Chen, N., Li, X. Y., Shi, H. B., Hu, Q., Zhang, Y. H., Sun, Y. N., et al. (2021). Simulation of maize crop growth using an improved crop model considering the disintegrated area of biodegradable film. *Field Crops Res.* 272, 108270. doi:10.1016/j.fcr.2021.108270
- Cirujeda, A., Anzalone, A., Aibar, J., Moreno, M. M., and Zaragoza, C. (2012). Purple nutsedge (*Cyperus rotundus* L.) control with paper mulch in processing tomato. *Crop Prot.* 39, 66–71. doi:10.1016/j.cropro.2012.03.028
- Deng, L., Yu, Y., Zhang, H. Y., Wang, Q., and Yu, R. D. (2019). The effects of biodegradable mulch film on the growth, yield, and water Use efficiency of cotton and maize in an arid region. *Sustainability* 11 (24), 7039. doi:10.3390/su11247039
- Douglas, G. S., Bence, A. E., Prince, R. C., McMillen, S. J., and Butler, E. L. (1996). Environmental stability of selected petroleum hydrocarbon source and weathering ratios. *Environ. Sci. Technol.* 30 (7), 2332–2339. doi:10.1021/es950751e
- Drumright, R. E., Gruber, P. R., and Henton, D. E. (2000). Polylactic acid technology. *Adv. Mat.* 12 (23), 1841–1846. doi:10.1002/1521-4095(200012)12:23<1841::aid-adma1841>3.0.co;2-e
- Durieux, V., and Gevenois, P. A. (2010). Bibliometric indicators: Quality Measurements of scientific publication. *Radiology* 255 (2), 342–351. doi:10.1148/radiol.09090626
- Eriksson, O., Reich, M. C., Frostell, B., Bjorklund, A., Assefa, G., Sundqvist, J. O., et al. (2005). Municipal solid waste management from a systems perspective. *J. Clean. Prod.* 13 (3), 241–252. doi:10.1016/j.jclepro.2004.02.018
- Galizia, M., and Bye, K. P. (2018). Advances in organic Solvent Nanofiltration rely on physical chemistry and polymer chemistry. *Front. Chem.* 6, 511. doi:10.3389/fchem.2018.00511
- Ge, J. J., Wu, R., Shi, X. H., Yu, H., Wang, M., and Li, W. J. (2002). Biodegradable polyurethane materials from bark and starch. II. Coating material for controlled-release fertilizer. *J. Appl. Polym. Sci.* 86 (12), 2948–2952. doi:10.1002/app.11211
- Ghisi, N. d. C., Zuanazzi, N. R., Carrenho Fabrin, T. M., and Oliveira, E. C. (2020). Glyphosate and its toxicology: A scientometric review. *Sci. Total Environ.* 733, 139359. doi:10.1016/j.scitotenv.2020.139359
- Gu, X.-B., Li, Y.-N., and Du, Y.-D. (2017). Biodegradable film mulching improves soil temperature, moisture and seed yield of winter oilseed rape (*Brassica napus* L.). *Soil Tillage Res.* 171, 42–50. doi:10.1016/j.still.2017.04.008
- Gueymard, C. A., Myers, D., and Emery, K. (2002). Proposed reference irradiance spectra for solar energy systems testing. *Sol. Energy* 73 (6), 443–467. doi:10.1016/s0038-092x(03)00005-7
- Harzing, A. W., and Alakangas, S. (2016). Google scholar, Scopus and the Web of science: A longitudinal and cross-disciplinary comparison. *Scientometrics* 106 (2), 787–804. doi:10.1007/s11192-015-1798-9
- Hayes, D. G., Wadsworth, L. C., Sintim, H. Y., Flury, M., English, M., Schaeffer, S., et al. (2017). Effect of diverse weathering conditions on the physicochemical properties of biodegradable plastic mulches. *Polym. Test.* 62, 454–467. doi:10.1016/j.polymertesting.2017.07.027
- Hirsch, J. E. (2005). An index to quantify an individual's scientific research output. *Proc. Natl. Acad. Sci. U. S. A.* 102 (46), 16569–16572. doi:10.1073/pnas.0507655102
- Huang, L., Zhou, M., Lv, J., and Chen, K. (2020). Trends in global research in forest carbon sequestration: A bibliometric analysis. *J. Clean. Prod.* 252, 119908. doi:10.1016/j.jclepro.2019.119908
- Immirzi, B., Malinconico, M., Romano, G., Russo, R., and Santagata, G. (2003). Biodegradable films of natural polysaccharides blends. *J. Mat. Sci. Lett.* 22 (20), 1389–1392. doi:10.1023/a:1025786708540
- Javadi, A., Kramschuster, A. J., Pilla, S., Lee, J., Gong, S. Q., and Turng, L. S. (2010). Processing and Characterization of Microcellular PHBV/PBAT blends. *Polym. Eng. Sci.* 50 (7), 1440–1448. doi:10.1002/pen.21661
- Jiang, F., Li, T., Li, Y. J., Zhang, Y., Gong, A., Dai, J. Q., et al. (2018). Wood-based Nanotechnologies toward sustainability. *Adv. Mat.* 30 (1), 1703453. doi:10.1002/adma.201703453
- Kader, M. A., Senge, M., Mojid, M. A., and Ito, K. (2017). Recent advances in mulching materials and methods for modifying soil environment. *Soil Tillage Res.* 168, 155–166. doi:10.1016/j.still.2017.01.001
- Kapanen, A., Schettini, E., Vox, G., and Itavaara, M. (2008). Performance and environmental impact of biodegradable films in agriculture: A field study on protected cultivation. *J. Polym. Environ.* 16 (2), 109–122. doi:10.1007/s10924-008-0091-x
- Kasirajan, S., and Ngouajio, M. (2012). Polyethylene and biodegradable mulches for agricultural applications: A review. *Agron. Sustain. Dev.* 32 (2), 501–529. doi:10.1007/s13593-011-0068-3
- Keesstra, S. D., Bouma, J., Wallinga, J., Titttonell, P., Smith, P., Cerda, A., et al. (2016). The significance of soils and soil science towards realization of the United Nations Sustainable Development Goals. *Soil* 2 (2), 111–128. doi:10.5194/soil-2-111-2016

- Kessler, F., Marconatto, L., Rodrigues, R. D. B., Lando, G. A., Schrank, A., Vainstein, M. H., et al. (2014). Biodegradation improvement of poly(3-hydroxybutyrate) films by entomopathogenic fungi and UV-assisted surface functionalization. *J. Photochem. Photobiol. B Biol.* 130, 57–67. doi:10.1016/j.jphotobiol.2013.11.002
- Lamont, W. J. (2005). Plastics: Modifying the microclimate for the production of vegetable crops. *Horttechnology* 15 (3), 477–481. doi:10.21273/horttech.15.3.0477
- Lewis, S. L., Lopez-Gonzalez, G., Sonke, B., Affum-Baffoe, K., Baker, T. R., Ojo, L. O., et al. (2009). Increasing carbon storage in intact African tropical forests. *Nature* 457 (7232), 1003–1006. doi:10.1038/nature07771
- Li, C. H., Moore-Kucera, J., Miles, C., Leonas, K., Lee, J., Corbin, A., et al. (2014). Degradation of potentially biodegradable plastic mulch films at three diverse U.S. Locations. *Agroecol. Sustain. Food Syst.* 38 (8), 861–889. doi:10.1080/21683565.2014.884515
- Li, R., Chai, S. X., Chai, Y. W., Li, Y. W., Lan, X. M., Ma, J. T., et al. (2021). Mulching optimizes water consumption characteristics and improves crop water productivity on the semi-arid Loess Plateau of China. *Agric. Water Manag.* 254, 106965. doi:10.1016/j.agwat.2021.106965
- Li, R., Hou, X. Q., Jia, Z. K., and Han, Q. F. (2016). Mulching materials improve soil properties and maize growth in the Northwestern Loess Plateau, China. *Soil Res.* 54 (6), 708–718. doi:10.1071/sr15175
- Li, Y. N., Fang, R. Y., Liu, Z. H., Jiang, L. P., Zhang, J. D., Li, H. H., et al. (2021). The association between toxic pesticide environmental exposure and Alzheimer's disease: A scientometric and visualization analysis. *Chemosphere* 263, 128238. doi:10.1016/j.chemosphere.2020.128238
- Liang, Y. L., Zhang, C. E., and Guo, D. W. (2002). Film types and their benefit in cropland ecosystems on the Loess Plateau in China. *J. Plant Nutr.* 25 (5), 945–955. doi:10.1081/pln-120003930
- Liu, E. K., He, W. Q., and Yan, C. R. (2014). 'White revolution' to 'white pollution'—Agricultural plastic film mulch in China. *Environ. Res. Lett.* 9 (9), 091001. doi:10.1088/1748-9326/9/9/091001
- Lu, P. F., Jia, C., Zhang, Y. F., Li, Y. F., Zhang, M., and Mao, Z. Q. (2016). Preparation and properties of starch-based polymer coated urea Granules. *J. Biobased Mat. Bioenergy* 10 (2), 113–118. doi:10.1166/jbmb.2016.1576
- Luo, J., Liu, Y. N., Fan, C. Z., Tang, L., Yang, S. J., Liu, M. L., et al. (2021). Direct Attack and Indirect transfer mechanisms Dominated by reactive Oxygen Species for Photocatalytic H₂O₂ production on g-C₃N₄ Possessing nitrogen Vacancies. *ACS Catal.* 11 (18), 11440–11450. doi:10.1021/acscatal.1c03103
- Ma, Z. F., Ma, Y. B., Qin, L. Z., Liu, J. X., and Su, H. J. (2016). Preparation and characteristics of biodegradable mulching films based on fermentation industry wastes. *Int. Biodeterior. Biodegrad.* 111, 54–61. doi:10.1016/j.ibiod.2016.04.024
- Malizia, A., and Monmany-Garzia, A. C. (2019). Terrestrial ecologists should stop ignoring plastic pollution in the Anthropocene time. *Sci. Total Environ.* 668, 1025–1029. doi:10.1016/j.scitotenv.2019.03.044
- Mari, A. I., Pardo, G., Aibar, J., and Cirujeda, A. (2020). Purple nutsedge (*Cyperus rotundus* L.) control with biodegradable mulches and its effect on fresh pepper production. *Sci. Hortic.* 263, 109111. doi:10.1016/j.scienta.2019.109111
- Masui, A., Ikawa, S., Fujiwara, N., and Hirai, H. (2011). Influence for soil environment by continuing use of biodegradable plastic. *J. Polym. Environ.* 19 (3), 622–627. doi:10.1007/s10924-011-0314-4
- Mongeon, P., and Paul-Hus, A. (2016). The journal coverage of Web of science and Scopus: A comparative analysis. *Scientometrics* 106 (1), 213–228. doi:10.1007/s11192-015-1765-5
- Moreno, M. M., and Moreno, A. (2008). Effect of different biodegradable and polyethylene mulches on soil properties and production in a tomato crop. *Sci. Hortic.* 116 (3), 256–263. doi:10.1016/j.scienta.2008.01.007
- Mueller, R. J. (2006). Biological degradation of synthetic polyesters - enzymes as potential catalysts for polyester recycling. *Process Biochem.* 41 (10), 2124–2128. doi:10.1016/j.procbio.2006.05.018
- Mujtaba, G., Hayat, R., Hussain, Q., and Ahmed, M. (2021). Physio-chemical Characterization of Biochar, compost and Co-composted Biochar derived from green waste. *Sustainability* 13 (9), 4628. doi:10.3390/su13094628
- Muroi, F., Tachibana, Y., Kobayashi, Y., Sakurai, T., and Kasuya, K. (2016). Influences of poly(butylene adipate-co-terephthalate) on soil microbiota and plant growth. *Polym. Degrad. Stab.* 129, 338–346. doi:10.1016/j.polymdegradstab.2016.05.018
- Nagashima, K., Kihara, N., and Iino, Y. (2012). Oxidative coupling polymerization of bishydrazide for the synthesis of poly(diacylhydrazine): Oxidative preparation of oxidatively degradable polymer. *J. Polym. Sci. A. Polym. Chem.* 50 (20), 4230–4238. doi:10.1002/pola.26225
- Orgiles-Calpena, E., Aran-Ais, F., Torro-Palau, A. M., and Orgiles-Barcelo, C. (2014). Biodegradable polyurethane adhesives based on polyols derived from renewable resources. *Proc. Institution Mech. Eng. Part L J. Mater. Des. Appl.* 228 (2), 125–136. doi:10.1177/1464420713517674
- Pignatello, J. J., Oliveros, E., and MacKay, A. (2006). Advanced oxidation processes for organic contaminant destruction based on the Fenton reaction and related chemistry. *Crit. Rev. Environ. Sci. Technol.* 36 (1), 1–84. doi:10.1080/10643380500326564
- Ping, Q., He, J. G., and Chen, C. M. (2017). How many ways to Use CiteSpace? A study of user interactive Events over 14 Months. *J. Assoc. Inf. Sci. Technol.* 68 (5), 1234–1256. doi:10.1002/asi.23770
- Purahong, W., Wahdan, S. F. M., Heinz, D., Jariyavidyanont, K., Sungkapreecha, C., Tanunchai, B., et al. (2021). Back to the future: Decomposability of a Biobased and biodegradable plastic in field soil environments and its Microbiome under Ambient and future Climates. *Environ. Sci. Technol.* 55 (18), 12337–12351. doi:10.1021/acs.est.1c02695
- Qi, Y. L., Beriot, N., Gort, G., Lwanga, E. H., Gooren, H., Yang, X. M., et al. (2020). Impact of plastic mulch film debris on soil physicochemical and hydrological properties. *Environ. Pollut.* 266, 115097. doi:10.1016/j.envpol.2020.115097
- Qi, Y. L., Yang, X. M., Pelaez, A. M., Lwanga, E. H., Beriot, N., Gertsen, H., et al. (2018). Macro- and micro- plastics in soil-plant system: Effects of plastic mulch film residues on wheat (*Triticum aestivum*) growth. *Sci. Total Environ.* 645, 1048–1056. doi:10.1016/j.scitotenv.2018.07.229
- Qi, Y., Ossowicki, A., Yang, X., Lwanga, E. H., Dini-Andreote, F., Geissen, V., et al. (2020). Effects of plastic mulch film residues on wheat rhizosphere and soil properties. *J. Hazard. Mater.* 387, 121711. doi:10.1016/j.jhazmat.2019.121711
- Raddadi, N., and Fava, F. (2019). Biodegradation of oil-based plastics in the environment: Existing knowledge and needs of research and innovation. *Sci. Total Environ.* 679, 148–158. doi:10.1016/j.scitotenv.2019.04.419
- Raquez, J. M., Nabar, Y., Narayan, R., and Dubois, P. (2008). Novel high-performance talc/poly (butylene adipate)-co-terephthalate hybrid materials. *Macromol. Mat. Eng.* 293 (4), 310–320. doi:10.1002/mame.200700352
- Rychter, P., Biczak, R., Herman, B., Smylla, A., Kurcok, P., Adamus, G., et al. (2006). Environmental degradation of polyester blends containing atactic poly(3-hydroxybutyrate). Biodegradation in soil and ecotoxicological impact. *Biomacromolecules* 7 (11), 3125–3131. doi:10.1021/bm060708r
- Saglam, M., Sintim, H. Y., Bary, A. I., Miles, C. A., Ghimire, S., Inglis, D. A., et al. (2017). Modeling the effect of biodegradable paper and plastic mulch on soil moisture dynamics. *Agric. Water Manag.* 193, 240–250. doi:10.1016/j.agwat.2017.08.011
- Sander, M. (2019). Biodegradation of polymeric mulch films in agricultural soils: Concepts, knowledge gaps, and future research directions. *Environ. Sci. Technol.* 53 (5), 2304–2315. doi:10.1021/acs.est.8b05208
- Sarmah, D., and Karak, N. (2020). Biodegradable superabsorbent hydrogel for water holding in soil and controlled-release fertilizer. *J. Appl. Polym. Sci.* 137 (13), 48495. doi:10.1002/app.48495
- Schonbeck, M. W., and Evanylo, G. K. (1998). Effects of mulches on soil properties and tomato production I. Soil temperature, soil moisture and Marketable yield. *J. Sustain. Agric.* 13 (1), 55–81. doi:10.1300/J064v13n01_06
- Serrano-Ruiz, H., Eras, J., Martin-Closas, L., and Pelacho, A. M. (2020). Compounds released from unused biodegradable mulch materials after contact with water. *Polym. Degrad. Stab.* 178, 109202. doi:10.1016/j.polymdegradstab.2020.109202
- Serrano-Ruiz, H., Martin-Closas, L., and Pelacho, A. M. (2018). Application of an *in vitro* plant ecotoxicity test to unused biodegradable mulches. *Polym. Degrad. Stab.* 158, 102–110. doi:10.1016/j.polymdegradstab.2018.10.016
- Sforzini, S., Governa, D., Boeri, M., Oliveri, L., Oldani, A., Vago, F., et al. (2016). Relevance of the bioavailable fraction of DDT and its metabolites in freshwater sediment toxicity: New insight into the mode of action of these chemicals on *Dictyostelium discoideum*. *Ecotoxicol. Environ. Saf.* 132, 240–249. doi:10.1016/j.ecoenv.2016.06.013
- Shen, L. X., Zhang, Y. M., Lan, Y. C., and Li, R. F. (2019). Effects of degradable films with different degradation cycles on soil temperature, moisture and maize yield. *Int. J. Agric. Biol. Eng.* 12 (3), 36–44. doi:10.25165/j.ijabe.20191203.4065
- Shen, S., Cheng, C., Yang, J., and Yang, S. (2018). Visualized analysis of developing trends and hot topics in natural disaster research. *Plos One* 13 (1), e0191250. doi:10.1371/journal.pone.0191250
- Siwek, P., Domagala-Swiatkiewicz, I., Bucki, P., and Puchalski, M. (2019). Biodegradable agroplastics in 21st century horticulture. *Polimery* 64 (7–8), 480–486. doi:10.14314/polimery.2019.7.2
- Song, J. H., Murphy, R. J., Narayan, R., and Davies, G. B. H. (2009). Biodegradable and compostable alternatives to conventional plastics. *Phil. Trans. R. Soc. B* 364 (1526), 2127–2139. doi:10.1098/rstb.2008.0289

- Sun, T., Li, G., Ning, T. Y., Zhang, Z. M., Mi, Q. H., and Lal, R. (2018). Suitability of mulching with biodegradable film to moderate soil temperature and moisture and to increase photosynthesis and yield in peanut. *Agric. Water Manag.* 208, 214–223. doi:10.1016/j.agwat.2018.06.027
- Sun, Y. Q., Wu, S. M., and Gong, G. Y. (2019). Trends of research on polycyclic aromatic hydrocarbons in food: A 20-year perspective from 1997 to 2017. *Trends Food Sci. Technol.* 83, 86–98. doi:10.1016/j.tifs.2018.11.015
- Tan, H., Li, J. L., He, M., Li, J. Y., Zhi, D., Qin, F. Z., et al. (2021). Global evolution of research on green energy and environmental technologies: A bibliometric study. *J. Environ. Manag.* 297, 113382. doi:10.1016/j.jenvman.2021.113382
- Tanunchai, B., Juncheed, K., Wahdan, S. F. M., Guliyev, V., Udovenko, M., Lehnert, A. S., et al. (2021). Analysis of microbial populations in plastic-soil systems after exposure to high poly(butylene succinate-co-adipate) load using high-resolution molecular technique. *Environ. Sci. Eur.* 33 (1), 105. doi:10.1186/s12302-021-00528-5
- Titirici, M. M., White, R. J., Brun, N., Budarin, V. L., Su, D. S., del Monte, F., et al. (2015). Sustainable carbon materials. *Chem. Soc. Rev.* 44 (1), 250–290. doi:10.1039/c4cs00232f
- Touchaleaume, F., Angellier-Coussy, H., Cesar, G., Raffard, G., Gontard, N., and Gastaldi, E. (2018). How performance and fate of biodegradable mulch films are impacted by field ageing. *J. Polym. Environ.* 26 (6), 2588–2600. doi:10.1007/s10924-017-1154-7
- Tremblay, J. F. (2018). AGRICULTURE Trying new films on Chinese lands Conventional plastic coverings are a boon to China's agriculture but are taking an environmental toll. *Chem. Eng. News* 96 (3), 18–19.
- van Eck, N. J., and Waltman, L. (2010). Software survey: VOSviewer, a computer program for bibliometric mapping. *Scientometrics* 84 (2), 523–538. doi:10.1007/s11192-009-0146-3
- Vroman, I., and Tighzert, L. (2009). Biodegradable polymers. *Materials* 2 (2), 307–344. doi:10.3390/ma2020307
- Wang, W., Han, L., Zhang, X., and Wei, K. (2021). Plastic film mulching affects N₂O emission and ammonia oxidizers in drip irrigated potato soil in northwest China. *Sci. Total Environ.* 754, 142113. doi:10.1016/j.scitotenv.2020.142113
- Wang, Z. H., Wu, Q., Fan, B. H., Zheng, X. R., Zhang, J. Z., Li, W. H., et al. (2019). Effects of mulching biodegradable films under drip irrigation on soil hydrothermal conditions and cotton (*Gossypium hirsutum* L.) yield. *Agric. Water Manag.* 213, 477–485. doi:10.1016/j.agwat.2018.10.036
- Weber, C. A. (2003). Biodegradable mulch films for weed suppression in the Establishment Year of Matted-row Strawberries. *Horttechnology* 13 (4), 665–668. doi:10.21273/horttech.13.4.0665
- Weng, Y. X., Jin, Y. J., Meng, Q. Y., Wang, L., Zhang, M., and Wang, Y. Z. (2013). Biodegradation behavior of poly(butylene adipate-co-terephthalate) (PBAT), poly(lactic acid) (PLA), and their blend under soil conditions. *Polym. Test.* 32 (5), 918–926. doi:10.1016/j.polymertesting.2013.05.001
- Witt, U., Muller, R. J., and Deckwer, W. D. (1997). Biodegradation behavior and material properties of aliphatic/aromatic polyesters of commercial importance. *J. Environ. Polym. Degrad.* 5 (2), 81–89. doi:10.1007/bf02763591
- Xiang, Y., Li, C. Y., Hao, H. B., Tong, Y. F., Chen, W. J., Zhao, G. Z., et al. (2021). Performances of biodegradable polymer composites with functions of nutrient slow-release and water retention in simulating heavy metal contaminated soil: Biodegradability and nutrient release characteristics. *J. Clean. Prod.* 294, 126278. doi:10.1016/j.jclepro.2021.126278
- Xie, P. (2015). Study of international anticancer research trends via co-word and document co-citation visualization analysis. *Scientometrics* 105 (1), 611–622. doi:10.1007/s11192-015-1689-0
- Yamamoto-Tamura, K., Hiradate, S., Watanabe, T., Koitabashi, M., Sameshima-Yamashita, Y., Yarimizu, T., et al. (2015). Contribution of soil esterase to biodegradation of aliphatic polyester agricultural mulch film in cultivated soils. *Amb. Express* 5, 10. doi:10.1186/s13568-014-0088-x
- Yin, M., Li, Y., Fang, H., and Chen, P. (2019). Biodegradable mulching film with an optimum degradation rate improves soil environment and enhances maize growth. *Agric. Water Manag.* 216, 127–137. doi:10.1016/j.agwat.2019.02.004
- Zhang, C., Tian, S. H., Qin, F. Z., Yu, Y. L., Huang, D. L., Duan, A. B., et al. (2021). Catalyst-free activation of permanganate under visible light irradiation for sulfamethazine degradation: Experiments and theoretical calculation. *Water Res.* 194, 116915. doi:10.1016/j.watres.2021.116915
- Zhao, X. B. (2017). A scientometric review of global BIM research: Analysis and visualization. *Automation Constr.* 80, 37–47. doi:10.1016/j.autcon.2017.04.002
- Zhou, X. Q., Li, Z. F., Zheng, T. L., Yan, Y. C., Li, P. Y., Odey, E. A., et al. (2018). Review of global sanitation development. *Environ. Int.* 120, 246–261. doi:10.1016/j.envint.2018.07.047



OPEN ACCESS

EDITED BY
Yunbing Wang,
Sichuan University, China

REVIEWED BY
Jennifer Patterson,
Instituto IMDEA Materiales, Spain

*CORRESPONDENCE
Ruben Michael Ceballos,
ceballos@uark.edu
Chenguang Fan,
cf021@uark.edu

SPECIALTY SECTION
This article was submitted to
Biomaterials,
a section of the journal
Frontiers in Bioengineering and
Biotechnology

RECEIVED 14 July 2022
ACCEPTED 24 October 2022
PUBLISHED 03 November 2022

CITATION
Fatema N, Ceballos RM and Fan C
(2022), Modifications of cellulose-based
biomaterials for
biomedical applications.
Front. Bioeng. Biotechnol. 10:993711.
doi: 10.3389/fbioe.2022.993711

COPYRIGHT
© 2022 Fatema, Ceballos and Fan. This
is an open-access article distributed
under the terms of the [Creative
Commons Attribution License \(CC BY\)](#).
The use, distribution or reproduction in
other forums is permitted, provided the
original author(s) and the copyright
owner(s) are credited and that the
original publication in this journal is
cited, in accordance with accepted
academic practice. No use, distribution
or reproduction is permitted which does
not comply with these terms.

Modifications of cellulose-based biomaterials for biomedical applications

Nour Fatema¹, Ruben Michael Ceballos^{1,2*} and
Chenguang Fan^{1,3*}

¹Cell and Molecular Biology Program, University of Arkansas, Fayetteville, AR, United States,

²Department of Biological Sciences, University of Arkansas, Fayetteville, AR, United States,

³Department of Chemistry and Biochemistry, University of Arkansas, Fayetteville, AR, United States

Cellulose is one of the most abundant organic compounds in nature and is available from diverse sources. Cellulose features tunable properties, making it a promising substrate for biomaterial development. In this review, we highlight advances in the physical processes and chemical modifications of cellulose that enhance its properties for use as a biomaterial. Three cellulosic products are discussed, including nanofibrillated, nanocrystalline, and bacterial cellulose, with a focus on how each may serve as a platform for the development of advanced cellulose-based biomaterials for Biomedical applications. In addition to associating mechanical and chemical properties of cellulosic materials to specific applications, a prospectus is offered for the future development of cellulose-based biomaterials for biomedicine.

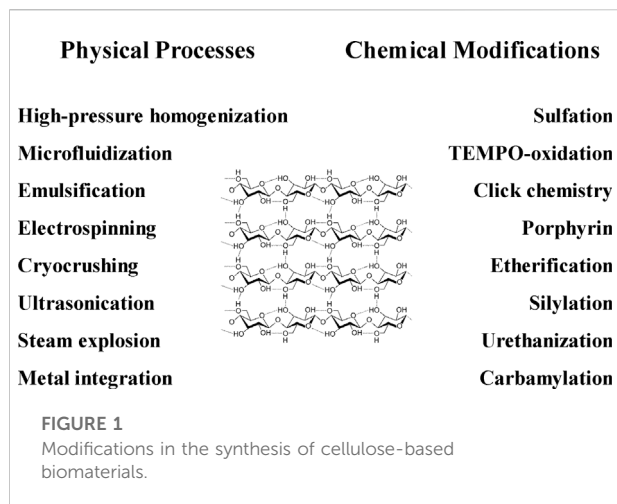
KEYWORDS

cellulose, nanocellulose, hydrogel, biomaterial, biomedicine

Introduction

Cellulose is the most abundant, broadly-distributed natural polymer in the world (Moon et al., 2011). It is composed of glucose residues linked by β -1,4-glycosidic bonds. Natural fibers from cellulosic feedstock and synthetic cellulose are used in textiles, food, construction, and many other industries (Zhu et al., 2016; Yang et al., 2021). The biocompatibility, biodegradability, water-retention capacity, renewability, and tunability of cellulose make it an ideal biopolymer for use as a biomaterial (Bhaladhare and Das, 2022). In general, cellulosic materials are considered to be environment-friendly and are low-cost when compared to other conventional synthetic materials (Hickey and Pelling, 2019). Cellulose polymers for biomaterials may be produced either by chemical synthesis or biosynthesis. Feedstock from a variety of sources (e.g., plants, animals, and microbes) serve as substrates to produce cellulose-based materials (He et al., 2016; Okeyoshi et al., 2018).

Over the past decade, there has been renewed interest in the use of cellulosic feedstocks to produce biofuels as fuel prices fluctuate erratically and use of fossil fuels continue to contribute to geopolitical instability and climate change (Ceballos, 2017; Kumar et al., 2020; Saravanan et al., 2022). In addition, other research has focused on the physical and chemical properties of cellulose for the development of cellulose-based



biomaterials (Habibi, 2014; Agarwal and Csóka, 2019; Tarrahi et al., 2022). It has been shown that cellulose fibers produce elongated fibrillary structures or intact rod-like crystalline particles in the nanoscale range when subjected to mechanical shearing or controlled acid hydrolysis (Klemm et al., 2011). This is advantageous because it permits useful modifications to the macromolecular structure of cellulose (through a variety of chemistries) with nanoscale tunability for a myriad of sophisticated applications (Habibi, 2014).

Several reviews are published on using nanoscale, structured cellulosic substrates (i.e., nanocellulose) in biomaterials. These are mainly focused on sourcing, isolation, fabrication, and surface modifications to cellulose (Hickey and Pelling, 2019; Moohan et al., 2020; Sood et al., 2021; Mali and Sherje, 2022). Although these reports offer details regarding synthesis of cellulosic materials, forming composites, and current applications for cellulosic biomaterials (Agarwal and Csóka, 2019; Tarrahi et al., 2022), few is focused on the compatibility between particular physical processes and chemical properties and the suitability of the resulting nanocellulose-based materials for specific biomedical applications. Here, we aim to connect the features of cellulose-based materials based on their physical and chemical properties to biomedical applications. This review addresses different types of cellulose-based substrates (e.g., nanofibrillated, nanocrystalline, and bacterial cellulose) and the benefits of selected chemical and physical treatments that are amenable for biomedical applications of cellulose-based materials.

Modifications in the synthesis of cellulose-based biomaterials

Over the last decade, improvements for the use of cellulose as a biomaterial have included modifying surface properties and

constructing cellulose-based composites to serve a wider range of applications (Habibi, 2014; Jorfi and Foster, 2015). Structured cellulose with nanoscale features (i.e., nanocellulose) that include a high aspect (i.e., length-to-width) ratio and a large (micro- to macroscopic) surface area (Agarwal and Csóka, 2019) can be broadly classified as either nanofibrillated cellulose (NFC), nanocrystalline cellulose (NCC), or bacterial cellulose (BC) depending upon its source and properties (Lin and Dufresne, 2014). Functionality of cellulosic materials can be modified surface alterations, including physical adsorption of molecules, attachment of chemical moieties, and derivatization by one or more functional groups (Figure 1).

Modifications by physical or mechanical processes

Mechanical shearing laterally disintegrates cellulose fibers into sub-structural nanoscale units, called nanofibrils, resulting in nanofibrillated cellulose (NFC) (Habibi, 2014). Rigorous mechanical disruption produces NFC, which features fibrils on the order of several microns (Orlando et al., 2020). Three main technologies, homogenization, microfluidization, and microgrinding, are widely used for mechanical treatment of substrate leading to NFC. For example, a high-pressure homogenization method, which combines a homogenizer and a microfluidizer, is one of the most common substrate treatments due high defibrillation efficiency and relatively short isolation times compared to other methods. During high-pressure homogenization, high shear forces produce defibrillated cellulose fibers from both crystalline and amorphous domains of the cellulose substrate (Kose et al., 2011; Habibi, 2014). Another method to produce NFC is emulsification in which agitation of a multi-phase mixture yields small aqueous droplets of hydrogel precursors in a hydrophobic medium (i.e., oil or organic solvent). This is a proven strategy to produce of nano- or micro-sphere gels (El-Sherbiny and Yacoub, 2013).

NFC may also be produce by other methods including cryocrushing, ultrasonication, and steam explosion (Uetani and Yano, 2011). Cryocrushing involves a combination of severe shearing of cellulose in a refiner, followed by high-impact crushing under liquid nitrogen. Resulting microfibrils are useful in the production of high strength and high stiffness composites for high-performance applications like bone tissue and prosthetics engineering (Chakraborty et al., 2005). In ultrasonication, purified cellulose is soaked in deionized water and then subjected to ultrasonic fibrillation to isolate nanofibers. The process can be performed at a different frequencies and output power levels depending upon the purpose of the process (Xie et al., 2016). Ultrasonication yields nanofibers with desired properties, such as high crystallinity and thermal resistance (Chen et al., 2011), which are used as nanocomposites, filtration media, or films that feature optical transparency

(Chakraborty et al., 2005; Chen et al., 2011). Steam explosion is another alternative process for NFC production, in which saturated steam is used to treat cellulosic feedstock. NFC derived from steam explosion exhibits a notable increase in tensile strength as well as improvement in other properties, such as reduced lignin content (Chakraborty et al., 2005).

For BC, silver has been integrated into cellulose by soaking feedstock with various substances, including silver salts (Chen et al., 2019), silver sulfadiazine (Aris et al., 2019), and silver-based fluorescent complexes (deBoer et al., 2015). Other metals such as titanium oxide (Ullah M. W. et al., 2016b), zinc or zinc oxide (Wahid et al., 2019; Dharmalingam and Anandalakshmi, 2020; Dinca et al., 2020), and zeolites or montmorillonite (Horue et al., 2020) have also been integrated into BC biomaterials. BC acts as stabilizing agent to control particle nucleation. Therefore, integration of metal nanoparticles into BC is promising strategy homogeneously incorporating metal nanoparticles and controlling particle formation. In general, the biocompatibility, high specific surface area, and non-toxicity of BC are properties that have prompted rapid development of BC-based biomaterials (Sureshkumar et al., 2010).

Modifications by chemical alteration

In addition to physical processes, chemical modifications have also been used to develop cellulose-based biomaterials for specific applications. For example, sulfation introduces highly negative sulfate esters on the surface of NCC. This, in turn, can enhance adsorption of select biomolecules such as enzymes (Chen et al., 2013). The 2,2,6,6-tetramethylpiperidine-1-oxyl (TEMPO)-mediated oxidation of cellulose is a widely used method to change the hydroxymethyl groups of cellulose to carboxylic forms while conserving secondary hydroxyls (Besbes et al., 2011; Isogai et al., 2011). Cellulose has also been explored as a substrate for carrying out reactions by click chemistry. Click chemistry produces a group of reactions that are fast, simple to use, easy to purify, versatile, regiospecific, and give high product yields (Hein et al., 2008). For example, porphyrin was covalently immobilized to NCC via a 1,3-dipolar cycloaddition catalyzed by Cu(I), which resulted in photodynamic inactivation of *Mycobacterium smegmatis* and *Staphylococcus aureus*. *Escherichia coli* was also inactivated but at lower efficacy (Feese et al., 2011). Etherification has been used as a cost effective and highly efficient chemical treatment step to facilitate the defibrillation of the fibers (Hasani et al., 2008; Eyholzer et al., 2012). Etherification of cellulose by aqueous sodium hydroxide may be followed by cationic surface functionalization of NCC or NFC with ammonium groups via the addition of a nucleophile. Surface modifications to NCC or NFC have also been done through silylation with alkyltrimethylchlorosilanes followed by isocyanate treatment (Gousse et al., 2002; Andresen et al., 2007). Either NCC or

NFC can be treated with isocyanate, which results in urethane linkages via urethanization or carbamylation. This enhances the molecular hydrophobicity of the material (Siqueira et al., 2013).

Chemical modification of a cellulose substrate either alone or in conjunction with mechanical or physical treatment may endow the emerging cellulose-based material with a unique set of properties. Selection of manufacturing processes yields biomaterial with desired thermal stability, tensile strength, crystallinity, and other factors. Different material profiles can be matched to compatible applications.

Modifications of cellulose-based biomaterials for biomedical applications

The use of cellulose as a biomaterial has a long history. Physical processes or chemical modifications of cellulose (Orlando et al., 2020), derivatization of cellulose (Yang et al., 2021), or mixing cellulose with other materials to produce composites (Aris et al., 2019; Wahid et al., 2019) have all resulted in the development of innovative and useful biomaterials. These cellulose-based materials are becoming increasingly useful in biomedicine, including diagnosis, treatment, prevention, and analysis of disease and disease progression (Figure 2).

Drug delivery

Cellulose and nanocellulose have been used in the form of gels, membranes, spheres, and crystals as excipients for a wide range of drugs (Agarwal and Csóka, 2019). Early literature reports that periodate-oxidized cellulose can be used to immobilize insulin or *p*-amino salicylic acid for prolonged drug delivery (Singh et al., 1981; Bala et al., 1982). In addition, by copolymerizing methacrylic acid, N-isopropyl acrylamide, or ethylene glycol dimethacrylate and employing silica microspheres modified by 3-methacryloxypropyltrimethoxysilane as a template, cellulose-coated hollow microspheres have been engineered to enable prolonged (i.e., slow release) drug delivery (Agarwal and Csóka, 2019). In contrast, for a rapid and controlled drug delivery, oxidized cellulose beads have been developed. Specifically, TEMPO-mediated oxidation provides a pH-responsive system for drug release from beads cellulose beads, which can be tuned to retain drug at pH 1.2 and release drug at pH 7.0 (Xie et al., 2021). The release rate is controlled by changes in oxidation state, allowing drug release at different locations with strategic timing (Xie et al., 2021). Cellulose beads can also be derived from BC. For example, a high-absorbance BC membrane was developed for sustained release of the anti-inflammatory drug diclofenac in transdermal systems (Silva et al., 2014). Using

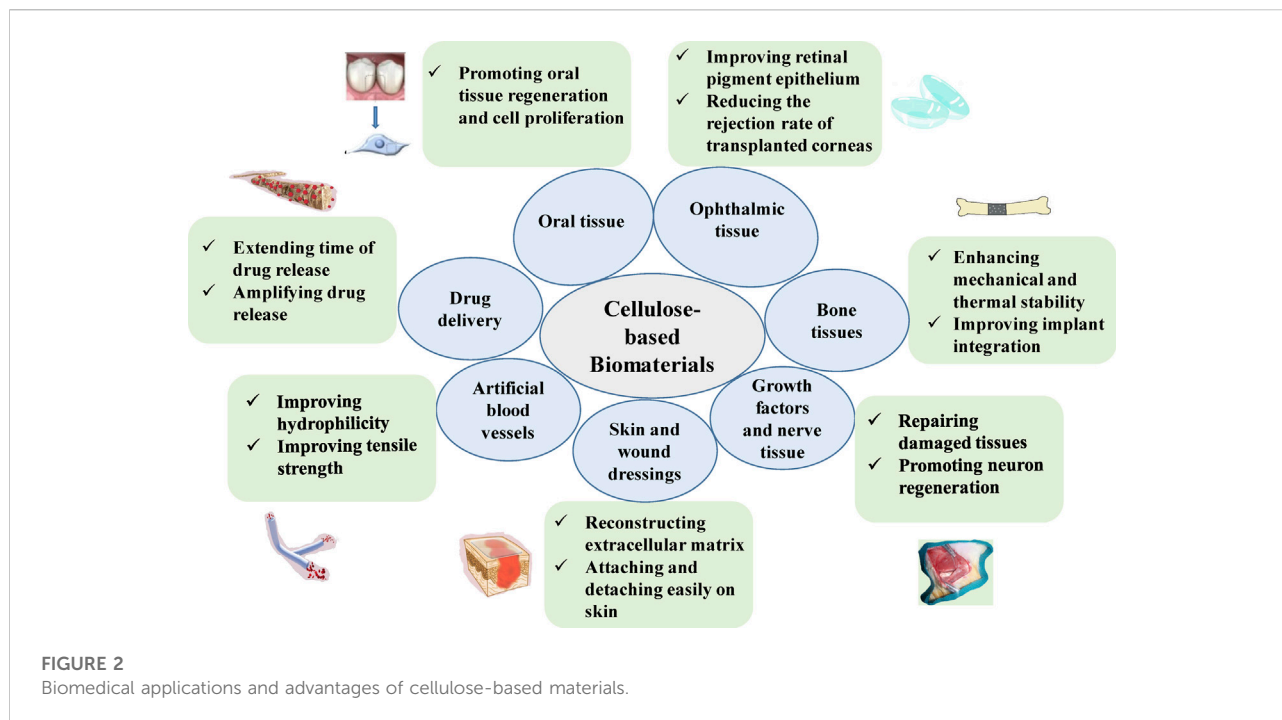


FIGURE 2
Biomedical applications and advantages of cellulose-based materials.

glycerol to facilitate drug absorption and enhance membrane malleability, diclofenac was more readily absorbed (Agarwal and Csóka, 2019). In another report, benzalkonium chloride-treated BC dry films were found to have high drug-loading capacity and enhanced drug efficacy for at least 24 h against *Staphylococcus aureus* and *Bacillus subtilis* when applied to wounds (Ullah H. et al., 2016a).

Skin and wound dressings

Cellulose-based materials have been used in wound healing to mimic skin, facilitate rapid regeneration of skin cells, and minimize scarring (Hickey and Pelling, 2019). Among the most advanced materials used in wound dressings are those produced *via* bioprinting. Nanocellulose can be an ideal component of bio-ink. For example, nanocellulose fibrils derived from TEMPO-mediated oxidation reduce viscosity in bioprinting yielding advantageous rheological properties (Rees et al., 2015). Bioprinting with nanocellulose-based bio-ink also permits the construction of porous nanostructures to stabilize functionalized molecules. For example, carboxymethylated-periodate nanocellulose has been used in bioprinting to produce 3D porous structures with the capacity to carry and launch microbicides (Rees et al., 2015). Electrospinning is a useful method for the production of 3D porous matrices that mimic the natural structures of layers within skin. Mixtures of cellulose acetate and hydrogel (e.g., gelatin and poly urethane) have been used in electrospinning processes to form scaffolds (Vatankhah

et al., 2014). By varying the ratio of nanocellulose-to-hydrogel, parameters such as porosity, stiffness, hydrophobicity, absorption, and surface area can be tuned to improve efficiency in wound healing applications (Liu et al., 2012). The high specific surface area and hydrophilicity of NFC allows it to hold large amounts of water (relative to its dry mass). When dispersed in water, NFC yields a hydrogel that can be modified for a variety of purposes including the production of wound dressing products. It has been shown that functionalized cellulose dressings are superior to existing commercial products such as Suprathel (Hakkarainen et al., 2016).

Bone tissue engineering

Cellulose has been used in bone tissue engineering because cellulose fibers resemble the collagen fibers of bone tissue and are compatible with the stiff, mechanical environment found in bone systems (Torgbo and Sukyai, 2018; Vallejo et al., 2021). Because the mechanical properties of hydrogels cannot withstand mechanical stresses seen on bone, they are often reinforced with nanocellulose (e.g., NFC). Cellulose nanocrystals (e.g., NCC) serve as support in electrospun matrices of polylactic acid (PLA) or polyvinyl alcohol (PVA) hydrogels (Chalal et al., 2014; Rescignano et al., 2014; Zhang et al., 2015). It has been demonstrated that adhesion between PLA and cellulose in electrospinning can be enhanced by maleic anhydride grafting, polyethylene glycol grafting (PEG), and sodium dodecyl sulfate (SDS). This

process modifies the nanocrystals to produce matrices with smaller diameters and polydispersity (Zhou et al., 2013). It also increases mechanical and thermal stability. For example, it has been reported that PLA-cellulose scaffolds can exhibit tensile strengths greater than 10 MPa (Zhang et al., 2015). Fibrous nanocellulose has been used with bioactive glass to coat metal implants resulting in rapid mineralization (e.g., hydroxyapatite formation) to facilitate cell attachment and proliferation around the implants (Chen et al., 2015). Thus, high mechanical strength cellulose and cellulose composites are being successfully implemented in bone tissue regeneration applications.

Nerve tissue repair and growth factor delivery

Cellulosic materials have been used as scaffolds for nerve cell and stem cell culturing as well as for the delivery of growth factors into tissues of the nervous system (Wang et al., 2013; Du et al., 2014; Kuzmenko et al., 2016). For example, cellulose-based biomaterials have been shown to promote the regeneration of neurons after spinal cord injury. NFC scaffolds are used in research to promote *in vitro* neural stem cell differentiation. *In vivo*, the tunable porosity of NFC scaffolds can facilitate optimal release of growth factors into injured spinal cord regions (Tsai et al., 2006; Hackett et al., 2010). For targeted delivery into micro-environments surrounding neural stem cells, cellulose-based scaffolds have been used to transport and release growth factors. This is useful for heterogeneous neural differentiation of large populations of stem cells and for repairing damaged nerve tissues (Wang et al., 2013).

Ophthalmic tissue repair

Cellulose-based materials have been developed for several ophthalmic applications. For example, BC/polyvinyl alcohol (PVA) composites are being developed to mimic properties of the natural cornea, which offers a transparent structure with high light transmittance, flexibility but with mechanical strength, and desirable thermal properties (Wang et al., 2010). BC-based contact lens and lens components can be doped with antibiotics, such as ciprofloxacin/ γ -cyclodextrin to prevent infection or to treat active bacterial infections (Cavicchioli et al., 2015). BC biomaterials that are modified with chitosan and carboxymethyl cellulose to maximize hydrophilicity have been shown to facilitate enhances propagation of retinal pigment epithelial cells (Goncalves et al., 2015). This offers new prospects in the treatment of multiple eyes diseases including age-related macular degeneration.

Oral tissue repair

Nanocellulose-based materials have also been developed for oral tissue repair and post-surgical recovery. For example, a blend of BC with calcium chloride and sodium alginate has resulted in the construction of a cellulosic “sponge”. This material has been shown to promote the proliferation of gingival fibroblast cells (Chiaoprakobkij et al., 2011). Similar BC-based materials have shown utility in recovery regimens in root canal surgeries. Specifically, BC biomaterials for plugging cavities from dental root canals showed the ability to expand and cover the entire canal space with the added benefit of sterilizing and removing residue from the canal space (Yoshino et al., 2013).

Artificial blood vessels

Cellulosic biomaterials have also been used in the regeneration and replacement of vasculature. BC can be molded to very different shapes during its synthesis to generate substrates optimized for enhancing cell attachment and proliferation (Mohite and Patil, 2014; Picheth et al., 2017). Studies have demonstrated that in vascular grafting, materials made with BC induce a reduction in thrombin at target surfaces thus inhibiting clot formation (Fink et al., 2010). This is a notable advantage over other commonly materials commonly used for vascular grafting (e.g., PET and PTFE). In addition, BC-derived composites have emerged as a major alternative in the replacement of atherosclerotic blood vessels. For example, blending BC nanocrystals with PVA (Polyvinyl alcohol) results in an artificial vessel with high tensile strength, low cytotoxicity, and enhanced suture retention profile (Tang et al., 2015). A key issue in implants is optimizing cell adhesion. The development of hydrophilic BC-based biomaterials with polyethylene glycol (PEG) grafted into the cellulosic base have shown favorable compatibility for cell proliferation and adhesion (e.g., fibroblasts), reduced propensity for complement activation, and resistance to bacterial adhesion (da Silva et al., 2016). The development of such hydrophilic BC composites offers notable advances in the development of novel artificial blood vessels implants, coatings for cardiovascular stents (resistant to bacterial adhesion), and the replacement heart valves.

Prospectus

Development of nanocellulose-based biomaterials is a robust area of current research and engineering. From feedstock choice to defining properties of different cellulosic substrates and matching pretreatment and manufacturing processes to specific applications, the diversity and number of cellulosic biomaterials is growing. In this review, we have summarized

general properties of three common cellulosic materials (i.e., NCC, NFC, BC) and discussed physical and chemical processes used to produce or modify each. We have provided examples of how these starting materials are being used in different biomedical applications and why the unique properties of each cellulose substrate are suitable to each application. Due to the sensitivity of biological systems to foreign materials and the tunability of cellulosic substrates, the use of cellulose-based biomaterials for biomedical applications is a robust area of research and development. The sheer abundance of cellulose as a raw material and its status as a sustainable resource make cellulosic materials even more attractive. Efforts to understand the limitations of cellulosic biomaterials in biomedicine, such as the potential for immunological rejection, facilitating disease transmission, and enhancing risks for future malignancies are valuable as cellulose-based products become more widely used in biomedicine (Savoji et al., 2018). The potential is great, indeed. Cellulose is being used in bio-ink that serves to produce scaffolds for the regeneration of tissues or entire organs (Weng et al., 2021). Cellulose matrices are being used to stabilize differentiating stem cells and in tissue engineering. Cellulose-based drug delivery systems (e.g., cellulose microspheres and nanobeads) are used to regulate the controlled release of medications and growth factors with high resolution and specificity. Thus, despite some limitations such as production costs for advanced cellulosic substrates (Tornello et al., 2016) and special transportation/storage conditions (Guan et al., 2020), the future looks promising for the use of cellulose-based biomaterials in biomedicine.

References

- Agarwal, C., and Csóka, L. (2019). "Chapter 6 - surface-modified cellulose in biomedical engineering," in *Materials for biomedical engineering*. Editors V. Grumezescu and A. M. Grumezescu (Elsevier), Amsterdam, Netherlands 215–261. doi:10.1016/B978-0-12-818431-8.00007-6
- Andresen, M., Stenstad, P., Moretro, T., Langsrud, S., Syverud, K., Johansson, L. S., et al. (2007). Nonleaching antimicrobial films prepared from surface-modified microfibrillated cellulose. *Biomacromolecules* 8 (7), 2149–2155. doi:10.1021/bm070304e
- Aris, F. A. F., Fauzi, F., Tong, W. Y., and Abdullah, S. S. S. (2019). Interaction of silver sulfadiazine with bacterial cellulose via *ex-situ* modification method as an alternative diabetic wound healing. *Biocatal. Agric. Biotechnol.* 21, 101332. doi:10.1016/j.bcab.2019.101332
- Bala, K., Guha, S. K., and Vasudevan, P. (1982). p-Amino salicylic acid — oxidized cellulose system: a model for long term drug delivery. *Biomaterials* 3 (2), 97–100. doi:10.1016/0142-9612(82)90041-2
- Besbes, I., Alila, S., and Boufi, S. (2011). Nanofibrillated cellulose from TEMPO-oxidized eucalyptus fibres: Effect of the carboxyl content. *Carbohydr. Polym.* 84 (3), 975–983. doi:10.1016/j.carbpol.2010.12.052
- Bhaladhare, S., and Das, D. (2022). Cellulose: A fascinating biopolymer for hydrogel synthesis. *J. Mat. Chem. B* 10, 1923–1945. doi:10.1039/d1tb02848k
- Cavicchioli, M., Corso, C. T., Coelho, F., Mendes, L., Saska, S., Soares, C. P., et al. (2015). Characterization and cytotoxic, genotoxic and mutagenic evaluations of bacterial cellulose membranes incorporated with ciprofloxacin: A potential material for use as therapeutic contact lens. *World J. Pharm. Pharm. Sci.* 4, 1626–1647.
- Ceballos, R. M. (2017). *Bioethanol and natural resources: Substrates, chemistry and engineered systems*. Boca Raton, FL: CRC Press. doi:10.1201/9781315154299
- Chakraborty, A., Sain, M., and Kortschot, M. (2005). Cellulose microfibrils: A novel method of preparation using high shear refining and cryocrushing. *Holzforchung* 59 (1), 102–107. doi:10.1515/hf.2005.016
- Chalal, S., Hussain, F. S. J., and Yusoff, M. B. M. (2014). Biomimetic growth of bone-like apatite via simulated body fluid on hydroxyethyl cellulose/polyvinyl alcohol electrospun nanofibers. *Biomed. Mat. Eng.* 24 (1), 799–806. doi:10.3233/bme-130871
- Chen, G., Zhang, B., Zhao, J., and Chen, H. W. (2013). Improved process for the production of cellulose sulfate using sulfuric acid/ethanol solution. *Carbohydr. Polym.* 95 (1), 332–337. doi:10.1016/j.carbpol.2013.03.003
- Chen, H., Cheng, R. Y., Zhao, X., Zhang, Y. H., Tam, A., Yan, Y. F., et al. (2019). An injectable self-healing coordinative hydrogel with antibacterial and angiogenic properties for diabetic skin wound repair. *NPG Asia Mat.* 11, 3. doi:10.1038/s41427-018-0103-9
- Chen, Q., Garcia, R. P., Munoz, J., de Larraya, U. P., Garmendia, N., Yao, Q. Q., et al. (2015). Cellulose nanocrystals-bioactive glass hybrid coating as bone substitutes by electrophoretic Co-deposition: *In situ* control of mineralization of bioactive glass and enhancement of osteoblastic performance. *ACS Appl. Mat. Interfaces* 7 (44), 24715–24725. doi:10.1021/acsami.5b07294
- Chen, W. S., Yu, H. P., Liu, Y. X., Hai, Y. F., Zhang, M. X., and Chen, P. (2011). Isolation and characterization of cellulose nanofibers from four plant cellulose fibers using a chemical-ultrasonic process. *Cellulose* 18 (2), 433–442. doi:10.1007/s10570-011-9497-z
- Chiaoprakobkij, N., Sanchavanakit, N., Subbalekha, K., Pavasant, P., and Phisalaphong, M. (2011). Characterization and biocompatibility of bacterial cellulose/alginate composite sponges with human keratinocytes and gingival fibroblasts. *Carbohydr. Polym.* 85 (3), 548–553. doi:10.1016/j.carbpol.2011.03.011

Author contributions

NF, RC, and CF wrote and edited the manuscript. All authors contributed to the article and approved the submitted version.

Funding

This work was funded by the National Institutes of Health (R15GM140433 to CF and P20GM139768 to CF) and the National Science Foundation (MCB 1818346 to RC).

Conflict of interest

The authors declare that the research was conducted in the absence of any commercial or financial relationships that could be construed as a potential conflict of interest.

Publisher's note

All claims expressed in this article are solely those of the authors and do not necessarily represent those of their affiliated organizations, or those of the publisher, the editors and the reviewers. Any product that may be evaluated in this article, or claim that may be made by its manufacturer, is not guaranteed or endorsed by the publisher.

- da Silva, R., Sierakowski, M. R., Bassani, H. P., Zawadzki, S. F., Pirich, C. L., Ono, L., et al. (2016). Hydrophilicity improvement of mercerized bacterial cellulose films by polyethylene glycol graft. *Int. J. Biol. Macromol.* 86, 599–605. doi:10.1016/j.ijbiomac.2016.01.115
- deBoer, T. R., Chakraborty, I., and Mascharak, P. K. (2015). Design and construction of a silver(I)-loaded cellulose-based wound dressing: Trackable and sustained release of silver for controlled therapeutic delivery to wound sites. *J. Mater. Science-Materials Med.* 26 (10), 9. doi:10.1007/s10856-015-5577-1
- Dharmalingam, K., and Anandalakshmi, R. (2020). Functionalization of cellulose-based nanocomposite hydrogel films with zinc oxide complex and grapefruit seed extract for potential applications in treating chronic wounds. *Polymer* 202, 122620. doi:10.1016/j.polymer.2020.122620
- Dinca, V., Mocanu, A., Isopencu, G., Busuioc, C., Brajnicov, S., Vlad, A., et al. (2020). Biocompatible pure ZnO nanoparticles-3D bacterial cellulose biointerfaces with antibacterial properties. *Arabian J. Chem.* 13 (1), 3521–3533. doi:10.1016/j.arabj.2018.12.003
- Du, J., Tan, E., Kim, H. J., Zhang, A., Bhattacharya, R., and Yarema, K. J. (2014). Comparative evaluation of chitosan, cellulose acetate, and polyethersulfone nanofiber scaffolds for neural differentiation. *Carbohydr. Polym.* 99, 483–490. doi:10.1016/j.carbpol.2013.08.050
- El-Sherbiny, I. M., and Yacoub, M. H. (2013). Hydrogel scaffolds for tissue engineering: Progress and challenges. *Glob. Cardiol. Sci. Pract.* 2013 (3), 38–342. doi:10.5339/gcsp.2013.38
- Eyholzer, C., Tingaut, P., Zimmermann, T., and Oksman, K. (2012). Dispersion and reinforcing potential of carboxymethylated nanofibrillated cellulose powders modified with 1-hexanol in extruded poly(lactic acid) (PLA) composites. *J. Polym. Environ.* 20 (4), 1052–1062. doi:10.1007/s10924-012-0508-4
- Feese, E., Sadeghifar, H., Gracz, H. S., Argyropoulos, D. S., and Ghiladi, R. A. (2011). Photobactericidal porphyrin-cellulose nanocrystals: Synthesis, characterization, and antimicrobial properties. *Biomacromolecules* 12 (10), 3528–3539. doi:10.1021/bm200718s
- Fink, H., Faxalv, L., Molnar, G. F., Drotz, K., Risberg, B., Lindahl, T. L., et al. (2010). Real-time measurements of coagulation on bacterial cellulose and conventional vascular graft materials. *Acta Biomater.* 6 (3), 1125–1130. doi:10.1016/j.actbio.2009.09.019
- Goncalves, S., Padrao, J., Rodrigues, I. P., Silva, J. P., Sencadas, V., Lanceros-Mendez, S., et al. (2015). Bacterial cellulose as a support for the growth of retinal pigment epithelium. *Biomacromolecules* 16 (4), 1341–1351. doi:10.1021/acs.biomac.5b00129
- Gousse, C., Chanzy, H., Excoffier, G., Soubeyrand, L., and Fleury, E. (2002). Stable suspensions of partially silylated cellulose whiskers dispersed in organic solvents. *Polymer* 43 (9), 2645–2651. doi:10.1016/s0032-3861(02)00051-4
- Guan, N., Liu, Z. H., Zhao, Y. H., Li, Q., and Wang, Y. T. (2020). Engineered biomaterial strategies for controlling growth factors in tissue engineering. *Drug Deliv.* 27 (1), 1438–1451. doi:10.1080/10717544.2020.1831104
- Habibi, Y. (2014). Key advances in the chemical modification of nanocelluloses. *Chem. Soc. Rev.* 43 (5), 1519–1542. doi:10.1039/c3cs60204d
- Hackett, J. M., Dang, T. T., Tsai, E. C., and Cao, X. D. (2010). Electrospun biocomposite polycaprolactone/collagen tubes as scaffolds for neural stem cell differentiation. *Materials* 3 (6), 3714–3728. doi:10.3390/ma3063714
- Hakkarainen, T., Koivuniemi, R., Kosonen, M., Escobedo-Lucea, C., Sanz-Garcia, A., Vuola, J., et al. (2016). Nanofibrillar cellulose wound dressing in skin graft donor site treatment. *J. Control. Release* 244, 292–301. doi:10.1016/j.jconrel.2016.07.053
- Hasani, M., Cranston, E. D., Westman, G., and Gray, D. G. (2008). Cationic surface functionalization of cellulose nanocrystals. *Soft Matter* 4 (11), 2238–2244. doi:10.1039/b806789a
- He, S. D., Wang, X., Zhang, Y., Wang, J., Sun, H. J., Wang, J. H., et al. (2016). Isolation and prebiotic activity of water-soluble polysaccharides fractions from the bamboo shoots (*Phyllostachys praecox*). *Carbohydr. Polym.* 151, 295–304. doi:10.1016/j.carbpol.2016.05.072
- Hein, C. D., Liu, X. M., and Wang, D. (2008). Click chemistry, a powerful tool for pharmaceutical sciences. *Pharm. Res.* 25 (10), 2216–2230. doi:10.1007/s11095-008-9616-1
- Hickey, R. J., and Pelling, A. E. (2019). Cellulose biomaterials for tissue engineering. *Front. Bioeng. Biotechnol.* 7, 45. doi:10.3389/fbioe.2019.00045
- Horue, M., Cacicedo, M. L., Fernandez, M. A., Rodenak-Kladniew, B., Sanchez, R. T. M., and Castro, G. R. (2020). Antimicrobial activities of bacterial cellulose - silver montmorillonite nanocomposites for wound healing. *Mater. Sci. Eng. C* 116, 111152. doi:10.1016/j.msec.2020.111152
- Isogai, A., Saito, T., and Fukuzumi, H. (2011). TEMPO-oxidized cellulose nanofibers. *Nanoscale* 3 (1), 71–85. doi:10.1039/c0nr00583e
- Jorfi, M., and Foster, E. J. (2015). Recent advances in nanocellulose for biomedical applications. *J. Appl. Polym. Sci.* 132 (14), 19. doi:10.1002/app.41719
- Klemm, D., Kramer, F., Moritz, S., Lindstrom, T., Ankerfors, M., Gray, D., et al. (2011). Nanocelluloses: A new family of nature-based materials. *Angew. Chem. Int. Ed.* 50 (24), 5438–5466. doi:10.1002/anie.201001273
- Kose, R., Mitani, I., Kasai, W., and Kondo, T. (2011). Nanocellulose" as a single nanofiber prepared from pellicle secreted by gluconacetobacter xylinus using aqueous counter collision. *Biomacromolecules* 12 (3), 716–720. doi:10.1021/bm1013469
- Kumar, M., Sun, Y. Q., Rathour, R., Pandey, A., Thakur, I. S., and Tsang, D. C. W. (2020). Algae as potential feedstock for the production of biofuels and value-added products: Opportunities and challenges. *Sci. Total Environ.* 716, 137116. doi:10.1016/j.scitotenv.2020.137116
- Kuzmenko, V., Kalogeropoulos, T., Thunberg, J., Johannesson, S., Hagg, D., Enoksson, P., et al. (2016). Enhanced growth of neural networks on conductive cellulose-derived nanofibrous scaffolds. *Mater. Sci. Eng. C* 58, 14–23. doi:10.1016/j.msec.2015.08.012
- Lin, N., and Dufresne, A. (2014). Nanocellulose in biomedicine: Current status and future prospect. *Eur. Polym. J.* 59, 302–325. doi:10.1016/j.eurpolymj.2014.07.025
- Liu, X., Lin, T., Gao, Y., Xu, Z. G., Huang, C., Yao, G., et al. (2012). Antimicrobial electrospun nanofibers of cellulose acetate and polyester urethane composite for wound dressing. *J. Biomed. Mat. Res.* 100B (6), 1556–1565. doi:10.1002/jbm.b.32724
- Mali, P., and Sherje, A. P. (2022). Cellulose nanocrystals: Fundamentals and biomedical applications. *Carbohydr. Polym.* 275, 118668. doi:10.1016/j.carbpol.2021.118668
- Mohite, B. V., and Patil, S. V. (2014). A novel biomaterial: Bacterial cellulose and its new era applications. *Biotechnol. Appl. Biochem.* 61 (2), 101–110. doi:10.1002/bab.1148
- Moohan, J., Stewart, S. A., Espinosa, E., Rosal, A., Rodriguez, A., Larraneta, E., et al. (2020). Cellulose nanofibers and other biopolymers for biomedical applications. A review. *Appl. Sci. (Basel)* 10 (1), 65. doi:10.3390/app10010065
- Moon, R. J., Martini, A., Nairn, J., Simonsen, J., and Youngblood, J. (2011). Cellulose nanomaterials review: Structure, properties and nanocomposites. *Chem. Soc. Rev.* 40 (7), 3941–3994. doi:10.1039/c0cs00108b
- Okeyoshi, K., Joshi, G., Okajima, M. K., and Kaneko, T. (2018). Formation of polysaccharide membranes by splitting of evaporative air-LC interface. *Adv. Mat. Interfaces* 5 (3), 1701219. doi:10.1002/admi.201701219
- Orlando, I., Basnett, P., Nigmatullin, R., Wang, W. X., Knowles, J. C., and Roy, I. (2020). Chemical modification of bacterial cellulose for the development of an antibacterial wound dressing. *Front. Bioeng. Biotechnol.* 8, 557885. doi:10.3389/fbioe.2020.557885
- Picheth, G. F., Pirich, C. L., Sierakowski, M. R., Woehl, M. A., Sakakibara, C. N., de Souza, C. F., et al. (2017). Bacterial cellulose in biomedical applications: A review. *Int. J. Biol. Macromol.* 104, 97–106. doi:10.1016/j.ijbiomac.2017.05.171
- Rees, A., Powell, L. C., Chinga-Carrasco, G., Gethin, D. T., Syverud, K., Hill, K. E., et al. (2015). 3D bioprinting of carboxymethylated-periodate oxidized nanocellulose constructs for wound dressing applications. *Biomed. Res. Int.* 7, 1–7. doi:10.1155/2015/925757
- Rescignano, N., Fortunati, E., Montesano, S., Emiliani, C., Kenny, J. M., Martino, S., et al. (2014). PVA bio-nanocomposites: A new take-off using cellulose nanocrystals and plga nanoparticles. *Carbohydr. Polym.* 99, 47–58. doi:10.1016/j.carbpol.2013.08.061
- Saravanan, A., Kumar, P. S., Jeevanantham, S., Karishma, S., and Vo, D. V. N. (2022). Recent advances and sustainable development of biofuels production from lignocellulosic biomass. *Bioresour. Technol.* 344, 126203. doi:10.1016/j.biortech.2021.126203
- Savoji, H., Godau, B., Hassani, M. S., and Akbari, M. (2018). Skin tissue substitutes and biomaterial risk assessment and testing. *Front. Bioeng. Biotechnol.* 6, 86. doi:10.3389/fbioe.2018.00086
- Silva, N. H., Rodrigues, A. F., Almeida, I. F., Costa, P. C., Rosado, C., Neto, C. P., et al. (2014). Bacterial cellulose membranes as transdermal delivery systems for diclofenac: *In vitro* dissolution and permeation studies. *Carbohydr. Polym.* 106, 264–269. doi:10.1016/j.carbpol.2014.02.014
- Singh, M., Vasudevan, P., Sinha, T. J. M., Ray, A. R., Misro, M. M., and Guha, K. (1981). AN insulin delivery system from oxidized cellulose. *J. Biomed. Mat. Res.* 15 (5), 655–661. doi:10.1002/jbm.820150504
- Siqueira, G., Bras, J., Follain, N., Belbekhouche, S., Marais, S., and Dufresne, A. (2013). Thermal and mechanical properties of bio-nanocomposites reinforced by Luffa cylindrical cellulose nanocrystals. *Carbohydr. Polym.* 91 (2), 711–717. doi:10.1016/j.carbpol.2012.08.057
- Sood, A., Gupta, A., and Agrawal, G. (2021). Recent advances in polysaccharides based biomaterials for drug delivery and tissue engineering applications. *Carbohydr. Polym. Technol. Appl.* 2, 100067. doi:10.1016/j.carpta.2021.100067
- Sureshkumar, M., Siswanto, D. Y., and Lee, C. K. (2010). Magnetic antimicrobial nanocomposite based on bacterial cellulose and silver nanoparticles. *J. Mat. Chem.* 20 (33), 6948–6955. doi:10.1039/c0jm00565g

- Tang, J. Y., Bao, L. H., Li, X., Chen, L., and Hong, F. F. (2015). Potential of PVA-doped bacterial nano-cellulose tubular composites for artificial blood vessels. *J. Mat. Chem. B* 3 (43), 8537–8547. doi:10.1039/c5tb01144b
- Tarrahi, R., Khataee, A., Karimi, A., and Yoon, Y. (2022). The latest achievements in plant cellulose-based biomaterials for tissue engineering focusing on skin repair. *Chemosphere* 288, 132529. doi:10.1016/j.chemosphere.2021.132529
- Torgbo, S., and Sukyai, P. (2018). Bacterial cellulose-based scaffold materials for bone tissue engineering. *Appl. Mater. Today* 11, 34–49. doi:10.1016/j.apmt.2018.01.004
- Tornello, P. R. C., Ballarin, F. M., Caracciolo, P. C., and Abraham, G. A. (2016). Micro/nanofiber-based scaffolds for soft tissue engineering applications: Potential and current challenges. *Nanobiomaterials soft tissue Eng.* 5, 201–229. doi:10.1016/B978-0-323-42865-1.00008-8
- Tsai, E. C., Dalton, P. D., Shoichet, M. S., and Tator, C. H. (2006). Matrix inclusion within synthetic hydrogel guidance channels improves specific supraspinal and local axonal regeneration after complete spinal cord transection. *Biomaterials* 27 (3), 519–533. doi:10.1016/j.biomaterials.2005.07.025
- Uetani, K., and Yano, H. (2011). Nanofibrillation of wood pulp using a high-speed blender. *Biomacromolecules* 12 (2), 348–353. doi:10.1021/bm101103p
- Ullah, H., Santos, H. A., and Khan, T. (2016a). Applications of bacterial cellulose in food, cosmetics and drug delivery. *Cellulose* 23 (4), 2291–2314. doi:10.1007/s10570-016-0986-y
- Ullah, M. W., Ul-Islam, M., Khan, S., Kim, Y., Jang, J. H., and Park, J. K. (2016b). *In situ* synthesis of a bio-cellulose/titanium dioxide nanocomposite by using a cell-free system. *RSC Adv.* 6 (27), 22424–22435. doi:10.1039/c5ra26704h
- Vallejo, M., Cordeiro, R., Dias, P. A. N., Moura, C., Henriques, M., Seabra, I. J., et al. (2021). Recovery and evaluation of cellulose from agroindustrial residues of corn, grape, pomegranate, strawberry-tree fruit and fava. *Bioresour. Bioprocess.* 8 (1), 25. doi:10.1186/s40643-021-00377-3
- Vatankhah, E., Prabhakaran, M. P., Jin, G. R., Mobarakeh, L. G., and Ramakrishna, S. (2014). Development of nanofibrous cellulose acetate/gelatin skin substitutes for variety wound treatment applications. *J. Biomater. Appl.* 28 (6), 909–921. doi:10.1177/0885328213486527
- Wahid, F., Duan, Y. X., Hu, X. H., Chu, L. Q., Jia, S. R., Cui, J. D., et al. (2019). A facile construction of bacterial cellulose/ZnO nanocomposite films and their photocatalytic and antibacterial properties. *Int. J. Biol. Macromol.* 132, 692–700. doi:10.1016/j.ijbiomac.2019.03.240
- Wang, J. H., Gao, C., Zhang, Y. S., and Wan, Y. Z. (2010). Preparation and *in vitro* characterization of BC/PVA hydrogel composite for its potential use as artificial cornea biomaterial. *Mater. Sci. Eng. C* 30 (1), 214–218. doi:10.1016/j.msec.2009.10.006
- Wang, Y. F., Cooke, M. J., Sachewsky, N., Morshead, C. M., and Shoichet, M. S. (2013). Bioengineered sequential growth factor delivery stimulates brain tissue regeneration after stroke. *J. Control. Release* 172 (1), 1–11. doi:10.1016/j.jconrel.2013.07.032
- Weng, T. T., Zhang, W., Xia, Y. L., Wu, P., Yang, M., Jin, R. H., et al. (2021). 3D bioprinting for skin tissue engineering: Current status and perspectives. *J. Tissue Eng.* 12, 204173142110285. doi:10.1177/20417314211028574
- Xie, F., De Wever, P., Fardim, P., and van den Mooter, G. (2021). TEMPO-oxidized cellulose beads as potential pH-responsive carriers for site-specific drug delivery in the gastrointestinal tract. *Molecules* 26 (4), 1030. doi:10.3390/molecules26041030
- Xie, J. L., Hse, C. Y., De Hoop, C. F., Hu, T. X., Qi, J. Q., and Shupe, T. F. (2016). Isolation and characterization of cellulose nanofibers from bamboo using microwave liquefaction combined with chemical treatment and ultrasonication. *Carbohydr. Polym.* 151, 725–734. doi:10.1016/j.carbpol.2016.06.011
- Yang, Y., Lu, Y. T., Zeng, K., Heinze, T., Groth, T., and Zhang, K. (2021). Recent progress on cellulose-based ionic compounds for biomaterials. *Adv. Mat.* 33 (28), 2000717. doi:10.1002/adma.202000717
- Yoshino, A., Tabuchi, M., Uo, M., Tatsumi, H., Hideshima, K., Kondo, S., et al. (2013). Applicability of bacterial cellulose as an alternative to paper points in endodontic treatment. *Acta Biomater.* 9 (4), 6116–6122. doi:10.1016/j.actbio.2012.12.022
- Zhang, C. M., Salick, M. R., Cordie, T. M., Effingham, T., Dan, Y., and Turng, L. S. (2015). Incorporation of poly(ethylene glycol) grafted cellulose nanocrystals in poly(lactic acid) electrospun nanocomposite fibers as potential scaffolds for bone tissue engineering. *Mater. Sci. Eng. C* 49, 463–471. doi:10.1016/j.msec.2015.01.024
- Zhou, C. J., Shi, Q. F., Guo, W. H., Terrell, L., Qureshi, A. T., Hayes, D. J., et al. (2013). Electrospun bio-nanocomposite scaffolds for bone tissue engineering by cellulose nanocrystals reinforcing maleic anhydride grafted PLA. *ACS Appl. Mat. Interfaces* 5 (9), 3847–3854. doi:10.1021/am4005072
- Zhu, H. L., Luo, W., Ciesielski, P. N., Fang, Z. Q., Zhu, J. Y., Henriksson, G., et al. (2016). Wood-derived materials for green electronics, biological devices, and energy applications. *Chem. Rev.* 116 (16), 9305–9374. doi:10.1021/acs.chemrev.6b00225



OPEN ACCESS

EDITED BY

Candan Tamerler,
University of Kansas, United States

REVIEWED BY

Geert-Jan W. Graulus,
University of Hasselt, Belgium
Silvia Joana Bidarra,
Universidade do Porto, Portugal

*CORRESPONDENCE

Carlos Mas-Moruno,
✉ carles.mas.moruno@upc.edu

RECEIVED 23 March 2023

ACCEPTED 23 May 2023

PUBLISHED 01 June 2023

CITATION

Oliver-Cervelló L, Martin-Gómez H,
Gonzalez-Garcia C,
Salmeron-Sanchez M, Ginebra M-P and
Mas-Moruno C (2023), Protease-
degradable hydrogels with
multifunctional biomimetic peptides for
bone tissue engineering.
Front. Bioeng. Biotechnol. 11:1192436.
doi: 10.3389/fbioe.2023.1192436

COPYRIGHT

© 2023 Oliver-Cervelló, Martin-Gómez,
Gonzalez-Garcia, Salmeron-Sanchez,
Ginebra and Mas-Moruno. This is an
open-access article distributed under the
terms of the [Creative Commons
Attribution License \(CC BY\)](#). The use,
distribution or reproduction in other
forums is permitted, provided the original
author(s) and the copyright owner(s) are
credited and that the original publication
in this journal is cited, in accordance with
accepted academic practice. No use,
distribution or reproduction is permitted
which does not comply with these terms.

Protease-degradable hydrogels with multifunctional biomimetic peptides for bone tissue engineering

Lluís Oliver-Cervelló^{1,2}, Helena Martin-Gómez^{1,2},
Cristina Gonzalez-Garcia³, Manuel Salmeron-Sanchez³,
Maria-Pau Ginebra^{1,2,4} and Carlos Mas-Moruno^{1,2*}

¹Biomaterials, Biomechanics and Tissue Engineering Group, Department of Materials Science and Engineering, Universitat Politècnica de Catalunya (UPC), Barcelona, Spain, ²Barcelona Research Center in Multiscale Science and Engineering, UPC, Barcelona, Spain, ³Centre for the Cellular Microenvironment, Advanced Research Centre, University of Glasgow, Glasgow, United Kingdom, ⁴Institute for Bioengineering of Catalonia (IBEC), Barcelona Institute of Science and Technology (BIST), Barcelona, Spain

Mimicking bone extracellular matrix (ECM) is paramount to develop novel biomaterials for bone tissue engineering. In this regard, the combination of integrin-binding ligands together with osteogenic peptides represents a powerful approach to recapitulate the healing microenvironment of bone. In the present work, we designed polyethylene glycol (PEG)-based hydrogels functionalized with cell instructive multifunctional biomimetic peptides (either with cyclic RGD-DWIVA or cyclic RGD-cyclic DWIVA) and cross-linked with matrix metalloproteinases (MMPs)-degradable sequences to enable dynamic enzymatic biodegradation and cell spreading and differentiation. The analysis of the intrinsic properties of the hydrogel revealed relevant mechanical properties, porosity, swelling and degradability to engineer hydrogels for bone tissue engineering. Moreover, the engineered hydrogels were able to promote human mesenchymal stem cells (MSCs) spreading and significantly improve their osteogenic differentiation. Thus, these novel hydrogels could be a promising candidate for applications in bone tissue engineering, such as acellular systems to be implanted and regenerate bone or in stem cells therapy.

KEYWORDS

biomimetic peptides, DWIVA, hydrogel, functionalization, osteogenic differentiation, multifunctionality

1 Introduction

Stem cells have the capacity to differentiate into multiple cell types, which makes stem-cell-based therapies a promising approach to treat degenerative diseases and injuries as well as to promote tissue regeneration. Nonetheless, these therapies present a major drawback associated to the low cell retention and survival rate of the cells at the administration site, decreasing the effectivity of the treatment (Zhang, Gupte, and Ma, 2013; Zhao, Cui, and Li, 2019). A powerful solution to overcome such shortcomings may be the combination of stem cells with material-based approaches. In this way, it is possible to regulate the administration of the cells through a supporting material with well-defined biophysical and biomechanical properties, thus allowing a better control of the cell behavior. In addition, recreating the *in*

vivo microenvironment of stem cells is paramount to differentiate them into a particular lineage. In this regard, the use of biomaterials is a potential tool to mimic and to reproduce the extracellular matrix (ECM) of stem cells, triggering the desired cell response (Lutolf and Hubbell, 2005; Hussey et al., 2018).

Although autografts and allografts are still the most used strategies to repair bone, they both present disadvantages that limit their use. For instance, autografts are subjected to inflammation and pain at the extraction site and there are constraints in the obtainable quantities, whereas in the case of allografts, there is a risk of disease transmission and immunogenic response (Habibovic, 2017; Iaquinata et al., 2019).

Synthetic hydrogels are a promising alternative in bone regenerative medicine, as they are easily produced by chemical methods and can be fine-tuned, allowing to provide the material with the desired mechanical properties and biochemical signals. Furthermore, they are cytocompatible, versatile and may be injected into the defect site (Catoira et al., 2019; Clark et al., 2020). Nonetheless, most synthetic hydrogels lack bioactivity, meaning that they do not have the capacity to actively modulate cell fate. Consequently, hydrogels have to be equipped with biochemical cues. The incorporation of such biologically active molecules, together with the intrinsic characteristics of synthetic hydrogels, makes them potential candidates for mimicking bone ECM and, thus, not only serving as scaffolds for stem cells, but also to trigger osteogenic differentiation and inducing bone regeneration (Lo et al., 2012; Brown and Anseth, 2017).

In this regard, growth factors (GFs) can be used in combination with hydrogels and other materials (Mitchell et al., 2016). A clear example is the use of bone morphogenetic protein 2 (BMP-2) to induce osteogenic differentiation. For instance, absorbable collagen sponges or calcium phosphate scaffolds have been used as carriers for BMP-2 (Krishnan et al., 2017; Han et al., 2021). Nonetheless, the low affinity of such biomaterials to adsorb BMP-2, together with the burst release of the protein upon implantation, greatly limit their use. Alternatively, it is possible to immobilize BMP-2 to the hydrogel, allowing a better control of its release (Chen Xin et al., 2021). In this regard, Park et al. developed a hydrogel of methoxy poly (ethylene glycol)-poly (caprolactone) block copolymers, in which BMP-2 was covalently immobilized. Such system had the capacity to promote osteogenic differentiation of human periodontal ligament stem cells *in vivo*, as shown by the high mineralization and overexpression of osteogenic genes in comparison to the hydrogels that did not present BMP-2 (Park et al., 2017). BMP-2 has also been combined with platelet derived growth factor BB (PDGF-BB) in smart PEG hydrogels. The fast release of PDGF-BB allowed the recruitment of mesenchymal progenitor cells, while the sustained delivery of BMP-2 promoted the healing of bone defects (Lienemann et al., 2020).

Despite the extensive use of GFs together with biomaterials and, in particular, with hydrogels, GFs still have to be administered at supra-physiological doses due to their short half-life and quick clearance *in vivo*, causing some adverse effects in the patient, like inflammation, ectopic bone formation, cancer or in severe cases death (James et al., 2016). A feasible alternative to mimic bone ECM is the combination of peptides derived from its ECM. Indeed, it has been observed that BMP-2 receptors may synergistically crosstalk with integrins (Dalby et al., 2018). Consequently, the incorporation

of BMP-2-derived peptides together with cell adhesive sequences (mainly RGD) in a well-defined manner is a promising approach to provide hydrogels with osteogenic activity (Oliver-Cervelló et al., 2021). In this regard, we recently developed a multifunctional biomimetic peptide incorporating the RGD and DWIVA (a sequence derived from the wrist epitope of BMP-2) peptides with the capacity to synergistically promote cell adhesion and osteogenic differentiation on model 2D materials *in vitro* and promote new bone formation on titanium implants *in vivo* (Oliver-Cervelló et al., 2021; Oliver-Cervelló et al., 2022).

In addition to endowing cell instructive properties, another challenge when designing hydrogels for cell differentiation is to understand the influence of the intrinsic hydrogel properties in stem cell behavior in comparison to 2D systems. Although these systems are very useful for understanding fundamental biological processes, the employed culturing conditions differ from 3D environments. For instance, on flat surfaces, cells do not have any constrain and can easily establish cell-cell interactions (Carletti et al., 2011). Moreover, relatively stiff surfaces (more than 20 kPa) are known to promote osteogenic differentiation through the mechanotransduction phenomenon, in which cells are able to sense mechanical stimuli and transduce them into biochemical signals that mediate gene expression (Monteiro et al., 2018). On the contrary, in 3D-stiff hydrogels, cell movement is restricted and thus, osteogenic differentiation may be hindered as there may not be enough physical space for cell growth, migration and proliferation (Thiele et al., 2014; Liu et al., 2018).

Such steric hindrance may be overcome with the incorporation of biodegradable sequences on the engineered hydrogels. This is crucial in tissue engineering to allow for timely degradation of the hydrogels during the process of cell differentiation. Of note, such events should be synchronized to ensure that the differentiated cells have sufficient space to proliferate and migrate but also a matrix supporting them (Khetan et al., 2013; Bao et al., 2017). In this regard, the use of matrix metalloproteinases (MMP)-degradable sequences allows the controlled degradation of the hydrogels as cells differentiate. For instance, Wei et al. developed degradable and soft PEG hydrogels incorporating MMP-cleavage sites, the cell adhesive RGD sequence and the osteodifferentiation promoter BMP-2. Such soft hydrogels triggered mesenchymal stem cells (MSCs) spreading and proliferation, and once the hydrogels were degraded and the cells released to a stiff surface, they differentiated towards the osteogenic lineage (Wei et al., 2020). Similarly, the group of Salmeron-Sanchez also engineered degradable PEG-based hydrogels with high affinity for BMP-2, being able to reproduce bone tissue microenvironments with the required biological and mechanical properties to promote MSCs osteogenic differentiation (Trujillo et al., 2020; Dobre et al., 2021).

Nevertheless, finding the optimal proportion of all the elements of the hydrogel (i.e., bioactive cues, degradation sequences and the material itself) to ensure degradation while triggering differentiation and to maintain the required mechanical and chemical properties is not trivial.

In the present work, we engineered a PEG-based hydrogel with the capacity to promote human MSCs spreading and osteogenic differentiation. In detail, the hydrogel was composed of 4-arm poly (ethylene glycol)-maleimide (PEG-4Mal), which was functionalized with a biomimetic peptide recently developed by us containing the

cyclic RGD cell adhesive motif (cRGD) and a BMP-2 derived peptide (DWIVA or its cyclic variant cDWIVA) in a chemically-defined manner (Oliver-Cervelló et al., 2022). Moreover, the hydrogels also incorporated MMP-degradable sequences to allow for a cell-mediated degradation to direct cell differentiation. *In vitro* results demonstrated the capacity of such hydrogel to support cell growth and spreading and to trigger human MSCs osteodifferentiation. This hydrogel may be a promising candidate for stem cell therapies in the field of bone regeneration as well as an implant to promote osteogenic differentiation of bone host cells.

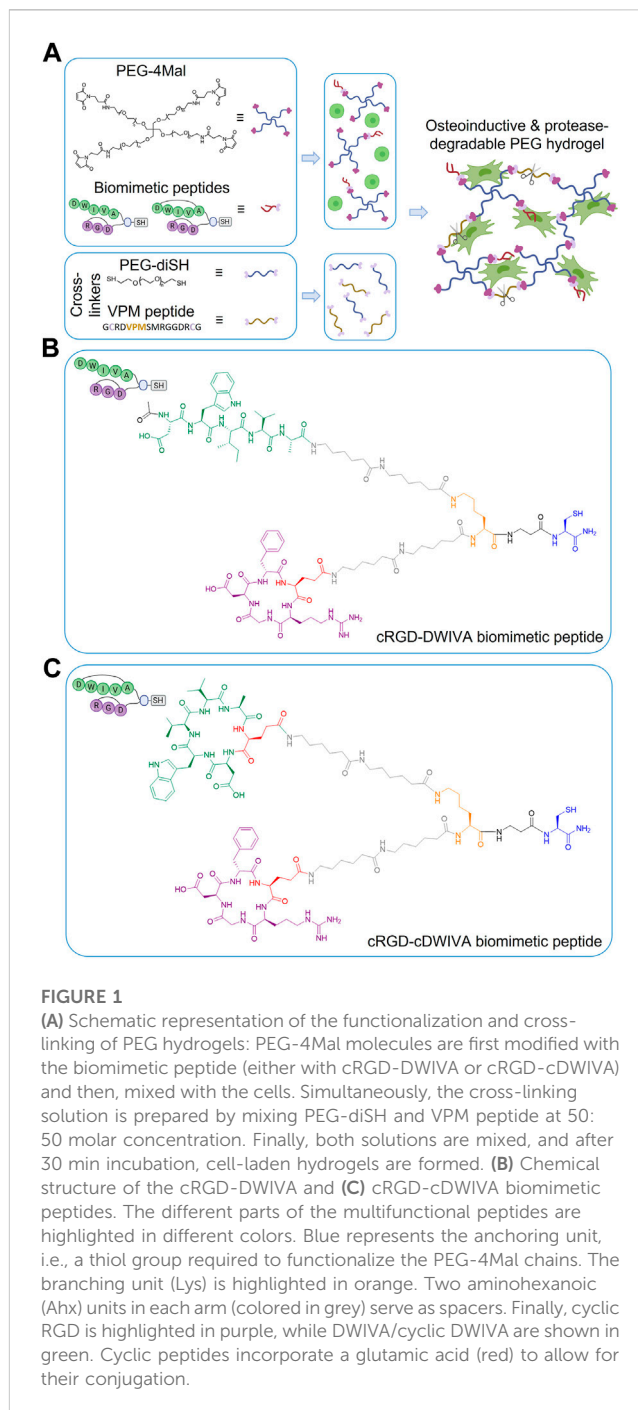
2 Materials and methods

2.1 Peptide synthesis

The synthesis of the cRGD-DWIVA {[cyclic(Arg-Gly-Asp-D-Phe-Glu)-Ahx-Ahx] (Ac-Asp-Trp-Ile-Val-Ala-Ahx-Ahx)-Lys-βAla-Cys-NH₂] and cRGD-cDWIVA {[cyclic(Arg-Gly-Asp-D-Phe-Glu)-Ahx-Ahx] (cyclic(Asp-Trp-Ile-Val-Ala-Glu)-Ahx-Ahx)-Lys-βAla-Cys-NH₂] biomimetic peptides was performed by solid-phase peptide synthesis (SPPS). Fmoc-Rink Amide MBHA resin (164 mg, 0.4 mmol/g for the cRGD-DWIVA, and 150 mg, 0.04 mmol/g for the cRGD/cDWIVA) was used as a solid support. After placing the resin in a propylene syringe, the Fmoc group was removed with piperidine (20% piperidine in DMF, v/v) (1 × 1 min, 1 × 5 min and 1 × 10 min), followed by the addition of Fmoc-Cys (Trt)-OH (0.5 eq.), using OxymaPure (0.5 eq.) and DIC (0.5 eq.) for 90 min in DMF. The excess of reactive positions of the resin were capped with 31 μL of Ac₂O and 57 μL DIEA in DMF for 30 min. Subsequently, the building block (Fmoc-Ahx-Ahx-Lys (Alloc)-βAla) was incorporated stepwise using standard Fmoc/tBu chemistry (5 eq. of each Fmoc-protected amino acid) and OxymaPure/DIC as coupling reagents (5 eq. each).

In the case of the cRGD-DWIVA peptide, the partially protected cyclic RGD peptide [cyclic [R(Pbf)GD(OtBu)]fE], 2.5 eq.—its synthesis and characterization were already published in (Oliver-Cervelló et al., 2022)—was incorporated using PyBOP (4 eq.), HOAt (4 eq.) and DIEA (8 eq.) at pH = 8 for 1 h in DMF. To ensure a quantitative yield, this reaction was followed by a resin washing and a re-coupling of the cyclic peptide [PyBOP (2 eq.), HOAt (2 eq.) and DIEA (4 eq.)]. The Alloc group of the Lys was then removed using catalytic amounts of palladium and two units of Fmoc-Ahx-OH were sequentially coupled to build the second peptidic branch. Finally, the DWIVA sequence was elongated using standard Fmoc/tBu chemistry and the N-terminus acetylated by treatment with Ac₂O/DIEA/DMF (1:2:7, v/v/v) (1 × 5, 2 × 10 min). Cleavage and side-chain deprotection of the peptide were done with TFA/TIS/H₂O (95:2.5:2.5, v/v/v) for 90 min. The obtained crude was dissolved in H₂O/ACN (1:1, v/v) and lyophilized to yield 96.2 mg of crude peptide. The peptide was purified by semipreparative HPLC.

For the cRGD-cDWIVA peptide, the coupling of cyclic RGD, Alloc removal and the insertion of Fmoc-Ahx-OH residues was performed as described for cRGD-DWIVA above. Next, 3 eq. of the partially protected cyclic [D(OtBu)W(Boc)IVAE] [details published elsewhere (Oliver-Cervelló et al., 2022)] were coupled to the peptidyl-resin using PyBOP (4 eq.), HOAt (4 eq.) and DIEA (8 eq.) in DMF for 90 min. A recoupling of the cyclic peptide



using the same conditions was performed to ensure the reaction completion. Finally, the cleavage of the peptide was carried out as previously described yielding 76.6 mg of the crude peptide, which was purified by semipreparative HPLC.

2.1.1 Characterization of the peptides

Matrix-assisted laser desorption/ionization–time of flight (MALDI-TOF) was performed on an Applied Biosystems/MDS SCIEX 4800 Plus with a N₂ laser of 337 nm using α-cyano-4-hydroxycinnamic acid (ACH) matrix (10 mg/mL of ACH in ACN-H₂O (1:1, v/v) containing 0.1% TFA). Sample preparation:

TABLE 1 Hydrogel compositions, considering PEG density, peptide concentration and the PEG-diSH:VPM molar ratio.

Hydrogel code	PEG-4Mal (%)	Peptide (mM)	PEG-diSH:VPM (molar ratio)
PEG-0	5	0	100:0
PEG-50	5	0	50:50
cRGD-DWIVA	5	1	50:50
cRGD-cDWIVA	5	1	50:50

1 μ L of sample solution mixed with 1 μ L matrix were seeded on the MALDI-TOF plate and air-dried.

2.1.2 cRGD-DWIVA

RP-HPLC (linear gradient from 20:100 [0.036% TFA in ACN/0.045% TFA in H₂O] in 8 min: t_R = 6.118 min, >99% purity). MALDI-TOF (m/z): [M + H]⁺ Calcd. For C₉₃H₁₄₅N₂₃O₂₃S 1985.38, found 1985.02.

2.1.3 cRGD-cDWIVA

RP-HPLC (linear gradient from 30:90 [0.036% TFA in ACN/0.045% TFA in H₂O] in 8 min: t_R = 5.253 min, 95% purity). MALDI-TOF (m/z): [M + H]⁺ Calcd. For C₉₆H₁₄₈N₂₄O₂₄S 2054.44, found 2054.06.

The chemical structures of the two peptides are shown in [Figures 1B, C](#). Their MALDI-TOF spectra and HPLC chromatograms can be found in the [Supplementary Material \(Supplementary Figure S1\)](#).

2.2 PEG hydrogel preparation and functionalization

PEG hydrogels were fabricated by Michael-type addition reaction between maleimide-functionalized 4-arm PEG (PEG-4Mal) and dithiol cross-linkers, following a modified protocol described elsewhere ([Trujillo et al., 2020](#)). In detail, the required amount of PEG-4Mal (20 kDa, Biochempeg, United States) was weighted and dissolved in phosphate buffered saline (PBS) to have a final hydrogel concentration of 5% (w/v). Then, the corresponding amount of either cRGD-DWIVA or cRGD-cDWIVA biomimetic peptides was added to the PEG-4Mal solution to have a final concentration of 1 mM of peptide in the hydrogel. The functionalized PEG-4Mal solution was quickly mixed and incubated during 15 min at room temperature (RT) to ensure the peptide-maleimide reaction. Simultaneously, cross-linking solutions of PEG-diSH (3.4 kDa, CreativePEGWorks, United States) or mixtures of 50:50 molar ratio of PEG-diSH and a protease-degradable peptide (VPM peptide, GCRDVPMSMRGGDRCG, purity 95.5%, 1,696.96 g/mol, GenScript, United States) were prepared. Afterwards, 50 μ L hydrogels (or 400 μ L hydrogels for rheological measurements) were produced by mixing PEG-4Mal or functionalized PEG-4Mal with the cross-linking solutions to have a 1:1 molar ratio between thiols and maleimide groups. After adding the cross-linkers, hydrogels were allowed to gel during 30 min at RT. For biological assays, cells were always mixed with the PEG-4Mal-peptide before adding the cross-linker at a density of 30,000 cells/hydrogel (600,000 cells/mL). Biomimetic hydrogels, i.e., hydrogels

functionalized with either the cRGD-DWIVA or the cRGD-cDWIVA, were always cross-linked at 50:50 molar ratio PEG-diSH:VPM. As negative controls, non-functionalized but protease-degradable PEG hydrogels at 50:50 molar ratio PEG-diSH:VPM (PEG-50 condition), and PEG-only hydrogels (without VPM nor peptides, PEG-0 condition) were also designed. Of note, all hydrogel conditions were designed to present the same degree of cross-linking. [Table 1](#) summarizes all the hydrogel conditions used in the present study.

2.3 Physicochemical characterization of PEG hydrogels

2.3.1 Hydrogel porosity and structure

Porosity of hydrogels was calculated by measuring the dry weight of the samples and the wet weight after overnight incubation with PBS as follows:

$$\text{Porosity (\%)} = \frac{m_s - m_0}{m_s} 100$$

Where m_s is the mass of the hydrogel after overnight incubation (swelling equilibrium) and m_0 is the dry mass of the hydrogel.

Afterwards, samples were frozen with liquid nitrogen and lyophilized (Lyobench-85, Noxair, Spain). Then, samples were coated with carbon and the structure of the hydrogels examined by scanning electron microscopy (SEM) (Phenom XL Desktop SEM, PhenomWorld, Netherlands).

2.3.2 Rheological behaviour

Rheological analysis of hydrogels was performed using a Rheometer Discovery RH-2 (TA Instruments, United States) and with samples of 400 μ L volume, which were overnight incubated at 37°C with PBS prior to the measurements to ensure total hydration. The rheometer was equipped with a rough parallel plate geometry (upper plate diameter 20 mm) and measurements were carried out at 37°C. To ensure the hydration of the hydrogels during the measurements, PBS was added to the outer part of the samples. Prior to the measurements, a frequency sweep was performed to determine the angular frequency (ω) range in which the storage modulus (G') was stable, i.e., in the linear viscoelastic region (LVR). Subsequently, strain sweeps from 0.1% to 10% with an angular frequency of 10 rad/s were performed. The gap between the geometry plate and the rheometer base was set in the way that the applied normal force to the hydrogel was always 0.5 N.

TABLE 2 Characteristic parameters used for the calculations of the mesh size of the hydrogels.

Parameter	Value (units)
N_A	$6.022 \cdot 10^{23}$ (1/mol)
R	8.31 ($m^3 Pa/K mol$)
T	309 (K)
l	0.146 (nm) (Cruise et al., 1998)
M_r	44 (g/mol) (Merrill et al., 1993)
C_n	4 (Merrill et al., 1993)
\bar{M}_c	$11,800$ (g/mol) (Raeber et al., 2005)
\bar{M}_n	$20,000$ (g/mol)
\bar{v}	0.893
V_1	18 (cm^3/mol)
χ	0.4 (Clark et al., 2020)

2.3.3 Hydrogel swelling

Hydrogels were weighted and incubated with distilled water during 24 h to study the swelling of the hydrogels. The mass of the hydrogels was measured at 5, 10, 20, 90, 240, and 1,440 min and their swelling capacity calculated as:

$$Q_s (\%) = \frac{m_s - m_0}{m_0} \cdot 100$$

Where Q_s is the swelling ratio in percentage, m_s is the mass of the hydrogel at each time point (after removing the liquid excess) and m_0 is the initial mass of the hydrogel previous to the swelling.

2.3.4 Mesh size calculations

The mesh size (ξ , linear distance between two adjacent cross-links) of the hydrogels was calculated following two different methods. The first one was based on the rubber elasticity theory (Welzel et al., 2011) and the G' obtained from the rheological measurements, and was calculated following the next equation:

$$\xi = \left(\frac{G' N_A}{RT} \right)^{-1/3}$$

Where N_A is the Avogadro's number, R the molar gas constant and T the temperature at which the rheological measurements were performed.

The second method considered the swelling measurements together with the Flory-Rehner theory and the following equations modified by Peppas and Merrill (Canal and Peppas, 1989):

$$\xi = v_{2,s}^{-1/3} (\bar{r}_0^2)^{1/2}$$

Where $v_{2,s}$ is the polymer fraction after swelling and the $(\bar{r}_0^2)^{1/2}$ is the unperturbed mean-square end-to-end distance of the PEG, calculated as:

$$(\bar{r}_0^2)^{1/2} = l \left(\frac{2\bar{M}_c}{M_r} \right)^{1/2} C_n^{1/2}$$

Where l is the average bond length between C-C and C-O bonds in the repeat unit of PEG [-O-CH₂-CH₂-], M_r is the PEG repeating unit molecular mass, C_n is the characteristic ratio of the PEG polymer and \bar{M}_c is the average molecular mass between the cross-links in the network, which can be calculated by:

$$\frac{1}{\bar{M}_c} = \frac{2}{\bar{M}_n} - \frac{\left(\frac{\bar{v}}{V_1} \right) \left[\ln(1 - v_{2,s}) + v_{2,s} + \chi v_{2,s}^2 \right]}{v_{2,r} \left[\left(\frac{v_{2,s}}{v_{2,r}} \right)^{1/3} - \frac{1}{2} \left(\frac{v_{2,s}}{v_{2,r}} \right) \right]}$$

Where \bar{M}_n is the molecular mass of the PEG polymer, \bar{v} is the specific PEG volume ($\bar{v} = \frac{\rho_{H_2O}}{\rho_{PEG}}$), V_1 is the molar volume of the water, χ is the Flory PEG-water interaction parameter, and $v_{2,r}$ is the polymer volume fraction before swelling. All the characteristic parameters for the calculations are included in Table 2.

2.3.5 Hydrogel degradation

After hydrogel formation, hydrogels were incubated with PBS overnight at 37°C to allow them to swell and reach equilibrium. Prior to the degradation assay, all samples were weighted and then, hydrogels were incubated with collagenase at 1 mg/mL (Roche, Switzerland) in PBS. At each time point (1, 2, 4, 8, 24, 48, 72, and 144 h), the liquid excess was removed, and hydrogels were weighted. Afterwards, samples were placed in a new container and fresh collagenase solution was added. The mass loss of the samples was calculated as:

$$m_{loss} (\%) = \frac{m_0 - m_t}{m_0} \cdot 100$$

Where m_{loss} is the percentage of mass lost, m_0 is the mass of the hydrogel after the overnight swelling and m_t is the mass of the hydrogel at each time point.

2.4 Biological characterization of PEG hydrogels

2.4.1 Cell culture

Human MSCs (ATTC, United States) were cultured in Advanced DMEM with D-glucose, non-essential amino acids, sodium pyruvate, and supplemented with 10% FBS, 20 mM HEPES, 2 mM L-glutamine and penicillin/streptomycin (50 U/mL and 50 µg/mL, respectively). When cells reached 80% confluence, they were detached with trypsin-EDTA and plated in new flasks. MSCs were used between passage 4 and 6. Human aortic smooth muscle cells (AoSMCs) were cultured in Growth Medium ready to use (Cell applications, United States). When AoSMCs reached 60%–70% confluence, they were detached following the same steps as in MSCs. AoSMCs were used at passage 11. Cells were maintained at 37°C in a humidified atmosphere with 5% of CO₂. Culture medium was replaced every 2 days.

2.4.2 Viability studies

Human MSCs (30,000 cells/hydrogel) were embedded on the hydrogels and cultured for 1, 3, 7, and 14 days on standard conditions. At each time point, hydrogels were stained for Calcein-AM (3 µM) (Santa Cruz Biotechnology, United States) for live MSCs and propidium iodide (4 µM) (PI, Sigma-Aldrich,

United States) for dead cells. Human MSC-laden hydrogels were incubated for 30 min and afterwards gels were imaged using a fluorescent microscope (Carl ZEISS LSM 800, Germany). Fiji/ImageJ was used to quantify the number of viable cells in relation to the total number of cells (Schindelin et al., 2012).

2.4.3 Cell morphology

After 7 or 14 days in culture, hydrogels loaded with human MSCs were washed with PBS for 15 min at 37°C. Then, cells were fixed with 4% PFA in PBS (v/v) for 60 min and permeabilized with 0.05% Triton X-100 in PBS for 30 min. Afterwards, cells were blocked with 1% BSA in PBS for 60 min. Cytoskeletal actin filament (F-actin) were stained with phalloidin-Alexa Fluor 546 (1:400) in permeabilization buffer for 1 h and nuclei were staining with DAPI (1:1,000) in PBS-Glycine for 15 min. Washing between treatments were done with PBS-Glycine (two times for 7.5 min each). Samples were finally imaged with a fluorescent microscope (Carl ZEISS LSM 800, Germany) and analyzed with Fiji/ImageJ.

2.4.4 Myosin expression

After 7 days in culture, hydrogels loaded with human MSCs were stained with myosin heavy chain (MHC) staining to analyze the differentiation of the cells towards the myogenic lineage. The procedure was similar as previously explained (section 2.4.3), but in this case, myotubes were stained with monoclonal anti-MHC (1:250) primary antibody in BSA 1% for 2 h, followed by Alexa 488 anti-mouse IgG antibody (1:2000) in 0.05% Triton for 1 h.

2.4.5 Alkaline phosphatase (ALP) activity

After incubating the cells 14 days, hydrogels were washed with PBS for 15 min at 37°C. Then, hydrogels were transferred to an Eppendorf and frozen at −20°C until their use. Hydrogels were thawed and M-PER (Thermo Fisher Scientific, United States) was added to obtain the cell lysis and incubated for 30 min at RT. Afterwards to ensure a total extraction of the cell lysis from the hydrogels, samples were destroyed by passing them 10 times through a needle. Then, the lysate was filtered through a column with a filter (GeneMATRIX Universal RNA Purification kit, EURx, Poland) to remove the hydrogel. ALP activity was then quantified using the Sensolyte pNPP Alkaline Phosphatase Activity Kit (AnaSpec Inc., United States). In brief, cells were incubated for 60 min at 37°C with the reagents described in the kit protocol. After stopping the reaction, ALP levels were obtained by measuring the absorbance at 405 nm using a Synergy HTX multimode reader (Bio-Tek, United States). For each condition, ALP activity was normalized to cell number, which was measured by quantifying the released LDH using the Cytotoxicity Detection kitPLUS (Roche, United States). After 7 min incubation at RT with the kit reagents, absorbance values at 492 nm were measured with a microplate reader (Infinite M200 PRO, Tecan Group Ltd., Switzerland).

2.4.6 Gene expression

After incubating the cells during 7 or 14 days, gene expression of osteogenic markers was evaluated by RT-qPCR. At each time point, samples were washed with PBS for 15 min at 37°C and then samples were transferred to an Eppendorf. RNA was extracted using TRIzol Reagent (Invitrogen, United States), following the manufacturer's protocol, with some modifications. In detail, 1 mL of TRIzol was

TABLE 3 List of primer sequences used in RT-qPCR.

Gene	Type	Primer (5' → 3')
GAPDH	Forward	TTGCCATCAATGACCCCTTCA
	Reverse	CGCCCCACTTGATTGTGA
RUNX2	Forward	AAATGCCTCCGCTGTTATGAA
	Reverse	GCTCCGGCCCAAAATCT
COL1A1	Forward	AGGTCCCCCTGGAAAGAA
	Reverse	AATCCTCGAGCACCTGA
ALP	Forward	ATCTTTGGTCTGGCTCCCATG
	Reverse	TTTCCCGTTTACCGTCCAC
Osterix	Forward	TGCTTGAGGAGGAAGTTCAC
	Reverse	AGGTCACTGCCACAGAGTA
OPN	Forward	AGCTGGATGACCAGAGTGCT
	Reverse	TGAAATTATCGGCTGTGGAA
MMP2	Forward	CGGTTTCTCGAATCCATGA
	Reverse	GGTATCCATCGCCATGCT
MyoD	Forward	GGGAAGAGTGCGGCGGTGTCGAG
	Reverse	TCCGAGAAGGGTGCTGCGTGGAA
Desmin	Forward	TCGGCTCTAAGGGCTCCT
	Reverse	CGTGGTCAGAACTCCTGGTT

added to the samples and incubated for 20 min at RT. Then, TRIzol was transferred to a new Eppendorf and RNA isolation was performed adding 0.2 mL of chloroform per mL of TRIzol. The solution was mixed thoroughly by shaking it and incubated for 15 min at RT. Afterwards, samples were centrifuged for 15 min at 12,000 g at 4°C. The obtained aqueous phase containing the RNA was transferred to a new Eppendorf and 1 mL of EtOH 70% was added. To complete RNA isolation, RNA samples were purified using the RNeasy Mini Kit columns (Qiagen, Germany). RNA quantification was performed using a Take3 micro-volume plate (Bio-Tek, United States). cDNA synthesis was obtained using the QuantiTect Reverse Transcription kit (Bio Molecular Systems, Australia). RT-qPCR was carried out on a Mic real time PCR cyclor (Bio Molecular Systems, Australia) and gene expression was assessed by QuantiFast SYBR Green PCR Kit (Qiagen, Germany). GAPDH was used as a housekeeping gene and the relative gene expression levels were evaluated using the $2^{-\Delta\Delta C_t}$ method. Primer sequences are shown in Table 3.

2.5 Statistical analysis

All data presented in this work are given as mean values ± standard deviation. SPSS Statistics 24.0 software (IBM, United States) was used for statistical analysis. When normal distribution was satisfied, one-way ANOVA test with a *post hoc* pairwise comparison using Tukey's (for homogeneous variances) or Tamhane test (for non-homogeneous variances) was performed.

Otherwise, the non-parametric Kruskal–Wallis test was used. p values were considered significant if $p < 0.05$. For physicochemical characterization three ($n = 3$) samples per condition were used, while for biological characterization, each condition was replicated in triplets in each experiment ($n = 3$) and, for quantification, five pictures per sample were used to calculate cell area and viability.

3 Results and discussion

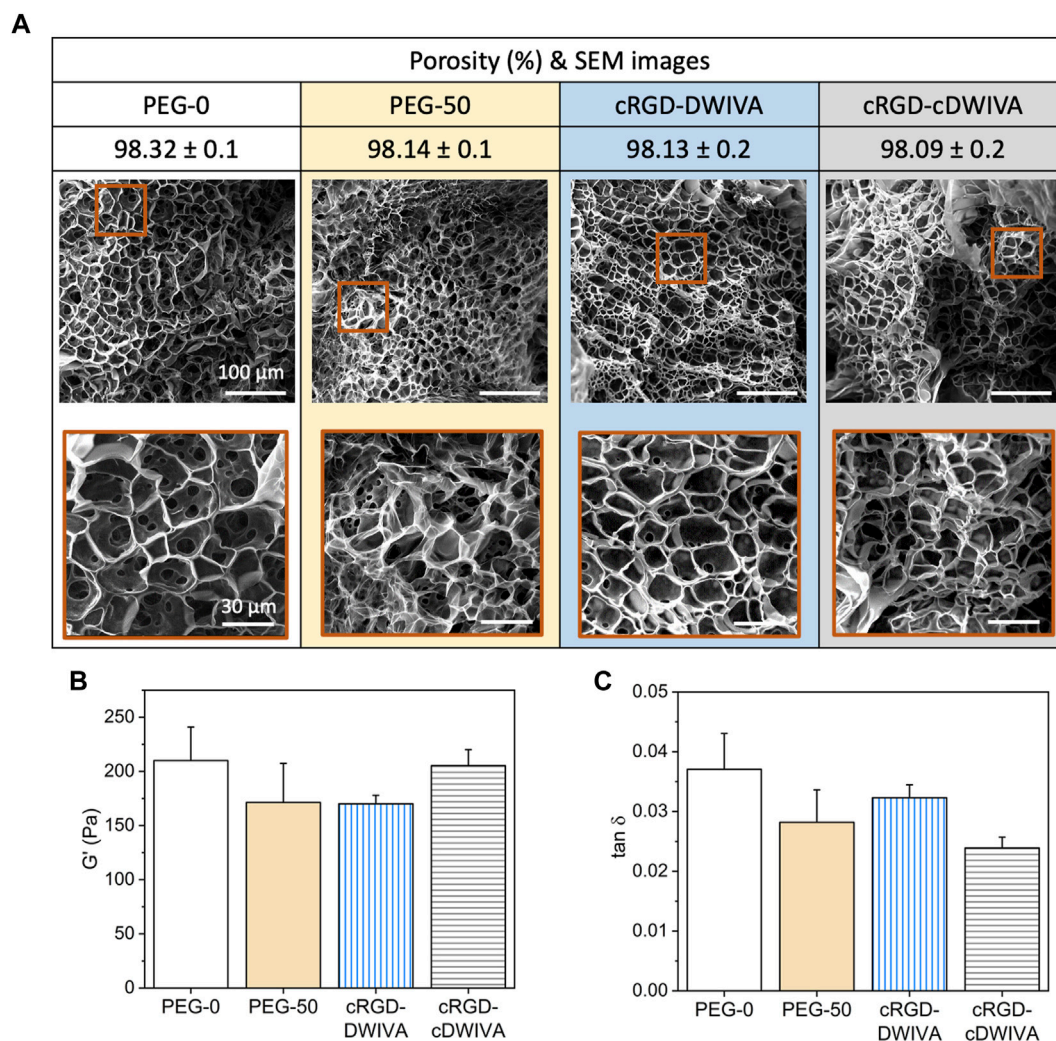
3.1 Design, synthesis and physicochemical properties of the biomimetic hydrogels

Protease-degradable PEG hydrogels were designed with the main objective of recreating the 3D microenvironment of bone ECM. To this end, the hydrogels incorporated i) cell instructive peptides combining the integrin binding peptide RGD and the BMP-2-derived peptide DWIVA, previously shown by us to promote synergistic integrin-growth factor signaling (Oliver-Cervelló et al., 2021); and ii) the MMP-degradable sequence VPM (Turk et al., 2001). Thus, in order to produce the hydrogels, PEG-4Mal was first modified with the thiolated multifunctional biomimetic peptides (either with cRGD-DWIVA or cRGD-cDWIVA, Figure 1). Of note the use of the individual peptides (either RGD or DWIVA) or their combination as a mixture, without controlling their geometrical disposition, failed to support synergistic signaling (Oliver-Cervelló et al., 2021; Oliver-Cervelló et al., 2022), and thus these peptides were not included in the present study. The rationale for using cyclic peptides relies on the fact that conformational restriction is known to enhance the peptide's receptor affinity and provide higher biological potential. Indeed, cyclization of RGD has been demonstrated to enhance the selectivity of this peptide towards integrins involved in cell adhesion and osteodifferentiation, such as $\alpha v \beta 3$ (Mas-Moruno et al., 2016). On the other hand, cyclization of the BMP-2-derived DWIVA was shown to retain or even enhance the potential of the linear counterpart, although the exact effect of the conformation in its binding to BMP receptors has not been elucidated (Oliver-Cervelló et al., 2022). The peptide-functionalized PEG-4Mal was then cross-linked with dithiolated cross-linkers (PEG-diSH and/or VPM peptide—Figure 1A) according to a recently published protocol (Trujillo et al., 2020), to allow hydrogel formation and endow the system with protease-degradable properties. It should be mentioned that biodegradable hydrogels were always fabricated at a 50:50 molar ratio between the PEG-diSH and VPM cross-linkers. Non-degradable PEG hydrogels (PEG-0) were also used as negative (non-degradable) controls with the same degree of cross-linking as the functionalized hydrogels. Moreover, non-functionalized but biodegradable PEG hydrogels, i.e., with the VPM sequence (PEG-50), were also included as controls. It is important to remark that all hydrogels were always formed using the same concentration of cross-linkers, ensuring both the same degree of cross-linking for all hydrogel conditions and a stoichiometric balance between the free thiols present in the cross-linkers and the remaining free maleimide groups (unreacted) on the PEG-functionalized molecules. PEG hydrogels were formed by Michael-type addition, which is considered a very efficient reaction (Darling et al., 2016;

Martínez-Jothar et al., 2018; Ravasco et al., 2019). In this regard, the thiol-maleimide conjugation is a click reaction, being fast, straight forward and easily controlled by pH modification (Darling et al., 2016; Martínez-Jothar et al., 2018; Ravasco et al., 2019). Interestingly, such Michael-type addition has been previously used in PEG-based hydrogels without having any detrimental effect in the bioactivity, compatibility and cell viability, mainly, because the reaction takes place under physiological conditions, without generating any by-products and with no requirements of adding initiating chemicals (which may be toxic) to control the reaction (Nair et al., 2014; Kim et al., 2016; Jansen et al., 2018). The high efficiency of the Michael reaction allows the control of the hydrogel stiffness, resulting in broader stiffness ranges compared to other cross-linking reactions (Phelps et al., 2012). It should also be mentioned that the thiol-maleimide reaction is not only used to cross-link the hydrogels, but also to functionalize them (as in the present study). Thus, cysteine-containing molecules, i.e., proteins, peptides or GFs, have commonly been used to modify the bulk PEG structure, providing hydrogels with high bioactivity (Lutolf and Hubbell, 2003; Cambria et al., 2015). In this regard, functionalized PEG hydrogels have been widely employed in biomedical applications, including drug delivery, regenerative strategies or surface modifications (Peyton et al., 2006; Zhu, 2010; Li et al., 2018; Jansen et al., 2022). For instance, VEGF-loaded-PEG hydrogels were engineered as a release platform to promote pancreatic islet vascularization (Phelps et al., 2015), while PEG-based systems modified with chitosan, enhanced proliferation and differentiation of neurospheres-like progenitors cultured in the self-healing hydrogels (Tseng et al., 2015). Furthermore, PEG is characterized by its high biocompatibility, easily tunable mechanical properties, resistance to protein adsorption and non-immunogenic reactions, which makes it an ideal candidate for tissue engineering (Alcantar et al., 2000; Zhu and Marchant, 2011; Chang et al., 2019; Mandal et al., 2020).

Physicochemical properties of the engineered hydrogels were first evaluated by SEM (Figure 2A). It is worth noting that the porosity values obtained from SEM images do not probably correspond to the actual porosity of the samples in the hydrated state due to the freeze-drying of hydrogels. However, SEM images allowed us to compare the internal structure and pore sizes in the different hydrogel conditions. The four hydrogels showed similar structural morphology with interconnectivity between different pores, indicating that neither the functionalization of the PEG with the biomimetic peptides nor the addition of the VPM during the cross-linking process had any significant effect in terms of structural morphology. Furthermore, the hydrogels were highly porous, with values about 98% of bulk porosity (Figure 2A). These results ensure that the possible different cellular behavior observed in the functionalized hydrogels can be attributed to the presence of the biomimetic peptides and not to their structure or porosity.

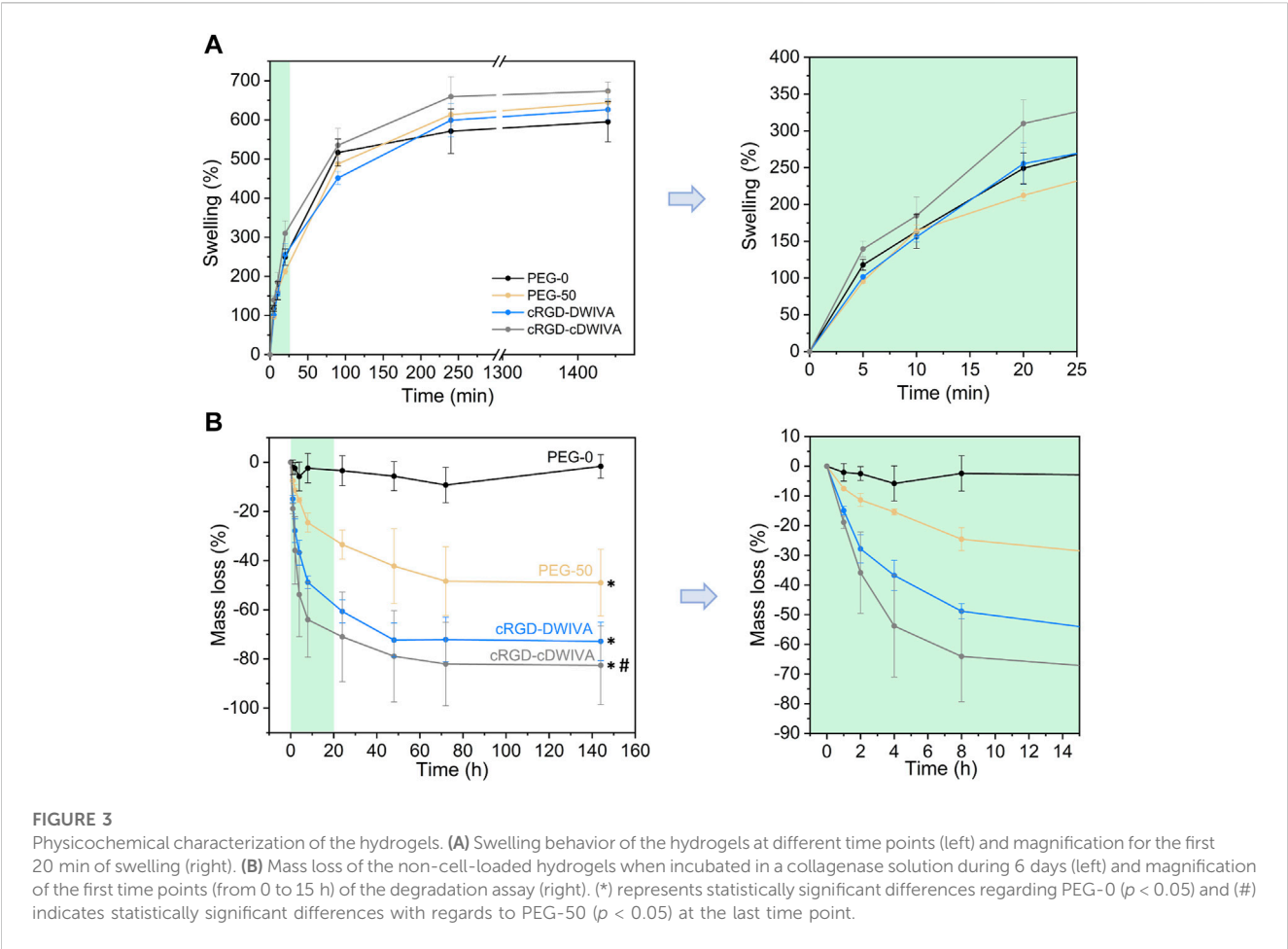
Rheological measurements were next performed to assess the viscoelastic properties of the hydrogels (Figures 2B, C). Such viscoelasticity is characteristic of this kind of materials, due to the intrinsic properties of the polymer and the great amount of water entrapped in its network. Having systems with viscoelastic properties may be a great advantage, as it has been demonstrated that many soft tissues and ECMs in the human

**FIGURE 2**

Physicochemical and mechanical characterization of the hydrogels. (A) Porosity and structural morphology of the hydrogels obtained by SEM analysis, showing the general structure (scale bar = 100 μ m) and a higher magnification area (scale bar = 30 μ m) for each condition. (B) Storage modulus (G') and (C) damping factor ($\tan \delta$) of the four hydrogel conditions obtained by strain sweeps in the range of 0.1%–10% strain. Statistically significant differences ($p < 0.05$) were not observed between any of the conditions.

body present this type of mechanical behavior (Chaudhuri et al., 2016; 2020; Chaudhuri, 2017). Thus, strain sweep measurements in the LVR were performed, showing that bulk non-degradable PEG hydrogels without functionalization exhibited a G' of about 200 Pa (Figure 2B), which corresponds to a stiffness of about 600 Pa. Similar values were obtained when adding the biodegradable cross-linker and/or the biomimetic peptides in the hydrogels, indicating that none of both components had any significant effect in the G' values. This value of stiffness may seem rather low for designing hydrogels for bone tissue engineering. Indeed, hydrogel stiffnesses for bone regeneration have been traditionally set in the range of >20 kPa, with values much more similar to the ones presented by osteoid tissues (Sen et al., 2009; Huebsch et al., 2015). Although such values may have a positive effect in the mechanotransduction phenomenon, at such range of stiffness, the ability of the cells to spread, grow and initiate osteodifferentiation through biochemical cues may

be hindered. (Bao et al., 2017; Major et al., 2019). Furthermore, such difference in stiffness between our hydrogels ($G' \approx 200$ Pa) and the traditional ones for bone regeneration ($G' > 20$ kPa) is probably translated in differences in degradability and structure of the systems, both having an important effect in cell traction forces developed during hydrogel degradation and the remodeling process of the cells. These cellular tractions have been demonstrated to be crucial in MSCs osteogenic differentiation, being mediated by the cell degradation process of the matrices and, more important, being independent of matrix mechanics (Khetan et al., 2013; Clark et al., 2020). Of note, finding the best approach depending on the application is paramount to ensure the successful performance of the hydrogel. Another interesting feature derived from the rheological measurements, is the similar damping factor presented by the different hydrogels (Figure 2C), indicating that the ratio between G'' and G' for all the conditions was very similar, without



observing statistically significant differences. Thus, the viscoelastic properties of the four conditions were comparable, obtaining G'' values of about 5 Pa for the four conditions.

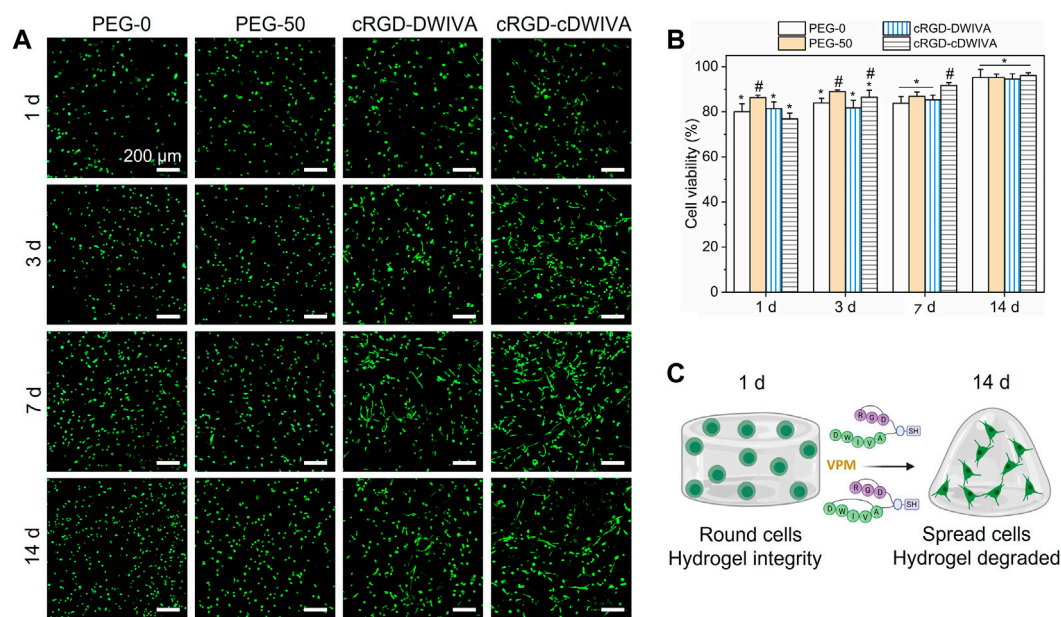
The swelling ratio of the hydrogels was also measured (Figure 3A). This parameter is important to shed light on the hydrogel network structure as well as on how the distance between cross-linking affects the structure. In our system, the four hydrogels presented a similar swelling behavior, reaching values of 600%–650% at 24 h, with no statistically significant differences between conditions. In general, longer cross-linkers (PEG-diSH) will restrain less the swelling capacity of the hydrogels in comparison to shorter chains (VPM). Hence, degradable hydrogels (PEG-50, cRGD-DWIVA and cRGD-cDWIVA) would be expected to swell less than the PEG-0; however, this was not the case. On one hand, this could be explained by the fact that the differences in molecular weight between cross-linkers are not large enough to be reflected on the swelling of the hydrogels. In addition, the VPM peptide is slightly positive charged, which may enhance the affinity for water molecules in comparison to the PEG-diSH. Nonetheless, the swelling ratios obtained in this study are in the same order of magnitude than the ones found in the literature working with PEG-4Mal networks with similar concentrations as ours (Clark et al., 2020; Wei et al., 2020).

Moreover, mesh size of the hydrogels was also calculated either by applying the rubber elasticity theory combined with the G'

TABLE 4 Mesh size (ξ) calculations for the different hydrogel conditions.^a Mesh size calculated by rubber elasticity theory and with G' from rheology.^b Mesh size calculated by Flory-Rehner equations using theoretical \bar{M}_c .^c Mesh size calculated by Flory-Rehner equations using experimental \bar{M}_c from swelling experiments.

Hydrogel	$\xi \pm \text{SD}$ (nm) ^a	$\xi \pm \text{SD}$ (nm) ^b	$\xi \pm \text{SD}$ (nm) ^c
PEG-0	27.4 ± 1.3	29.6 ± 0.5	24.7 ± 0.7
PEG-50	29.4 ± 2.0	30.8 ± 0.2	26.0 ± 0.1
cRGD-DWIVA	29.3 ± 0.4	30.2 ± 1.6	25.2 ± 1.7
cRGD-cDWIVA	27.5 ± 0.7	32.0 ± 0.1	27.4 ± 0.2

values from rheology or by the Flory-Rehner equations and the \bar{M}_c values (either theoretical or experimental—obtained from swelling assays). The results are summarized in Table 4. Mesh sizes calculated by the rubber elasticity theory were of ≈ 27 – 29 nm for all the conditions, with no differences between them. Interestingly, from the Flory-Rehner equation, slightly bigger mesh sizes for each condition were obtained using the theoretical \bar{M}_c in comparison to the experimental one. Nonetheless, the mesh size obtained by the three different approaches were very similar, indicating a good correlation between the assays. Of note, the mesh size of the hydrogels is in accordance with other works (Clark et al., 2020;

**FIGURE 4**

Cell viability on the hydrogels. (A) Live/dead staining (live in green and dead in red) at 1, 3, 7, and 14 days in culture (scale bar = 200 μ m). (B) Quantification of cell viability expressed by the ratio of live cells respect to the total number of cells. Different symbols denote statistically significant differences between conditions for each time point ($p < 0.05$). (C) Schematic representation of cell behavior over time in the presence of VPM and the biomimetic peptides (figure created with BioRender).

Dobre et al., 2021). Such mesh sizes would allow the diffusion of nutrients and oxygen through the hydrogels and thus, support cell growth.

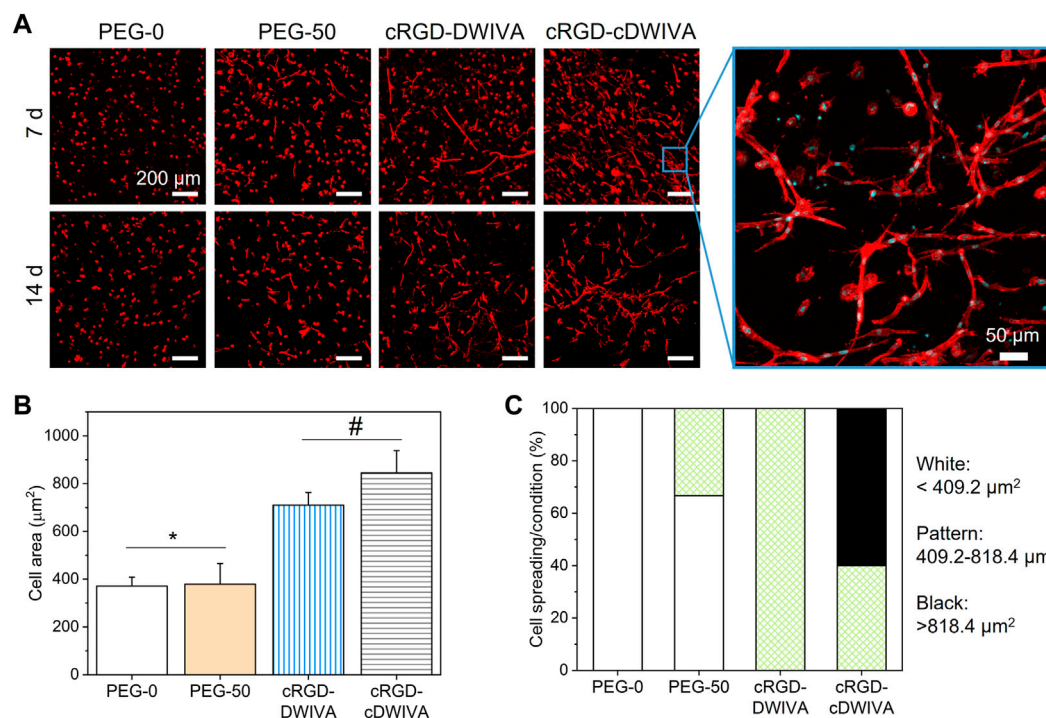
In addition, degradability of the hydrogels was studied by incubating them in a collagenase type I solution (Figure 3B). The degradation assay was initiated when hydrogels reached swelling equilibrium (after overnight incubation), considering the mass of the swollen hydrogels as the initial mass for the experiment. As expected, non-degradable hydrogels (PEG-0) were stable during 6 days of incubation. However, when introducing the VPM cross-linker, which is a protease-degradable sequence, hydrogels (PEG-50, cRGD-DWIVA and cRGD-cDWIVA) began to degrade, reaching a plateau at 72 h. After 2 h, the degradation rate was already noticeable, and PEG-50 hydrogels exhibited about 8% of mass loss, whereas cRGD-DWIVA and cRGD-cDWIVA hydrogels presented a higher, 15% of degradation. Of note, the differences observed in the degradation rate between PEG-50 and the biomimetic hydrogels (cRGD-DWIVA and cRGD-cDWIVA) were more evident with increasing incubation times, and, for instance, at 8 h, PEG-50 had a $\approx 25\%$ of mass loss in contrast to the $\approx 55\%$ of the biomimetic hydrogels, being twice faster their degradation behavior. Indeed, after 6 days, PEG-50 exhibited about 50% of mass loss, while the biomimetic hydrogels showed about 80% degradation. More insights would be required to better understand such differences in degradability; nonetheless, similar degradation rates have been observed in PEG hydrogels modified with biological cues and cross-linked with the VPM sequence (Trujillo et al., 2020).

Together, the data obtained from the physicochemical characterization of the hydrogels demonstrated the capacity to

modify the intrinsic properties of the systems to control their stiffness, swelling and degradation rates. Of note, the similar properties, i.e., swelling, porosity and stiffness, shown in the different hydrogel conditions ensure that the possible changes observed in the biological characterization can be attributed to the presence of the protease-degradable sequences as well as the biomimetic peptides, and not to the physicochemical properties of the hydrogels.

3.2 Biomimetic hydrogels support cell viability and spreading

After the physicochemical characterization, hydrogels laden with human MSCs were produced and their biocompatibility was assessed by cell viability studies (Figure 4). The hydrogels were prepared similarly to the ones for physicochemical assays, but in this case, cells were mixed directly in the PEG-4Mal solution (already functionalized with the biomimetic peptides) previous to cross-linking (see section 2.2 for details). Notably, the encapsulation of the cells in the hydrogels did not have any effect in the cross-linking process. Then, live/dead staining (live cells in green and dead cells in red) at 1, 3, 7, and 14 days was performed (Figure 4A). At each time point, most of the cells were alive, indicating the great biocompatibility of PEG. The highest number of dead cells was observed at day 1, which was associated to the fabrication process of the hydrogels, in which cells were subjected to high stress. On one hand, gelation of the hydrogels was allowed during 30 min at RT, and additionally, cells were thoroughly mixed with the PEG-4Mal solutions to achieve homogeneous distribution of the cells in the

**FIGURE 5**

Cell morphology on the hydrogels. (A) Actin staining of the embedded human MSCs after 7 and 14 days in culture (scale bar = 200 μm) together with a high magnification image showing cell morphology (scale bar = 50 μm). (B) Quantification of cell spreading after culturing the cells 7 days inside the hydrogel. (C) Cell area classification in round, spread and super spread after 7 days in culture. A round cell was considered every cell with smaller area than the biggest one in the PEG-0 condition (409.2 μm²). All cells between the biggest area of the cells in the PEG-0 condition but smaller than twice that area (818.4 μm²) were considered spread, while the super spread cells were the ones bigger than 818.4 μm². Different symbols denote statistically significant differences between conditions ($p < 0.05$).

loaded hydrogels, both processes decreasing cell viability. For quantification purposes, cell viability was calculated as the ratio between live cells and the total number of cells within the hydrogel (Figure 4B). As expected, the lowest cell viability was observed at day 1, with values of about 80% for all the conditions. Nevertheless, cell viability improved over time, reaching values higher than 95% after 14 days in culture, with no significant differences observed between conditions. Furthermore, in PEG-0 hydrogels (not degradable nor biomimetic) cells presented a roundish-like morphology, characteristic of 3D microenvironments where physical constraints due to the polymeric dense matrix do not allow cell spreading (Major et al., 2019). However, from day 3 onwards, biomimetic hydrogels, i.e., cRGD-DWIVA and cRGD-cDWIVA, exhibited cell spreading, especially at 7 and 14 days (Figure 4C). Also, PEG-50 at day 7 started to present some spread cells, although to a lower extent in comparison to the biomimetic peptides, which confirms the importance of installing both biodegradability and bioactivity in the hydrogels to promote cell spreading.

To further study cell morphology, actin staining was performed at day 7 and 14 (Figure 5A). Cytoskeletal actin labeling confirmed the capacity of the cRGD-DWIVA and cRGD-cDWIVA biomimetic peptides to promote cell spreading due to the degradation of the hydrogel as well as the stimulation of the cells, showing well-defined actin fibers. On the contrary, cells embedded in PEG-0 were totally round. Although at 7 days PEG-50 hydrogels presented some spread

cells, degradability alone was not enough to promote cell spreading and it was only when combined with the biomimetic peptides that cells were able to effectively spread. Indeed, quantification of cell morphology at day 7 (Figure 5B) showed that both biomimetic peptides promoted the highest cell spreading, reaching cell area values of about two times bigger than the PEG-50 control. Notably, no significant differences were observed between PEG-0 and PEG-50, verifying that degradability is not enough to support cell spreading if bioactive cues are not present in the systems. Moreover, cells were classified as round, spread and super spread depending on their area at day 7, considering a round cell every cell with smaller area than the biggest one in the PEG-0 condition (Figure 5C). Such classification showed that introducing degradability alone increased up to 33% the number of spread cells. Interestingly, when functionalizing the hydrogels with the cRGD-DWIVA all the cells were classified as spread, while the modification with the cRGD-cDWIVA resulted in 40% of spread cells and 60% of super spread cells, indicating a positive effect in cell area by the cyclization of DWIVA.

Interestingly, higher magnification of the embedded cells in the biomimetic conditions showed the characteristic morphology of osteoblasts, which is an initial indicator of the successful differentiation of the human MSCs towards the osteogenic lineage. Such cell morphologies have been also observed in PEG hydrogels loaded with MSCs with comparable stiffness values to our systems and presenting osteogenic differentiation cues (Shekaran et al., 2014; Clark et al., 2020; Nasello et al., 2020). Of note, only in the biomimetic

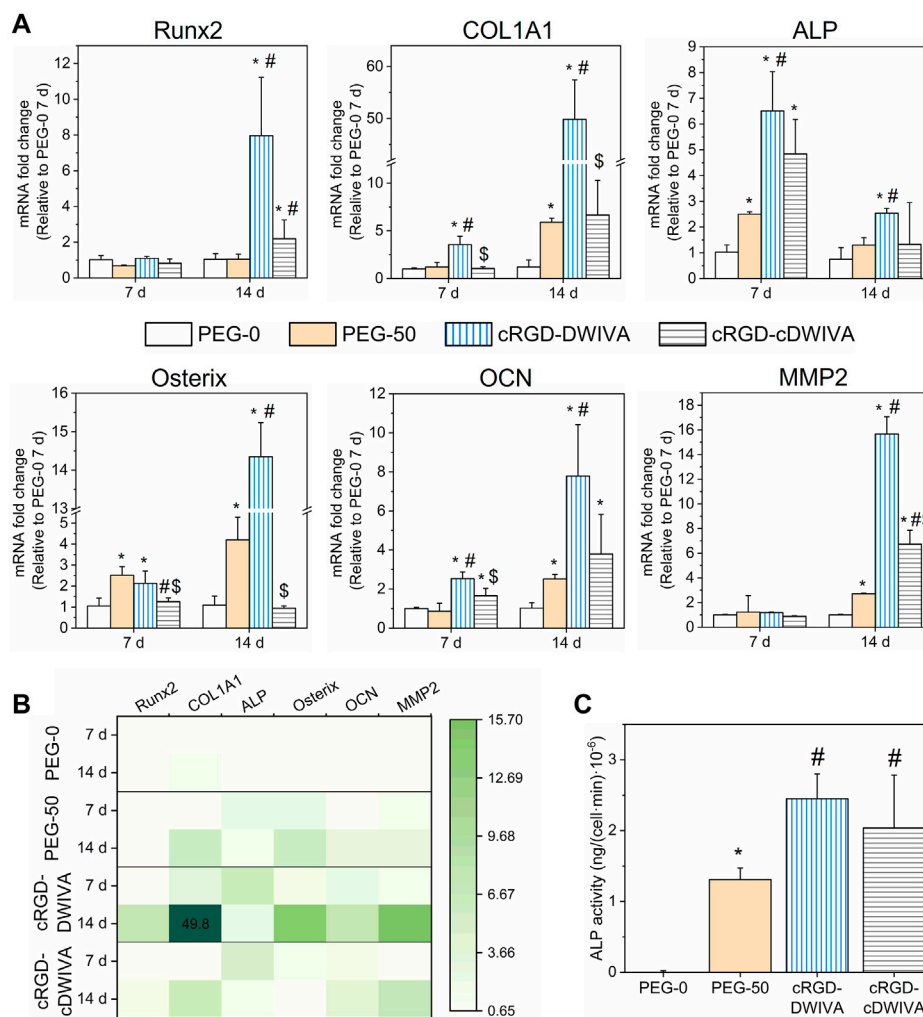


FIGURE 6

Osteogenic differentiation of human MSCs in the laden hydrogels. **(A)** Expression of Runx2, COL1A1, ALP, Osterix, OCN and MMP2 genes obtained by RT-qPCR analysis at 7 and 14 days. (*) represents statistically significant differences regarding PEG-0, (#) expresses statistically significant differences with respect to PEG-50, and (\$) indicates statistically significant differences with regards to cRGD-DWIVA ($p < 0.05$). **(B)** Heatmap of the studied genes, summarizing the expression of each gene, condition and time point. **(C)** ALP activity after 14 days in culture of the different hydrogel conditions. Different symbols denote statistical significance difference between conditions ($p < 0.05$).

hydrogels, MSCs were able to form “cell branches,” a characteristic phenomenon that has been also observed in other soft hydrogels for bone tissue engineering (Campos et al., 2016). We hypothesize that such “cell branches” may be related with the mesh size of the hydrogels, which was of $\approx 24\text{--}30\text{ nm}$. This mesh size is not big enough to initially allow cell migration around the hydrogel. However, cell protrusions may be generated through the mesh due to the degradation process of the hydrogels (in which mesh size will progressively become bigger) and the presence of the biomimetic peptides.

3.3 Biomimetic hydrogels promote human MSCs osteogenic differentiation

The osteogenic lineage commitment of human MSCs was first evaluated by studying osteospecific gene expression at 7 and

14 days by means of RT-qPCR. In detail, Runx2, COL1A1, ALP, Osterix and OCN genes were measured (Figure 6A). At day 7, an overexpression of COL1A1, ALP, Osterix and OCN genes was observed for the cRGD-DWIVA condition in comparison to the negative PEG-0 control. Such differences were also statistically significant in comparison to the biodegradable hydrogels without peptides (PEG-50), except for the Osterix gene, which was also overexpressed in PEG-50, reaching similar values to the cRGD-DWIVA. Nonetheless, the overexpression of Osterix in PEG-50 hydrogels was not surprising, as some studies have related the overexpression of such gene with the activation of some MMPs, such as MMP13, MMP9 or MMP2, the last two highly involved in matrix remodeling (Dai et al., 2015; Liu et al., 2020; Nishimura et al., 2012). On the other hand, only ALP and OCN genes were overexpressed for cRGD-cDWIVA, indicating that cyclization of the DWIVA motif

may have a detrimental effect (at least at 7 days) on the osteogenic capacity of the biomimetic peptide. The highest osteogenic expression at day 7 was observed for the ALP gene, for both cRGD-DWIVA (with almost a 7-fold increase compared to PEG-0) and cRGD-cDWIVA (with a 5-fold change). Remarkably, Runx2 was not expressed in any of the conditions at 7 days, although at day 14, it was observed an 8-fold increase for the cRGD-DWIVA and 2-fold for cRGD-cDWIVA, both showing a significant increase in comparison to PEG-0 and PEG-50. Noteworthy, at day 14, cRGD-DWIVA promoted a high expression of all the characteristic osteogenic genes, reaching values of 50-fold change for COL1A1. These results demonstrate the osteogenic capacity of the cRGD-DWIVA biomimetic peptide. However, the cRGD-cDWIVA was only able to express Runx2 at day 14, confirming the previous observation at day 7, in which the cDWIVA lost its bioactivity in terms of osteodifferentiation. We previously reported that in 2D (Oliver-Cervelló et al., 2022), the cRGD-cDWIVA peptide was able to maintain the osteogenic differentiation capacity in comparison to cRGD-DWIVA and, in some cases, even improve it. Such discrepancies reflect how critical is the translation of *in vitro* testing from 2D to 3D environments, in which cell behavior may substantially vary (Duval et al., 2017; Mirbagheri et al., 2019; Jensen and Teng, 2020).

Moreover, the overexpression of ALP and Osterix genes is paramount in our system, as they are involved in the Smad-independent pathway (Wei et al., 2015; Sano et al., 2017) [pathway triggered by our biomimetic peptides (Oliver-Cervelló et al., 2021)]. This is in agreement with the high expression of ALP at day 7 and Osterix at day 14 for the cRGD-DWIVA. Interestingly, PEG-50 hydrogels (incorporating the biodegradable cross-linker but not the biomimetic peptides), were also able to promote ALP expression, especially at day 7, which could be explained by the fact that such gene has been demonstrated to be involved in the formation of the organic phase of bone ECM. In this regard, COL1A1 and OCN genes are also influenced by bone ECM formation, which contributes to the high expression of both genes for the cRGD-DWIVA condition at day 14 (Frank et al., 2002; Granéli et al., 2014; Viti et al., 2016).

As biodegradable hydrogels containing the VPM sequence were engineered in this study, MMPs expression was also assessed. The full degradable sequence incorporated in the hydrogels was the GCRDVPMS↓MRGGDRCG peptide, the ↓ indicating the cleavable site for MMPs. Among the MMP family, MMP2 and MMP9 have been reported for being highly sensitive to the VPM cleavable site (Jha et al., 2016; Chen Weikai et al., 2021). Thus, MMP2 gene expression was also analyzed by RT-qPCR. In this regard, no expression of MMP2 was observed after 7 days in culture, which could be explained by the fact that cells did not have enough time to degrade the hydrogel network and produce new ECM. Indeed, at day 7, hydrogels still presented a good consistency. On the contrary, at day 14, PEG-50 hydrogels showed a 3-fold expression in comparison to PEG-0 (which did not include the degradable sequence), suggesting the activation of MMP2 and ultimately leading to VPM cleavage. More relevantly, the incorporation of both biomimetic peptides, either cRGD-

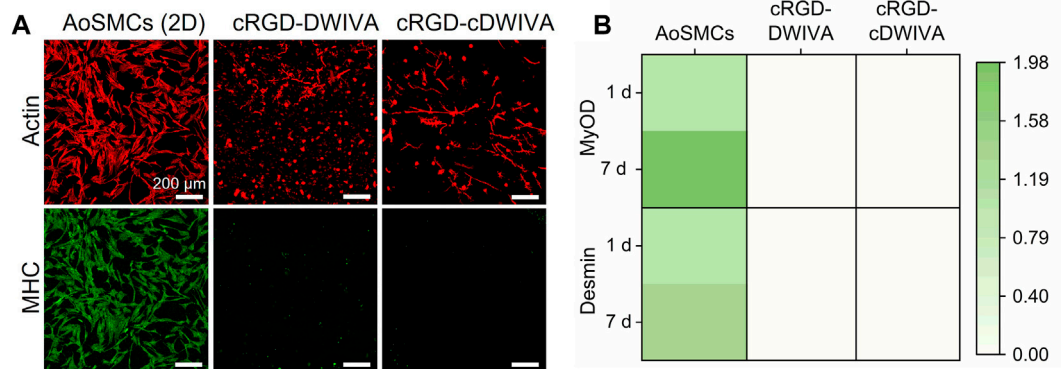
DWIVA or cRGD-cDWIVA, significantly increased the MMP2 gene expression, highlighting the importance of adding biologically active cues, i.e., cRGD and DWIVA/cDWIVA, to stimulate cell behavior. These results are in accordance with the cell spreading data (Figure 5), in which it was shown that the degradation of the hydrogel (and consequently decreasing the physical restriction for the cells) was not enough to promote full cell spreading and that the presence of the biomimetic peptides was paramount to orchestrate cell behavior. However, the 3-fold expression of MMP2 observed in the PEG-50 at 14 days (as well as the 5-fold change expression of COL1A1) could be an indication of nascent protein secretion by the cells due to the presence of the VPM sequence, as both genes are involved in the remodeling of ECM and the production of proteins, which could contribute (together with the degradation—and thus the softening of the hydrogel) to the spreading of some cells in that condition (Figure 5). Of note, MMPs are transcriptional targets of Runx2 (Wessely et al., 2019). Hence, MMP2 expression may be dependent on Runx2 expression, as observed at day 14. Moreover, at that time point, cells have been able to degrade to a higher extent the hydrogels and thus, produce more ECM, contributing to the higher expression of MMP2, especially in the biomimetic conditions.

Gene expression results were summarized in a heatmap (Figure 6B), clearly showing the activation of a higher number of genes for the cRGD-DWIVA and cRGD-cDWIVA conditions, especially for the former at day 14.

To further verify the osteogenic differentiation as well as to correlate the change of the cell genotype with a modification of its phenotype, ALP activity was measured at 14 days (Figure 6C). The biomimetic peptides significantly enhanced ALP activity with regards to PEG-0. However, PEG-50 also expressed ALP activity, although to a lower extent compared to the biomimetic conditions. cRGD-DWIVA and cRGD-cDWIVA exhibited the highest ALP activity values, both presenting statistically significant differences in comparison to PEG-50. These ALP activity results are in accordance with the ones from RT-qPCR.

The results presented here differ from the work of Madl et al., where alginate hydrogels functionalized with an RGD and DWIVA mixture were not able to promote ALP activity (Madl et al., 2014). However, in their work, the spatial disposition between both motifs was not controlled, which seemed to be a key factor to promote synergistic signaling between both peptides, as we recently demonstrated (Oliver-Cervelló et al., 2021). Moreover, the biomaterial employed to produce the hydrogels was also different, which may influence cell behavior as well.

Very recent studies have demonstrated the importance of installing biodegradability in hydrogels for bone tissue engineering, being such parameter even more critical than the material stiffness to regulate osteogenesis (Sun et al., 2022). In this regard, Peng et al. showed that fast degradation of soft PEG hydrogels was essential to stimulate MSCs and to further trigger their osteogenic commitment (Peng et al., 2018). Similarly, Lutolf et al. demonstrated that bone remodeling in a critical defect in rat cranium was totally dependent on the proteolytic sensitivity of the gels (Lutolf

**FIGURE 7**

Myogenic differentiation of the human MSCs embedded in the PEG hydrogels. **(A)** Actin and myosin heavy chain staining at 7 days. Human AoSMCs cultured on glass were used as positive controls (scale bar = 200 μ m). **(B)** Heatmap representing the expression of characteristic genes of myogenesis (MyOD and Desmin) at 1 and 7 days. The mRNA expression levels were normalized to the housekeeping gene GAPDH.

et al., 2003). Moreover, the degradation of the hydrogels facilitated cell spreading and cellular traction, which contributed to the human MSCs osteogenic differentiation (Khetan et al., 2013). Such findings have not only been observed in bone regeneration but also in neurogenesis, where neural progenitor cell stemness was strongly related to the hydrogel biodegradability rather than the matrix stiffness, revealing that degradability may enhance cell-mediated matrix remodeling and thus, influence cell mechanoresponse (Madl et al., 2017). All these examples support our findings, in which, with low stiffness hydrogels, osteogenic differentiation is possible due to both the presence of the biomimetic peptides (that act as biochemical cues for the cells) and degradability (that allows cell spreading and induces cellular traction). Indeed, other hydrogels with soft properties have also shown the capacity to differentiate cells towards the osteogenic lineage (Mullen et al., 2013; Jha et al., 2014; Clark et al., 2020; Wei et al., 2020; Sun et al., 2022).

On the whole, our PCR data and the values of ALP activity clearly indicate the osteogenic commitment of MSCs on the functionalized hydrogels; nonetheless, taking into account that MSCs showed a notable elongated morphology and numerous cell-cell contacts, we wanted to exclude any possible (partial) differentiation towards the myogenic lineage. Thus, characteristic myogenic markers, namely, MHC staining and MyOD and Desmin gene expression, were also studied (Figure 7) (Xu et al., 2015; Yi et al., 2017). Human AoSMCs cultured on glass were used as positive control. MHC staining of the cells demonstrated that only the AoSMCs cultured on glass exhibited myosin, while the biomimetic hydrogels functionalized with either the cRGD-DWIVA or the cRGD-cDWIVA did not present any. The expression of the characteristic myogenic genes MyOD and Desmin was also investigated. Interestingly, none of the biomimetic hydrogels expressed these myogenic genes. Similar results were obtained by Wei et al., in which soft PEG hydrogels containing osteogenic cues, i.e., BMP-2, did not express myogenic markers (Wei et al., 2020).

All in all, these biological results demonstrate the capacity of the protease-degradable and biomimetic PEG hydrogels to promote cell spreading and human MSCs osteogenic differentiation.

4 Conclusion

In conclusion, the functionalization of PEG hydrogels with biomimetic peptides combining the cRGD sequence with BMP-2-derived motifs (DWIVA or cDWIVA) in a chemically-defined manner resulted in a novel class of 3D biomaterials with unique features: i) fine-control of the physicochemical properties; ii) protease-dependent degradability; and iii) presentation of biochemical cues to recreate bone ECM. In particular, the hydrogels functionalized with cRGD-DWIVA were able to significantly trigger human MSCs spreading and osteogenic differentiation. Recently, we demonstrated the capacity of these two peptides to promote integrin and BMPR synergistic signaling on 2D materials, notably only when presented in a geometrically controlled fashion, but not when exposed individually or as mixture (Oliver-Cervelló et al., 2021; Oliver-Cervelló et al., 2022). In this work, such spatially-tuned signaling is translated to 3D matrices and coupled with protease-sensitive linkers allowing for a timely degradation of the hydrogels during the process of cell differentiation. Thus, these hydrogels stand out as novel systems to reproduce bone ECM *in vitro*, with potential to be used as alternative to current stem cell therapies or as implantable 3D matrices to stimulate the osteogenic differentiation of host human MSCs in damaged bone.

Data availability statement

The original contributions presented in the study are included in the article/Supplementary Material, further inquiries can be directed to the corresponding author.

Author contributions

LO-C: conceptualization, methodology, formal analysis, investigation, writing—original draft, writing—review and editing, visualization. HM-G: methodology, formal analysis, investigation, writing—original draft. CG-G: methodology, writing—review and editing. MS-S: methodology, writing—review and editing. M-PG: writing—review and editing, funding acquisition. CM-M: conceptualization, methodology, writing—original draft, writing—review and editing, visualization, supervision, funding acquisition. All authors contributed to the article and approved the submitted version.

Funding

This work was supported by the Spanish State Research Agency (PID 2020-114019RB-I00/AEI/10.13039/501100011033), the AGAUR (2021 SGR 01368 and FI-2018 predoctoral fellowship of LO-C) and the Generalitat of Catalunya (ICREA Academia Award of MP-G). This work has also received funding from the European Union's Horizon 2020 research and innovation Programme under the Marie Skłodowska-Curie Grant Agreement No. 872869 (project Bio-Tune, RISE).

References

- Alcantar, N. A., Aydil, E. S., and Israelachvili, J. N. (2000). Polyethylene glycol-coated biocompatible surfaces. *J. Biomed. Mater. Res.* 51 (3), 343–351. doi:10.1002/1097-4636(20000905)51:3<343::AID-JBM7>3.0.CO;2-D
- Bao, M., Xie, J., Piruska, A., and Huck, W. T. S. (2017). 3D microniches reveal the importance of cell size and shape. *Nat. Commun.* 8 (1), 1962. doi:10.1038/s41467-017-02163-2
- Brown, T. E., and Anseth, K. S. (2017). Spatiotemporal hydrogel biomaterials for regenerative medicine. *Chem. Soc. Rev.* 46 (21), 6532–6552. doi:10.1039/c7cs00445a
- Cambria, E., Kasper, R., Ahrens, C. C., Cook, C. D., Kroll, C., Krueger, A. T., et al. (2015). Covalent modification of synthetic hydrogels with bioactive proteins via sortase-mediated ligation. *Biomacromolecules* 16 (8), 2316–2326. doi:10.1021/acs.biomac.5b00549
- Campos, D., Filipa, D., Blaeser, A., Buellesbach, K., Sen, K. S., Xun, W., et al. (2016). Bioprinting organotypic hydrogels with improved mesenchymal stem cell remodeling and mineralization properties for bone tissue engineering. *Adv. Healthc. Mater.* 5 (11), 1336–1345. doi:10.1002/adhm.201501033
- Canal, T., and Peppas, N. A. (1989). Correlation between mesh size and equilibrium degree of swelling of polymeric networks. *J. Biomed. Mater. Res.* 23 (10), 1183–1193. doi:10.1002/jbm.820231007
- Carletti, E., Motta, A., and Migliaresi, C. (2011). Scaffolds for tissue engineering and 3D cell culture. *Methods Mol. Biol.* 695, 17–39. doi:10.1007/978-1-60761-984-0_2
- Catoira, M. C., Fusaro, L., Di Francesco, D., Ramella, M., and Boccafroschi, F. (2019). Overview of natural hydrogels for regenerative medicine applications. *J. Mater. Sci. Mater. Med.* 30, 115. doi:10.1007/s10856-019-6318-7
- Chang, H., Li, C., Huang, R., Su, R., Qi, W., and He, Z. (2019). Amphiphilic hydrogels for biomedical applications. *J. Mater. Chem. B* 7 (18), 2899–2910. doi:10.1039/C9TB00073A
- Chaudhuri, O., Cooper-White, J., Janmey, P. A., Mooney, D. J., and Shenoy, Vivek B. (2020). Effects of extracellular matrix viscoelasticity on cellular behaviour. *Nature* 584 (7822), 535–546. doi:10.1038/s41586-020-2612-2
- Chaudhuri, O., Gu, L., Klumpers, D., Darnell, M., Bencherif, S. A., Weaver, J., et al. (2016). Hydrogels with tunable stress relaxation regulate stem cell fate and activity. *Nat. Mater.* 15 (3), 326–334. doi:10.1038/nmat4489
- Chaudhuri, O. (2017). Viscoelastic hydrogels for 3D cell culture. *Biomaterials Sci.* 5 (8), 1480–1490. doi:10.1039/C7BM00261K
- Chen, W., Zhou, Z., Chen, D., Li, Y., Zhang, Q., and Su, J. (2021a). Bone regeneration using MMP-cleavable peptides-based hydrogels. *Gels* 7 (4), 199. doi:10.3390/gels7040199
- Chen, X., Tan, B., Bao, Z., Wang, S., Tang, R., Wang, Z., et al. (2021b). Enhanced bone regeneration via spatiotemporal and controlled delivery of a genetically engineered BMP-2 in a composite hydrogel. *Biomaterials* 277 (October), 121117. doi:10.1016/j.biomaterials.2021.121117
- Clark, A. Y., Martin, K. E., García, J. R., and García, A. J. (2020). Integrin-specific hydrogels modulate transplanted human bone marrow-derived mesenchymal stem cell survival, engraftment, and reparative activities. *Nat. Commun.* 11 (1), 1–14. doi:10.1038/s41467-019-14000-9
- Cruise, G. M., Scharp, D. S., and Hubbell, J. A. (1998). Characterization of permeability and network structure of interfacially photopolymerized poly(ethylene glycol) diacrylate hydrogels. *Biomaterials* 19 (14), 1287–1294. doi:10.1016/S0142-9612(98)00025-8
- Dai, Q.-S., Zhou, H.-Y., Wu, Z.-H., Long, J.-T., Shao, N., Cheang, T.-Y., et al. (2015). Osterix transcriptional factor is involved in the metastasis of human breast cancers. *Oncol. Lett.* 10 (3), 1870–1874. doi:10.3892/ol.2015.3448
- Dalby, M. J., García, A. J., and Salmeron-Sanchez, M. (2018). Receptor control in mesenchymal stem cell engineering. *Nat. Rev. Mater.* 3 (3), 17091. doi:10.1038/natrevmats.2017.91
- Darling, N. J., Hung, Y.-S., Sharma, S., and Segura, T. (2016). Controlling the kinetics of thiol-maleimide michael-type addition gelation kinetics for the generation of homogenous poly(ethylene glycol) hydrogels. *Biomaterials* 101 (September), 199–206. doi:10.1016/j.biomaterials.2016.05.053
- Dobre, O., Oliva, M. A. G., Giuseppe CicconeTrujillo, S., Rodrigo-Navarro, A., DouglasVentes, C., et al. (2021). A hydrogel platform that incorporates laminin isoforms for efficient presentation of growth factors – neural growth and osteogenesis. *Adv. Funct. Mater.* 31 (21), 2010225. doi:10.1002/ADFM.202010225
- Duval, K., Grover, H., Han, L.-H., Mou, Y., Pegoraro, A. F., Jeffery, F., et al. (2017). Modeling physiological events in 2D vs. 3D cell culture. *Physiology* 32 (4), 266–277. doi:10.1152/physiol.00036.2016
- Frank, O., Heim, M., Jakob, M., Barbero, A., Schäfer, D., Bendik, I., et al. (2002). Real-time quantitative RT-PCR analysis of human bone marrow stromal cells during osteogenic differentiation *in vitro*. *J. Cell. Biochem.* 85 (4), 737–746. doi:10.1002/jcb.10174
- Granéli, C., Anna, T., Ruetschi, U., Brisby, H., Thomsen, P., Lindahl, A., et al. (2014). Novel markers of osteogenic and adipogenic differentiation of human bone marrow stromal cells identified using a quantitative proteomics approach. *Stem Cell Res.* 12 (1), 153–165. doi:10.1016/j.scr.2013.09.009
- Habibovic, P. (2017). Strategic directions in osteoinduction and biomimetics. *Tissue Eng. - Part A* 23 (23–24), 1295–1296. doi:10.1089/TEN.TEA.2017.0430

Conflict of interest

The authors declare that the research was conducted in the absence of any commercial or financial relationships that could be construed as a potential conflict of interest.

Publisher's note

All claims expressed in this article are solely those of the authors and do not necessarily represent those of their affiliated organizations, or those of the publisher, the editors and the reviewers. Any product that may be evaluated in this article, or claim that may be made by its manufacturer, is not guaranteed or endorsed by the publisher.

Supplementary material

The Supplementary Material for this article can be found online at: <https://www.frontiersin.org/articles/10.3389/fbioe.2023.1192436/full#supplementary-material>

- Han, S., Won Paeng, K., Park, S., Jung, U. W., Cha, J. K., and Hong, J. (2021). Programmed BMP-2 release from biphasic calcium phosphates for optimal bone regeneration. *Biomaterials* 272, 120785. doi:10.1016/j.biomaterials.2021.120785
- Huebsch, N., Lippens, E., Lee, K., Mehta, M., Koshy, S. T., Darnell, M. C., et al. (2015). Matrix elasticity of void-forming hydrogels controls transplanted stem-cell-mediated bone formation. *Nat. Mater.* 14 (12), 1269–1277. doi:10.1038/nmat4407
- Hussey, G. S., Dziki, J. L., and Badylak, S. F. (2018). Extracellular matrix-based materials for regenerative medicine. *Nat. Rev. Mater.* 3 (7), 159–173. doi:10.1038/s41578-018-0023-x
- Iaquinta, M. R., Mazzoni, E., Bononi, I., Rotondo, J. C., Mazziotta, C., Montes, M., et al. (2019). Adult stem cells for bone regeneration and repair. *Front. Cell Dev. Biol.* 7, 268. doi:10.3389/fcell.2019.00268
- James, A. W., LaChaud, G., Jia, S., Asatrian, G., Nguyen, V., Zhang, X., et al. (2016). A Review of the clinical side effects of bone morphogenetic protein-2. *Tissue Eng. Part B Rev.* 22 (4), 284–297. doi:10.1089/ten.teb.2015.0357
- Jansen, L. E., Kim, H., Hall, C. L., McCarthy, T. P., Lee, M. J., and Peyton, S. R. (2022). A poly(ethylene glycol) three-dimensional bone marrow hydrogel. *Biomaterials* 280 (January), 121270. doi:10.1016/j.biomaterials.2021.121270
- Jansen, L. E., Negrón-Piñero, L. J., Galarza, S., and Peyton, S. R. (2018). Control of thiol-maleimide reaction kinetics in PEG hydrogel networks. *Acta Biomater.* 70 (April), 120–128. doi:10.1016/j.actbio.2018.01.043
- Jensen, C., and Teng, Y. (2020). Is it time to start transitioning from 2D to 3D cell culture? *Front. Mol. Biosci.* 7 (March), 33. doi:10.3389/fmolb.2020.00033
- Jha, A. K., Jackson, W. M., and Healy, K. E. (2014). Controlling osteogenic stem cell differentiation via soft bioinspired hydrogels. *PLoS ONE* 9 (6), e98640. doi:10.1371/journal.pone.0098640
- Jha, A. K., Tharp, K. M., Browne, S., Ye, J., Stahl, A., Yeghiazarians, Y., et al. (2016). Matrix metalloproteinase-13 mediated degradation of hyaluronic acid-based matrices orchestrates stem cell engraftment through vascular integration. *Biomaterials* 89 (May), 136–147. doi:10.1016/j.biomaterials.2016.02.023
- Khetan, S., Guvendiren, M., Legant, W. R., Cohen, D. M., Burdick, J. A., and Burdick, J. A. (2013). Degradation-mediated cellular traction directs stem cell fate in covalently crosslinked three-dimensional hydrogels. *Nat. Mater.* 12 (5), 458–465. doi:10.1038/nmat3586
- Kim, J., Kong, Y. P., Niedzielski, S. M., Singh, R. K., Putnam, A. J., and Shikanov, A. (2016). Characterization of the crosslinking kinetics of multi-arm poly(ethylene glycol) hydrogels formed via michael-type addition. *Soft Matter* 12 (7), 2076–2085. doi:10.1039/C5SM02668G
- Krishnan, L., Priddy, L. B., Esancy, C., Klosterhoff, B. S., Stevens, H. Y., Tran, L., et al. (2017). Delivery vehicle effects on bone regeneration and heterotopic ossification induced by high dose BMP-2. *Acta Biomater.* 49, 101–112. doi:10.1016/j.actbio.2016.12.012
- Li, X., Sun, Q., Qian, L., Kawazoe, N., and Chen, G. (2018). Functional hydrogels with tunable structures and properties for tissue engineering applications. *Front. Chem.* 6 (October), 499. doi:10.3389/fchem.2018.00499
- Lienemann, P. S., Vallmajo-Martin, Q., Papageorgiou, P., Blache, U., Metzger, S., Kiveliö, A., et al. (2020). Smart hydrogels for the augmentation of bone regeneration by endogenous mesenchymal progenitor cell recruitment. *Adv. Sci.* 7, 1903395. doi:10.1002/ADVS.201903395
- Liu, Q., Li, M., Wang, S., Xiao, Z., Xiong, Y., and Wang, G. (2020). Recent advances of Osterix transcription factor in osteoblast differentiation and bone formation. *Front. Cell Dev. Biol.* 8 (December), 601224. doi:10.3389/fcell.2020.601224
- Liu, Z., Tang, M., Zhao, J., Chai, R., and Kang, J. (2018). Looking into the future: Toward advanced 3D biomaterials for stem-cell-based regenerative medicine. *Adv. Mater.* 30, 1705388. doi:10.1002/adma.201705388
- Lo, K. W. H., Ulery, B. D., Ashe, K. M., and Laurencin, C. T. (2012). Studies of bone morphogenetic protein-based surgical repair. *Adv. Drug Deliv. Rev.* 64 (12), 1277–1291. doi:10.1016/j.addr.2012.03.014
- Lutolf, M. P., and Hubbell, J. A. (2003). Synthesis and physicochemical characterization of end-linked poly(ethylene glycol)-Co-peptide hydrogels formed by michael-type addition. *Biomacromolecules* 4 (3), 713–722. doi:10.1021/bm025744e
- Lutolf, M. P., and Hubbell, J. A. (2005). Synthetic biomaterials as instructive extracellular microenvironments for morphogenesis in tissue engineering. *Nat. Biotechnol.* 23 (1), 47–55. doi:10.1038/nbt1055
- Lutolf, M. P., Lauer-Fields, J. L., Schmoekel, H. G., Metters, A. T., Weber, F. E., Fields, G. B., et al. (2003). Synthetic matrix metalloproteinase-sensitive hydrogels for the conduction of tissue regeneration: Engineering cell-invasion characteristics. *Proc. Natl. Acad. Sci.* 100 (9), 5413–5418. doi:10.1073/pnas.0737381100
- Madl, C. M., LeSavage, B. L., Dewi, R. E., Dinh, C. B., RyanStowers, S., Khariton, M., et al. (2017). Maintenance of neural progenitor cell stemness in 3D hydrogels requires matrix remodelling. *Nat. Mater.* 16 (12), 1233–1242. doi:10.1038/nmat5020
- Madl, C. M., Mehta, M., Duda, G. N., Heilshorn, S. C., and Mooney, D. J. (2014). Presentation of BMP-2 mimicking peptides in 3D hydrogels directs cell fate commitment in osteoblasts and mesenchymal stem cells. *Biomacromolecules* 15 (2), 445–455. doi:10.1021/bm401726u
- Major, L. G., Holle, A. W., JenniferYoung, L., Hepburn, M. S., Jeong, K., Chin, I. L., et al. (2019). Volume adaptation controls stem cell mechanotransduction. *ACS Appl. Mater. Interfaces* 11 (49), 45520–45530. doi:10.1021/acsami.9b19770
- Mandal, A., John, R., Clegg, A. C. A., and Mitragotri, S. (2020). Hydrogels in the clinic. *Bioeng. Transl. Med.* 5 (2), 1–12. doi:10.1002/btm2.10158
- Martínez-Jothar, L., Doukeridou, S., RaymondSchiffelers, M., Sastre Torano, J., Oliveira, S., Corneliusvan Nostrum, F., et al. (2018). Insights into maleimide-thiol conjugation chemistry: Conditions for efficient surface functionalization of nanoparticles for receptor targeting. *J. Control. Release* 282 (July), 101–109. doi:10.1016/j.jconrel.2018.03.002
- Mas-Moruno, C., Fraioli, R., Rechenmacher, F., Neubauer, S., Kapp, T. G., et al. (2016). Avβ3-or α5β1-integrin-selective peptidomimetics for surface coating. *Angew. Chem. Int. Ed.* 55 (25), 7048–7067. doi:10.1002/anie.201509782
- Merrill, E., Dennison, K., and Sung, C. (1993). Partitioning and diffusion of solutes in hydrogels of poly(ethylene oxide). *Biomaterials* 14 (15), 1117–1126. doi:10.1016/0142-9612(93)90154-T
- Mirbagheri, M., Adibnia, V., Hughes, B. R., Waldman, S. D., Banquy, X., and Hwang, D. K. (2019). Advanced cell culture platforms: A growing quest for emulating natural tissues. *Mater. Horizons* 6 (1), 45–71. doi:10.1039/C8MH00803E
- Mitchell, A. C., Briquez, P. S., Hubbell, J. A., and Cochran, J. R. (2016). Engineering growth factors for regenerative medicine applications. *Acta Biomater.* 30, 1–12. doi:10.1016/j.actbio.2015.11.007
- Monteiro, A., Isabela, T. K., and Jenny, M. (2018). Engineered systems to study the synergistic signaling between integrin-mediated mechanotransduction and growth factors (Review). *Biointerphases* 13 (6), 06D302. doi:10.1116/1.5045231
- Mullen, C. A., Haugh, M. G., Schaffler, M. B., Majeska, R. J., and McNamara, L. M. (2013). Osteocyte differentiation is regulated by extracellular matrix stiffness and intercellular separation. *J. Mech. Behav. Biomed. Mater.* 28 (December), 183–194. doi:10.1016/j.jmbbm.2013.06.013
- Nair, D. P., Podgórski, M., Chatani, S., Gong, T., Xi, W., Fenoli, C. R., et al. (2014). The thiol-michael addition click reaction: A powerful and widely used tool in materials chemistry. *Chem. Mater.* 26 (1), 724–744. doi:10.1021/cm402180t
- Nasello, G., Alamán-Díez, P., Schiavi, J., Ángeles Pérez, M., McNamara, L., and García-Aznar, J. M. (2020). Primary human osteoblasts cultured in a 3D microenvironment create a unique representative model of their differentiation into osteocytes. *Front. Bioeng. Biotechnol.* 8 (April), 336. doi:10.3389/fbioe.2020.00336
- Nishimura, R., Wakabayashi, M., Hata, K., Matsubara, T., Honma, S., Wakisaka, S., et al. (2012). Osterix regulates calcification and degradation of chondrogenic matrices through matrix metalloproteinase 13 (MMP13) expression in association with transcription factor Runx2 during endochondral ossification. *J. Biol. Chem.* 287 (40), 33179–33190. doi:10.1074/jbc.M111.337063
- Oliver-Cervelló, L., Martín-Gómez, H., Mandakhbayar, N., Jo, Y.-W., Cavalcanti-Adam, E. A., Kim, H.-W., et al. (2022). Mimicking bone extracellular matrix: From BMP-2-derived sequences to osteogenic-multifunctional coatings. *Adv. Healthc. Mater.* August, 2201339. doi:10.1002/adhm.202201339
- Oliver-Cervelló, L., Martín-Gómez, H., Reyes, L., Noureddine, F., Ginebra, M. P., Mas-Moruno, C., et al. (2021). An engineered biomimetic peptide regulates cell behavior by synergistic integrin and growth factor signaling. *Adv. Healthc. Mater.* 10 (7), 2001757. doi:10.1002/adhm.202001757
- Park, H., Jin Seon Kwon, S., Sung Lee, B., Hoon Park, J., Lee, B. K., Yun, J.-H., et al. (2017). BMP2-modified injectable hydrogel for osteogenic differentiation of human periodontal ligament stem cells. *Sci. Rep.* 7 (6603), 6603. doi:10.1038/s41598-017-06911-8
- Peng, Y., Liu, Q.-J., He, T., Ye, K., Yao, X., and Ding, J. (2018). Degradation rate affords a dynamic cue to regulate stem cells beyond varied matrix stiffness. *Biomaterials* 178 (September), 467–480. doi:10.1016/j.biomaterials.2018.04.021
- Peyton, S. R., Raub, C. B., Keschrumer, V. P., and Putnam, A. J. (2006). The use of poly(ethylene glycol) hydrogels to investigate the impact of ECM chemistry and mechanics on smooth muscle cells. *Biomaterials* 27 (28), 4881–4893. doi:10.1016/j.biomaterials.2006.05.012
- Phelps, E. A., KellieTempleman, L., PeterThulé, M., and AndrésGarcía, J. (2015). Engineered VEGF-releasing PEG-MAL hydrogel for pancreatic islet vascularization. *Drug Deliv. Transl. Res.* 5 (2), 125–136. doi:10.1007/s13346-013-0142-2
- Phelps, E. A., Enemchukwu, N. O., Vincent, F., Fiore, J. C., Murthy, N., Sulchek, T., et al. (2012). Maleimide cross-linked bioactive PEG hydrogel exhibits improved reaction kinetics and cross-linking for cell encapsulation and *in situ* delivery. *Adv. Mater.* 24 (1), 64–70. doi:10.1002/adma.201103574
- Raeber, G. P., Lutolf, M. P., and Hubbell, J. A. (2005). Molecularly engineered PEG hydrogels: A novel model system for proteolytically mediated cell migration. *Biophysical J.* 89 (2), 1374–1388. doi:10.1529/biophysj.104.050682
- Ravasco, J. M. J. M., Faustino, H., Alexandre, T., and Gois, P. M. P. (2019). Bioconjugation with maleimides: A useful tool for chemical biology. *Chem. – A Eur. J.* 25 (1), 43–59. doi:10.1002/chem.201803174
- Sano, R., Nakajima, A., Kawato, T., Maeno, M., and Shimizu, N. (2017). Effect of compressive force on TGF-β1/2 signaling pathway in mc3t3-E1 cells. *J. Hard Tissue Biol.* 26 (2), 177–186. doi:10.2485/jhtb.26.177

- Schindelin, J., Arganda-Carreras, I., Frise, E., Kaynig, V., Longair, M., Tobias, P., et al. (2012). Fiji: An open-source platform for biological-image analysis. *Nat. Methods* 9 (7), 676–682. doi:10.1038/nmeth.2019
- Sen, S., AdamEngler, J., and E Discher, D. (2009). Matrix strains induced by cells: Computing how far cells can feel. *Cell. Mol. Bioeng.* 2 (1), 39–48. doi:10.1007/s12195-009-0052-z
- Shekaran, A., García, J. R., Clark, A. Y., Kavanaugh, T. E., Angela, S., et al. (2014). Bone regeneration using an alpha 2 beta 1 integrin-specific hydrogel as a BMP-2 delivery vehicle. *Biomaterials* 35 (21), 5453–5461. doi:10.1016/j.biomaterials.2014.03.055
- Sun, Q., Hou, Y., Chu, Z., and Qiang, W. (2022). Soft overcomes the hard: Flexible materials adapt to cell adhesion to promote cell mechanotransduction. *Bioact. Mater.* 10 (April), 397–404. doi:10.1016/j.bioactmat.2021.08.026
- Thiele, J., Ma, Y., Stéphanie, M., Bruekers, C., Ma, S., and Huck, W. T. S. (2014). 25th anniversary article: Designer hydrogels for cell cultures: A materials selection guide. *Adv. Mater.* 26 (1), 125–148. doi:10.1002/adma.201302958
- Trujillo, S., Gonzalez-Garcia, C., Rico, P., Reid, A., James, W., Dalby, M. J., et al. (2020). Engineered 3D hydrogels with full-length fibronectin that sequester and present growth factors. *Biomaterials* 252 (September), 120104. doi:10.1016/j.biomaterials.2020.120104
- Tseng, T.-C., Tao, L., Hsieh, F.-Y., Yen, W., Chiu, I.-M., and Hsu, S.-H. (2015). An injectable, self-healing hydrogel to repair the central nervous system. *Adv. Mater.* 27 (23), 3518–3524. doi:10.1002/adma.201500762
- Turk, B. E., Huang, L. L., Elizabeth, T. P., Cantley, L. C., and Cantley, L. C. (2001). Determination of protease cleavage site motifs using mixture-based oriented peptide libraries. *Nat. Biotechnol.* 19 (7), 661–667. doi:10.1038/90273
- Viti, F. M. L., Mezzelani, A., Petecchia, L., Milanesi, L., and Scaglione, S. (2016). Osteogenic differentiation of MSC through calcium signaling activation: Transcriptomics and functional analysis. *PLoS ONE* 11 (2), 148173. doi:10.1371/journal.pone.0148173
- Wei, Q., Pohl, T. L. M., Seckinger, A., Spatz, J. P., and Cavalcanti-Adam, E. A. (2015). Regulation of integrin and growth factor signaling in biomaterials for osteodifferentiation. *Beilstein J. Org. Chem.* 11, 773–783. doi:10.3762/bjoc.11.87
- Wei, Q., Young, J., Holle, A., Li, J., Bieback, K., Inman, G., et al. (2020). Soft hydrogels for balancing cell proliferation and differentiation. *ACS Biomaterials Sci. Eng.* 6 (8), 4687–4701. doi:10.1021/acsbmaterials.0c00854
- Welzel, P.B., Prokoph, S., Zieris, A., Grimmer, M., Zschoche, S., et al. (2011). Modulating biofunctional StarPEG heparin hydrogels by varying size and ratio of the constituents. *Polymers* 3 (1), 602–620. doi:10.3390/polym3010602
- Wessely, A., Anna, W., Reichert, T. E., Grässel, S., and RichardBauer, J. (2019). Induction of ALP and MMP9 activity facilitates invasive behavior in heterogeneous human BMSC and HNSCC 3D spheroids. *FASEB J.* 33 (11), 11884–11893. doi:10.1096/fj.201900925R
- Xu, Y., Li, Z., Li, X., Fan, Z., Liu, Z., Xie, X., et al. (2015). Regulating myogenic differentiation of mesenchymal stem cells using thermosensitive hydrogels. *Acta Biomater.* 26 (October), 23–33. doi:10.1016/j.actbio.2015.08.010
- Yi, H., Steven, F., He, Y., Liu, Q., Geng, X., Wei, S., et al. (2017). Tissue-specific extracellular matrix promotes myogenic differentiation of human muscle progenitor cells on gelatin and heparin conjugated alginate hydrogels. *Acta Biomater.* 62 (October), 222–233. doi:10.1016/j.actbio.2017.08.022
- Zhang, Z., Gupte, M. J., and Ma, P. X. (2013). Biomaterials and stem cells for tissue engineering. *Expert Opin. Biol. Ther.* 13 (4), 527–540. doi:10.1517/14712598.2013.756468
- Zhao, X., Cui, K., and Li, Z. (2019). The role of biomaterials in stem cell-based regenerative medicine. *Future Med. Chem.* 11 (14), 1777–1790. doi:10.4155/fmc-2018-0347
- Zhu, J. (2010). Bioactive modification of poly(ethylene glycol) hydrogels for tissue engineering. *Biomaterials* 31 (17), 4639–4656. doi:10.1016/j.biomaterials.2010.02.044
- Zhu, J., and Marchant, R. E. (2011). Design properties of hydrogel tissue-engineering scaffolds. *Expert Rev. Med. Devices* 8 (5), 607–626. doi:10.1586/erd.11.27



OPEN ACCESS

EDITED BY

Hasan Uludag,
University of Alberta, Canada

REVIEWED BY

Jonghyun Oh,
Jeonbuk National University, Republic of
Korea
Chandra Kothapalli,
Cleveland State University, United States

*CORRESPONDENCE

Yunbing Wang,
✉ yunbing.wang@scu.edu.cn
Xingdong Zhang,
✉ zhangxd@scu.edu.cn

RECEIVED 24 February 2023

ACCEPTED 19 May 2023

PUBLISHED 02 June 2023

CITATION

Zhang T, Dou Y, Luo R, Yang L, Zhang W,
Ma K, Wang Y and Zhang X (2023), A
review of the development of
interventional devices for mitral valve
repair with the implantation of
artificial chords.
Front. Bioeng. Biotechnol. 11:1173413.
doi: 10.3389/fbioe.2023.1173413

COPYRIGHT

© 2023 Zhang, Dou, Luo, Yang, Zhang,
Ma, Wang and Zhang. This is an open-
access article distributed under the terms
of the [Creative Commons Attribution
License \(CC BY\)](#). The use, distribution or
reproduction in other forums is
permitted, provided the original author(s)
and the copyright owner(s) are credited
and that the original publication in this
journal is cited, in accordance with
accepted academic practice. No use,
distribution or reproduction is permitted
which does not comply with these terms.

A review of the development of interventional devices for mitral valve repair with the implantation of artificial chords

Tingchao Zhang^{1,2}, Yichen Dou¹, Rifang Luo¹, Li Yang¹,
Weiwei Zhang², Kangmu Ma², Yunbing Wang^{1*} and
Xingdong Zhang^{1*}

¹National Engineering Research Center for Biomaterials, College of Biomedical Engineering, Sichuan University, Chengdu, China, ²Hangzhou Valgen Medtech Co., Ltd., Hangzhou, China

Mitral regurgitation (MR) was the most common heart valve disease. Surgical repair with artificial chordal replacement had become one of the standard treatments for mitral regurgitation. Expanded polytetrafluoroethylene (ePTFE) was currently the most commonly used artificial chordae material due to its unique physicochemical and biocompatible properties. Interventional artificial chordal implantation techniques had emerged as an alternative treatment option for physicians and patients in treating mitral regurgitation. Using either a transapical or a transcatheter approach with interventional devices, a chordal replacement could be performed transcatheter in the beating heart without cardiopulmonary bypass, and the acute effect on the resolution of mitral regurgitation could be monitored in real-time by transesophageal echo imaging during the procedure. Despite the *in vitro* durability of the expanded polytetrafluoroethylene material, artificial chordal rupture occasionally occurred. In this article, we reviewed the development and therapeutic results of interventional devices for chordal implantation and discuss the possible clinical factors responsible for the rupture of the artificial chordal material.

KEYWORDS

mitral regurgitation, artificial chordal implantation, expanded polytetrafluoroethylene (ePTFE), chordal ruptures, transapical, transcatheter, interventional devices

1 Introduction

Mitral regurgitation (MR) was a common heart valve disease in clinical practice and was characterized by the backflow of blood from the left ventricle to the left atrium during diastole (Enriquez-Sarano et al., 2009; Xu et al., 2022). A large number of patients require urgent treatment (Li et al., 2016). The mitral apparatus consisted of the mitral annulus, leaflets, commissures, chordae tendineae, posterior left atrium, LV free wall, and papillary muscles; dysfunction of any of these components may lead to mitral valve pathology, including MR (Figure 1A, Figure 1B) (Ali et al., 2020). Among them, degenerative MR (DMR) caused by structural lesions of the valve itself, such as mitral valve stenosis or prolapse due to redundancy or chordal rupture, was one of the main etiologies of MR (Soulat-Dufour and Addetia, 2020). Different treatment modalities were chosen clinically depending on the etiology of MR, which was divided into mitral valve replacement and repair. With better long-term outcomes, fewer valve-related

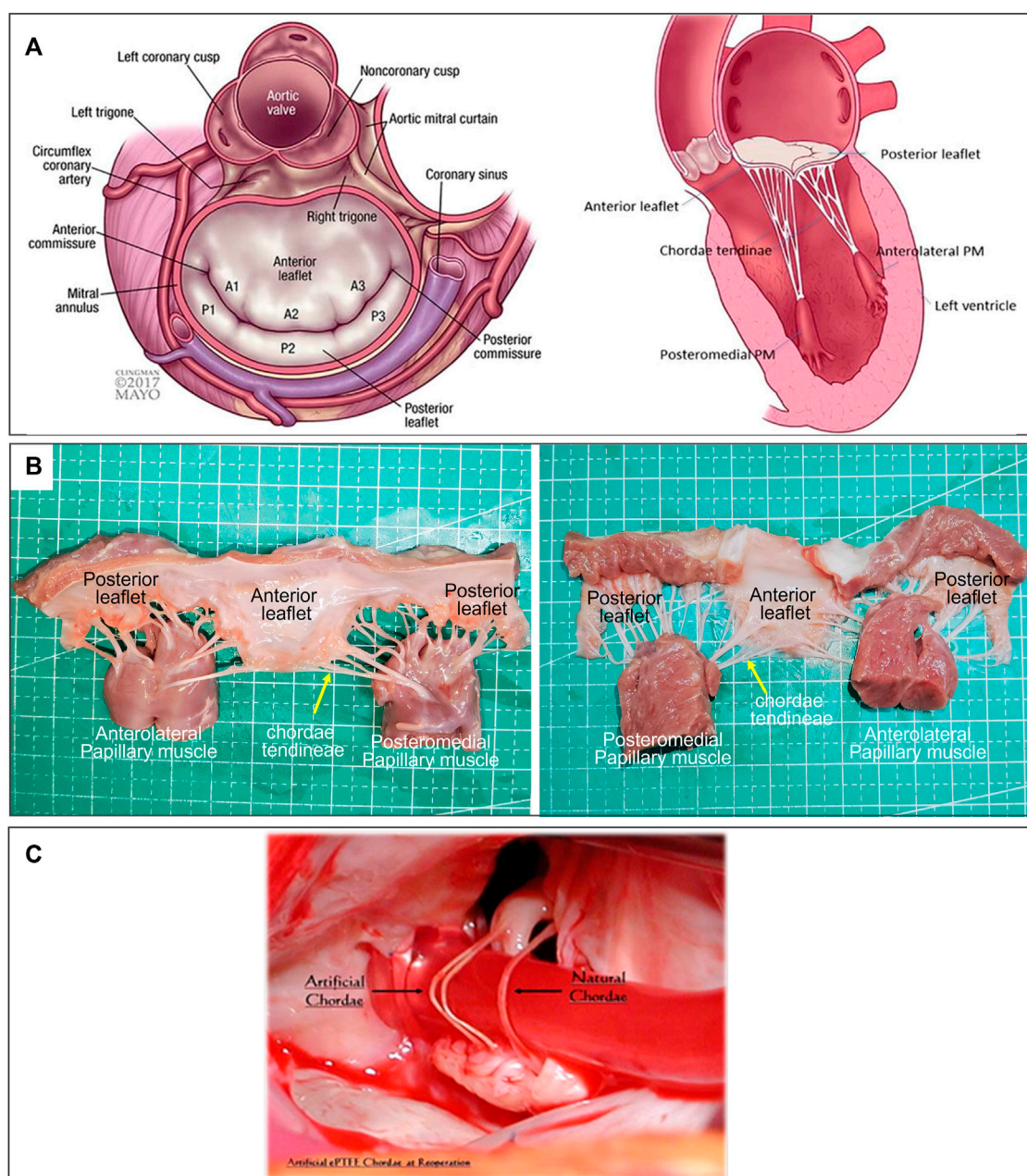


FIGURE 1

(A) Atrial and sagittal views of mitral valve. Left, P1-A1 was anterolateral, P3-A3 was posteromedial. Right, Sagittal view showing subvalvular supporting structures. A indicates anterior; P, posterior; and PM, papillary muscle (Ali et al., 2020). (B) Mitral Valve Anatomical Map. (C) Comparison of artificial and native chordae, reoperation after 12 years (Salvador et al., 2008).

complications, and lower mortality (Gillinov et al., 2008), mitral valve repair has emerged as a treatment option for patients with DMR.

Mitral valve repair mainly consists of annuloplasty (96.1%), leaflet resection (58.9%), and prosthetic chordae repair (29.2%) (Gammie et al., 2018b). With the development of technology, “preservation without resection” was the principle of mitral valve repair surgery. This allows complete preservation of lobular tissue and subvalvular structure to better preserve left ventricular function. A meta-analysis of 6,046 patients in 17 studies of mitral valve repair

by Ibrahim et al. (2012) showed that the “preserved method” was superior to the “resected method.”

Artificial chordae surgery repairs mitral prolapse or flail leaflets by replacing the diseased chords with a string-like material. This approach does not affect the surrounding valve structure and was more in keeping with the physiological anatomy of the valve. It has become the standard of care for DMR (Bortolotti et al., 2012b).

Although surgical mitral valve repair has a good long-term therapeutic effect, it must be performed under the conditions of thoracotomy and extracorporeal circulation, which were more

invasive. Compared with surgical thoracotomy, minimally invasive interventional repair devices can be performed under non-extracorporeal circulation and continuous heartbeat, with the advantages of less trauma and faster postoperative recovery (Ahmed et al., 2021).

The artificial chord intervention instrument was a minimally invasive interventional technique based on surgical mitral valve chordal repair, which may be divided into transapical chordal repair and transcatheter chordal repair according to the surgical approach. It could capture the prolapsed or tethered leaflet under ultrasound and/or x-ray guidance and implant the prosthetic chordae. It could also be readjusted to the appropriate length to restore leaflet alignment and reduce or eliminate MR (Fiocco et al., 2019). Many artificial chordae interventional devices have been developed based on this principle (Maisano et al., 2013), and some of them have entered the clinical or commercial application stage.

This review reports the development of artificial chordae materials, the principles of two routes of artificial chordae intervention devices, implantation methods, force differentials, and their clinical application effects and failure modes.

2 Development history of artificial chordae materials

The selection of materials was particularly critical for chordal replacement. The selection and research of artificial chordal materials began as early as the mid-20th century (David, 2004). To have a stable function under the complex physiological environment and long-term stress conditions *in vivo*, the ideal material should have the following properties: 1) High tensile strength and inelasticity to avoid fracture or deformation under the action of stress. 2) Resistance to calcification and mineral deposition to prevent hardening or fracture of the artificial chord after calcification. 3) Good fatigue properties, resistant to creep or fracture. 4) Fine, pliable, and capable of retaining this property long after implantation. 5) Porous structure that allows tissue growth to form a stable fibrous envelope and endothelial layer. 6) Good biocompatibility, resulting in producing an acceptable inflammatory response and resistance to thrombosis (Kunzelman and Cochran, 1990; David, 2004; Casado et al., 2012).

Initially, silk sutures, polyester sutures, polypropylene sutures, and pericardium were used to be artificial chords; however, they all had certain limitations and were abandoned due to changes in length and thrombosis after implant (January et al., 1962; Kay and Egerton, 1963; Morris et al., 1964; David, 2004). Among the pericardial materials, thickening, and stiffening, and contracture were found early after implantation of the autologous pericardium (Rittenhouse et al., 1978); while for allogeneic pericardial materials, a certain degree of flexibility was maintained in the early stage of implantation, but they showed insufficient long-term effects with fibrous hyperplasia, calcification, thickening and stiffness 3 years later (Frater et al., 1983). These materials must experience more than hundreds of millions of cardiac contractions. Because they had less flexibility, tensile strength, histocompatibility, and durability, they were difficult to fully meet the application requirements, so they have not been used and commercialized in large-scale clinical applications.

TABLE 1 GORE-TEX® ePTFE suture.

Specification	Diameter (mm)	Tensile strength (kg)
CV-4	0.404	1.79
CV-5	0.321	1.62

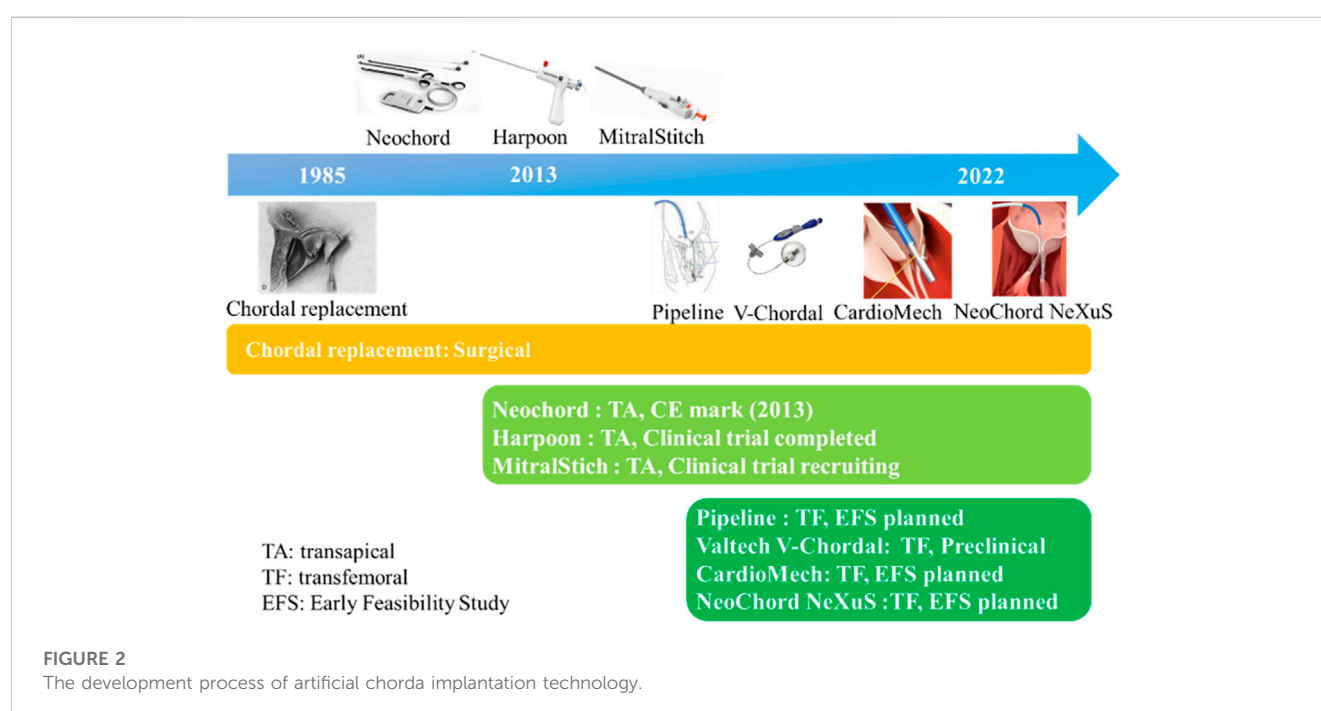
It was reported that expanded polytetrafluoroethylene (ePTFE) sutures were the gold standard in current clinical practice for the use of artificial chordae (David, 2022). The ePTFE suture was a microporous, non-absorbable monofilament suture made of PTFE that can stretch and expand, and also had many other unique properties. The molecular formula of ePTFE was the same as PTFE. Its chemical structure was very stable and resistant to hydrolysis and aging. The expanded and stretched ePTFE suture had good flexibility and tensile strength. It also had good biocompatibility and carries negative surface charges consistent with endothelial cells, making it less prone to thrombosis (Wang G. et al., 2022). The surface of the microporous structure was conducive to tissue growth, and the degree of inflammation was lower than that of the multifilament braided sutures (Nistal et al., 1990).

Gore's GORE-TEX® ePTFE product was commercially used in clinical practice and was approved by the FDA in 1985. Two major sizes were shown in Table 1.

When ePTFE was used for artificial tendons, it was found that after a few months of implantation, the surface was covered with fibers and endothelial tissue. This discovery was a major stimulus for ePTFE research. The two pioneers who extensively tested ePTFE on animals were Frater and Revuelta (Pomar et al., 2013). Revuelta et al. (1989) used ePTFE sutures as artificial chordae to replace the chordae of the ovine mitral valve. They resected one or two marginal chordae of the anterior leaflet of the mitral valve in 35 sheep and replaced them with a double-armed, pledget-supported, expanded polytetrafluoroethylene suture. The 30 surviving animals were hemodynamically studied and euthanized 3, 6, 9, 18, and 24 months after surgery. None of the sheep experienced mitral insufficiency. All specimens had normal mitral valves without thrombosis. The polytetrafluoroethylene suture remained pliable and was incorporated into the anterior leaflet and papillary muscle. Scanning and transmission electron microscopy showed that the suture was completely covered by a sheath of tissue with a collagen structure remarkably similar to that of native chordae. There was no evidence of calcification in the new chordae. This reproducible and safe technique may greatly simplify the difficult repair of chordae anomalies. This result was also confirmed in an authoritative article on chordal replacement published by Zussa (1996). Based on discussions with Frater, David began using the ePTFE suture as an artificial chord in the clinical treatment of DMR patients in 1989, and has done so for over 30 years (David, 1989). David et al. (2013) reviewed the long-term outcomes of 606 patients with ePTFE artificial chordal between 1986 and 2004. During the 18-year follow-up period, the cardiogenic mortality rate related to valvular disease was 8.5%. The reoperation rates at 1 year, 10 years, and 18 years were 1.4%, 5.3%, and 9.8%, respectively, and recurrent moderate/severe MR was 1.5%, 12.2%, and 32.5%. Hata et al. (2014) also reported on the long-term

TABLE 2 Advantages and disadvantages of the interventional repair techniques.

	Surgical	Transapical	Transcatheter
Material	ePTFE	ePTFE	ePTFE + metal anchor
Therapy method	Conventional thoracotomy and cardiopulmonary bypass	Minimally invasive, beating heart	Interventional and transseptal treatment
Risk and prognosis	The surgical risk was relatively high, and the postoperative prognosis was relatively slow	Risk was lower than surgical, and the prognosis was faster than surgical	Risk was relatively low, and the prognosis was relatively fast
Applicable patients	Younger patients with low surgical risk	Patients unable to undergo conventional surgical procedures	Patients unable to undergo conventional surgical procedures
Location of prolapse	Posterior leaflet prolapses, anterior leaflet prolapses or bileaflet prolapse	Isolated posterior leaflet prolapses	Isolated posterior leaflet prolapses



outcomes of 224 patients who received ePTFE artificial chordae between 1988 and 2013. Over 20 years, the mortality rate related to cardiac and valvular disease was 3.1%. The reoperation rates at 1, 10, and 20 years were 7%, 16%, and 26%, respectively, and recurrent moderate/severe MR were 9%, 18%, and 41%. These studies demonstrated that the clinical efficacy of early and long-term use of ePTFE suture as an artificial chord to repair DMR valve prolapse was effective.

The long-term durability of ePTFE artificial chordae was closely related to their biocompatibility. This has been confirmed by the histopathology of many ePTFE chordae taken removed during reoperations. The ePTFE sutures implanted *in vivo* remained macroscopically smooth and pliable, with a morphology close to that of native chordae (Figure 1C) (Salvador et al., 2008). Histopathologic examination showed that protein infiltrated into the internal microporous structure of ePTFE, and the surface was covered with fibrous tissue and endothelium by histopathological

examination. These tissue-material composite artificial chordae were formed by the interaction between the material and the organism. It improved the suture and reduced the inflammatory response and thrombosis, ensuring its long-term stability in the body (Hata et al., 2014).

3 Implantation methods and differences between artificial chords

ePTFE sutures have been used as artificial chordae for more than 35 years with proven durability and clinical efficacy. Currently, ePTFE sutures were used in both surgical and minimally invasive interventional devices. There were three methods of implantation: 1) surgical thoracotomy; 2) minimally invasive transapical implantation; and 3) transfemoral vein/atrial septal implantation (David, 2004; Fiocco et al., 2019). The advantages and disadvantages

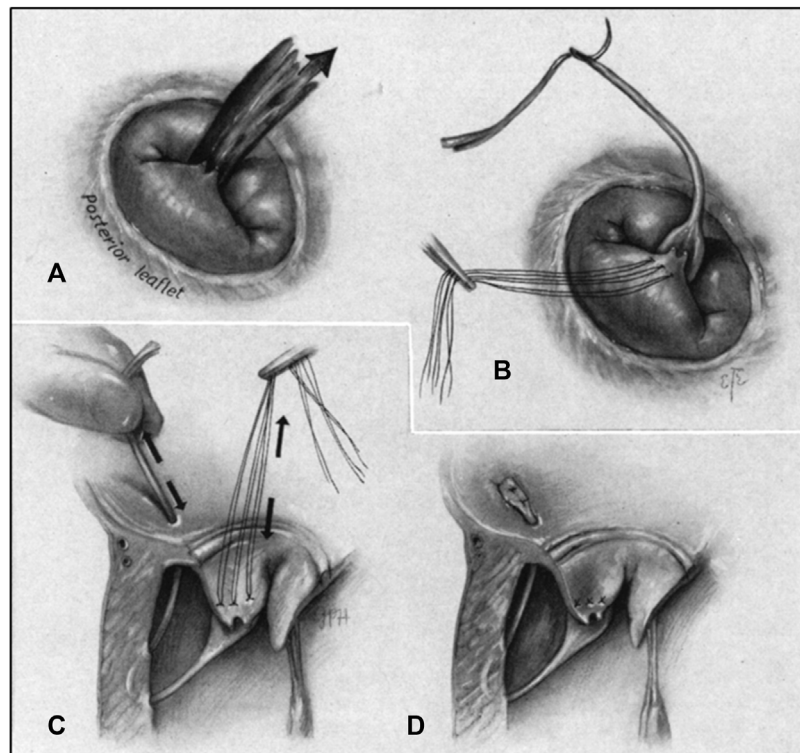


FIGURE 3

(A) Regurgitant jet produced by chordal rupture attached to posterior leaflet as seen from right thoracotomy. (B) Prosthetic chordal attached to flailing leaflet. (C) Pulley stitch completed in the ventricular wall. Tension adjusted on chordal, restoring leaflet position. (D) Prosthetic chordal anchored at the atrial wall and excess length excised (Morris et al., 1964).

of the above repair techniques were listed in Table 2 and Figure 2 summarized the development process of artificial chordae implantation technology and various representative devices.

3.1 Surgical thoracotomy implantation

The surgical method of artificial chordae implantation was to stop the heart beating with the support of extracorporeal circulation, then fully exposed the heart through a median sternotomy. The mitral valve was exposed through the right atrium-atrial septal incision or a combined right atrium-atrial septal-left atrial apex incision, and artificial chordae were implanted under direct visualization (Figure 3) (Morris et al., 1964).

Due to cardiac arrest, the suture length cannot be adjusted in real time to determine whether to eliminate regurgitation, and the smoothness of the ePTFE suture made tying the knot difficult. Therefore, surgeon experience was very important (Madhurapantula et al., 2020). The position of the chordae anchor was at the edge of the valve leaflet and the papillary muscle, which corresponded to the physiological and anatomical structure and had a good long-term effect. However, it was very traumatic for patients, and the postoperative recovery period could be as long as 6 weeks (Oh et al., 2020). A study of 449 patients who underwent mitral valve surgery from January 1995 to December 1999 showed that the operative mortality rate was 4.4%. Therefore, it

may not applied to many patients at high surgical risk patients due to poor cardiac function, high comorbidity, advanced age, and other factors (Bech-Hanssen et al., 2003).

3.2 Minimally invasive transapical implantation

Minimally invasive apical implantation was the implantation of ePTFE artificial chordae under 2D and 3D transesophageal echocardiographic (TEE) guidance without cardiopulmonary bypass while the heart continued to beat. In this method, only a small incision of approximately 4 cm was made in the fifth or sixth intercostal space to expose the cardiac apex of the heart, followed by deployment of the apical load and a ventriculotomy to establish the apical access (Figure 4) (Colli et al., 2018a). The artificial chordae were implanted and anchored to the edge/root of the leaflets and the apical part of the epicardium, guided by TEE. As the heart beats continuously during the procedure, the suture length can be adjusted in real-time to determine the optimal length. Because the access of the transapical minimally invasive repair device was short, it had advantages such as short operation time, easy operation and high success rate. Although this approach was less traumatic for patients than surgical thoracotomy, it was prone to complications such as pericardial adhesions or left ventricular rupture due to

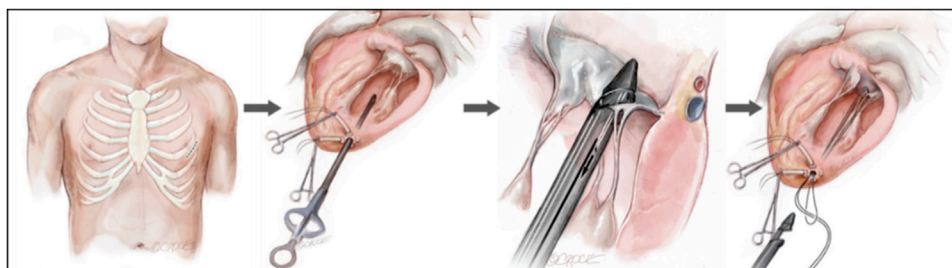


FIGURE 4
Transapical NeoChord mitral valve repair (Colli et al., 2018a).

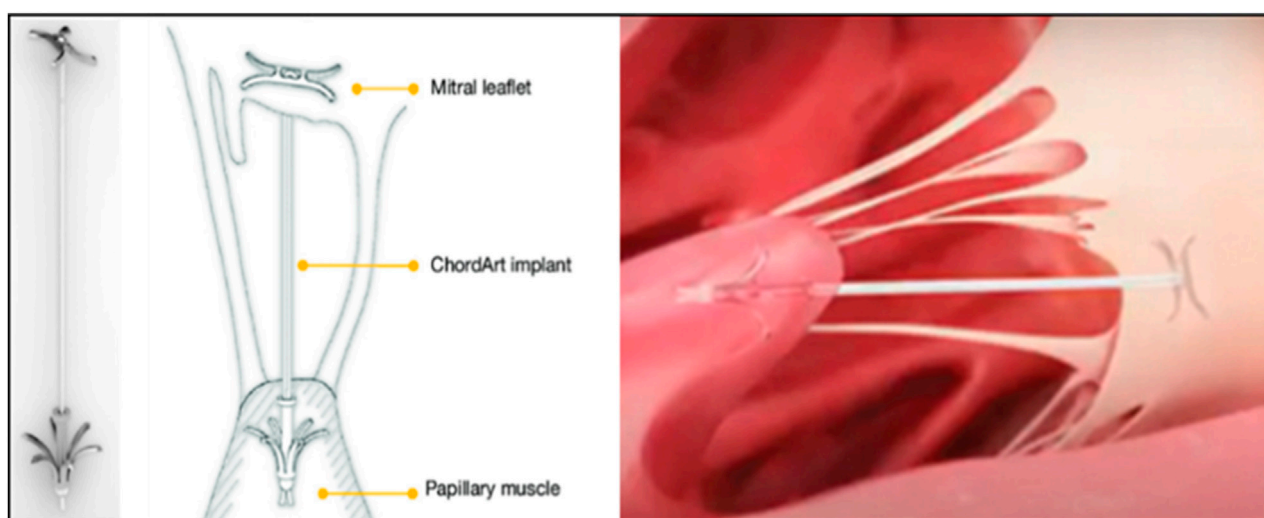


FIGURE 5
ChordArt implant. There were nitinol leaflets and papillary muscle anchors with an ePTFE chord (Rogers and Bolling, 2021; Weber et al., 2021).

damage to the apical and pericardial tissues (Blumenstein et al., 2012; Simões Costa et al., 2021).

3.3 Transcatheter implantation

Transcatheter implantation meant that the device entered through the femoral vein, punctures the interatrial septum, and then entered the left atrium and ventricle to complete the implantation of artificial chordae anchored at the edge of the valve leaflets and the papillary muscle under the guidance of echocardiography and digital subtraction techniques (Figure 5) (Rogers and Bolling, 2021; Weber et al., 2021). This approach allowed real-time adjustment of chordal length without the need for cardiac arrest or extracorporeal circulatory support. It also required no thoracic or cardiac incision, which was minimally traumatic for the patient, who recovered quickly and was discharged 2–3 days postoperatively (Oh et al., 2020).

However, the success rate of transcatheter chordae implantation was low due to the length of the approach, the complexity of the

mitral valve anatomy, the difficulty of the technique, and the narrow indication. It was currently in the early stages of development.

3.4 Differences of surgical, transapical and transcatheter repair

3.4.1 How many and where to place the artificial chordae

Depending on the extent and location of the prolapsed area, the number and placement of the artificial chordae may vary. One study found that the artificial chordae tendineae technology could preserve the effective opening area of the valve leaflet to the maximum extent, and could effectively cope with large-scale pathological changes by inserting a plurality of artificial chordae tendineae, better preserving the systolic and diastolic function of the left ventricle (Perier et al., 2008). A few studies have reported outcomes after mitral valve repair with artificial chordae including surgical repair and transapical repair (Table 3).

TABLE 3 Differences of mitral valve repair therapeutic strategy.

Therapeutic strategy	Repair method	Patient number	Area of lesion	Number of artificial chordae implanted	References
Surgical	Posterior leaflet repair using chordae alone	192	PML	1–6	Lange et al. (2010)
	Double-armed approach using ePTFE chordae and Carpentier resection	608	PML, AML, Bi-ML	4–8	Salvador et al. (2008)
	Loop technique	129	PML	3–4	Falk et al. (2008)
	Simple chordae replacement	74	PML, AML, Bi-ML	2–12	Kobayashi et al. (2000)
Transapical Neochord	Transapical off-pump MVr	10	PML (58.3%), AML (26.7%), Bi-ML (25%)	3–6	Kavakli et al. (2016)
	Transapical off-pump MVr	213	PML (90.6%), AML (5.2%), Bi-ML (4.2%)	3–4	Colli et al. (2018b)
	Transapical off-pump MVr	7	PML	3–4	Grinberg et al. (2019b)
	Transapical off-pump MVr	7	PML	3–5	Heuts et al. (2018)
	Transapical off-pump MVr	6	PML	3 or 3+	Kiefer et al. (2018)
	Transapical off-pump MVr	4	PML	2–3	Wang et al. (2019)
Transapical Harpoon	Transapical off-pump MVr	11	PML	3–5	Gammie et al. (2016)
	Transapical off-pump MVr	65	PML	0–7	Gammie et al. (2021)

AML, anterior mitral leaflet; PML, posterior mitral leaflet; Bi-ML, bilateral mitral leaflet (Figures 1A, B).

3.4.2 The position of the artificial chordae tendineae fixation

Surgical implantation of artificial chordae was a technique that was gaining acceptance. This technique involved suturing one or more artificial chordae to the head of a papillary muscle and the other end of the artificial chordae to the prolapsed leaflet (Aubert and Flecher, 2010). The length of the artificial chordae was appropriately adjusted to maintain the free edge of the anterior mitral leaflet at the same level as the free edge of the posterior leaflet below the annular plane to obtain an adequate area of apposition (Zussa et al., 1997). All chords attached directly to the papillary muscle (PM). The posteromedial PM gave chords to the medial half of both leaflets (i.e., posteromedial commissure, P3, A3 and half of P2 and A2) (Figure 1A). Similarly, the anterolateral PM chords attached to the lateral half of the MV leaflets (i.e., anterolateral commissure, A1, P1 and half of P2 and A2). During surgical mitral valve repair, the physician attached another segment of the artificial chordae tendineae to the papillary muscle following the normal anatomy.

In minimally invasive apical implantation, ePTFE artificial chordae were implanted on the leaflet and the chordae were stretched until adequate leaflet coaptation was achieved and then all chordae free ends were secured to the LV wall (Colli et al., 2018a). Annabel M et al. performed an *in vivo* biomechanical study of apical versus papillary neochordal anchoring for mitral regurgitation. Force tracings were compiled for each class of chordae at baseline, after prolapse, and after both repair techniques. Baseline forces were recorded for primary ($0.18 \text{ N} \pm 0.08 \text{ N}$) and secondary ($0.94 \text{ N} \pm 0.31 \text{ N}$). Echocardiographic and hemodynamic data

confirmed that the repairs restored physiological hemodynamics. Forces on the chordae and neochord were lower with papillary fixation than with apical fixation ($p = 0.003$). In addition, the maximum rate of change of force on the chordae and neochordae was higher for apical fixation than for papillary fixation (mean difference of 4.7 N/s , $p = 0.028$). Annabel M highlighted the impact of the anchoring position of artificial neochordae and might help guide strategies to increase durability. Although the development of minimally invasive and percutaneous devices for mitral valve repair was benefiting patients by providing superior survival and freedom from reoperation, adjustments to reduce leaflet stress were essential to fully utilize these new devices.

3.4.3 Chordal replacement in combination with partial leaflet resection

Chordal replacement with ePTFE strings to correct leaflet prolapse in patients with DMR was initially used for prolapse of the anterior leaflet, but over the years it was used to correct prolapse of all segments of the MV. The use of Gore-Tex sutures as artificial chords to replace native chordal has largely been used to correct prolapse of the anterior leaflet, commissural areas, and posterior leaflet with heights of 20 mm or less. However, large, voluminous posterior leaflets with prolapse must first be treated with partial resection followed by chordal replacement. Patients with advanced myxomatous degeneration often had large posterior leaflets and associated posterior displacement of the posterior mitral annulus. In these cases, the posterior leaflet was usually trimmed to a height of 15–18 mm, and the posterior leaflet was sutured back to the endocardium of the left ventricle with running 4-

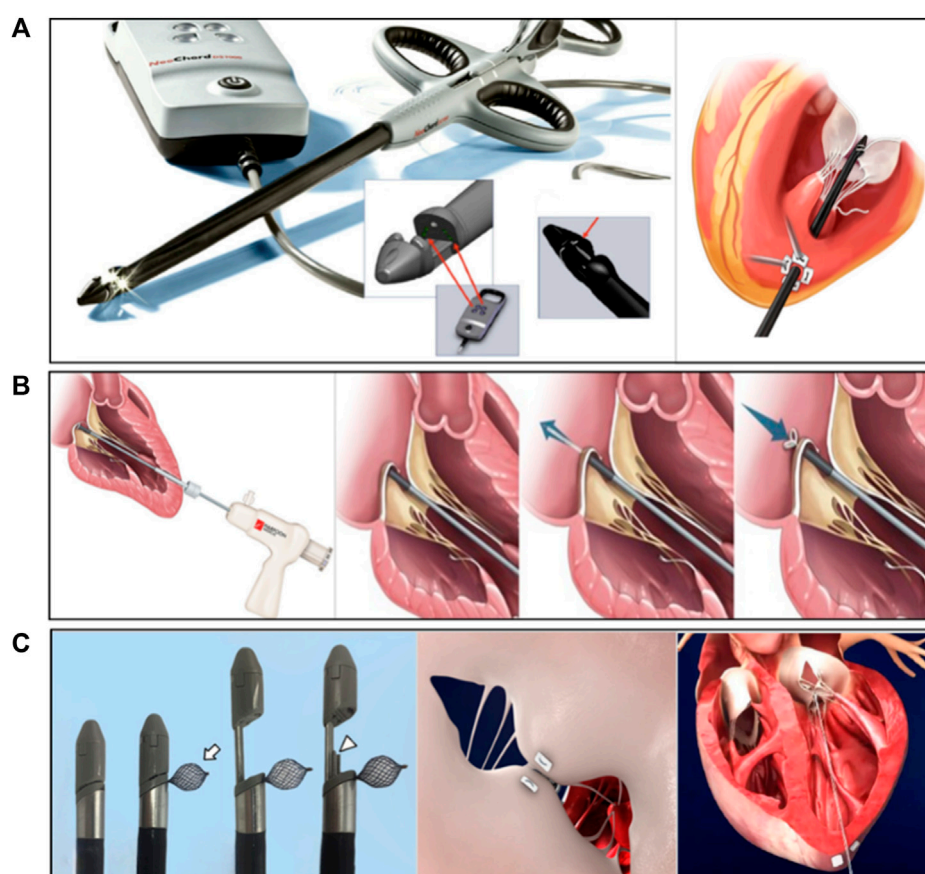


FIGURE 6

(A) The NeoChord DS 1000 system (Rucinkas et al., 2014; Fernando et al., 2020), (B) The Harpoon TSD-5 system (Gammie et al., 2016), (C) The MitralStitch system (Wang et al., 2018). Courtesy of (<http://www.dinovamedtech.com>).

0 polypropylene sutures (David et al., 2020). In David's study, isolated chordal replacement was used to correct prolapse in 186 (24.9%) patients and combined with leaflet resection in 560 (75.1%) patients. In their practice, chordal replacement with ePTFE sutures did not provide better results than MV repair using the established techniques of leaflet resection and chordal transfer, but it has dramatically increased the likelihood of MV repair in patients with MR due to leaflet prolapse.

Finite element results (Choi et al., 2017) showed that both repair techniques revealed reduced leaflet prolapse, decreased stress concentration, and restored leaflet coaptation. While neochordoplasty demonstrated further improved leaflet coaptation and superior posterior leaflet mobility, leaflet resection showed more uniform leaflet stress distributions. Virtual MV repair simulation has the ability to predict and quantify biomechanical and functional improvement after MV repair.

It could be said that chordal replacement with ePTFE sutures to correct mitral valve leaflet prolapse, either alone or in combination with leaflet resection all allowed a low probability of mitral valve reoperation and recurrent mitral regurgitation.

3.4.4 Concomitant combination therapy (COMBO)

A cohort of 595 (278 women, mean age 65 ± 16 years) consecutive patients with isolated mitral valve prolapse, with

comprehensive clinical, rhythmic, Doppler echocardiographic, and consistent mitral annular disjunction assessment. The presence of mitral annular disjunction was common [$n = 186$ (31%)] in patients with mitral valve prolapse, generally in younger patients, and was not random but was independently associated with severe myxomatous disease with bileaflet mitral valve prolapse and marked leaflet redundancy (Essayagh et al., 2021). Javier G reported that 744 consecutive patients with degenerative mitral regurgitation and prolapse underwent mitral valve surgery from January 2002 to December 2010 (Castillo et al., 2012). All patients underwent mitral valve repair with concomitant annuloplasty with a median ring size of 32 mm, and 175 patients (23.5%) underwent PTFE chordoplasty. Mitral ring annuloplasty could reverse annular dilation and restored the zone of coaptation in appropriately selected patients (Yap et al., 2021). If neochordae were implanted, concomitant annular reduction might help restore better systolic leaflet coaptation and reduced neochord forces. For transapical and transcatheter devices, there were several types of transcatheter mitral valve repair (TMVr) that targeted the leaflets, annulus and chordae. Concomitant combination (COMBO) therapy of TMVrs was rarely used as a treatment and there were very few publications about this therapeutic strategy (Yokoyama et al., 2023), only transcatheter edge-to-edge repair has been combined with other interventional repair methods to treat mitral regurgitation.

One could speculate that the COMBO approach might be a better option for patients suffering from severe MR with a selected anatomy where the combined devices could best play out their advantages, simultaneous mitral ring annuloplasty and PTFE chordoplasty as in surgical treatments.

4 Artificial chordae interventional implantation devices

Artificial chordae interventional repair was based on the proven chordae implantation technique, which used special devices to repair the valve while the heart was beating. The following section described the principle, implantation methods, force differences, and therapeutic effects of the artificial chordae interventional devices.

4.1 Transapical artificial chordal intervention implantation devices

At present, the apical chordae repair devices that have entered the clinical stage included NeoChord DS1000 (NeoChord, United States), Harpoon TSD-5 (Edwards Life Science, United States), MitralStitch (Hangzhou Valgen Medtech Co., Ltd., China), and other products. The technical difference was mainly in the method of anchoring the chordae. NeoChord and Harpoon have received CE certification (Savic et al., 2018).

4.1.1 Neochord DS1000 system

The Neochord DS1000 system was the first CE-marked transapical minimally invasive chordae repair product with over 1,700 patients implanted and was currently in FDA pivotal clinical trials. The system consisted of the Gore-Tex CV-4 size ePTFE suture. The conveyor has the following functions: valve leaf capture, optical fiber sensor detection of valve leaf capture, and artificial chordal anchor valve leaf (Figure 6A) (Rucinskas et al., 2014; Fernando et al., 2020). The procedure consisted of entering the left ventricle through the apical channel, crossing the mitral valve into the left atrium under TEE guidance, and then opening the collet to capture the leaflet. After the fiber optic sensor confirmed the capture, the leaflet was punctured and one end of the artificial chord was anchored to the leaflet edge, and the other end was withdrawn from the heart and fixed apically after real-time adjustment of the chord length to eliminate regurgitation under TEE guidance (Rucinskas et al., 2014).

Gerosa et al. (2021) reported a 3-year follow-up experience of a patients who underwent NeoChord DS1000 surgery for severe DMR due to single/bipartite leaflet mitral valve prolapse or flail between November 2013 and June 2019. The study enrolled 203 patients with severe DMR, of whom 200 (99%) had successful surgery (implantation of ≥ 2 pairs of chords and $MR \leq 1$); patient survival rates and primary endpoints (successful surgery, $MR \leq 2+$ and no major adverse events) were 91.2%, 89.7%, and 81.2% at 1, 2, and 3 years, respectively. Survival and re-intervention rates at 3 years were 94.0% and 6.4%, respectively. This suggested that the NeoChord DS1000 system for minimally invasive repair early to mid-term DMR was safe, effective, and reproducible. Early clinical

and echocardiographic results showed reduction in MR and significant improvement in symptoms with good left ventricular remodeling and low reintervention rates. However, the long-term effects needed to be confirmed with more clinical data and longer follow-up. The authors also examined the effect of different anatomic types (type A, isolated central posterior leaflet prolapse and/or flail; type B, posterior multisegmental prolapse; type C, anterior and/or bi-leaflet prolapse; and type D, paracommissural prolapse and/or flail and/or significant leaflet and/or annular calcifications) on repair outcomes, with probabilities of achieving effective end points of 88%, 83%, 72%, and 57%, respectively. This suggested that transapical chordal repair might be more appropriate for patients with posterior leaflet prolapse.

D'Onofrio et al. (2022) reviewed the treatment outcomes comparing the NeoChord DS1000 device group to the surgical group. A propensity analysis selected 88 matched pairs. Kaplan-Meier analysis showed similar 5-year survival in the 2 groups. The ratio of moderate/severe MR in patients who underwent instrumentation versus surgery was: $MR > 2+$ (42.4% vs. 15.4%) and $MR \geq 3+$ (21.6% vs. 10.3%), respectively; the reoperation rate was 21.1% vs. 8%, with a significant difference. However, in type A patients, moderate/severe MR (63.9% vs. 74.6% and 79.3% vs. 79%) and reoperation rates (79.7% vs. 85%) were close with no significant difference. Demonstrating that transapical beating-heart mitral valve chordae implantation can be considered as an alternative treatment for degenerative mitral regurgitation, especially in patients with isolated P2 (central posterior leaflet) region prolapse.

4.1.2 Harpoon system

The Harpoon system was another transapical chordal repair device (Figure 6B) (Gammie et al., 2016) that differed from the NeoChord DS1000 in that the chord was anchored to the root of the valve leaflet. The Harpoon system (Edwards Lifesciences, Irvine, CA, United States) was a 14-Fr, echo-guided, transapical chordal replacement device that allowed for the implantation of multiple and adjustable PTFE chordae. The Harpoon device was inserted and precisely navigated to the target. The prolapsed segment was punctured and an ePTFE chord was knotted on the atrial side of the prolapsed segment. The cord was externalized through the introducer (Gackowski et al., 2022). Safety and feasibility were demonstrated in the initial feasibility study in 30 patients with severe degenerative MR. At 1 month, MR was mild or less in 89% of patients and moderate in 11% of patients. At 6 months, MR was mild or less in 85% of patients, moderate in 8% of patients, and severe in 8% of patients (Gammie et al., 2021). Gammie et al. (2021) reported the results of a 1-year CE Mark clinical trial of the Harpoon system, mean study follow-up 1.4 ± 0.6 years, 1-year clinical follow-up was 100%, 1-year echo core lab follow-up for 52 patients at 1 year was 100%. 65 patients were enrolled and 62 (95%) achieved procedural success. Only two patients required conversion to surgery and one patient discontinued the procedure. Total procedure time was 126 ± 36 (72–222) min, and the introducer time was 42 ± 18 (18–126) min. Intraoperative blood loss was 272 ± 182 (50–949) ml and this data was collected for TRACER CE Mark study only ($n = 51$). The number of chords implanted was 4.0 ± 1.1 (0–7). During the perioperative period (from procedure to discharge), the rate of mortality, stroke rate,

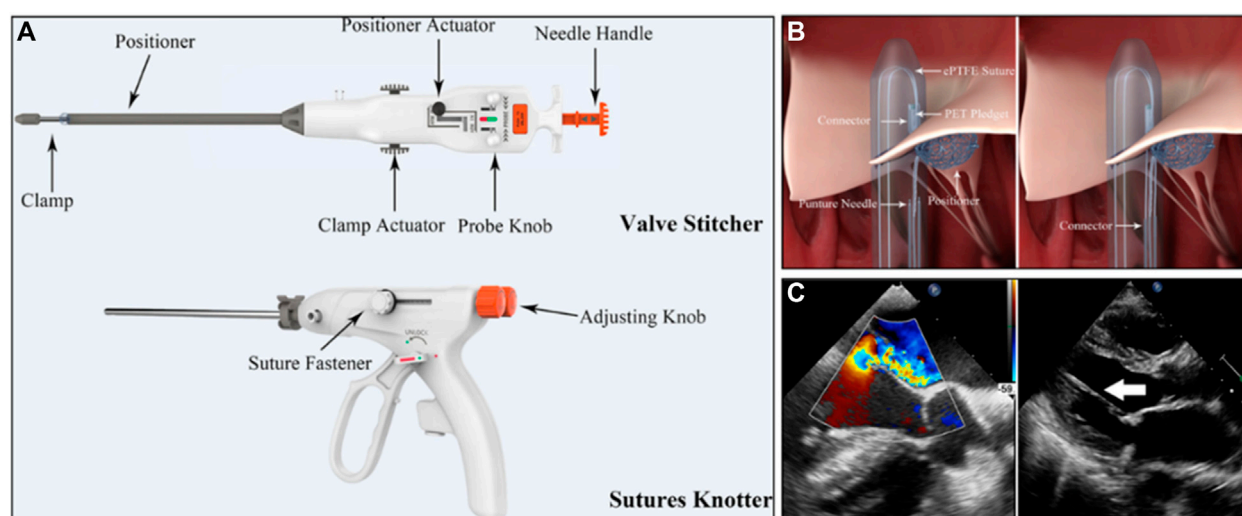


FIGURE 7

(A) The MitralStitch™ system device, Valve Stitcher and Sutures Knotter. The suture and pledget were preloaded in the head of the Valve Stitcher. (B) Mechanism of artificial chordae implantation by Valve Stitcher. (C) (Left) Intraprocedural two dimensional and color TEE image showing severe MR due to P2 region leaflet prolapse. (right) TTE view showing the implanted artificial chordae (arrow) (Wang S. et al., 2022).

renal failure, and atrial fibrillation rate were 0%, 0%, 0%, and 18%, respectively. Atrial fibrillation was pooled only for those without baseline atrial fibrillation ($n = 50$). At 1 year, 2 of the 62 patients died (3%) and 8 (13%) others required reoperation. At 1 year, 98% of patients with Harpoon cords were in New York Heart Association class I or II, and mitral regurgitation was none/trace in 52% ($n = 27$), mild in 23% ($n = 12$), moderate in 23% ($n = 12$), and severe in 2% ($n = 1$). Favorable cardiac remodeling outcome at 1 year included decreased end-diastolic left ventricular volume (153 ± 41 to 119 ± 28 ml) and diameter (53 ± 5 to 47 ± 6 mm), and a mean transmitral gradient of 1.4 ± 0.7 mmHg. This early clinical experience with the Harpoon beating heart mitral valve repair system demonstrated encouraging early safety and performance.

4.1.3 MitralStitch system

MitralStitch was the first product to offer both edge-to-edge repair and chordae repair. For edge-to-edge repair, a pair of chordae was implanted in each anterior and posterior leaflet, and the two chordae were locked together with titanium staples, resulting in a double-hole structure in the anterior and posterior leaflets (Figure 6C) (Wang et al., 2018). It was similar to NeoChord for chordae repair (Figure 7A). The chord was implanted at the edge of the leaflet and anchored to the apex of the heart (Figure 7B). Wang S. et al. (2022) reported the first-in-human (FIH) experience with MitralStitch, which was successful in all 10 patients with severe MR, including 9 patients who underwent chordae repair, and 1 patient who received chordae repair and edge-to-edge repair. At discharge, MR decreased from severe to trace in 5 patients and was mild in the other 5 patients (Figure 7C).

In conclusion, the transcatheter apical chordae repair device was easy to operate and had a high technical success rate. Theoretically, this technique can treat not only high-risk patients who were ineligible for surgery but also young patients with low surgical risk, which could largely replace traditional surgery and has a

promising application prospect. Appropriate patient inclusion criteria were also a key factor in achieving the best results. In some complex MR anatomies, surgical repair was superior. In type A patients with isolated P2 prolapse/flail, minimally invasive implantation via the apical approach was close to the early and mid-term results of surgery. Therefore, it was an ideal entry point for transapical chordal implantation as an adjunct to surgery. However, the transcatheter approach remained the ultimate approach for artificial chordae, as the apical approach was still traumatic and carried the risk of long-term pericardial adhesion.

4.2 Transcatheter intervention artificial chordae repair devices

Transcatheter chordae repair devices had attracted much attention due to their lower trauma and better compliance with the physiological and anatomical structure. However, due to their technical difficulties, the products were currently in animal experiments or early clinical stages, including NeoChord NeXus (NeoChord, United States), CardioMech (CardioMech, Norway) (Figure 8A) (Rogers and Bolling, 2021), and Pipeline (Gore, USA) (Figure 8B) (Fiocco et al., 2019), which have performed animal experiments and early clinical experiments. The transcatheter chordae repair device was composed of implants and a delivery system. The implants included ePTFE sutures (artificial chordae), papillary muscle anchor pieces, and leaflet anchor pieces connected at both ends. The delivery system included the large sheath for spacer puncture, the adjustable curved middle sheath, and the chordae implantation components (leaflet suture device, papillary muscle anchor device, chordae length adjustment, locking and cut-off devices, etc.). In addition, stents were included to assist in device stabilization procedures.

Unlike transapical artificial chordae devices, transcatheter devices required the implantation of metal anchors to hold sutures to the

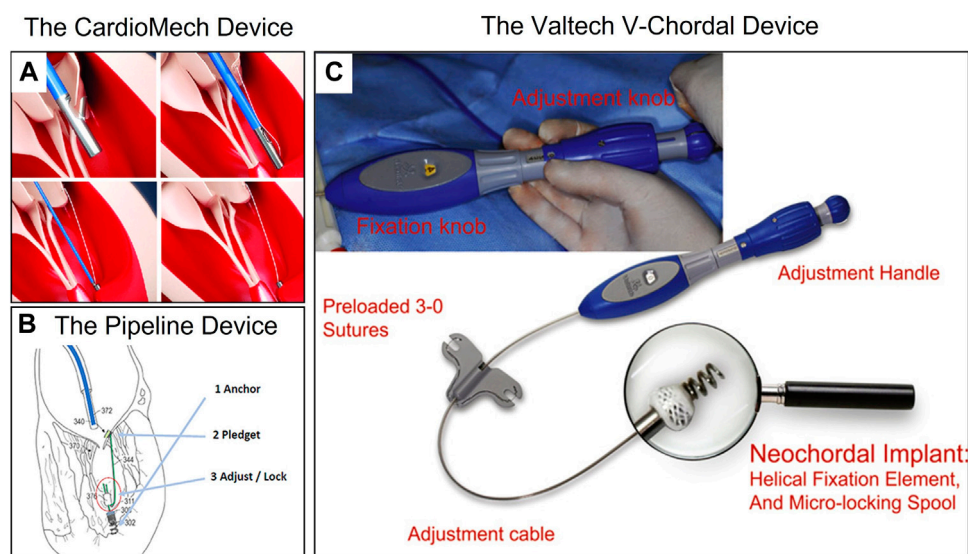


FIGURE 8

(A) The CardioMech Device. Courtesy of (CardioMech, Oslo, Norway) (Rogers and Bolling, 2021). (B) The Pipeline Device. Courtesy of (Pipeline Medical Technologies, Inc. a wholly-owned subsidiary of W.L. Gore & Associates, Inc., Santa Rosa, California) (Fiocco et al., 2019). (C) The Valtech V-Chordal Device. Courtesy of (Valtech, Or Yehuda, Israel) (Maisano et al., 2011).

papillary muscle, which may carry the risk of damaging the papillary muscle. Animal studies of the Neochord NeXuS system reported at the Transcatheter Cardiovascular Therapeutics (TCT) conference showed that the anchor nail on the papillary muscle was covered by fibrous tissue and endothelium at 90 days. Overall, the papillary muscle healed well overall and no obvious necrosis was observed. Maisano et al. (2011) compared the healing difference between metal screw anchors and surgical sutures anchoring the papillary muscle in the V-chordal system (Figure 8C) through *in vivo* experiments in sheep, and both showed good healing of at 90 days. Animal experiments with the Pipeline system also confirmed that the metal anchors did not damage the papillary muscle. These experiments provided preliminary confirmation of the *in vivo* safety of metal anchors for anchoring the papillary muscle.

Transcatheter chordae repair devices were still in the early stages of development due to their technical difficulty, and only a few clinical trials were reported. Rogers et al. (2020) reported in 2020 the first human trial of the Pipeline system (Figure 8B) in a 56-year-old male patient with severe MR due to prolapse in the P2 region, in which two artificial chords were successfully implanted transcatheterly and attached to a papillary muscle base anchor, eliminating MR intraoperatively. However, the papillary muscle anchor was found to be dislodged prior to discharge, resulting in recurrent MR, and the patient ultimately underwent mitral valve replacement. The authors concluded that the anchor nail displacement was related to the device technique and planned to reopen the clinical trial.

Unlike other solutions, the CardioMech system (Figure 8C) protocol implanted only a piece of chordal to treat MR, with metal pieces connected at both ends of the suture to anchor the leaflet and papillary muscle. Rinaldi reported three clinical trials of the CardioMech system at the TCT 2021 conference, and all three patients with P2 region prolapse had a reduction in MR from 4+ to <2+ after successful implantation of one chord, with no serious

adverse events occurring during the operation. However, postoperative dislodgement of the leaflet anchor nail occurred in all three patients and was ultimately unsuccessful.

The Neochord NeXuS system was a product based on the DS1000 for transfemoral/interatrial septal access that accessed the left atrium through a large 28F sheath via the femoral vein, captured the leaflet under the guidance of TEE and confirmed by a fiber optic sensor, and finally achieved multiple chords attached to a papillary muscle metal screw anchor. Currently, Latib et al. (2022) completed the FIH clinical trial with the Neochord NeXuS system in 2021 and reported 6-month follow-up results. Two pairs of artificial chords implanted in the leaflet and anchored to the anterior papillary muscle in a 55-year-old patient with prolapsed MR in the P2 region successfully reduced MR and maintained mild or trace MR at 1/3/6 months with firm anchoring of the papillary muscles without displacement.

Transcatheter chordae repair devices might be a viable and feasible option for the treatment of isolated single-leaflet prolapse in the future, with a good risk-benefit ratio. However, the technique and procedures were more complex with many steps and were still in the early stages of development, requiring stable devices, long-term follow-up, and more cases to confirm these preliminary results.

5 Artificial chordae rupture cases and failure factors

Transapical implantation of ePTFE chordae under beating heart condition was a minimally invasive interventional therapy with a very low rupture rate and proven durability and long-term results in a 25-year study published in 2013 (David et al., 2013), showing a bright prospect for the treatment of DMR. However, in early clinical trials, there were still reports of artificial chordae rupture cases,

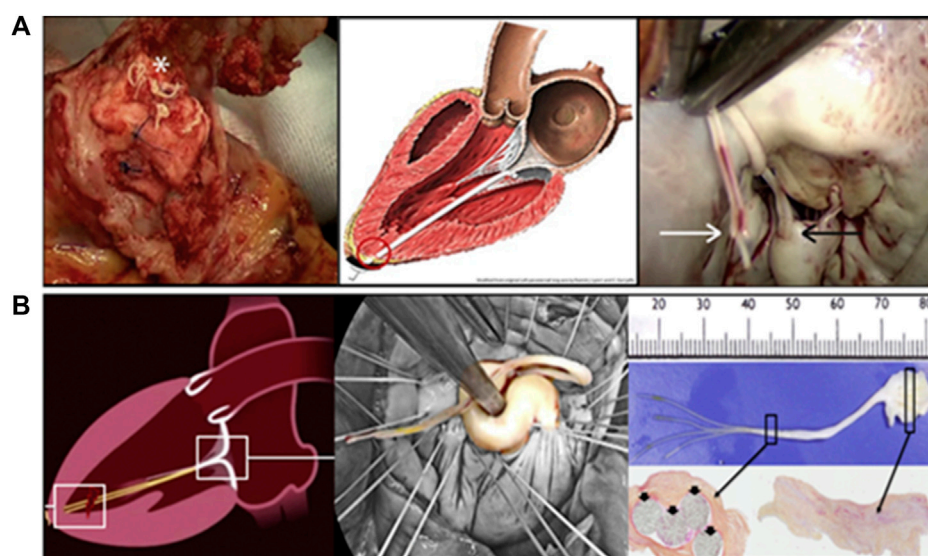


FIGURE 9
(A) A rupture in an implanted NeoChord below the knot and the pledget (Heuts et al., 2019). (B) Surgical view and histologic analysis of the resected ruptured neochords (Grinberg et al., 2019a).

whether in traditional surgery or intervention, (Mori et al., 2017). Although rare, the rupture of the artificial chordae might cause recurrent mitral regurgitation, endangering patients' health. We reviewed the cases of recurrent MR caused by rupture of ePTFE artificial chordae and discussed the possible causes of rupture.

Heuts et al. (2019) reported in 2019 that a female patient's implanted artificial chordae ruptured at the top of the apex knot (Figure 9A) during cycling 5 months after NeoChord treatment, resulting in acute MR. Grinberg et al. (2019a) reported two cases of chordae ruptured 1 year and 3 year after the implantation of the NeoChord DS1000 system in 2019. Both of them underwent second surgeries (Figure 9B). Bortolotti presented one patient with 2 pairs of CV-5 ePTFE implanted in the anterior leaflet that ruptured after 11 years postoperatively. In one case, only minimal calcification was observed, and the chordal rupture was therefore considered to be most likely related to weakening of the ePTFE by collagen infiltration and fatigue-induced lesions (Bortolotti et al., 2012a).

The long-term durability of transapical artificial chordae implantation was still unknown, so it was very important to understand the potential mechanism of chordal rupture.

5.1 Analysis of the force difference of artificial chordae between different anchorage positions

The durability and long-term effects of artificial chordae were closely related to the amount of force applied to them, and excessive force could lead to chordae rupture. The anchoring position and the length of the artificial chordae influenced their force. Surgical thoracotomy and transcatheter artificial chordae tended to be anchored to the leaflet and papillary muscles, whereas transapical chordae implantations tended to be leaflet and the apex. Since

artificial chordae implantation led to post-reconstruction shrinkage of the left ventricle, the length of the artificial chordae was often shortened somewhat from the optimal length to avoid recurrent MR (Bortolotti et al., 2012b). For apical anchoring, it was often clinically tightened by 5% from the optimal length; for papillary muscle-anchored chordae, it was shortened by 1–2 mm (Kasegawa et al., 1994).

Caballero et al. (2020) analyzed the effect of transapical anterolateral and posterolateral approaches and length on the force of artificial chordae through computer simulation. Their results showed that the forces on the artificial chordae with the anchoring position in the anterolateral apical region were generally greater than those in the posterolateral region, reaching more than 80% at the peak systolic period. Therefore, the postero-lateral approach was preferred for transapical minimally invasive instrumentation. Four artificial chordae were implanted in a model of severe MR due to prolapse the P2 region, and the total force was 2.68 N when the chordae were at their optimal length, which increased significantly with 5% tension, reaching a maximum total force of 12.2 N and a maximum force of 4.2 N for a single chord. Sturla et al. (2015) investigated the effect of the length of the artificial chords anchored to the papillary muscles on their force. The optimal length and the maximum force of 2 mm tightening were 1.31 and 1.62 N, respectively; when two artificial chordae were implanted, the maximum total force was 1.54 N for the optimal length and 1.92 N for the 2 mm tightening. According to the simulation force analysis, the force of the artificial chordae anchored at the apex was significantly higher than that of the papillary muscle, which might pose a challenge for the long-term durability of the artificial chordae implanted by transapical devices. Grinberg et al. (2019b) measured forces on the neochordae when implanted apically using the DS1000 system in humans. After all the neochordae were implanted, tracked the neochordae respectively. First, the neochordae implanted in the ideal location (in the middle of the

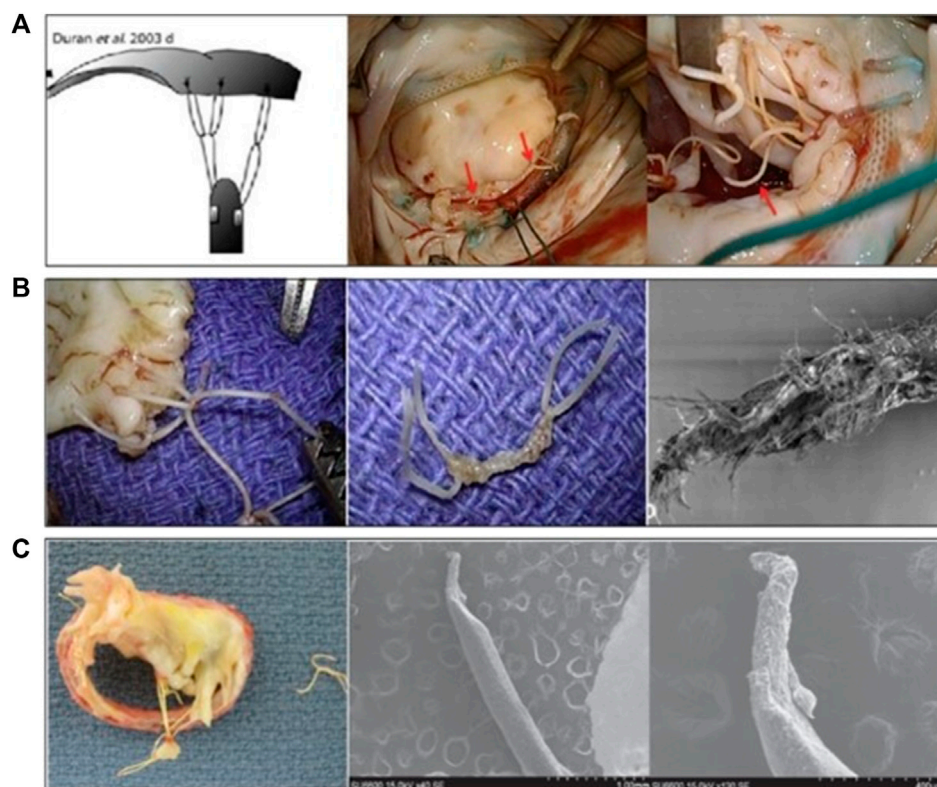


FIGURE 10

(A) The “loop” artificial chordal Implantation Technology (Duran and Pekar, 2003; Kudo et al., 2014), (B,C) Macro and SEM images of the partial fracture of the ePTFE loop (Castillo et al., 2013; Kudo et al., 2014).

prolapse) were tracked alone until the best TEE control was obtained. The tension was measured at between 0.7 and 0.9 N, and the oscillation in the amplitude of tension of about 13% that followed the respiratory cycles; second, the other neochordae were then tracked one by one with a single screw to achieve an equivalent tension on all neochordae, the tension of the neochordae tracked first was reduced from 0.8 N to 0.2–0.3 N when 4 neochordae were put in tension. The tension ($F = 0.98 \pm 0.08$ N) of all neochordae was higher than the previous tension ($F = 0.8$ N) of the tracked neochordae; then all neochordae were tracked together under TEE control until the optimal condition was reached. When the optimal TEE results were obtained, the tension of all neochordae was reduced to 0.87 ± 0.07 N, about $12\% \pm 2\%$ decrease; and finally all the neochordae were fixed at the apex of the left ventricle at the optimal length. During all the steps, neochordae tension, electrocardiogram, radial blood pressure, 3-D TEE, and surgical view were recorded. The author said in the section of study limitation that relative to the resistance, the length and direction of tension of the neochordae (from the leaflet free edge to the apex) were more important, which were different from those of the native chordae.

5.2 Differences in chordae implantation techniques in the leaflet

Differences in chordae implantation techniques might have a significant impact on the durability of the ePTFE artificial chordae.

We found several cases of chordae rupture in the “loop” implantation technique (Figure 10A) (Duran and Pekar, 2003; Kudo et al., 2014), probably due to frictional damage to the suture caused by the relative motion of the two loops during the cardiac cycle. This frictional rupture often occurred in the early and middle stages. Castillo described a case in which the “loop” technology was used for repair. Ultimately, the CV-5 ePTFE suture ruptured, which was analyzed by scanning electron microscopy (SEM) and found to be weakened at the point of contact between the two suture rings, which the author believed was caused by relative friction (Figure 10B) (Castillo et al., 2013). Kudo reported a case of CV-5 ePTFE suture loop rupture, which was found to be thinning by SEM, with a rupture time of 3 years, also using the “loop” technique (Figure 10C) (Kudo et al., 2014). Yamashita and Skarsgard (2011) reported two cases of early CV-5 ePTFE rupture at 14 and 2 months postoperatively, respectively, using the “loop” technique in both patients.

5.3 Calcification

Calcification might be one of the causes of the late rupture of ePTFE artificial chordae. Butany et al. (2004) reported a case of rupture after 14 years postoperatively. Histopathology showed that the ePTFE sutures ruptured due to calcification, but no inflammatory cells were found inside and around the sutures

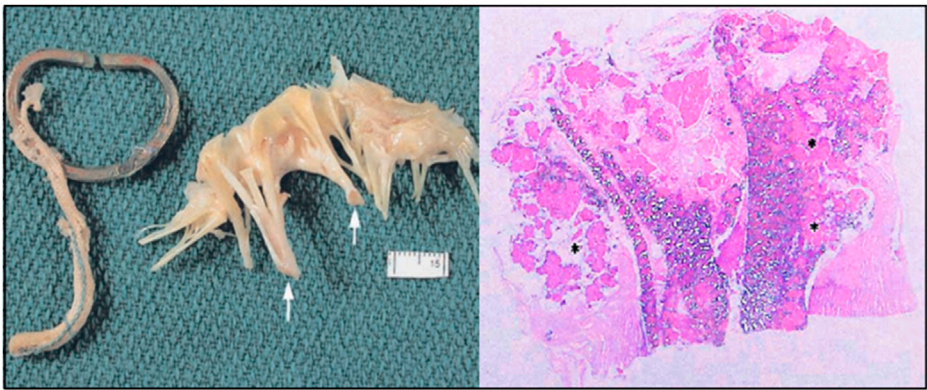


FIGURE 11
The anterior leaflets showed thickening chordae tendineae (white arrows). Longitudinal sections through the ruptured ePTFE suture. Large areas of mineralization were seen within the graft interstices and in the areas surrounding the graft (asterisk) (stain: hematoxylin and eosin, tissue viewed with polarized light, original magnification = $\times 1.6$) (Butany et al., 2004).

(Figure 11). Luthra et al. (2022) reported a 76-year-old woman who presented with severe mitral regurgitation 6 years after Neochord artificial chordae repair with Gore-Tex, the explanted sutures were found to be ruptured and stiff. Electron microscopy revealed microstructural disruption with extensive calcium infiltration at the site of rupture. Farivar et al. (2009) reported a case of rupture of two pairs of CV-5 chords after 11 years after the implantation in which the ePTFE was thickened and hardened. Coutinho et al. (2007) reported two cases of rupture; one patient had two pairs of CV-5 sutures implanted with a rupture time of 6 years and an unknown cause of rupture; the other patient also had two pairs of CV-5 sutures implanted with 1 pair of chords ruptured after 11 years due to calcification.

5.4 Specification of sutures

The rupture of the ePTFE artificial chordae might also be related to the suture specification. First, in all of the above cases, the sutures that ruptured were mainly CV-5 ePTFE sutures. Mutsuga reviewed the failure cases of using ePTFE artificial chordae from 2002 to 2020. One (0.5%) of 186 patients using CV-4 ruptured at 78 months. In addition, 6 (3.9%) of 154 patients using CV-5 ruptured at 44–201 months. The durability of CV-4 specification ePTFE suture might be better than CV-5 (Table 4) (Mutsuga et al., 2022). Therefore, there was a growing preference among physicians to use CV-4 with a thicker line diameter and stronger mechanical properties, and to increase the number of sutures to distribute the force on a single suture (David et al., 2020).

5.5 Other factors

There were also some cases where fracture factors were not described. Nakaoka reported a patient with three pairs of CV-5 ePTFE implanted in the anterior leaflet, in which one pair of ePTFE ruptured after 7 years, and the suture was thickened (Nakaoka et al., 2017). Yeo described a patient with chordal rupture at 4 months

TABLE 4 Distribution of use of expanded polytetrafluoroethylene suture on each mitral valve (Mutsuga et al., 2022).

Suture	AML	PML	AML + PML	Others
CV-4				
Ruptured ePTFE	1	0	0	0
Number	186	238	116	84
patients	45	59	18	17
Rupture rate, %	0.5	0	0	0
CV-5				
Ruptured ePTFE	6	9	0	0
Number	154	394	96	176
patients	41	95	16	23
Rupture rate, %	3.9	2.3	0	0
p-value	.03	.019

AML, anterior mitral leaflet; PML, posterior mitral leaflet.

postoperatively (Yeo et al., 1998), and Lam reported a case with an unknown rupture time, neither of which mentioned the cause of the rupture (Lam et al., 2004).

6 Conclusion and outlook

At present, the use of ePTFE artificial chordae to resolve mitral valve prolapse caused by extended or ruptured native chordae has become a mature method with a clinical history of more than 35 years, providing stable valve function and clinical outcomes in most patients with DMR. The long-term durability of ePTFE played a key role, which was closely related to its physicochemical properties and biocompatibility. Although this technology was safe and effective, there were still cases of ePTFE artificial suture rupture occurring due to chordae calcification, friction, surgical injury, and excessive force. Therefore, when performed artificial chordae repair, some measures could be taken to reduce the probability of this adverse event, such as 1) paying attention to chordae implantation and suturing techniques to avoid frictional

damage to the sutures; 2) increasing the number of chords to reduce the force distributed on each suture; and 3) using CV-4 instead of CV-5, which had a thicker string diameter and stronger mechanical properties.

Artificial chordae interventional devices had gradually become a substitute therapy for high-risk DMR patients, providing physicians with a variety of options. The two different types of devices had their own advantages and disadvantages. Among them, the transapical chordae repair devices had more clinical data, relatively simple technique and operation, and a high success rate, but it was traumatic, and the force on the chordae was greater than the papillary muscle anchoring. Transcatheter chordae repair devices were in the early investigational phase with limited clinical data. Their advantages include less trauma and anchoring of the chordae to the papillary muscle, which was closer to the physiologic and anatomic structure. However, they had narrow indications and anatomical limitations, and the technique and operation were relatively complex. In the future, clinical studies with larger sample size and longer follow-up are necessary to confirm the long-term outcomes and patient selection criteria.

As an important part of the interventional mitral valve treatment technology, transcatheter chordae repair technology will continue to be a mainstream development direction in the field of interventional mitral valve treatment in the future, which has unparalleled advantages over interventional mitral valve replacement such as:

- (1) More physiological.
- (2) Less impact on mitral valve hemodynamics.
- (3) No interference with future secondary surgical procedures.
- (4) Feasibility for low-risk, low-grade patients.

The continued emergence of interventional transcatheter chordae repair devices via the femoral vein also meant that a solid step had been taken in this technical field and that it still had a wild prospective.

For the patients with prolapse but no significant dilatation of the valve ring, whose cardiac function was still good, interventional transcatheter chordae repair devices were the most beneficial for them at that time.

However, in high-risk patients with severe mitral regurgitation leading to the stage of heart failure, the lack of clinical experience

with simple interventional artificial chordae repair and the existence of distant recurrent regurgitation risk, which to some extent limits the application of artificial chordae, but we still have reason to believe that with the accumulation of experience and the progress of technology, the complete intervention of mitral valve repair will no longer be an unattainable dream.

Author contributions

Conceptualization, TZ, YW, LY, and RL; methodology, investigation, TZ and WZ; data analyses, resources, and writing (original draft), TZ and YD; review, editing and supervision, YW and KM; funding acquisition, YW; supervision, resources, XZ. All authors contributed to the article and approved the submitted version.

Funding

This work was financially supported by the National Key Research and Development Programs, China (Grant No. 2022YFC2409100), the CAMS Innovation Fund for Medical Sciences (Grant No. 2021-I2M-5-013).

Conflict of interest

Authors TZ, WZ, and KM were employed by Hangzhou Valgen Medtech Co., Ltd., China.

The remaining authors declare that the research was conducted in the absence of any commercial or financial relationships that could be construed as a potential conflict of interest.

Publisher's note

All claims expressed in this article are solely those of the authors and do not necessarily represent those of their affiliated organizations, or those of the publisher, the editors and the reviewers. Any product that may be evaluated in this article, or claim that may be made by its manufacturer, is not guaranteed or endorsed by the publisher.

References

- Ahmed, A., Abdel-Aziz, T. A., AlAsaad, M. M. R., and Majthoob, M. (2021). Transapical off-pump mitral valve repair with NeoChord implantation: A systematic review. *J. Card. Surg.* 36 (4), 1492–1498. doi:10.1111/jocs.15350
- Ali, M., Shreenivas, S. S., Pratt, D. N., Lynch, D. R., and Kereiakes, D. J. (2020). Percutaneous interventions for secondary mitral regurgitation. *Circ. Cardiovasc. Interv.* 13 (8), e008998. doi:10.1161/CIRCINTERVENTIONS.120.008998
- Aubert, S., and Flecher, E. (2010). Is an anterior mitral leaflet prolapse still a challenge? *Arch. Cardiovasc. Dis.* 103 (3), 192–195. doi:10.1016/j.acvd.2009.12.002
- Bech-Hanssen, O., Rydén, T., Scherstén, H., Odén, A., Nilsson, F., and Jeppsson, A. (2003). Mortality after mitral regurgitation surgery: Importance of clinical and echocardiographic variables. *Eur. J. Cardiothorac. Surg.* 24 (5), 723–730. doi:10.1016/s1010-7940(03)00502-5
- Blumenstein, J., Van Linden, A., Arsalan, M., Moellmann, H., Liebrau, C., Walther, T., et al. (2012). Transapical access: Current status and future directions. *Expert Rev. Med. Devices* 9 (1), 15–22. doi:10.1586/erd.11.66
- Bortolotti, U., Celiento, M., Pratali, S., Anastasio, G., and Pucci, A. (2012a). Recurrent mitral regurgitation due to ruptured artificial chordae: Case report and review of the literature. *J. Heart Valve Dis.* 21 (4), 440–443. PMID: 22953668.
- Bortolotti, U., Milano, A. D., and Frater, R. W. M. (2012b). Mitral valve repair with artificial chordae: A review of its history, technical details, long-term results, and pathology. *Ann. Thorac. Surg.* 93 (2), 684–691. doi:10.1016/j.athoracsur.2011.09.015
- Butany, J., Collins, M. J., and David, T. E. (2004). Ruptured synthetic expanded polytetrafluoroethylene chordae tendinae. *Cardiovasc. Pathol.* 13 (3), 182–184. doi:10.1016/S1054-8807(04)00006-7
- Caballero, A., Mao, W., McKay, R., and Sun, W. (2020). Transapical mitral valve repair with neochordae implantation: FSI analysis of neochordae number and complexity of leaflet prolapse. *Int. J. Numer. Method. Biomed. Eng.* 36 (3), e3297. doi:10.1002/cnm.3297
- Casado, J. A., Diego, S., Ferreño, D., Ruiz, E., Carrascal, I., Méndez, D., et al. (2012). Determination of the mechanical properties of normal and calcified human mitral

- chordae tendineae. *J. Mech. Behav. Biomed. Mater.* 13 (0), 1–13. doi:10.1016/j.jmbbm.2012.03.016
- Castillo, J. G., Anyanwu, A. C., Fuster, V., and Adams, D. H. (2012). A near 100% repair rate for mitral valve prolapse is achievable in a reference center: Implications for future guidelines. *J. Thorac. Cardiovasc. Surg.* 144 (2), 308–312. doi:10.1016/j.jtcvs.2011.12.054
- Castillo, J. G., Anyanwu, A. C., El-Eshmawi, A., Gordon, R. E., and Adams, D. H. (2013). Early rupture of an expanded polytetrafluoroethylene neochord after complex mitral valve repair: An electron microscopic analysis. *J. Thorac. Cardiovasc. Surg.* 145 (3), e29–e31. doi:10.1016/j.jtcvs.2012.12.011
- Choi, A., McPherson, D. D., and Kim, H. (2017). Neochordoplasty versus leaflet resection for ruptured mitral chordae treatment: Virtual mitral valve repair. *Comput. Biol. Med.* 90, 50–58. doi:10.1016/j.combiomed.2017.09.006
- Colli, A., Adams, D., Fiocco, A., Pradegan, N., Longinotti, L., Nadali, M., et al. (2018a). Transapical NeoChord mitral valve repair. *Ann. Cardiothorac. Surg.* 7 (6), 812–820. doi:10.21037/acs.2018.11.04
- Colli, A., Manzan, E., Aidietis, A., Rucinskas, K., Bizzotto, E., Besola, L., et al. (2018b). An early European experience with transapical off-pump mitral valve repair with NeoChord implantation. *Eur. J. Cardiothorac. Surg.* 54 (3), 460–466. doi:10.1093/ejcts/ezy064
- Coutinho, G., Carvalho, L., and Antunes, M. (2007). Acute mitral regurgitation due to ruptured ePTFE neo-chordae. *J. Heart Valve Dis.* 16 (3), 278–281. PMID: 17578048
- David, T. E., Armstrong, S., and Ivanov, J. (2013). Chordal replacement with polytetrafluoroethylene sutures for mitral valve repair: A 25-year experience. *J. Thorac. Cardiovasc. Surg.* 145 (6), 1563–1569. doi:10.1016/j.jtcvs.2012.05.030
- David, T. E., David, C. M., Lafreniere-Roula, M., and Manliot, C. (2020). Long-term outcomes of chordal replacement with expanded polytetrafluoroethylene sutures to repair mitral leaflet prolapse. *J. Thorac. Cardiovasc. Surg.* 160 (2), 385–394.e1. doi:10.1016/j.jtcvs.2019.08.006
- David, T. E. (1989). Replacement of chordae tendineae with expanded polytetrafluoroethylene sutures. *J. Card. Surg.* 4 (4), 286–290. doi:10.1111/j.1540-8191.1989.tb00291.x
- David, T. E. (2004). Artificial chordae. *Semin. Thorac. Cardiovasc. Surg.* 16 (2), 161–168. doi:10.1053/j.semthor.2004.03.004
- David, T. E. (2022). Chordal replacement with expanded polytetrafluoroethylene sutures to correct leaflet prolapse. *Ann. Thorac. Surg.* 115, 103–104. doi:10.1016/j.athoracsur.2022.06.002
- D'Onofrio, A., Mastro, F., Nadali, M., Fiocco, A., Pittarello, D., Aruta, P., et al. (2022). Transapical beating heart mitral valve repair versus conventional surgery: A propensity-matched study. *Interact. Cardiovasc. Thorac. Surg.* 35 (1), ivac053. doi:10.1093/icvts/ivac053
- Duran, C. M. G., and Pekar, F. (2003). Techniques for ensuring the correct length of new mitral chords. *J. Heart Valve Dis.* 12 (2), 156–161. PMID: 12701786
- Enriquez-Sarano, M., Atkins, C. W., and Vahanian, A. (2009). Mitral regurgitation. *Lancet* 373 (9672), 1382–1394. doi:10.1016/S0140-6736(09)60692-9
- Essayagh, B., Sabbag, A., Antoine, C., Benfari, G., Batista, R., Yang, L.-T., et al. (2021). The mitral annular disjunction of mitral valve prolapse: Presentation and outcome. *JACC Cardiovasc. Imaging* 14 (11), 2073–2087. doi:10.1016/j.jcmg.2021.04.029
- Falk, V., Seeburger, J., Czesla, M., Borger, M. A., Willige, J., Kuntze, T., et al. (2008). How does the use of polytetrafluoroethylene neochordae for posterior mitral valve prolapse (loop technique) compare with leaflet resection? A prospective randomized trial. *J. Thorac. Cardiovasc. Surg.* 136 (5), 1200–1206. doi:10.1016/j.jtcvs.2008.07.028
- Farivar, R. S., Shernan, S. K., and Cohn, L. H. (2009). Late rupture of polytetrafluoroethylene neochordae after mitral valve repair. *J. Thorac. Cardiovasc. Surg.* 137 (2), 504–506. doi:10.1016/j.jtcvs.2008.02.053
- Fernando, R. J., Shah, R., Yang, Y., Goeddel, L. A., Villablanca, P. A., Núñez-Gil, I. J., et al. (2020). Transcatheter mitral valve repair and replacement: Analysis of recent data and outcomes. *J. Cardiothorac. Vasc. Anesth.* 34 (10), 2793–2806. doi:10.1053/j.jvca.2020.01.009
- Fiocco, A., Nadali, M., Speziali, G., and Colli, A. (2019). Transcatheter mitral valve chordal repair: Current indications and future perspectives. *Front. Cardiovasc. Med.* 6, 128–138. doi:10.3389/fcvm.2019.00128
- Frazer, R. W. M., Gabbay, S., Shore, D., Factor, S., and Strom, J. (1983). Reproducible replacement of elongated or ruptured mitral valve chordae. *Ann. Thorac. Surg.* 35 (1), 14–28. doi:10.1016/S0003-4975(10)61426-9
- Gackowski, A., D'Ambra, M. N., Diprose, P., Szymański, P., Duncan, A., Bartus, K., et al. (2022). Echocardiographic guidance for HARPOON beating-heart mitral valve repair. *Eur. Heart J. - Cardiovasc. Imaging* 23 (2), 294–297. doi:10.1093/ehjci/jeab044
- Gammie, J. S., Wilson, P., Bartus, K., Gackowski, A., Hung, J., D'Ambra, M. N., et al. (2016). Transapical beating-heart mitral valve repair with an expanded polytetrafluoroethylene cordal implantation device. *Circulation* 134 (3), 189–197. doi:10.1161/CIRCULATIONAHA.116.022010
- Gammie, J. S., Chikwe, J., Badhwar, V., Thibault, D. P., Vemulapalli, S., Thourani, V. H., et al. (2018b). Isolated mitral valve surgery: The society of thoracic surgeons adult cardiac surgery database analysis. *Ann. Thorac. Surg.* 106 (3), 716–727. doi:10.1016/j.athoracsur.2018.03.086
- Gammie, J. S., Bartus, K., Gackowski, A., Szymanski, P., Bilewska, A., Kusmierczyk, M., et al. (2021). Safety and performance of a novel transventricular beating heart mitral valve repair system: 1-year outcomes. *Eur. J. Cardiothorac. Surg.* 59 (1), 199–206. doi:10.1093/ejcts/ezaa256
- Gerosa, G., Nadali, M., Longinotti, L., Ponzone, M., Caraffa, R., Fiocco, A., et al. (2021). Transapical off-pump echo-guided mitral valve repair with neochordae implantation mid-term outcomes. *Ann. Cardiothorac. Surg.* 10 (1), 131–140. doi:10.21037/acs-2020-mv-86
- Gillinov, A. M., Blackstone, E. H., Nowicki, E. R., Slisatkov, W., Al-Dossari, G., Johnston, D. R., et al. (2008). Valve repair versus valve replacement for degenerative mitral valve disease. *J. Thorac. Cardiovasc. Surg.* 135 (4), 885–893.e2. doi:10.1016/j.jtcvs.2007.11.039
- Grinberg, D., Adamou Nouhou, K., Pozzi, M., and Obadia, J.-F. (2019a). Artificial mitral chordae: When length matters. *J. Thorac. Cardiovasc. Surg.* 157 (2), e23–e25. doi:10.1016/j.jtcvs.2018.09.015
- Grinberg, D., Cottinet, P.-J., Thivolet, S., Audigier, D., Capsal, J.-F., Le, M.-Q., et al. (2019b). Measuring chordae tension during transapical neochordae implantation: Toward understanding objective consequences of mitral valve repair. *J. Thorac. Cardiovasc. Surg.* 158 (3), 746–755. doi:10.1016/j.jtcvs.2018.10.029
- Hata, H., Fujita, T., Shimahara, Y., Sato, S., Ishibashi-Ueda, H., and Kobayashi, J. (2014). A 25-year study of chordal replacement with expanded polytetrafluoroethylene in mitral valve repair. *Interact. Cardiovasc. Thorac. Surg.* 20 (4), 463–469. doi:10.1093/icvts/ivu441
- Heuts, S., Daemen, J. H. T., Streukens, S. A. F., Olsthoorn, J. R., Vainer, J., Cheriex, E. C., et al. (2018). Preoperative planning of transapical beating heart mitral valve repair for safe adaptation in clinical practice. *Innovations* 13 (3), 200–206. doi:10.1097/imv.0000000000000506
- Heuts, S., Kawczynski, M., Olsthoorn, J. R., and Sardari Nia, P. (2019). Late rupture of transapically beating heart implanted neochords. *J. Thorac. Cardiovasc. Surg.* 157 (2), e27–e29. doi:10.1016/j.jtcvs.2018.07.106
- Ibrahim, M., Rao, C., and Athanasios, T. (2012). Artificial chordae for degenerative mitral valve disease: Critical analysis of current techniques. *Interact. Cardiovasc. Thorac. Surg.* 15 (6), 1019–1032. doi:10.1093/icvts/ivs387
- January, L. E., Fisher, J. M., and Ehrenhaft, J. L. (1962). Mitral insufficiency resulting from rupture of normal chordae tendineae: Report of a surgically corrected case. *Circulation* 26 (0), 1329–1333. doi:10.1161/01.cir.26.6.1329
- Kasegawa, H., Kamata, S., Hirata, S., Kobayashi, N., Mannouji, E., Ida, T., et al. (1994). Simple method for determining proper length of artificial chordae in mitral valve repair. *Ann. Thorac. Surg.* 57 (1), 237–238. doi:10.1016/0003-4975(94)90413-8
- Kavakli, A. S., Ozturk, N. K., Ayoglu, R. U., Emmiler, M., Ozyurek, L., Inanoglu, K., et al. (2016). Anesthetic management of transapical off-pump mitral valve repair with NeoChord implantation. *J. Cardiothorac. Vasc. Anesth.* 30 (6), 1587–1593. doi:10.1053/j.jvca.2016.06.031
- Kay, J. H., and Egerton, W. S. (1963). The repair of mitral insufficiency associated with ruptured chordae tendineae. *Ann. Surg.* 157 (3), 351–360. doi:10.1097/0000658-196303000-00005
- Kiefer, P., Meier, S., Noack, T., Borger, M. A., Ender, J., Hoyer, A., et al. (2018). Good 5-year durability of transapical beating heart off-pump mitral valve repair with neochordae. *Ann. Thorac. Surg.* 106 (2), 440–445. doi:10.1016/j.athoracsur.2018.01.092
- Kobayashi, J., Sasako, Y., Bando, K., Minatoya, K., Niwaya, K., and Kitamura, S. (2000). Ten-year experience of chordal replacement with expanded polytetrafluoroethylene in mitral valve repair. *Circulation* 102(Suppl. 1_3), III30–III34–34. doi:10.1161/01.cir.102.suppl_3.iii-30
- Kudo, M., Yozu, R., and Okamoto, K. (2014). Recurrent mitral regurgitation due to ruptured ePTFE neochordae after mitral valve repair by the loop technique: A report of case. *Ann. Thorac. Cardiovasc. Surg.* 20 (Suppl. ment), 746–749. doi:10.5761/atcs.cr.13-00240
- Kunzelman, K. S., and Cochran, R. P. (1990). Mechanical properties of basal and marginal mitral valve chordae tendineae. *ASAIO Trans.* 36 (3), M405–M408. PMID: 2252712
- Lam, B.-K., Cosgrove, D. M., Bhudia, S. K., and Gillinov, A. M. (2004). Hemolysis after mitral valve repair: Mechanisms and treatment. *Ann. Thorac. Surg.* 77 (1), 191–195. doi:10.1016/S0003-4975(03)01455-3
- Lange, R., Guenther, T., Noebauer, C., Kiefer, B., Eichinger, W., Voss, B., et al. (2010). Chordal replacement versus quadrangular resection for repair of isolated posterior mitral leaflet prolapse. *Ann. Thorac. Surg.* 89 (4), 1163–1170. doi:10.1016/j.athoracsur.2009.12.057
- Latib, A., Ho, E. C., Scotti, A., Modine, T., Shaburishvili, T., Zirkashvili, T., et al. (2022). First-in-Human transseptal transcatheter mitral chordal repair. *JACC Cardiovasc. Interv.* 15 (17), 1768–1769. doi:10.1016/j.jcin.2022.05.020
- Li, J., Pan, W., Yin, Y., Cheng, L., and Shu, X. (2016). Prevalence and correlates of mitral regurgitation in the current era: An echocardiography study of a Chinese patient population. *Acta Cardiol.* 71 (1), 55–60. doi:10.1080/AC.71.1.3132098

- Luthra, S., Eissa, A., Malvindi, P. G., and Tsang, G. M. (2022). Calcification of gore-tex neochord after mitral repair: Electron microscopy. *Ann. Thorac. Surg.* 114 (1), e1–e3. doi:10.1016/j.athoracsur.2021.08.057
- Madhurapantula, R. S., Krell, G., Morfin, B., Roy, R., Lister, K., and Orgel, J. P. R. O. (2020). Advanced methodology and preliminary measurements of molecular and mechanical properties of heart valves under dynamic strain. *Int. J. Mol. Sci.* 21 (3), 763–779. doi:10.3390/ijms21030763
- Maisano, F., Cioni, M., Seeburger, J., Falk, V., Mohr, F. W., Mack, M. J., et al. (2011). Beating-heart implantation of adjustable length mitral valve chordae: Acute and chronic experience in an animal model. *Eur. J. Cardiothorac. Surg.* 40 (4), 840–847. doi:10.1016/j.jcts.2011.01.021
- Maisano, F., Buzzatti, N., Taramasso, M., and Alfieri, O. (2013). Mitral transcatheter Technologies. *Rambam Maimonides Med. J.* 4 (3), e0015. doi:10.5041/RMMJ.10115
- Mori, M., Pang, P., and Hashim, S. (2017). Rupture of GORE-TEX neochordae 10 years after mitral valve repair. *J. Thorac. Dis.* 9 (4), E343–E345. doi:10.21037/jtd.2017.03.64
- Morris, J. D., Penner, D. A., and Brandt, R. L. (1964). Surgical correction of ruptured chordae tendineae. *J. Thorac. Cardiovasc. Surg.* 48 (5), 772–780. doi:10.1016/S0022-5223(19)33360-4
- Mutsuga, M., Narita, Y., Tokuda, Y., Uchida, W., Ito, H., Terazawa, S., et al. (2022). Predictors of failure of mitral valve repair using artificial chordae. *Ann. Thorac. Surg.* 113 (4), 1136–1143. doi:10.1016/j.athoracsur.2021.04.084
- Nakaoka, Y., Kubokawa, S.-i., Yamashina, S., Yamamoto, S., Teshima, H., Irie, H., et al. (2017). Late rupture of artificial neochordae associated with hemolytic anemia. *J. Cardiol. Cases* 16 (4), 123–125. doi:10.1016/j.jccase.2017.06.007
- Nistal, F., García-Martínez, V., Arbe, E., Fernández, D., Artiñano, E., Mazorra, F., et al. (1990). *In vivo* experimental assessment of polytetrafluoroethylene trileaflet heart valve prosthesis. *J. Thorac. Cardiovasc. Surg.* 99 (6), 1074–1081. doi:10.1016/S0022-5223(20)31464-1
- Oh, N., Kampaktsis, P., Gallo, M., Guariento, A., Weixler, V., Staffa, S., et al. (2020). An updated meta-analysis of MitraClip versus surgery for mitral regurgitation. *ACS* 10 (1), 1–14. doi:10.21037/acs-2020-mv-24
- Perier, P., Hohenberger, W., Lakew, F., Batz, G., Urbanski, P., Zacher, M., et al. (2008). Toward a new paradigm for the reconstruction of posterior leaflet prolapse: Midterm results of the “respect rather than resect” approach. *Ann. Thorac. Surg.* 86 (3), 718–725. doi:10.1016/j.athoracsur.2008.05.015
- Pomar, J. L., Revuelta, J. M., and Frater, R. (2013). Cuerdas artificiales de ePTFE: ¿imprescindibles en las técnicas de preservación mitral actuales? *Cirugía Cardiovasc.* 20 (3), 119–121. doi:10.1016/j.circv.2013.09.001
- Revuelta, J. M., Garcia-Rinaldi, R., Gaité, L., Val, F., and Garijo, F. (1989). Generation of chordae tendineae with polytetrafluoroethylene stents: Results of mitral valve chordal replacement in sheep. *J. Thorac. Cardiovasc. Surg.* 97 (1), 98–103. doi:10.1016/S0022-5223(19)35132-3
- Rittenhouse, E. A., Davis, C. C., Wood, S. J., and Sauvage, L. R. (1978). Replacement of ruptured chordae tendineae of the mitral valve with autologous pericardial chordae. *J. Thorac. Cardiovasc. Surg.* 75 (6), 870–876. doi:10.1016/S0022-5223(19)39602-3
- Rogers, J. H., and Bolling, S. F. (2021). Transseptal chordal replacement: Early experience. *Ann. Cardiothorac. Surg.* 10 (1), 50–56. doi:10.21037/acs-2020-mv-10
- Rogers, J. H., Ebner, A. A., Boyd, W. D., Lim, S., Reardon, M. J., Smith, T. W., et al. (2020). First-in-Human transfemoral transseptal mitral valve chordal repair. *JACC Cardiovasc. Interv.* 13 (11), 1383–1385. doi:10.1016/j.jcin.2019.12.019
- Rucinskas, K., Janauskas, V., Zakarkaitė, D., Aidietienė, S., Samalavicius, R., Speziali, G., et al. (2014). Off-pump transapical implantation of artificial chordae to correct mitral regurgitation: Early results of a single-center experience. *J. Thorac. Cardiovasc. Surg.* 147 (1), 95–99. doi:10.1016/j.jtcvs.2013.08.012
- Salvador, L., Mirone, S., Bianchini, R., Regesta, T., Patelli, F., Minniti, G., et al. (2008). A 20-year experience with mitral valve repair with artificial chordae in 608 patients. *J. Thorac. Cardiovasc. Surg.* 135 (6), 1280–1287.e1. doi:10.1016/j.jtcvs.2007.12.026
- Savic, V., Pozzoli, A., Gülmez, G., Demir, H., Batinkov, N., Kuwata, S., et al. (2018). Transcatheter mitral valve chord repair. *Ann. Cardiothorac. Surg.* 7 (6), 881–740. doi:10.21037/asvide.2018.881
- Simões Costa, S., Brandão, M., and Martins, D. (2021). A potentially catastrophic complication of transapical mitral neochordoplasty. *Rev. Española Cardiol. (English Ed.)* 74 (11), 984–985. doi:10.1016/j.rec.2021.03.004
- Soulut-Dufour, L., and Addetia, K. (2020). Degenerative mitral regurgitation. *Curr. Opin. Cardiol.* 35 (5), 454–463. doi:10.1097/hco.0000000000000769
- Sturla, F., Votta, E., Onorati, F., Pechlivanidis, K., Pappalardo, O. A., Gottin, L., et al. (2015). Biomechanical drawbacks of different techniques of mitral neochordal implantation: When an apparently optimal repair can fail. *J. Thorac. Cardiovasc. Surg.* 150 (5), 1303–1312.e4. doi:10.1016/j.jtcvs.2015.07.014
- Wang, S., Meng, X., Luo, Z., and Pan, X. (2018). Transapical beating-heart mitral valve repair using a novel artificial chordae implantation system. *Ann. Thorac. Surg.* 106 (5), e265–e267. doi:10.1016/j.athoracsur.2018.05.031
- Wang, L. H., Pu, Z. X., Kong, M. J., Jiang, J. B., Ren, K. D., Gao, F., et al. (2019). The first four cases of successful NeoChord procedure in mainland China. *World J. Emerg. Med.* 10 (3), 133–137. doi:10.5847/wjem.j.1920-8642.2019.03.001
- Wang, G., Gao, C., Xiao, B., Zhang, J., Jiang, X., Wang, Q., et al. (2022a). Research and clinical translation of trilayer stent-graft of expanded polytetrafluoroethylene for interventional treatment of aortic dissection. *Regen. Biomater.* 9, rabc049–064. doi:10.1093/rb/rbac049
- Wang, S., Meng, X., Hu, S., Sievert, H., Xie, Y., Hu, X., et al. (2022b). Initial experiences of transapical beating-heart mitral valve repair with a novel artificial chordal implantation device. *J. Card. Surg.* 37 (5), 1242–1249. doi:10.1111/jocs.16342
- Weber, A., Taramasso, M., Podkopajev, A., Janauskas, V., Zakarkaitė, D., Vogel, R., et al. (2021). Mitral valve repair with a device for artificial chordal implantation at 2 years. *JTCVS Open* 8, 280–289. doi:10.1016/j.xjon.2021.08.041
- Xu, H., Liu, Q., Cao, K., Ye, Y., Zhang, B., Li, Z., et al. (2022). Distribution, characteristics, and management of older patients with valvular heart disease in China: China-DVD study. *JACC Asia* 2, 354–365. doi:10.1016/j.jacasi.2021.11.013
- Yamashita, M. H., and Skarsgard, P. L. (2011). Intermediate and early rupture of expanded polytetrafluoroethylene neochordae after mitral valve repair. *Ann. Thorac. Surg.* 92 (1), 341–343. doi:10.1016/j.athoracsur.2011.01.042
- Yap, J., Bolling, S. F., and Rogers, J. H. (2021). Contemporary review in interventional cardiology: Mitral annuloplasty in secondary mitral regurgitation. *Struct. Heart* 5 (3), 247–262. doi:10.1080/24748706.2021.1895457
- Yeo, T. C., Freeman, W. K., Schaff, H. V., and Orszulak, T. A. (1998). Mechanisms of hemolysis after mitral valve repair: Assessment by serial echocardiography. *J. Am. Coll. Cardiol.* 32 (3), 717–723. doi:10.1016/S0735-1097(98)00294-0
- Yokoyama, H., Ruf, T. F., Geyer, M., Tamm, A. R., Da Rocha E Silva, J. G., Gößler, T. A. M., et al. (2023). Reverse cardiac remodeling in patients undergoing combination therapy of transcatheter mitral valve repair. *Front. Cardiovasc. Med.* 10, 1029103–1029109. doi:10.3389/fcvm.2023.1029103
- Zussa, C., Polesel, E., Rocco, F., and Valfrè, C. (1997). Artificial chordae in the treatment of anterior mitral leaflet pathology. *Cardiovasc. Surg.* 5 (1), 125–128. doi:10.1016/S0967-2109(96)00066-X
- Zussa, C. (1996). Different applications of ePTFE valve chordae: Surgical technique. *J. Heart Valve Dis.* 5 (4), 356–361.



OPEN ACCESS

EDITED BY

Chandra Kothapalli,
Cleveland State University, United States

REVIEWED BY

Siwei Zhao,
University of Nebraska Medical Center,
United States
Prabha Sikder,
Cleveland State University, United States

*CORRESPONDENCE

Monica A. Serban,
✉ monica.serban@umontana.edu

RECEIVED 19 April 2023

ACCEPTED 31 May 2023

PUBLISHED 08 June 2023

CITATION

Veit JGS, Weidow M and Serban MA (2023), A versatile, bioengineered skin reconstruction device designed for use in austere environments.
Front. Bioeng. Biotechnol. 11:1208322.
doi: 10.3389/fbioe.2023.1208322

COPYRIGHT

© 2023 Veit, Weidow and Serban. This is an open-access article distributed under the terms of the [Creative Commons Attribution License \(CC BY\)](https://creativecommons.org/licenses/by/4.0/). The use, distribution or reproduction in other forums is permitted, provided the original author(s) and the copyright owner(s) are credited and that the original publication in this journal is cited, in accordance with accepted academic practice. No use, distribution or reproduction is permitted which does not comply with these terms.

A versatile, bioengineered skin reconstruction device designed for use in austere environments

Joachim G. S. Veit^{1,2}, Morgan Weidow¹ and Monica A. Serban^{1,2*}

¹Serban Lab, Department of Biomedical and Pharmaceutical Sciences, University of Montana, Missoula, MT, United States, ²Montana Biotechnology Center (BIOTECH), University of Montana, Missoula, MT, United States

Austere environments in which access to medical facilities, medical personnel, or even water and electricity is limited or unavailable pose unique challenges for medical device product design. Currently existing skin substitutes are severely inadequate for the treatment of severe burns, chronic wounds, battlefield injuries, or work-related injuries in resource-limited settings. For such settings, an ideal device should be biocompatible, bioresorbable, promote tissue healing, not require trained medical personnel for deployment and use, and should enable topical drug delivery. As proof of concept for such a device, silk fibroin and an antioxidant hyaluronic acid derivative were chosen as primary constituents. The final formulation was selected to optimize tensile strength while retaining mechanical compliance and protection from reactive oxygen species (ROS). The ultimate tensile strength of the device was 438.0 KPa. Viability of dermal fibroblasts challenged with ROS-generating menadione decreased to 49.7% of control, which was rescued by pre-treatment with the hyaluronic acid derivative to 85.0% of control. The final device formulation was also tested in a standardized, validated, *in vitro* skin irritation test which revealed no tissue damage or statistical difference from control. Improved topical drug delivery was achieved via an integrated silk fibroin microneedle array and selective device processing to generate crosslinked/through pores. The final device including these features showed a 223% increase in small molecule epidermal permeation relative to the control. Scaffold porosity and microneedle integrity before and after application were confirmed by electron microscopy. Next, the device was designed to be self-adherent to enable deployment without the need of traditional fixation methods. Device tissue adhesive strength (12.0 MPa) was evaluated and shown to be comparable to a commercial adhesive surgical drape (12.9 MPa) and superior to an over-the-counter liquid bandage (4.1 MPa). Finally, the device's wound healing potential was assessed in an *in vitro* full-thickness skin wound model which showed promising device integration into the tissue and cellular migration into and above the device. Overall, these results suggest that this prototype, specifically designed for use in austere environments, is mechanically robust, is cytocompatible, protects from ROS damage, is self-adherent without traditional fixation methods, and promotes tissue repair.

KEYWORDS

austere environment, skin reconstruction device, wound healing, biomaterial, microneedles, silk fibroin, hyaluronic acid

1 Introduction

Skin functions as our primary barrier to the environment and provides protection from pathogens, allergens, radiation, and mechanical injury. It also plays an important role in metabolism, fluid regulation, and thermal homeostasis. Disruption of the skin's integrity can be life-threatening and as such, repairing damage from insults such as burns, trauma, medical procedures, and others, is critical. Civilian modern medical facilities or military tertiary care facilities are well equipped to successfully handle such procedures. However, wound repair and skin reconstruction in resource-limited settings poses unique challenges and drastically changes design requirements for adequate solutions. As an example, in combat areas, repair and reconstructive care is typically delayed until transfer to adequately equipped tertiary care centers rather than being addressed in primary or secondary care centers. This delayed care can lead to severe wound deterioration and is associated with increased morbidity and mortality (Bhandari et al., 2012; Driscoll et al., 2018). Within a civilian context, rural areas and communities of lower socioeconomic status report a higher incidence and severity of burn injuries than wealthy or urban areas, which is exacerbated by a lack of specialized care centers and trained medical personnel (Vidal-Trecan et al., 2000; Chamania, 2010). The World Health Organization reports that 180,000 deaths occur every year due to burns, primarily in low- and middle-income countries, and burns are a leading cause of disability-adjusted life-years in these areas (World Health Organization, 2018). Regarding chronic wounds, a similar disparity is observed in these underserved populations in which the risk of major amputation associated with chronic wounds is 50% higher in rural patients when compared to their urban counterparts, which is further accentuated in low-income countries by ulcerative skin diseases and neglected tropical diseases (Sutherland et al., 2020; Sen, 2021; Toppino et al., 2022). These facts clearly underline the need for products and wound care mitigation strategies specific to austere, resource-limited settings, while producing optimal therapeutic outcomes.

Although there are numerous wound healing products on the market today, none are suitable as critical care products for use in resource-limited settings (Jeschke et al., 2018; Snyder et al., 2020). Allografts, autografts, synthetic, and semi-synthetic devices are commercially available, but all require application and use in a properly equipped medical facility by highly trained medical personnel. Additionally, many of them require multiple surgical steps which are unfeasible in resource-limited settings.

We sought to develop a skin reconstruction device which acts as a protective barrier upon application while promoting concurrent tissue healing and device biodegradation to allow autologous remodeling of wounded tissue. Designed specifically for resource-limited settings, the device aims to simplify deployment, increase user-friendliness by removing requirements for sutures or other traditional fixation methods, allow patient-specific topical drug application, facilitate biointegration into healing tissue to reduce the need for sequential surgical procedures, and allow for use by any first responder or care provider.

For the device formulation, we chose well-characterized biodegradable natural polymers with good environmental stability, specifically silk fibroin (SF) and hyaluronic acid (HA) for optimal tissue integration, therapeutic outcome, and cold-

chain independence (Holland et al., 2019). We also used another well-characterized material, polyvinyl alcohol (PVA), as a transient structural stabilizer and porogen. To ensure accelerated tissue healing, we tailored the properties of HA via chemical conjugation with D-methionine (Dmet) to yield an HA-methionine conjugate (HAM) capable of mitigating oxidative stress, which often is associated with inflammation and delayed wound healing (Deng et al., 2021; Wang et al., 2023). To enable topical drug delivery, the device scaffold was processed to be macro- and micro-porous, and was equipped with an integrated microneedle array for profound tissue access. This prototype was intentionally designed drug-free to allow for user and patient-specific drug selection, which translates to increased versatility within austere environments by avoiding the need to possess multiple formulations of the device. Moreover, from a product perspective, the drug-free design would be regulated by the US Food and Drug Administration as a biomedical device rather than a combination product (Serban, 2016). Finally, to maximize user-friendliness and ease of deployment, the device was rendered self-adherent upon contact with the wound and can be easily set in place without the need for traditional fixation systems.

To optimize this concept's utility for resource-limited settings, the formulation and assembly processes were intended to be simple, efficient, and effective, thus ensuring downstream cost-efficiency, easy scalability and, ideally, cold-chain independence, although this was not evaluated in the current study. The data presented here serves as proof of concept for a unique skin reconstruction device purposely designed to address the unique unmet needs of critical wound care and skin reconstruction in settings where currently existing products and technologies are irrelevant.

2 Materials and methods

2.1 Chemicals and antibodies

The following chemicals were used in this study: polydimethylsiloxane (PDMS) (Dow Silicones Corporation, Sylgard 184); polyethylene glycol (PEG) 10 kDa (Sigma-Aldrich, 81280); Anhydrous Sodium Carbonate (EMD, SX0395-1); polyvinyl alcohol (PVA) 146–186 kDa (Acros Organics, 183160010); anhydrous lithium bromide (Acros Organics, 453980010); Dulbecco's phosphate buffered saline (Corning, 21-031-CV); fluorescein disodium (Alfa Aesar, J61549.22); D-methionine (Alfa Aesar, B21213); hyaluronic acid (Lifecore, HA1M-5); iodoacetic acid (Acros Organics, 122280250); BupH MES buffered saline (Thermo, 28390); 1-Ethyl-3-(3-dimethylaminopropyl) carbodiimide (EDC) (Thermo, 22980); (3-4,5-dimethyl thiazole 2-yl) 2,5-diphenyltetrazoliumbromide (MTT); Mowiol 4-88 (EMD Millipore, 475904); glycerol (Fisherbrand, G33-500); 1,4-diazobicyclo-[2.2.2]-octane (Alfa Aesar, A14003); O-phthalaldehyde (OPA) (TCI, P0280); mercaptoacetic acid (Fisherbrand, AC125430010); 1-heptanesulfonate monohydrate (Fisherbrand, AA1521418).

The following antibodies were used in this study: mouse anti-human keratin 14 (Abcam, ab7800, RRID:AB_306091) was diluted 1:1000; rabbit anti-human vimentin (Abcam, ab92547, RRID:AB_10562134) was diluted 1:250; both secondary antibodies, donkey

anti-rabbit Alexa Fluor Plus 555 (Invitrogen, A32794, RRID:AB_2762834) and goat anti-mouse Alexa Fluor 647 (Abcam, ab150115, RRID:AB_2687948), were diluted 1:1000; DAPI (Thermo Scientific, 62248) was diluted 1:1000.

2.2 Silk isolation

Silk fibroin (SF) was extracted from *Bombyx mori* silk yarn (Bratac, Brazil) as previously described (Rockwood et al., 2011; Johnston et al., 2018). Briefly, yarn was boiled for 30 min in sodium carbonate (0.02 M) to remove sericin, then rinsed and dried. Extracted SF was then dissolved in lithium bromide (9.3 M) at 20% w/v for 4 h at 60°C. This was then transferred to a Slide-A-Lyzer G2 3.5k MWCO dialysis cassette (Thermo Scientific, 87725) and dialyzed against deionized water (3–4 L) for 48 h (8–10 water changes) to yield 6%–8% (w/v) SF. To further concentrate, the cassette was then transferred to a solution of 10 kDa PEG (20% w/v) in deionized water until the desired concentration (14%–15% SF) was reached. Any precipitated solids were removed from the solution by centrifugation at 4°C, 3600 RCF for 2 × 20 min and decanting the solution. Concentration was determined by adding SF solution (1.0 mL) into a MJ33 moisture analyzer (Mettler Toledo) and recording the mass of the solid remaining after drying. Concentrated SF solutions were stored at 4°C until use.

2.3 HAM synthesis

Carboxy methyl hyaluronic acid (CMHA) was synthesized as previously described (Arrigali and Serban, 2022) from HA, which increases available carboxy moieties for subsequent d-methionine (Dmet) conjugation. Briefly, HA (0.4 g) was ground into a fine powder in a glass mortar and pestle, then dissolved in sodium hydroxide (4 mL, 45% w/v) with stirring for 2 h at room temperature (RT). Isopropanol (30 mL) was then added followed by iodoacetic acid (0.423 M) in isopropanol (10 mL) and stirred for 2 h at RT. Isopropanol was removed by vacuum filtration. Then, the resulting solid was dissolved in deionized (DI) water (40 mL) and the pH was neutralized (~7.0) before the solution was dialyzed against DI water for 72 h (12–15 water changes) with a Slide-A-Lyzer 3.5k MWCO dialysis cassette (Thermo Scientific, 66130). After dialysis, the solution was frozen, lyophilized, and stored at –20°C in an airtight container until use.

Conjugation of Dmet to CMHA (HAM) was done as previously described (Arrigali and Serban, 2022). Briefly, CMHA (50 mg) was dissolved in MES buffer (10 mL). Dmet (220 mg) was then added, followed by EDC (100 mg). This mixture was allowed to react overnight with stirring at RT, then was neutralized with NaOH (1 M) and dialyzed against DI water for 72 h. After dialysis, the HAM solution was frozen, lyophilized, and stored at –20°C in an airtight container until use.

Modification of CMHA and HAM was confirmed by ¹H-NMR on a Bruker 400 MHz using product in deuterated water (10 mg mL⁻¹). Carboxymethylation efficiency was determined using quantitative ¹H-NMR to normalize the three carboxymethyl methylene protons (4.1 ppm) to the two methyl

protons of the N-acetylglucosamine of HA (1.95 ppm) (Supplementary Figure S1).

2.4 Scaffold casting

Varying concentrations of SF and HAM were combined in conical tubes by gently pipetting up and down followed by brief immersion in a sonicating water bath to homogenize. A 32 × 32 × 1 mm (or 32 × 32 × 0.5 mm) deep well was cast in PDMS from a simple template made in Fusion 360 software and printed on a Form 3 (Formlabs) SLA 3D printer using Clear V4 photopolymer ink. These PDMS molds were pre-chilled, then used to cast 1 mm (or 0.5 mm for wound healing) thick SF/HAM scaffolds. The scaffolds were frozen in a –80°C freezer overnight, then lyophilized for 24 h. Following lyophilization, the SF was made water insoluble by inducing physical crosslinking via β-sheet formation by soaking in 90% ethanol for 1 h (scaffolds used for tension testing were soaked overnight to match ethanol treatment of final device). β-sheet formation (Chen et al., 2009; Love et al., 2019) indicated by the amide I peak at 1620 cm⁻¹ was confirmed by FTIR using a Nicolet iS50 FTIR with ATR (Supplementary Figure S2).

2.5 Microneedle array

A microneedle (MN) array template was designed using Fusion 360 software (Autodesk). The 21 × 36 MN array consisted of 400 μm tall conical MNs with a base diameter of 120 μm and pitch of 600 μm. The needle profile consists of 3 facets: the first 110 μm from the tip has walls angled at 15° from vertical to allow for a sharp, low-penetration force tip; this transitions to a main shaft with more gradually sloped sides, 6° from vertical, to provide increased compressive support and lateral rigidity; finally, a 25 μm radius fillet was placed at the intersection of the MN shaft and the base to prevent stress concentrations. This design was sent to the University of Utah Nanofabrication Lab (Salt Lake City, UT) for two-photon polymerization (2PP) 3D printing on a Photonic Pro GT2 (Nanoscribe) using IP-S resin and a ×10 objective. Following printing, a negative of the MN array was cast using Sylgard 184 polydimethylsiloxane (PDMS) as per manufacturer's recommendation and allowed to fully cure overnight at 35°C before separating from the MN template.

PVA was dissolved at 8% (w/v) in nanopure water and stirred at 90°C until solubilized. Concentrated SF was diluted to 8% and combined with PVA at a 7:3 (SF:PVA) ratio by volume, pipetted to mix, then submerged 15–20 s in sonicating water bath to emulsify and degas the mixture. This SF:PVA solution was then cast into the PDMS MN negative mold and centrifuged at 3600 RCF for 5 min to completely fill the MN negative mold and remove any trapped air. This was then allowed to air dry overnight to form a film.

Characterization of MN and MN equipped devices was performed by scanning electron microscopy (SEM) on a Thermo Scientific Phenom ProX SEM with SED/EDS. Some SEM samples were coated in 5 nm gold by plasma deposition in air using a LUXOR Goldcoater to improve image resolution. Uncoated

samples were also imaged to confirm that no changes were induced by gold coating.

2.6 Device assembly

SF scaffolds were lightly brushed with a solution of SF (6%–8% w/v) on one side, placed on the backside of the MN film still within the PDMS mold, then pressed with a glass coverslip (to provide even pressure) and a 30 g weight while it dries. After drying, the entire assembly is submerged in 90% ethanol overnight to induce β -sheet formation. The device is then allowed to air dry completely. A final thin layer of tissue adhesive aerosolized SF was applied to the surface of the MN using a TLC reagent sprayer (Kimble, 422530-0025) loaded with a SF solution (6%–8% w/v), then allowed to air dry. This random coil-abundant, water soluble layer of SF reactivates when exposed to moisture and acts as an adhesive, as has been previously demonstrated (Johnston et al., 2018), to secure the device.

2.7 Tensile strength testing

Scaffolds or assembled devices were cut into $10 \times 30 \times 1$ mm dog bone-shaped sheets for tension testing using a hobby knife and custom 3D-printed stencil. Samples were soaked for 30 min in PBS, lightly pressed between two lab tissues to remove all excess liquid, then the sample was clamped into the tension fixture (Supplementary Figure S3A) of a Discovery HR-2 hybrid rheometer (TA Instruments, New Castle, DE). Tensile force was evaluated at room temperature with a constant linear rate of $166.67 \mu\text{m s}^{-1}$ until failure. Any samples which failed at the fixture interface were considered invalid and removed from the data. Ultimate tensile strength (UTS) testing was performed on eight distinct sample replicates.

2.8 Reactive oxygen species protection assay

Primary neonatal fibroblasts were purchased from ATCC (PCS-201-010) and cultured in fibroblast basal medium supplemented with low-serum fibroblast growth kit and 0.5% penicillin-streptomycin-amphotericin B (ATCC: PCS-201-030, PCS-201-041, PCS-999-002, respectively) using manufacturer's protocols. After trypsinization and counting using a Countess automated cell counter (Thermo Scientific), fibroblasts were seeded at 6.0×10^3 cells per well into a 96-well plate, incubated in a 37°C , 5% CO_2 humidified incubator for 24 h before beginning treating with appropriate treatment for 24 h. After 24 h, the treatment was replaced with menadione ($10 \mu\text{M}$), or vehicle (0.1% ethanol in media) in control group, and returned to incubator for 5 h. Wells were rinsed with growth media then the Cell-titer 96 Aqueous One Solution Cell Proliferation Assay kit (Promega, G3580) was run using manufacturer's protocol and absorbance at 490 nm was read on a Cytation 5 microplate reader (Biotek). Reactive oxygen species (ROS) protection assay was performed in biological quadruplicates measured in technical duplicates.

2.9 Skin irritation testing

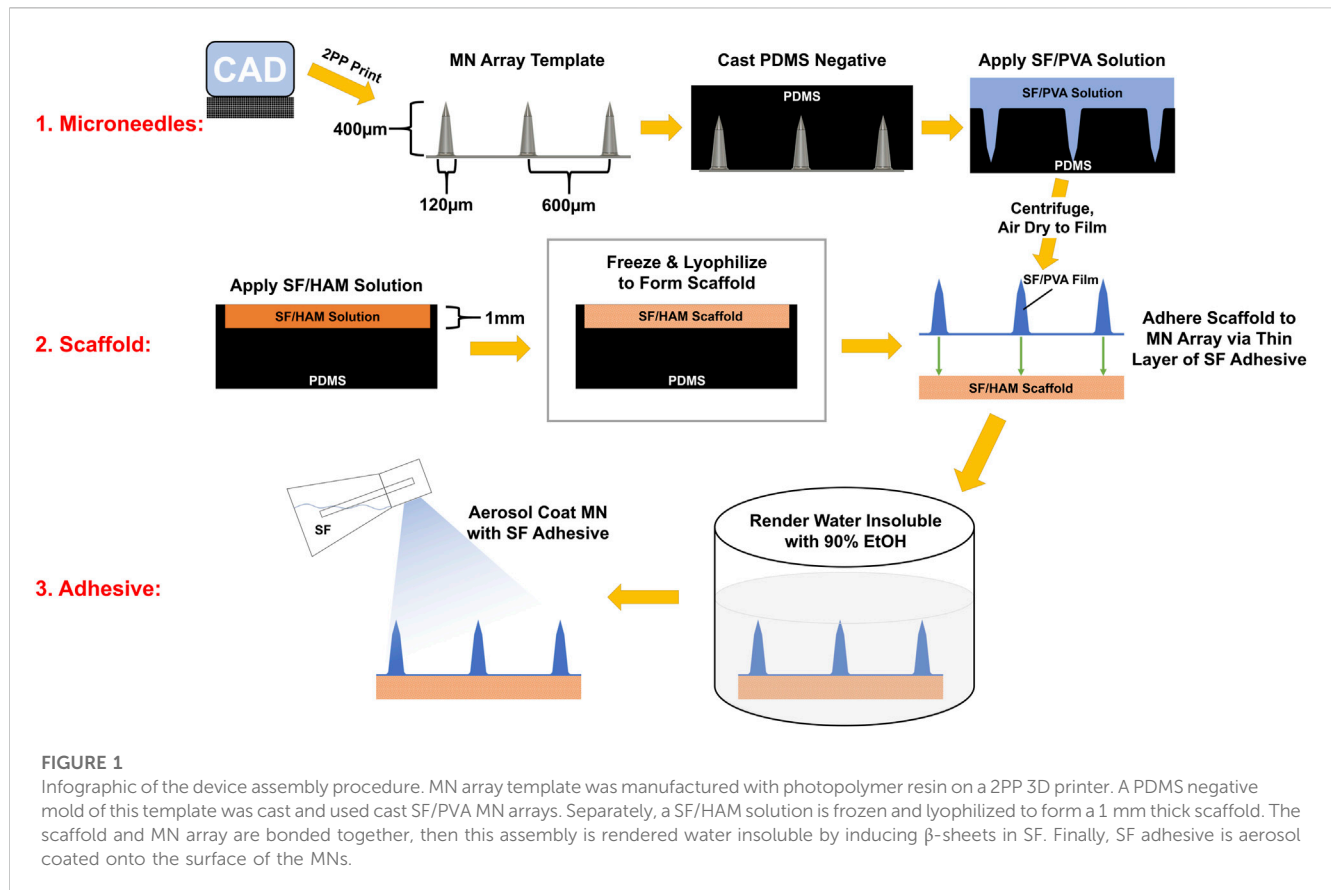
Skin irritation testing (SIT) was performed following OECD TG439 protocols and using *in vitro* EpiDerm tissues (Mattek Corporation, EPI-200-SIT). Briefly, complete devices were frozen in liquid nitrogen, then ground into a fine powder using a glass mortar and pestle. A drop of DPBS (25 μL) was placed on the epidermal surface of each test tissue, followed by 25 mg of the powdered device. Tissues were exposed to a negative control (DPBS), positive control (5% SDS solution), or the test substance for 60 ± 1 min, thoroughly washed, then further incubated for 42 h. Cell viability was then determined by reduction of MTT using absorbance at 570 nm on a Cytation5 microplate reader. SIT was performed as directed by the standardized protocol in biological triplicates measured in technical duplicates.

2.10 Fibroblast migration

Scaffolds (1 mm thickness) were prepared from a solution of SF (12% w/v) with HAM (0.2% w/v), frozen and lyophilized as described above, then rendered insoluble in 90% ethanol. Disks (8 mm diameter) were punched from the scaffolds, then transferred to sterile 24-well plates in a laminar flow cell culture hood where they were allowed to completely dry in sterile conditions for 3 days. The scaffolds were pre-soaked in fibroblast growth media for 1 h and placed in cell culture inserts (Millipore PIHP01250) to keep the scaffold surface above the surface of the media. A 5 μL drop containing 4.0×10^5 fibroblasts was gently pipetted onto the center of the scaffold. These were placed in a 37°C , 5% CO_2 humidified incubator overnight to allow cells to properly adhere, then additional media was added to each well to fully submerge the scaffolds. Growth media was subsequently changed every 2 days. Scaffolds were collected on day 2 and day 7 after initial seeding, fixed, then immuno-labeled for confocal imaging (see below). Fibroblast migration was performed on four distinct samples for each collection day.

2.11 Adhesive testing

Complete devices were prepared as indicated before. Circular 8 mm diameter patches of the devices or Steri-DrapeTM (3M Healthcare, St. Paul, MN) were cut out with a biopsy punch (Accuderm, Fort Lauderdale, FL). A small square of natural sheep chamois leather (Amazon, Seattle, WA) was cut out, moistened, then all extra water was squeezed out with a lab tissue. The samples were then placed onto the leather with the adhesive against the leather and a ~ 30 g weight was placed onto the device to provide downward pressure as it dried overnight. The following day, a small drop of cyanoacrylate glue (Gorilla Glue Company, Cincinnati, OH) was placed onto a custom 3D printed adapter (Supplementary Figure S3B) and stuck to the top of the adhered sample. For the New-SkinTM liquid bandage (Advantice Health, Cedar Knolls, NJ) samples, a thin coating of liquid bandage was applied directly to the 3D printed adapter, which was then pressed onto a square of chamois leather and allowed to dry for the manufacturer-recommended 5 min. The



samples were clamped into the top of the tension fixture of the DHR-2, then a small drop of glue was placed onto a similar 3D printed adapter clamped to the bottom of the tension fixture. The fixture was automatically lowered until the glue contacted the chamois leather. This was then held at a constant force of 0.5 N for 15 min to allow the glue to dry. After 15 min, the tension fixtures began to separate at a rate of $100 \mu\text{m s}^{-1}$ until the device had completely separated from the leather. All samples were only considered valid if the separation occurred at the interface of the adhesive and the leather (this was true for all device samples tested; none failed at any other location). The absolute value of the peak tension (N) experienced before failure was divided by the adhesive surface area of the device (m^2) to calculate the tensile strength (in Pa) of the adhesive. Adhesive testing was performed on six distinct sample replicates.

2.12 Drug permeation *in vitro* reconstructed human epidermis

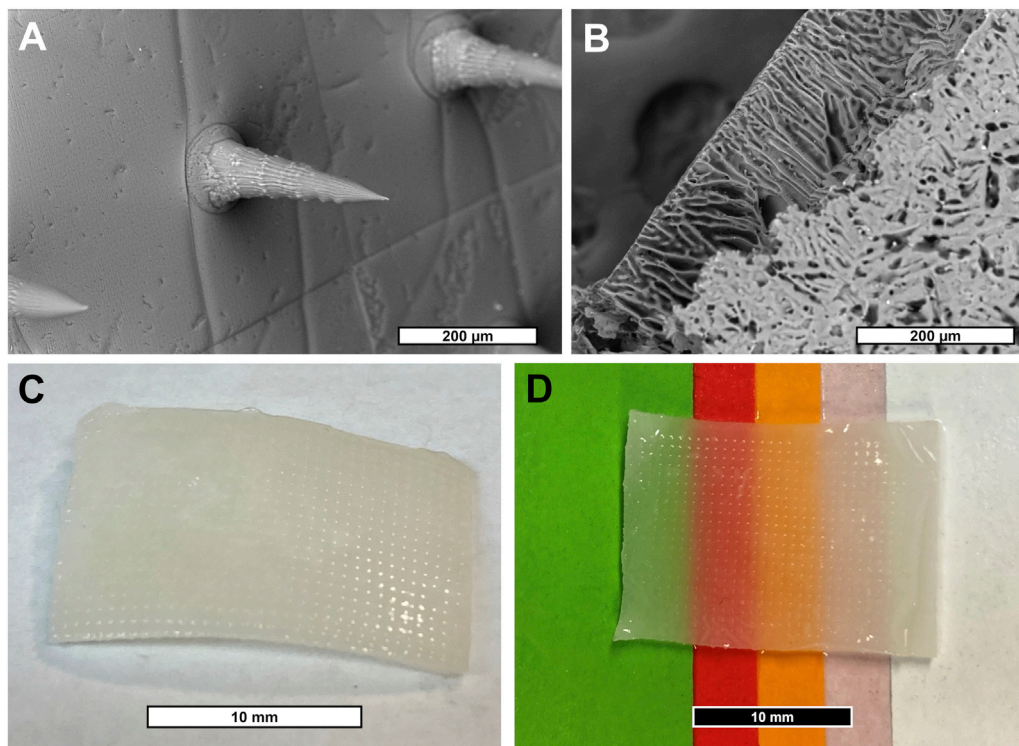
Reconstructed human epidermis (RHE) were grown *in vitro* and cultured at air-liquid interface for 11 days as previously described in detail (Veit et al., 2021a; Veit et al., 2021b) using primary neonatal epidermal keratinocytes (Gibco, C-001-5C). The fully developed RHE were transferred to a 12-well plate containing 600 μL DPBS per well. A 4 mm diameter device was placed into the center of the RHE and gently pressed down with a cotton tipped swab to puncture the skin with the MN. The MN-

free scaffold group was also pressed with a cotton swab with equal force to control for any non-MN associated damage affecting drug permeation. Fluorescein disodium (1 mM) in DPBS (10 μL) was applied onto the top of each scaffold and the tissues were incubated between timepoints in a dark, humidified, 37°C incubator. At each timepoint, the RHE were transferred to a new well containing fresh DPBS. The previous timepoint was collected in a microcentrifuge tube and stored at -20°C until analysis. When necessary, samples were diluted to within the linear range of the standard curve and the total fluorescein permeated was determined by fluorescence on a Cytation5 (Biotek) microplate reader (ex. 490 nm; em. 515 nm). Drug permeation assay was performed in biological quadruplicates measured in technical duplicates.

2.13 Full-thickness *in vitro* skin wound healing assay

Complete devices were punched into 3 mm diameter disks during the 90% EtOH soaking step of production, then transferred into a covered, sterile TC plate in a flowing tissue culture hood to dry overnight.

EpiDerm full-thickness (EFT) *in vitro* skin models were purchased from Mattek Corporation (EFT-412). Following the manufacturer's recommended overnight equilibration period in a 37°C , 5% CO_2 humidified incubator, tissues were wounded using a 3 mm biopsy punch (Accuderm, Fort Lauderdale, FL) and the

**FIGURE 2**

(A) SEM micrograph of SF/PVA MN array. (B) SEM micrograph of SF/HAM scaffold surface and partial cross section. (C) Photograph of hydrated device showing MN surface and (D) demonstrating the devices' translucent property allowing it to inherit the underlying colors.

resulting tissue plug was removed with fine-tipped sterile tweezers. The prepared sterile 3 mm devices were briefly soaked in DPBS, then gently placed into the induced EFT wounds.

These tissues were allowed to grow for 20 days, with media changes every 1–2 days using the supplied manufacturer's media. The tissues were then fixed and processed for histological analysis (see below).

2.14 Histology and immuno-labeling of tissues

RHE and EFT tissues were fixed overnight (4% formaldehyde with 1% acetic acid in DPBS), transferred to histology cassettes, then processed for paraffin embedding in an ASP300S tissue processor (Leica Biosystems, Deer Park, IL). Paraffin embedded tissues were cut down on a microtome until the device was just exposed, then an additional 1.0 mm was removed to allow for a series of 6–10 μm sections to be made in the approximate center of the applied device. The slide-mounted sections were then either stained with hematoxylin and eosin (H&E) or deparaffinized and rehydrated for immuno-labeling using an Autostainer XL (Leica) robot. All tissue processing and sectioning equipment was provided by the Center for Environmental Health Sciences Molecular Histology and Fluorescent Imaging Core at the University of Montana.

Antigen retrieval of deparaffinized sections was done by placing slides in pH 6.0 citric acid (2.2 g L^{-1}) within a double boiler for 20 min. Slides were rinsed in PBS, then blocked for 1 h in a buffer containing glycine (0.1 M), bovine serum albumin (BSA) (1% w/v), and triton X-100 (0.02% v/v), in PBS. Primary antibodies were diluted in BSA (0.2%) and triton X-100 (0.02%) in PBS (PBT buffer) and applied to the slides for overnight incubation at 4°C in a humidity chamber. The following day, slides were rinsed 3×3 min in PBT buffer with gentle orbital shaking. Secondary antibodies diluted in PBT buffer were incubated for 1 h at room temperature in a humidity chamber. Slides were again rinsed 3×3 min in PBT buffer, then incubated for 10 min with DAPI in PBT buffer before a final 3×5 min rise in PBS. Coverslips were mounted with Mowiol + DABCO mounting media (10% w/v Mowiol 4-88, 25% w/v glycerol, 0.1 M Tris (pH 8.5), and 2.5% w/v 1,4-diazobicyclo-[2.2.2]-octane).

H&E stained tissues were imaged on a DMI3000B (Leica Microsystems, Deerfield, IL) inverted widefield microscope with a Leica DFC450C camera. Immuno-labeled samples were imaged on a Leica Stellaris 5 confocal microscope.

2.15 Statistical analysis

Statistical analysis was performed as described in respective figure captions using GraphPad Prism software (v9.4.1). Sample

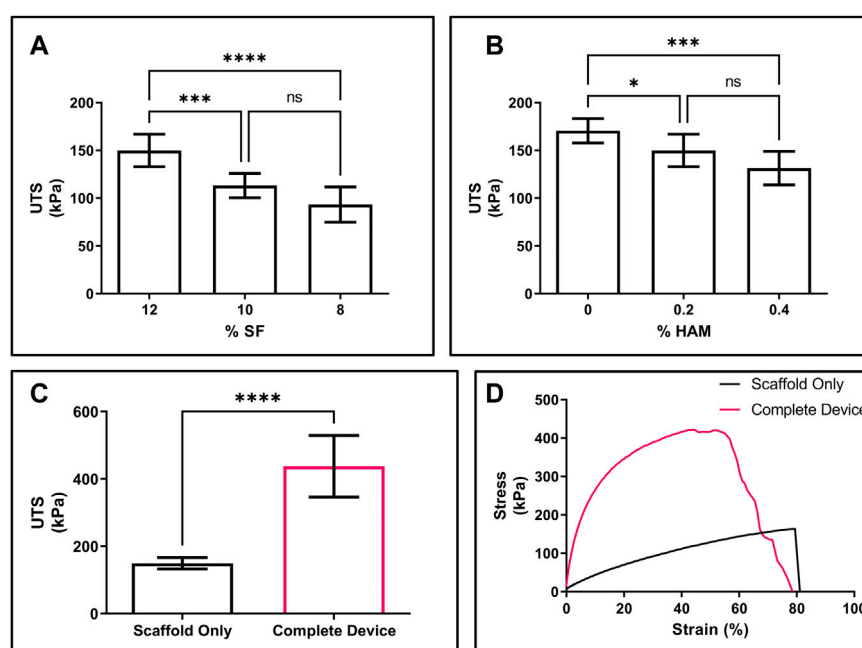


FIGURE 3

Mechanical properties of scaffold and device. **(A)** UTS of scaffold made from solutions containing varying concentrations of SF with 0.2% HAM. **(B)** UTS of scaffold from solutions containing 12% SF and varying concentrations of HAM. **(C)** UTS of the final formations of the scaffold only (black) compared to the complete device (pink). **(D)** Representative stress-strain curve for scaffold only (black) compared to the complete device (pink). **(A,B)** $n = 8$; one-way ANOVA with Dunnett's correction for multiple comparisons; * $p < 0.05$, *** $p < 0.001$, **** $p < 0.0001$. **(C)** $n = 8$; 2-sided t -test; **** $p < 0.0001$. NS, not significant.

sizes in figure captions refer to the number of distinct sample replicates and do not include technical replicates. Technical replicates were combined prior to statistical analysis.

3 Results

3.1 Device design and production

The complete device formulation consists of SF as the main structural component, HAM as the main bioactive component, and PVA for transient structural stability and porosity. Physical and biological properties of HAM can be found in Supplementary Materials (Supplementary Figures S4, S5).

As a first step in creating a complete device, a negative mold of conical MNs was designed and manufactured as described in Section 2.5 from a micron-scale 3D printed template (Figure 1). Next, a mixture of SF and PVA was cast into a negative MN mold and allowed to dry into a film of sharp MNs with a tip radius of $\sim 2 \mu\text{m}$ (Figure 2A, Supplementary Figure S6). Separately, a porous scaffold (Figure 2B) was generated by freezing and lyophilizing a solution of SF and HAM placed in a 1 mm deep cuboidal negative mold. This scaffold was subsequently adhered to the dried MN array with SF adhesive, rendered water-insoluble by ethanol-induced β -sheet formation (confirmed by FTIR, Supplementary Figure S2), then coated with a thin layer of aerosolized SF tissue adhesive. This three-component complete device (scaffold, bonded MN array, and aerosolized SF adhesive)

is stored dry until ready for use when it can be quickly activated by rehydration. For the purposes of this study, “complete device” (Figure 2C), refers to the final selected formulation of the device which consists of a scaffold made from a solution of 12% (w/v) SF and 0.2% (w/v) HAM which is adhered to a MN array containing a 7:3 mass ratio of SF to PVA, which has been rendered water insoluble then coated in SF adhesive. Interestingly, once hydrated, the complete device appears translucent and capable of adopting any underlying colors (Figure 2D).

3.2 Device characterization

3.2.1 Mechanical properties

To determine the best balance between tensile strength, porosity, and HAM content, while retaining a compliant, skin-like feel (Supplementary Video S1), scaffolds were made with solutions containing varying concentrations of SF and HAM. For the scaffolds, both a decrease in SF (Figure 3A) and an increase in HAM (Figure 3B) content resulted in decreased UTS. The elongation at break for the final scaffold formation (12% SF + 0.2% HAM) was $78.3\% \pm 10.3\%$ (mean \pm SD), and there were no statistically significant differences in elongation at break from varying SF or HAM content in the scaffold (Supplementary Figures S7A, B). The complete device showed a significant increase in UTS (438.0 ± 91.5 KPa; mean \pm SD) compared to the scaffold alone (149.9 ± 17.0 KPa) (Figure 3C) and displayed a steeper rise in the stress-strain curve, indicating a larger elastic

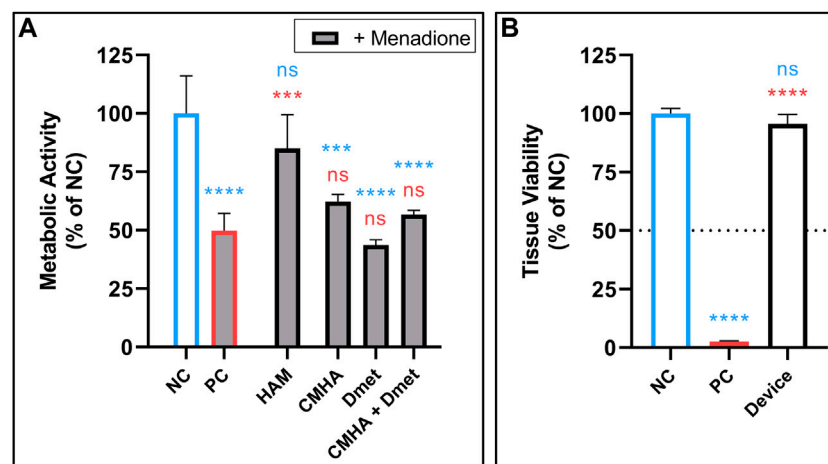


FIGURE 4

(A) ROS protection of fibroblasts by treatment with 2 mg mL⁻¹ HAM or equivalent concentrations of CMHA alone, Dmet alone, or a blend of CMHA + Dmet. Followed by treatment with ROS-generating menadione (indicated by grey fill). *n* = 4. (B) Skin irritation test of NC (vehicle), PC (5% SDS), and final device formulation (25 mg, powdered) performed in 3D *in vitro* human epidermis. Dotted line shows cutoff threshold indicating whether test compound is considered a possible irritant. *n* = 3. (A,B) Mean +SD; one-way ANOVA with Tukey's correction for multiple comparisons vs. NC (blue) or PC (red); ***p* < 0.01, ****p* < 0.001, *****p* < 0.0001. NC, negative control; NS, not significant; PC, positive control; SDS, sodium dodecyl sulfate.

modulus (Figure 3D) due to the additional components (MN array film and SF adhesive). Compared to the scaffold only, the elongation at break of the complete device was 42.9% ± 12.5% (Supplementary Figure S7C), likely due to the lower elasticity of the MN film.

3.2.2 ROS protection, cytocompatibility, and skin irritation testing

The ability of HAM to protect against ROS was evaluated using an MTS colorimetric assay, which measures metabolic activity and is reflective of cell viability. Primary human fibroblasts were pretreated with the indicated material or a vehicle control, then challenged by treatment with ROS-generating menadione. The menadione-challenged positive control (PC) significantly reduced fibroblast activity relative to the negative control (NC). This reduced activity was reversed and no longer significantly different than NC in the cells pre-treated with either 2 or 1 mg mL⁻¹ HAM (Figure 4A, Supplementary Figures S5B). CMHA-alone, Dmet-alone, and a non-conjugated blend of the two, all in HAM-equivalent concentrations (based on mass ratio of CMHA to Dmet in HAM), were found to have no significant protective effect, highlighting the importance of chemical conjugation between HA and Dmet.

Next, SIT was performed according to validated protocols (OECD TG439) using 25 mg of the complete device in powdered form. No evidence of skin irritation was found, nor was any statistically significant change in cell viability detected relative to the untreated control (Figure 4B).

In addition, the device's ability to support fibroblast proliferation and migration was also tested by seeding an 8 mm diameter, 1 mm thick scaffold made from a solution of 12% (w/v) SF and 0.2% (w/v) HAM, with a 5 µL drop of primary fibroblasts placed into the center of the scaffold top. Scaffolds

were collected 2 and 7 days after seeding and immuno-stained with anti-vimentin to visualize fibroblasts (Figure 5, Supplementary Figure S8). On day 2, only a small number of fibroblasts have begun to migrate away from the initial seeding area. However, by day 7, nearly the entire top and bottom of the scaffold is fully covered in fibroblasts.

3.2.3 Device Adherence

To test the adhesive strength of the device, 8 mm diameter complete devices, which included the tissue adhesive SF coated MNs, were adhered to chamois leather (as a skin analog) and pulled apart on a tensile testing fixture. The device demonstrated bonding of complete device to the skin analog in the MPa range, which was nearly identical to the adhesive strength of a commercially available adhesive surgical drape and significantly stronger than an over-the-counter liquid bandage formulation (Figure 6).

3.2.4 Drug delivery capabilities

To assess the skin penetration performance and drug permeability of the devices, 4 mm diameter complete devices were applied onto the surface of *in vitro* human epidermis models with gentle pressure from a sterile cotton swab. The MNs were found to easily penetrate the epidermis in a pattern consistent with the designed MN array (Figures 7A,B). After 24 h *in situ* residence in the human epidermis models, the water-soluble PVA in the MN array film surface appears to have dissolved away from the SF structure, as evidenced by the appearance of abundant pores (Figures 7C,D). To test the topical drug delivery effectiveness of the complete devices, fluorescein disodium was applied onto scaffolds containing scaffold only (S), scaffold with MNs (S + MN), and scaffold with MNs and the SF adhesive coating (complete device, S + MN + A). Relative to S alone, S + MN and S + MN + A both significantly increased topical drug permeation (Figures 7E,F).

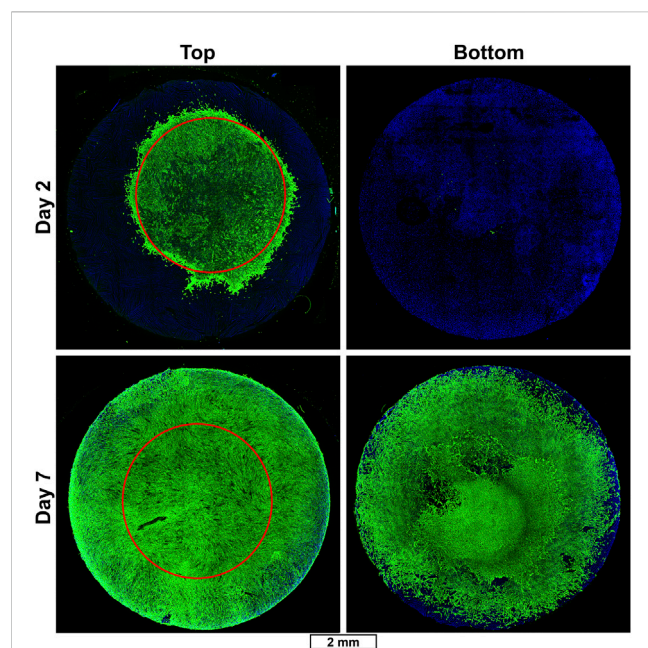


FIGURE 5

Fibroblast migration in SF/HAM scaffold. Representative immunofluorescent confocal micrographs of SF/HAM scaffolds cultured for 2 (top row) or 7 (bottom row) days following initial seeding with a 5 μ L drop of primary fibroblasts directly onto the top center surface of the scaffold. Red circle shows approximate initial seeding area to illustrate extent of migration. Scale bar applies to all images. DAPI and auto-fluorescent SF (blue); vimentin staining identifies fibroblasts (green).

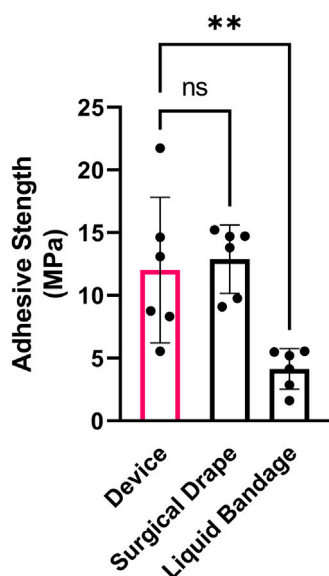


FIGURE 6

Device adhesive strength. Adhesive tensile strength of SF adhesive-coated complete device compared to a commercial surgical isolation drape and liquid bandage bonded to chamois leather (as skin analog) and pulled apart perpendicularly. $n = 6$; Mean \pm SD; one-way ANOVA with Dunnett's correction for multiple comparisons; $**p < 0.01$.

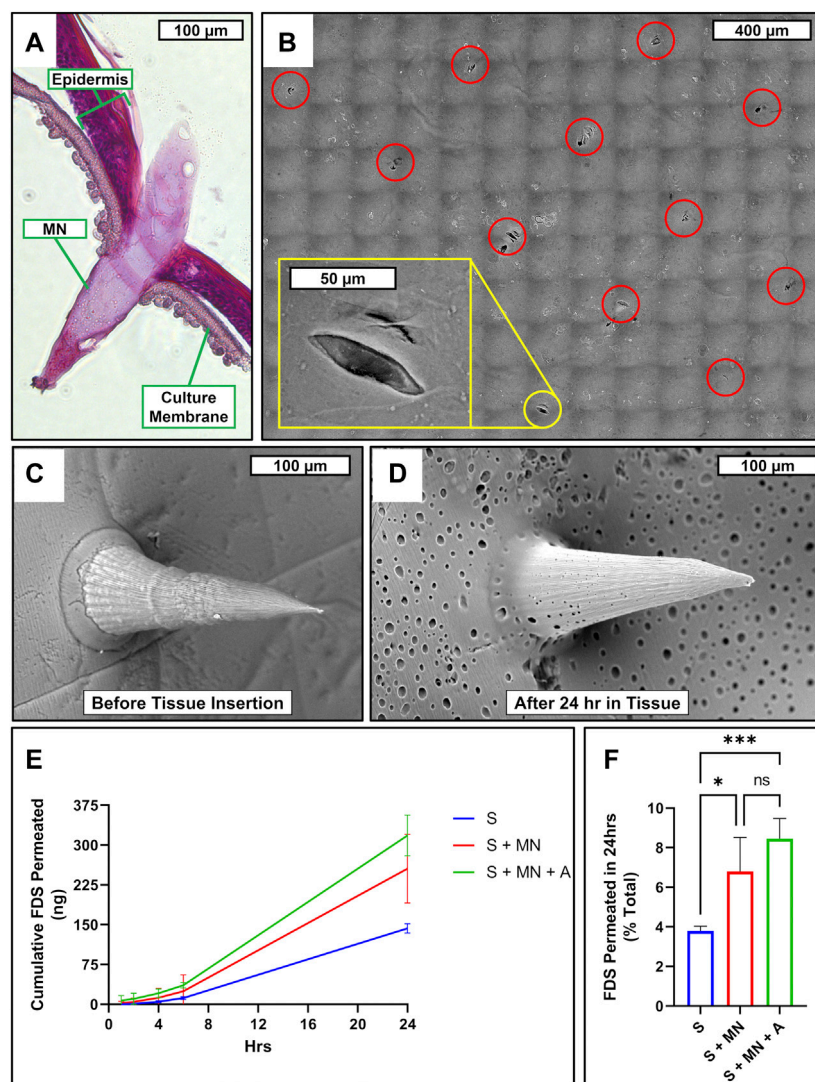
3.3 Wound healing

To investigate the device's effect on wound healing, *in vitro* full-thickness human skin equivalents were wounded with a 3 mm biopsy punch and a 3 mm diameter complete device was placed into the wound (Figure 8A), which was then allowed to heal for 20 days. The control tissue which was not treated with a device showed migration of epidermal keratinocytes across the base of the cell culture insert, but there remained an obvious tissue gap in the dermis which could not heal naturally (Figure 8B). The tissues treated with the devices provided a dermal scaffold and appeared to integrate well into the healing wound (Figure 8C). Epidermal keratinocytes (red) are seen forming a continuous epidermis across a majority of the device surface (blue) and fibroblasts (green) are observed migrating deep into the scaffold of the device (Figure 8D).

4 Discussion

With the deliberate intent to design a skin regeneration device for austere, resource-limited settings, each component was carefully considered and selected for incorporation into the final formulation. SF, a well-characterized, natural polymeric protein which is widely employed in biomedical applications, was chosen as the primary structural component for both the scaffold and MN array due to its biocompatibility, biodegradability, environmental stability, and the ease of tailoring its mechanical properties via structural changes (Vepari and Kaplan, 2007; Holland et al., 2019). PVA, a biocompatible, water-soluble synthetic polymer was added to the MN film to increase device porosity while transiently maintaining the initial mechanical robustness of the MN. Specifically, the microneedles are non-porous at the time of deployment but reveal micropores within 24 h as the PVA microdroplets dissolve out of the MN array. Although not tested in our studies, previous reports suggest that the addition of PVA to SF may also improve cytocompatibility relative to SF alone (Ulloa Rojas et al., 2022).

The final component of the complete device, HAM, is a hyaluronan-conjugate previously developed by our group and shown to decrease oxidative stress (Arrigali and Serban, 2022). HAM builds on HA's excellent intrinsic biocompatibility and ease of chemical modification (Serban and Skardal, 2019; Graça et al., 2020; Marinho et al., 2021). HA, a natural polymeric glycosaminoglycan, has been extensively characterized for its role in wound healing (Chen and Abatangelo, 1999; Schanté et al., 2011; Neuman et al., 2015). Endogenous HA is known to have size-dependent biological effects on wound healing processes, with high molecular weight HA having been reported to be anti-inflammatory, anti-angiogenic, and anti-proliferative, while low molecular weight HA has been found to be pro-inflammatory, pro-angiogenic, and pro-wound healing (Chen and Abatangelo, 1999; Aya and Stern, 2014; Neuman et al., 2015). Interestingly, each of these extremes possess both desirable and undesirable properties in the context of skin reconstruction. While the exact range of what is considered high- and low-molecular weight HA varies across studies, our HAM characterization data indicates that the conjugate's molecular weight (192 KDa) appears to fall

**FIGURE 7**

Microneedle skin penetration, drug permeability, and porosity. **(A)** Cross-sectional micrograph of RHE penetrated by SF/PVA MNs. **(B)** SEM micrograph mosaic of RHE surface following MN insertion and removal. Red circles highlight perforations caused by microneedle array; yellow inset zooms in on a single perforation. SEM micrograph of SF/PVA MN film surface before **(C)** and after **(D)** being inserted in RHE for 24 h. **(E)** Cumulative permeated FDS at each timepoint and **(F)** percent of total applied FDS permeated over 24 h after application to the surface of each sample consisting of scaffold only (S; blue), scaffold with MN (S + MN; red), or scaffold with MN and SF adhesive coating (S + MN + A; green), which had been applied to the surface of an RHE. $n = 4$; one-way ANOVA with Tukey's correction for multiple comparisons; * $p < 0.05$; *** $p < 0.001$. FDS, fluorescein disodium; NS, not significant.

consistently between the two groups, which may reduce the risk of significant detrimental effects seen at each extreme, and in our experiments showed beneficial biological effects. However, if pertinent, adaptation of HAM synthesis to generate significantly higher or lower molecular weight forms could be explored in future iterations to target the various biological effects as needed.

The overall assembly of the skin reconstruction device follows a deconstructed and easily scalable method which separately produces a porous SF/HAM scaffold adhered to a MN array made from a SF/PVA blend. The assembled device is rendered water insoluble via a simple physical cross-linking process, dried, then a thin coating of adhesive SF (Johnston et al., 2018) is sprayed onto the surface of the MNs and allowed to dry. Upon MN insertion into tissue, the

adhesive is rehydrated by physiological moisture, forming a strong bond between the device and tissue surface. In contrast to traditional grafts and skin reconstruction systems, the self-adherent nature of this device eliminates the need for sutures or traditional invasive fixation methods and can be deployed without the need for trained medical personnel. Our comparison with a commercially available adhesive surgical drape and an over-the-counter liquid bandage formulation offers some insight into the adhesiveness of our device and suggests it should provide adequate adhesion *in situ*. Although this study did not investigate shorter adhesion times, our previously published work (Johnston et al., 2018) investigated the properties of this SF adhesive given shorter setting times. This work assessed both wet adhesive (60 s equilibration) and partially dried

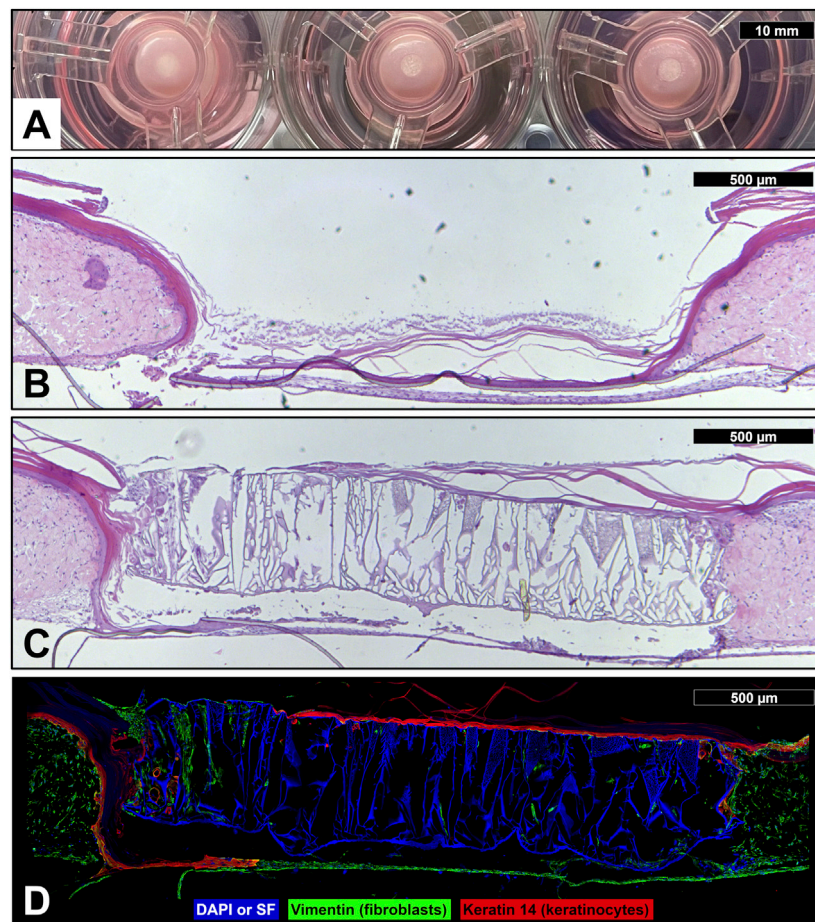


FIGURE 8

Device wound healing in vitro skin model. **(A)** Photograph of wounded human skin equivalents (3 mm full-thickness wound) treated with reconstruction devices at the start of the wound healing experiment (day 0). Micrographs of sectioned and hematoxylin and eosin stained full-thickness human skin equivalent which was wounded with a 3 mm biopsy punch, then left untreated as a control **(B)** or treated with a skin reconstruction device **(C)**, and allowed to heal for 20 days. **(D)** Immunofluorescent micrograph of wounded human skin equivalent treated with skin reconstruction device. DAPI and auto-fluorescent SF (blue); vimentin staining identifies fibroblasts (green); keratin 14 staining identifies keratinocytes (red).

adhesive (3 h equilibration) strength, which could be used to extrapolate some level of confidence in the time-dependent adhesive potential of the device.

Our mechanical characterization data indicate that a device formulation comprising of 12% (w/v) SF and 0.2% (w/v) HAM provides the ideal balance between mechanical strength and ROS protection. It is important to underline that our device design was focused on the development of a robust, easy-to-handle system that would provide a sufficient mechanical barrier during handling and wound healing, while facilitating tissue-mediated device degradation and resorption, and a match of the exact mechanical properties of native skin was not deemed relevant. As is, the device provides a sufficiently strong protective barrier which allows for reasonable flexibility and ease of motion of wounded tissue throughout the device handling and healing process. Although we did not investigate this in our study, the device composition leads us to expect device degradation as the wound heals and subsequent studies will be focused on assessing the exact timeline of this process.

Based on the well-understood properties and previous studies of the constituent materials, our devices are expected to be fully

biocompatible, although this will also need to be confirmed in subsequent preclinical studies. The data presented herein supports our expectations as standardized skin irritation tests following OECD TG439 guidelines showed that exposure to neither the device nor excess HAM resulted in any decrease in epidermal tissue viability relative to control. This *in vitro* organotypic test is considered equivalent to traditional *in vivo* preclinical models and has been shown to be accurately predictive of *in vivo* performance (OECD, 2021).

The antioxidant effects of HAM, and its ability to improve Dmet cellular internalization over unconjugated Dmet, have been previously described by our group in cochlear cells (Arrigali and Serban, 2022). Although Dmet is intrinsically antioxidant, it is not readily internalized by cells in efficacious concentrations. By conjugating Dmet to HA, we can leverage HA-receptor mediated internalization to increase intracellular Dmet. This effect is clearly demonstrated in this study, which shows ROS protecting effects by HAM but not by equivalent concentrations of unconjugated Dmet. As literature reported *in vivo* data indicates that elevated and sustained ROS levels are detrimental to wound healing (Dunnill

et al., 2017), we evaluated the effect of HAM on primary human fibroblasts treated with menadione, a compound which strongly induces cellular production of ROS (Singh and Husain, 2018), then quantified cellular metabolic activity by MTS reduction assay, which is commonly used as a cell viability assay. The results indicate that HAM strongly protects against cellular damage by ROS, while equivalent amounts of CMHA, Dmet, or a blend of the two in the unconjugated form, do not.

Next, since fibroblast migration and proliferation are critical steps in proper wound healing (Saghazadeh et al., 2018), we sought to evaluate these processes in our devices. Our data show that the SF/HAM scaffold facilitates generous fibroblast migration and proliferation *in vitro*. We also show that the skin reconstruction device is able to integrate into *in vitro* human skin equivalents following full-thickness (epidermis and dermis) wounding. Due to the thinness of the *in vitro* human skin equivalent used, a device made from 0.5 mm thick scaffold was used in place of the 1.0 mm thick scaffold used in the rest of the study. This was needed to allow the adjacent epidermal keratinocytes to migrate over the device in a manner more representative of the real-world conditions expected in deeper *in vivo* wounds. This preliminary data showed that, despite the lack of underlying tissue in this *in vitro* model (relative to *in vivo* skin), within 20 days the device was able to integrate into the tissue to act as a dermal scaffold within the wound. Epidermal keratinocytes migrated across the surface and continued to produce a protective stratum corneum, while fibroblasts had begun to migrate deep into the scaffold. We anticipate that, in an extended form of this study, the wound healing response will overlap with proteolytic degradation (Holland et al., 2019) of the device. This process should involve the device being increasingly replaced by the endogenous extracellular matrix components, such as collagen and elastin which are secreted by the native fibroblasts, and we hope to investigate these device integration aspects in subsequent studies. Within austere environments, existing skin substitutes, if available, would likely only be applied days after the initial wounding once the patient reaches a properly equipped medical facility. Given that the device detailed in this study is intended to offer a rapid, more immediate treatment option than currently exists in austere environments, we opted to compare this device's *in vitro* wound healing performance relative to a control wound which received no treatment as opposed to an existing skin reconstruction product. We postulate this comparison to be more representative of the actual outcomes which would be seen in the field.

Another essential consideration for the device design was its ability to enable topical drug delivery. This feature is intended to allow patient/situationally-specific antibiotics, local anesthetics, or any other therapeutics deemed appropriate for care, to be simply applied to the surface of the device to directly treat the targeted tissue, thus reducing or eliminating the adverse effects associated with systemic treatments (Holtman and Jellish, 2012; Carmichael et al., 2018; Negut et al., 2018). Previous studies have also suggested that MNs, in addition to enhancing drug permeation, may also inherently aid wound healing by stabilizing the wound or mechanically promoting debridement and cell proliferation (Barnum et al., 2020). Our approach to facilitating topical drug treatments was to incorporate a dense MN array as well as macro- and micro-pores into the device design.

The results of this study show that our custom MN arrays can fully and efficiently penetrate the tough epidermis and even break through the underlying polycarbonate membrane of the cell culture inserts used in the *in vitro* epidermis model. Although this study utilized *in vitro* epidermis models commonly used for preliminary drug permeation and skin barrier assessments (Agonia et al., 2022) and SF MN have been previously shown to be effective in animal models (Tsioris et al., 2012; Stinson et al., 2017), future *in vivo* or skin explant studies are required to confirm efficacy of this device's MN array. We also show that the MN array with adhesive coating more than doubles drug delivery across the epidermis relative to the scaffold alone. Although only about 8% of the total drug applied permeated over the initial 24-h period, we suspect that a significant portion of the drug was absorbed into the scaffold and, upon saturation, subsequent doses applied to the device would likely result in significantly more drug permeating more rapidly. The results also indicate that within 24 h of being inserted into a tissue, the PVA component of the MN film dissipates leaving the insoluble SF film with sufficient porosity to facilitate drug permeation and cellular infiltration.

Of note, in line with the Food and Drug Administration's initiative to reduce animal testing and promote the use of qualified alternative methods for product testing (FDA, 2023), this study employed validated, standardized *in vitro* testing methods for the initial assessments of cytocompatibility, tissue interaction, and wound healing efficiency. Our data now positions these devices to be confidently advanced to subsequent targeted preclinical studies that would seek to address their biodegradation, bioresorption, and overall *in vivo* performance.

5 Conclusion

Altogether, this study describes the conceptualization, development, and proof of concept of a unique, user-friendly, effective, biomaterial-based skin reconstruction system specifically targeting the needs of patients in resource-limited settings. We demonstrated that this device is cytocompatible and non-irritant, displays favorable mechanical properties, protects cells from ROS damage, facilitates cell migration and wound healing *in vitro*, and improves topical drug permeability. The device formulation is expected to translate into a biocompatible, highly stable, cold-chain independent product, although these aspects will be specifically addressed in subsequent studies. Future iterations of the device concept presented herein will seek to address the issue of eschar and wound debridement via similar minimalist approaches. However, in its current form, the device appears to represent a viable option for secondary care centers and rural clinics. Overall, this work highlights the unique considerations associated with the generation of treatment options for austere environments where minimalist but versatile designs may be better suited than traditionally innovated concepts.

Data availability statement

The raw data supporting the conclusions of this article will be made available by the authors, without undue reservation.

Author contributions

JV led data curation, formal analysis, investigation, methodology, validation, visualization, and original manuscript preparation. JV also contributed to conceptualization, resource acquisition, and supervision. MW contributed to investigation, validation, and manuscript revision and review. MS led conceptualization, funding acquisition, project administration, and supervision, and contributed to methodology, resource acquisition, and manuscript revision and review. All authors contributed to the article and approved the submitted version.

Funding

This work was supported by the M. J. Murdock Charitable Trust via a commercialization initiation grant [CI-UM202015818] to MS.

Acknowledgments

We would like to thank Brian Baker at the University of Utah Nanofabrication Lab for his advice and assistance in manufacturing the 2PP 3D-printed microneedle templates used in this project. We would also like to acknowledge the help provided by Daniel Decato from the Center for Biomolecular Structure and Dynamics Magnetic

Resonance Core Facility at the University of Montana for his assistance with ^1H -NMR.

Conflict of interest

The authors declare that the research was conducted in the absence of any commercial or financial relationships that could be construed as a potential conflict of interest.

Publisher's note

All claims expressed in this article are solely those of the authors and do not necessarily represent those of their affiliated organizations, or those of the publisher, the editors and the reviewers. Any product that may be evaluated in this article, or claim that may be made by its manufacturer, is not guaranteed or endorsed by the publisher.

Supplementary material

The Supplementary Material for this article can be found online at: <https://www.frontiersin.org/articles/10.3389/fbioe.2023.1208322/full#supplementary-material>

References

- Agonia, A. S., Palmeira-de-Oliveira, A., Cardoso, C., Augusto, C., Pellevoisin, C., Videau, C., et al. (2022). Reconstructed human epidermis: An alternative approach for *in vitro* bioequivalence testing of topical products. *Pharmaceutics* 14, 1554. doi:10.3390/pharmaceutics14081554
- Arrigali, E. M., and Serban, M. A. (2022). Development and characterization of a topically deliverable prophylactic against oxidative damage in cochlear cells. *Front. Pharmacol.* 13, 907516. doi:10.3389/fphar.2022.907516
- Aya, K. L., and Stern, R. (2014). Hyaluronan in wound healing: Rediscovering a major player. *Wound Repair Regen.* 22, 579–593. doi:10.1111/wrr.12214
- Barnum, L., Samandari, M., Schmidt, T. A., and Tamayol, A. (2020). Microneedle arrays for the treatment of chronic wounds. *Expert Opin. Drug Deliv.* 17, 1767–1780. doi:10.1080/17425247.2020.1819787
- Bhandari, P., Maurya, S., and Mukherjee, M. (2012). Reconstructive challenges in war wounds. *Indian J. Plast. Surg.* 45, 332–339. doi:10.4103/0970-0358.101316
- Carmichael, H., Wiktor, A. J., Wagner, A. L., and Velopulos, C. G. (2018). High risk of developing long-term opioid use after burn injury. *J. Am. Coll. Surg.* 227, S264. doi:10.1016/j.jamcollsurg.2018.07.543
- Chamania, S. (2010). Training and burn care in rural India. *Indian J. Plast. Surg.* 43, 126–130. doi:10.4103/0970-0358.70735
- Chen, W. Y. J., and Abatangelo, G. (1999). Functions of hyaluronan in wound repair. *Wound Repair Regen.* 7, 79–89. doi:10.1046/j.1524-475X.1999.00079.x
- Chen, X., Knight, D. P., and Shao, Z. (2009). B-turn formation during the conformation transition in silk fibroin. *Soft Matter* 5, 2777–2781. doi:10.1039/b900908f
- Deng, L., Du, C., Song, P., Chen, T., Rui, S., Armstrong, D. G., et al. (2021). The role of oxidative stress and antioxidants in diabetic wound healing. *Oxid. Med. Cell. Longev.* 2021, 1–11. doi:10.1155/2021/8852759
- Driscoll, I. R., Mann-Salinas, E. A., Boyer, N. L., Pamplin, J. C., Serio-Melvin, M. L., Salinas, J., et al. (2018). Burn casualty care in the deployed setting. *Mil. Med.* 183, 161–167. doi:10.1093/milmed/usy076
- Dunnill, C., Patton, T., Brennan, J., Barrett, J., Dryden, M., Cooke, J., et al. (2017). Reactive oxygen species (ROS) and wound healing: The functional role of ROS and emerging ROS-modulating technologies for augmentation of the healing process. *Int. Wound J.* 14, 89–96. doi:10.1111/iwj.12557
- FDA (2023). *FDA seeks \$8.4 billion to further investments in critical public health modernization, Core Food and medical product safety programs*. Silver Spring, MD: Resonance Core Facility at the University of Montana for his assistance with ^1H -NMR.
- FDA News Release. Available at: <https://www.fda.gov/news-events/press-announcements/fda-seeks-84-billion-further-investments-critical-public-health-modernization-core-food-and-medical>.
- Graça, M. F. P., Miguel, S. P., Cabral, C. S. D., and Correia, I. J. (2020). Hyaluronic acid—based wound dressings: A review. *Carbohydr. Polym.* 241, 116364. doi:10.1016/j.carbpol.2020.116364
- Holland, C., Numata, K., Rnjak-Kovacina, J., and Seib, F. P. (2019). The biomedical use of silk: Past, present, future. *Adv. Healthc. Mat.* 8, 1800465. doi:10.1002/adhm.201800465
- Holtman, J. R., and Jellish, W. S. (2012). Opioid-induced hyperalgesia and burn pain. *J. Burn Care Res.* 33, 692–701. doi:10.1097/BCR.0b013e31825adcb0
- Jeschke, M. G., Shahrokhi, S., Finnerty, C. C., Branski, L. K., and Dibildox, M. (2018). Wound coverage technologies in burn care: Established techniques. *J. Burn Care Res.* 39, 313–318. doi:10.1097/BCR.0b013e3182920d29
- Johnston, E. R., Miyagi, Y., Chuah, J. A., Numata, K., and Serban, M. A. (2018). Interplay between silk fibroin's structure and its adhesive properties. *ACS Biomater. Sci. Eng.* 4, 2815–2824. doi:10.1021/acsbiomaterials.8b00544
- Love, C. J., Serban, B. A., Katashima, T., Numata, K., and Serban, M. A. (2019). Mechanistic insights into silk fibroin's adhesive properties via chemical functionalization of serine side chains. *ACS Biomater. Sci. Eng.* 5, 5960–5967. doi:10.1021/acsbiomaterials.9b01014
- Marinho, A., Nunes, C., and Reis, S. (2021). Hyaluronic acid: A key ingredient in the therapy of inflammation. *Biomolecules* 11, 1518. doi:10.3390/biom11101518
- Negut, I., Grumezescu, V., and Grumezescu, A. M. (2018). Treatment strategies for infected wounds. *Molecules* 23, 2392. doi:10.3390/molecules23092392
- Neuman, M. G., Nanau, R. M., Oruña-Sánchez, L., and Coto, G. (2015). Hyaluronic acid and wound healing. *J. Pharm. Pharm. Sci.* 18, 53–60. doi:10.18433/j3k89d
- OECD (2021). *Test No. 439: In vitro skin irritation: Reconstructed human epidermis test method*. Paris, FR: OECD. doi:10.1787/9789264242845-en
- Rockwood, D. N., Preda, R. C., Yücel, T., Wang, X., Lovett, M. L., and Kaplan, D. L. (2011). Materials fabrication from *Bombyx mori* silk fibroin. *Nat. Protoc.* 6, 1612–1631. doi:10.1038/nprot.2011.379
- Saghazadeh, S., Rinoldi, C., Schot, M., Kashaf, S. S., Sharifi, F., Jalilian, E., et al. (2018). Drug delivery systems and materials for wound healing applications. *Adv. Drug Deliv. Rev.* 127, 138–166. doi:10.1016/j.addr.2018.04.008

- Schanté, C. E., Zuber, G., Herlin, C., and Vandamme, T. F. (2011). Chemical modifications of hyaluronic acid for the synthesis of derivatives for a broad range of biomedical applications. *Carbohydr. Polym.* 85, 469–489. doi:10.1016/j.carbpol.2011.03.019
- Sen, C. K. (2021). Human wound and its burden: Updated 2020 compendium of estimates. *Adv. Wound Care* 10, 281–292. doi:10.1089/wound.2021.0026
- Serban, M. A., and Skardal, A. (2019). Hyaluronan chemistries for three-dimensional matrix applications. *Matrix Biol.* 78–79, 337–345. doi:10.1016/j.matbio.2018.02.010
- Serban, M. A. (2016). Translational biomaterials - the journey from the bench to the market - think “product”. *Curr. Opin. Biotechnol.* 40, 31–34. doi:10.1016/j.copbio.2016.02.009
- Singh, S. K., and Husain, S. M. (2018). A redox-based superoxide generation system using quinone/quinone reductase. *ChemBioChem* 19, 1657–1663. doi:10.1002/cbic.201800071
- Snyder, D., Sullivan, N., Margolis, B. D., and Schoelles, K. (2020). *Skin substitutes for treating chronic wounds*. Rockville, MD: Technology Assessment Program. Available at: <https://www.cms.gov/Medicare/Coverage/DeterminationProcess/downloads/id109TA.pdf>.
- Stinson, J. A., Raja, W. K., Lee, S., Kim, H. B., Diwan, I., Tutunjian, S., et al. (2017). Silk fibroin microneedles for transdermal vaccine delivery. *ACS Biomater. Sci. Eng.* 3, 360–369. doi:10.1021/acsbomaterials.6b00515
- Sutherland, B. L., Pecanac, K., Bartels, C. M., and Brennan, M. B. (2020). Expect delays: Poor connections between rural and urban health systems challenge multidisciplinary care for rural Americans with diabetic foot ulcers. *J. Foot Ankle Res.* 13, 32–10. doi:10.1186/s13047-020-00395-y
- Toppino, S., Koffi, D. Y., Kone, B. V., N'krumah, R. T. A. S., Coulibaly, I. D., Tobian, F., et al. (2022). Community-based wound management in a rural setting of Côte d'Ivoire. *PLoS Negl. Trop. Dis.* 16, 00107300. doi:10.1371/journal.pntd.0010730
- Tsioris, K., Raja, W. K., Pritchard, E. M., Panilaitis, B., Kaplan, D. L., and Omenetto, F. G. (2012). Fabrication of silk microneedles for controlled-release drug delivery. *Adv. Funct. Mat.* 22, 330–335. doi:10.1002/adfm.201102012
- Ulloa Rojas, J. E., Oliveira, V. L. De, De Araujo, D. R., Tofoli, G. R., De Oliveira, M. M., Carastan, D. J., et al. (2022). Silk fibroin/poly(vinyl alcohol) microneedles as carriers for the delivery of singlet oxygen photosensitizers. *ACS Biomater. Sci. Eng.* 8, 128–139. doi:10.1021/acsbomaterials.1c00913
- Veit, J. G. S., De Glas, V., Balau, B., Liu, H., Bourlond, F., Paller, A. S., et al. (2021a). Characterization of CYP26B1-selective inhibitor, DX314, as a potential therapeutic for keratinization disorders. *J. Invest. Dermatol.* 141, 72–83.e6. doi:10.1016/j.jid.2020.05.090
- Veit, J. G. S., Poumay, Y., Mendes, D., Kreitinger, J., Walker, L., Paquet, A., et al. (2021b). Preclinical assessment of dual CYP26[A1/B1] inhibitor, DX308, as an improved treatment for keratinization disorders. *Ski. Heal. Dis.* 22, e22. doi:10.1002/ski.22
- Vepari, C., and Kaplan, D. L. (2007). Silk as a biomaterial. *Prog. Polym. Sci.* 32, 991–1007. doi:10.1016/j.progpolymsci.2007.05.013
- Vidal-Trecan, G., Tcherny-Lessenot, S., Grossin, C., Devaux, S., Pages, M., Laguerre, J., et al. (2000). Differences between burns in rural and in urban areas: Implications for prevention. *Burns* 26, 351–358. doi:10.1016/S0305-4179(99)00175-8
- Wang, G., Yang, F., Zhou, W., Xiao, N., Luo, M., and Tang, Z. (2023). The initiation of oxidative stress and therapeutic strategies in wound healing. *Biomed. Pharmacother.* 157, 114004. doi:10.1016/j.biopha.2022.114004
- World Health Organization (2018). *Burns*. Geneva, CH: WHO. Available at: <https://www.who.int/en/news-room/fact-sheets/detail/burns> (Accessed March 13, 2023).



OPEN ACCESS

EDITED BY

Jinjin Chen,
Sun Yat-sen University, China

REVIEWED BY

Tianshu Li,
Musashi University, Japan
Jonghyun Oh,
Jeonbuk National University, Republic of
Korea

*CORRESPONDENCE

Hasan Uludag,
✉ huludag@ualberta.ca

[†]These authors have contributed equally
to this work

RECEIVED 21 June 2023

ACCEPTED 14 August 2023

PUBLISHED 28 August 2023

CITATION

Nasrullah M, Meenakshi Sundaram DN,
Claerhout J, Ha K, Demirkaya E and
Uludag H (2023), Nanoparticles and
cytokine response.
Front. Bioeng. Biotechnol. 11:1243651.
doi: 10.3389/fbioe.2023.1243651

COPYRIGHT

© 2023 Nasrullah, Meenakshi Sundaram,
Claerhout, Ha, Demirkaya and Uludag.
This is an open-access article distributed
under the terms of the [Creative
Commons Attribution License \(CC BY\)](#).
The use, distribution or reproduction in
other forums is permitted, provided the
original author(s) and the copyright
owner(s) are credited and that the original
publication in this journal is cited, in
accordance with accepted academic
practice. No use, distribution or
reproduction is permitted which does not
comply with these terms.

Nanoparticles and cytokine response

Mohammad Nasrullah^{1†}, Daniel Nisakar Meenakshi Sundaram^{2†},
Jillian Claerhout¹, Khanh Ha¹, Erkan Demirkaya³ and
Hasan Uludag^{1,2,4*}

¹Faculty of Pharmacy and Pharmaceutical Sciences, University of Alberta, Edmonton, AB, Canada,

²Department of Chemical and Materials Engineering, Faculty of Engineering, University of Alberta,
Edmonton, AB, Canada, ³Department of Paediatrics, Schulich School of Medicine & Dentistry, Western

University, London, ON, Canada, ⁴Department of Biomedical Engineering, Faculty of Medicine and
Dentistry, University of Alberta, Edmonton, AB, Canada

Synthetic nanoparticles (NPs) are non-viral equivalents of viral gene delivery systems that are actively explored to deliver a spectrum of nucleic acids for diverse range of therapies. The success of the nanoparticulate delivery systems, in the form of efficacy and safety, depends on various factors related to the physicochemical features of the NPs, as well as their ability to remain “stealth” in the host environment. The initial cytokine response upon exposure to nucleic acid bearing NPs is a critical component of the host response and, unless desired, should be minimized to prevent the unintended consequences of NP administration. In this review article, we will summarize the most recent literature on cytokine responses to nanoparticulate delivery systems and identify the main factors affecting this response. The NP features responsible for eliciting the cytokine response are articulated along with other factors related to the mode of therapeutic administration. For diseases arising from altered cytokine pathophysiology, attempts to silence the individual components of cytokine response are summarized in the context of different diseases, and the roles of NP features on this respect are presented. We finish with the authors’ perspective on the possibility of engineering NP systems with controlled cytokine responses. This review is intended to sensitize the reader with important issues related to cytokine elicitation of non-viral NPs and the means of controlling them to design improved interventions in the clinical setting.

KEYWORDS

cytokine response, nanoparticle, inflammatory response, non-viral delivery, biocompatibility

1 Introduction

Nucleic acid-based therapies utilize a range of endogenous and altered nucleic acids derived from DNA and RNA to target specific genes and modify their expression or activity, which lead to therapeutic benefits. A handful of nucleic acid therapies have gained entry into the clinical practice while a large range of nucleic acids are now undergoing clinical testing for regulatory approval. They offer several advantages over conventional drugs (i.e., small organic molecules) and provide activities that cannot be matched by such drugs. They can be designed to be highly specific, avoiding off-target effects that can occur with the current drugs. Rather than simply suppressing the symptoms, these therapies have the potential to treat diseases at the genetic level by altering the root-cause of the disease with long-lasting effects, allowing targeted and precise treatments (Kulkarni et al., 2021). Nucleic acid-based

therapies derived from plasmid DNA (pDNA), messenger RNA (mRNA), small interfering RNA (siRNA), and antisense oligonucleotides (ASOs), have shown promise in treating a range of diseases, including those that are currently considered “incurable”. The siRNA-based drug Vutrisiran, to treat the rare genetic disease polyneuropathy of hereditary transthyretin-mediated amyloidosis (Mullard, 2022) and the mRNA-based COVID-19 vaccines (Watson et al., 2022) are leading examples of nucleic acid therapies.

With the help of recent technological advancements, nucleic acid therapies have become progressively feasible in terms of both production and accessibility, hence, they are explored in clinics for many indications. A critical challenge in exploring new indications lies in the efficiency of the delivery system (Uludag et al., 2019). Administering nucleic acids without a carrier or delivery system is not desirable since they cannot enter cells on their own (at least without significant chemical modifications). These nucleic acids are also prone to undergo rapid degradation due to systemic nucleases, and elicit immune responses due to similarities with the genetic make-up of foreign entities. Nanoparticles (NPs), i.e., delivery vesicles structured at the nm-scale, have emerged as the most promising candidates for delivering nucleic acid-based drugs to overcome such challenges. Their success depends on their ability to efficiently reach the target cells and release their payload without inducing significant toxicity. The NPs are non-viral in nature, but they could still interact with the immune system and subsequently trigger immune responses that can lead to adverse effects. Cytokine response is considered as one of the key immune responses to the NPs (Zolnik et al., 2010) and it is imperative for NPs to remain in “stealth” model when it comes to cytokine response upon administration in a host.

Cytokines are a class of proteins with essential functions in immunity, and other physiological processes such as cellular proliferation, differentiation, apoptosis and inflammatory reactions. They are produced and secreted by various cells in the body, including immune cells and endothelial cells in response to a variety of physiological events and pathological processes. They act as chemical messengers, which bind to specific receptors on the surface of target cells, triggering a range of downstream signaling pathways, and facilitating communications between cells of the immune system, as well as other cells in the body. Cytokines can be broadly classified into several categories, including growth factors, interleukins (ILs), interferons (IFNs), tumor necrosis factors (TNFs), and chemokines (Deckers et al., 2023). Abnormal cytokines levels can trigger a pro-inflammatory or anti-inflammatory response and are associated with a wide range of diseases. Excessive secretion of certain cytokines has been linked to the development of autoimmune diseases such as rheumatoid arthritis, lupus, and multiple sclerosis, in which the body's immune system erroneously targets healthy cells and tissues (Moudgil and Choubey, 2011). Sepsis is induced by overproduction of cytokines in response to foreign invaders and can lead to death if uncontrolled. Certain cytokines, such as IL-15 and M-CSF may promote tumorigenesis, whereas others, such as IFN- γ , may inhibit it (Dranoff, 2004). Cytokines can typically display multiple roles, such as TNF- α and IFN- γ , which can either promote tumor growth or suppress it (Wang and Lin, 2008). Cytokine alterations are also the root-cause of certain

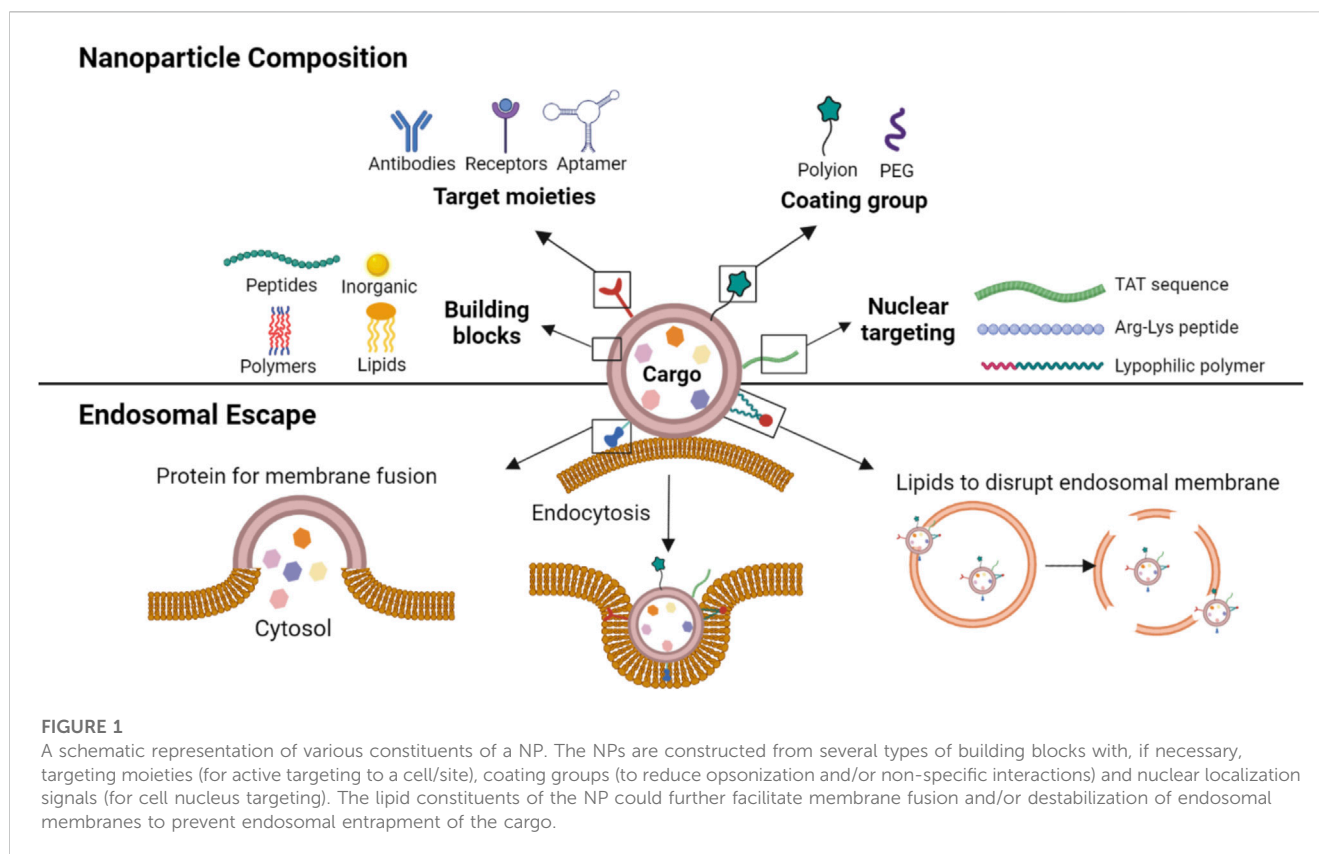
chronic inflammatory disorders such as ulcerative colitis, Crohn's disease, and inflammatory bowel disease. Depression and other mood disorders have been linked to elevated levels of pro-inflammatory cytokines (Raison et al., 2006).

When NPs enter the body bearing nucleic acids, they can be recognized by the immune system as foreign invaders like viruses, which can activate monocytes, macrophages, and dendritic cells to release defensive cytokines. Several factors related to the physicochemical features of the NPs, the nucleic acid cargo, administration regimen (location, dose, etc.) and patients' genetic profile can influence the nature and the intensity of the cytokine response (Gonçalves et al., 2020; Bila et al., 2021; Gu et al., 2021). In extreme cases, a cytokine storm, also known as cytokine release storm (Fajgenbaum and June, 2020) may be triggered. On the other hand, a controlled cytokine response with modulation of desired cytokines, can be beneficial by enhancing immune responses against tumors or pathogens, which leads to better therapeutic outcomes. Hence, understanding the cytokine response to NPs is essential to investigate the safety and efficacy of nucleic acid-based drugs.

In this report, we cover the latest developments in the cytokine response to NP-based non-viral delivery systems. We provide a brief insight into the premises behind different NP formulations, highlight their technological features that make them promising for clinical translation and survey the information on their cytokine response. We discuss ideas that may pave the way to interfere specifically with abnormal cytokine physiology and develop improved formulations with minimal adverse effects.

2 Nanoparticle-based nucleic acid delivery systems

A diverse range of materials has been explored as the foundation for NP fabrication in delivery of nucleic acids (Figure 1). These include peptide/protein derived natural or synthetic biomolecules, lipid-based compounds (natural and synthetic), polymeric and dendrimeric materials, inorganic frameworks (Paunovska et al., 2022), and more recently exosomes (El-Andaloussi et al., 2012). Cationic biomaterials are used to take advantage of the anionic nature of the nucleic acids to form ionic complexes for NP formation and/or entrapment, while the neutral biomaterials have been used for simple entrapment or encapsulation of nucleic acids. Some NPs are derived from a single (homogenous) component, which allows a simple fabrication process but may limit functional features of the NPs. On the other hand, the leading NP formulation, lipid NPs (LNPs) that formed the basis of the recent SARS-CoV-2 vaccines, are formed from a cocktail of lipids: a neutral lipid (e.g., distearoylphosphatidylcholine, DSPC) for nucleic acid entrapment, cholesterol for structure integrity, PEGylated lipid (DSPE-PEG) to create a hydrophilic, non-opsonizing surface, and an ionizable lipid (e.g., DLin MC3-DMA) for membrane fusion (Verbeke et al., 2019; Wang et al., 2023). Having multiple components enhances the functionality of NPs but may require specialized fabrication techniques not readily amenable for scale-up. Advanced polymers may incorporate some of these features into a single component, such as cationic and PEG moieties, lipidic side-groups and bioactive peptides capable of controlling intracellular trafficking (Suk et al., 2016), so that NPs formulations can be



conveniently prepared as long as the single component polymer is fabricated in a reproducible manner.

Irrespective of the building block, the NPs can facilitate nucleic acid delivery into cells through various uptake mechanisms, including cell membrane penetration and receptor-mediated internalization, and further binding to nucleic acids to protect them from degradation in the extracellular environment. Where necessary, cell/tissue/organ tropism can be built into the NPs by selective binding ligands that include biosynthetic antibodies against desired molecules (e.g., Her2), particular receptor ligands (e.g., folate) (Xu et al., 2017) or aptamers, to name a few. Such targeted systems aim to concentrate the nucleic acids at sites of action, and are expected to elicit minimal host response that can prevent the NPs from functioning.

Since endosomal membranes pose a significant barrier to the transport and release of the nucleic acids, NPs with endosomal escape mechanisms are preferred in the design of the carriers. Several strategies have been utilized to this end; if possible, endosomal entrapment could be avoided by using “fusogenic” NPs that can fuse with the cell membrane and release their cargo into the cytoplasm (Chen et al., 2013; Joubert et al., 2023). Lipid NPs (LNPs), in particular, can fuse with cell membranes to release their cargo into the cytoplasm directly. However, all NPs are likely to undergo some extent of endosomal uptake and the primary approach to overcome this barrier is to incorporate specific signals that facilitate endosomal escape such as the fusogenic peptides (Samec et al., 2022; Joubert et al., 2023), or lipids that disrupt the endosomal membrane order (Lam et al., 2023). Alternatively, some polymers can display “proton sponge” effect,

in which the cationic moieties absorb H^+ and produce osmotic swelling of the endosomes, resulting in rupture and discharge of the nucleic acids into the cytoplasm (Pei and Buyanova, 2019). The release of the cargo from endosomes might be sufficient for nucleic acids that function in cytoplasm, for example, mRNA and non-coding RNAs such as short interfering RNA (siRNA), but additional measures might be needed to enhance the nuclear uptake of the nucleic acid. The nuclear uptake can be facilitated with lysine-arginine rich synthetic polypeptides (Li et al., 2022), viral-derived TAT peptides, ionizable lipids or lipophilic polymers whose mechanism of nuclear uptake remains to be elucidated can function along the same lines and increase nucleic acid uptake into cells.

3 Cytokine response to nanoparticles

The ability of a host to mount a significant cytokine release in response to administered nucleic acids with various delivery platforms has been appreciated. The most common clinical approach to circumvent immune response is through the administration of immunosuppressive agents to block immune cell interaction (Zhang C et al., 2021). Figure 2 provides a summary of various pharmacological approaches to interfere with the cytokine response in a clinical setting, not necessarily tailored for the NP systems. Some of the utilized agents are broad acting such as the use of corticosteroids, while others are quite specific such as the use of Anakinra™ to inhibit IL-1 β activity. Early clinical studies using viral delivery of gene medicines indicated the cytokine

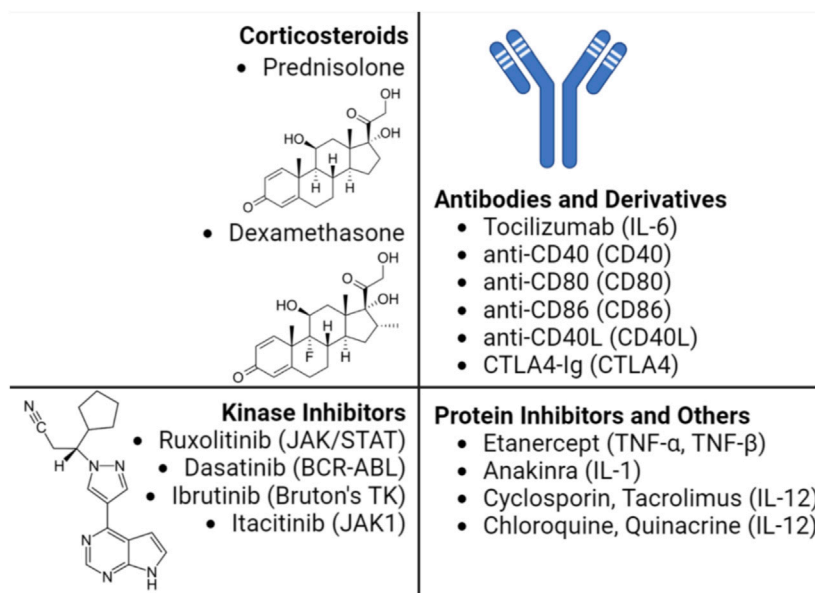


FIGURE 2

Main pharmacological agents employed to control cytokine storm in a clinical setting. The mediators targeted by the pharmacological agent is shown in parenthesis. The immunosuppressive properties of the corticosteroids are attributed to their ability to bind glucocorticoid receptors to block various signaling pathways affecting cytokine production in immune cells. The humanized antibody Tocilizumab predominantly used in treating rheumatoid arthritis also received approval to address cytokine release syndrome (CRS) following a CAR-T therapy based on AAV (Le et al., 2018). The kinase inhibitors with indicated target enzyme displayed immuno suppressive properties, including suppression of CRS, some of which are being investigated in T-cell therapies (Fraietta et al., 2016; Huarte et al., 2020; Xiang et al., 2022). Etanercept and Anakinra was successfully used to address CRS in patients without altering the therapeutic effect of CAR-T therapy in treatment of multiple myeloma (Zhang L et al., 2021) and B-cell lymphoma (Strati et al., 2020), respectively. Other molecules such as cyclosporin and tacrolimus, which inhibit the phosphatase calcineurin, can downregulate the IL-2 cytokine levels (Chu and Ng, 2021).

response to be significant; following an adenovirus-based infusion protocol into the right hepatic artery for the treatment of ornithine transcarbamylase deficiency, 1 patient (out of 19) exhibited peak levels of IL-6 (~4,500 pg/mL) at 8 h post injection that remained high until the passing of the patient (Chatenoud et al., 1989; Raper et al., 2003). Although one other patient also exhibited high IL-6 level, it subsequently dropped helping in complete recovery. Another study with an adenovirus vector in 2009 carrying human hepatocyte growth factor (Ad-HGF) proved successful involving 21 patients with severe coronary artery disease. While IL-4 levels remained unaffected by the treatment, IL-10 was upregulated in the first 24 h, but later decreasing to control levels (Yang et al., 2009). To improve the safety, a non-viral approach was employed for cystic fibrosis correction with lipid (DOPE: DMPE-PEG₅₀₀₀)/DNA complexes in an aerosolized form; 4 out of 8 patients experienced fever, muscle, and joint aches along with myalgias and arthralgia in some of them. Serum IL-6 levels were elevated in all patients ranging between ~10 and ~50 pg/mL although no causality was reported, while IL-1, IL-8, TNF α and IFN- γ levels were unaltered (Ruiz et al., 2001). A polymeric NP, CALAA-01 consisting of i) a cationic cyclodextrin, ii) a hydrophilic stabilizer adamantane-PEG and iii) a targeting ligand for human transferrin receptor, was used to carry a siRNA against an anti-cancer target, ribonucleotide reductase M2 subunit (RRM2). The serum cytokine studies in primates recorded an upregulation of IL-6, IL-12 and IFN- γ levels which correlated with patient clinical trials ($n = 24$). The cytokine levels peaked mostly between 2 and 6 h post

injection with IL-6 and IL-10 reaching ~600 pg/mL, TNF α ~200 pg/mL and IFN- γ ~50 pg/mL, but the levels dropped back to normal/baseline in 24 h. It was evident that the polymeric CALAA-01 induced an inflammatory response but was tolerated to some extent by the patients (Zuckerman et al., 2014).

Recent studies in preclinical models have provided alternative, non-pharmacological approaches to control the cytokine response to non-viral carriers. Dose is an important contributing factor as higher doses correlate with higher cytokine induction in several models. Although no major cytokine upregulation was reported with cell penetrating peptides (CPPs), a slight upregulation could be seen in TNF- α levels between 1 and 5 mg/kg doses of CPPs TP10, stearyl-(R_xR)₄, PF3 and PF4 *in vivo* (Suhorutsenko et al., 2011). Similarly, the levels of IL-1 β /-6/-8 secretion from keratinocytes/fibroblasts increased with increase in the dose of PAMAM *in vitro* (Czarnomysy et al., 2019) as well as cytokine secretion (MIP-2, TNF- α and IL-6) from macrophage cells to G4-G6 PAMAMs (Naha et al., 2010). Among 7 different lipid-modified LMW bPEI, one polymer showed increased IL-6/TNF- α secretion at higher polymer dose (~20 pg/mL vs. < 5 pg/mL) (Meenakshi Sundaram et al., 2022).

Increase in pDNA dose from 30 μ g to 80 μ g increased the serum TNF- α levels from ~5 to ~40 pg/mL (Kawakami et al., 2006). Similar observations were reported with oligodeoxynucleotides having CpG motifs as the levels of IL-6 and IFN- α increased from ~500 to ~1,250 pg/mL and ~80–~180 pg/mL, respectively, with increase in the concentration of the oligodeoxynucleotides delivered by a 1.8 kDa PEI (Cheng et al., 2018). Such a dose-dependent increase

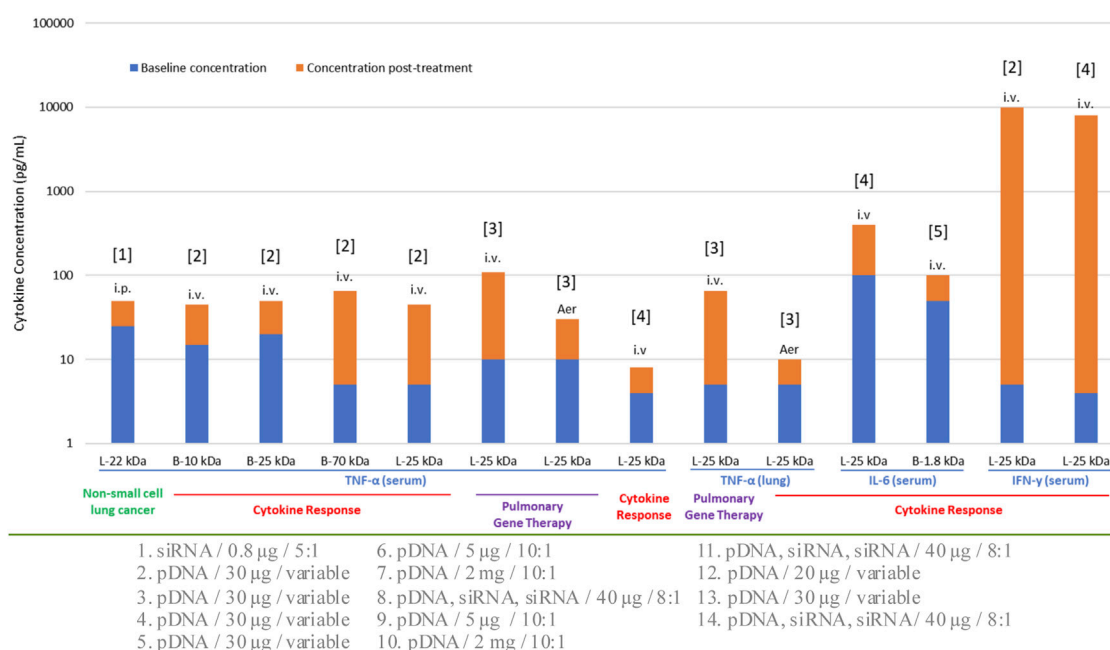


FIGURE 3

Cytokine response to various formulations of PEI in preclinical animal models. The specific cytokine investigated, the administration route (IV, IP, AER; intravenous, intraperitoneal and aerosolized, respectively) and the normal/disease model employed are indicated for each study. L: Linear PEI, B: Branched PEI. The numbers on the horizontal axis indicate the molecular weight (kDa) of the PEI used. The nature of the nucleic acid cargo, the dose administered and the N:P ratio employed in the formulations were variable; this information is provided below the graph and numbered according to the bar number from left to right. References for the studies are: [1]: Zhang et al., 2013, [2]: Kawakami et al., 2006, [3]: Gautam et al., 2001, [4]: Bonnet et al., 2008, [5]: Cheng et al., 2018.

in cytokine levels was also seen with CALAA-01 NPs, as patients treated with 10 mg/m² (dose of siRNA) displayed negligible cytokine response, while with 20–30 mg/m² dose, there was a maximum increase of 200-fold for IL-6, 100-fold for IL-10, 15-fold for TNF-α and 20-fold for IFN-γ (Brockstedt et al., 1999; Zuckerman et al., 2014). Use of a low dose should be a key consideration irrespective of the therapy and should be implemented even at the earliest stages of discovery and validation studies in *in vitro* and *in vivo* bioassays.

Selection of administration route is normally dependent on the type of therapeutic intervention in addition to the anatomical site being targeted. Local routes would be more beneficial to confine the NPs, thereby avoiding unwanted systemic side effects. Commonly utilized IV route has the advantage of targeting systemic diseases as it can reach various organs. The influence of administration route on immune response was recognized early when using recombinant adeno-associated viral vectors (AAV) in C57BL/6 mice for ovalbumin delivery. The immune response following IM injection showed the lowest response through the development of cytotoxic T lymphocytes (CTL) (Brockstedt et al., 1999), while contrasting effects were observed in other studies where IM route triggered a high immune response compared to other routes of administration. Additional studies on the difference in immune responses upon different routes of administration (oral, IV and IM) have been reported with AAV through CTL (Sun et al., 2003; Shirley et al., 2020). Relatively fewer studies could be found with non-viral gene delivery systems. Routes such as IM, intradermal (ID), intralymphatic (ILy), and SC were compared in BALB/c mice with a model antigen (ovalbumin). All systems showed an

antibody response with ILy administration. The ID and IM routes induced a moderate response, whereas the SC route did not elicit any response with T-helper (Th) cells being a major player in this study. Re-stimulation of the mice splenocytes (*in vitro*) was performed to better understand the cellular response based on IFN-γ, IL-4 and IL-10 cytokine secretion. With liposomes, the ILy route showed an elevated IFN-γ secretion compared to the SC, ID and IM routes. The chitosan and PLGA NPs did not show any major differences between the route of administrations and IFN-γ/IL-10 induction, while the route of administration was important for chitosan NPs for the IL-4 secretion (IM < SC < ID < ILy) (Mohan et al., 2010). Although this was a vaccination study, the findings could be extrapolated to gain an insight on the immunogenicity of non-viral NPs. With liposome-based vectors, several animal studies were reported for nucleic acid NPs derived from this carrier (Figure 3) and different routes did not appear to make a significant difference in the elicited response in this case. Within this limited data set, i) some cytokines (IFN-γ) appeared to be more stimulated with this particular carrier, and ii) the cytokine response appeared to be similar in normal vs. disease models. Different types of NPs other than LNPs and polymeric systems also found to contribute to cytokine responses (Table 1).

With viral delivery systems, pre-exposure to viruses could explain the stronger cytokine responses in some individuals, but this should not be an issue with NPs. In Phase Ia/Ib studies with CALAA-01, 19 (M) Phase Ia patients had good tolerance to dose escalation, while 3 (F) out of 5 (F) Phase Ib patients experienced dose-limiting toxic events (DLTs) along with grade 3 toxicities.

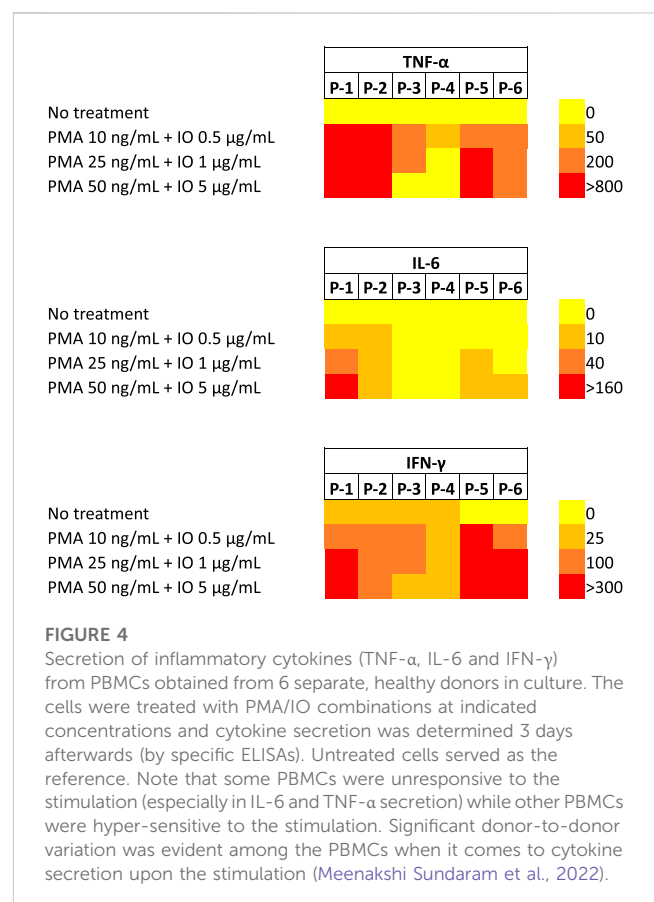
TABLE 1 Cytokines responses by NPs with/without cargos other LNPs and polymeric systems.

Type of NPs	Composition of NP (+/-) cargo	Cytokine and functional response
Carbon nanotube (CN)	Multi-wall CN with a mixture of 5.6 wt% ferrocene in toluene	Induces pro-inflammatory cytokines (Boyles et al., 2015)
	Single-wall CN with amine-functionalized group	Induces TNF α and IL-1 β (Gao et al., 2021a)
Graphene oxide (GO)	GO from Asbury Mills 3061 grade graphite	GO with larger lateral size enhances the production of IL-6, TNF α and IL-1 β (Ma et al., 2015)
	Vanillin-functionalized NP from a mixture of vanillin with GO	Releases significantly higher level of IL1- β , TNF- α , GM-CSF, IL-6, IL-8 (Gurunathan et al., 2019)
Dendrimers	Non-modified native PAMAM dendrimer	Triggers secretion of TNF α and IL-1 β (Gao et al., 2021b)
Magnetic nanoparticle (MNP)	MNP prepared by dissolving iron(III) acetylacetonate, 1,2-hexadecanediol, oleic acid, and oleylamine in benzyl ether	Suppresses chronic inflammatory response and activates acute inflammatory response (Zhu et al., 2019)
Gold NP (GNP)	<i>Ephedra sinica</i> Stapf extract-capped GNP	Helped <i>Ephedra sinica</i> Stapf to silence upstream signaling pathways of pro-inflammatory mediators and cytokines (Park et al., 2019)
Gold NP (GNP)	<i>Hypericum perforatum</i> extract-capped GNP	Helped <i>Hypericum perforatum</i> to downregulate pro-inflammatory cytokines (IFN- γ , IL-17A and IL-6) and upregulate anti-inflammatory cytokines (TGF- β , IL-10 and IL-4) (Mahmoudi et al., 2022)
Silica NP (SNP)	Mesoporous SNP	Induces the expression pro-inflammatory cytokine genes (IL-1, IL-8 and TNF- α) (Ghasemi et al., 2022)
SNP		Induces pro-inflammatory cytokines CXCL8 and IL-6 (Låg et al., 2018)
Calcium phosphate NP (CaPNP)	CapNP by incubating BSA and CaCl ₂ in Dulbecco's Modified Eagle Medium	Facilitated delivery of TNF-stimulated gene 6 knocked mesenchymal stem cells into liver and silences cytokines (Wang et al., 2020)
Exosome	Obtained from adipose-derived mesenchymal stem cells	Induces higher expression of anti-inflammatory cytokines (Heo et al., 2020)

Some patients exhibited slight cytokine response mediated by Th2 cells. (Zuckerman et al., 2014). Substantial variation in cytokine induction was observed among 307 participants (children) towards virus and bacterial infection with differences as high as 1000-fold. Twenty-eight separate cytokines were evaluated against 15 different stimuli including various pathogens using peripheral blood mononuclear cells (PBMC) isolated from 307 participants. The reason(s) for the difference could be due to i) different receptors being recognized among the participants, ii) failure to determine the specific cell type present in PBMCs before undertaking the study, iii) use of PBMCs stored in liquid nitrogen and iv) the difference in the time of sample collection along with genetic differences among the cells (Lin et al., 2022). We also noted such differences in *vitro* studies performed with PBMC obtained from otherwise healthy individuals (i.e., blood donors) (Figure 4); only 3 out of 6 donor PBMC exhibited very high levels with the “stimulatory” treatment of PMA/IO (phorbol 12-myristate 13-acetate/ionomycin).

4 Management of cytokine response: possibility of precision intervention

Novel approaches are being explored to formulate minimally immunogenic NP carriers and for therapeutic purpose in diseases involving cytokine dis-regulation. The collective effort is paving the way for a personalized approach to cytokine therapy whereby very specific interventions, mainly based on RNA Interference (RNAi),



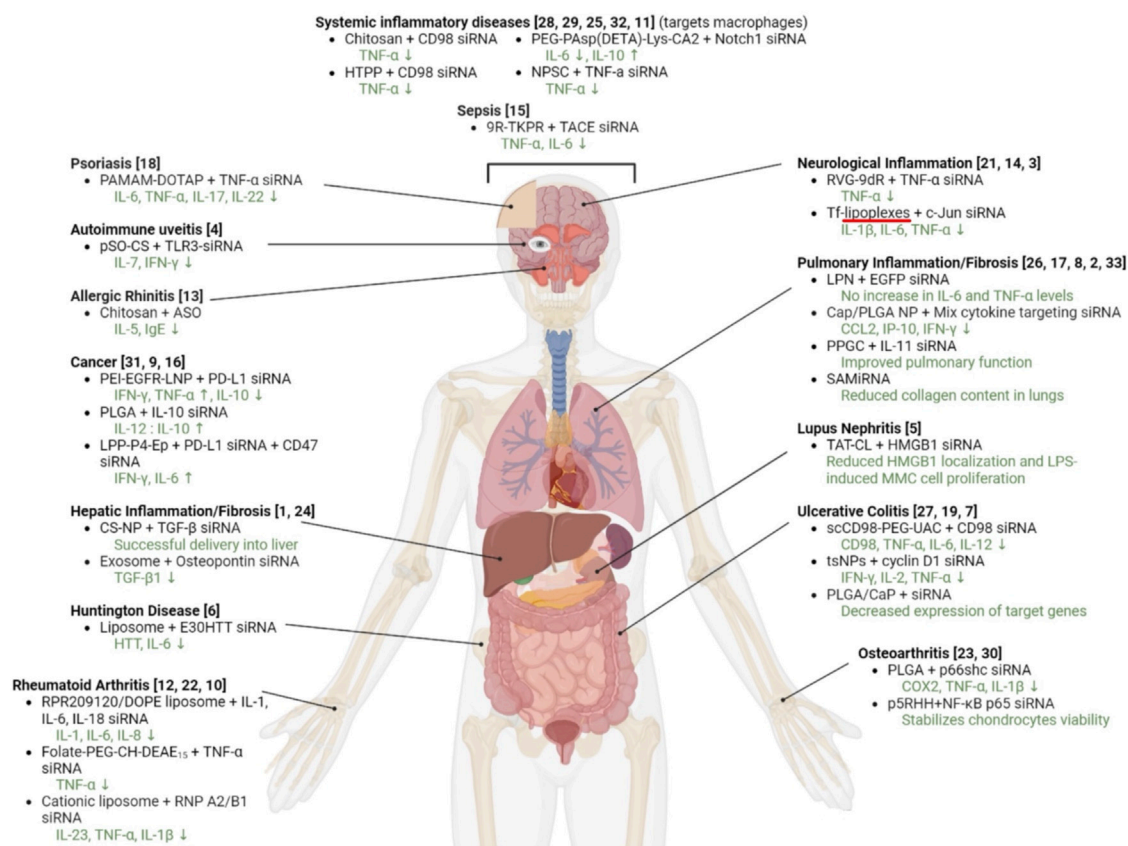


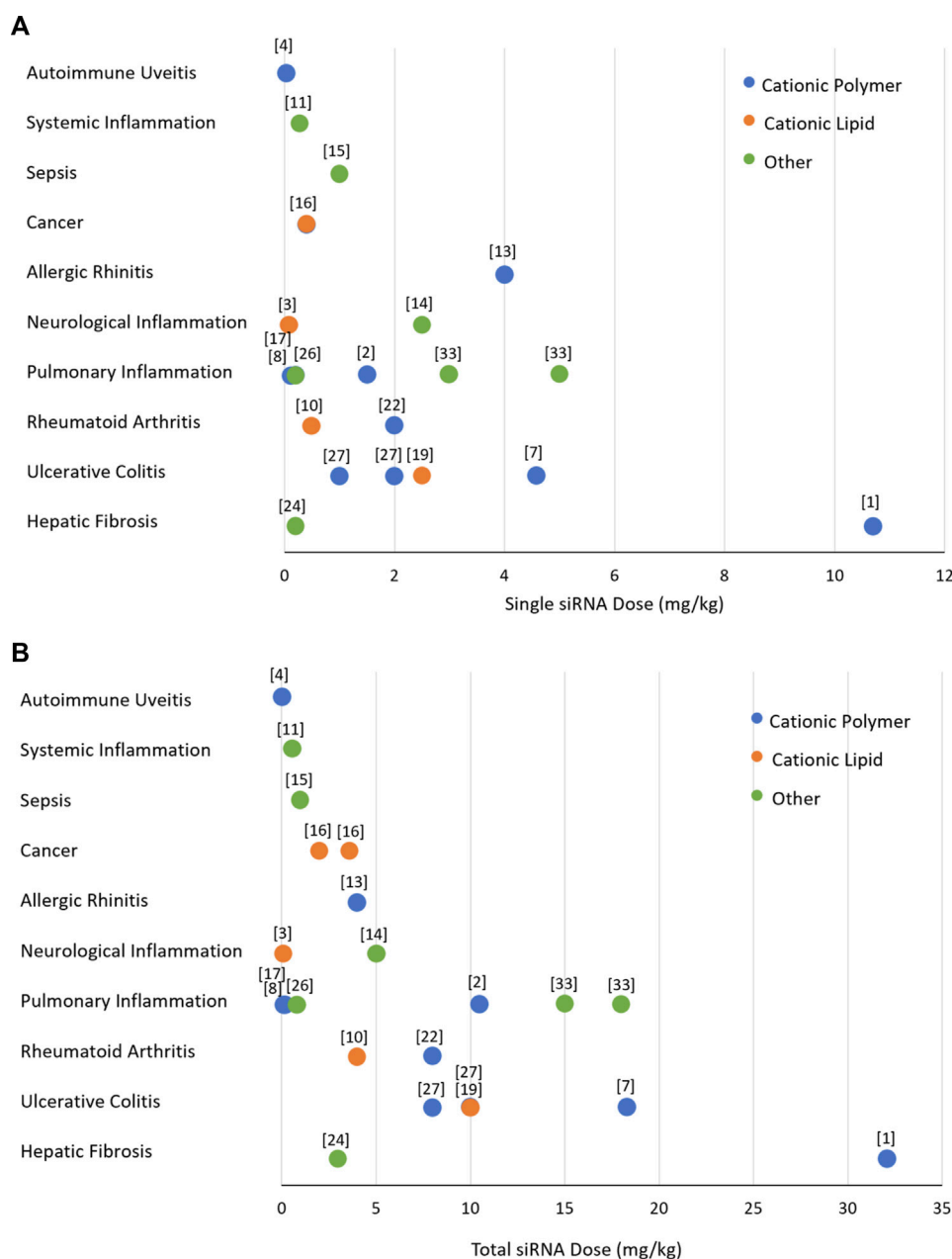
FIGURE 5

Attempts to implement RNAi in various disease models involving cytokine mediators. The specific siRNA target and the delivery system used are indicated. The references to the specific study are numbered as follows: 1: (Azzam, El Safy, et al., 2020). 2: (Bai et al., 2022). 3: (Cardoso et al., 2010). 4: (Chen et al., 2013). 5: (Diao et al., 2019). 6: (Fihurka et al., 2022). 7: (Frede et al., 2016). 8: (Frede et al., 2017). 9: (Heo et al., 2015). 10: (Herman et al., 2015). 11: (Jiang et al., 2018). 12: (Khouri et al., 2008). 13: (Kim and Kim, 2007). 14: (Kim et al., 2010). 15: (Lee et al., 2021). 16: (Lian et al., 2019). 17: (Okuda et al., 2018). 18: (Pandi et al., 2018). 19: (Peer et al., 2008). 20: (Rudd et al., 2020). 21: (Kim et al., 2011). 22: (Shi et al., 2018). 23: (Shin et al., 2020). 24: (Tang et al., 2022). 25: (Wu et al., 2018). 26: (Wu et al., 2021). 27: (Xiao et al., 2014). 28: (Xiao et al., 2016). 29: (Xiao et al., 2017). 30: (Yan et al., 2019). 31: (Yang et al., 2022). 32: (Jiang et al., 2018). 33: (Yoon et al., 2016).

significant inflammatory cytokines and care is needed in polymer design to reduce reactive species (Beyerle et al., 2010), beyond simple PEGylation. Low MW PEIs (<2 kDa), either in native form or modified with various lipids, seems to be relatively free from cytokine elicitation (Meenakshi Sundaram et al., 2022). With a high MW (22 kDa) PEIs tested in a murine model, blood cytokine levels were elevated to between ~ 4 and $\sim 10^3$ pg/mL with different batches of polymers, indicating the importance of a reproducible manufacturing process for the NP materials (Bonnet et al., 2008).

A close inspection of the reported RNAi studies in cytokine disorders indicated a significant variation in the administered dose (Figure 6). We expect a dose of ~ 1 mg/kg in preclinical (animal) models to be reasonable for clinical translation to human patients. The doses used in most animal models are <5 mg/kg, with cationic polymers as well as lipids being effective at the lower dose of the spectrum. It is obviously not possible to directly assign the observed potencies (given by effective doses summarized in Figure 6) to the efficiency of the delivery system, since the target characteristics as well as the intrinsic potency of the siRNA to silence the intended target contribute to the overall potency. Head-to-head comparison

are missing in most studies since the focus is to demonstrate the feasibility of a particulate nanoparticulate system in the intended indication. Dose response studies is a must in this regard, but admittedly as in our work, the feasibility of the therapeutic approach is commonly explored at a single “efficacious” dose rather than a dose range. It is noteworthy that the most efficacious systems (given by single and total doses administered) are polymeric chitosan and poly(lactide-co-glycolide), Transferrin-decorated and EpCAM (epithelial cell adhesion molecule)-decorated cationic liposomes, calcium phosphate, and arginine-functionalized AuNP (Cardoso et al., 2010; Chen et al., 2013; Frede et al., 2017; Jiang et al., 2018; Lian et al., 2019; Wu et al., 2021) indicating no preferential delivery system emerging among the effective systems. It appears that NPs of diverse compositions could be made to implement RNAi in preclinical models of cytokine disorders. Among these apparently more efficacious systems, the majority of the delivery systems were applied locally (Cardoso et al., 2010; Chen et al., 2013; Frede et al., 2017; Wu et al., 2021) that justified the relatively low dose, but some systemically (intravenous) as well (Jiang et al., 2018; Lian et al., 2019), making them promising for systems disorders.

**FIGURE 6**

The doses of siRNA treatments used in preclinical models of inflammatory diseases. **(A)** The dose of individual siRNA injections. **(B)** Total dose injected based on the individual injection dose and the numbers of injections undertaken. The data is from studies summarized in Figure 5, excluding *in vitro*/cell culture studies. The numbers refer to the study references shown in the legend of Figure 5. The nature of delivery system used was classified as polymeric (blue), lipid (orange) and others (green).

5 Interpersonal differences in immune response

Inter-individual variations in human immune response, even among those considered as healthy, are widely accepted (as evident by differential responses in clinical studies), yet to which extent and for what reasons, not much is known. Using a systems-level analysis of 210 healthy twins between 8 and 82 years old, homeostatic cytokines such as IL-2 and IL-7 (crucial in T-cell proliferation) were found to be highly

heritable whereas most signaling cytokines such as IL-6 and IL-21 were highly non-heritable (Brodin et al., 2015). This is in alignment with prior studies that demonstrated the low impact of heritability on variation in inter-individual T-cells and dendritic cell responses (Brodin and Davis, 2017). With age, genetic similarity in immune responses also decreased even in identical twins, with non-heritable influences contributing more to the variations (Brodin et al., 2015). These non-heritable impacts include environmental exposure (e.g., vaccines, infections, pollution, etc.), but can also extend to effects by

pathogens, symbiotic microbiome and *de novo* mutations (Brodin and Davis, 2017). For example, a common environmental risk factor is cigarette smoke, which has been shown to correlate to higher autoantibodies as well as lower immunoglobulins and NK-cell functional activity (Brodin and Davis, 2017). Given the cross-talk between immune cell populations, a recent study has proposed a framework to view human immune systems in terms of immunotypes categorized based on key combinations of immune cell composition (Kaczorowski et al., 2017). The study found that variation in human immune systems is more continuous than discrete, and suggested that certain combinations of immune cell populations can predict functional responses to different stimuli (Kaczorowski et al., 2017). However, it should be noted that these analyses were limited to blood cell types, thus, an expansion of the measurements including serum cytokines and chemokines are necessary to validate and improve their predictive capacities (Kaczorowski et al., 2017).

The human immune responses to adenoviruses (AVs) were considered stereotypical, short-lasting and non-threatening, however, they manifest in a spectrum with diverse levels of length and severity (Atasheva and Shayakhmetov, 2022). Not surprisingly, patients with more severe diseases would exhibit more serious immune reactions after exposure to natural AV infections. Upon administration of AV therapies, IL-1 elevation was noted only 3 h after IV-administration, while early response cytokines such as IL-6, TNF- α , and IFN- γ and the CCL2 chemokine would show maximal levels at 6 h, with a return to baseline levels within 24 h. The presence of AV-specific antibodies can heighten the immune response by enabling viruses to gain entry into dendritic cells, which causes release of inflammatory cytokines (Atasheva and Shayakhmetov, 2022). It was the elevation of AV-specific antibodies that was suggested to potentially contribute to the lethal immune response in a patient after virus administration (Somanathan et al., 2020).

Regarding immune responses triggered by non-viral therapies, de Braganca and others have outlined both acute and long-term effects of the NP systems in the lung tissue (De Braganca, 2021). These effects can manifest locally such as edema and inflammation, but can also spread to organs beyond the pulmonary system. Immune side effects vary depending on the NP features such as size, geometry, stiffness, and hydrophobicity. Interestingly, higher toxicity is associated with smaller particles due to higher surface-volume ratio enabling more opportunities to interact with the immune system (De Braganca, 2021). Cationic NPs have been shown to trigger dendritic cell-activated release of pro-inflammatory factors such as IL-1 β , IL-6, MCP-1, MIP-1 α and TNF- α (Barillet et al., 2019), potentially due to interactions with the negative charges on the cell surface (De Braganca, 2021). Silica NPs also displayed immunotoxicity both *in vitro* and *in vivo*; genotoxicity and cytotoxicity were observed in RAW 264.7 cells upon exposure to such NPs at 200 μ g/mL (Chen et al., 2018). Silica NP exposure also triggers size-independent injuries in mouse lung tissues as well as oxidative stress and cardiac inflammation in zebrafish embryos (Chen et al., 2018). Another reason behind adverse immunological side effects lies in the mechanism of NP administration. Commonly administered through inhalation, NPs can activate dendritic cells, whose pattern recognition receptors

recognize the nucleic acid in the NPs as foreign (De Braganca, 2021). This triggers release of pro-inflammatory cytokines and chemokines and can cause cellular and organ damage (De Braganca, 2021). Non-viral gene therapeutics have been also shown to trigger immune responses in the ocular space. A recent review article by Ren and coworkers summarizes clinical findings that demonstrate even the widely considered immune-privileged ocular space is still subject to unwanted inflammatory effects elicited by retinal gene editing tools (Ren et al., 2022). Non-viral vectors such as chitosan showed inflammation and retinal damage while PCEP (poly(((cholesteryloxocarbonylamidoethyl) methylbis(ethylene) ammonium iodide) ethyl phosphate)) showed 15% retinal degeneration in rabbits (Ren et al., 2022). Similarly, lipoplexes carrying high amount of ribonucleoprotein showed toxicity in mice via subretinal delivery (Ren et al., 2022).

6 Conclusion and perspectives

The concerns related to cytokine release syndrome have been well appreciated in early gene therapy work with viral vectors, but this issue is also critical when it comes to non-viral systems. Although it has been possible to fine-tune this response and minimize it at times (Cron et al., 2023), it is still a concern with some non-viral NP systems. Non-viral NPs have lagged viral systems for clinical entry, and this is likely due to lower efficacy issues rather than the immunological reactions. Relatively minor measures can be taken to adjust the dose, administration route and especially to pre-screen patients to cytokine sensitivity, which will ultimately help with the host response. It may be possible to intervene with the cytokine responses very precisely, by relying on transient suppression of gene expression by using RNAi or more permanent measures such as CRISPR/Cas9 system (Ottaviano et al., 2022). Transient expression may be sufficient for controlling initial host response, which tends to subside if not life-threatening. A permanent stoppage of any cytokine response may give additional complications on the long term in managing host response to foreign invaders and/or other physiological and pathological events. RNAi can make it possible to intervene with a spectrum of cytokines in a convenient way, by using a mixture of specific siRNAs (early attempts have been made as noted in Figure 5). Considering the spectrum of attempts undertaken in several disease models, it is clear that there is a wide range of inflammatory and cytokine-associated diseases that will directly benefit from the RNAi approach. Where localized application is feasible (e.g., colitis with defined anatomical involvement), it may be safer to utilize nanoparticulate systems to locally deliver the cytokine interfering agents. Where systemic intervention might be required (e.g., sepsis), it is preferred to utilize “stealth” nanoparticulate systems that do not exacerbate the disease any further. While PEG incorporation into NPs (or NP building blocks) has been the “go-to” approach for this end, this modification typically reduced the efficacy of NPs and needs to be implemented in a way that the dose administered are not compromised due to lower efficacy. The PEG itself, within the 2–10 kDa region, did not appear to induce proinflammatory cytokines with silica NP incubated primary murine macrophages and dendritic cells (Storjohann et al., 2023). However, other types of NPs and/or dose used were

reported to significantly affect this response (Tehrani et al., 2022; Zamorina et al., 2023). Coating the surface of NPs or including additives that change the zeta-potential (from highly cationic surface to neutral surface, in our hands) could be a simpler measure to reduce inflammatory cytokine response (Meenakshi Sundaram et al., 2022). The exact role of NP features when attempting to modulate cytokine secretion needs to be better controlled. Clearly, the collective experience in various preclinical models indicated that the cytokine response is a significant issue with all of the NP delivery systems (Godinho et al., 2014). When RNAi is attempted to be implemented, the NP delivery system should not be viewed as a simple 'passive' carrier; it may elicit or help to reduce cytokine levels independently. It is likely that particular NPs in the spectrum of NPs used (Figure 5) will be more suitable for certain applications. Efforts to elucidate this relationship is worthwhile since it will critically impact the efficacy and the course of pharmacodynamic response in the investigated pathophysiology.

Using human PBMCs rather than animal models is important in assessing the cytokine response. We found cells lines such as Jurkat T-cells to be much more sensitive than the primary PBMC, which may lead to an erroneous assessment of the cytokine response if used routinely. Individual variations in cytokine response are obviously better modeled by the use of PBMC in culture (Figure 3). It will be important to tackle this with a representative sampling of PBMCs to estimate the true potential of delivery systems to induce inflammatory cytokines. Ultimately, this will save much effort to select minimally reactive delivery systems, where the clinical safety is utmost important.

While a great deal of efforts have been placed on minimizing cytokine response, it may be useful in certain indications to utilize NPs that can elicit a specific cytokine response. As eluted in experimental cancer applications above, induction of cytokine response can aid in therapeutic effects for certain kinds of cancers, as in the case of sensitizing malignant cells to chemotherapy. In that way, better understanding of structural features of the NPs that can elicit a strong and/or selective cytokine response will help to design novel systems for therapy. Induction of a certain cytokine cocktail has the potential to alter the physiology of local immune cells so that the effects might be long lasting and more potent upon such an 'engineered' cytokine response. For example, with lipid-substituted PEI polymers, we

have observed that cytotoxicity, hemocompatibility (i.e., RBC lysis potency) and inflammatory cytokine (TNF- α , IL-6 and IFN- γ) secretion was differentially dependent on the nature of the lipid substituted on the PEI (Meenakshi Sundaram et al., 2022). Hence it may be possible to fine-tune these properties independent of each other. While these cytokines are lumped as inflammatory cytokines, we also saw differential upregulation of the cytokines in response to non-viral carrier exposure, in that one or more of this class of cytokines could be selectively stimulated, so that it may be possible to fine tune the response among a physiologically similar group of cytokines as a function of carrier features. Individual variations in cytokine response and its determinants constitute another aspect of NP technology that will require more attention to develop personalized therapies and optimize NPs for gene delivery, so that research efforts need to continue to shed more light on this important issue.

Author contributions

MN, DM, JC, KH, and HU drafted the manuscript, ED and HU edited the manuscript, MN, DM, JC, and KH generated the Figures. All authors contributed to the article and approved the submitted version.

Conflict of interest

The authors declare that the research was conducted in the absence of any commercial or financial relationships that could be construed as a potential conflict of interest.

Publisher's note

All claims expressed in this article are solely those of the authors and do not necessarily represent those of their affiliated organizations, or those of the publisher, the editors and the reviewers. Any product that may be evaluated in this article, or claim that may be made by its manufacturer, is not guaranteed or endorsed by the publisher.

References

- Atasheva, S., and Shayakhmetov, D. M. (2022). Cytokine responses to adenovirus and adenovirus vectors. *Viruses* 14, 888. doi:10.3390/V14050888
- Azzam, M., El Safy, S., Abdelgelil, S. A., Weiskirchen, R., Asimakopoulou, A., de Lorenzi, F., et al. (2020). Targeting activated hepatic stellate cells using collagen-binding chitosan nanoparticles for siRNA delivery to fibrotic livers. *Pharmaceutics* 12 (6), 590. doi:10.3390/PHARMACEUTICS12060590
- Bai, X., Zhao, G., Chen, Q., Li, Z., Gao, M., Ho, W., et al. (2022). Inhaled siRNA nanoparticles targeting IL11 inhibit lung fibrosis and improve pulmonary function post-bleomycin challenge. *Sci. Adv.* 8 (25), eabn7162. doi:10.1126/SCIADV.ABN7162
- Barillet, S., Fattal, E., Mura, S., Tsapis, N., Pallardy, M., Hillaireau, H., et al. (2019). Immunotoxicity of poly (lactic-co-glycolic acid) nanoparticles: influence of surface properties on dendritic cell activation 13, 606–622. doi:10.1080/17435390.2018.1564078
- Beyerle, A., Merkel, O., Stoeger, T., and Kissel, T. (2010). Pegylation affects cytotoxicity and cell-compatibility of poly(ethylene imine) for lung application: structure-function relationships. *Toxicol. Appl. Pharmacol.* 242 (2), 146–154. doi:10.1016/J.TAAP.2009.10.001
- Bila, D., Radwan, Y., Dobrovolskaia, M. A., Panigaj, M., and Afonin, K. A. (2021). The recognition of and reactions to nucleic acid nanoparticles by human immune cells. *Molecules* 26 (14), 4231. doi:10.3390/MOLECULES26144231
- Bonnet, M. E., Erbacher, P., and Bolcato-Bellemin, A. L. (2008). Systemic delivery of DNA or siRNA mediated by linear polyethylenimine (L-PEI) does not induce an inflammatory response. *Pharm. Res.* 25 (12), 2972–2982. doi:10.1007/s11095-008-9693-1
- Boyles, M. S. P., Young, L., Brown, D. M., MacCalman, L., Cowie, H., Moiala, A., et al. (2015). Multi-walled carbon nanotube induced frustrated phagocytosis, cytotoxicity and pro-inflammatory conditions in macrophages are length dependent and greater than that of asbestos. *Toxicol. Vitro* 29, 1513–1528. doi:10.1016/J.TIV.2015.06.012
- Brockstedt, D. G., Podsakoff, G. M., Fong, L., Kurtzman, G., Mueller-Ruchholtz, W., and Engleman, E. G. (1999). Induction of immunity to antigens expressed by recombinant adeno-associated virus depends on the route of administration. *Clin. Immunol.* 92 (1), 67–75. doi:10.1006/clim.1999.4724
- Brodin, P., and Davis, M. M. (2017). Human immune system variation. *Nat. Rev. Immunol.* 17, 21–29. doi:10.1038/NRI.2016.125

- Brodin, P., Jovic, V., Gao, T., Bhattacharya, S., Angel, C. J. L., Furman, D., et al. (2015). Variation in the human immune system is largely driven by non-heritable influences. *Cell* 160, 37–47. doi:10.1016/j.cell.2014.12.020
- Cardoso, A. L. C., Costa, P., de Almeida, L. P., Simões, S., Plesnila, N., Culmsee, C., et al. (2010). Tf-lipoplex-mediated c-Jun silencing improves neuronal survival following excitotoxic damage *in vivo*. *J. Control Release* 142 (3), 392–403. doi:10.1016/j.jconrel.2009.11.004
- Carter, E., Lau, C. Y., Tosh, D., Ward, S. G., and Mrsny, R. J. (2013). Cell penetrating peptides fail to induce an innate immune response in epithelial cells *in vitro*: implications for continued therapeutic use. *Eur. J. Pharm. Biopharm.* 85 (1), 12–19. doi:10.1016/j.ejpb.2013.03.024
- Chatenoud, L., Ferran, C., Reuter, A., Legendre, C., Gevaert, Y., Kreis, H., et al. (1989). Systemic reaction to the anti-T-cell monoclonal antibody OKT3 in relation to serum levels of tumor necrosis factor and interferon-gamma [corrected]. *N. Engl. J. Med.* 320 (21), 1420–1421. doi:10.1056/NEJM198905253202117
- Chen, L., Liu, J., Zhang, Y., Zhang, G., Kang, Y., Chen, A., et al. (2018). The toxicity of silica nanoparticles to the immune system. *Nanomedicine (Lond)* 13, 1939–1962. doi:10.2217/NNM-2018-0076
- Chen, S., Yan, H., Sun, B., Zuo, A., and Liang, D. (2013). Subretinal transfection of chitosan-loaded TLR3-siRNA for the treatment of experimental autoimmune uveitis. *Eur. J. Pharm. Biopharm.* 85 (3 Pt A), 726–735. doi:10.1016/j.ejpb.2013.09.005
- Cheng, T., Miao, J., Kai, D., and Zhang, H. (2018). Polyethyleneimine-mediated CpG oligodeoxynucleotide delivery stimulates bifurcated cytokine induction. *ACS Biomater. Sci. Eng.* 4 (3), 1013–1018. doi:10.1021/acsbomaterials.8b00049
- Chu, W. S., and Ng, J. (2021). Immunomodulation in administration of rAAV: preclinical and clinical adjuvant pharmacotherapies. *Front. Immunol.* 12, 658038. doi:10.3389/fimmu.2021.658038
- Cron, R. Q., Goyal, G., and Chatham, W. W. (2023). Cytokine storm syndrome. *Annu. Rev. Med.* 74, 321–337. doi:10.1146/annurev-med-042921-112837
- Czarnomys, R., Bielawska, A., and Bielawski, K. (2019). Effect of 2nd and 3rd generation PAMAM dendrimers on proliferation, differentiation, and pro-inflammatory cytokines in human keratinocytes and fibroblasts. *Int. J. Nanomedicine* 14, 7123–7139. doi:10.2147/IJN.S211682
- De Bragance, L. (2021). A study of the immune responses to therapeutic inhaled nanoparticles by lung alveolar macrophages — research explorer. The University of Manchester. Available at: <https://research.manchester.ac.uk/en/studentTheses/a-study-of-the-immune-responses-to-therapeutic-inhaled-nanoparticles> (Accessed August 17, 2023).
- Deckers, J., Anbergen, T., Hokke, A. M., de Dreu, A., Schrijver, D. P., de Bruin, K., et al. (2023). Engineering cytokine therapeutics. *Nat. Rev. Bioeng.* 2023, 286–303. doi:10.1038/s44222-023-00030-y
- Diao, L., Tao, J., Wang, Y., Hu, Y., and He, W. (2019). Co-Delivery of dihydroartemisinin and HMGB1 siRNA by TAT-modified cationic liposomes through the TLR4 signaling pathway for treatment of lupus nephritis. *Int. J. Nanomedicine* 14, 8627–8645. doi:10.2147/IJN.S220754
- Dranoff, G. (2004). Cytokines in cancer pathogenesis and cancer therapy. *Nat. Rev. Cancer* 4 (1), 11–22. doi:10.1038/nrc1252
- El-Andaloussi, S., Lee, Y., Lakhal-Littleton, S., Li, J., Seow, Y., Gardiner, C., et al. (2012). Exosome-mediated delivery of siRNA *in vitro* and *in vivo*. *Nat. Protoc.* 7 (12), 2112–2126. doi:10.1038/nprot.2012.131
- Elisabhy, M., and Wooley, K. L. (2013). Cytokines as biomarkers of nanoparticle immunotoxicity. *Chem. Soc. Rev.* 42 (12), 5552–5576. doi:10.1039/C3CS60064E
- Fajgenbaum, D. C., and June, C. H. (2020). Cytokine storm. *N. Engl. J. Med.* 383, 2255–2273. doi:10.1056/NEJMRA2026131
- Fihurka, O., Sava, V., and Sanchez-Ramos, J. (2022). Dual-function hybrid nanoparticles with gene silencing and anti-inflammatory effects. *Nanomedicine Lond. Engl.* 17 (9), 577–590. doi:10.2217/NNM-2021-0458
- Fraietta, J. A., Beckwith, K. A., Patel, P. R., Ruella, M., Zheng, Z., Barrett, D. M., et al. (2016). Ibrutinib enhances chimeric antigen receptor T-cell engraftment and efficacy in leukemia. *Blood* 127 (9), 1117–1127. doi:10.1182/blood-2015-11-679134
- Frede, A., Neuhaus, B., Klopffleisch, R., Walker, C., Buer, J., Müller, W., et al. (2016). Colonic gene silencing using siRNA-loaded calcium phosphate/PLGA nanoparticles ameliorates intestinal inflammation *in vivo*. *J. Control Release* 222, 86–96. doi:10.1016/j.jconrel.2015.12.021
- Frede, A., Neuhaus, B., Knuschke, T., Wadwa, M., Kollenda, S., Klopffleisch, R., et al. (2017). Local delivery of siRNA-loaded calcium phosphate nanoparticles abates pulmonary inflammation. *Nanomedicine* 13 (8), 2395–2403. doi:10.1016/j.nano.2017.08.001
- Gao, X., Zheng, X., Gao, S., Huang, Y., Xiong, J., and Ren, H. (2021a). Toxicity of amine-functionalized single-carbon nanotube (NH₂ f-SWCNT) to channel catfish (*Ictalurus punctatus*): organ pathologies, oxidative stress, inflammation, and apoptosis. *Chemosphere* 282, 131133. doi:10.1016/j.chemosphere.2021.131133
- Gao, Y., Shen, M., and Shi, X. (2021b). Interaction of dendrimers with the immune system: an insight into cancer nanotherapeutics. *View* 2, 20200120. doi:10.1002/VTW.20200120
- Gautam, A., Densmore, C. L., and Waldrep, J. C. (2001). Pulmonary cytokine responses associated with PEI-DNA aerosol gene therapy. *Gene Ther.* 8 (3), 254–257. doi:10.1038/sj.gt.3301369
- Ghasemi, M., Bakhshi, B., Khashei, R., and Soudi, S. (2022). Mesoporous silica nano-adjuvant triggers pro-inflammatory responses in Caco-2/peripheral blood mononuclear cell (PBMC) co-cultures. *Nanobiomedicine* 9, 184954352210883. doi:10.1177/18495435221088374
- Godinho, B. M. D. C., McCarthy, D. J., Torres-Fuentes, C., Beltrán, C. J., McCarthy, J., Quinlan, A., et al. (2014). Differential nanotoxicological and neuroinflammatory liabilities of non-viral vectors for RNA interference in the central nervous system. *Biomaterials* 35 (1), 489–499. doi:10.1016/j.biomaterials.2013.09.068
- Gonçalves, A., Machado, R., Gomes, A. C., and Costa, A. D. (2020). Nanotechnology solutions for controlled cytokine delivery: an applied perspective. *Appl. Sci.* 10 (20), 7098. doi:10.3390/app10207098
- Gu, P., Zhang, Y., Cai, G., Liu, Z., Hu, Y., Liu, J., et al. (2021). Administration routes of polyethyleneimine-coated PLGA nanoparticles encapsulating Angelica sinensis polysaccharide vaccine delivery system affect immune responses. *Mol. Pharm.* 18 (6), 2274–2284. doi:10.1021/acs.molpharmaceut.1c00090
- Gurunathan, S., Kang, M. H., Jeyaraj, M., and Kim, J. H. (2019). Differential immunomodulatory effect of graphene oxide and vanillin-functionalized graphene oxide nanoparticles in human acute monocytic leukemia cell line (THP-1). *Int. J. Mol. Sci.* 20, 247. doi:10.3390/ijms20020247
- Hassett, K. J., Higgins, J., Woods, A., Levy, B., Xia, Y., Hsiao, C. J., et al. (2021). Impact of lipid nanoparticle size on mRNA vaccine immunogenicity. *J. Control Release* 335, 237–246. doi:10.1016/j.jconrel.2021.05.021
- Heo, J. S., Lim, J. Y., Yoon, D. W., Pyo, S., and Kim, J. (2020). Exosome and melatonin additively attenuates inflammation by transferring miR-34a, miR-124, and miR-135b. *Biomed. Res. Int.* 2020, 1–9. doi:10.1155/2020/1621394
- Heo, M. B., Kim, S. Y., Yun, W. S., and Lim, Y. T. (2015). Sequential delivery of an anticancer drug and combined immunomodulatory nanoparticles for efficient chemimmunotherapy. *Int. J. Nanomedicine* 10, 5981–5992. doi:10.2147/IJN.S90104
- Herman, S., Fischer, A., Presumey, J., Hoffmann, M., Koenders, M. I., Escrivi, V., et al. (2015). Inhibition of inflammation and bone erosion by RNA interference-mediated silencing of heterogeneous nuclear RNP A2/B1 in two experimental models of rheumatoid arthritis. *Arthritis Rheumatol.* 67 (9), 2536–2546. doi:10.1002/art.39223
- Huarte, E., O'Connor, R. S., Peel, M. T., Nunez-Cruz, S., Leferovich, J., Juvekar, A., et al. (2020). Itacitinib (INC039110), a JAK1 inhibitor, reduces cytokines associated with cytokine release syndrome induced by CAR T-cell therapy. *Clin. Cancer Res.* 26 (23), 6299–6309. doi:10.1158/1078-0432.CCR-20-1739
- Jiang, Y., Hardie, J., Liu, Y., Ray, M., Luo, X., Das, R., et al. (2018). Nanocapsule-mediated cytosolic siRNA delivery for anti-inflammatory treatment. *J. Control Release* 283, 235–240. doi:10.1016/j.jconrel.2018.06.001
- Joubert, F., Munson, M. J., Sabirsh, A., England, R. M., Hemmerling, M., Alexander, C., et al. (2023). Precise and systematic end group chemistry modifications on PAMAM and poly(l-lysine) dendrimers to improve cytosolic delivery of mRNA. *J. Control. Release* 356, 580–594. doi:10.1016/j.jconrel.2023.03.011
- Kaczorowski, K. J., Shekhar, K., Nkulikiyimfura, D., Dekker, C. L., Maecker, H., Davis, M. M., et al. (2017). Continuous immunotypes describe human immune variation and predict diverse responses. *Proc. Natl. Acad. Sci. U. S. A.* 114, E6097–E6106–E6106. doi:10.1073/pnas.1705065114
- Kawakami, S., Ito, Y., Charoensit, P., Yamashita, F., and Hashida, M. (2006). Evaluation of proinflammatory cytokine production induced by linear and branched polyethyleneimine/plasmid DNA complexes in mice. *J. Pharmacol. Exp. Ther.* 317 (3), 1382–1390. doi:10.1124/jpet.105.100669
- Khoury, M., et al. (2008). Combined anti-inflammatory therapy using a novel siRNA formulation successfully prevents and cures mice from arthritis. *Mol. Ther.* 16, S386. doi:10.1016/s1525-0016(16)40431-4
- Kim, H. O., Kim, H. S., Youn, J. C., Shin, E. C., and Park, S. (2011). Serum cytokine profiles in healthy young and elderly population assessed using multiplexed bead-based immunoassays. *J. Transl. Med.* 9, 113. doi:10.1186/1479-5876-9-113
- Kim, S. S., Ye, C., Kumar, P., Chiu, L., Subramanya, S., Wu, H., et al. (2010). Targeted delivery of siRNA to macrophages for anti-inflammatory treatment. *Mol. Ther.* 18 (5), 993–1001. doi:10.1038/mt.2010.27
- Kim, S. T., and Kim, C. K. (2007). Water-soluble chitosan-based antisense oligodeoxynucleotide of interleukin-5 for treatment of allergic rhinitis. *Biomaterials* 28 (22), 3360–3368. doi:10.1016/j.biomaterials.2007.03.029
- Kulkarni, J. A., Witzigmann, D., Thomson, S. B., Chen, S., Leavitt, B. R., Cullis, P. R., et al. (2021). The current landscape of nucleic acid therapeutics. *Nat. Nanotechnol.* 16 (6), 630–643. doi:10.1038/s41565-021-00898-0
- Läg, M., Skuland, T., Godymchuk, A., Nguyen, T. H. T., Pham, H. L. T., and Refsnes, M. (2018). Silica nanoparticle-induced cytokine responses in BEAS-2B and HBEC3-KT cells: significance of particle size and signalling pathways in different lung cell cultures. *Basic Clin. Pharmacol. Toxicol.* 122, 620–632. doi:10.1111/bcpt.12963
- Lam, K., Leung, A., Martin, A., Wood, M., Schreiner, P., Palmer, L., et al. (2023). Unsaturated, trialkyl ionizable lipids are versatile lipid-nanoparticle components for

therapeutic and vaccine applications. *Adv. Mater* 35, e2209624. doi:10.1002/adma.202209624

Le, R. Q., Li, L., Yuan, W., Shord, S. S., Nie, L., Habtemariam, B. A., et al. (2018). FDA approval summary: tocilizumab for treatment of chimeric antigen receptor T cell-induced severe or life-threatening cytokine release syndrome. *Oncologist* 23 (8), 943–947. doi:10.1634/theoncologist.2018-0028

Lee, J., Son, W., Hong, J., Song, Y., Yang, C. S., and Kim, Y. H. (2021). Down-regulation of TNF- α via macrophage-targeted RNAi system for the treatment of acute inflammatory sepsis. *J. Control Release* 336, 344–353. doi:10.1016/J.JCONREL.2021.06.022

Li, P., Holliger, P., and Tagami, S. (2022). Hydrophobic-cationic peptides modulate RNA polymerase ribozyme activity by accretion. *Nat. Commun.* 13 (1), 3050. doi:10.1038/s41467-022-30590-3

Lian, S., Xie, R., Ye, Y., Xie, X., Li, S., Lu, Y., et al. (2019). Simultaneous blocking of CD47 and PD-L1 increases innate and adaptive cancer immune responses and cytokine release. *EBiomedicine* 42, 281–295. doi:10.1016/J.EBIOM.2019.03.018

Lin, L., Curtin, J. A., Regis, E., Hirsman, A., Howard, R., Tutino, M., et al. (2022). A systems immunology approach to investigate cytokine responses to viruses and bacteria and their association with disease. *Sci. Rep.* 12 (1), 13463. doi:10.1038/s41598-022-16509-4

Ma, J., Liu, R., Wang, X., Liu, Q., Chen, Y., Valle, R. P., et al. (2015). Crucial role of lateral size for graphene oxide in activating macrophages and stimulating pro-inflammatory responses in cells and animals. *ACS Nano* 9, 10498–10515. doi:10.1021/ACS.NANO.5B04751

Mahmoudi, M., Rastin, M., Arababadi, M. K., Anaeigoudari, A., and Nosratabadi, R. (2022). Enhancing the efficacy of *Hypericum perforatum* in the treatment of an experimental model of multiple sclerosis using gold nanoparticles: an *in vivo* study. *Avicenna J. Phytomedicine* 12, 325–336. doi:10.22038/AJP.2022.19574

Meenakshi Sundaram, D. N., Plianwong, S., Kc, R., Ostergaard, H., and Uludağ, H. (2022). *In vitro* cytotoxicity and cytokine production by lipid-substituted low molecular weight branched PEIs used for gene delivery. *Acta Biomater.* 148, 279–297. doi:10.1016/j.actbio.2022.06.030

Mohanan, D., Slütter, B., Henriksen-Lacey, M., Jiskoot, W., Bouwstra, J. A., Perrie, Y., et al. (2010). Administration routes affect the quality of immune responses: A cross-sectional evaluation of particulate antigen-delivery systems. *J. Control Release* 147 (3), 342–349. doi:10.1016/j.jconrel.2010.08.012

Moreira, D. A., Santos, S. D., Leiro, V., and Pêgo, A. P. (2023). Dendrimers and derivatives as multifunctional nanotherapeutics for Alzheimer's disease. *Pharmaceutics* 15 (4), 1054. doi:10.3390/PHARMACEUTICS15041054

Moudgil, K. D., and Choubey, D. (2011). Cytokines in autoimmunity: role in induction, regulation, and treatment. *J. Interferon Cytokine Res.* 31 (10), 695–703. doi:10.1089/JIR.2011.0065

Mullard, A. (2022). FDA approves fifth RNAi drug — alnylam's next-gen hATTR treatment. *Nat. Rev. Drug Discov.* 21 (8), 548–549. doi:10.1038/D41573-022-00118-X

Naha, P. C., Davoren, M., Lyng, F. M., and Byrne, H. J. (2010). Reactive oxygen species (ROS) induced cytokine production and cytotoxicity of PAMAM dendrimers in J774A.1 cells. *Toxicol. Appl. Pharmacol.* 246 (1–2), 91–99. doi:10.1016/j.taap.2010.04.014

Okuda, T., Morishita, M., Mizutani, K., Shibayama, A., Okazaki, M., and Okamoto, H. (2018). Development of spray-freeze-dried siRNA/PEI powder for inhalation with high aerosol performance and strong pulmonary gene silencing activity. *J. Control Release* 279, 99–113. doi:10.1016/J.JCONREL.2018.04.003

Ottaviano, G., Georgiadis, C., Gkazi, S. A., Syed, F., Zhan, H., Etuk, A., et al. (2022). Phase 1 clinical trial of CRISPR-engineered CAR19 universal T cells for treatment of children with refractory B cell leukemia. *Sci. Transl. Med.* 14 (668), eabq3010. doi:10.1126/scitranslmed.abq3010

Pandi, P., Jain, A., Kommineni, N., Ionov, M., Bryszewska, M., and Khan, W. (2018). Dendrimer as a new potential carrier for topical delivery of siRNA: A comparative study of dendriplex vs. lipoplex for delivery of TNF- α siRNA. *Int. J. Pharm.* 550 (1–2), 240–250. doi:10.1016/J.IJPHARM.2018.08.024

Park, S. Y., Yi, E. H., Kim, Y., and Park, G. (2019). Anti-neuroinflammatory effects of *Ephedra sinica* Stapf extract-capped gold nanoparticles in microglia. *Int. J. Nanomedicine* 14, 2861–2877. doi:10.2147/IJN.S195218

Paunovska, K., Loughrey, D., and Dahlman, J. E. (2022). Drug delivery systems for RNA therapeutics. *Nat. Rev. Genet.* 23 (5), 265–280. doi:10.1038/s41576-021-00439-4

Peer, D., Park, E. J., Morishita, Y., Carman, C. V., and Shimaoka, M. (2008). Systemic leukocyte-directed siRNA delivery revealing cyclin D1 as an anti-inflammatory target. *Science* 319 (5863), 627–630. doi:10.1126/SCIENCE.1149859

Pei, D., and Buyanova, M. (2019). Overcoming endosomal entrapment in drug delivery. *Bioconjug Chem.* 30 (2), 273–283. doi:10.1021/ACS.BIOCONJCHEM.8B00778

Raison, C. L., Capuron, L., and Miller, A. H. (2006). Cytokines sing the blues: inflammation and the pathogenesis of depression. *Trends Immunol.* 27 (1), 24–31. doi:10.1016/j.it.2005.11.006

Raper, S. E., Chirmule, N., Lee, F. S., Wivel, N. A., Bagg, A., Gao, G. P., et al. (2003). Fatal systemic inflammatory response syndrome in a ornithine transcarbamylase deficient patient following adenoviral gene transfer. *Mol. Genet. Metab.* 80 (1–2), 148–158. doi:10.1016/j.ymgme.2003.08.016

Ren, D., Fisson, S., Dalkara, D., and Ail, D. (2022). Immune responses to gene editing by viral and non-viral delivery vectors used in retinal gene therapy. *Pharmaceutics* 14, 1973. doi:10.3390/PHARMACEUTICS14091973

Rudd, K. E., Johnson, S. C., Agesa, K. M., Shackelford, K. A., Tsoi, D., Kievlan, D. R., et al. (2020). Global, regional, and national sepsis incidence and mortality, 1990–2017: analysis for the global burden of disease study. *Lancet* 395 (10219), 200–211. doi:10.1016/S0140-6736(19)32989-7

Ruiz, F. E., Clancy, J. P., Perricone, M. A., Bebok, Z., Hong, J. S., Cheng, S. H., et al. (2021). A clinical inflammatory syndrome attributable to aerosolized lipid-DNA administration in cystic fibrosis. *Hum. Gene Ther.* 12 (7), 751–761. doi:10.1089/104303401750148667

Sakurai, F., Terada, T., Yasuda, K., Yamashita, F., Takakura, Y., and Hashida, M. (2002). The role of tissue macrophages in the induction of proinflammatory cytokine production following intravenous injection of lipoplexes. *Gene Ther.* 9 (16), 1120–1126. doi:10.1038/sj.gt.3301784

Samec, T., Alati, K. L., Boulos, J., Gilmore, S., Hazelton, A., Coffin, C., et al. (2022). Fusogenic peptide delivery of bioactive siRNAs targeting CSNK2A1 for treatment of ovarian cancer. *Mol. Ther. - Nucleic Acids* 30, 95–111. doi:10.1016/J.OMTN.2022.09.012

Santos, A., Veiga, F., and Figueiras, A. (2020). Dendrimers as pharmaceutical excipients: synthesis, properties, toxicity and biomedical applications. *Mater. (Basel)* 13 (1), 65. doi:10.3390/MA13010065

Shi, Q., Rondon-Cavanzo, E. P., Dalla Picola, I. P., Tiera, M. J., Zhang, X., Dai, K., et al. (2018). *In vivo* therapeutic efficacy of TNF α ; silencing by folate-PEG-chitosan-DEAE/siRNA nanoparticles in arthritic mice. *Int. J. Nanomedicine* 13, 387–402. doi:10.2147/IJN.S146942

Shin, H. J., Park, H., Shin, N., Shin, J., Gwon, D. H., Kwon, H. H., et al. (2020). p66shc siRNA Nanoparticles Ameliorate Chondrocytic Mitochondrial Dysfunction in Osteoarthritis. *Int. J. Nanomedicine* 15, 2379–2390. doi:10.2147/IJN.S234198

Shirley, J. L., de Jong, Y. P., Terhorst, C., and Herzog, R. W. (2020). Immune responses to viral gene therapy vectors. *Mol. Ther.* 28 (3), 709–722. doi:10.1016/j.jymth.2020.01.001

Somanathan, S., Calcedo, R., and Wilson, J. M. (2020). Adenovirus-antibody complexes contributed to lethal systemic inflammation in a gene therapy trial. *Mol. Ther.* 28, 784–793. doi:10.1016/J.YMTHE.2020.01.006

Storjohann, R., Gericke, B., Reifensath, J., Herrmann, T., Behrens, P., Oltmanns, H., et al. (2023). Influence of PEG chain length of functionalized magnetic nanoparticles on the cytocompatibility and immune competence of primary murine macrophages and dendritic cells. *J. Int. J. Mol. Sci.* 24, 2565. doi:10.3390/ijms24032565

Strati, P., Ahmed, S., Kebriaei, P., Nastoupil, L. J., Claussen, C. M., Watson, G., et al. (2020). Clinical efficacy of anakinra to mitigate CAR T-cell therapy-associated toxicity in large B-cell lymphoma. *Blood Adv.* 4 (13), 3123–3127. doi:10.1182/bloodadvances.2020002328

Suhrutsenko, J., Oskolkov, N., Arukuusk, P., Kurrikoff, K., Eriste, E., Copolovici, D. M., et al. (2011). Cell-penetrating peptides, PepFects, show no evidence of toxicity and immunogenicity *in vitro* and *in vivo*. *Bioconjug Chem.* 22 (11), 2255–2262. doi:10.1021/bc200293d

Suk, J. S., Xu, Q., Kim, N., Hanes, J., and Ensign, L. M. (2016). PEGylation as a strategy for improving nanoparticle-based drug and gene delivery. *Adv. Drug Deliv. Rev.* 99, 28–51. doi:10.1016/J.ADDR.2015.09.012

Sun, J. Y., Anand-Jawa, V., Chatterjee, S., and Wong, K. K. (2003). Immune responses to adeno-associated virus and its recombinant vectors. *Gene Ther.* 10 (11), 964–976. doi:10.1038/sj.gt.3302039

Tahtinen, S., Tong, A. J., Himmels, P., Oh, J., Paler-Martinez, A., Kim, L., et al. (2022). IL-1 and IL-1RA are key regulators of the inflammatory response to RNA vaccines. *Nat. Immunol.* 23 (4), 532–542. doi:10.1038/s41590-022-01160-y

Tang, M., Guo, C., Sun, M., Zhou, H., Peng, X., Dai, J., et al. (2022). Effective delivery of osteopontin small interference RNA using exosomes suppresses liver fibrosis via TGF- β 1 signaling. *Front. Pharmacol.* 13, 882243. doi:10.3389/FPHAR.2022.882243

Tehrani, S. F., Rabanel, J. M., Legeay, S., Cayon, J., Riou, J., Saulnier, P., et al. (2022). Tailoring PEGylated nanoparticle surface modulates inflammatory response in vascular endothelial cells. *Eur. J. Pharm. Biopharm.* 174, 155–166. PMID: 35413403. doi:10.1016/j.ejpb.2022.04.003

Tsai, S. J., Black, S. K., and Jewell, C. M. (2020). Leveraging the modularity of biomaterial carriers to tune immune responses. *Adv. Funct. Mater* 30 (48), 2004119. doi:10.1002/ADFM.202004119

Uludağ, H., Ubeda, A., and Ansari, A. (2019). At the intersection of biomaterials and gene therapy: progress in non-viral delivery of nucleic acids. *Front. Bioeng. Biotechnol.* 7 (JUN), 131. doi:10.3389/FBIOE.2019.00131

Verbeke, R., Lentacker, I., De Smedt, S. C., and Dewitte, H. (2019). Three decades of messenger RNA vaccine development. *Nano Today* 28, 100766. doi:10.1016/J.NANTOD.2019.100766

- Wang, M., Zhang, M., Fu, L., Lin, J., Zhou, X., Zhou, P., et al. (2020). Liver-targeted delivery of TSG-6 by calcium phosphate nanoparticles for the management of liver fibrosis. *Theranostics* 10, 36–49. doi:10.7150/THNO.37301
- Wang, X., and Lin, Y. (2008). Tumor necrosis factor and cancer, buddies or foes? *Acta Pharmacol. Sin.* 29 (11), 1275–1288. doi:10.1111/J.1745-7254.2008.00889.X
- Wang, X., Liu, S., Sun, Y., Yu, X., Lee, S. M., Cheng, Q., et al. (2023). Preparation of selective organ-targeting (SORT) lipid nanoparticles (LNPs) using multiple technical methods for tissue-specific mRNA delivery. *Nat. Protoc.* 18 (1), 265–291. doi:10.1038/s41596-022-00755-x
- Watson, O. J., Barnsley, G., Toor, J., Hogan, A. B., Winskill, P., and Ghani, A. C. (2022). Global impact of the first year of COVID-19 vaccination: A mathematical modelling study. *Lancet Infect. Dis.* 22 (9), 1293–1302. doi:10.1016/S1473-3099(22)00320-6
- Weiss, M., Fan, J., Claudel, M., Sonntag, T., Didier, P., Ronzani, C., et al. (2021). Density of surface charge is a more predictive factor of the toxicity of cationic carbon nanoparticles than zeta potential. *J. Nanobiotechnology* 19 (1), 5. doi:10.1186/s12951-020-00747-7
- Wu, L., Wu, L. P., Wu, J., Sun, J., He, Z., Rodríguez-Rodríguez, C., et al. (2021). Poly(lactide-co-glycolide) nanoparticles mediate sustained gene silencing and improved biocompatibility of siRNA delivery systems in mouse lungs after pulmonary administration. *ACS Appl. Mater. Interfaces* 13 (3), 3722–3737. doi:10.1021/ACSAMI.0C21259
- Wu, T., Tan, M., Gong, H., Wang, Y., and Shuai, X. (2018). Co-delivery of andrographolide and Notch1-targeted siRNA to macrophages with polymer-based nanocarrier for enhanced anti-inflammation. *Chin. J. Polym. Sci.* 36 (12), 1312–1320. doi:10.1007/s10118-018-2158-z
- Xiang, Z., Kuranda, K., Quinn, W., Chekaoui, A., Ambrose, R., Hasanpourghai, M., et al. (2022). The effect of rapamycin and ibrutinib on antibody responses to adeno-associated virus vector-mediated gene transfer. *Hum. Gene Ther.* 33 (11–12), 614–624. doi:10.1089/hum.2021.258
- Xiao, B., Laroui, H., Viennois, E., Ayyadurai, S., Charania, M. A., Zhang, Y., et al. (2014). Nanoparticles with surface antibody against CD98 and carrying CD98 small interfering RNA reduce colitis in mice. *Gastroenterology* 146 (5), 1289–1300.e19. doi:10.1053/J.GASTRO.2014.01.056
- Xiao, B., Ma, P., Ma, L., Chen, Q., Si, X., Walter, L., et al. (2017). Effects of tripolyphosphate on cellular uptake and RNA interference efficiency of chitosan-based nanoparticles in Raw 264.7 macrophages. *J. Colloid Interface Sci.* 490, 520–528. doi:10.1016/J.JCIS.2016.11.088
- Xiao, B., Ma, P., Viennois, E., and Merlin, D. (2016). Urocanic acid-modified chitosan nanoparticles can confer anti-inflammatory effect by delivering CD98 siRNA to macrophages. *Colloids Surf. B Biointerfaces* 143, 186–193. doi:10.1016/J.COLSURFB.2016.03.035
- Xu, L., Yeudall, W. A., and Yang, H. (2017). Folic acid-decorated polyamidoamine dendrimer exhibits high tumor uptake and sustained highly localized retention in solid tumors: its utility for local siRNA delivery. *Acta Biomater.* 57, 251–261. doi:10.1016/J.ACTBIO.2017.04.023
- Yan, H., Duan, X., Pan, H., Akk, A., Sandell, L. J., Wickline, S. A., et al. (2019). Development of a peptide-siRNA nanocomplex targeting NF- κ B for efficient cartilage delivery. *Sci. Rep.* 9 (1), 442. doi:10.1038/S41598-018-37018-3
- Yang, G., Zhou, D., Dai, Y., Li, Y., Wu, J., Liu, Q., et al. (2022). Construction of PEI-EGFR-PD-L1-siRNA dual functional nano-vaccine and therapeutic efficacy evaluation for lung cancer. *Thorac. Cancer* 13 (21), 2941–2950. doi:10.1111/1759-7714.14618
- Yang, Z. J., Xu, S. L., Chen, B., Zhang, S. L., Zhang, Y. L., Wei, W., et al. (2009). Hepatocyte growth factor plays a critical role in the regulation of cytokine production and induction of endothelial progenitor cell mobilization: A pilot gene therapy study in patients with coronary heart disease. *Clin. Exp. Pharmacol. Physiol.* 36 (8), 790–796. doi:10.1111/j.1440-1681.2009.05151.x
- Yoon, P. O., Park, J. W., Lee, C. M., Kim, S. H., Kim, H. N., Ko, Y., et al. (2016). Self-assembled micelle interfering RNA for effective and safe targeting of dysregulated genes in pulmonary fibrosis. *J. Biol. Chem.* 291 (12), 6433–6446. doi:10.1074/jbc.M115.693671
- Zamorina, S., Timganova, V., Bochkova, M., Shardina, K., Uzhviyuk, S., Khramtsov, P., et al. (2023). The effect of PEGylated graphene oxide nanoparticles on the Th17-Polarization of activated T helpers. *Mater. (Basel)* 16 (2), 877. doi:10.3390/ma16020877
- Zhang, C., Delawary, M., Huang, P., Korchak, J. A., Suda, K., and Zubair, A. C. (2021). IL-10 mRNA engineered MSCs demonstrate enhanced anti-inflammation in an acute GvHD model. *Cells* 10 (11), 3101. doi:10.3390/CELLS10113101
- Zhang, L., Wang, S., Xu, J., Zhang, R., Zhu, H., Wu, Y., et al. (2021). Etanercept as a new therapeutic option for cytokine release syndrome following chimeric antigen receptor T cell therapy. *Exp. Hematol. Oncol.* 10 (1), 16. doi:10.1186/s40164-021-00209-2
- Zhang, P., Xu, N., Zhou, L., Xu, X., Wang, Y., Li, K., et al. (2013). A linear polyethylenimine mediated siRNA-based therapy targeting human epidermal growth factor receptor in SPC-A1 xenograft mice. *Transl. Respir. Med.* 1 (1), 2. doi:10.1186/2213-0802-1-2
- Zhu, Y., Jiang, P., Luo, B., Lan, F., He, J., and Wu, Y. (2019). Dynamic protein corona influences immune-modulating osteogenesis in magnetic nanoparticle (MNP)-infiltrated bone regeneration scaffolds *in vivo*. *Nanoscale* 11, 6817–6827. doi:10.1039/C8NR08614A
- Zolnik, B. S., González-Fernández, A., Sadrieh, N., and Dobrovolskaia, M. A. (2010). Minireview: nanoparticles and the immune system. *Endocrinology* 151 (2), 458–465. doi:10.1210/EN.2009-1082
- Zuckerman, J. E., Gritli, I., Tolcher, A., Heide, J. D., Lim, D., Morgan, R., et al. (2014). Correlating animal and human phase Ia/Ib clinical data with CALAA-01, a targeted, polymer-based nanoparticle containing siRNA. *Proc. Natl. Acad. Sci. U. S. A.* 111 (31), 11449–11454. doi:10.1073/pnas.1411393111



OPEN ACCESS

EDITED BY

Babatunde Okesola,
University of Nottingham,
United Kingdom

REVIEWED BY

Cosimo Ligorio,
University of Nottingham,
United Kingdom

*CORRESPONDENCE

Herbert P. Jennissen,
✉ hp.jennissen@uni-due.de

RECEIVED 22 May 2023

ACCEPTED 22 June 2023

PUBLISHED 07 September 2023

CITATION

Jennissen HP (2023), Camouflaged
angiogenic BMP-2 functions exposed by
pico-paracrine biohybrids.
Front. Bioeng. Biotechnol. 11:1226649.
doi: 10.3389/fbioe.2023.1226649

COPYRIGHT

© 2023 Jennissen. This is an open-access
article distributed under the terms of the
[Creative Commons Attribution License](#)
(CC BY). The use, distribution or
reproduction in other forums is
permitted, provided the original author(s)
and the copyright owner(s) are credited
and that the original publication in this
journal is cited, in accordance with
accepted academic practice. No use,
distribution or reproduction is permitted
which does not comply with these terms.

Camouflaged angiogenic BMP-2 functions exposed by pico-paracrine biohybrids

Herbert P. Jennissen*

Institute of Physiological Chemistry, Faculty of Medicine, University of Duisburg-Essen, Essen, Germany

The constant release of human bone morphogenetic protein 2 (rhBMP-2) in the picomolar range (Pico-Stat) from PDLLA-biohybrids led to the detection of intrinsic novel pro- and anti-angiogenic functions of this cytokine. As integrant part in this perspective of previous work, first evidence for the binding of rhBMP-2, as an *inverse agonist*, to allosteric angiogenic receptors in cocultures of human endothelial cells is reported.

KEYWORDS

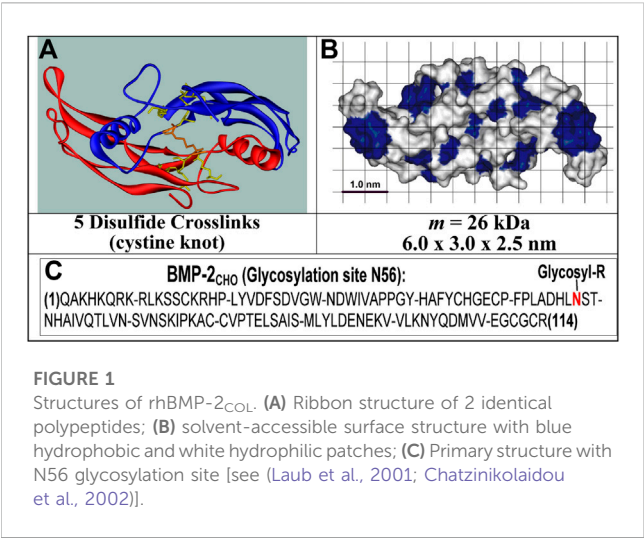
angioiduction, osteoinduction, pico-technology, constitutive receptor activity, allosteric inverse agonist, orthosteric agonist, inverse concentration dependence, proangiogenic and antiangiogenic factors

1 Introduction

BMP-2 initiates osteogenesis requiring angiogenesis, with the ingrowth of mesenchymal stem cells and osteoblasts. The global market size (MRI, 2023) of the recombinant form (rhBMP-2) [INFUSE® Bone Graft (Food and Drug Administration, 2004)] reached USD 498.1 million in 2021 (MRI, 2023). This protein, rhBMP-2_{CHO}, is produced by a genetically engineered Chinese hamster ovary cell line, as a disulfide-linked heterodimeric protein mixture of two different polypeptide chains of 114 and 131 amino acids. Each chain is glycosylated at one site with high-mannose-type glycans (Food and Drug Administration, 2004; Committee for Medicinal Products for Human use, 2014; Kenley et al., 1993). As applied, BMP-2_{CHO} comprises a microheterogeneous mixture of three different BMP-2 isoforms and up to 15 additional different glycoforms (Kenley et al., 1993).

In contrast, the non-glycosylated rhBMP-2_{COL} second species (Schlüter et al., 2009) from *E. coli* (Figure 1) is homodimeric and displays no microheterogeneity (Jennissen et al., 1999; Laub et al., 2007). The molecular masses of the commercial glycosylated (rhBMP-2_{CHO}) and the non-glycosylated rhBMP-2 species (rhBMP-2_{COL}) correspond to 33–36 kDa for the former and 26 kDa for the latter, respectively (Laub et al., 2007). In humans, 12 mg of rhBMP-2_{CHO} must be applied for osteoinduction in a concentration of 1.5 mg/mL (~44 μM) in an absorbable collagen sponge (ACS). After intravenous injection, rhBMP-2 is eliminated with a half-life of $t_{1/2} = 6.7$ min in nonhuman primates (Food and Drug Administration, 2004). Physiological serum levels of BMP-2 in healthy human controls are reported to be 17.1 ± 0.6 pg/mL ($= 4.8 \times 10^{-13}$ M) (Kercheva et al., 2020).

In receptor-binding studies, the binding function (θ) and the state function (r) are distinguished (Laub et al., 2007). The binding function (θ) of rhBMP-2 is a direct measure of receptor occupation by the ligand with K^0_D in the range of ~0.45 nM (Mayer et al., 1996). The state function (r) (Wiemann et al., 2001; Laub et al., 2007) of rhBMP-2 correlates with the receptor activity state by monitoring downstream products (e.g., alkaline phosphatase) in activity tests in MC3T3-E1 cell cultures, with both species of rhBMP-2_{CHO} and rhBMP-2_{COL} having indistinguishable biological activities of nanomolar




affinities ($K'_D \sim 2\text{--}10\text{ nM}$ (Laub et al., 2007)). BMP-2 also specifically binds to its prodomain for ECM targeting, presumably with a similar affinity constant ($K'_D \sim 4\text{--}8\text{ nM}$) as BMP-7 (Spanou et al., 2023). RhBMP-2 is known to indirectly initiate angiogenesis in the nanomolar range ($0.38\text{--}3.8\text{ nM}$) (Deckers et al., 2002) by activating paracrine VEGF-mediated osteoblast-endothelial cell cross-talk (Kulikauskas and Bautch, 2022). The combination of biomolecular materials, such as rhBMP-2, with the other biomaterial classes such as metals, polymers, or ceramics, forms a biohybrid material [see (Jennissen, 2019)]. In protein immobilization, we distinguish adsorbates (adsorption), covalates (covalent binding), and inclusates (encapsulated biohybrids) (Jennissen, 2019). A biohybrid is classed as bioactive if it has been “designed to induce a specific biological activity” (Williams et al., 1987). A paracrine biohybrid is, e.g., a growth factor releasing biomaterial. Recently, we reported the first evidence of a direct influence of rhBMP-2_{COL} on angiogenesis in co-cultures at picomolar concentrations (Dohle et al., 2021). Applications of rhBMP-2 in solute and PDLLA solid-phase forms are described.

2 Methods

RhBMP-2_{COL} from *E. coli* (Morphoplant GmbH Bochum, D) and rhBMP-2_{CHO} from CHO-cells (InductOs®, Medtronic BioPharma B.V., Heerlen, NL) were employed (Laub et al., 2007). The dose-response derived biological equivalent activity equals $K'_D \sim 5\text{--}15\text{ nM}$ for both species of rhBMP-2 (Laub et al., 2007). The for many weeks stable PDLLA nanofiber fleece preparation is described in (Sowislok and Jennissen, 2022). Labeled ¹²⁵I-rhBMP-2 (Dohle et al., 2021) was for the analytical preparation of adsorbate PDLLA biohybrids. Non-isotope biohybrids were made in parallel for the other experiments. In a 24-well cell culture plate, the single well volume corresponds to 0.5–1.0 mL. Human outgrowth endothelial cells (OECs) and human primary osteoblasts (pOBs) were prepared as described (Dohle et al., 2021).

TABLE 1 Preparation of rhBMP-2-PDLLA-adsorbate biohybrids*.

		
BMP-2 [μg/mL] concentration	Adsorbed amount [mg/g]	
	rhBMP-2 _{COL}	rhBMP-2 _{CHO}
10 (low)	0.33 ± 0.06	0.58 ± 0.10
30 (high)	2.61 ± 0.81	3.40 ± 0.61

*The adsorbed load (high and low) to the nanofiber fleece from the adsorption solution (10 and 30 μg/mL) was determined at room temperature after 10–20 h of adsorption by tracer detection with ¹²⁵I-rhBMP-2 (Dohle et al., 2021). Mean ± SD, n = 3.

TABLE 2 ¹²⁵I-rhBMP-2_{COL} release kinetics from biohybrids (Table 1).

Initial Γ_{BMP-2}^S	Burst			Sustained release		
	k'_{-1}	$t_{1/2}$	K'_D	k'_{-2}	$t_{1/2}$	K'_D
mg/g	$10^{-4} [s^{-1}]$	[d]	nM	$10^{-8} [s^{-1}]$	[d]	pM
8.97	5.34			3.86		
±	±	0.015	8.2	±	208	0.59
1.53	0.16			2.91		

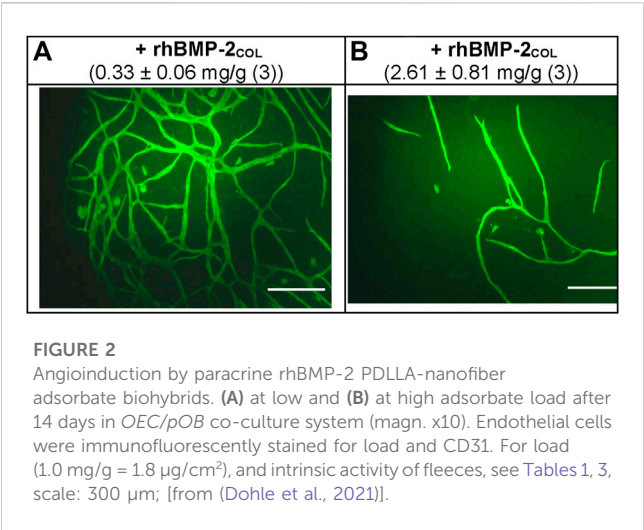
*Data are derived from desorption kinetics of a 22-day duration [for details see (Sänger et al., 2014)] $\bar{x} \pm \text{SEM}$; for $k_{+1} = 6.5 \pm 0.4 \times 10^4\text{ M}^{-1}\text{ s}^{-1}$ see (Dohle et al., 2020).

Cocultures consisted of endothelial cells (130.000/well) and primary osteoblasts (20.000/well). Relative gene expressions (RQ) of mRNA for various proteins are described in (Dohle et al., 2021). In dose-response experiments, rhBMP-2_{COL} was added in defined concentrations to the OEC/pOB co-culture system and harvested after 7 days of incubation for fluorescence microscopy and quantitative Nikon NIS image processing as described (Dohle et al., 2021). The pixel values were converted to length according to 1 pixel = 0.46 μm. Cell viability was tested by the LDH cytotoxicity assay CyQUANT™ as described (Dohle et al., 2021). In desorption experiments, 1 cm² (1 mg) fleeces with an rhBMP-2_{COL} loads of ~ 6.98 mg/g PDLLA were placed in 1.5 mL flow-through chambers (Sänger et al., 2014). They were perfused with sterile phosphate-buffered saline (PBS) pH 7.4 at a flow rate of 10 mL/h in a 16-channel Watson-Marlow peristaltic pump for 22 days at ca. 22°C–26°C. Statistical calculations were done with the PC program GraphPad Prism 4/5 (La Jolla, CA). Prism software fails in exponential decays with r^2 -values of <0.2 when decays parallel the abscissa at $t_{1/2} > 100\text{--}200\text{ days}$ (slope ~ zero). Kinetic and thermodynamic constants under non-standard conditions are termed “apparent” (K' , k'). Equilibrium dissociation constants (K_D , $K_{0.5}$) represent affinity constants (Landry et al., 2015).

3 Results

3.1 Pico-paracrine biohybrids

In preparing solid-state paracrine adsorbate biohybrids, rhBMP-2_{COL} was adsorbed to the surface of a non-woven fleece



composed of PDLLA nanofibers ($\varnothing = \sim 100$ nm), prepared by electrospinning (Dohle et al., 2021; Sowislok and Jennissen, 2022) (see Table 1).

Decisive is the 22-day rhBMP-2_{COL} adsorbate release kinetics from biohybrids loaded with ~ 8.9 mg/g Table 2. The two-phase exponential decay function displays a half-life of 3–4 h for the burst phase ($K'_D = 8.2$ nM) and a half-life of 208 days for sustained high-affinity release ($K'_D = k_{-2}/k_{+1} = 0.59 \times 10^{-12}$ M; = pico paracrine biohybrid). Such rhBMP-2_{COL} adsorbate PDLLA biohybrids (Table 1) were incubated in OEC/pOB co-cultures for 14 days and led to large numbers of capillary-like microvessels with no VEGF-A gene activation (Dohle et al., 2021) (Figure 2A; 0.33 mg/g). Fewer microvessels, but more than in controls, form at an 8-fold higher rhBMP-2_{COL} adsorbate load (Figure 2B).

In contrast to the pro-angiogenic activities of rhBMP-2_{COL}, the glycosylated species rhBMP-2_{CHO} was anti-angiogenic, fully inhibiting control angiogenesis (Dohle et al., 2021) and forming instead a cobblestone layer of endothelial cells [not shown, see (Dohle et al., 2021)].

These results were confirmed in Table 3. At a low rhBMP-2_{COL}, adsorbate loads of 0.33 mg/g and a total length of microvessels of 23.9 ± 5.1 mm formed without an increased expression of VEGF-A (Dohle et al., 2021). At high adsorbate loads of 2.6 mg/g, the total length decreased 5-fold to 4.7 ± 0.44 mm, and in controls lacking adsorbate down 10-fold to intrinsic 2.4 ± 0.046 mm. The knots in the microvessel mesh paralleled the length changes. At low concentrations of rhBMP-2_{COL}, they totaled a high of 51.9 ± 11.5 knots, decreasing 4.3-fold to 12.2 ± 0.6 at higher concentrations and 12-fold less in controls of 4.3 ± 1.1 knots. These changes were statistically significant (Table 3).

3.2 Solution studies

In the following, concentration-response experiments in solution are shown. Instead of correlating with rising concentrations, the pro-angiogenic microvessel response

TABLE 3 Length and knot data of capillary-like structures induced by rhBMP-2_{COL} adsorbate biohybrids after 14 days in co-culture*.

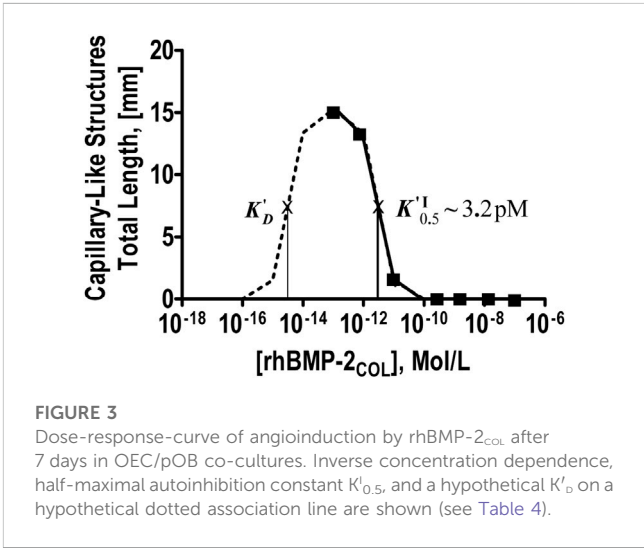
rhBMP-2 _{COL} Biohybrid	Adsorbed amount of rhBMP-2 _{COL}		
	\varnothing mg/g Controls	0.33 mg/g	2.6 mg/g
(After 14 days)	(intrinsic activity)	(pro-angiogenic activity)	
Length Analysis (mm)	2.4 ± 0.046	23.9 ± 5.1	4.7 ± 0.44
Knot Analysis (dimensionless)	4.3 ± 1.1	51.9 ± 11.5	12.2 ± 0.6

*mean \pm SD, $n = 4$; in t-tests all values of a series differ significantly $p < 0.001$ from one-another [see (Dohle et al., 2021) Table 1 and Figure 2].

TABLE 4 Dose-response angioinduction in OEC/pOB co-cultures after 7 days by decreasing concentrations of rhBMP-2_{COL} in solution*.

[rhBMP-2 _{COL}]	Microvessel total length		
	Gross, pixel	Net, pixel	Net, mm
Control, 0	$13,070 \pm 1,456$	-	-
1×10^{-7} M	8 ± 0.6	0	0
1×10^{-8} M	12 ± 3	0	0
1×10^{-9} M	22 ± 1	0	0
1×10^{-10} M	$1,217 \pm 436$	0	0
1×10^{-11} M	$16,360 \pm 377$	$3,290 \pm 75$	1.5 ± 0.015
1×10^{-12} M	$42,103 \pm 4,276$	$29,034 \pm 2,961$	13.4 ± 1.4
1×10^{-13} M	$46,245 \pm 3,978$	$33,175 \pm 2,853$	15.3 ± 1.3

*Microvessels (capillary-like structures) were determined by quantitative histologic staining (CD31; 1 pixel ~ 0.46 µm). For further details see Figure 2, (mean \pm SD, $n = 3$). [data from (Dohle et al., 2021)].



increased as a function of factor-10 graded dilutions of rhBMP-2_{COL} (Table 4). Microvessel formation thus followed an inverse concentration gradient, exposing a hitherto unseen

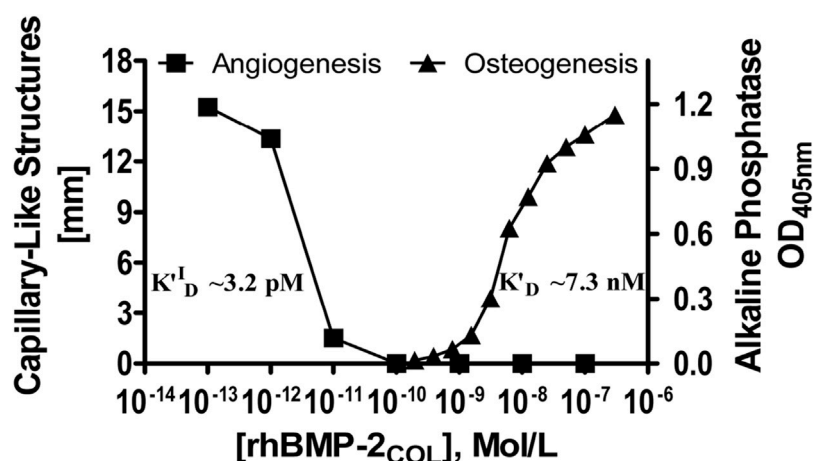


FIGURE 4

Dose-response curves of rhBMP-2_{COL} for the induction of angiogenic (inverse agonist) and osteogenic activities. Cocultures of OEC/pOB cells (Dohle et al., 2021) and mono-cultures of MC3T3-E1 cells (Laub et al., 2007) were employed respectively with corresponding affinity constants K'_D (see also legends to Table 4 and Figure 3).

angiogenic activity by rhBMP-2_{COL} in the picomolar range, confirming results in Figure 2 and Table 3. Anti-angiogenic concentrations of rhBMP-2_{COL} >10 pM fully abolished pro-angiogenic responses.

The data of Table 4 are plotted in Figure 3 down to concentrations of 10⁻¹⁶ M for a classical receptor type. Inhibition increases with the concentration of rhBMP-2_{COL}. The apparent half-saturation constant is not a classical affinity constant but an “autoinhibition” constant ($K'^{I}_{0.5}$) with a value of 3.2 pM. The hypothetical (see dotted line) dissociation constant (K'_D) for the presumed association of rhBMP-2_{COL} to endothelial cell receptors lies in the subpicomolar range ~10⁻¹⁴ M. The anti-angiogenic regulation by rhBMP-2_{COL} prevents too many blood vessels from being formed as a “high concentration cut-off regulation”, in which an apparent agonist turns into an antagonist at high concentrations.

Figure 4 shows a compound extended dose-response plot comprising the data of Table 4 on inverse related angioinduction (Dohle et al., 2021) together with data on direct related osteoinduction [derived from activity measurements with MC3T3-E1 cells in culture (Laub et al., 2007)] and their respective affinity constants. The inverse angiogenic branch saturates at ca. 15 mm and the direct osteogenic branch at 1.2 OD units. The apparent half-saturation autoinhibition constant ($K'^{I}_{0.5}$) can now be termed as an inverse-related affinity constant (K'^{I-R}_D) for angiogenesis with a value of 3.2 pM which contrasts with the direct-related affinity constant (K'_D) for osteoinduction at 7.3 nM. Since the constants of the two activities are separated by three and more orders of magnitude, identical receptors, shared, cross-reactive receptors and homologous desensitization (Popovic and Wilson, 2010) of receptors are improbable, strongly indicating an angiogenic receptor with constitutive activity

(Berg and Clarke, 2018) (see saturation in Figure 4) and rhBMP-2_{COL} as a full inverse agonist in a typical dose response curve in Figure 4.

Control of local picomolar concentrations of rhBMP-2_{COL} in solute form (Table 4) are short-term and difficult, but via solid-state technology, e.g., as rhBMP-2_{COL}-PDLLA biohybrids (Figure 2; Table 3), are simple and long-term by sustained release (Table 2), comparable to a pH-Stat. In this study, not the pH but the growth factor concentration in the pico- or subpicomolar range is maintained as constant and guaranteed by high-affinity dissociation constants K'_D (= Pico-Stat) (Jennissen, 2023).

3.3 rhBMP-2 an angiogenesis inhibitor

As shown, the microvessel control values in the absence of rhBMP-2 (experiments of Tables 3, 4) are not zero but exhibit a significant spontaneous, endogenous pro-angiogenic control activity in the OEC/pOB cultures by VEGF-A (Dohle et al., 2021). This endogenous activity is inhibited by both species of rhBMP-2 (Dohle et al., 2021), for rhBMP-2_{COL} by concentrations above 10–20 pM (see Figures 3, 4). Thus it could be argued that the observed proangiogenic activity of rhBMP-2_{COL} (Figures 2, 3) is not of a stimulatory but only of a deinhibitory nature on dilution. However such a “deinhibition” neither accounts for a 9-fold net higher angiogenic biohybrid activity *in vitro* (Table 3) nor for a severalfold net higher vessel density *in vivo* (21 days, rats) in low versus high load comparison (Al-Maawi et al., 2023) (see Tables 1, 3). The above paradox angiogenic activity agrees with the evidence of rhBMP-2_{COL} being a full inverse agonist of a novel allosteric receptor complex together with an as yet unknown orthosteric agonist (see: Berg and Clarke, 2018; de Vries et al., 2021).

4 Conclusion

Adsorbate load-dependent pro- and anti-angiogenic functions of the considered inverse agonist rh-BMP-2_{COL} on endothelial cells, has been determined by the novel method of solid-state biohybrids as nano- or pico-stats.

Data availability statement

The original contributions presented in the study are included in the article/supplementary material, further inquiries can be directed to the corresponding author.

Author contributions

The author confirms being the sole contributor of this work and has approved it for publication.

References

- Al-Maawi, S., Sowislo, A., Dohle, E., Lach, R., Henning, S., Michler, G. H., et al. (2023). Electrospun PDLLA nanofiber fleece loaded with low concentrated rhBMP-2 enhances bone regeneration by activating both angiogenesis and osteogenesis *in vivo*. *Manuscript in preparation*.
- Berg, K. A., and Clarke, W. P. (2018). Making sense of pharmacology: inverse agonism and functional selectivity. *Int. J. Neuropsychopharmacol.* 21, 962–977. doi:10.1093/ijnp/pty071
- Chatzinikolaïdou, M., Laub, M., Rumpf, H. M., and Jennissen, H. P. (2002). Biocoating of electropolished and ultra-hydrophilic titanium and cobalt chromium molybdenum alloy surfaces with proteins. *Mater. Werkst. Mat. Sci. Eng. Technol.* 33, 720–727. doi:10.1002/mawe.200290002
- Committee for Medicinal Products for Human use (Chmp) (2014). “InductOs-EMEA/H/C/000408-II/0100 EMA/CHMP/649027/2014,” Assessment Report. 1–60.
- Deckers, M. M., van Bezooijen, R. L., van der, H. G., Hoogendam, J., van Der, B. C., Papapoulos, S. E., et al. (2002). Bone morphogenetic proteins stimulate angiogenesis through osteoblast-derived vascular endothelial growth factor A. *Endocrinology* 143, 1545–1553. doi:10.1210/endo.143.4.8719
- de Vries, R. M. J. M., Meijer, F. A., Doveston, R. G., Leijten-van de Gevel, I. A., and Brunsveld, L. (2021). Cooperativity between the orthosteric and allosteric ligand binding sites of RORgammat. *Proc. Natl. Acad. Sci. U.S.A.* 118, 1–9.
- Dohle, D. S., Zumbrink, T., Meißner, M., and Jennissen, H. P. (2020). Protein adsorption hysteresis and transient states of fibrinogen and BMP-2 as model mechanisms for proteome binding to implants. *Curr. Dir. Biomed. Eng.* 6, 1–4. doi:10.1515/cdbme-2020-3046
- Dohle, E., Sowislo, A., Ghanaati, S., and Jennissen, H. P. (2021). Angiogenesis by BMP-2-PDLLA-biohybrids in Co-culture with osteoblasts and endothelia. *Curr. Dir. Biomed. Eng.* 7, 835–838. doi:10.1515/cdbme-2021-2213
- Food and Drug Administration (2004). *INFUSE® bone Graft: Summary of safety and effectiveness data*. Maryland: Access Data FDA, 1–29.
- Jennissen, H. P. (2019). Aspects of multimodal hybrid biomaterials. *Curr. Dir. Biomed. Eng.* 5, 303–305. doi:10.1515/cdbme-2019-0076
- Jennissen, H. P. (2023). Pharmaceutical composition for promoting osteoinduction and angiogenesis. Patent Application WO2023/052554A1, pp. 1–18.
- Jennissen, H. P., Zumbrink, T., Chatzinikolaïdou, M., and Steppuhn, J. (1999). Biocoating of implants with mediator molecules: surface enhancement of metals by treatment with chromosulfuric acid. *Mater. Werkst. Mat. Sci. Eng. Technol.* 30, 838–845. doi:10.1002/(sici)1521-4052(199912)30:12<838:aid-mawe838>3.0.co;2-w
- Kenley, R. A., Yim, K., Abrams, J., Ron, E., Turek, T., Marden, L. J., et al. (1993). Biotechnology and bone graft substitutes. *Pharm. Res.* 10, 1393–1401. doi:10.1023/a:1018902720816
- Kercheva, M., Gusakova, A. M., Ryabova, T. R., Suslova, T. E., Kzhyshkowska, J., and Ryabov, V. V. (2020). Serum levels of bone morphogenetic proteins 2 and 4 in patients with acute myocardial infarction. *Cells* 9, 2179. doi:10.3390/cells9102179
- Kulikauskas, M. R., and Bautch, V. L. (2022). The versatility and paradox of BMP signaling in endothelial cell behaviors and blood vessel function. *Cell Mol. Life Sci.* 79, 77. doi:10.1007/s00018-021-04033-z
- Landry, J. P., Ke, Y., Yu, G. L., and Zhu, X. D. (2015). Measuring affinity constants of 1450 monoclonal antibodies to peptide targets with a microarray-based label-free assay platform. *J. Immunol. Methods* 417, 86–96. doi:10.1016/j.jim.2014.12.011
- Laub, M., Chatzinikolaïdou, M., and Jennissen, H. P. (2007). Aspects of BMP-2 binding to receptors and collagen: influence of cell senescence on receptor binding and absence of high-affinity stoichiometric binding to collagen. *Mater. Werkst. Mat. Sci. Eng. Technol.* 38, 1020–1026. doi:10.1002/mawe.200700238
- Laub, M., Seul, T., Schmachtenberg, E., and Jennissen, H. P. (2001). Molecular modelling of bone morphogenetic protein 2 (BMP-2) by 3D-rapid prototyping. *Mater. Werkst. Mat. Sci. Eng. Technol.* 32, 926–930. doi:10.1002/1521-4052(200112)32:12<926:aid-mawe926>3.0.co;2-1
- Mayer, H., Scutt, A. M., and Ankenbauer, T. (1996). Subtle differences in the mitogenic effects of recombinant human bone morphogenetic proteins -2 to -7 on DNA synthesis on primary bone-forming cells and identification of BMP-2/4 receptor. *Calcif. Tissue Int.* 58, 249–255. doi:10.1007/bf02508644
- MRI (2023). “Global bone morphogenetic protein (BMP) 2 market size & forecast 2023-2028 report,” Market research Report No:2023-2028, 1–160.
- Popovic, N., and Wilson, E. (2010). “Cell surface receptors,” in *Comprehensive toxicology*. Editor C. McQueen (Amsterdam: Elsevier), 81–91. doi:10.1016/B978-0-08-046884-6.00206-2
- Sänger, T., Asran, A. S., Laub, M., Michler, G. H., and Jennissen, H. P. (2014). Release dynamics and biological activity of PDLLA nanofiber composites of rhBMP-2 and rhVEGF₁₆₅ as scaffolds for tissue engineering. *Biomed. Tech. Berl.* 59 (S1), 69–72. doi:10.1515/bmt-2014-5000
- Schlüter, H., Apweiler, R., Holzthutter, H. G., and Jungblut, P. R. (2009). Finding one's way in proteomics: a protein species nomenclature. *Chem. Cent. J.* 3, 11. doi:10.1186/1752-153X-3-11
- Sowislo, A., and Jennissen, H. P. (2022). Bioengineering of tubes, rings and panels for guided bone and vascular regeneration. *Curr. Dir. Biomed. Eng.* 8, 620–623. doi:10.1515/cdbme-2022-1158
- Spanou, C. E. S., Wohl, A. P., Doherr, S., Correns, A., Sonntag, N., Lutke, S., et al. (2023). Targeting of bone morphogenetic protein complexes to heparin/heparan sulfate glycosaminoglycans in bioactive conformation. *FASEB J.* 37, e22717. doi:10.1096/fj.202200904r
- Wiemann, M., Rumpf, H. M., Bingmann, D., and Jennissen, H. P. (2001). The binding of rhBMP-2 to the receptors of viable MC3T3 cells and the question of cooperativity. *Mater. Werkst. Mat. Sci. Eng. Technol.* 32, 931–936. doi:10.1002/1521-4052(200112)32:12<931:aid-mawe931>3.0.co;2-h
- Williams, D. F., Albrektsson, T., Black, J., Christei, P., Glantz, P.-O., Gross, U., et al. (1987). “Definitions in biomaterials,” in *Proceedings of a Consensus Conference of the ESB, Progress in Biomedical Engineering*, Chester, England, March 3-5, 1986. Editor D. F. Williams (Elsevier Sci), pp. 66–68.

Funding

This study was funded by Deutsche Forschungsgemeinschaft Grant JE 84/15-3.

Conflict of interest

The author declares that the research was conducted in the absence of any commercial or financial relationships that could be construed as a potential conflict of interest.

Publisher's note

All claims expressed in this article are solely those of the authors and do not necessarily represent those of their affiliated organizations, or those of the publisher, the editors and the reviewers. Any product that may be evaluated in this article, or claim that may be made by its manufacturer, is not guaranteed or endorsed by the publisher.



OPEN ACCESS

EDITED BY

Yunbing Wang,
Sichuan University, China

REVIEWED BY

Kui Xu,
Anhui University of Chinese Medicine,
China
Bo Yuan,
Sichuan University, China

*CORRESPONDENCE

Hongtao Wei,
✉ htwei@jlu.edu.cn

RECEIVED 02 August 2023

ACCEPTED 05 October 2023

PUBLISHED 19 October 2023

CITATION

Chen M, Ren M, Shi Y, Liu X and Wei H (2023), State-of-the-art polyetheretherketone three-dimensional printing and multifunctional modification for dental implants. *Front. Bioeng. Biotechnol.* 11:1271629. doi: 10.3389/fbioe.2023.1271629

COPYRIGHT

© 2023 Chen, Ren, Shi, Liu and Wei. This is an open-access article distributed under the terms of the [Creative Commons Attribution License \(CC BY\)](#). The use, distribution or reproduction in other forums is permitted, provided the original author(s) and the copyright owner(s) are credited and that the original publication in this journal is cited, in accordance with accepted academic practice. No use, distribution or reproduction is permitted which does not comply with these terms.

State-of-the-art polyetheretherketone three-dimensional printing and multifunctional modification for dental implants

Meiqing Chen¹, Mei Ren¹, Yingqi Shi¹, Xiuyu Liu² and Hongtao Wei^{1*}

¹Department of Stomatology, China-Japan Union Hospital of Jilin University, Changchun, China, ²Hospital of Stomatology, Jilin University, Changchun, China

Polyetheretherketone (PEEK) is a high-performance thermoplastic polymer with an elastic modulus close to that of the jawbone. PEEK has the potential to become a new dental implant material for special patients due to its radiolucency, chemical stability, color similarity to teeth, and low allergy rate. However, the aromatic main chain and lack of surface charge and chemical functional groups make PEEK hydrophobic and biologically inert, which hinders subsequent protein adsorption and osteoblast adhesion and differentiation. This will be detrimental to the deposition and mineralization of apatite on the surface of PEEK and limit its clinical application. Researchers have explored different modification methods to effectively improve the biomechanical, antibacterial, immunomodulatory, angiogenic, antioxidative, osteogenic and anti-osteoclastogenic, and soft tissue adhesion properties. This review comprehensively summarizes the latest research progress in material property advantages, three-dimensional printing synthesis, and functional modification of PEEK in the fields of implant dentistry and provides solutions for existing difficulties. We confirm the broad prospects of PEEK as a dental implant material to promote the clinical conversion of PEEK-based dental implants.

KEYWORDS

polyetheretherketone, dental implants, three-dimensional printing, functional modification, biological activity

1 Introduction

In the field of dentistry, the primary goal is to reconstruct missing teeth to restore original function and maximize esthetic performance. With the rapid development of social economy and the improvement in esthetic concepts, dental implants—the rebirth of teeth—have become the most eye-catching repair option in stomatology. The superiority of dental implants has led to a mushroomed increase in their demand worldwide. It has been reported that the number of dental implants being used exceeded a million per year over a decade ago, and the global dental implant market is expected to reach \$6.81 billion by 2024 (Jiang et al., 2020). The enormous demand of society and the limitations of existing materials have greatly promoted the interest in developing alternative materials for dental implants. Polyetheretherketone (PEEK) is a widely used standard biopolymer material for

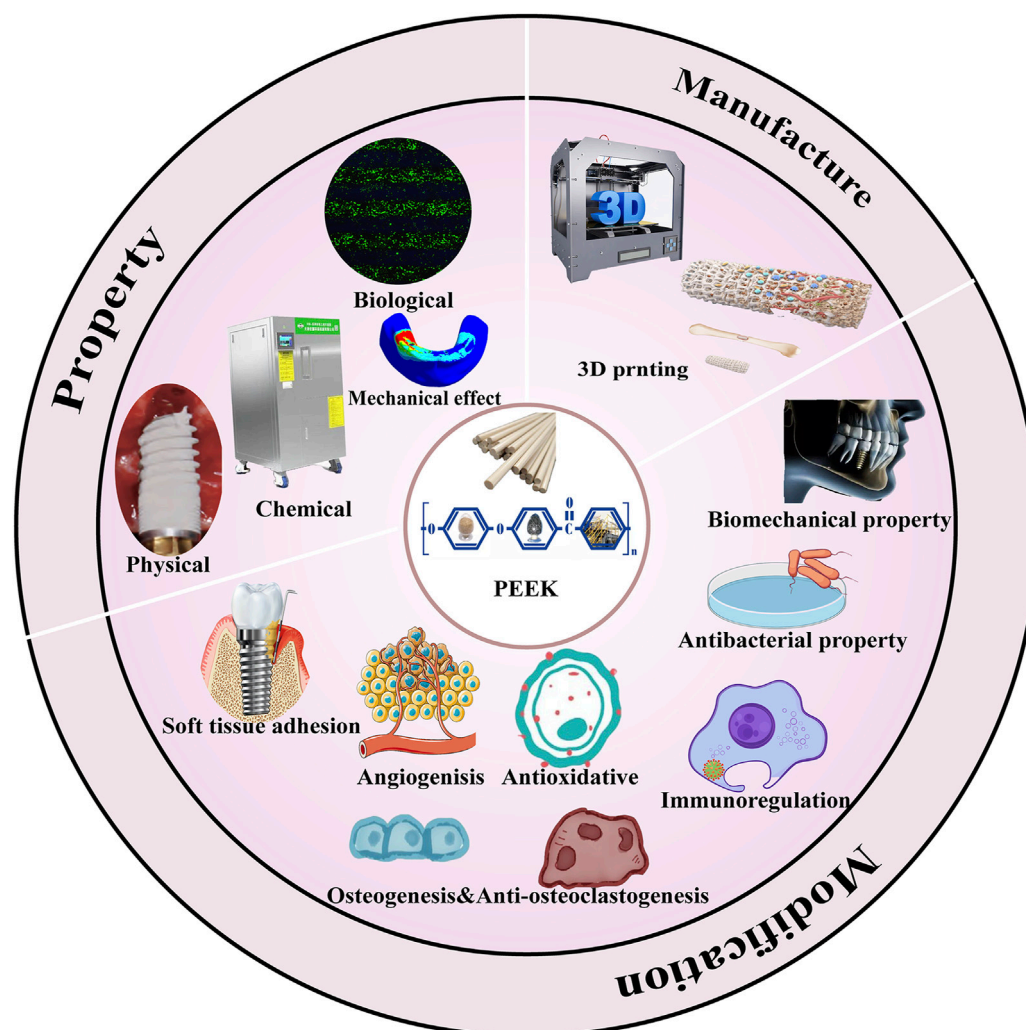


FIGURE 1
PEEK property, manufacture, and modification.

implantation. It has excellent esthetic properties, and the elastic modulus of reinforced PEEK can be comparable to that of human bones. A British scientist first produced PEEK in 1978, and in the 1980s, PEEK was approved by the US Food and Drug Administration (FDA) as an *in vivo* implantable material. It was also during this period that the role of material surface properties in osseointegration was revealed and recognized. Until April 1998, Thornton Cleveleys first proposed the use of implantable PEEK as a commercial biomaterial. Since then, the application of PEEK in biomedicine has grown exponentially, becoming a substitute for metal implants and the preferred material in plastic and trauma surgery (Mishra and Chowdhary, 2019; AlOtaibi et al., 2020; He et al., 2021; Ma et al., 2023). At present, PEEK is developed to be used not only as dental implants but also in the fields of maxillofacial/cranial implants, general orthopedic surgery, spinal surgery, and cardiac surgery (Panayotov et al., 2016).

The key factor for successful dental implantation is excellent osseointegration with surrounding bone tissues. Osseointegration, proposed by R. Branemark, refers to the direct contact and mechanical bonding between dental implants and the jawbone

without any interference from fibers or connective tissue (Kadambi et al., 2021). Clinically, osseointegration is defined as the asymptomatic rigid fixation of allograft implants in bone under functional load. In 2017, a study described osseointegration as a response to isolating foreign implants (AlOtaibi et al., 2020). By dividing molecular and cellular communication of post-implantation, osseointegration is divided into four stages: homeostasis, the inflammatory phase, the proliferative phase, and the remodeling phase (Pidhatika et al., 2022). Effective osseointegration provides support and structural stability for dental implants. However, as PEEK does not have bone induction ability in essence, it lacks the capacity to induce osteogenic differentiation and stimulate new bone formation, which affects osseointegration between PEEK implants and the surrounding alveolar bone. Therefore, PEEK urgently requires modification methods to improve its biological activity to achieve osseointegration.

This paper provides a detailed comparison of traditional metal implant materials and PEEK in terms of physical, chemical, and biological properties for the first time. Three-dimensional finite

TABLE 1 Limitations of Ti.

Limitations	Consequence/mechanism	References
Common metal problems—wear, metal fatigue, and fretting corrosion	Affect its service life	Guo et al. (2022b)
Metallic heterocurrent	When other kinds of metals are around in oral, it is formed	da Cruz et al. (2021)
Metal allergy (rate is about 0.6%)	It can cause cellular sensitization; clinical manifestations are hypersensitivity and anaphylaxis; specific manifestations can be eczema, urticaria, edema, pruritus of skin, facial erythema, necrosis, pain, and hyperplastic tissues	Sicilia et al. (2008); Guo et al. (2021a)
Galvanic corrode	It slowly leaks out trace amounts of elements that can be toxic to humans, such as aluminum and vanadium. At the same time, the release of Ti ions can upregulate the pro-inflammatory factor, inhibit the activity of osteoblasts, promote osteoclast activity, and change the microbial composition of the biofilm then cause peri-implantitis	Ren et al. (2020a); Kim et al. (2019); Noronha Oliveira et al. (2018); Alves et al. (2022)
Metallic color and gray appearance	It can be seen in thin gingival types or high-smile line patients, which greatly affects the esthetic effect that has been valued at present	Azizi et al. (2018); Schwitala and Müller (2013)
Metal design limitations	Slender central screw used to connect the abutment to the metal implant is prone to fatigue and fracture when subjected to non-axial forces and cyclic occlusion. At this time, the rigid Ti implant cannot drill a hole with a dental drill to remove the snapped screw	Jiang et al. (2020)
Density of 4.506 g/cm ³	It is about three times the average human bone density	Fu et al. (2021a)
Poor biological activity, slow healing, porosity, thermal and electrical conductivity, complex manufacturing processes, and expensive production costs	-	Sagomonyants et al. (2008); Carpenter et al. (2018); Jovanović et al. (2021)

element analysis (FEA) also indicates the mechanical advantages of PEEK at the implant–bone interface. The aforementioned points confirm the feasibility and reasons of PEEK being used as a novel implant substitute material. Second, we introduce the most suitable method for manufacturing PEEK dental implants—3D printing—and discuss methods to solve existing research hotspots in 3D printing, such as the research progress in improving the interlayer adhesion of 3D-printed PEEK. In addition, as an important aspect, we comprehensively summarize different modification strategies for improving the biomechanical properties, antibacterial properties, soft tissue adhesion ability, immunoregulation ability, and antioxidative, osteogenic and anti-osteoclastogenic, and angiogenic properties of PEEK. This review aims to comprehensively analyze in detail the clinical application potential of PEEK-based dental implant materials and summarize the latest progress in improving their different activities from a functional perspective. Figure 1 summarizes the article content.

2 Property advantages of PEEK

2.1 Limitations of metal implants

Currently, the vast majority of dental implants are made of metals, such as titanium (Ti) and Ti alloys (principally Ti6Al4V)—the current gold standard in dentistry. However, the high elastic modulus of Ti affects the stress adjustment of bone tissue and a series of problems, which eventually cause stress shielding (Sumner, 2015). Since the elastic modulus of a Ti implant is more than five times that of cortical bone (14 GPa), most of the pressure will be transferred to

the implant and reduce the load of cortical bone; according to Wolff's law, there is a positive correlation between the load and bone growth, so it will gradually lead to the decrease in bone mineral density and chronic osteoporosis (Liu et al., 2021a; Kruse et al., 2021; Manzoor et al., 2021). Marginal bone loss of Ti implants can reach a certain extent after the first year of stress (Najeeb et al., 2016b). Therefore, the mechanical binding of the bone–implant interface is affected, and the implant becomes loose, leading to implantation failure (Nagels et al., 2003). Some other limitations of Ti have been found in clinical use and manufacturing, as given in Table 1.

2.2 Property advantages of PEEK as an implant

Because of the defects of metal and ceramic-based materials, there is an urgent need for a new implant alternative multifunctional material to adapt to the rapid development of material and oral medical systems. Poly(oxy-1,4-phenyleneoxy-1,4-phenylenecarbonyl-1,4-phenylene), abbreviated as PEEK, combines excellent physical, chemical, and biological properties (Searle and Pfeiffer, 1985). PEEK is a leading high-performance thermoplastic polymer in the polyaryl-ether-ketone (PAEK) family used in dental biomedical sciences (Jung et al., 2019; Araújo Nobre et al., 2021). Compared with traditional thermosets such as epoxy, thermoplastics not only have equivalent mechanical properties but also have low manufacturing time and cost, high toughness, less crosslinks, easier repair and recycling, and easily undergo secondary processing through melting and reconsolidation (Boon et al., 2021; Chen et al., 2021). The sequence and proportion of phenylene rings

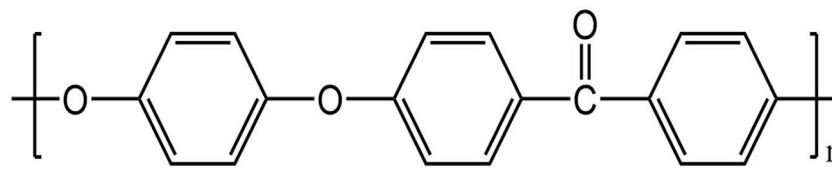


FIGURE 2
Molecular structure of PEEK (Ma et al., 2020).

(aryl), carbonyl sets (R-CO-R), and ether bonds (R-O-R) in the molecular backbone of the PAEK family are different. Flexibility and rigidity are provided by R-O-R and R-CO-R, respectively, which enhance the inter-molecular interactions and aryl (Toth et al., 2006; Alqurashi et al., 2021). The main chain of PEEK is composed of repeating units of a single ketone bond and double ether bonds (Figure 2). As we all know, structure determines property. The structure of PEEK not only makes it the only polymer material that can support repetitive loading without plastic deformation and fracture (Yakufu et al., 2020) but also makes it highly hydrophobic (Lee et al., 2012).

As a special organic plastic, it is tooth-colored, which meets esthetic requirements, and overcomes the problem of gingival staining caused by alloys (Najeeb et al., 2016b; Benli et al., 2020). When the implant is screwed into bone tissue or subjected to complex occlusion force, it experiences wear and tear, and excellent abrasion resistance can reduce the production of fragments that stimulate surrounding tissues and cause inflammation. Chen et al. (2020b) prepared PEEK coating on a central screw thread through thermal spraying and measured the friction coefficient and clamping force of the screw thread pair. It turned out that PEEK coating could reduce the friction coefficient and increase clamping force and preload under large-scale sliding, improving anti-loosening performance of screws under dynamic load. The aforementioned results show that PEEK has good abrasion resistance. PEEK is radiolucent and does not affect the nuclear magnetic resonance imaging (MRI) examination, so the healing of soft and hard tissues around the implant can be clearly observed (Korn et al., 2015). Köse et al. (2021) produced a polymethylmethacrylate phantom and placed prosthetic material cylinders (Co-Cr, Ti, zirconia, and PEEK) into a hole to compare artifacts in cone beam computed tomography (CBCT) images. They evaluated the presence of artifacts by calculating the standard deviation (SD) of grayscale values in regions of interest (ROIs) around each material. Since PEEK has the lowest density and atomic number, it absorbs the least radiation. The experimental result proved that the artifacts of PEEK are similar to the empty phantom (control group), which are significantly lower than those of the zirconia, Co-Cr, and Ti groups ($p < .05$). From the perspective of precise radiographic images, PEEK is the preferred dental implant material. Natural periodontal ligament has shock absorption function, and there is a lack of similar tissue around the implant and direct contact with bone tissue. After absorbing the occlusion force received, PEEK gently and smoothly transmits it to the surrounding bone tissue, thereby achieving shock absorption and protecting bone tissue from heavy loads to avoid implant failure, which can extend the lifespan of the implant (Anguiano-Sanchez

et al., 2016; Zhao et al., 2020). Significantly, the long-term success rate of implants depends on whether they can minimize marginal bone loss after functional loading. According to Hooke's law, similar mechanical properties of PEEK and bone distribute stress evenly and they share a similar amount of modulus to minimize disuse bone resorption caused by stress shielding, which also improves implant stability by enhancing the bond between implants and bone (Steenberghe et al., 2001; Chen et al., 2012; Jiang et al., 2020). Interestingly, a similar elastic modulus can also be used to provide a damping effect for PEEK restorations (Papathanasiou et al., 2020). Research has shown that carbon fiber-reinforced PEEK (CFR-PEEK) can withstand maximum chewing pressure (306 N) under oral physiological conditions (Wang et al., 2023). The specific strength (strength-to-weight ratio) of pure PEEK also gives it excellent mechanical strength (Marin et al., 2020). PEEK also has excellent chemical stability, thermal stability, and biocompatibility, which can be proved by resisting all chemical reagents except 98% sulfuric acid, and long-term stable mechanical performance in a 120 °C environment (Kurtz and Devine, 2007). In a previous study, PEEK resisted *in vivo* degradation and damage simulated by lipid exposure (AlOtaibi et al., 2020). In addition, during the initial healing phase, a clinical controlled trial using Ti and polymer abutments did not show an increasing risk of marginal bone resorption or soft tissue decline (Koutouzis et al., 2011). These properties are shown in Table 2. In addition, creep resistance, nonmagnetic property, high bending and compression resistance, no exothermic reaction, low solubility and water absorption, and self-lubrication also make it an attractive biological engineering material (Wang et al., 2023).

Due to the continuous and irreversible impact of stress and strain on the microstructure of alveolar bone, osseointegration is strongly influenced by the stress and strain distribution of the implant–bone interface, which is a key factor for long-term success in implantation (Bins-Ely et al., 2020). FEA is a method used to predict stress and strain at any point in any given geometric shape via theoretical models (Chokaree et al., 2022). In the field of stomatology, FEA has been recognized as a well-established research method for predicting the von Mises equivalent stress and strain, compressive/tensile stress, and strain energy density (SED) of various dental implants and peri-implant alveolar bone (Frost, 2004). Implant prosthesis repair of mandibular edentulous patients is usually a mixed-support All-on-4 treatment, consisting of a bar, top cap and four implants, screws, and abutments (Maló et al., 2003). Shash et al. (2022) found that the stress and strain changes in PEEK implants and surrounding bone tissue were smaller than those in Ti, so the chewing force on mixed-support dentures could be transferred to acrylic dentures and mucosa. The

TABLE 2 Chemical and biological properties of PEEK.

	Property advantages	Application significance	References
Chemical properties	Resistance to chemical, thermal, and bio-degradation	It can be applied to complex oral environments through various manufacturing methods	Fu et al. (2021a)
	Superior processability	It enables PEEK to accurately manufacture various complex structures of implants	Ma et al. (2020)
	Resistance to ethylene oxide gas, γ radiation, and steam	It can withstand repeated sterilization	Singh et al. (2019)
Biological properties	PEEK has a two-phase semi-crystalline structure which does not provide any kind of cytotoxicity or mutagenicity	It shows high compatibility with soft and hard tissues	Lethaus et al. (2012); Maloo et al. (2022)
	Low plaque affinity	Inhibition of peri-implant inflammation	Najeeb et al. (2016b)

maximum von Mises stress (σ_M) also did not exceed the pain threshold (0.63–1.2 MPa) and yield strength (140–170 MPa), which would not cause part breakage and mucosal pain. Therefore, PEEK is more suitable for use as an All-on-4 implant, which can reduce the burden on the implant and alveolar bone, especially in the cases of poor bone quality. For the impact of the implant itself, the von Mises in CFR-PEEK implants will not exceed its ultimate strength, so there is no risk of fracture or yielding (Al-Mortadi et al., 2022). In addition, von Mises stresses of Ti implants are prone to concentrate in the neck, which may lead to postoperative fracture, while CFR-PEEK with Young's modulus 19 GPa can avoid such problems (Sarot et al., 2010). For the implant–bone interface, Lee et al. (2012) found that 5*0.5 mm² PEEK coating could increase the SED level of bone tissue around the implant, thus having a smaller stress-shielding effect compared to Ti and zirconium.

In summary, PEEK is a new implant material that can potentially replace Ti and zirconia, with reasons including improving aesthetics, reducing risks caused by mechanical properties, higher design freedom, reducing system costs, and more optional manufacturing methods (Shash et al., 2022). Although Ti and zirconia are the best known implant materials in dental applications among the biomedical alloys, PEEK takes it to the next level in some special circumstances, such as bruxism, metal allergy, and higher esthetic requirement (Lijnev et al., 2022).

3 Manufacture of PEEK implants—3D printing

In order to further improve the bioactivity and performance of implants, scholars start from the manufacturing process to search for suitable methods and parameters. Aiming to improve the efficiency of manufacturing oral restoration and the size accuracy of implants, while reducing the workload of dentists, a fully digital product manufacturing process—additive manufacturing (AM) technology (also known as 3D printing technology)—was created (Barazanchi et al., 2017). Such a digital procedure uses data flow to integrate disease diagnosis, treatment planning, and prosthesis production (Salmi, 2021). The working principle of AM is discrete stacking. The continuous superposition of a discrete process is transformed into a 3D digital model of a two-dimensional sheet model, and the entire process is sequentially stacked layer by layer by a computer program (Kessler et al.,

2020). AM is not a type but a class of technology, and seven 3D printing categories are included in the American Society for Testing and Materials classification standard. Traditional subtractive machining technology (also known as numerical control processing technology, NC) of PEEK includes injection molding, thermal compression molding, and computer-aided design and computer-aided manufacturing (CAD/CAM) milling. Injection molding injects PEEK and/or its composites into a pre-designed mold under highly evaluated temperature and shear force to form a product with customized geometry. As for thermal compression molding, heat and pressure are applied to the molten state of PEEK in a platen mold of a given thickness to form products (He et al., 2021). Compared with NC, AM is suitable for the mass production of complex implants in a short period of time and can also reuse unformed raw materials to reduce costs (Tian et al., 2021). Among AM, commonly used methods in the field of PEEK oral implants include selective laser sintering (SLS) and fused filament fabrication (FFF) or fused deposition modeling (FDM) (Huang et al., 2023). SLS has the longest using time and the greatest potential for large-scale production (Luo et al., 2023). It selectively melts PEEK powder at high temperatures (i.e., > T_m of PEEK) generated by laser or electron beam irradiation, and the solid structure is fused together in a layer-by-layer manner (Ligon et al., 2017). Nevertheless, SLS wastes a large amount of PEEK powder, which may be potentially contaminated and cannot be reused as raw material. It also requires additional safety measures (Rodzeń et al., 2021b). Due to minimal waste and easy operation, FDM is considered the best printing method for PEEK. In FDM, PEEK powders are spun into filaments as raw material by FFF, and then, the molten filaments are extruded through the orifice of the nozzle and merged with the previously deposited material to form predetermined 3D porous scaffolds (Yang et al., 2017). Unfortunately, the PEEK scaffold generated by FDM has weak interior bonding strength and mechanical properties. The solutions are introduced in the following.

3.1 Solutions to enhance mechanical properties

The unique porous structure on the surface of the 3D-printed scaffold provides high roughness and a large usable surface area, thereby increasing the accumulation of cells in these grooves, which may promote intercellular contact and improve cell viability (Yu

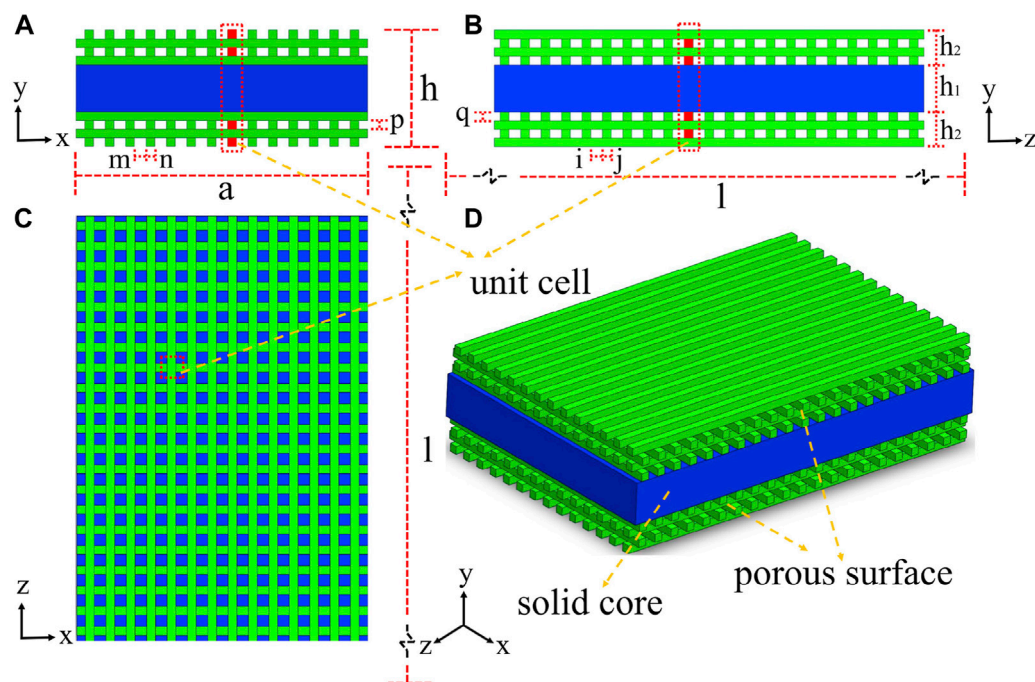


FIGURE 3
Surface porous PEEK structure with a solid interior by FDM. (A) Left view. (B) Front view. (C) Top view. (D) Isometric view.

et al., 2022). However, the internal pore of the implant reduces its mechanical properties. To balance the mechanical and osseointegration properties of PEEK, Li et al. (2021) designed a surface porous PEEK (SP-PEEK) structure with a solid interior by FDM (Figure 3). It has a variable porous layer number and pore diameter ($m = 0.4$ mm, 0.6 mm, 0.8 mm, and 1.0 mm). When the pore layer number varied from 2 to 8, SP-PEEK retained the modulus of solid PEEK from 96.78% to 45.59%. When the pore diameter varied from 0.4 to 1.0 mm, SP-PEEK retained the modulus of solid PEEK from 91.58% to 48.00%. In addition to retaining most of the mechanical properties of PEEK, SP-PEEK also exhibited excellent *in vitro* osteogenic behavior. The authors found that the group with $m = 0.6$ mm had the highest osteogenic activity ($p \leq 0.05$). It is reported that printing parameters such as nozzle temperature, plate temperature, layer thickness, printing speed, infill ratio, and raster angle also affect the mechanical properties of a 3D-printed material significantly (Wang et al., 2020). Therefore, changing the printing parameters is one of the methods to solve the problem of insufficient mechanical properties of materials. The optimal set of printing parameters for achieving the best mechanical performance has not yet been found. Wang et al. (2021c) designed a three-factor experiment based on the Box-Behnken design and used the response surface methodology (RSM) to find the optimal printing parameters. Among the parameters involved in the experiment, the nozzle diameter had the greatest impact on the mechanical properties of 3D-printed material, followed by printing speed and nozzle temperature. In addition, the authors also proposed a set of parameters that are meaningful for the application of dental implants: the parameter combination of a nozzle diameter of 0.5 mm, a nozzle temperature of 420°C , and a printing speed of 5 mm/s tends to form the best

bending strength and elastic modulus simultaneously. A compression test showed that the larger the nozzle diameter (>0.6 mm), the better the compression performance of the 3D-printed material. Sonaye et al. (2022) also found a set of suitable processing conditions to produce FFF-based PEEK with excellent mechanical properties: bedplate temperature 150°C , nozzle temperature 450°C , chamber temperature 90°C , layer thickness 0.1 mm, and printing speed 30 mm/s. They also used an autoclave at 134°C for 15 h (134°C for 1 h in the autoclave is equivalent to 37°C for 1–4 years) to conduct an accelerated aging test. The average fatigue strength of aged PEEK and non-aged PEEK is 27.86 MPa and 32.09 MPa, respectively, so they both can withstand force greater than the maximum oral masticatory force (306 N). This study breaks through the shortcoming of FFF in manufacturing small but robust implants and demonstrates their long-term mechanical durability. In terms of PEEK composites, both printing temperature and composite content can affect the mechanical properties of the printed product. Wang et al. (2021b) found that the tensile and flexural strengths of 5 wt% of CF-reinforced PEEK (CFR-PEEK) in FDM increased with the rise in nozzle and platform temperatures. However, as the introduction of fibers increased, the impact strength of PEEK composites decreased. The aforementioned phenomenon can be explained as the printing material has better melt flow and formability at higher temperatures. In addition, higher temperature provides more energy to increase penetration and diffusion between the filaments and interlayer. The increase in fiber content leads to the formation of pores and the degradation of molecular chain properties during filament preparation. However, temperature requirements for the chamber, print bed, and hot end of FDM-printed PEEK are higher than those for most available commercial FFF printers.

Rodzeń et al. (2021b) successfully printed PEEK/hydroxyapatite (PEEK/HA) composites (up to 30 wt% HA) by using a custom-modified commercial printer Ultimaker 2+ (UM2+) with high-temperature capabilities. X-ray diffraction (XRD) showed crystallinity up to 50%, and crystalline domains can be clearly observed using a scanning electron microscope (SEM) and by high-resolution transmission electron microscopy (HR-TEM) analyses. Such high crystallinity significantly enhanced the mechanical properties of 3D-printed samples through delivering continuous crystalline domains in all directions.

3.2 Strategies for increasing interlayer adhesion

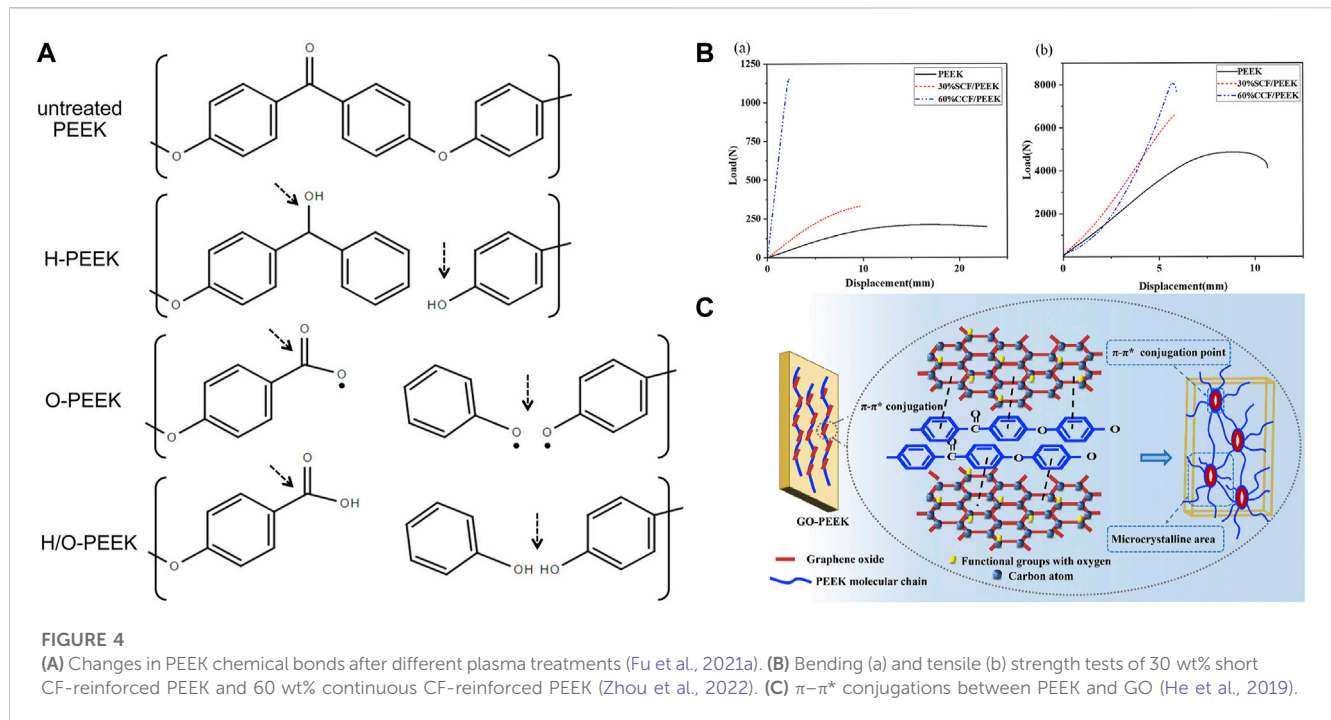
Compared to injection molding and milling, molecular chains between layers of FDM-based PEEK are less crosslinked and entangled, leading to only small interlayer forces (Guo et al., 2022a). In addition, PEEK has a large melt viscosity and a high melting temperature, which makes interlaminar interface cracking or delamination become one of the most common failure types during clinical use (Lv et al., 2022). Therefore, increasing the fluidity is a key step in improving interlayer adhesion. Nevertheless, the raw materials for FDM are usually PEEK–fiber composites, which are added to enhance the mechanical properties of the scaffold. Rigid fibers such as glass fibers have high hardness, coupled with nozzle size limitations, resulting in an orientation distribution parallel to the interlayer interface rather than a directional distribution, making it impossible to bridge the indirect interface of the printed layer. In addition, adding fibers can further reduce the fluidity of the slurry and reduce interlayer adhesion (Lv et al., 2022). However, if flexible fibers are added, interlayer bridging can be achieved. Adding inorganic fullerene tungsten sulfide (IF-WS) nanoparticles during the production of the fusion filament can reduce the melt viscosity of the polymer by 25% (Golbang et al., 2020). Similar to the layer-by-layer laying process of FDM, Wu et al. (2022) generated CFR-PEEK laminates via laser-assisted forming with a repress treatment. Because of the repress treatment on the top surface of the laminate through laser heating and roller compaction, percolation flow and squeeze flow of the resin and reheating of the laminate body were generated. The interlaminar shear strength (ILSS) of laminates, which had less voids and a higher degree of crystallinity, was improved by 32.87% more than that of the laminates without repress treatment. Post-heat treatment is also suitable for increasing the interlayer mechanical strength of FDM 3D-printed PEEK composites by increasing crystallinity and interfacial bonding properties. Treatment at 250°C for 6 h reduces inter-fiber drawbacks and at 230°C potentially increases the interlaminar tensile strength from 6.96 MPa to 36.28 MPa (Rodzeń et al., 2021a). Since printing parameters can improve the mechanical properties of 3D-printed PEEK, perhaps its mechanism is to increase interlayer adhesion. Basgul et al. (2021) developed a one-dimensional (1D) transient heat transfer-based non-isothermal polymer healing model to predict the interlayer strength of FFF-based PEEK. According to the model, they found an association between nozzle temperature, bed temperature, and environment temperature (TN, TB, and TC, respectively) and the interlayer strength in FDM. The most significant impact on interlayer healing was TN. Decreasing the

TN by 20°C–465°C almost halved completely healed layers (47% less), and below 445°C (TN), none of the layers could achieve 100% healing. Increasing TB could increase the number of healing layers by 100%. Although TC had little effect on the lower area near the printing bed, it increased the number of 100% healed layers by heating up. In order to solve the layer delamination and the mechanical performance shortage caused by FDM-based 3D printing and promote its deeper and wider development in the medical field, we should continuously try other methods such as proper material formulation, improving printing parameters, improving compactness of the layer interface and adjustment of the printing interval, and optimization of the printing path (Lv et al., 2022).

Although 3D printing technology has been able to produce customized scaffolds with a complex intrinsic porous structure and different surface roughness, its high cost and low productivity limit its application in large-scale production. The resolution achievable to date also poses a challenge when applying 3D printing to dental implants with a diameter less than 5 mm (He et al., 2021). More importantly, the impact of AM technology and the post-treatment process on crystallinity is difficult to control. Low crystallinity may be due to the insufficient mechanical strength of the material, while high crystallinity can cause deformation of the material (Yi et al., 2021). In the future, we should focus on finding a new manufacturing method that simultaneously improves stiffness and ductility that 3D printing cannot achieve. A solid-state pressure-induced flow (PIF) process uses a mold to apply pressure to a solid material and forces the sample to flow in one direction within the confinement of both sides. PIF can prepare a bioinspired nacre-like PEEK material which has high stiffness and excellent ductility at the same time (Luo et al., 2023).

4 Modification for enhanced bioproperties

The aromatic main chain and lack of surface charge and chemical functional groups make pure PEEK exhibit hydrophobicity, low surface energy, and biological inertness. Poor adhesion and proliferation of cells, as well as weak absorption of protein on such an inset surface, lead to reduced osteogenic differentiation of progenitor cells and the production of inflammatory environments which tend to generate apoptosis and necrosis. Finally, fibrous tissue wrapping the implant hinders bone integration, which manifests implantation failure (Olivares-Navarrete et al., 2015; Wan et al., 2020). In recent years, scholars have spared no effort in researching PEEK modification and made it a hot topic, especially for the methods of comprehensive biological response related to bone reconstruction after implantation, including biocompatibility, bacterial resistance, immunoregulation, angiogenesis, antioxidation, osteogenesis and anti-osteoclastogenesis, and soft tissue adhesion. Biocompatibility of dental implants is the basis for affecting protein adsorption and osteoblast adhesion and differentiation. However, insufficient antibacterial activity of the material can lead to the formation of dental plaque on its surface, which, in turn, reduces the biocompatibility of the material surface (Renvert et al., 2008). In addition, bacterial infections around implants can cause bone



resorption. Materials prevent inflammation by regulating the body's immune response, thereby affecting bone remodeling and absorption (Takayanagi, 2007). The unique periodontal soft tissue sealing of dental implants is the first line of defense against external stimuli. During bone regeneration around the implant, it is essential to generate blood vessels. Vascular regeneration ability and blood supply ensure sufficient nutrient supply during osseointegration, which is also a prerequisite for the formation of osseointegration by pre-osteoblasts and mesenchymal stem cells (Ding et al., 2021). It is worth noting that early inflammation caused by implants is beneficial for early angiogenesis and tissue regeneration, while subsequent controlled inflammation can promote bone regeneration (Kargozar et al., 2020). This section comprehensively analyzes and discusses innovative modification methods to achieve separate or simultaneous enhancement of the aforementioned activities, promoting the feasibility and long-term stability of PEEK application in human oral environment.

4.1 Biomechanical property

Plasma is an ionized gas with an equal density of positive and negative charges, commonly known as the fourth state substance. They exist in a high-energy state, including electrons, ions, free radicals, and excited species (Wang et al., 2019). Plasma immersion ion implantation (PIII) treatment usually uses high-voltage electricity to accelerate plasma particles and implant them onto the surface of the materials. Such bombardment of the surface can locally heat up at the nano-scale and activate chemical reactions (Comyn et al., 1996). At a more detailed molecular level, strike not only damages the polymer chains on the surface of materials but also leads to microetching, removal of organic residues, and cross-linking. Differences in functional groups and activities introduced

by various plasmas attract researchers' attention. Fu et al. (2021b) found that oxygen plasma-treated PEEK took 5 min to reduce the contact angle of PEEK to 3° , while hydrogen/oxygen-treated PEEK only took 1 min, indicating that H/O plasma worked fastest to achieve the same effects. The author believed it was related to the differences in fracture sites and reformation of functional groups (Figure 4A). During hydrogen plasma treatment, the C-O-C bond and C=O bond of PEEK fractured to form C-OH, and there was a small amount of benzene rings cleaved and volatilized, which were the reasons for hydrophilicity improvement. In oxygen plasma treatment, after the cleavage of C-O-C bonds, an O atom/radical was added to form C-O-O-C, and a benzene ring and the C=O group broke to form unstable O=C-O• and C-O• which reacted with the humidity of air to form O=C-OH and C-OH finally. The generation of these functional polar groups resulted in a smaller contact angle for oxygen plasma treatment compared to hydrogen plasma treatment. The H/O-PEEK group combined the advantages of the aforementioned two types of plasma to produce the fastest working speed. However, the mixture of hydrogen and oxygen was theoretically explosive. The low pressure under study and the safety valves in the system perfectly ensured safety. However, the study did not include the gold implant material standard, Ti, as a control. Other research studies found that ammonia or N_2 plasma treatment produces nitrogen-containing functional groups, while water plasma treatment produces OH groups (Yu et al., 2022). Although plasma treatment has been proven to optimize the properties of PEEK, the time taken for plasma treatment to generate maximum surface crystallinity, whether it can resist implantation process wear by increasing surface hardness, and the role of bone integration *in vivo* are still a significant focus of future research (Delgado-Ruiz and Romanos, 2018).

In recent years, many studies have focused on synthesizing composite materials of PEEK and fillers. Fillers dispersed in

PEEK matrices can significantly improve their mechanical properties, such as elastic modulus, bending strength, and micro-hardness (Zhong et al., 2021). The type and content of fillers determine the characteristics of composite materials. Due to high mechanical performance and low density, carbon fiber (CF) became the most commonly used reinforcing fiber for PEEK (Chua et al., 2021). Different length, thickness, and weight fractions of CF added to PEEK can produce CFR-PEEK with different elastic moduli, which are within the elastic modulus range of human bones (Guo et al., 2022c). Zhou et al. (2022) proposed that the bending and tensile strength and elastic modulus of 30 wt% short CF-reinforced PEEK were close to those of human bones, while the bending strength of 60 wt% continuous CF-reinforced PEEK was 644 MPa (Figure 4B), which is even higher than that of pure Ti. Therefore, such materials with high strength and appropriate elastic modulus are suitable for use as oral implants. The type of CF should be selected based on the application and process. Short CF increases the wear resistance of PEEK but reduces ductility (Ji et al., 2020). Long CFs have strong mechanical properties and can be braided in various ways (Zhao et al., 2021). Continuous CF has the best performance and low cost, but its processing efficiency is low (Chang et al., 2020). However, the cytotoxicity of CFR-PEEK is controversial. Some studies have found that CFR-PEEK has mild cytotoxicity and increases with the increase in CF content (Qin et al., 2019). The differences in manufacturing technology may be the reason for the inconsistent cytotoxicity of CFR-PEEK; therefore, more *in vivo* experiments are needed to determine the biocompatibility of CFR-PEEK.

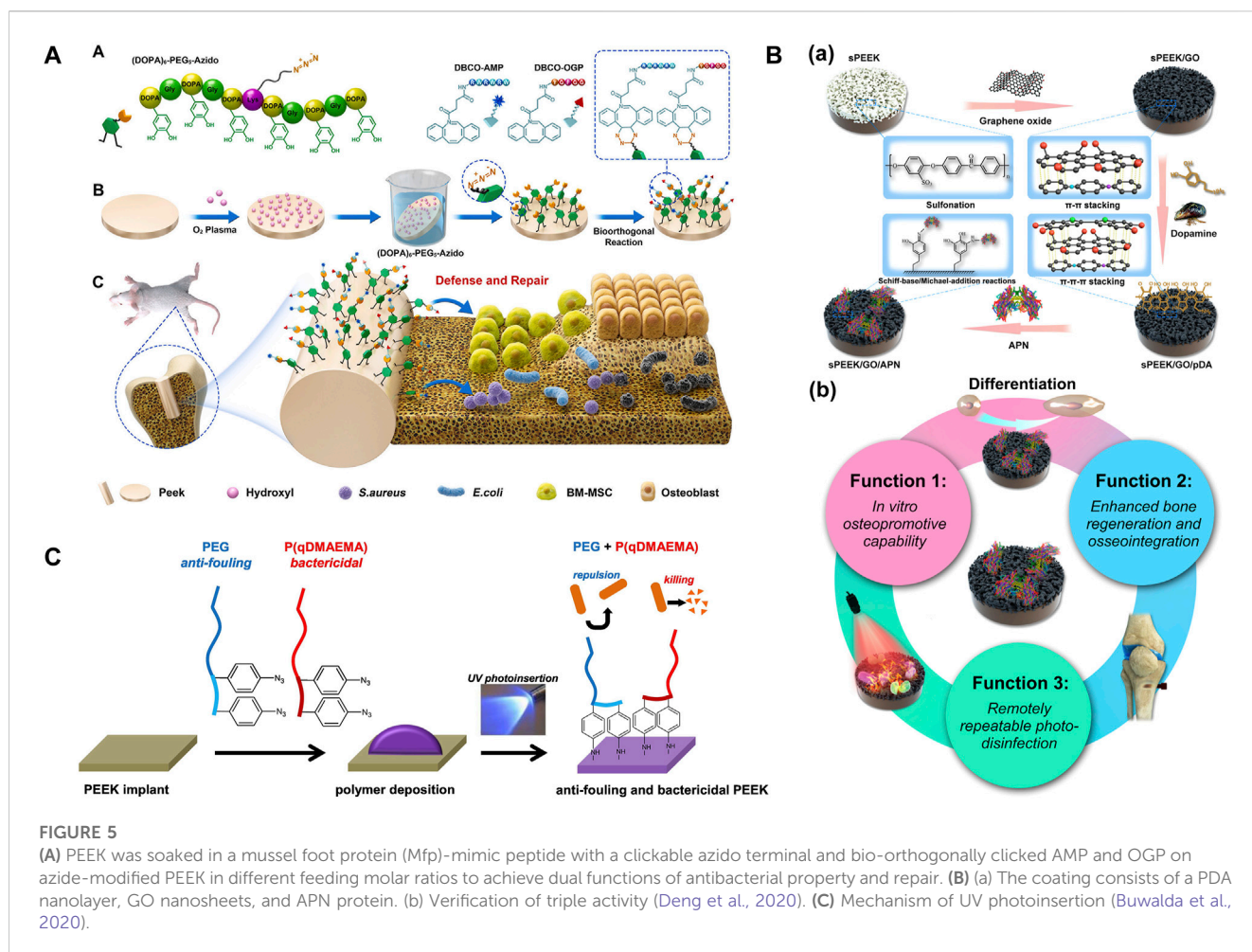
It is worth noting that when PEEK is reinforced or functionally modified, its mechanical strengths, such as stiffness, tensile strength, flexural strength, and hardness, increase, but its toughness is difficult to balance. Researchers usually functionalize fillers on the surface to evenly disperse or increase interfacial bonding strength in the PEEK matrix, which can promote load transfer but may confine the motion of interfacial polymer segments and lead to a substantial decrease in ductility (He et al., 2019). Graphene (G) and graphene oxide (GO) are low-dimensional nanomaterials which are widely used as reinforcing fillers for polymers. He et al. (2021) manufactured GO-reinforced PEEK (GO/PEEK) nanocomposites with different GO loading through injection molding. The compressive modulus of all composites reached a level similar to that of natural cancellous bone. The 0.5% GO loading had the maximum increase in elongation at break (increased by 86.32% compared to PEEK) and remarkable toughness (increased by 127.20% compared to PEEK). The adhesion and spreading of bone marrow stromal stem cells were also enhanced by the addition of GO. This might be attributed to the structural similarity between PEEK and GO, which enabled them to achieve strong interaction through the formation of π - π^* conjugations (Figure 4C). They provided uniform dispersion of GO in the PEEK matrix, nucleation sites for the oriented crystallization zone of PEEK, and increased molecular chain alignment along the GO plane.

4.2 Antibacterial property

Currently, about 20% failed implantation surgeries are caused by infections (Deng et al., 2017). Collagen fiber degradation and

marginal bone resorption in peri-implantitis are caused by host overreaction and the direct action of bacteria (Abranches et al., 2018). Therefore, the influence of PEEK as a dental implant material on bacterial adhesion and biofilm formation as well as its bactericidal ability is very important. Although many studies have shown that PEEK has an excellent antibacterial rate of about 50%, which is better than that of Ti, bacteria still adhere to the surface of PEEK under SEM observation, and the number increases over time. Therefore, the antibacterial performance of PEEK itself is not sufficient to resist infection, which can cause inflammatory fibrous tissue to wrap around PEEK and hinder bone integration (Najeeb et al., 2016a), affecting the stability and functional load of the dental implant. The following introduces novel antibacterial modification methods of PEEK.

Subgingival plaque is composed of *Streptococcus sanguinis* (*S. sanguinis*) and *Porphyromonas gingivalis* (*P. gingivalis*) and is the initiating factor of peri-implantitis. They are the early and late colonized bacteria in the dental plaque biofilm, respectively (Periasamy and Kolenbrander, 2010). Some metal cations can inhibit pathogenic bacteria of peri-implantitis, such as silver (Ag^+), zinc (Zn^{2+}), magnesium (Mg^{2+}), and copper (Cu^{2+}) ions. However, the potential toxicity of metal ions and the antibiotic resistance mutations of bacteria no longer make them perfect antibacterial agents, and people are increasingly in urgent need of antibacterial agents with strong antibacterial effects, few side effects, and no drug resistance. Efficient and aggressive antimicrobial peptides (AMPs) have become a new kind of antibacterial agents because of their biogenic nature (Jiang et al., 2021). AMPs not only exert bactericidal effects by targeting bacterial cytoplasmic membranes and dislocating the adhesion of mussel-like molecules to PEEK but also left azide groups that could undergo orthogonal reactions (Wenzel et al., 2014; Chen et al., 2020a). Li et al. (2022a) bio-orthogonally clicked AMP and an osteogenic growth peptide (OGP) on azide-modified PEEK (DBCO-AMP and DBCO-OGP) in different and accurate feeding molar ratios to achieve dual functions of defense and repair (Figure 5A). *In vitro* and *in vivo* experiments had shown that the AMP-containing group could degrade *Escherichia coli* (*E. coli*) and *Staphylococcus aureus* (*S. aureus*) and integrated better with surrounding tissues, even synergistically enhancing bone integration in the case of postoperative infection. The study drew heatmaps with various standardized performances and found that PEEK- A_2O_2 (the feeding molar ratio of AMP/OGP was 2:2) had the best dual activity. Due to the limited active site on the surface of PEEK, antibacterial and osteogenic modifications are contradictory in most cases (Yakufu et al., 2020), so it is important to find a balance between them. Simply increasing the content of osteogenic-inducing active substances does not significantly enhance the bone integration effect *in vivo* as antibacterial activity is a prerequisite for osteogenesis. This study may be a promising solution in the field of surface bioengineering modification of inert dental implants. Yuan et al. (2019) decorated mouse beta-defensin-14 (MBD-14) on porous PEEK via lyophilization, and the modified PEEK was verified to have broad-spectrum antibacterial ability through *in vitro* and *in vivo* experiments. Proliferation and osteogenic differentiation of bone mesenchymal stem cells were also enhanced. Although antibiotics are one of the most commonly used antibacterial agents, one in every 15 people is allergic. Furthermore, the form of dental



bacterial biofilm has antibiotic resistance which is 1,000–1,500 times greater than that of planktonic bacteria. Photodynamic therapy (PDT) is a light-based alternative therapy for peri-implantitis and peri-implant mucositis, especially when patients are allergic to antibiotics (Sibata et al., 2000). PDT uses photosensitizers that can be activated when exposed to specific wavelengths of light in the presence of oxygen (typically using visible red light at 620–690 nm). Focusing the light on the infected lesion, the photosensitizer transfers energy to oxygen molecules, converting them into strongly oxidizing singlet oxygen. Ultimately, the production of reactive oxygen species (ROS) leads to bacterial death (Robertson et al., 2009; Azizi et al., 2018; Ren et al., 2020b; Hou et al., 2020). Peng et al. (2021a) compared the antibacterial effects of PDT and ampicillin through biofilm removal assay. Different concentrations of temoporfin were selected as photosensitizers. The results showed that both the PDT and ampicillin groups had good removal effects on *Streptococcus mutans* (*S. mutans*) and actinomycetes ($p < 0.05$), with high doses of temoporfin having better biofilm removal effects ($p < 0.01$). The osteoblast activity of PEEK was comparable to that of other groups. Deng et al. (2020) prepared a coating consisting of a PDA nanolayer, GO nanosheets, and adiponectin (APN) protein on the surface of sulfonated PEEK using π - π interaction (Figure 5B). After irradiation with 808-nm NIR light, the coated PEEK produced antibacterial rates of 99.49% and 92.4% for *S. aureus* and *E. coli*,

respectively. However, the damage of high temperature and ROS to surrounding tissues and cells limits its clinical application (Ren et al., 2020b). In the future, how to improve the absorption rate and penetration ability of photosensitizers and develop light sources that can reduce irradiation time are urgent issues that need to be solved.

It is reasonable to achieve antibacterial performance by changing the PEEK surface (morphology and chemical composition). The rigid cell walls of bacteria limit their deformability. When the nanopore size of the porous morphology formed on the surface of PEEK is smaller than bacteria, they cannot stick, while combining other modification methods can kill bacteria with smaller pore sizes. In addition, nanoporosity structures can damage bacterial cell membranes (Wang et al., 2017; Wang et al., 2018; Yang et al., 2021). In order to improve the competitive adhesion of cells against bacteria, it is important to comprehensively consider the structure and morphology of bacteria and cells, as well as the properties of materials. Changes in chemical composition usually refer to the combination of PEEK with antibacterial chemicals. The diphenylketone groups on the PEEK main chain are converted to semi-benzopinacol radicals under ultraviolet (UV) irradiation, and then, antibacterial monomers can be grafted spontaneously onto the free radicals (Kyomoto and Ishihara, 2009). There are usually two methods for endowing PEEK with antibacterial activity: (1) reducing bacterial adhesion and (2) killing bacteria. Buwalda et al. (2020) achieved the aforementioned two aspects simultaneously through a

one-step approach. They covalently grafted bactericidal quaternized poly(dimethylaminoethyl acrylate) (P (qDMAEMA)) polymers and aryl-azide-containing modified anti-fouling PEG onto the surface of PEEK through UV photoinserterion (Figure 5C). Although such functionalized PEEK had no obvious effect on Gram-negative *E. coli*, it had a good inhibitory effect on Gram-positive *S. aureus*, which increased with PEG chain length. It is worth noting that only when the lengths of PEG and P (qDMAEMA) were roughly equal could they exert a synergistic effect. The method of inserting aryl-azide groups through UV photoinserterion had “spectral significance” because most polymer substrates with carbon-hydrogen bonds could form covalent bonds with reactive nitrene intermediates. Therefore, this chemical method can be extended to other polymer implants. Positive antibacterial groups, such as $-\text{SO}_3\text{H}$, $-\text{OH}$, and $-\text{COOH}$, can also be introduced on the surface of PEEK, which can cause electrostatic repulsion and negatively charged bacterial cell membranes to generate a zeta potential difference (Liu et al., 2021a; Zhang et al., 2022). However, the introduction of these functional groups lacks long-term *in vivo* experimental verification.

In addition to changing the surface properties of PEEK, blending modification can enhance its antibacterial activity. Studies have confirmed that functionalized ceramic nanoparticles such as titanium dioxide (T-NPs) and silicon dioxide (S-NPs) had antibacterial activity under UV and dark conditions (Bokare et al., 2013). In the absence of UV irradiation, ceramic particles can produce exogenous ROS to exert bactericidal effects (Diez-Pascual and Diez-Vicente, 2015). Muthusamy Subramanian and Thanigachalam, (2022) used T-NP- and S-NP-reinforced PEEK (T/PEEK and S/PEEK) with good compressive strength and hardness values to test antibacterial activity *in vitro*. The average diameter of the inhibitory zone of 16 wt% T/PEEK, 12 wt% S/PEEK, and 16 wt% TS/PEEK on *E. coli* was 10.5, 11.9, and 18.299 mm, respectively, and the average diameter of the inhibitory zone on *Bacillus subtilis* was 12.25, 13.65, and 16.125 mm, respectively. The inhibitory zone diameters of pure PEEK were 9.213 mm and 10.452 mm, respectively. Therefore, it was confirmed that even without UV irradiation, the antibacterial ability of T-NP- and S-NP-reinforced PEEK composites can be significantly improved. Pezzotti et al. (2018) mixed silicon nitride (Si_3N_4) of three phases and PEEK by high-temperature melting. *In vitro* experiments found that PEEK/ β - Si_3N_4 had the best antibacterial effect against *Staphylococcus epidermidis* (*S. epidermidis*), while there was no obvious difference in the performance of PEEK/ α - Si_3N_4 compared to pure PEEK. The authors explained that the eluted NH_4^+ increased the pH value around the implant and damaged the bacterial cell membrane. Although antibacterial fillers can avoid the uncertain long-term bonding stability of coatings, they can alter the overall mechanical properties of the composite material. In addition, there is also a problem of weak bonding between the filler and PEEK interface. It is necessary to evaluate the functional loading of PEEK composite materials after implantation *in vivo*, and finding suitable filler dosage and size is also a key research point.

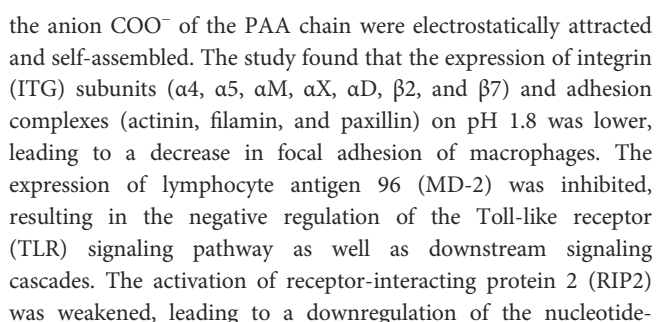
Most modification strategies of PEEK are to increase its activity by improving hydrophilicity, but as hydrophilicity increases, bacterial adhesion to its surface increases subsequently. Lijnev et al. (2022) incubated PEEK in 10 M sodium hydroxide for 24 h at 37°C. As expected, the enriched $-\text{OH}$ increased the hydrophilicity

of PEEK, thereby increasing its protein adsorption, mineral deposition, and human bone mesenchymal stem cell (hBMSC) adhesion. However, the disc diffusion method and *in vitro* bacterial attachment assay results showed a surprisingly significant decrease in the antibacterial activity of PEEK against *S. aureus* strains after the coating treatment. Thus, in order to find better ways to improve the antibacterial performance of dental implants, it is necessary to first understand the mechanism of infection, then evaluate the overall performance of the modification method, and finally, conduct animal and clinical experiments.

4.3 Immunoregulation

Inflammation begins with bacterial infection, followed by an excessive immune response mediated by autoimmune cells. When dental implants are screwed into the maxilla and (or) mandible, macrophages play a core regulatory role in mediating the immune response of the host and releasing cytokines and growth factors, leading to the formation of a pro-inflammatory M1 phenotype or anti-inflammatory M2 phenotype through polarization (Brown et al., 2012; Klopffleisch, 2016). The M1 phenotype enhances inflammatory response in the early stage to control infection, while the M2 phenotype promotes tissue regeneration and repair in the later stage (Shen et al., 2021). For the surface of PEEK, macrophages typically polarize toward the pro-inflammatory M1 phenotype and fuse into multinucleated giant cells, releasing fibrosis-enhancing cytokines, ultimately blocking osseointegration by fiber encapsulation (Sridharan et al., 2015). Therefore, PEEK is extremely desirable to be endowed with immunomodulatory ability, enabling it to transition from transient M1 polarization to an anti-inflammatory M2 phenotype in a timely manner, which can release chemokines to recruit osteoprogenitor cells and activate osseointegration (Chen et al., 2016). Based on the aforementioned mechanism, some studies loaded interleukin-4 (IL-4) on the implant surface to polarize macrophages to the M2 phenotype (Spiller et al., 2015) or used covalent modification of clusters of differentiation 47 (CD47) protein to “camouflage” which could not be identified by the autoimmune system (Gao et al., 2017). However, these expensive, short-life, and complex preparation processes of growth factor proteins are not easy to come by. Enabling dental implant materials to induce M2 phenotype macrophage polarization and creating a suitable osteogenic microenvironment have attracted extensive interest recently.

As a cost-effective technology, layer-by-layer (LBL) self-assembly can form films with specific structure and composition on the surface of materials by continuously dipping in polyelectrolytes with opposite charges (Costa and Mano, 2014). The films formed on the surface of PEEK through electrostatic interactions change its surface morphology, which can not only induce hBMSCs to differentiate into osteogenic lineage but also selectively polarize macrophages to reduce the secretion of pro-inflammatory cytokines, endowing PEEK with immunomodulatory ability (Gao et al., 2020). Gao et al. (2020) repeatedly immersed negatively charged PEEK into 2-mercaptoethanol, phorbol-12-myristate-13-acetate (PAH), and poly(acrylic acid) (PAA) weak polyelectrolyte solutions. The cation NH_4^+ of the PAH chain and



Excluding coatings, changing the physical and chemical properties of the PEEK surface, such as morphology (Lee et al., 2018), functional group types (Vassey et al., 2020), and elemental composition (Guo et al., 2021b), can endow PEEK with unique characteristics and improve its hydrophilicity. Subsequently, the polarization of adherent immune cells will be directly affected, which regulates the host immune response (Qin et al., 2020). Designing micro/nano-morphological structures of PEEK is one of the most commonly used and valuable strategies for improving immune regulatory ability. Surface physical structure and chemical composition modification of PEEK definitely exhibit better synergistic effects than single modification. Liu et al. (2022) sulfonated PEEK/hydroxyapatite (HA) (SPHA) composites to obtain both 3D porous physical and Ca^{2+} chemical signal surfaces. High concentration of extracellular calcium could reduce inflammation via activating the calcium-sensing receptor signal cascade to inhibit tumor necrosis factor alpha (TNF- α) expression and the wingless type 5a/receptor tyrosine kinase-like orphan receptor 2 (Wnt5a/Ror2) signaling pathway (Chen et al., 2016). Therefore, the high Ca^{2+} concentration and hydrophilicity of sulfonated PEEK/HA resulted in a low M1 phenotype-macrophage ratio. In addition, SPHA downregulated the expression of the inducible nitric oxide synthase (iNOS) protein, resulting in a nitric oxide (NO) concentration decrease (Zhou et al., 2021). In the co-culture medium of SPHA and mouse bone marrow mesenchymal stem cells (mBMSCs), due to low NO concentration, the expression of osteogenic-related osterix (OSX, the downstream gene of runt-related transcription factor 2 (IRUNX2)) and alkaline phosphatase (ALP) genes was increased in 4 days (Figure 6B) through the cyclic adenosine monophosphate-protein kinase A (cAMP-PKA) pathway (Kim et al., 2021), while the expression of osteoclast-related matrix metalloproteinase-9 (MMP-9) and MMP-13 (MMPs degrading the mineralized matrix) genes was reduced in 7 days. Some studies combine porous surfaces with the direct loading of immunomodulatory bioactive molecules or substances. BMSCs play a strong role in osteoimmunomodulation because of BMSC-derived exosomes (Exos) which carry biosignal molecules in paracrine secretion (Li et al., 2020). Exos regulate the transformation of macrophages from the M1 phenotype to M2 phenotype after binding to target cells. In addition, Exos carry a variety of miRNAs related to regulating osteogenesis, which can directly induce internal and external osteogenesis in the absence of cells (Zhai et al., 2020). Fan et al. (2021) bridged BMSC-derived Exos coating onto 3D porous PEEK via tannic acid (TA). RT-PCR and immunofluorescence results showed that the Exo-coated TA-SPEEK group could inhibit the expression of M1 surface markers (TNF- α and iNOS) and promoted the

expression of M2 surface markers (Arg-1 and IL-10). The study also found that compared with other groups, the expression of activator phosphorylated I κ B (p-I κ B) of nuclear factor-kappa B (NF- κ B) and the protein phosphorylation degree of downstream factor NF- κ B p65 in the Exo-loaded TA-SPEEK group were significantly downregulated, which fully proved that Exo-loaded TA-SPEEK promoted the anti-inflammatory M2 polarization of macrophages through the negative regulation of the NF- κ B pathway. Gut microbiota (GM) is crucial in regulating systemic health as its fermentation metabolite short-chain fatty acids (SCFAs) contain butyrate, which is known to have anti-inflammatory and immunomodulatory effects (Geva-Zatorsky et al., 2017). Yue et al. (2018) loaded sodium butyrate (SB) on the surface of SPEEK to study its regulation on macrophages under different stimuli. *In vitro* macrophage polarization assay showed that SB-SPEEK at low concentrations (≤ 1.0 mM) could increase the expression of M2 phenotype-related cytokines IL-4, IL-10, bone morphogenetic protein-2 (BMP-2), and VEGF (immunomodulatory mechanisms are shown in Figure 6C). However, it is important to pay attention to the potential cytotoxicity hazards of high SB concentrations.

Although there have been many studies on macrophage polarization, the mechanism is too complex and difficult to figure out, including M1/M2 phenotype interconversion, promotion or inhibition of the M1/M2 phenotype, and change in macrophage activity (Murray, 2017). It is worth noting that specific directional polarization M2 phenotype macrophages contain many subtypes, including M2a, M2b, M2c and M2d, and M2a, among which M2c can cause fibrous tissue proliferation (Lescoat et al., 2020). Therefore, in the future, we should find a new regulatory cellular signaling pathway and deeply explore the mechanism of macrophage polarization. Changing the host immune response to materials can determine the fate of dental implants and the outcome of bone integration.

4.4 Antioxidative property

Our biological system produces highly active molecules such as ROS and reactive nitrogen species (RNS) during fatty acid metabolism, aerobic metabolism, and when encountering environmental stimuli (Yu and Wang, 2022). The implantation inevitably leads to the release of ROS, such as hydroxyl radical (OH \cdot), hydrogen peroxide (H $_2$ O $_2$), and superoxide anion (O $_2^{\cdot-}$), thereby clearing aging cell debris, resisting pathogens, and protecting body homeostasis (Li et al., 2023). The human body's self-antioxidant defense system can maintain a balance between the oxidative and antioxidative modes by timely removing oxidation–reduction products but lacks the ability to reverse imbalance. Once factors cause imbalance, such as diabetes mellitus (DM), it will cause oxidative stress (OS) in the bone microenvironment around the implants. The excessive ROS produced by OS not only inhibits cell proliferation and differentiation, resulting in tissue damage, but also suppresses the release of VEGF, resulting in impaired capillary formation. In more severe cases, it can damage proteins and DNA (Wang et al., 2021a). Therefore, endowing PEEK dental implants with antioxidative capacity, reducing the impact of OS on nutrient supply, and

providing a stable microenvironment for bone integration are as important as osteogenic induction.

Chitosan (CS) has been proven to have antioxidant property that can quench hydroxyl and superoxide radicals (Li et al., 2012). Borgolte et al. (2022) proposed that coating CS with a 30% degree of substitution of benzophenone (30%BP-CS) on PEEK had the best free radical-quenching effect, which could increase the quenching of OH \cdot by three times compared to the control group. Furthermore, the quenching effect of 30%BP-CS was 1.5 times higher than that of CS (Figure 7A). The study found that the oxidation resistance of 30%BP-CS coating was not a good solution because the free radical quenching active surface of the coating was relatively smaller. Bone integration includes three synergistic and sequential processes: macrophage-mediated immune response, EC-induced angiogenesis, and osteoblast-induced osteogenesis (Patel et al., 2020). CS can control the multi-stage release of Zn $^{2+}$ and match it with various steps of bone integration. A covalently grafted multifunctional sustained-release coating composed of carboxylated graphene oxide (GC), Zn $^{2+}$, and CS on the surface of CFR-PEEK (CP/GC@Zn/CS) was achieved by Zhao et al. (2023), which completed the rapid release of Zn $^{2+}$ in the initial stage, sustained release of Zn $^{2+}$ in the middle stage, and slow release of Zn $^{2+}$ in the late stage. The coating played a role in immune regulation, angiogenesis, and osteogenesis in stages. The study found that the levels of ROS and RNS in macrophages of CP/GC@Zn/CS were the lowest, thus confirming that the coating can effectively inhibit OS in macrophages. During the removal of H $_2$ O $_2$, cerium dioxide nanoparticles (CeO $_2$ NPs) have been confirmed to have catalase-like activity and co-act as an oxygen buffer. Li et al. (2023) uniformly doped CeO $_2$ NPs in PEEK, and its ability to significantly reduce ROS levels in osteoblasts *in vitro* (Figure 7B shows antioxidant capacity tests) and better induce osteogenesis *in vivo* was verified. DM is an extremely common chronic disease, and the mitochondrial dynamics in the microenvironment surrounding the implant are imbalanced due to its sustained hyperglycemia and excessive ROS production (Willems et al., 2015). Therefore, the antioxidant activity of dental implants in DM patients is particularly important. Under high-glucose conditions, dynamin-related protein 1 (Drp1) produces excessive ROS and mitochondrial breakage, while the balance of mitochondrial membrane potential (MMP) resurgence protects the mitochondrial ultrastructure. Based on mitochondrial dynamics and DM osteogenesis, Wang et al. (2021a) loaded ZnO and Sr(OH) $_2$ on SPEEK. The study proposed for the first time that the release of Zn and Sr downregulated the Drp1 gene, restored MMP, eliminated ROS, and enhanced bone integration *in vivo* under DM conditions (Figures 7C, D show the mechanisms). Such a development of new PEEK implants targeting the mitochondrial regulatory ability of DM patients is of great significance.

In summary, reducing the degree of intracellular OS through PEEK modification is crucial for creating a favorable bone integration microenvironment. The production of ROS not only directly damages periodontal tissue but also releases chemokines that affect macrophage polarization and activate inflammatory response. Some studies suggest that the reduction of ROS can inhibit the M1 phenotype and promote the M2 phenotype (Yu and Wang, 2022). Therefore, regulating the body immune response by controlling the ROS level is worth further exploration. In

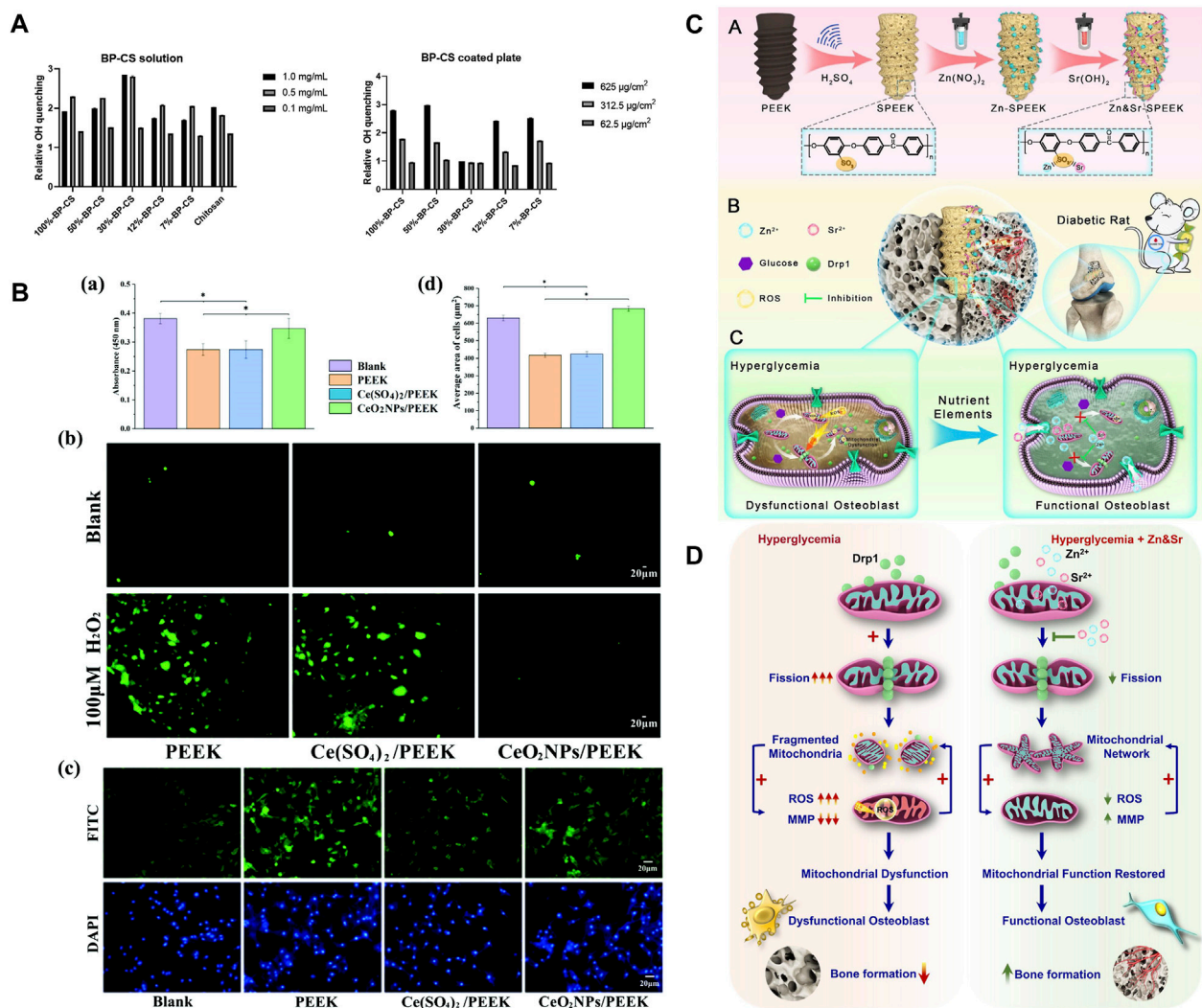


FIGURE 7

(A) Quenching of OH radicals by 30%BP-CS solutions (left) and coatings (right) (Borgolte et al., 2022). (B) Under OS conditions: (a) Cell viability, (b) ROS in cells, (c) cell morphology staining, and (d) average cell area (Li et al., 2023). (C) Material preparation and *in vivo* bone integration (Wang et al., 2021a). (D) Mechanism of tissue damage and targeting mitochondria to promote osteogenesis in DM (Wang et al., 2021b).

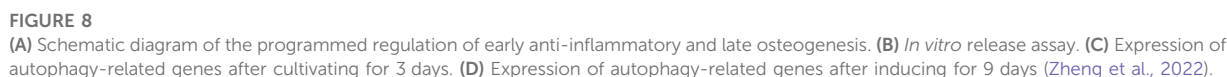
addition, antioxidant activity is particularly important in some special patients, such as elderly patients with high OS in the bone microenvironment and DM patients with mitochondrial dynamic imbalance.

4.5 Osteogenesis and anti-osteoclastogenesis

Targeting the recruitment of BMSCs around dental implants, promoting cell migration, adhesion, proliferation, and differentiation, and further promoting extracellular matrix (ECM) mineralization are eternal topics and the ultimate goal of dental implant materials. During bone integration, the formation of mineralized bone and the absorption and degradation of the bone matrix are inseparable factors that always work together. The modification of PEEK implants should not only focus on

inducing direct osteogenesis or anti-osteoclastogenesis but also on the immune inflammatory response mediated by macrophages that occurs early after implantation. The cross-regulation between the skeletal and immune systems is crucial for the dynamic balance between bone formation and bone resorption which guides successful bone integration (Chen et al., 2016). Therefore, this section introduces PEEK implant modification methods from the perspective of bone immunology that can simultaneously promote osteogenesis and anti-osteoclastogenesis.

The unique surface characteristics of implants have a direct impact on the proliferation and differentiation behavior of BMSCs. Yang et al. (2022) constructed a titanate nano-network structure on the PEEK surface (PEEK-TNS) by plasma sputtering and alkali treatment. PEEK-TNS significantly downregulated pro-inflammatory genes (TNF- α and IL-6) and upregulated anti-inflammatory genes (IL-10 and Arg-1), inducing the macrophages transformation from M1 to M2. While the



Bone integration is a delicate balance between bone resorption and bone regeneration. The improvement in the bone integration ability of PEEK dental implants should involve both osteogenesis and osteoclasts. Osteoclasts are produced by the monocyte macrophage system, so modification strategies targeting the

immune system can affect bone remodeling around implants. Such a modification strategy is particularly effective for OP patients as OP typically manifests as overactive osteoclast bone resorption (Zhao et al., 2022).

4.6 Angiogenesis

If an appropriate inflammatory response of the implant is a prerequisite for successful osseointegration, then angiogenesis is a concurrent event that assists osseointegration (Kusumbe et al., 2014). Being one of the key factors in osseointegration, angiogenesis is the process of vascular endothelial cell (EC) proliferation in pre-existing vessels to form sufficient blood vessels (Wang et al., 2013). As transportation pipelines, these new blood vessels deliver various nutrients, oxygen, stem cells, and even osteoinductive factors required for the new bone around the implant (Ito et al., 2006; Hutton and Grayson, 2014). However, research studies on PEEK modification methods dedicated to enhancing its angiogenic ability currently are not as extensive as inducing osteogenic differentiation.

Currently, the effects of most PEEK angiogenic modification methods are significant, but they do not take into account the basic health status of the host. It is well known that the successful rate of bone defect implantation in diabetes mellitus is low, partly due to the relatively high possibility of infection in the diabetes microenvironment (Mangialardi et al., 2019). Another important reason is that patients with diabetes usually produce excessive ROS, resulting in oxidative stress in the microenvironment around the implant (Rendra et al., 2019). This phenomenon can have a negative impact on the release of VEGF from ECs, thereby affecting angiogenesis and nutrient supply around the implant, ultimately resulting in failed osseointegration and implant loosening. Therefore, loading antioxidants on the PEEK surface is an important means to promote angiogenesis in diabetes patients. Huang et al. (2022) first loaded TA, Pluronic F127 (PF127), and gentamicin sulfate (GS) on sulfonated PEEK (SP@ (TA-GS/PF)*3) by LBL. TA is a natural antioxidant with five diethylene glycol ester groups, which not only has high stability and activity but also has been proven to be an effective drug therapy for clearing ROS (Wu et al., 2021). The results obtained by Huang showed that H₂O₂ in the SP@ (TA-GS/PF)*3 group caused the weakest damage to human umbilical vein endothelial cells (HUVECs) and promoted the secretion of VEGF by HUVECs after injury. Immunohistochemical staining and analysis further revealed that SP@ (TA-GS/PF)*3 exhibited excellent angiogenesis-promoting ability by enhancing the expression of angiogenic-related cytokines (CD31 and vWF). In addition, osteoblast differentiation was also enhanced, which was beneficial to osseointegration under diabetic conditions. For patients with hypercholesterolemia or cardiovascular disease, stable and easily available small-molecule statins are widely used because of their function of protecting ECs. In recent years, it has been proven that statins can regulate angiogenesis and osteogenesis through miRNAs (Li et al., 2016). Sun et al. (2022) loaded simvastatin on SPEEK (concentrations 0.55, 1.1, and 2.2 mg/mL, groups SP-SimL, SP-SimM, and SP-SimH, respectively). The porous structure of sulfonated PEEK can achieve the sustained release of drugs, and this local drug

delivery platform can suppress the systemic side effects of high-dose statins (such as hepatotoxicity and nephrotoxicity) and improve bioavailability (Liao, 2019). The drug release depended on the content and superficial area (Grassi et al., 2003), which was confirmed by the highest drug release rate of SP-SimM measured in the study. The drug concentration of SP-SimM was higher than that of SP-SimL, and the surface area was larger than SP-SimH. SP-SimM also had the strongest promoting effect on the formation of type-H vessels that regulated angiogenic-osteogenic coupling, which was contrary to the results of the miRNA-29cb² knockout (miR29cb^{2-/-}) mouse implantation experiment *in vivo*. This result provided direct evidence for the mechanism of simvastatin enhancing vascular regeneration. Previous studies by the author have shown that miRNA-29cb² regulates type-H vessels to achieve angiogenesis and bone regeneration by targeting hypoxia-inducible factor-3α (HIF-3α), while other studies have suggested that HIF-3α and hypoxia-inducible factor-1β (HIF-1β) are in a competitively binding relationship. The hypoxic environment can stimulate the binding of hypoxia response elements (HREs) of HIF-1β and the promoter regions of angiogenic-related genes (VEGF and collagen-2α (Col-2α)) which can promote neovascularization (Duan, 2016; Zhang and Kong, 2023). In this study, SP and SP-SimM were implanted into WT and miR29cb^{2-/-} mice, and quantitative analysis of HIF-3α and HIF-1β around implants revealed that miR29cb² knockout mice impaired the decreased HIF-3α expression in WT mice induced by simvastatin (Figure 9A). However, the mechanism of simvastatin on miRNA-29cb² is very complex; thus, more analysis factors and observation time are needed to obtain more reliable evidence. The implant adjustment strategies for other common systemic diseases are worth in-depth research, which will provide great convenience for mixing with other systemic disease patients and broaden the indications for dental implants.

Drugs for systemic diseases usually have low stability, less amount of active drugs reaching the implant area after first-pass elimination, and damage to the liver and kidney. Therefore, topical modified implants can suppress their controversy in bone healing.

Bioactive metal elements (Cu and Mg) have multiple functions such as antibacterial activity, promoting angiogenesis, and enhancing bone regeneration. It is a novel modification method to assemble metal and catecholamine on the surface of PEEK. As a member of catecholamine, PDA can respond to pH by changing charge and degradation, so it can mediate the controlled release of metal elements (Yan et al., 2021). This on-demand release avoids high doses and premature elution of metal ions, thereby alleviating concerns about metal toxicity and bacterial drug resistance (Yan et al., 2020). The PDA structure contains abundant hydrophilic groups, such as amino, imino, and carboxyl groups, which can not only reduce the contact angle of PEEK but also serve as a bridge to bond the coating of metal ions (Wei et al., 2023). Most importantly, when the pH changes, amino groups in the PDA are protonated, which weakens its internal force, and the grafted metal elements are released and eluted (Yan et al., 2021). Therefore, PDA is an excellent adhesive candidate for binding metal elements. Cu has been proven to maintain the stability of the hypoxia-inducible factor-1α (HIF-1α) structure, which can simulate a hypoxia stimulate and then increase VEGF secretion and activate endothelial nitric oxide synthase (eNOS) to release NO which can accelerate the maturation of

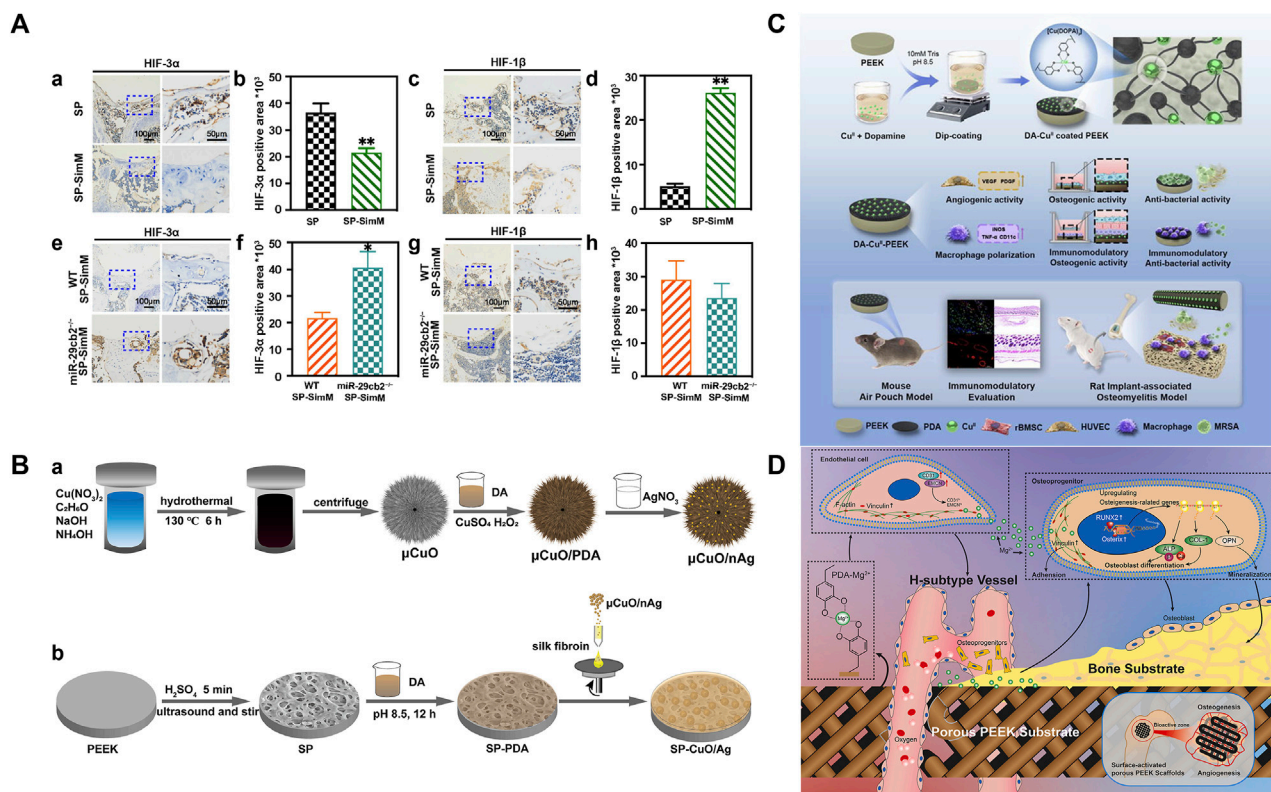


FIGURE 9

(A) Expression and quantification of HIF-3α in wild-type mice (a and b). Expression and quantification of HIF-1β in wild-type mice (c and d). Expression and quantification of HIF-3α in 29cb2^{-/-} mice (e and f). Expression and quantification of HIF-1β in 29cb2^{-/-} mice (g and h) (Huang et al., 2022). (B) Silver nanoparticles (nAg) are coated onto copper oxide microspheres (μCuO) through PDA; then, μCuO/nAg was loaded onto silk fibroin (SF) and spun onto the surface of SPEEK with polymerized PDA (SP-CuO/Ag) (Yan et al., 2020). (C) Schematic diagram of material synthesis and evaluation (Lyu, 2022). (D) Mechanism of Mg²⁺-PEEK scaffold osteogenesis and angiogenesis (Wei et al., 2023).

ECs (Murohara and Asahara, 2002; Urso and Maffia, 2015). Yan et al. (2020) coated silver nanoparticles (nAg) onto copper oxide microspheres (μCuO) through PDA; then, μCuO/nAg was spun onto the surface of SPEEK (Figures 9B). The study measured the production of NO, and the NO content of SP-CuO/Ag was more than twice that of the PEEK group, and the proliferation activity of HUVEC by the MTT method could also surpass that of the PEEK group on day 3. Furthermore, micro-computed tomography (micro-CT) showed that the coating was strong enough to withstand the stress generated by mechanical motion because there was no detachment after 12 weeks of implantation in the rabbit tibia. The author also invented another pH-responsive coating PDA-mediated co-deposition of citrate-copper nanoclusters (CCuNs) (Yan et al., 2021). It was unique in that the pH responsiveness was provided by PDA, and citrate also can induce angiogenesis, which could synergistically interact with Cu. The study found that the expression levels of HIF-1α, NO, VEGF, and iNOS in CCuNs were twice as high as those in Cu-loaded only samples, which might be related to the doubling of intracellular Cu levels caused by citrate (Finney et al., 2008). Due to angiogenesis and bone regeneration being coupled, there must be communication and crosstalk between ECs and osteoblastic cells (OBs) (Ramamany et al., 2016). A co-culture system of adipose-derived mesenchymal stem cells (Ad-MSCs) and HUVECs simulating the real *in vivo* environment was

established to evaluate the effect of CCuN-SPEEK on cell crosstalk. Compared with the single culture of Ad-MSCs, the secretion of ALP activity and collagen in the co-culture system increased by 20 times, while there was no calcium deposition on the surface of CCuN-PEEK. There is also a simple and efficient “one-pot” method for assembling Cu and DOPA on the surface of PEEK. Lyu (2022) directly coated a layer of PDA and CuII coordination complexes on the surface of PEEK (Figures 9C). If the concentration of metal ions exceeds a specific value, it will have cytotoxicity, and the critical concentration varies for different types of cells. The inductively coupled plasma-mass spectrometry (ICP-MS) results in the study showed that the highest concentration of Cu released by DA-CuII-coated PEEK was 0.2 ppm (not exceeding the toxicity level of most cells) (Kaplan and Maryon, 2016; Ning et al., 2016). In addition, all samples could promote the formation of tubes *in vitro* and the expression of angiogenic-related genes (VEGF, VEGF-A, and platelet-derived growth factor). There is increasing evidence that Mg²⁺, which is the fourth most abundant cation in the human body, can induce angiogenesis (Stegen et al., 2015). Wei et al. (2023) deposited Mg²⁺ on the surface of FDM-based PEEK using PDA as an adhesive. The pore size of PEEK scaffolds was 429 ± 37 μm, within the range of 300–500 μm, which was fully in favor of capillary ingrowth and substance exchange (Hutmacher, 2000). Type-H vessel is a special subtype of capillaries that couple angiogenesis

and osteogenesis at both time and space levels in a bone homeostasis environment (Peng et al., 2020). High expression levels of CD31 and endomucin (CD31hiEMCNhi) are their characteristics (Xu et al., 2018). The study found that Mg²⁺-PDA PEEK significantly upregulated the expression of CD31 and endomucin (EMCN) compared to uncoated PEEK. More importantly, micro-CT of rabbit femoral condyles implanted with scaffolds showed that the diameter and volume fraction of blood vessels were the highest at all detection time points in the Mg²⁺-PDA PEEK group. The results of observing the number, thickness, and morphology of blood vessels in hard tissue sectioning under the microscope were consistent with these (Figure 9D demonstrates the mechanism of sample osteogenesis and angiogenesis). In recent years, PDA has been widely used for the functional modification of material surfaces due to its good biocompatibility and simple production process. Even though the material substrate has a complex shape with 3D pores, the dense coating of the PDA film will not be affected. The metal ions grafted on the surface of PDA promote angiogenesis at low concentrations and play a bactericidal role at high concentrations. Therefore, strictly controlling the critical concentration of metal ions is of utmost importance. The development of a coating on the surface of PEEK that releases appropriate concentrations will effectively avoid problems of bacterial resistance and metal toxicity.

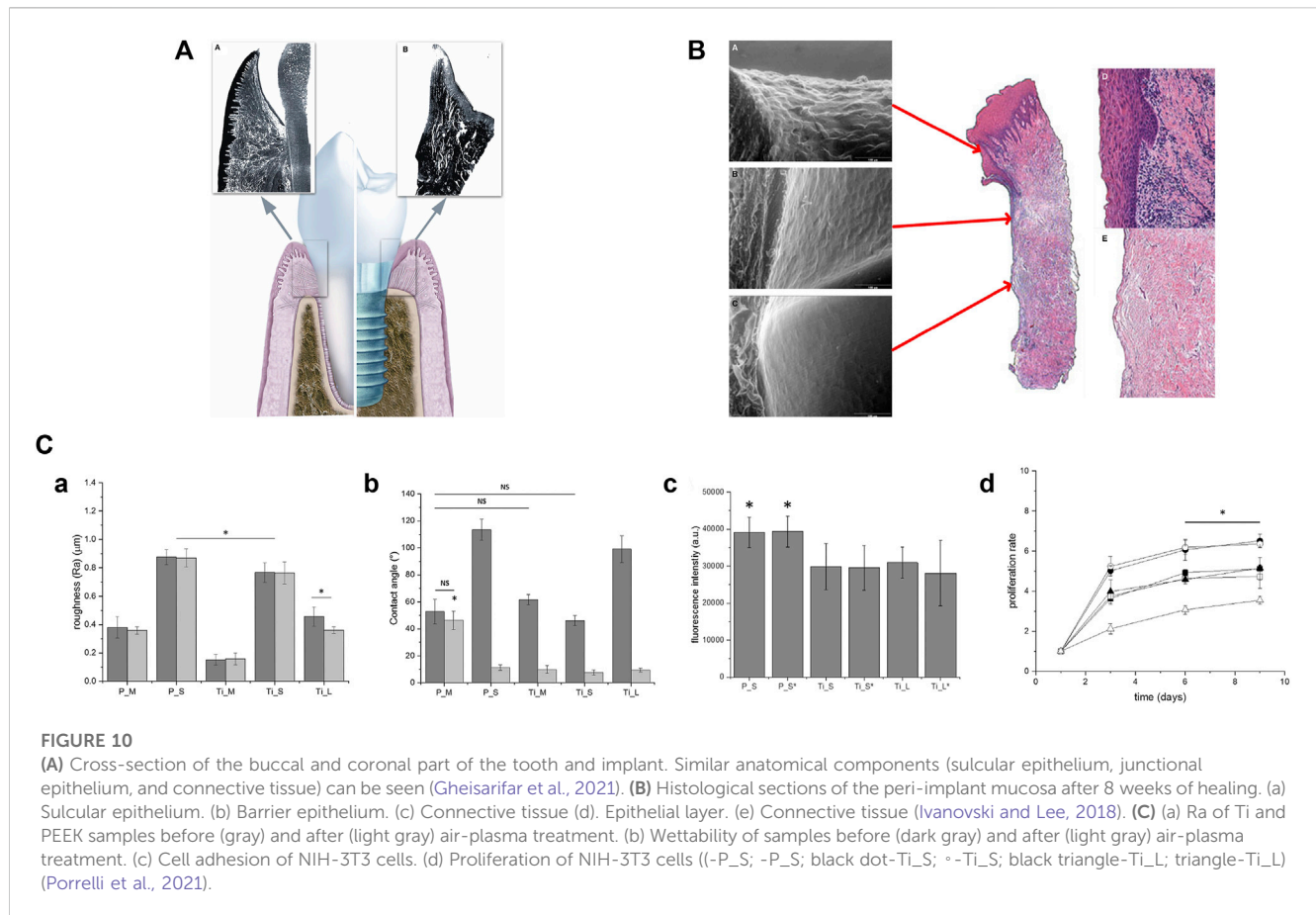
Vascular regeneration is one of the prerequisite steps to promote the initial stability of osseointegration, and the cortical intraductal network within the cortical bone is composed of transversal Volkmann's canals and longitudinal Haversian canals, which are intertwined with capillaries (Xie et al., 2014). Therefore, providing PEEK implants with the ability to generate blood vessels is crucial. Nevertheless, the chemical inertness of PEEK limits the reactive activity of ECs. At present, there are two main chains to enhance functional angiogenic response to PEEK implants: loading angiogenesis-related cytokines and stimulating endothelial cell autocrine VEGF. Obviously, the latter is a more advanced strategy because the loaded protein or polypeptide is easy to denature and inactivate after entering the complex internal environment and may also lead to ectopic vascularization. In addition, by combining modification methods to enhance the ability of angiogenesis and osteogenesis, solutions to the clinical application challenges of PEEK implants can be achieved, twice the result with half the effort.

4.7 Soft tissue adhesion

The long-term stability of dental implants is achieved not only by combining with bone tissue but also by adhering to periodontal soft tissue to achieve biological sealing. The epithelial junction is the first barrier of tissue around the implant (the histological structure of the periodontal tissue around the implant is shown in Figures 10A, B), which can effectively prevent bacterial invasion and prevent the occurrence of implantitis. Peng et al. (2021b) compared the adhesion of human oral fibroblast (HOF) cells on the surface of CAD-CAM bare PEEK and traditional implant materials Ti6Al4V and Y-TZP. The pseudopodium structures of HOF cells were apparent on the surface of PEEK, which showed

significant affinity. This is because the oxygen atoms with non-bonding pairs in the ether molecules of PEEK provide high polarity to increase the adhesion of cell receptors (integrins) on the cell membrane through adhesion proteins (fibronectin and collagen) (Ivanovski and Lee, 2018; Gheisarifar et al., 2021). However, due to the lack of biological activity of pure PEEK, which cannot be directly applied, scientists have explored many modification methods that can simultaneously improve the ability of osteogenesis and soft tissue adhesion.

It is known that laser etching, plasma treatment, and sandblasting can alter the surface morphology or introduce functional groups of PEEK and enhance its surface soft tissue cell adhesion. However, the three treatment methods have different effects. Femtosecond laser (FSL) uses a focused laser beam to form periodic features with micro/nano morphology on the material surface with high spatial and temporal resolution. For polymer materials, the maximum inhibition of surface oxidation is the greatest advantage of FSL. Xie et al. (2021) compared the effects of different powers of FSL (80 mW and 160 mW) on the behavior of soft tissue cells. SEM showed that unique submicro-nano structures were formed, and the number, adhesion, and proliferation of gingival epithelial (GE) cells were higher than those of pure PEEK; furthermore, the activity of 160FPK was more enhanced than that of 80FPK. At the same time, the adhesion, proliferation, and osteogenic-related gene expression of osteoblasts were also significantly enhanced. Consequently, laser etching plays an important role in increasing soft tissue sealing and bone regeneration. In order to compare the differences in the effects of laser etching and plasma treatment on human gingival fibroblasts (HGFs), Gheisarifar et al. (2021) treated PEEK with laser (PL), plasma (PP), and laser + plasma (PLP), respectively. It was found that laser etching had a stronger ability to improve HGF adhesion by increasing Ra, while plasma treatment had a better ability to increase HGF proliferation by reducing the water contact angle (WCA). However, some studies have shown that hydrophilicity is not conducive to the adhesion and diffusion of fibroblasts, which has been more clearly confirmed in the study of Porrelli et al. (2021). They proposed that, similar to laser etching, sandblasting also changed surface morphology to increase roughness. The adhesion of mouse embryonic fibroblast cells (NIH-3T3 cells) on the sandblasted PEEK surface was strongest and independent of hydrophilicity, while the proliferation of NIH-3T3 cells on the sandblasted Ti surface was strongest and only slightly dependent on hydrophilicity (Figure 10C). Therefore, roughness can affect the adhesion and proliferation of fibroblasts more than hydrophilicity. However, just as the study found that sandblasting PEEK could not inhibit biofilm formation, rough surfaces were also prone to bacterial adhesion, so multiple modification methods needed to be combined to achieve good bone integration of PEEK. Recently, a novel laser ablation (SyntheGra®, Geass s. r. l., Italy) has been applied to Ti, which forms micro particles that can simultaneously promote eukaryotic cell adhesion and inhibit bacterial adhesion (Ionescu et al., 2018). The effect of this treatment on PEEK surface is still unknown. There are also some coating techniques that can promote soft tissue adhesion. Pang et al. (2021) deposited a 400-nm-thick nanotantalum pentoxide (TP) coating on the surface of PEEK (PKTP) by vacuum evaporation (VE). The bioactive TP coating exhibited a



10-nm irregular protrusion on the surface of PEEK, which provided more sites for cell attachment. This was consistent with the enhanced adhesion and proliferation of HGEs on the PKTP surface. By the enhanced adhesion and proliferation of rBMSC, it could be seen that bone integration is also promoted. In addition to changing the morphology, preparing a tooth protein biomimetic coating can promote the adsorption of ECs. Periodontal tissue sealing is achieved by adhesion of epithelial cells to dentin and cementum. However, hemidesmosomes (HDs) and collagen I in dentin and cementum are in direct contact; furthermore, the basement membrane (BM) protein layer secreted by epithelial cells in HD is actually in direct contact with collagen I (Borradori and Sonnenberg, 1999; Bertassoni et al., 2012). Based on the aforementioned adhesion mechanism, Saad et al. (2022) prepared a layer of biomimetic collagen I coating on the surface of PEEK (Col-COOH-PEEK), with a Ti alloy as the control (Col-COOH-Ti). Through the results of label-free mass spectrometry (proteomics), it was found that the average protein score on Col-COOH-PEEK was five times that of Col-COOH-Ti, and the absorption of all BM proteins (laminin, nidogen, and fibronectin) was improved. Most importantly, laminins are proteins with the highest score and the only one with higher adsorption rates for Col-COOH-PEEK and Col-COOH-Ti than PEEK and Ti, which corresponded to the survival ability of keratinocyte epithelial cells on Col-COOH-PEEK being twice that of PEEK. That is, specific proteins have specific binding sites on collagen, and increasing the adsorption of specific

proteins is of great significance for the adhesion of epithelial cells. The method of covalently coupling proteins may increase their long-term applicability. However, in order to ensure its stability, it is worth exploring the protein stability in an enzyme-containing environment. In addition, it will be of great significance to compare the binding strength with physically adsorbed proteins in the future.

All together, we provided a comprehensive introduction to the modification methods of biomechanical, anti-inflammatory, antibacterial, angiogenic, antioxidant, osteogenic and anti-osteoclastogenic, and soft tissue adhesion properties of PEEK, which can greatly expand the practical clinical application of PEEK. In order to apply it to the human body, we should also further understand the mechanism of implant osseointegration to help explore more strategies to comprehensively improve the biological activity of PEEK, which requires the joint efforts of medicine, chemistry, regenerative medicine, and other disciplines. Future research focuses are as follows: (1) *in vitro* testing of biocompatibility and chemical stability requires simulating the dynamic environment *in vivo*; (2) preclinical research should strictly select animal models and try to select large animal models for testing; (3) in order to simulate the natural oral environment, cyclic loading should be added to the stability assessment of bone integration. This can be achieved through three-dimensional finite element analysis mentioned in the following section; and (4) conducting randomized controlled clinical trials.

5 Discussion and conclusion

At present, a large number of experiments have confirmed that PEEK can overcome the limitations brought about by biological inertness through surface or blending modification. This makes PEEK frequently seen in the biomedical field, such as spinal interbody fusion cages, artificial hip joints, and artificial knee joints in spinal surgery and orthopedics, as well as dental removable partial dentures, fixed dentures, implant abutments, and orthodontic arch wires in stomatology. However, it cannot be ignored that PEEK dental implants discussed in this article seem to be limited to the initial exploration stage and lack effective clinical implantation research and data. In other words, so far, no research has applied modified PEEK to humans, and only a small portion has studied its osseointegration in dog jaws. A considerable number of studies have reported successful cases of PEEK as other jawbone implant materials. EL Morsy et al. (2020) used PEEK as a barrier material for guided bone regeneration, while Li et al. (2022b) used PEEK for the treatment of mandibular segmental bone defects. Due to the excellent biocompatibility, mechanical properties, and processability of PEEK, there were no postoperative complications such as infection or displacement due to bearing chewing power in both studies. In the past decade, only two studies reported the effectiveness of PEEK dental implants. Marya et al. (2011) demonstrated three cases of PEEK dental implants. The author believed that the implants had the potential for osseointegration during the 6-month follow-up period. However, the report had a small number of participants and did not introduce evaluation methods. On the contrary, the report by Khonsari et al. (2014) showed three cases with severe postoperative infections, resulting in failed osseointegration and, ultimately, implant loosening. In summary, it still takes some time to translate the results created in the laboratory into practical clinical treatment, and this process may face many challenges, for example, the stability of surface chemical coating and the activity maintenance *in vivo*, whether degradable components can be accurately released at the target site, whether implants can play a role in the constantly changing oral environment, and the differences in habits and bones between patients. These issues are both crucial and difficult to solve. Therefore, animal models with strict standards should be established for testing to maximize the homogeneity of preclinical analysis.

Within the scope of this review, it can be concluded that PEEK is expected to replace traditional dental implant materials. Its aesthetics and low stress shielding make it have greater

application advantages in special patient groups. In addition, the stress distribution in the bone tissue around PEEK is not inferior to traditional implants and is even more suitable for patients with poor bone conditions. Furthermore, we summarized a series of parameters to optimize the performance of 3D-printed PEEK with complex porous structures. Finally, different functionalization strategies are proposed to enable patients to benefit from non-metallic implants. Currently, PEEK research studies usually lack large-scale animal testing and randomized controlled clinical trials. Combining with the complex specific dynamic environment of the human body, future research should focus on animal experiments and clinical research with cyclic loading and long observation time and combine multidisciplinary efforts to achieve a broader application of PEEK.

Author contributions

MC: writing—original draft. MR: investigation and writing—review and editing. YS: supervision and writing—review and editing. XL: supervision and writing—review and editing. HW: writing—review and editing.

Funding

The authors declare that no financial support was received for the research, authorship, and/or publication of this article.

Conflict of interest

The authors declare that the research was conducted in the absence of any commercial or financial relationships that could be construed as a potential conflict of interest.

Publisher's note

All claims expressed in this article are solely those of the authors and do not necessarily represent those of their affiliated organizations, or those of the publisher, the editors, and the reviewers. Any product that may be evaluated in this article, or claim that may be made by its manufacturer, is not guaranteed or endorsed by the publisher.

References

- Abranches, J., Zeng, L., Kajfasz, J. K., Palmer, S. R., Chakraborty, B., Wen, Z. T., et al. (2018). Biology of oral streptococci. *Microbiol. Spectr.* 6, 6–11. doi:10.1128/microbiolspec.GPP3-0042-2018
- Al-Mortadi, N., Bataineh, K., and Albakri, I. (2022). A three – dimensional finite element analysis of polyetheretherketone PEEK in dental implant prosthesis: a novel implant system. *TODENTJ* 16, e187421062203040. doi:10.2174/18742106-v16-e2203040
- AlOtaibi, N., Naudi, K., Conway, D., and Ayoub, A. (2020). The current state of PEEK implant osseointegration and future perspectives: a systematic review. *Eur. Cell Mater* 40, 1–20. doi:10.22203/eCM.v040a01
- Alqurashi, H., Khurshid, Z., Syed, A. U. Y., Rashid Habib, S., Rokaya, D., and Zafar, M. S. (2021). Polyetherketoneketone (PEKK): an emerging biomaterial for oral implants and dental prostheses. *J. Adv. Res.* 28, 87–95. doi:10.1016/j.jare.2020.09.004
- Alves, C. H., Russi, K. L., Rocha, N. C., Bastos, F., Darrieux, M., Parisotto, T. M., et al. (2022). Host-microbiome interactions regarding peri-implantitis and dental implant loss. *J. Transl. Med.* 20, 425. doi:10.1186/s12967-022-03636-9
- Anguiano-Sanchez, J., Martinez-Romero, O., Siller, H. R., Diaz-Elizondo, J. A., Flores-Villalba, E., and Rodriguez, C. A. (2016). Influence of PEEK coating on hip implant stress shielding: a finite element analysis. *Comput. Math. Methods Med.* 2016, 1–10. doi:10.1155/2016/6183679

- Araújo Nobre, M., Moura Guedes, C., Almeida, R., and Silva, A. (2021). Poly-ether-ether-ketone and implant dentistry: the future of mimicking natural dentition is now. *Polym. Int.* 70, 999–1001. doi:10.1002/pi.6212
- Azizi, B., Budimir, A., Bago, I., Mehmeti, B., Jakovljević, S., Kelmendi, J., et al. (2018). Antimicrobial efficacy of photodynamic therapy and light-activated disinfection on contaminated zirconia implants: an *in vitro* study. *Photodiagnosis Photodyn. Ther.* 21, 328–333. doi:10.1016/j.pdpdt.2018.01.017
- Bai, X., Zhang, X., Zhang, R., Chen, W., Wang, H., Xiao, J., et al. (2023). Immobilizing enoxacin on implant by polyvinyl butyral coating to promote osseointegration in osteoporosis with infection. *Mat. Des.* 227, 111749. doi:10.1016/j.matdes.2023.111749
- Barazanchi, A., Li, K. C., Al-Amleh, B., Lyons, K., and Waddell, J. N. (2017). Additive technology: update on current materials and applications in dentistry. *J. Prosthodont* 26, 156–163. doi:10.1111/jopr.12510
- Basgul, C., Thieringer, F. M., and Kurtz, S. M. (2021). Heat transfer-based non-isothermal healing model for the interfacial bonding strength of fused filament fabricated polyetheretherketone. *Addit. Manuf.* 46, 102097. doi:10.1016/j.addma.2021.102097
- Benli, M., Eker Gümüş, B., Kahraman, Y., Huck, O., and Özcan, M. (2020). Surface characterization and bonding properties of milled polyetheretherketone dental posts. *Odontology* 108, 596–606. doi:10.1007/s10266-020-00484-1
- Bertassoni, L. E., Orgel, J. P. R., Antipova, O., and Swain, M. V. (2012). The dentin organic matrix – limitations of restorative dentistry hidden on the nanometer scale. *Acta Biomater.* 8, 2419–2433. doi:10.1016/j.actbio.2012.02.022
- Bins-Ely, L., Suzuki, D., Magini, R., Benfatti, C. A. M., Teughels, W., Henriques, B., et al. (2020). Enhancing the bone healing on electrical stimuli through the dental implant. *Comput. Methods Biomech. Biomed. Engin* 23, 1041–1051. doi:10.1080/10255842.2020.1785437
- Bokare, A., Sanap, A., Pai, M., Sabharwal, S., and Athawale, A. A. (2013). Antibacterial activities of Nd doped and Ag coated TiO₂ nanoparticles under solar light irradiation. *Colloids Surf. B Biointerfaces* 102, 273–280. doi:10.1016/j.colsurfb.2012.08.030
- Boon, Y. D., Joshi, S. C., and Bhudolia, S. K. (2021). Review: filament winding and automated fiber placement with *in situ* consolidation for fiber reinforced thermoplastic polymer composites. *Polym. (Basel)* 13, 1951. doi:10.3390/polym13121951
- Borgolte, M., Riester, O., Quint, I., Blendinger, F., Bucher, V., Laufer, S., et al. (2022). Synthesis of a biocompatible benzophenone-substituted chitosan hydrogel as novel coating for PEEK with extraordinary strong antibacterial and anti-biofilm properties. *Mat. Today Chem.* 26, 101176. doi:10.1016/j.mtchem.2022.101176
- Borradori, L., and Sonnenberg, A. (1999). Structure and function of hemidesmosomes: more than simple adhesion complexes. *J. Invest. Dermatol* 112, 411–418. doi:10.1046/j.1523-1747.1999.00546.x
- Brown, B. N., Ratner, B. D., Goodman, S. B., Amar, S., and Badylak, S. F. (2012). Macrophage polarization: an opportunity for improved outcomes in biomaterials and regenerative medicine. *Biomaterials* 33, 3792–3802. doi:10.1016/j.biomaterials.2012.02.034
- Buwalda, S., Rotman, S., Eglin, D., Moriarty, F., Bethry, A., Garric, X., et al. (2020). Synergistic anti-fouling and bactericidal poly(ether ether ketone) surfaces via a one-step photomodification. *Mater Sci. Eng. C Mater Biol. Appl.* 111, 110811. doi:10.1016/j.msec.2020.110811
- Carpenter, R. D., Klosterhoff, B. S., Torstrick, F. B., Foley, K. T., Burkus, J. K., Lee, C. S. D., et al. (2018). Effect of porous orthopaedic implant material and structure on load sharing with simulated bone ingrowth: a finite element analysis comparing titanium and PEEK. *J. Mech. Behav. Biomed. Mater* 80, 68–76. doi:10.1016/j.jmbbm.2018.01.017
- Chai, H., Sang, S., Luo, Y., He, R., Yuan, X., and Zhang, X. (2022). Icarin-loaded sulfonated polyetheretherketone with osteogenesis promotion and osteoclastogenesis inhibition properties via immunomodulation for advanced osseointegration. *J. Mat. Chem. B* 10, 3531–3540. doi:10.1039/D1TB02802B
- Chang, B., Li, X., Parandoush, P., Ruan, S., Shen, C., and Lin, D. (2020). Additive manufacturing of continuous carbon fiber reinforced poly-ether-ether-ketone with ultrahigh mechanical properties. *Polym. Test.* 88, 106563. doi:10.1016/j.polymertesting.2020.106563
- Chen, D., Li, J., Yuan, Y., Gao, C., Cui, Y., Li, S., et al. (2021). A review of the polymer for cryogenic application: methods, mechanisms and perspectives. *Polymers* 13, 320. doi:10.3390/polym13030320
- Chen, J., Shi, X., Zhu, Y., Chen, Y., Gao, M., Gao, H., et al. (2020a). On-demand storage and release of antimicrobial peptides using Pandora's box-like nanotubes gated with a bacterial infection-responsive polymer. *Theranostics* 10, 109–122. doi:10.7150/thno.38388
- Chen, Q., Zhu, C., and Thouas, G. A. (2012). Progress and challenges in biomaterials used for bone tissue engineering: bioactive glasses and elastomeric composites. *Prog. Biomater.* 1, 2. doi:10.1186/2194-0517-1-2
- Chen, X., Ma, R., Min, J., Li, Z., Yu, P., and Yu, H. (2020b). Effect of PEEK and PTFE coatings in fatigue performance of dental implant retaining screw joint: an *in vitro* study. *J. Mech. Behav. Biomed. Mater* 103, 103530. doi:10.1016/j.jmbbm.2019.103530
- Chen, Z., Klein, T., Murray, R. Z., Crawford, R., Chang, J., Wu, C., et al. (2016). Osteoimmunomodulation for the development of advanced bone biomaterials. *Mat. Today.* 19, 304–321. doi:10.1016/j.mattod.2015.11.004
- Chokaree, P., Poovarodom, P., Chaijareenont, P., Yavirach, A., and Rungsiyakul, P. (2022). Biomaterials and clinical applications of customized healing abutment—a narrative review. *J. Funct. Biomater.* 13, 291. doi:10.3390/jfb13040291
- Chua, C. Y. X., Liu, H.-C., Di Trani, N., Susnjari, A., Ho, J., Scorrano, G., et al. (2021). Carbon fiber reinforced polymers for implantable medical devices. *Biomaterials* 271, 120719. doi:10.1016/j.biomaterials.2021.120719
- Comyn, J., Mascia, L., Xiao, G., and Parker, B. M. (1996). Plasma-treatment of polyetheretherketone (PEEK) for adhesive bonding. *Int. J. Adhes. Adhes.* 16, 97–104. doi:10.1016/0143-7496(96)89798-3
- Costa, R. R., and Mano, J. F. (2014). Polyelectrolyte multilayered assemblies in biomedical technologies. *Chem. Soc. Rev.* 43, 3453. doi:10.1039/c3cs60393h
- da Cruz, M. B., Marques, J. F., Peñarrieta-Juanito, G. M., Costa, M., Souza, J. C. M., Magini, R. S., et al. (2021). Bioactive-enhanced polyetheretherketone dental implant materials: mechanical characterization and cellular responses. *J. Oral Implantol.* 47, 9–17. doi:10.1563/aaid-joi-D-19-00172
- Delgado-Ruiz, R., and Romanos, G. (2018). Potential causes of titanium particle and ion release in implant dentistry: a systematic review. *Int. J. Mol. Sci.* 19, 3585. doi:10.3390/ijms19113585
- Deng, L., Deng, Y., and Xie, K. (2017). AgNPs-decorated 3D printed PEEK implant for infection control and bone repair. *Colloids Surf. B Biointerfaces* 160, 483–492. doi:10.1016/j.colsurfb.2017.09.061
- Deng, Y., Gao, X., Shi, X.-L., Lu, S., Yang, W., Duan, C., et al. (2020). Graphene oxide and adiponectin-functionalized sulfonated poly(etheretherketone) with effective osteogenicity and remotely repeatable photodisinfection. *Chem. Mat.* 32, 2180–2193. doi:10.1021/acs.chemmater.0c00290
- Diez-Pascual, A. M., and Diez-Vicente, A. L. (2015). Nano-TiO₂ reinforced PEEK/PEI blends as biomaterials for load-bearing implant applications. *ACS Appl. Mat. Interfaces* 7, 5561–5573. doi:10.1021/acsami.5b00210
- Ding, T., Kang, W., Li, J., Yu, L., and Ge, S. (2021). An *in situ* tissue engineering scaffold with growth factors combining angiogenesis and osteoimmunomodulatory functions for advanced periodontal bone regeneration. *J. Nanobiotechnol.* 19, 247. doi:10.1186/s12951-021-00992-4
- Duan, C. (2016). Hypoxia-inducible factor 3 biology: complexities and emerging themes. *Am. J. Physiol. Cell Physiol.* 310, C260–C269. doi:10.1152/ajpcell.00315.2015
- El Morsy, O. A., Barakat, A., Mekhemer, S., and Mounir, M. (2020). Assessment of 3-dimensional bone augmentation of severely atrophied maxillary alveolar ridges using patient-specific poly ether-ether ketone (PEEK) sheets. *Clin. Implant Dent. Relat. Res.* 22, 148–155. doi:10.1111/cid.12890
- Fan, L., Guan, P., Xiao, C., Wen, H., Wang, Q., Liu, C., et al. (2021). Exosome-functionalized polyetheretherketone-based implant with immunomodulatory property for enhancing osseointegration. *Bioact. Mater* 6, 2754–2766. doi:10.1016/j.bioactmat.2021.02.005
- Finney, L., Vogt, S., Fukai, T., and Glesne, D. (2008). COPPER AND ANGIOGENESIS: UNRAVELLING A RELATIONSHIP KEY TO CANCER PROGRESSION. *Clin. Exp. Pharmacol. Physiol.* 36 (1), 88–94. doi:10.1111/j.1440-1681.2008.04969.x
- Frost, H. M. (2004). A 2003 update of bone physiology and Wolff's law for clinicians. *Angle Orthod.* 74 (1), 3–15. doi:10.1043/0003-3219(2004)074<0003:AUOBPA>2.0.CO;2
- Fu, L., Jafari, H., Gießl, M., Yerneni, S. S., Sun, M., Wang, Z., et al. (2021a). Grafting polymer brushes by ATRP from functionalized poly(ether ether ketone) microparticles. *Polym. Adv. Technol.* 32, 3948–3954. doi:10.1002/pat.5405
- Fu, Q., Gabriel, M., Schmidt, F., Müller, W.-D., and Schwitala, A. D. (2021b). The impact of different low-pressure plasma types on the physical, chemical and biological surface properties of PEEK. *Dent. Mater* 37, e15–e22. doi:10.1016/j.dental.2020.09.020
- Gao, A., Hang, R., Li, W., Zhang, W., Li, P., Wang, G., et al. (2017). Linker-free covalent immobilization of heparin, SDF-1 α , and CD47 on PTFE surface for antithrombogenicity, endothelialization and anti-inflammation. *Biomaterials* 140, 201–211. doi:10.1016/j.biomaterials.2017.06.023
- Gao, A., Liao, Q., Xie, L., Wang, G., Zhang, W., Wu, Y., et al. (2020). Tuning the surface immunomodulatory functions of polyetheretherketone for enhanced osseointegration. *Biomaterials* 230, 119642. doi:10.1016/j.biomaterials.2019.119642
- Geva-Zatorsky, N., Sefik, E., Kua, L., Pasman, L., Tan, T. G., Ortiz-Lopez, A., et al. (2017). Mining the human gut microbiota for immunomodulatory organisms. *Cell* 168, 928–943.e11. doi:10.1016/j.cell.2017.01.022
- Gheisarifar, M., Thompson, G. A., Drago, C., Tabatabaei, F., and Rasoulianboroujeni, M. (2021). *In vitro* study of surface alterations to polyetheretherketone and titanium and their effect upon human gingival fibroblasts. *J. Prosthet. Dent.* 125, 155–164. doi:10.1016/j.prosdent.2019.12.012
- Golbang, A., Harkin-Jones, E., Wegryzn, M., Campbell, G., Archer, E., and McIlhagger, A. (2020). Production and characterization of PEEK/IF-WS2 nanocomposites for additive manufacturing: simultaneous improvement in processing characteristics and material properties. *Addit. Manuf.* 31, 100920. doi:10.1016/j.addma.2019.100920

- Grassi, M., Voinovich, D., Moneghini, M., Franceschini, E., Perissutti, B., and Filipovic-Grcic, J. (2003). Preparation and evaluation of a melt pelletised paracetamol/stearic acid sustained release delivery system. *J. Control Release* 88 (3), 381–391. doi:10.1016/s0168-3659(03)00011-7
- Guo, C., Lu, R., Wang, X., and Chen, S. (2021a). Antibacterial activity, biocompatibility and osteogenic differentiation of graphene oxide coating on 3D-network poly-ether-ether-ketone for orthopaedic implants. *J. Mater. Sci. Mater. Med.* 32, 135. doi:10.1007/s10856-021-06614-7
- Guo, F., Huang, S., Liu, N., Hu, M., Shi, C., Li, D., et al. (2022a). Evaluation of the mechanical properties and fit of 3D-printed polyetheretherketone removable partial dentures. *Dent. Mater. J.* 41, 816–823. doi:10.4012/dmj.2022-063
- Guo, G., Xu, Q., Zhu, C., Yu, J., Wang, Q., Tang, J., et al. (2021b). Dual-temporal bidirectional immunomodulation of PEEK-PEEK implants in vascular regeneration for sequentially enhancing antibacterial activity and osteogenesis. *Appl. Mat. Today*. 22, 100888. doi:10.1016/j.apmt.2020.100888
- Guo, L., Zou, Z., Smeets, R., Kluwe, L., Hartjen, P., Gosau, M., et al. (2022b). Attachment and osteogenic potential of dental pulp stem cells on non-thermal plasma and UV light treated titanium, zirconia and modified PEEK surfaces. *Materials* 15, 2225. doi:10.3390/ma15062225
- Guo, Y., Chen, C., Zhang, S., Ren, L., Zhao, Y., and Guo, W. (2022c). Mediation of mechanically adapted TiCu/TiCuN/CFR-PEEK implants in vascular regeneration to promote bone repair *in vitro* and *in vivo*. *J. Orthop. Transl.* 33, 107–119. doi:10.1016/j.jot.2022.02.008
- He, M., Chen, X., Guo, Z., Qiu, X., Yang, Y., Su, C., et al. (2019). Super tough graphene oxide reinforced polyetheretherketone for potential hard tissue repair applications. *Compos. Sci. Technol.* 174, 194–201. doi:10.1016/j.compscitech.2019.02.028
- He, M., Huang, Y., Xu, H., Feng, G., Liu, L., Li, Y., et al. (2021). Modification of polyetheretherketone implants: from enhancing bone integration to enabling multimodal therapeutics. *Acta Biomater.* 129, 18–32. doi:10.1016/j.actbio.2021.05.009
- Hou, Y., Yang, X., Liu, R., Zhao, D., Guo, C., Zhu, A., et al. (2020). Pathological mechanism of photodynamic therapy and photothermal therapy based on nanoparticles. *Int. J. Nanomedicine* 15, 6827–6838. doi:10.2147/IJN.S269321
- Huang, J., Lin, S., Bai, X., Li, W., Zhang, R., Miao, C., et al. (2022). Decorated polyetheretherketone implants with antibacterial and antioxidative effects through layer-by-layer nanoarchitectonics facilitate diabetic bone integration with infection. *ACS Appl. Mat. Interfaces* 14, 52579–52598. doi:10.1021/acsami.2c11574
- Huang, S., Wei, H., and Li, D. (2023). Additive manufacturing technologies in the oral implant clinic: a review of current applications and progress. *Front. Bioeng. Biotechnol.* 11, 1100155. doi:10.3389/fbioe.2023.1100155
- Hutmacher, D. W. (2000). Scaffolds in tissue engineering bone and cartilage. *Biomaterials* 21 (24), 2529–2543. doi:10.1016/s0142-9612(00)00121-6
- Hutton, D. L., and Grayson, W. L. (2014). Stem cell-based approaches to engineering vascularized bone. *Curr. Opin. Chem. Eng.* 3, 75–82. doi:10.1016/j.coche.2013.12.002
- Ionescu, A. C., Brambilla, E., Azzola, F., Ottobelli, M., Pellegrini, G., and Francetti, L. A. (2018). Laser microtextured titanium implant surfaces reduce *in vitro* and *in situ* oral biofilm formation. *PLoS One* 13, e0202262. doi:10.1371/journal.pone.0202262
- Ito, K., Yamada, Y., Naiki, T., and Ueda, M. (2006). Simultaneous implant placement and bone regeneration around dental implants using tissue-engineered bone with fibrin glue, mesenchymal stem cells and platelet-rich plasma. *Clin. Oral Implants Res.* 17, 579–586. doi:10.1111/j.1600-0501.2006.01246.x
- Ivanovski, S., and Lee, R. (2018). Comparison of peri-implant and periodontal marginal soft tissues in health and disease. *Periodontol.* 2000 76, 116–130. doi:10.1111/prd.12150
- Ji, C., Wang, B., Hu, J., Zhang, C., and Sun, Y. (2020). Effect of different preparation methods on mechanical behaviors of carbon fiber-reinforced PEEK-Titanium hybrid laminates. *Polym. Test.* 85, 106462. doi:10.1016/j.polymertesting.2020.106462
- Jiang, X., Yao, Y., Tang, W., Han, D., Zhang, L., Zhao, K., et al. (2020). Design of dental implants at materials level: an overview. *J. Biomed. Mater. Res.* 108, 1634–1661. doi:10.1002/jbm.a.36931
- Jiang, Y., Chen, Y., Song, Z., Tan, Z., and Cheng, J. (2021). Recent advances in design of antimicrobial peptides and polypeptides toward clinical translation. *Adv. Drug Deliv. Rev.* 170, 261–280. doi:10.1016/j.addr.2020.12.016
- Jovanović, M., Živić, M., and Milosavljević, M. (2021). A potential application of materials based on a polymer and CAD/CAM composite resins in prosthetic dentistry. *J. Prosthodont Res.* 65, 137–147. doi:10.2186/jpr.JPOR_2019_404
- Jung, H.-D., Jang, T.-S., Lee, J. E., Park, S. J., Son, Y., and Park, S.-H. (2019). Enhanced bioactivity of titanium-coated polyetheretherketone implants created by a high-temperature 3D printing process. *Biofabrication* 11, 045014. doi:10.1088/1758-5090/ab376b
- Kadambi, P., Luniya, P., and Dhatrik, P. (2021). Current advancements in polymer/polymer matrix composites for dental implants: a systematic review. *Mat. Today*. 46, 740–745. doi:10.1016/j.matpr.2020.12.396
- Kaplan, J. H., and Maryon, E. B. (2016). How mammalian cells acquire copper: an essential but potentially toxic metal. *Biophys. J.* 110, 7–13. doi:10.1016/j.bpj.2015.11.025
- Kargozar, S., Baino, F., Hamzehlou, S., Hamblin, M. R., and Mozafari, M. (2020). Nanotechnology for angiogenesis: opportunities and challenges. *Chem. Soc. Rev.* 49, 5008–5057. doi:10.1039/C8CS01021H
- Kessler, A., Hickel, R., and Reymus, M. (2020). 3D printing in dentistry—state of the art. *Oper. Dent.* 45, 30–40. doi:10.2341/18-229-L
- Khonsari, R. H., Berthier, P., Rouillon, T., Perrin, J.-P., and Corre, P. (2014). Severe infectious complications after PEEK-derived implant placement: report of three cases. *J. Oral Maxillofac. Surg.* 26, 477–482. doi:10.1016/j.joms.2013.04.006
- Kim, K. T., Eo, M. Y., Nguyen, T. T. H., and Kim, S. M. (2019). General review of titanium toxicity. *Int. J. Implant Dent.* 5, 10. doi:10.1186/s40729-019-0162-x
- Kim, S., Yuen, T., Iqbal, J., Rubin, M. R., and Zaidi, M. (2021). The NO-cGMP-PKG pathway in skeletal remodeling. *Ann. N. Y. Acad. Sci.* 1487, 21–30. doi:10.1111/nyas.14486
- Klopfleisch, R. (2016). Macrophage reaction against biomaterials in the mouse model – phenotypes, functions and markers. *Acta Biomater.* 43, 3–13. doi:10.1016/j.actbio.2016.07.003
- Korn, P., Elschner, C., Schulz, M. C., Range, U., Mai, R., and Scheler, U. (2015). MRI and dental implantology: two which do not exclude each other. *Biomaterials* 53, 634–645. doi:10.1016/j.biomaterials.2015.02.114
- Köse, T. E., Günaçar, D. N., Ateş, S. M., and Çağlar, İ. (2021). Artifact expression of polyetheretherketone in cone beam computed tomography: an *in vitro* study. *J. Prosthet. Dent.* 126, 793.e1–793.e5. doi:10.1016/j.prosdent.2021.09.028
- Koutouzis, T., Richardson, J., and Lundgren, T. (2011). Comparative soft and hard tissue responses to titanium and polymer healing abutments. *J. Oral Implantol.* 37, 174–182. doi:10.1563/AAID-JOI-D-09-00102.1
- Kruse, H. V., McKenzie, D. R., Clark, J. R., and Suchowerska, N. (2021). Plasma ion implantation of 3D-printed PEEK creates optimal host conditions for bone ongrowth and mineralisation. *Plasma Process. Polym.* 18, 2000219. doi:10.1002/ppap.202000219
- Kubo, Y., Wruck, C. J., Fragoulis, A., Drescher, W., Pape, H. C., Lichte, P., et al. (2019). Role of Nrf2 in fracture healing: clinical aspects of oxidative stress. *Calcif. Tissue Int.* 105, 341–352. doi:10.1007/s00223-019-00576-3
- Kurtz, S. M., and Devine, J. N. (2007). PEEK biomaterials in trauma, orthopedic, and spinal implants. *Biomaterials* 28, 4845–4869. doi:10.1016/j.biomaterials.2007.07.013
- Kusumbe, A. P., Ramasamy, S. K., and Adams, R. H. (2014). Coupling of angiogenesis and osteogenesis by a specific vessel subtype in bone. *Nature* 507, 323–328. doi:10.1038/nature13145
- Kyomoto, M., and Ishihara, K. (2009). Self-initiated surface graft polymerization of 2-methacryloyloxyethyl phosphorylcholine on poly(ether ether ketone) by photoirradiation. *ACS Appl. Mat. Interfaces* 1, 537–542. doi:10.1021/am800260t
- Lecaille, F., Chazeirat, T., Bojarski, K. K., Renault, J., Saidi, A., Prasad, V. G. N. V., et al. (2020). Rat cathepsin K: enzymatic specificity and regulation of its collagenolytic activity. *Biochim. Biophys. Acta Proteins Proteom* 1868, 140318. doi:10.1016/j.bbapap.2019.140318
- Lee, J., Byun, H., Madhurakkat Perikamana, S. K., Lee, S., and Shin, H. (2018). Current advances in immunomodulatory biomaterials for bone regeneration. *Adv. Healthc. Mater* 8 (4), e1801106. doi:10.1002/adhm.201801106
- Lee, W.-T., Koak, J.-Y., Lim, Y.-J., Kim, S.-K., Kwon, H.-B., and Kim, M.-J. (2012). Stress shielding and fatigue limits of poly-ether-ether-ketone dental implants. *J. Biomed. Mater. Res. B Appl. Biomater.* 100 (4), 1044–1052. doi:10.1002/jbm.b.32669
- Lescoat, A., Lelong, M., Jeljel, M., Piquet-Pellorce, C., Morzadec, C., Ballerie, A., et al. (2020). Combined anti-fibrotic and anti-inflammatory properties of JAK-inhibitors on macrophages *in vitro* and *in vivo*: perspectives for scleroderma-associated interstitial lung disease. *Biochem. Pharmacol.* 178, 114103. doi:10.1016/j.bcp.2020.114103
- Lethaus, B., Safi, Y., Ter Laak-Poort, M., Kloss-Brandstätter, A., Banki, F., Robbenmenke, C., et al. (2012). Cranioplasty with customized titanium and PEEK implants in a mechanical stress model. *J. Neurotrauma* 29, 1077–1083. doi:10.1089/neu.2011.1794
- Li, H., Wang, Z., Song, Q., Guo, M., Jiao, Z., Wang, Y., et al. (2023). Polyetheretherketone microspheres loaded with cerium dioxide nanoparticles mitigate damage from cellular oxidative stress and promote bone repair. *Mat. Des.* 225, 111426. doi:10.1016/j.matdes.2022.111426
- Li, K., Xing, R., Liu, S., Li, R., Qin, Y., Meng, X., et al. (2012). Separation of chito-oligomers with several degrees of polymerization and study of their antioxidant activity. *Carbohydr. Polym.* 88, 896–903. doi:10.1016/j.carbpol.2012.01.033
- Li, L., Zhang, Y., Mu, J., Chen, J., Zhang, C., Cao, H., et al. (2020). Transplantation of human mesenchymal stem-cell-derived exosomes immobilized in an adhesive hydrogel for effective treatment of spinal cord injury. *Nano Lett.* 20, 4298–4305. doi:10.1021/acs.nanolett.0c00929
- Li, M., Bai, J., Tao, H., Hao, L., Yin, W., Ren, X., et al. (2022a). Rational integration of defense and repair synergy on PEEK osteoimplants via biomimetic peptide clicking strategy. *Bioact. Mater* 8, 309–324. doi:10.1016/j.bioactmat.2021.07.002
- Li, P., Yin, Y.-L., Guo, T., Sun, X.-Y., Ma, H., Zhu, M.-L., et al. (2016). Inhibition of aberrant MicroRNA-133a expression in endothelial cells by statin prevents endothelial dysfunction by targeting GTP cyclohydrolase 1 *in vivo*. *Circulation* 134, 1752–1765. doi:10.1161/CIRCULATIONAHA.116.017949

- Li, S., Wang, T., Hu, J., Li, Z., Wang, B., Wang, L., et al. (2021). Surface porous polyether-ether-ketone based on three-dimensional printing for load-bearing orthopedic implant. *J. Mech. Behav. Biomed. Mater* 120, 104561. doi:10.1016/j.jmbbm.2021.104561
- Li, Y., Li, Z., Tian, L., Li, D., Lu, B., Shi, C., et al. (2022b). Clinical application of 3D-printed PEEK implants for repairing mandibular defects. *J. Craniomaxillofac Surg.* 50, 621–626. doi:10.1016/j.jcms.2022.06.002
- Liao, Y., Ouyang, L., Ci, L., Chen, B., Lv, D., Li, Q., et al. (2019). Pravastatin regulates host foreign-body reaction to polyetheretherketone implants via miR-29ab1-mediated SLIT3 upregulation. *Biomaterials* 203, 12–22. doi:10.1016/j.biomaterials.2019.02.027
- Ligon, S. C., Liska, R., Stampfl, J., Gurr, M., and Mülhaupt, R. (2017). Polymers for 3D printing and customized additive manufacturing. *Chem. Rev.* 117, 10212–10290. doi:10.1021/acs.chemrev.7b00074
- Lijnev, A., Elango, J., Gómez-López, V. M., Pérez-Albacete Martínez, C., Granero Marín, J. M., and Maté Sánchez De Val, J. E. (2022). Antibacterial and proliferative effects of NaOH-coated titanium, zirconia, and ceramic-reinforced PEEK dental composites on bone marrow mesenchymal stem cells. *Pharmaceutics* 15, 98. doi:10.3390/pharmaceutics15010098
- Liu, C., Bai, J., Wang, Y., Chen, L., Wang, D., Ni, S., et al. (2021a). The effects of three cold plasma treatments on the osteogenic activity and antibacterial property of PEEK. *Dent. Mater* 37, 81–93. doi:10.1016/j.dental.2020.10.007
- Liu, C., Lin, J., Tang, L., Liu, Z., Jiang, Z., and Lian, K. (2021b). Design of metal-polymer structure for dental implants with stiffness adaptable to alveolar bone. *Compos. Commun.* 24, 100660. doi:10.1016/j.coco.2021.100660
- Liu, X., Ouyang, L., Chen, L., Qiao, Y., Ma, X., Xu, G., et al. (2022). Hydroxyapatite composited PEEK with 3D porous surface enhances osteoblast differentiation through mediating NO by macrophage. *Regen. Biomater.* 9, rbab076. doi:10.1093/rb/rbab076
- Luo, C., Liu, Y., Peng, B., Chen, M., Liu, Z., Li, Z., et al. (2023). PEEK for oral applications: recent advances in mechanical and adhesive properties. *Polymers* 15, 386. doi:10.3390/polym15020386
- Lv, C., Shen, H., Liu, J., Wu, D., Qu, E., and Liu, S. (2022). Properties of 3D printing fiber-reinforced geopolymers based on interlayer bonding and anisotropy. *Materials* 15, 8032. doi:10.3390/ma15228032
- Ly, Z., Zhao, Y., Huo, S., Wang, F., Meng, X., Yuan, Z., et al. (2022). Mussel-inspired dopamine-CuII coated polyetheretherketone surface with direct and immunomodulatory effect to facilitate osteogenesis, angiogenesis, and antibacterial ability. *Mat. Des.* 222, 111069. doi:10.1016/j.matdes.2022.111069
- Ma, T., Zhang, J., Sun, S., Meng, W., Zhang, Y., and Wu, J. (2023). Current treatment methods to improve the bioactivity and bonding strength of PEEK for dental application: a systematic review. *Eur. Polym. J.* 183, 111757. doi:10.1016/j.eurpolymj.2022.111757
- Ma, Z., Zhao, X., Zhao, J., Zhao, Z., Wang, Q., and Zhang, C. (2020). Biologically modified polyether ether ketone as dental implant material. *Front. Bioeng. Biotechnol.* 8, 620537. doi:10.3389/fbioe.2020.620537
- Maló, P., Rangert, B., and Nobre, M. (2003). All-on-Four immediate-function concept with brånemark System® implants for completely edentulous mandibles: a retrospective clinical study. *Clin. Implant Dent. Relat. Res.* 5, 2–9. doi:10.1111/j.1708-8208.2003.tb00010.x
- Maloo, L. M., Toshiwal, S. H., Reche, A., Paul, P., and Wanjar, M. B. (2022). A sneak peek toward polyaryletherketone (PAEK) polymer: a review. *Cureus* 14, e31042. doi:10.7759/cureus.13042
- Mangialardi, G., Ferland-McCollough, D., Maselli, D., Santopalo, M., Cordaro, A., Spinetti, G., et al. (2019). Bone marrow pericyte dysfunction in individuals with type 2 diabetes. *Diabetologia* 62, 1275–1290. doi:10.1007/s00125-019-4865-6
- Manzoor, F., Golbang, A., Jindal, S., Dixon, D., McIlhagger, A., Harkin-Jones, E., et al. (2021). 3D printed PEEK/HA composites for bone tissue engineering applications: effect of material formulation on mechanical performance and bioactive potential. *J. Mech. Behav. Biomed. Mater* 121, 104601. doi:10.1016/j.jmbbm.2021.104601
- Marin, E., Boschetto, F., Zanolco, M., Adachi, T., Toyama, N., Zhu, W., et al. (2020). KUSA-A1 mesenchymal stem cells response to PEEK-Si3N4 composites. *Mat. Today Chem.* 17, 100316. doi:10.1016/j.mtchem.2020.100316
- Marya, K., Dua, J., Chawla, S., Sonoo, P. R., Aggarwal, A., and Singh, V. (2011). Polyetheretherketone (PEEK) dental implants: a case for immediate loading. *Int. J. Oral Implantol. Clin. Res.* 2, 97–103. doi:10.5005/jp-journals-10012-1043
- Mishra, S., and Chowdhary, R. (2019). PEEK materials as an alternative to titanium in dental implants: a systematic review. *Clin. Implant Dent. Relat. Res.* 21, 208–222. doi:10.1111/cid.12706
- Murohara, T., and Asahara, T. (2002). Nitric oxide and angiogenesis in cardiovascular disease. *Antioxid. Redox Signal* 4, 825–831. doi:10.1089/152308602760598981
- Murray, P. J. (2017). Macrophage polarization. *Annu. Rev. Physiol.* 79, 541–566. doi:10.1146/annurev-physiol-022516-034339
- Muthusamy Subramanian, A. V., and Thanigachalam, M. (2022). Mechanical performances, *in-vitro* antibacterial study and bone stress prediction of ceramic particulates filled polyether ether ketone nanocomposites for medical applications. *J. Polym. Res.* 29, 318. doi:10.1007/s10965-022-03180-6
- Nagels, J., Stokdijk, M., and Rozing, P. M. (2003). Stress shielding and bone resorption in shoulder arthroplasty. *J. Shoulder Elb. Surg.* 12, 35–39. doi:10.1067/mse.2003.22
- Najeeb, S., Bds, Z. K., Bds, S. Z., and Bds, M. S. Z. (2016a). Bioactivity and osseointegration of PEEK are inferior to those of titanium: a systematic review. *J. Oral Implantol.* 42, 512–516. doi:10.1563/aaid-joi-D-16-00072
- Najeeb, S., Zafar, M. S., Khurshid, Z., and Siddiqui, F. (2016b). Applications of polyetheretherketone (PEEK) in oral implantology and prosthodontics. *J. Prosthodont Res.* 60, 12–19. doi:10.1016/j.jpor.2015.10.001
- Ning, C., Wang, X., Li, L., Zhu, Y., Li, M., Yu, P., et al. (2016). Concentration ranges of antibacterial cations for showing the highest antibacterial efficacy but the least cytotoxicity against mammalian cells: implications for a new antibacterial mechanism. *Chem. Res. Toxicol.* 28 (9), 1815–1822. doi:10.1021/acs.chemrestox.5b00258
- Noronha Oliveira, M., Schunemann, W. V. H., Mathew, M. T., Henriques, B., Magini, R. S., Teughels, W., et al. (2018). Can degradation products released from dental implants affect peri-implant tissues? *J. Periodont Res.* 53, 1–11. doi:10.1111/jre.12479
- Olivares-Navarrete, R., Hyzy, S. L., Slosar, P. J., Schneider, J. M., Schwartz, Z., and Boyan, B. D. (2015). Implant materials generate different peri-implant inflammatory factors: poly-ether-ether-ketone promotes fibrosis and microtextured titanium promotes osteogenic factors. *Spine (Phila Pa 1976)* 40, 399–404. doi:10.1097/BRS.0000000000000778
- Panayotov, I. V., Orti, V., Cuisinier, F., and Yachouh, J. (2016). Polyetheretherketone (PEEK) for medical applications. *J. Mater Sci. Mater Med.* 27, 118. doi:10.1007/s10856-016-5731-4
- Pang, Z., Pan, Z., Ma, M., Xu, Z., Mei, S., Jiang, Z., et al. (2021). Nanostructured coating of non-crystalline tantalum pentoxide on polyetheretherketone enhances RBMS cells/HGE cells adhesion. *Int. J. Nanomedicine* 16, 725–740. doi:10.2147/IJN.S286643
- Papathanasiou, I., Kamposiora, P., Papavasiliou, G., and Ferrari, M. (2020). The use of PEEK in digital prosthodontics: a narrative review. *BMC Oral Health* 20, 217. doi:10.1186/s12903-020-01202-7
- Patel, K. D., Kim, T.-H., Mandakhbayar, N., Singh, R. K., Jang, J.-H., Lee, J.-H., et al. (2020). Coating biopolymer nanofibers with carbon nanotubes accelerates tissue healing and bone regeneration through orchestrated cell- and tissue-regulatory responses. *Acta Biomater.* 108, 97–110. doi:10.1016/j.actbio.2020.03.012
- Peng, T.-Y., Lin, D.-J., Mine, Y., Tasi, C.-Y., Li, P.-J., Shih, Y.-H., et al. (2021a). Biofilm Formation on the surface of (Poly)Ether-Ether-Ketone and *in vitro* antimicrobial efficacy of photodynamic therapy on peri-implant mucositis. *Polymers* 13, 940. doi:10.3390/polym13060940
- Peng, T.-Y., Shih, Y.-H., Hsia, S.-M., Wang, T.-H., Li, P.-J., Lin, D.-J., et al. (2021b). *In vitro* assessment of the cell metabolic activity, cytotoxicity, cell attachment, and inflammatory reaction of human oral fibroblasts on polyetheretherketone (PEEK) implant-abutment. *Polymers* 13, 2995. doi:10.3390/polym13172995
- Peng, Y., Wu, S., Li, Y., and Crane, J. L. (2020). Type H blood vessels in bone modeling and remodeling. *Theranostics* 10 (1), 426–436. doi:10.7150/thno.34126
- Periasamy, S., and Kolenbrander, P. E. (2010). Central role of the early colonizer veillonella sp. in establishing multispecies biofilm communities with initial, middle, and late colonizers of enamel. *J. Bacteriol.* 192, 2965–2972. doi:10.1128/JB.01631-09
- Pezzotti, G., Marin, E., Adachi, T., Lerussi, F., Rondinella, A., Boschetto, F., et al. (2018). Incorporating Si₃N₄ into PEEK to produce antibacterial, osteoconductive, and radiolucent spinal implants. *Macromol. Biosci.* 18, 1800033. doi:10.1002/mabi.201800033
- Pidhatika, B., Widayana, V. T., Nalam, P. C., Swasono, Y. A., and Ardhani, R. (2022). Surface modifications of high-performance polymer polyetheretherketone (PEEK) to improve its biological performance in dentistry. *Polymers* 14, 5526. doi:10.3390/polym14245526
- Porrelli, D., Mardirossian, M., Crapisi, N., Urban, M., Ulian, N. A., Bevilacqua, L., et al. (2021). Polyetheretherketone and titanium surface treatments to modify roughness and wettability – improvement of bioactivity and antibacterial properties. *J. Mater Sci. Technol.* 95, 213–224. doi:10.1016/j.jmst.2021.04.023
- Qin, W., Li, Y., Ma, J., Liang, Q., Cui, X., Jia, H., et al. (2020). Osseointegration and biosafety of graphene oxide wrapped porous CF/PEEK composites as implantable materials: the role of surface structure and chemistry. *Dent. Mater* 36, 1289–1302. doi:10.1016/j.dental.2020.06.004
- Qin, W., Li, Y., Ma, J., Liang, Q., and Tang, B. (2019). Mechanical properties and cytotoxicity of hierarchical carbon fiber-reinforced poly (ether-ether-ketone) composites used as implant materials. *J. Mech. Behav. Biomed. Mater* 89, 227–233. doi:10.1016/j.jmbbm.2018.09.040
- Ramasamy, S. K., Kusumbe, A. P., Wang, L., and Adams, R. H. (2016). Endothelial Notch activity promotes angiogenesis and osteogenesis in bone. *Nature* 507 (7492), 376–380. doi:10.1038/nature13146
- Ren, L., Tang, S., Shen, X., Gao, C., Jung, Y. K., Wang, D., et al. (2020a). Influences of sodium tantalite submicro-particles in polyetheretherketone based composites on behaviors of rBMSCs/HGE-1 cells for dental application. *Colloids Surf. B Biointerfaces* 188, 110723. doi:10.1016/j.colsurfb.2019.110723
- Ren, X., Gao, R., Van Der Mei, H. C., Ren, Y., Peterson, B. W., and Busscher, H. J. (2020b). Eradicating infecting bacteria while maintaining tissue integration on

photothermal nanoparticle-coated titanium surfaces. *ACS Appl. Mat. Interfaces*. 12, 34610–34619. doi:10.1021/acsaami.0c08592

Rendra, E., Riabov, V., Mossel, D. M., Sevastyanova, T., Harmsen, M. C., and Kzhyskowska, J. (2019). Reactive oxygen species (ROS) in macrophage activation and function in diabetes. *Immunobiology* 224, 242–253. doi:10.1016/j.imbio.2018.11.010

Renvert, S., Roos-Jansäker, A.-M., and Claffey, N. (2008). Non-surgical treatment of peri-implant mucositis and peri-implantitis: a literature review. *J. Clin. Periodontol.* 35, 305–315. doi:10.1111/j.1600-051X.2008.01276.x

Robertson, C. A., Evans, D. H., and Abrahamse, H. (2009). Photodynamic therapy (PDT): a short review on cellular mechanisms and cancer research applications for PDT. *J. Photochem Photobiol. B* 96, 1–8. doi:10.1016/j.jphotobiol.2009.04.001

Rodzeń, K., Harkin-Jones, E., Wegrzyn, M., Sharma, P. K., and Zhigunov, A. (2021a). Improvement of the layer-layer adhesion in FFF 3D printed PEEK/carbon fibre composites. *Compos. Part A Appl. Sci. Manuf.* 149, 106532. doi:10.1016/j.compositesa.2021.106532

Rodzeń, K., Sharma, P. K., McIlhagger, A., Mokhtari, M., Dave, F., Tormey, D., et al. (2021b). The direct 3D printing of functional PEEK/hydroxyapatite composites via a fused filament fabrication approach. *Polymers* 13, 545. doi:10.3390/polym13040545

Saad, A., Penaloza Arias, C., Wang, M., ElKashty, O., Brambilla, D., Tamimi, F., et al. (2022). Biomimetic strategy to enhance epithelial cell viability and spreading on PEEK implants. *ACS Biomater. Sci. Eng.* 8, 5129–5144. doi:10.1021/acsbmaterials.2c00764

Sagomonyants, K. B., Jarman-Smith, M. L., Devine, J. N., Aronow, M. S., and Gronowicz, G. A. (2008). The *in vitro* response of human osteoblasts to polyetheretherketone (PEEK) substrates compared to commercially pure titanium. *Biomaterials* 29, 1563–1572. doi:10.1016/j.biomaterials.2007.12.001

Salmi, M. (2021). Additive manufacturing processes in medical applications. *Materials* 14, 191. doi:10.3390/ma14010191

Sarot, J. R., Contar, C. M. M., Cruz, A. C. C. D., and De Souza Magini, R. (2010). Evaluation of the stress distribution in CFR-PEEK dental implants by the three-dimensional finite element method. *J. Mater. Sci. Mater. Med.* 21, 2079–2085. doi:10.1007/s10856-010-4084-7

Schwitalla, A. D., Abou-Emara, M., Spintig, T., Lackmann, J., and Müller, W. D. (2015). Finite element analysis of the biomechanical effects of PEEK dental implants on the peri-implant bone. *J. Biomech.* 48, 1–7. doi:10.1016/j.jbiomech.2014.11.017

Schwitalla, A., and Müller, W.-D. (2013). PEEK dental implants: a review of the literature. *J. Oral Implantol.* 39, 743–749. doi:10.1563/AAID-JOI-D-11-00002

Searle, O. B., and Pfeiffer, R. H. (1985). Victrex® poly(ethersulfone) (PES) and Victrex® poly(etheretherketone) (PEEK). *Polym. Eng. Sci.* 25, 474–476. doi:10.1002/pen.760250808

Shash, Y. H., El-Wakad, M. T., Eldosoky, M. A. A., and Dohiem, M. M. (2022). Evaluation of stress and strain on mandible caused using “All-on-Four” system from PEEK in hybrid prosthesis: finite-element analysis. *Odontology* 111 (3), 618–629. doi:10.1007/s10266-022-00771-z

Shen, H., Shi, J., Zhi, Y., Yang, X., Yuan, Y., Si, J., et al. (2021). Improved BMP2-CPC-stimulated osteogenesis *in vitro* and *in vivo* via modulation of macrophage polarization. *Mater. Sci. Eng. C Mater. Biol. Appl.* 118, 111471. doi:10.1016/j.msec.2020.111471

Sibata, C. H., Colussi, V. C., Oleinick, N. L., and Kinsella, T. J. (2000). Photodynamic therapy: a new concept in medical treatment. *Braz J. Med. Biol. Res.* 33 (8), 869–880. doi:10.1590/s0100-879x200000800002

Sicilia, A., Cuesta, S., Coma, G., Arregui, I., Guisasaola, C., Ruiz, E., et al. (2008). Titanium allergy in dental implant patients: a clinical study on 1500 consecutive patients. *Clin. Oral Implants Res.* 19, 823–835. doi:10.1111/j.1600-0501.2008.01544.x

Singh, S., Prakash, C., and Ramakrishna, S. (2019). 3D printing of polyether-etherketone for biomedical applications. *Eur. Polym. J.* 114, 234–248. doi:10.1016/j.eurpolymj.2019.02.035

Sonaye, S. Y., Bokam, V. K., Saini, A., Nayak, V. V., Witek, L., Coelho, P. G., et al. (2022). Patient-specific 3D printed Poly-ether-ether-ketone (PEEK) dental implant system. *J. Mech. Behav. Biomed. Mater* 136, 105510. doi:10.1016/j.jmbbm.2022.105510

Spiller, K. L., Nassiri, S., Witherel, C. E., Anfang, R. R., Ng, J., Nakazawa, K. R., et al. (2015). Sequential delivery of immunomodulatory cytokines to facilitate the M1-to-M2 transition of macrophages and enhance vascularization of bone scaffolds. *Biomaterials* 37, 194–207. doi:10.1016/j.biomaterials.2014.10.017

Sridharan, R., Cameron, A. R., Kelly, D. J., Kearney, C. J., and O'Brien, F. J. (2015). Biomaterial based modulation of macrophage polarization: a review and suggested design principles. *Mat. Today*. 18, 313–325. doi:10.1016/j.mattod.2015.01.019

Steenberghe, D. V., Quirynen, M., Naert, I., Maffei, G., and Jacobs, R. (2001). Marginal bone loss around implants retaining hinging mandibular overdentures, at 4-8- and 12-years follow-up: bone loss around implants retaining overdentures. *J. Clin. Periodontol.* 28, 628–633. doi:10.1034/j.1600-051x.2001.028007628.x

Stegen, S., Gastel, N. V., and Carmeliet, G. (2015). Bringing new life to damaged bone: the importance of angiogenesis in bone repair and regeneration. *Bone* 70, 19–27. doi:10.1016/j.bone.2014.09.017

Sumner, D. R. (2015). Long-term implant fixation and stress-shielding in total hip replacement. *J. Biomech.* 48, 797–800. doi:10.1016/j.jbiomech.2014.12.021

Sun, Y., Liu, X., Zeng, X., Wang, L., Jin, Z., Kelvin, W. K., et al. (2022). Simvastatin-loaded sulfonated PEEK enhances angiogenesis and osteogenesis via miR-29cb2-mediated HIF-3α downregulation. *Chem. Eng. J.* 448 (15), 137738. doi:10.1016/j.cej.2022.137738

Takayanagi, H. (2007). Osteoimmunology: shared mechanisms and crosstalk between the immune and bone systems. *Nat. Rev. Immunol.* 7, 292–304. doi:10.1038/nri2062

Tian, Y., Chen, C., Xu, X., Wang, J., Hou, X., Li, K., et al. (2021). A review of 3D printing in dentistry: technologies, affecting factors, and applications. *Scanning* 2021, 1–19. doi:10.1155/2021/9950131

Toth, J. M., Wang, M., Estes, B. T., Scifert, J. L., Seim, H. B., and Turner, A. S. (2006). Polyetheretherketone as a biomaterial for spinal applications. *Biomaterials* 27, 324–334. doi:10.1016/j.biomaterials.2005.07.011

Urso, E., and Maffia, M. (2015). Behind the link between copper and angiogenesis: established mechanisms and an overview on the role of vascular copper transport systems. *J. Vasc. Res.* 52, 172–196. doi:10.1159/000438485

Vassey, M. J., Figueredo, G. P., Scurr, D. J., Vasilevich, A. S., Vermeulen, S., Carlier, A., et al. (2020). Immune modulation by design: using topography to control human monocyte attachment and macrophage differentiation. *Adv. Sci. (Weinh.)* 7, 1903392. doi:10.1002/advs.201903392

Wan, T., Jiao, Z., Guo, M., Wang, Z., Wan, Y., Lin, K., et al. (2020). Gaseous sulfur trioxide induced controllable sulfonation promoting biomineralization and osseointegration of polyetheretherketone implants. *Bioact. Mat.* 5, 1004–1017. doi:10.1016/j.bioactmat.2020.06.011

Wang, C., Lin, K., Chang, J., and Sun, J. (2013). Osteogenesis and angiogenesis induced by porous β-CaSiO₃/PDLGA composite scaffold via activation of AMPK/ERK1/2 and PI3K/Akt pathways. *Biomaterials* 34, 64–77. doi:10.1016/j.biomaterials.2012.09.021

Wang, D., Zou, Y., Tao, L., Zhang, Y., Liu, Z., Du, S., et al. (2019). Low-temperature plasma technology for electrocatalysis. *Chin. Chem. Lett.* 30, 826–838. doi:10.1016/j.ccl.2019.03.051

Wang, H., Fu, X., Shi, J., Li, L., Sun, J., Zhang, X., et al. (2021a). Nutrient element decorated polyetheretherketone implants steer mitochondrial dynamics for boosted diabetic osseointegration. *Adv. Sci. (Weinh.)* 8, 2101778. doi:10.1002/advs.202101778

Wang, J., Yu, W., Shi, R., Yang, S., Zhang, J., Han, X., et al. (2023). Osseointegration behavior of carbon fiber reinforced polyetheretherketone composites modified with amino groups: an *in vivo* study. *J. Biomed. Mater. Res. B Appl. Biomater.* 111, 505–512. doi:10.1002/jbm.b.35167

Wang, M., Bhardwaj, G., and Webster, T. (2017). Antibacterial properties of PEKK for orthopedic applications. *Int. J. Nanomedicine* 12, 6471–6476. doi:10.2147/IJN.S134983

Wang, P., Zou, B., Ding, S., Li, L., and Huang, C. (2021b). Effects of FDM-3D printing parameters on mechanical properties and microstructure of CF/PEEK and GF/PEEK. *Chin. J. Aeronaut.* 34, 236–246. doi:10.1016/j.cja.2020.05.040

Wang, S., Deng, Y., Yang, L., Shi, X., Yang, W., and Chen, Z.-G. (2018). Enhanced antibacterial property and osteo-differentiation activity on plasma treated porous polyetheretherketone with hierarchical micro/nano-topography. *J. Biomater. Sci. Polym. Ed.* 29, 520–542. doi:10.1080/09205063.2018.1425181

Wang, Y., Müller, W.-D., Rumjahn, A., Schmidt, F., and Schwitalla, A. D. (2021c). Mechanical properties of fused filament fabricated PEEK for biomedical applications depending on additive manufacturing parameters. *J. Mech. Behav. Biomed. Mater* 115, 104250. doi:10.1016/j.jmbbm.2020.104250

Wang, Y., Müller, W.-D., Rumjahn, A., and Schwitalla, A. (2020). Parameters influencing the outcome of additive manufacturing of tiny medical devices based on PEEK. *Materials* 13, 466. doi:10.3390/ma13020466

Wei, X., Zhou, W., Tang, Z., Wu, H., Liu, Y., Dong, H., et al. (2023). Magnesium surface-activated 3D printed porous PEEK scaffolds for *in vivo* osseointegration by promoting angiogenesis and osteogenesis. *Bioact. Mater* 20, 16–28. doi:10.1016/j.bioactmat.2022.05.011

Wenzel, M., Chiriac, A. I., Otto, A., Zweytick, D., May, C., Schumacher, C., et al. (2014). Small cationic antimicrobial peptides delocalize peripheral membrane proteins. *Proc. Natl. Acad. Sci. U.S.A.* 111 (14), E1409–E1418. doi:10.1073/pnas.1319900111

Willems, P. H. G. M., Rossignol, R., Dieteren, C. E. J., Murphy, M. P., and Koopman, W. J. H. (2015). Redox homeostasis and mitochondrial dynamics. *Cell Metab.* 22, 207–218. doi:10.1016/j.cmet.2015.06.006

Wu, D., Miao, Q., Dai, Z., Niu, F., and Ma, G. (2022). Effect of voids and crystallinity on the interlaminar shear strength of *in-situ* manufactured CF/PEEK laminates using repass treatment. *Compos. Sci. Technol.* 224, 109448. doi:10.1016/j.compscitech.2022.109448

Wu, K., Wu, X., Guo, J., Jiao, Y., and Zhou, C. (2021). Facile polyphenol-europium assembly enabled functional poly(l-lactic acid) nanofiber mats with enhanced antioxidant and angiogenesis for accelerated wound healing. *Adv. Healthc. Mater* 10 (19), e2100793. doi:10.1002/adhm.202100793

Xie, D., Xu, C., Ye, C., Mei, S., Wang, L., Zhu, Q., et al. (2021). Fabrication of submicro-nano structures on polyetheretherketone surface by femtosecond laser for

- exciting cellular responses of mc3t3-E1 cells/gingival epithelial cells. *Int. J. Nanomedicine* 16, 3201–3216. doi:10.2147/IJN.S303411
- Xie, H., Cui, Z., Wang, L., Xia, Z., Hu, Y., Xian, L., et al. (2014). PDGF-BB secreted by preosteoclasts induces angiogenesis during coupling with osteogenesis. *Nat. Med.* 20 (11), 1270–1278. doi:10.1038/nm.3668
- Xu, R., Yallowitz, A., Qin, A., Wu, Z., Shin, D. Y., Kim, J.-M., et al. (2018). Targeting skeletal endothelium to ameliorate bone loss. *Nat. Med.* 24 (6), 823–833. doi:10.1038/s41591-018-0020-z
- Yakufu, M., Wang, Z., Wang, Y., Jiao, Z., Guo, M., Liu, J., et al. (2020). Covalently functionalized poly(etheretherketone) implants with osteogenic growth peptide (OGP) to improve osteogenesis activity. *RSC Adv.* 10, 9777–9785. doi:10.1039/D0RA00103A
- Yan, J., Xia, D., Zhou, W., Li, Y., Xion, P., Li, Q., et al. (2020). pH-responsive silk fibroin-based CuO/Ag micro/nano coating endows polyetheretherketone with synergistic antibacterial ability, osteogenesis, and angiogenesis. *Acta Biomater.* 115, 220–234. doi:10.1016/j.actbio.2020.07.062
- Yan, J., Xia, D., Zhou, W., Li, Y., Xion, P., Li, Q., et al. (2021). Polyetheretherketone with citrate potentiated influx of copper boosts osteogenesis, angiogenesis, and bacteria-triggered antibacterial abilities. *J. Mater. Sci. Technol.* 71, 31–43. doi:10.1016/j.jmst.2020.08.048
- Yang, C., Tian, X., Li, D., Cao, Y., Zhao, F., and Shi, C. (2017). Influence of thermal processing conditions in 3D printing on the crystallinity and mechanical properties of PEEK material. *J. Mater. Process Technol.* 248, 1–7. doi:10.1016/j.jmatprotec.2017.04.027
- Yang, X., Chai, H., Guo, L., Jiang, Y., Xu, L., Huang, W., et al. (2021). *In situ* preparation of porous metal-organic frameworks ZIF-8@Ag on poly-ether-etherketone with synergistic antibacterial activity. *Colloids Surf. B* 205, 111920. doi:10.1016/j.colsurfb.2021.111920
- Yang, Y., Zhang, H., Komasa, S., Kusumoto, T., Kuwamoto, S., Okunishi, T., et al. (2022). Immunomodulatory properties and osteogenic activity of polyetheretherketone coated with titanate nanonetwork structures. *Int. J. Mol. Sci.* 23, 612. doi:10.3390/ijms23020612
- Yi, N., Davies, R., Chaplin, A., McCutcheon, P., and Ghita, O. (2021). Slow and fast crystallising poly aryl ether ketones (PAEKs) in 3D printing: crystallisation kinetics, morphology, and mechanical properties. *Addit. Manuf.* 39, 101843. doi:10.1016/j.addma.2021.101843
- Yu, B., and Wang, C. (2022). Osteoporosis and periodontal diseases – an update on their association and mechanistic links. *Periodontol.* 2000 89, 99–113. doi:10.1111/prd.12422
- Yu, D., Lei, X., and Zhu, H. (2022). Modification of polyetheretherketone (PEEK) physical features to improve osteointegration. *J. Zhejiang Univ. Sci. B* 23, 189–203. doi:10.1631/jzus.B2100622
- Yuan, X., Ouyang, L., Luo, Y., Sun, Z., Yang, C., Wang, J., et al. (2019). Multifunctional sulfonated polyetheretherketone coating with beta-defensin-14 for yielding durable and broad-spectrum antibacterial activity and osseointegration. *Acta Biomater.* 86, 323–337. doi:10.1016/j.actbio.2019.01.016
- Yue, H., Yuan, L., Zhang, W., Zhang, S., Wei, W., and Ma, G. (2018). Macrophage responses to the physical burden of cell-sized particles. *J. Mat. Chem. B* 6, 393–400. doi:10.1039/C7TB01673E
- Zhai, M., Zhu, Y., Yang, M., and Mao, C. (2020). Human mesenchymal stem cell derived exosomes enhance cell-free bone regeneration by altering their miRNAs profiles. *Adv. Sci.* 7, 2001334. doi:10.1002/adv.202001334
- Zhang, S., Long, J., Chen, L., Zhang, J., Fan, Y., Shi, J., et al. (2022). Treatment methods toward improving the anti-infection ability of poly(etheretherketone) implants for medical applications. *Colloids Surf. B* 218, 112769. doi:10.1016/j.colsurfb.2022.112769
- Zhang, X.-A., and Kong, H. (2023). Mechanism of HIFs in osteoarthritis. *Front. Immunol.* 14, 1168799. doi:10.3389/fimmu.2023.1168799
- Zhao, M., Chen, G., Zhang, S., Chen, B., Wu, Z., and Zhang, C. (2022). A bioactive poly(ether-ether-ketone) nanocomposite scaffold regulates osteoblast/osteoclast activity for the regeneration of osteoporotic bone. *J. Mat. Chem. B* 10, 8719–8732. doi:10.1039/D2TB01387H
- Zhao, S., Dong, W., Wang, Y., Zhou, X., Jiang, J., Hu, R., et al. (2023). Construction of multifunctional zinc ion sustained-release biocoating on the surface of carbon fiber reinforced polyetheretherketone with enhanced anti-inflammatory activity, angiogenesis, and osteogenesis. *ACS Appl. Mat. Interfaces.* 15, 31256–31272. doi:10.1021/acsami.3c04948
- Zhao, W., Yu, R., Dong, W., Luan, J., Wang, G., Zhang, H., et al. (2021). The influence of long carbon fiber and its orientation on the properties of three-dimensional needle-punched CF/PEEK composites. *Compos. Sci. Technol.* 203, 108565. doi:10.1016/j.compscitech.2020.108565
- Zhao, X., Karthik, N., Xiong, D., and Liu, Y. (2020). Bio-inspired surface modification of PEEK through the dual cross-linked hydrogel layers. *J. Mech. Behav. Biomed. Mater.* 112, 104032. doi:10.1016/j.jmbbm.2020.104032
- Zheng, Y., Gao, A., Bai, J., Liao, Q., Wu, Y., Zhang, W., et al. (2022). A programmed surface on polyetheretherketone for sequentially dictating osteoimmunomodulation and bone regeneration to achieve ameliorative osseointegration under osteoporotic conditions. *Bioact. Mat.* 14, 364–376. doi:10.1016/j.bioactmat.2022.01.042
- Zhong, F., Xie, P., Hou, R., Niu, W., Huang, J., Hu, F., et al. (2021). Improved performance of sulfonated poly ether ether ketone/three-dimensional hierarchical molybdenum disulfide nanoflower composite proton exchange membrane for fuel cells. *J. Mater. Sci.* 56, 6531–6548. doi:10.1007/s10853-020-05716-x
- Zhou, S., Wen, H., Han, X., and Li, H. (2021). Phyllygenin protects against osteoarthritis by repressing inflammation via PI3K/Akt/NF- κ B signaling: *in vitro* and *vivo* studies. *J. Funct. Foods.* 80, 104456. doi:10.1016/j.jff.2021.104456
- Zhou, Z., Han, X., Gao, W., Li, Y., Yu, W., Yang, S., et al. (2022). Fabrication and mechanical properties of different types of carbon fiber reinforced polyetheretherketone: a comparative study. *J. Mech. Behav. Biomed. Mater.* 135, 105472. doi:10.1016/j.jmbbm.2022.105472



OPEN ACCESS

EDITED BY

Nihal Engin Vrana,
Sparta Medical, France

REVIEWED BY

Lidong Zhang,
East China Normal University, China
Miryam Criado-Gonzalez,
University of the Basque Country, Spain

*CORRESPONDENCE

Chaenyung Cha,
✉ ccha@unist.ac.kr

RECEIVED 28 August 2023

ACCEPTED 17 October 2023

PUBLISHED 30 October 2023

CITATION

Noh Y, Son E and Cha C (2023), Exploring stimuli-responsive elastin-like polypeptide for biomedicine and beyond: potential application as programmable soft actuators.
Front. Bioeng. Biotechnol. 11:1284226.
doi: 10.3389/fbioe.2023.1284226

COPYRIGHT

© 2023 Noh, Son and Cha. This is an open-access article distributed under the terms of the [Creative Commons Attribution License \(CC BY\)](https://creativecommons.org/licenses/by/4.0/). The use, distribution or reproduction in other forums is permitted, provided the original author(s) and the copyright owner(s) are credited and that the original publication in this journal is cited, in accordance with accepted academic practice. No use, distribution or reproduction is permitted which does not comply with these terms.

Exploring stimuli-responsive elastin-like polypeptide for biomedicine and beyond: potential application as programmable soft actuators

Yeongjin Noh, Eunjoo Son and Chaenyung Cha*

Center for Multidimensional Programmable Matter, Department of Materials Science and Engineering, Ulsan National Institute of Science and Technology (UNIST), Ulsan, Republic of Korea

With the emergence of soft robotics, there is a growing need to develop actuator systems that are lightweight, mechanically compliant, stimuli-responsive, and readily programmable for precise and intelligent operation. Therefore, “smart” polymeric materials that can precisely change their physicochemical properties in response to various external stimuli (e.g., pH, temperature, electromagnetic force) are increasingly investigated. Many different types of polymers demonstrating stimuli-responsiveness and shape memory effect have been developed over the years, but their focus has been mostly placed on controlling their mechanical properties. In order to impart complexity in actuation systems, there is a concerted effort to implement additional desired functionalities. For this purpose, elastin-like polypeptide (ELP), a class of genetically-engineered thermoresponsive polypeptides that have been mostly utilized for biomedical applications, is being increasingly investigated for stimuli-responsive actuation. Herein, unique characteristics and biomedical applications of ELP, and recent progress on utilizing ELP for programmable actuation are introduced.

KEYWORDS

elastin-like polypeptide, biomedicine, stimuli-responsiveness, soft actuator, shape deformation

1 Introduction

Soft robotics as a scientific field has grown tremendously over the last two decades. Compared to the traditional robotics that involves the design and fabrication of controllable electromechanical parts with hard materials such as metals and hard plastics, soft robotics rely more on flexible and mechanically compliant materials that allow much greater complexity in movement and device fabrication Kim et al. (2013). The importance of soft robotics is tied to the growing need for the robots to adapt and function under dynamic 3D environment (e.g., temperature, humidity, electromagnetic field, and topography) and safely interact with human and other sensitive objects. Coyle et al. (2018) Therefore, flexible polymeric materials whose mechanical properties and stimuli-responsive transformation can be tuned in a wide range are generally selected Shen et al. (2020). In addition, soft robotics are ideal for creating miniaturized devices usually intended for wearable biomedical devices Cianchetti et al. (2018).

More recently, stimuli-responsive and compliant materials are actively investigated for biomedical applications, such as drug delivery, biosensor, and tissue engineering, as they can impart complex control over their functionalities, which are not generally possible for

conventional materials. For example, drug release from soft materials, such as hydrogels and nanovesicles as drug delivery systems, is governed by the laws of diffusion. Even though the release rates can be controlled to a certain degree by controlling the mechanics of the materials, the release is continuous and not amenable for “switching on and off” under desired conditions. The stimuli-responsive polymers that undergo reversible phase transition between swollen and collapsed states under aqueous environment in response to changes in external stimuli, such as pH, temperature and ionic strength, have been widely adopted to develop the materials that allow more precisely block or facilitate the drug release at specific conditions [Wei et al. \(2017\)](#). The same stimuli-responsive materials can be used to detect biomarkers, as the binding of the biomarker elicit the change in the degree of stimuli-responsiveness in a scalable manner [Shu et al. \(2020\)](#).

A crucial factor for developing soft robotic systems is the proper actuation mechanism, which is also directly related to the type of material. [El-Atab et al. \(2020\)](#); [Ilami et al. \(2021\)](#); [Li et al. \(2022\)](#) The actuation of traditional robotics is mostly accomplished by integrating electromechanical and/or hydraulic devices to induce movement, so the type of material is generally not a primary concern. On the other hand, the material itself must act as the actuator for soft robotics, for the sake of developing compact and compliant devices that are able to change their physicochemical properties in response to external stimuli without the need for separate actuators. For this reason, much of the research effort has been geared towards developing stimuli-responsive polymers, most notably electroactive polymers (EAP) and shape memory polymers (SMP) which undergo physical transformation upon change in temperature and electric field, as “soft actuators” [Bar-Cohen, \(2005\)](#); [Lendlein, \(2018\)](#); [Xia et al. \(2021\)](#); [Maksimkin et al. \(2022\)](#). For biomedical applications, thermoresponsive polymers, such as poly (N-isopropylacrylamide) (PNIPAm) and poloxamers [i.e., block copolymers consisting of poly (ethylene glycol) and poly (propylene glycol) blocks], have been especially popular, as their transition temperatures nearing temperature could be effectively utilized to generate implantable biomedical devices [Roy et al. \(2013\)](#); [Bordat et al. \(2019\)](#).

2 Overview of stimuli-responsive polymers as soft actuators

For the actuator to undergo highly specific changes, the material must be designed so that there is a precise correlation between the amount of stimulation and the degree of shape deformation. In addition, this correlation must be completely reversible for repeated operations. This means it should be possible to “program” their stimuli-responsive physical change, while maintaining their structural integrity and processability.

2.1 Electroactive polymers

EAPs are defined broadly as the materials that can change their physical dimensions in response to externally applied electrical field [Bar-Cohen and Anderson, \(2019\)](#); [Maksimkin et al. \(2022\)](#). EAPs can be categorized into dielectric (“dry”) and

ionic (“wet”) types. The electric field applied to a thin dielectric material creates molecular rearrangement and charge polarization. The charge accumulation on opposite ends generates repulsive force, causing the material to deform ([Figure 1A](#)). For example, poly (vinylidene fluoride) (PVDF) is a well-known dielectric polymer having piezoelectric and ferroelectric properties. Due to these electromechanical properties, PVDF has been one of the most investigated EAPs for actuators. Dielectric elastomers such as polysiloxane are also widely used because of their flexibility and mechanical compliance allowing larger strain [Novelli et al. \(2023\)](#). For the actuator to deform freely in all directions, the electrode also must be flexible enough to undergo similar shape deformation. In addition, the actuators anchored to stationary or flexible object can undergo different degrees of deformation.

Ionic EAPs rely on the mobility of ions embedded in the polymeric material under the electric field [Chang et al. \(2018\)](#); [Neuhaus et al. \(2020\)](#); [Dong et al. \(2021\)](#). For example, a tri-layer actuator consisting of two conductive polymer layers (e.g., polypyrrole) separated by an electrolyte layer undergo oxidation at the anode and reduction at the cathode ([Figure 1B](#)). The oxidized conductive polymer attracts counteranions from the electrolyte layer, causing the layer to expand and the entire structure to deform. Ionic polymers have also been explored as actuators, in the form of ionic polymer-metal composites (IPMC) and ionic polymer gels, which also involve asymmetric accumulation of ions ([Figure 1C](#)). Ionic EAPs can be operated under low voltage and produce large strain, but the response time is relatively slow, as they involve the diffusion of ions in liquid media. Dielectric EAPs, on the other hand, require relatively high electric field for polarization and the resulting strain is low, but their response time is faster. Regardless of type of materials, EAPs must accompany electrodes to supply electric field, so they are not generally feasible for creating miniaturized devices.

2.2 Thermoresponsive polymers

In addition to electrical field, temperature has been another potent stimulus for inducing physical changes of soft actuators. [Tokudome et al. \(2016\)](#); [Agarwal et al. \(2019\)](#) Temperature change can be induced externally by using electrical heater/cooler systems. Alternatively, natural difference in temperature can be used to drive the actuation, such as bodily temperature for wearable/implantable device. Therefore, thermoresponsive materials that undergo physical change in response to temperature change have also been extensively studied as soft actuators. SMPs are the most widely explored class of programmable materials [Ratna and Karger-Kocsis, \(2008\)](#); [Scalet, \(2020\)](#); [Xia et al. \(2021\)](#). SMPs do not refer to a specific type of polymers, rather the polymers that can be deformed, or “programmed,” to a certain shape at an elevated temperature are induced to revert back to its original shape in response to a stimulus, usually temperature ([Figure 2A](#)). For a polymer to demonstrate the shape memory effect, it must have both the “soft” segment that can undergo stress-induced deformation usually above the glass transition temperature (T_g), and the “hard” segment that holds its original position to which the deformed polymer can revert. Therefore, thermoplastic polymers engineered to form physical or chemical crosslinking are generally explored as SMPs. This

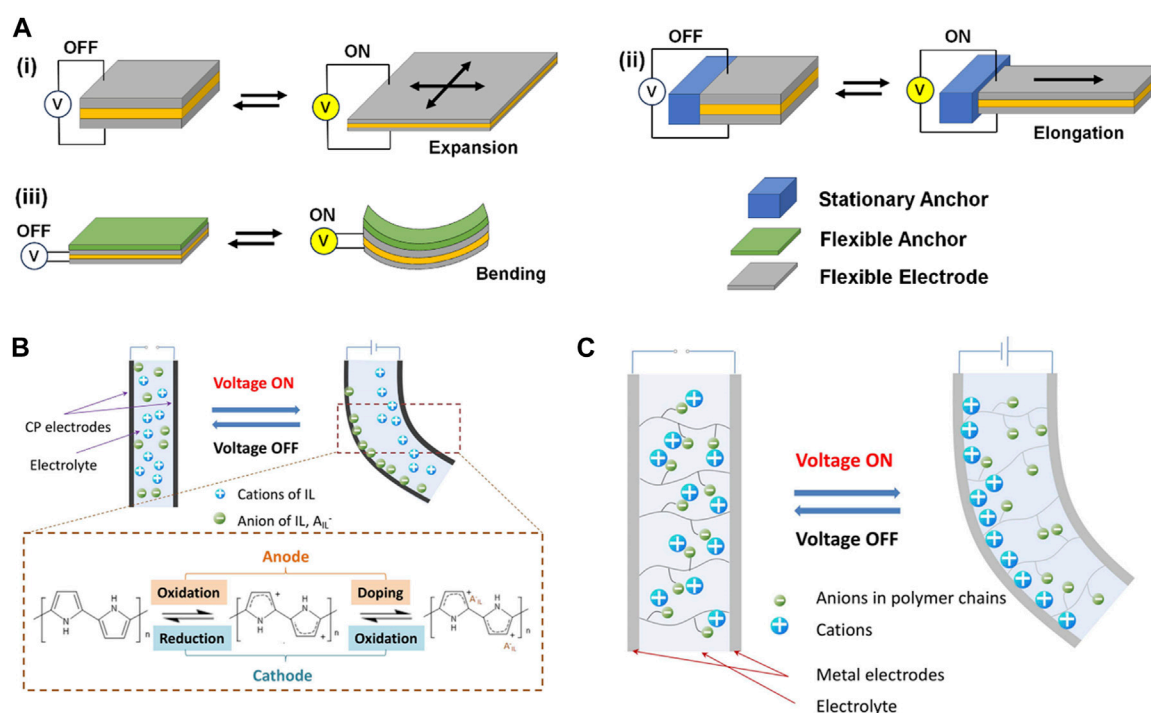


FIGURE 1

Schematic illustrations of actuators based on electroactive polymers undergoing shape deformation upon external electric field: (A) dielectric elastomer actuators, (B) conducting polymer actuator, and (C) ionic polymer-metal composite actuator. (B,C) are reproduced with permission from Dong et al. (2021), under the Creative Commons Attribution (CC-BY-4.0) license.

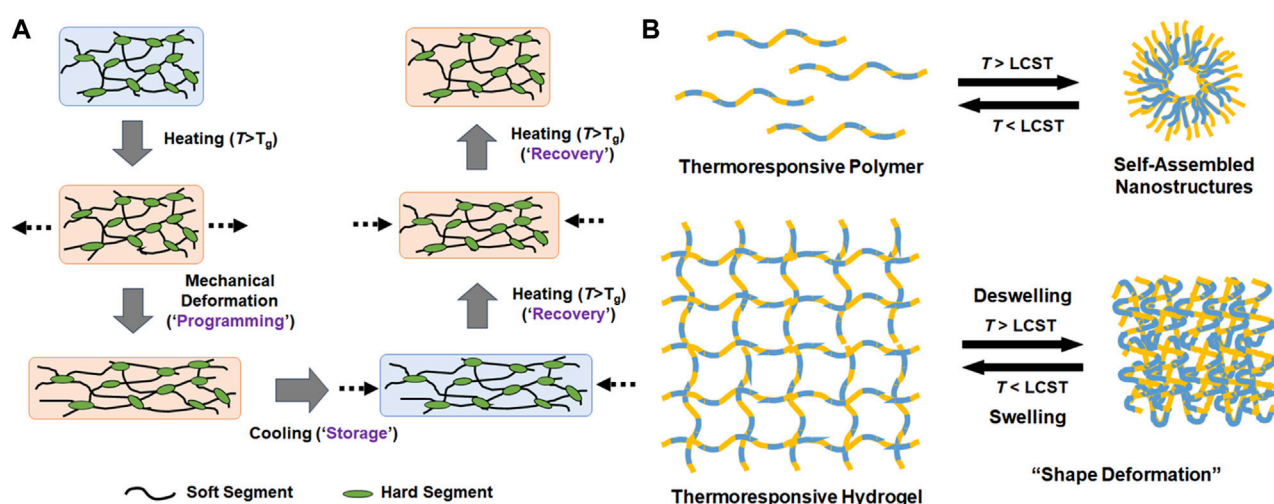


FIGURE 2

Schematic illustrations of the mechanisms of (A) shape memory polymers and (B) thermoresponsive self-assembled nanostructures and reversible swelling and deswelling of hydrogels.

actuation mechanism of SMP is entropically driven to the original disordered state. The most notable class of SMPs is polyurethane (PU) Huang et al. (2010); Menon et al. (2019). PU is generally synthesized by step-growth polymerization between diisocyanate and diol. The urethane bonds are capable of hydrogen bonding, which provides physical crosslinking. Most diisocyanate monomers,

such as 4,4'-methylenediphenyl diisocyanate, isophorone diisocyanate, and toluene diisocyanate, are rigid and serve as "hard segment" in PU to provide mechanical strength, while diols (or polyols) serve as "soft segment." By tailoring their combination, thermoplastic and elastomeric PUs having a wide range of physicochemical properties can be prepared. However, the shape change is not

naturally reversible, and it must be mechanically reprogrammed at the elevated temperature for repeated performance.

Thermoresponsive polymers that can undergo reversible phase transition at a particular temperature, called lower critical solution temperature (LCST), have received significant research interest (Figure 2B) Zhang et al. (2019). These polymers remain soluble in aqueous media at lower temperature surrounded by water molecules via hydrogen bonding, but strong intermolecular interaction between polymer chain usually via hydrophobic interaction dominates at higher temperature leading to chain collapse, diminished solubility, and the formation of self-assembled nanostructures above a certain concentration. When these polymers are integrated into hydrated structures such as hydrogels, this thermoresponsive phase transition can induce a shape deformation. One of the first and most widely investigated example is PNIPAm, whose thermoresponsive phase transition is driven by hydrophobic isopropyl pendant groups Liu et al. (2022). The LCST of PNIPAm is near bodily temperature (at 32°C), which makes it ideal for biomedical applications. Many structural analogs of PNIPAm, which contains functional groups capable of similar attractive physical interactions, have been developed over the years having a wide range of LCST's Roy et al. (2013). Block copolymers consisting of hydrophilic and hydrophobic blocks are another class of thermoresponsive polymers that can undergo phase transition via hydrophobic interaction. For example, poloxamers are triblock copolymers consisting of one hydrophobic poly (propylene glycol) midblock and two hydrophilic poly (ethylene glycol) endblocks that also demonstrate reversible phase transition whose LCST's can be tuned widely Zarrintaj et al. (2018); Zarrintaj et al. (2020). Unlike PNIPAm, block copolymers can form nanostructures or hydrogels by themselves via self-assembly above LCST at different concentrations.

The most important attribute of thermoresponsive polymers is the reversibility of actuation, which is a clear advantage over SMPs that need repeated thermomechanical reprogramming. In addition, because of this innate reversible thermoresponsiveness, these polymers can be easily hybridized with other polymers and nanomaterials to impart the thermoresponsive actuation capability. However, because of the low mechanical strength, it is difficult to fabricate actuators by themselves, and as a consequence, they generally need to be integrated with the existing platform for mechanical reinforcement. Furthermore, the actuation mechanism for the thermoresponsive polymers is mostly based on hydrophobic interaction and hydrogen bonding which are mostly realized under aqueous environment. Therefore, thermoresponsive polymers are ideally suited for materials used for biomedical applications, such as hydrogels, nanofibers, and nanovesicles Wei et al. (2017); Shu et al. (2020).

With the continued maturation of the field of bioengineering, there is a growing trend to develop and adopt new materials having unprecedented functionality. In this regard, materials that can function as soft actuators are extensively investigated to impart biomaterials with controllable properties. In addition to known polymers such as PNIPAm, there is a new class of biopolymers, called elastin-like polypeptide (ELP), which are steadily emerging as a biocompatible, stimuli-responsive material system that possesses similar thermoresponsive properties, while allowing more sophisticated control of their properties via genetic engineering.

In the following, the principles of genetic engineering technology to produce ELP and its basic properties are introduced. In addition, the notable examples of implementing ELP as a stimuli-responsive soft actuators for biomedical application are provided with a historical perspective.

2.3 pH and light-responsive polymers

As thermoresponsive polymers relied on the hydrophobic interaction at elevated temperature, there are polymers that can undergo phase transition in response to the changes in pH. For example, polyanions, the polymers containing numerous acidic functional groups such as carboxylic acid and sulfonic acid, can form hydrogen bonds at lower pH leading to chain collapse, while the deprotonation at higher pH leads to ionization and the loss of hydrogen bonding. Polycations, on the other hand, possess amino groups that acquire positive charge upon protonation at lower pH. In addition, these polymers can acquire charge at different pH's, making them ionic EAP's that can be actuated via external electrical potential. Olvera Bernal et al. develop a nanofiber-based soft actuator consisting of chitosan, a natural cationic polysaccharide, and poly (vinyl alcohol). Olvera Bernal et al. (2023) The nanofibers developed a net positive charge at lower pH due to the protonation of chitosan, thereby undergoing shape deformation in response to external electrical potential. Zhang et al. created a hybrid hydrogel consisting of cationic poly [2-(N,N'-dimethyl amino) ethyl methacrylate] (PDMAEMA) and anionic poly (acrylic acid) (PAAc) Zhang et al. (2020a). The hydrogels exhibited a wide range of pH-responsive swelling/deswelling based on the concentrations of PDMAEMA and PAAc.

There are photoactive polymers that can change their conformations in response to light at a specific range of wavelength. The most notable example is the polymer containing azobenzene moieties, which undergoes reversible trans-cis transition via UV light, called photoisomerization Mahimwalla et al. (2012); Chen et al. (2020). Compared to other stimuli, light has the advantage of more precise control of actuation by using a focused laser with a narrow wavelength. Xu et al. developed an azobenzene-containing liquid crystalline elastomer that can store the mechanical energy generated by trans-cis photoisomerization of azobenzene Lu et al. (2017). The release of mechanical energy by UV irradiation caused a large shape deformation.

3 Elastin-like polypeptide (ELP) as thermoresponsive biopolymer

It is truly fascinating to know that soft actuators based on EAP and thermoresponsive polymers are largely inspired based on human physiology. The movement of muscle tissue, contraction and relaxation of myofibers, is governed by the electrical signals relayed via neural network connected by neuromuscular junction, which is essentially the basis for EAPs Hannaford et al. (2001); Cui et al. (2020). A lesser-known fact about thermoresponsive polymer is that several types of bodily tissues also make use of a naturally thermoresponsive, fibrous protein, called elastin, to impart mechanical compliance and elasticity.

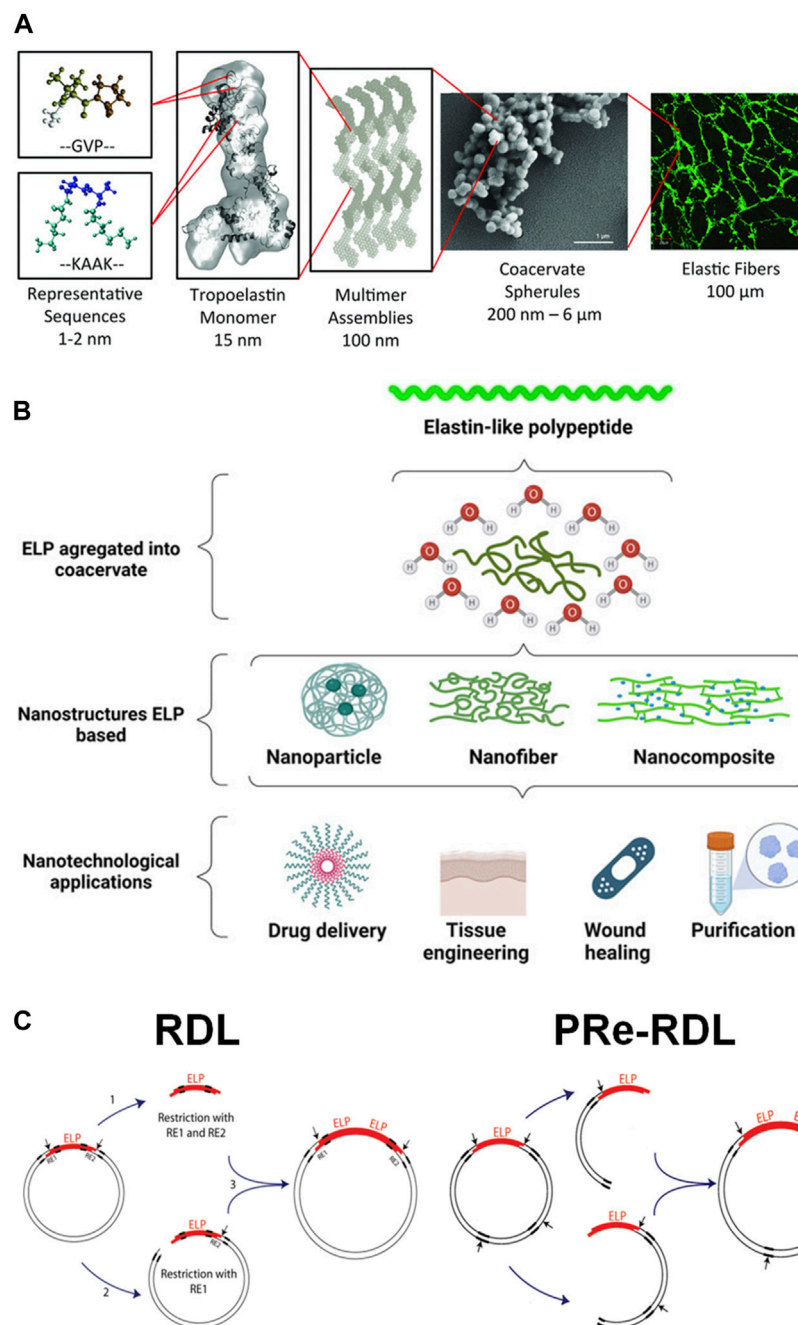


FIGURE 3

(A) The hierarchical assembly of tropoelastin molecules into crosslinked elastin fibers. Reproduced with permission from Tarakanova et al. (2019) under the Creative Commons Attribution (CC BY-NC 4.0) License. (B) The self-assembly of elastin-like polypeptide (ELP) to form various nanostructures for biomedical applications. Reproduced with permission from Lima et al. (2022) under Creative Commons Attribution (CC BY) License. (C) The construction of the plasmid DNA containing ELP gene by the conventional recursive directional ligation (RDL) or recursive directional ligation by plasmid reconstruction (Pre-RDL). Reproduced with permission from McDaniel et al. (2010). Copyright © 2010 American Chemical Society.

3.1 ELP: overview

Elastin is found in many soft connective tissues, such as skin, blood vessel, tendon and ligament, as well as those in larger internal organs such as lung and heart Oszvar et al. (2021). The common feature among these different tissues is the requirement for mechanical loading and compliance. Elastin is a crosslinked, fibrous network of large polypeptides (around 50–70 kDa) called

tropoelastin (TE) (Figure 3A) Almine et al. (2010); Tarakanova et al. (2019); Rodriguez-Cabello et al. (2021). TE has a very characteristic amino acid sequence, consisting of repeats of non-polar, hydrophobic pentapeptide units, a Val-Pro-Gly-X-Gly motif with X being any amino acid residue besides proline. Abundance of proline makes TE demonstrate helical secondary structure. The unique aspect of TE is the abundance of valine containing isopropyl group, which is essentially a structural analog of

PNIPAm. Therefore, much like PNIPAm, tropoelastin similarly demonstrates thermoresponsive chain collapse at elevated physiological temperature. These factors allow the tissue containing elastin fibers to undergo substantial mechanical deformation in response to external force without structural damage (Ozsvar et al. (2021)).

Because of this thermoresponsive properties as well as biocompatibility, there have been significant research efforts to utilize elastin for biomedical applications in addition to basic biochemical research (Figure 3B) Lima et al. (2022). However, it is technically challenging to extract elastin in its native form from biological tissue without structural damage in large quantities. Therefore, the production of TE via recombinant DNA technology has been viewed as a viable alternative. Sequencing of the mRNA and construction of different variations of complementary DNA (cDNA) of TE have been developed over the years Indik et al. (1987); Fazio et al. (1988); Martin et al. (1995). Recombinant tropoelastin (rTE) that retain their characteristic features (e.g., thermoresponsiveness, elasticity, enzymatic crosslinking, and cellular and biomolecular adhesions) could be produced in large quantities using the cDNA to implement recombinant technology Indik et al. (1990); Bedell-Hogan et al. (1993); Wu et al. (1999). More recently, rTE has been increasingly utilized for biomedical applications, including drug delivery and tissue engineering Wise et al. (2009). For example, Annabi et al. developed a mechanically-tough and biocompatible nanocomposite hydrogel consisting of graphene oxide embedded in radically crosslinked rTE hydrogel with methacrylate-functionalized rTD Annabi et al. (2016). The presence of GO improved not only the mechanical strength, but also the electrical conductivity, which provided optimal environment for cardiomyocyte functions.

Despite the recent success in the synthesis and application of rTE, there are several limitations that prevent more efficient production and application of rTE. The biosynthesis of rTE via recombinant technology is often technically challenging, as rTE often becomes degraded by the bacterial host or bacterial membrane, often requiring fusion with other protein using lysogenic host Indik et al. (1990). Since the rTE is mostly based on the native TE genes, it is not amenable to control the molecular weight and introduce other functional groups to modulate the physicochemical and bioactive properties of resulting materials. Alternatively, more recent research trend of recombinant technology for elastin has shifted its focus to developing polypeptides containing the characteristic pentapeptide moieties, now universally termed elastin-like polypeptide (ELP), rather than its full sequence. The first reported ELP was developed by solid-state peptide synthesis, which is not amenable to generating high molecular weight species with accuracy. Martino et al. (2000) Like rTE, the recombinant technology has become the standard method of producing ELP. Unlike rTE, on the other hand, the ELP expression can be accomplished using a variety of plasmids and transfection hosts, and it does not suffer from premature degradation and remain stable during the purification process Meyer and Chilkoti, (2002).

The advancement in the recombinant technology for ELP was remarkably boosted by a key experimental techniques, called recursive directional ligation (RDL), developed by Chilkoti and co-workers Meyer and Chilkoti, (2002). It is often challenging to ligate a large gene into a plasmid. Because of the repetitive nature of

ELP sequence, it is more efficient to construct a plasmid by inserting multiple copies of oligomers by repeated digestion and ligation. In a typical RDL process, one set of the parent plasmid vector containing ELP oligomeric insert is fully digested to obtain the oligomer insert, while the other set is only digested on one side of the oligomer to become a linearized vector (Figure 3C) McDaniel et al. (2010). The insert is then ligated with the linearized vector to reconstruct the plasmid vector with the dimerized gene. This process can be easily repeated to build a larger vector. More recently, a modified version of this technique has been developed, called recursive directional ligation by plasmid reconstruction (Pre-RDL), which could overcome the limitations of RDL McDaniel et al. (2010). Since RDL involves the full digestion and purification of the insert, it is quite time-consuming. Also, the restriction site required for this process could limit the choice of codons. The inserts can also self-ligate, making it difficult to control the number of repeats. In Pre-RDL, instead of utilizing inserts, two sets of parent plasmids are only digested on one side, and thus, without generating the inserts, ligated together. Therefore, the gene length (the number of repeats) can be precisely controlled. Also, it can be used to efficiently introduce other genes expressing desired functional peptides. Pre-RDL has been proven highly useful for synthesizing a plasmid having a large, repetitive oligomeric gene McDaniel et al. (2010).

Another advantage of recombinant technology for ELP production is the simple purification process. Because of the thermoresponsiveness, ELP undergoes aggregation at higher temperature above LCST. Therefore, after cell lysis to dissolve the expressed ELP in the aqueous buffer, the temperature is increased above LCST to induce the ELP aggregation which is then collected via centrifugation. This process can be repeated to maximize the yield. This process, called inverse transition cycling, is by far more efficient and less arduous than a typical polyhistidine tagging and liquid chromatography. Meyer and Chilkoti, (1999).

3.2 ELP-based materials for biomedical applications

The most important and distinguishable biological function of elastin is imparting elasticity and mechanical toughness to biological tissues. Naturally, ELP has been often adopted to generate a variety of biomaterials with improved mechanical and thermoresponsive properties for biomedical applications MacEwan and Chilkoti, (2010); Varanko et al. (2020). For example, Zhang et al. demonstrated that ELP hydrogel crosslinked by disulfide bonds of cysteine residues were highly extensible and showed little hysteresis against repeated mechanical stress Zhang et al. (2015). The biocompatibility of the hydrogel was confirmed by the high viability of mesenchymal stem cells (MSCs) and human umbilical vascular endothelial cells (HUVECs) cultured on the hydrogel, as well as the low immunogenic response after implantation into an animal model. ELP can also be hybridized with other polymers to tune the mechanical properties of resulting hydrogels. Wang et al. developed poly (ethylene glycol) (PEG)-ELP hybrid hydrogel by crosslinking amine-functionalized PEG and ELP with tris(hydroxymethyl)phosphine (Figure 4A) Wang et al. (2014). Mechanical stiffness could be controlled by the crosslinking density of PEG and ELP. In order to impart cell adhesion

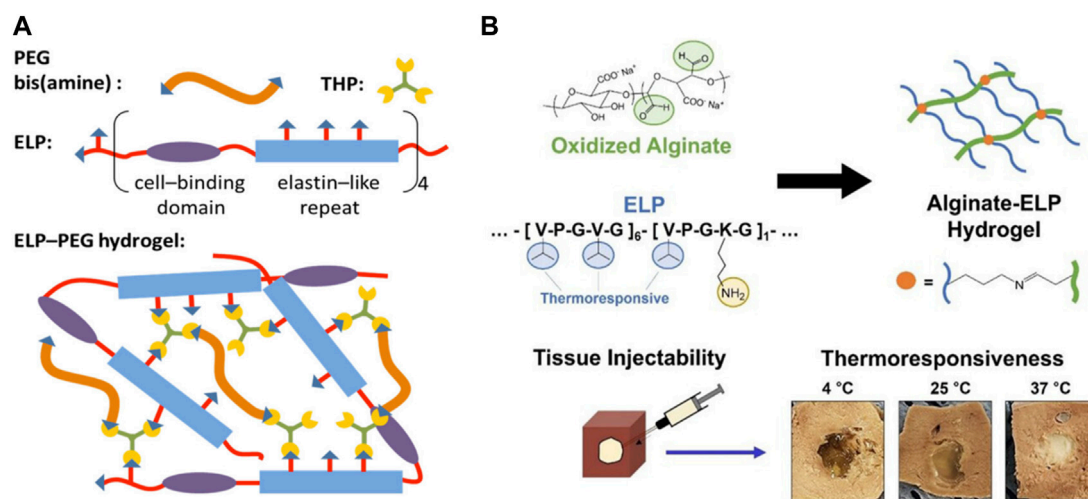


FIGURE 4

(A) Synthesis of poly(ethylene glycol) (PEG)-ELP hybrid hydrogel by crosslinking amine-functionalized PEG and ELP with tris (hydroxymethyl) phosphine (THP). ELP also contained cell-binding domain (RGD peptide) to utilize the hydrogel for tissue engineering applications. Reproduced with permission from Wang et al. (2014). Copyright © 2014 American Chemical Society. (B) Synthesis of tissue-injectable ELP-alginate hydrogel by Schiff base formation between lysine-rich ELP and aldehyde-presenting alginate. The hydrogel demonstrated hydrophobic phase transition at higher temperature, as evidenced by the decrease in size and increase in turbidity. Reproduced with permission from Lee et al. (2022b). Copyright © 2022 American Chemical Society.

properties to hydrogel, RGD peptide was conjugated to ELP by simply the fusion of RGD gene alongside the ELP gene to the plasmid, which is a clear advantage of recombinant technology. By keeping the RGD-ELP constant, the cell adhesion and mechanical properties of the hydrogel could be independently controlled. Similarly, Lee et al. demonstrated hydrogel formation via Schiff base reaction between lysine-rich ELP and aldehyde-functionalized alginate (Figure 4B) Lee et al. (2022b). Since the reaction occurred spontaneously without additional chemicals, this type of thermoresponsive gelation is ideally suited as a tissue-injectable delivery system, in which biocompatible, thermoresponsive gelation is induced upon injection followed by sustained release of bioactive molecules. Zhu et al. created ELP-hyaluronic acid (HA) hydrogel by Schiff base formation between aldehyde-presenting HA and hydrazine-presenting ELP Zhu et al. (2017). Increasing HA concentration resulted in increased cartilage phenotypes and reduced fibrocartilage phenotypes of encapsulated chondrocytes.

Since ELP is synthesized by recombinant DNA technology, it is feasible to develop fusion protein with other polypeptides and proteins to acquire synergistic properties. López Barreiro et al. (2023) For example, silk fibroin is a natural protein mostly procured from silkworm increasingly used as scaffold material for biomedical applications. Similar to ELP, silk fibroin also contains characteristic peptide repeats (e.g., GAGAX, X: guest residue). Therefore, there have been research efforts to develop the fusion polypeptide, “silk-elastin-like polypeptide (SELP),” via recombinant technology in order to control the physicochemical properties Huang et al. (2015); Gonzalez-Obeso et al. (2022). A similar strategy has been used to generate “collagen-elastin-like polypeptide” by incorporating the characteristic motif of collagen, glycine-proline-4-hydroxyproline Prhashanna et al. (2019).

Like other biopolymers, ELP can be processed into nanofibers via electrospinning Lee et al. (2011); Putzu et al. (2016). ELP has a

unique ability to form nanofibers, in addition to micelles and vesicles, by self-assembly of AB-type ELP block copolymers consisting of hydrophilic and hydrophobic blocks, taking advantage of its thermoresponsive properties and genetic engineering capability Saha et al. (2020). ELP block copolymers could be synthesized by modifying the guest residues of the pentapeptide units with either hydrophobic or hydrophilic amino acids. For example, alanine or glutamic acid having carboxylic acid is introduced as a guest residue to create hydrophilic blocks, while glycine, valine, or phenylalanine is introduced to generate hydrophobic blocks. Depending on the specific sequence and molecular weight, a wide range of nanostructures including nanofibers and micelles could be generated. For example, Dreher et al. developed ELP block copolymers consisting of alanine-rich hydrophilic and valine-rich hydrophobic blocks (Figure 5A) Dreher et al. (2008) This ELP block copolymer could self-assemble to form nanostructures above the body temperature. Interestingly, there were two distinct thermal transitions, which were attributed to the polymer-to-micelle and micelle-to-coacervate transitions. Furthermore, introducing tumor-targeting NGR peptide onto ELP helped facilitate the increased binding of ELP nanostructures to HT-1080 fibrosarcoma cells. McDaniel et al. induced self-assembled nanofiber formation of ELP copolymers by introducing the “assembly domain” to C-terminus of the alanine-rich hydrophilic domain. McDaniel et al. (2014) The assembly domain was a short hydrophobic domain, (XGG)₈, where X was tyrosine, phenylalanine or tryptophan. The size of the nanofibers as well as their LCSTs could be effectively controlled by the type of X residue. These ELP-based nanofibers have been utilized as scaffolds for tissue engineering applications. Natsume et al. developed the self-assembled ELP nanofibers presenting cell-adhesive REDV peptide as a scaffold for vascular graft generation Natsume et al. (2023). This REDV-presenting nanofibers demonstrated reduced

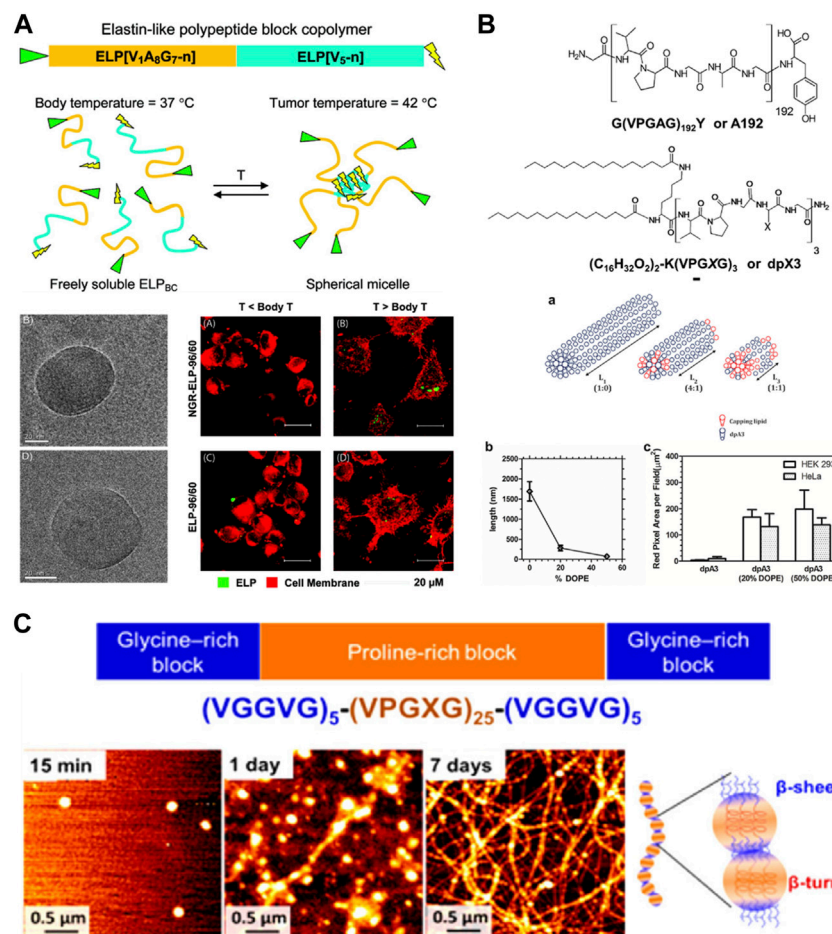


FIGURE 5

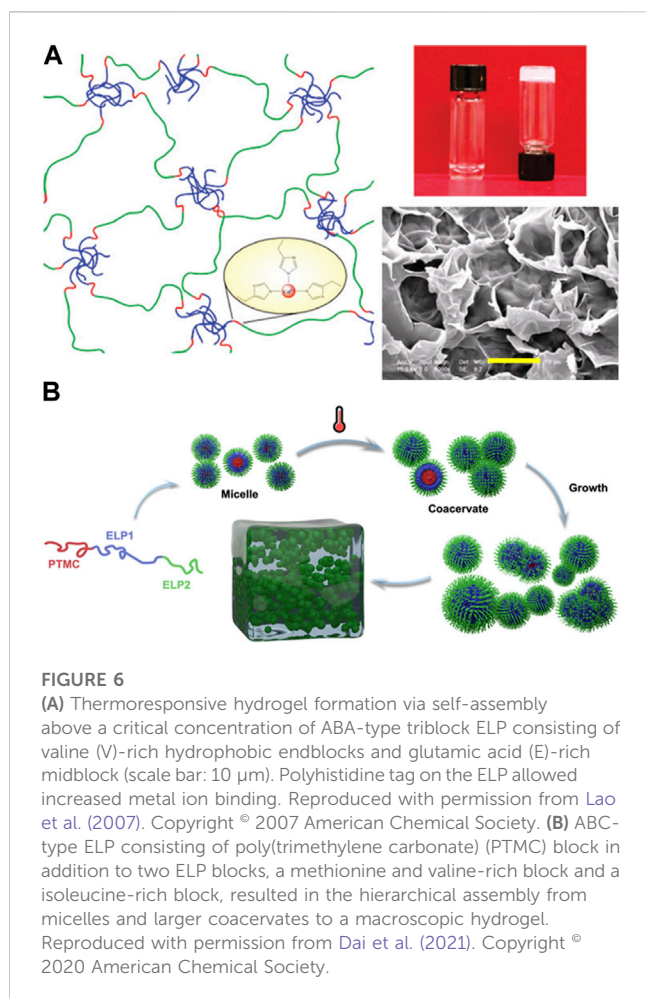
(A) ELP block copolymer consisting of alanine-rich hydrophilic and valine-rich hydrophobic blocks undergoing self-assembly to form micelles above body temperature. The micelles showed increased binding to tumor cells. Reproduced with permission from Dreher et al. (2008). Copyright © 2008 American Chemical Society. (B) ELP conjugated with a phospholipid, 1,2-dioleoyl-sn-glycero-3-phosphoethanolamine (DOPE), allowed the control of the size of self-assembled nanofibers. Reproduced with permission from Aluri et al. (2012). Copyright © 2012 American Chemical Society. (C) ABA-type triblock ELP consisting of proline (P)-rich midblock and glycine (G)-rich endblocks undergoing hierarchical assembly from micelles via beta-turn of P-blocks to nanofibers via beta-sheet formation of G-blocks. Reproduced with permission from Le et al. (2013). Copyright © 2013 American Chemical Society.

platelet adhesion, increased bioactivity of endothelial cells and smooth muscle cells.

Another advantage of thermoresponsive self-assembly of ELP nanofibers is the ability to precisely control their length and morphology, which is not generally feasible for electrospun nanofibers. These self-assembled nanofibers have been used to develop drug delivery vehicles and tissue engineering scaffolds. It is also possible to conjugate other polymers or lipids to tune nanofiber dimensions and morphologies. Aluri et al. demonstrated that the size of self-assembled nanofibers could be controlled by conjugating 1,2-dioleoyl-sn-glycero-3-phosphoethanolamine (DOPE), a phospholipid, to ELP (Figure 5B). Aluri et al. (2012) Increasing presence of DOPE provided stronger hydrophobic interaction, and as a result, led to shorter nanofibers. It has also been shown that even without hydrophilic blocks, nanofibers could be generated using ELP consisting of “double-hydrophobic” glycine (G)-rich and proline (P)-rich domains Le et al. (2013); Le et al. (2017). Le et al. demonstrated that the initial self-assembly by P-rich

domain results in nanoparticle formation by beta-turn formation, while subsequent increase in beta-sheet formation by G-rich domain connect the nanoparticles into a long nanofiber formation with beaded nanofiber morphology (Figure 5C).

ELP block copolymers above a certain critical concentration can form extended network structure via self-assembly to form hydrogels, similar to well-known poloxamers. For example, Lao et al. demonstrated thermoresponsive hydrogel formation of ABA-type triblock ELP consisting of valine (V)-rich hydrophobic endblocks and glutamic acid (E)-rich midblock, [(VPGVG)₂VPGE (VPGVG)₂]_n above a critical concentration of 6% (w/v) (Figure 6A) Lao et al. (2007). The hydrogel formation was thermally reversible, remaining gel state above room temperature and reverting to sol state upon cooling (4°C). Furthermore, polyhistidine tag on ELP also enhanced the metal ion binding. Ghoorchian et al. demonstrated that the micelle made from AB-type diblock ELP containing zinc-binding motif Ghoorchian et al. (2015). The addition of zinc could induce hydrogel formation. In addition to AB-type diblock



copolymers and ABA-type triblock copolymers, Dai et al. developed an ABC-type triblock copolymer consisting of a poly(trimethylene carbonate) (PTMC) block in addition to two ELP blocks having different degrees of hydrophobicity, a methionine and valine-rich block and a isoleucine-rich block (Figure 6B) Dai et al. (2021). Having additional degree of complexity in the ELP block copolymer allowed more intricate, hierarchical control of the morphology of resulting self-assembled structures, in which micelles first formed at low concentrations [0.1%–0.3% (w/v)] became larger coacervates at temperatures above the LCST. With further increase in concentration, the coacervates grew into micrometer-scale particles, which eventually undergo sol-gel transition to become macroscopic hydrogel [4% (w/v)].

3.3 Emerging role of ELP as thermoresponsive soft actuators: historical perspective and recent development

Naturally, being a polypeptide, most of the research on ELP has been focused on designing and implementing ELP for biomedical applications. The characteristic thermoresponsive properties are like those of widely explored PNIPAm, while the recombinant technology allows other peptide moieties to be integrated with ELP for added functionalities. This is a clear advantage over

synthetic polymers like PNIPAm, which need to be hybridized with other functional materials. As PNIPAm over the recent years has been widely explored as thermoresponsive soft actuators, there has been a rising research trend in adopting ELP for this purpose as well.

Urry and co-workers were one of the first to introduce the possibility of the mechanical actuation of chemically-crosslinked ELP hydrogels Urry, (1988); Urry et al. (1988). The hydrophobicity-driven phase transition of ELP hydrogel, as identified by the changes in mechanics and dimensions, was demonstrated by modulating pH and temperature, which was termed “mechanochemical coupling.” While these earlier attempts at developing ELP hydrogels for soft actuation presented in these studies were fabricated by non-specific radical crosslinking via gamma irradiation, more systematic approaches were taken in subsequent studies to develop ELP hydrogel by taking advantage of presenting specific amino acid sequences. Trabbic-Carlson et al. developed ELP hydrogel demonstrating reversible, thermoresponsive swelling/deswelling by crosslinking lysine-rich ELP (i.e., lysine as the guest residue) with tris-succinimidyl aminotriacetate as the crosslinker Trabbic-Carlson et al. (2003). Controlling the concentration, molecular weight and lysine content of ELP allowed more systematic modulation of the mechanical properties, and subsequent thermoresponsive shape change, of the ELP hydrogels.

While the study by Trabbic-Carlson et al. focused more on the basic mechanical characterization of ELP hydrogels, Valiaev et al. demonstrated the practical potential of ELP to modulate the actuation of microcantilever (Figure 7) Valiaev et al. (2007). The silicon nitride microcantilever used for atomic force microscopy and quartz crystal microbalance was grafted with ELP with varying molecular weights and guest residue compositions. The change in the deflection of the microcantilever in response to various parameters, such as temperature, ionic strength, and pH, could be tuned by ELP’s with varying molecular weights and guest residues. The degree of cantilever deflection was increased at lower pH and higher molecular weight. Even though ELP was only used for surface functionalization, the tunable thermoresponsive nature of ELP alone could effectively control the degree of actuation of existing actuators.

One common method of producing a soft actuator is to attach two layers consisting of stimuli-responsive “active” layer and a non-responsive “passive” layer, so the actuator can bend in one direction upon stimulation in a controlled manner based on the difference in mechanics. Kamada et al. developed a bilayer actuator consisting of polyacrylamide (PAAm)-ELP hydrogel layer and non-crosslinked ELP hydrogel Kamada et al. (2023). The degree of actuation could be controlled by the concentration of ELP and the ionic strength of the medium.

The ELP hydrogels that are structurally robust enough can also function as thermoresponsive soft actuators. Increasing the temperature above LCST to induce the shape deformation can be easily accomplished with a variety of heat sources. However, it is technically challenging to precisely control the thermoresponsive actuation in a localized manner using conventional heat sources. One innovative strategy to accomplish this task is by incorporating reduced graphene oxide (rGO) into the ELP hydrogel. rGO has been shown to display photothermal effect, in which thermal energy is generated upon photoexcitation using near IR (NIR) range. Wang

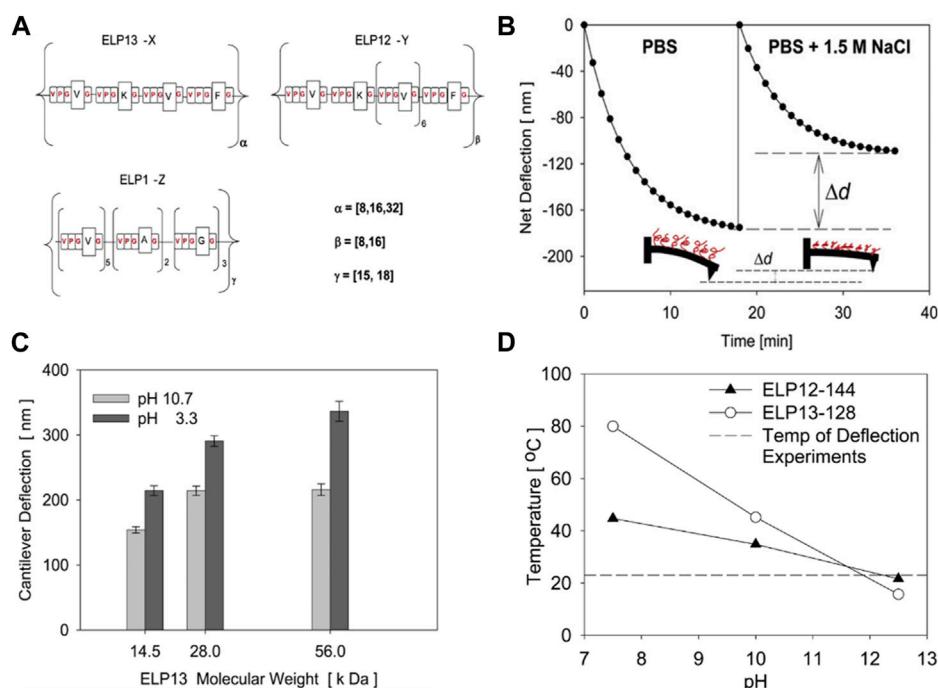


FIGURE 7

(A) ELP's having different molecular weights and pentapeptide compositions were prepared and coated on the surface of the cantilever used for atomic force microscopy (AFM). The degree of deflection of the ELP-coated cantilever under different (B) ionic strengths and (C) molecular weights of ELP and pH. (D) The transition temperatures of ELP's measured at different pH's. Reproduced with permission from Valiaev et al. (2007). Copyright © 2007 American Chemical Society.

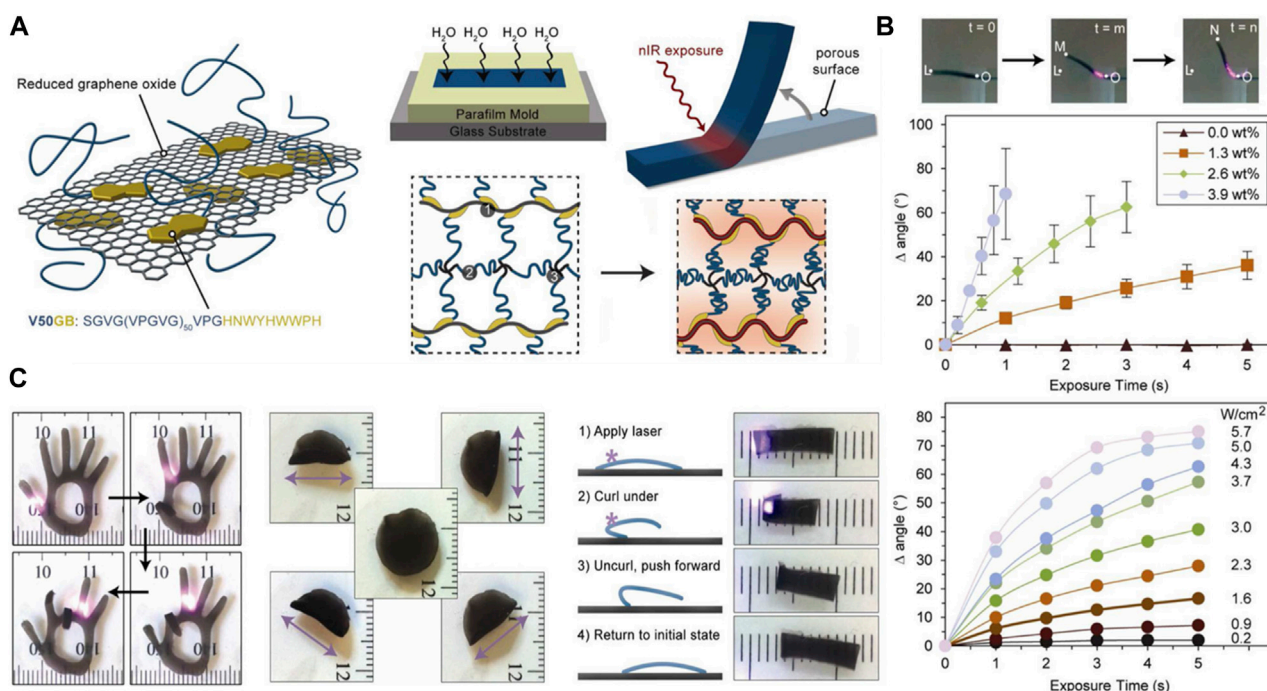


FIGURE 8

(A) Schematic illustration of the fabrication of near infrared (NIR)-responsive reduced graphene oxide (rGO)-ELP composite hydrogel actuator. (B) The degree of actuation (bending angle) controlled by the rGO concentration and NIR intensity. (C) The control of bending motions of various rGO-ELP soft actuators. Reproduced with permission from Wang et al. (2013). Copyright © 2013 American Chemical Society.

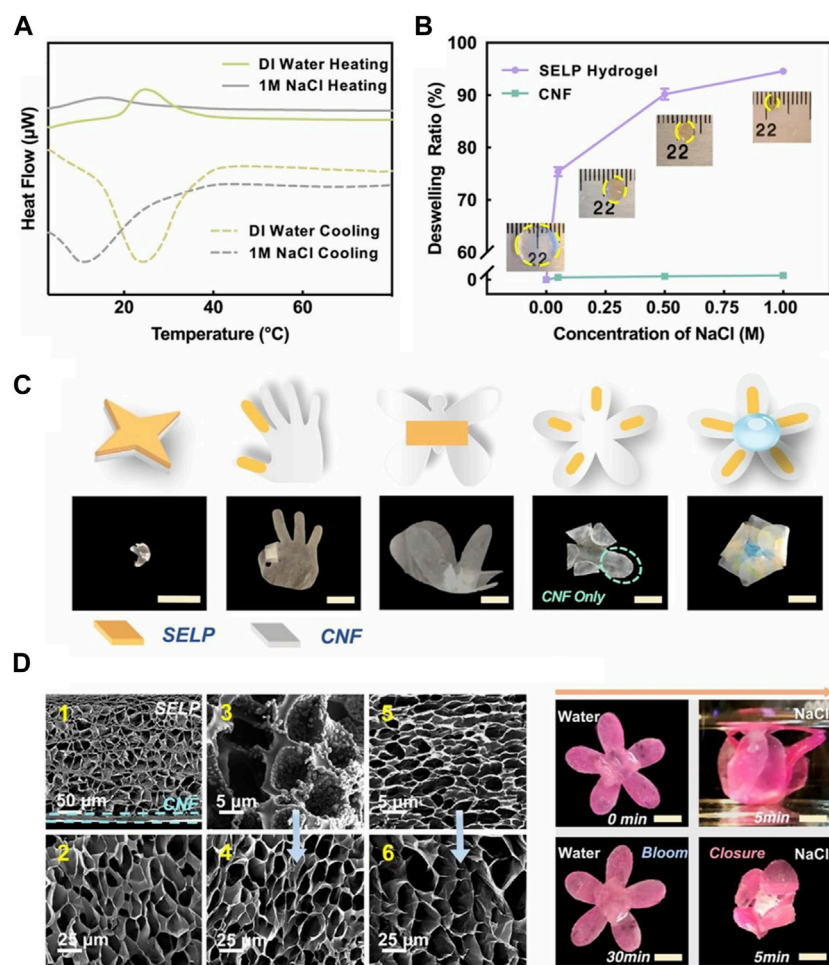


FIGURE 9

(A) Heat flux of silk fibroin-ELP (SELP) hydrogel measured in different ionic strength (deionized water vs. 1 M NaCl) by differential scanning calorimetry. (B) The deswelling ratios of SELP hydrogels measured under varying ionic strengths (up to 1 M NaCl). (C) The shape change of various soft bilayer actuators made of SELP hydrogel and cellulose nanofiber (CNF) membrane by 1 M NaCl. (D) Scanning electron microscopic images of (D1) SELP/CNF bilayer actuators and (D2) SELP hydrogels in swollen states at 4°C DI water, SELP hydrogels in contracted states at (D3) 1 M NaCl solutions at room temperature and (D5) 60°C DI water, respectively, and (D4 and D6) equilibrated back to 4°C DI water of (D3 and D5). Reproduced with permission from Wang et al. (2020). Copyright © 2020 National Academy of Sciences.

et al. successfully demonstrated that the irradiation of NIR laser upon rGO-ELP nanocomposite hydrogel generated enough heat at the area of the irradiation, causing the hydrogel to display highly coordinated motions (Figure 8) Wang et al. (2013). The degree and speed of actuation could be enhanced by the concentration of ELP and the intensity of NIR laser. The rGO-ELP hydrogel was then used to fabricate soft robots capable of sophisticated light-induced locomotion by selective irradiation.

More recently, Chiang et al. presented a more expansive exploration of rGO-laden ELP hydrogel as a soft actuator mediated by the photothermal effect Chiang et al. (2021). They controlled the composition of tetrakis (hydroxymethyl) phosphonium chloride (TMPC)-crosslinked ELP hydrogels by introducing either graphene oxide (GO) or rGO. In addition, ELP was copolymerized with silk fibroin (SF) to develop hybrid hydrogel. Using this dual approach, more comprehensive control of the mechanical properties was possible. For instance, hybridizing with SF alone increased the rigidity of the hydrogel, but it also became more brittle. Incorporating

GO or rGO into the ELP-SF hydrogel led to the significant increase in tensile strength and stretchability. They ultimately created a bilayer actuator consisting of one hydrogel layer containing GO and the other containing rGO. Because of the mechanical anisotropy between the layers, varying the ratio of GO to rGO could modulate bending motion of the bilayer actuator, which was further controlled by the intensity of NIR irradiation. Lo et al. demonstrated that the bioactivity of cardiomyocytes cultured on the rGO-laden ELP-SF hydrogel was well maintained, while being able to undergo the light-induced activation. Lo et al. (2017).

In addition to creating a hybridized network of silk fibroin and ELP by copolymerization, it is also possible to create a fusion protein of silk fibroin and ELP by recombinant DNA technology. While hybridization leads to randomized distribution of silk fibroin and ELP, it can be inferred that the silk fibroin unit directly attached to ELP would have more intimate effect on the thermoresponsive properties of ELP. Wang et al. developed a fusion protein consisting of the characteristic domain (GAGAGS) of silk fibroin

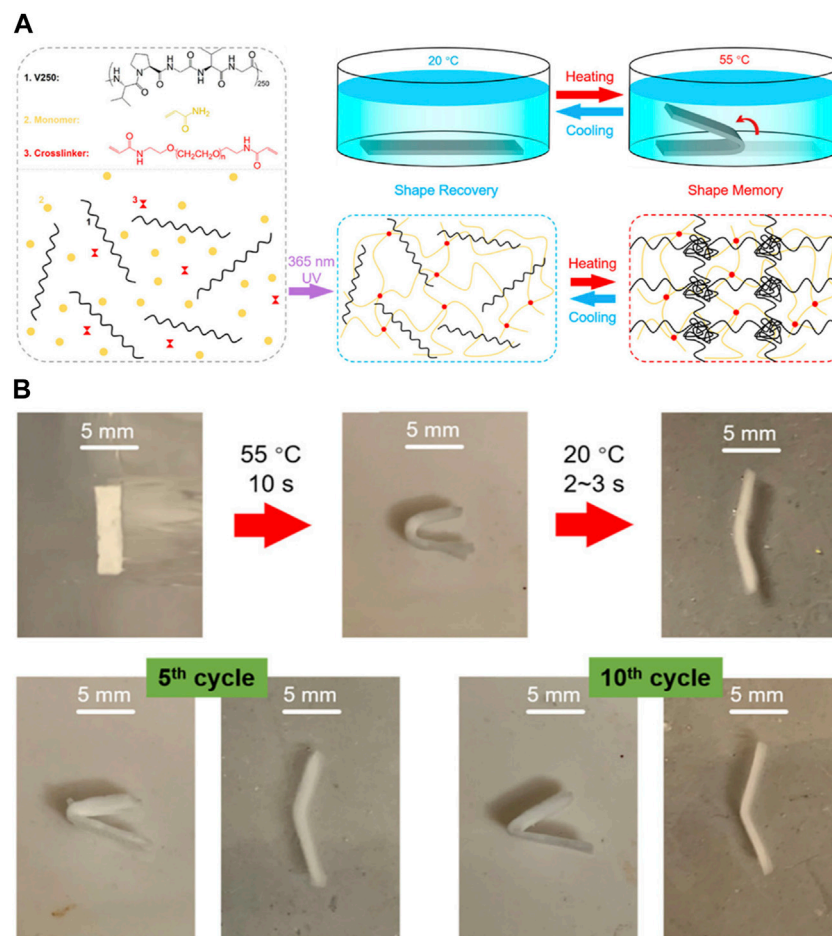


FIGURE 10

(A) Synthesis of semi-interpenetrating network hydrogel consisting of crosslinked polyacrylamide (PAAm) and ELP. ELP was physically incorporated into the PAAm network crosslinked by photoinitiated radical polymerization. Shape memory effect of the hydrogel could be imparted by programming the hydrogel at higher temperature via physical crosslinking between ELP molecules to hold the hydrogel in place. (B) Photographs of hydrogels demonstrating shape memory effect. The hydrogel could maintain the structure even after repeated shape deformations. Reproduced with permission from Zhang et al. (2020a). Copyright © 2020 American Chemical Society.

and ELP (“SELP”), in which the silk domain provided greater hydrophobicity and mechanical strength (Figure 9) Wang et al. (2020). The thermoresponsive phase transition of SELP hydrogel was shown to be influenced by both temperature and ionic strength. For example, the LCST was lowered to 15°C from 25°C when 1 M NaCl was added to deionized water. Also, the thermoresponsive deswelling became more pronounced in the presence of 1 M NaCl at the same temperature. Using this behavior, the bilayer actuators consisting of the active SELP hydrogel layer and the passive cellulose nanofiber (CNF) layer were developed, which allowed highly sophisticated motions upon the changes in temperature and ionic strength. These findings suggested that providing a functional moiety to ELP via genetic engineering could modulate the degree of actuation in a more refined manner.

ELP has also been used to generate SMPs, in which the ability of ELP to undergo phase transition above LCST and crosslinking could serve as the soft segment. For example, Zhang et al. developed a semi-interpenetrating network hydrogel consisting of chemically crosslinked PAAm and physically-crosslinked ELP (Figure 10) Zhang et al. (2020b). The hydrogel was shown to display higher tensile strength

at higher temperature, being able to maintain the structure without fracture and revert back to the original shape after extreme shape deformation. This indicated the strong physical crosslinking of ELP via hydrophobic interaction at higher temperature. In addition, the hydrogel could be programmed to a fixed shape without structural damage at 55°C above LCST, and the shape recovery took place at lower temperature. While synthetic polymers generally used for conventional SMPs have higher T_g , necessitating significant thermomechanical energy for shape deformation, the transition temperature of ELP is much lower and the thermoresponsive deformation occurs naturally at higher temperature, requiring much less external energy for shape programming. It should be noted that it differs from the traditional SMPs in that the deformed hydrogel at higher temperature could not maintain its structure and reverted to its original shape at lower temperature.

The biocompatible nature of ELP, being a natural biopolymer, also allows the ELP-based actuators to be used for biomedical applications. For example, the thermoresponsive shape change of ELP could be used as a “switch” to induce conformational changes of nanostructures for drug delivery and biosensing applications. Kim

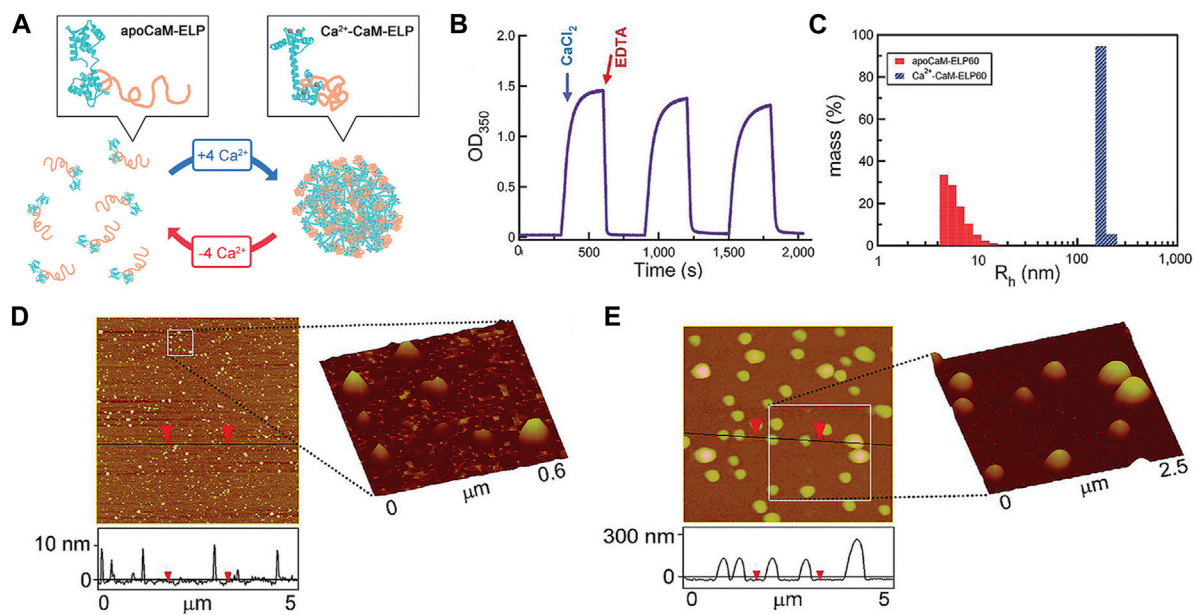


FIGURE 11

(A) Induction of self-assembly of apoCaM-ELP fusion protein to form large coacervates by binding with calcium (Ca²⁺-CaM-ELP). (B) The self-assembly by calcium and disassembly by removing calcium with chelation could be repeatedly performed. (C) The formation of self-assembled nanostructures was evaluated by the increase in the particle size (hydrodynamic radius). AFM images of (D) apoCaM-ELP and (E) Ca²⁺-CaM-ELP. Large coacervates were only detected for Ca²⁺-CaM-ELP. Reproduced with permission from Kim and Chilkoti, (2008). Copyright © 2008 American Chemical Society.

et al. developed a fusion protein consisting of calmodulin (CaM) and ELP via recombinant DNA technology to fuse two genes (Figure 11) Kim and Chilkoti, (2008). CaM module served as the ligand binding domain, in which selective binding of calcium induced to the simultaneous phase transition of ELP module. Without calcium, the CaM-ELP undergoes phase transition above LCST to form self-assembled nanoparticles. With the addition of calcium, the binding of calcium with CaM module caused more extensive phase transition of the ELP module, leading to the formation of larger, micrometer-scale aggregates. This process was shown to be reversible by removing the calcium via chelation. Since many biological processes involve calcium ions, it could be envisioned that this fusion protein as a “control switch” to modulate the processes. Lee et al. synthesized a ABA-triblock copolymer consisting of ELP endblocks and CaM midblock, capable of thermoresponsive hydrogel formation Lee et al. (2022a). The mechanical properties and conformational changes were controlled by the binding of calcium to CaM midblock. The release of trifluoperazine as a co-ligand with calcium from the hydrogel showed significant cytotoxic effect on the cancer cells, demonstrating the potential as a cancer therapy.

Photocrosslinking is one of the most popular methods to create hydrogels. Like other biopolymers, ELP has been modified with photolabile groups to generate hydrogel via photocrosslinking. Compared to physical crosslinking of ELP copolymers, mechanical properties of photocrosslinked ELP hydrogels can be more efficiently and broadly tuned. Guo et al. developed ELP hydrogel by photocrosslinking methacrylic functionalized ELP (“ELP-MA”) Guo et al. (2022). The mechanical properties and thermoresponsive shape deformation could be controlled by the

concentration and the degree of methacrylation of ELP. The hydrogel was demonstrated to be highly effective as a tissue adhesive and tissue engineering scaffolds.

4 Conclusion and perspective

Elastin has long fascinated biomedical researchers for its unique role in tissue physiology; controlling mechanical properties of ECM as well as providing biophysical cues to influence cellular behavior. Especially, elastin is largely responsible for the high mechanical strength and elasticity of biological tissue, which is originated from the coiled secondary structure of tropoelastin polypeptides that are enzymatically crosslinked. The tropoelastin consists of repeated pentapeptide units, rich in valine, glycine and proline that mediates hydrophobic interaction-driven coiled morphology above a certain transition temperature. Due to the difficulty of obtaining pure elastin from natural sources and the advantages of imparting desired functionalities, elastin-like polypeptide (ELP), which contains characteristic pentapeptide repeats and whose specific sequences can be precisely designed and produced by recombinant DNA technology, have been more widely utilized. The thermoresponsive phase transition behavior of ELP has proven to be quite useful for developing biomaterials, such as hydrogels, nanofibers and self-assembled nanostructures for biomedical applications including drug delivery and tissue engineering.

The ability of thermoresponsive polymeric materials to undergo shape deformation, such as widely popular poly(N-isopropylacrylamide) (PNIPAm), is being widely adopted to create actuators for soft robotics and multifunctional biomedical devices. Just as ELP has

followed the footsteps of PNIPAm in the field of biomedical engineering, the recent research trend regarding ELP is suggesting that it is also being seriously considered as thermoresponsive soft actuators. The number of published reports is not significant at this point to imply that it is becoming a broad trend, but it is not surprising given that ELP itself has not reached the status of more popular biopolymers, such as alginate, chitosan, and gelatin for biomedical applications, largely due to the fundamental limitation of mass producibility. However, with its unique thermoresponsive properties and precise control of physicochemical properties that other biopolymers do not possess, ELP has found its niche in the field of biomedicine as a stimuli-responsive biomaterial. In the same manner, ELP has the potential to provide the similar attributes to developing soft actuators by providing new functionalities afforded by the genetic engineering.

Even though ELP can be produced in relatively large quantities via recombinant technology, it is still not economically viable enough to develop large-scale actuators solely using ELP. Furthermore, the mechanical strength of ELP is not high enough to develop robust structures required for actuators. Therefore, ELP is more ideally suited as a functional moiety to impart thermoresponsiveness and bioactivity to a known material. As the direction of the research in soft actuators is shifting towards developing multifunctional actuators with different modes of actuation and a diverse array of properties, it is also expected that more hybridization strategies would be utilized to generate ELP-based composite materials. As a burgeoning material system for soft actuators, the ELP-based actuators developed thus far have been mostly geared toward biomedical applications. However, with further maturation, it can be envisioned that the ELP-based soft actuators could also find their place in other areas, such as electronics and environmental engineering.

Author contributions

YN: Conceptualization, Data curation, Investigation, Software, Writing–review and editing. ES: Data curation, Writing–review and

editing. CC: Conceptualization, Funding acquisition, Project administration, Resources, Software, Supervision, Writing–original draft, Writing–review and editing.

Funding

The author(s) declare financial support was received for the research, authorship, and/or publication of this article. This study was supported by Mid-Career Researcher Program through the National Research Foundation of Korea (NRF) funded by the Ministry of Science and ICT (2022R1A2C2009174) and the Technology Innovation Program (or Industrial Strategic Technology Development Program) (20009198, Development and demonstration of biodegradable bioplastic prototype) funded by the Ministry of Trade, Industry & Energy (MOTIE, Korea).

Conflict of interest

The authors declare that the research was conducted in the absence of any commercial or financial relationships that could be construed as a potential conflict of interest.

The author(s) declared that they were an editorial board member of Frontiers, at the time of submission. This had no impact on the peer review process and the final decision.

Publisher's note

All claims expressed in this article are solely those of the authors and do not necessarily represent those of their affiliated organizations, or those of the publisher, the editors and the reviewers. Any product that may be evaluated in this article, or claim that may be made by its manufacturer, is not guaranteed or endorsed by the publisher.

References

- Agarwal, S., Jiang, S., and Chen, Y. (2019). Progress in the field of water- and/or temperature-triggered polymer actuators. *Macromol. Mater. Eng.* 304 (2), 1800548. doi:10.1002/mame.201800548
- Almine, J. F., Bax, D. V., Mithieux, S. M., Nivison-Smith, L., Rnjak, J., Waterhouse, A., et al. (2010). Elastin-based materials. *Chem. Soc. Rev.* 39 (9), 3371–3379. doi:10.1039/B919452P
- Aluri, S., Pastuszka, M. K., Moses, A. S., and MacKay, J. A. (2012). Elastin-like peptide amphiphiles form nanofibers with tunable length. *Biomacromolecules* 13 (9), 2645–2654. doi:10.1021/bm300472y
- Annabi, N., Shin, S. R., Tamayol, A., Miscuglio, M., Bakooshi, M. A., Assmann, A., et al. (2016). Highly elastic and conductive human-based protein hybrid hydrogels. *Adv. Mater.* 28 (1), 40–49. doi:10.1002/adma.201503255
- Bar-Cohen, Y. (2005). Current and future developments in artificial muscles using electroactive polymers. *Expert Rev. Med. Devices* 2 (6), 731–740. doi:10.1586/17434440.2.6.731
- Bar-Cohen, Y., and Anderson, I. A. (2019). Electroactive polymer (EAP) actuators—background review. *Mech. Soft Mater.* 1 (1), 5. doi:10.1007/s42558-019-0005-1
- Bedell-Hogan, D., Trackman, P., Abrams, W., Rosenbloom, J., and Kagan, H. (1993). Oxidation, cross-linking, and insolubilization of recombinant tropoelastin by purified lysyl oxidase. *J. Biol. Chem.* 268 (14), 10345–10350. doi:10.1016/S0021-9258(18)82207-4
- Bordat, A., Boissenot, T., Nicolas, J., and Tsapis, N. (2019). Thermoresponsive polymer nanocarriers for biomedical applications. *Adv. Drug Deliv. Rev.* 138, 167–192. doi:10.1016/j.addr.2018.10.005
- Chang, L., Liu, Y., Yang, Q., Yu, L., Liu, J., Zhu, Z., et al. (2018). Ionic electroactive polymers used in bionic robots: a review. *J. Bionic Eng.* 15 (5), 765–782. doi:10.1007/s42235-018-0065-1
- Chen, M., Liang, S., Liu, C., Liu, Y., and Wu, S. (2020). Reconfigurable and recyclable photoactuators based on azobenzene-containing polymers. *Front. Chem.* 8, 706. doi:10.3389/fchem.2020.00706
- Chiang, M.-Y., Lo, Y.-C., Lai, Y.-H., Yong, Y.-Y. A., Chang, S.-J., Chen, W.-L., et al. (2021). Protein-based soft actuator with high photo-response and easy modulation for anisotropic cell alignment and proliferation in a liquid environment. *J. Mater. Chem. B* 9 (33), 6634–6645. doi:10.1039/D1TB01198G
- Cianchetti, M., Laschi, C., Menciassi, A., and Dario, P. (2018). Biomedical applications of soft robotics. *Nat. Rev. Mater.* 3 (6), 143–153. doi:10.1038/s41578-018-0022-y
- Coyle, S., Majidi, C., LeDuc, P., and Hsia, K. J. (2018). Bio-inspired soft robotics: material selection, actuation, and design. *Extreme Mech. Lett.* 22, 51–59. doi:10.1016/j.eml.2018.05.003
- Cui, H., Zhao, Q., Zhang, L., and Du, X. (2020). Intelligent polymer-based bioinspired actuators: from monofunction to multifunction. *Adv. Intell. Syst.* 2 (11), 2000138. doi:10.1002/aisy.202000138

- Dai, M., Goudounet, G., Zhao, H., Garbay, B., Garanger, E., Pecastaings, G., et al. (2021). Thermosensitive hybrid elastin-like polypeptide-based ABC triblock hydrogel. *Macromolecules* 54 (1), 327–340. doi:10.1021/acs.macromol.0c01744
- Dong, Y., Yeung, K.-W., Tang, C.-Y., Law, W.-C., Tsui, G.C.-P., and Xie, X. (2021). Development of ionic liquid-based electroactive polymer composites using nanotechnology. *Nanotechnol. Rev.* 10 (1), 99–116. doi:10.1515/ntrev-2021-0009
- Dreher, M. R., Simnick, A. J., Fischer, K., Smith, R. J., Patel, A., Schmidt, M., et al. (2008). Temperature triggered self-assembly of polypeptides into multivalent spherical micelles. *J. Am. Chem. Soc.* 130 (2), 687–694. doi:10.1021/ja0764862
- El-Atab, N., Mishra, R. B., Al-Modaf, F., Joharji, L., Alsharif, A. A., Alamoudi, H., et al. (2020). Soft actuators for soft robotic applications: a review. *Adv. Intell. Syst.* 2 (10), 2000128. doi:10.1002/aisy.202000128
- Fazio, M. J., Olsen, D. R., Kauh, E. A., Baldwin, C. T., Indik, Z., Ornstein-Goldstein, N., et al. (1988). Cloning of full-length elastin cDNAs from a human skin fibroblast recombinant cDNA library: further elucidation of alternative splicing utilizing exon-specific oligonucleotides. *J. Investigative Dermatology* 91 (5), 458–464. doi:10.1111/1523-1747.ep12476591
- Ghoorchian, A., Simon, J. R., Bharti, B., Han, W., Zhao, X., Chilkoti, A., et al. (2015). Bioinspired reversibly cross-linked hydrogels comprising polypeptide micelles exhibit enhanced mechanical properties. *Adv. Funct. Mater.* 25 (21), 3122–3130. doi:10.1002/adfm.201500699
- Gonzalez-Obeso, C., Rodriguez-Cabello, J. C., and Kaplan, D. L. (2022). Fast and reversible crosslinking of a silk elastin-like polymer. *Acta Biomater.* 141, 14–23. doi:10.1016/j.actbio.2021.12.031
- Guo, Z., Xu, Y., Dong, L., Desai, M. S., Xia, J., Liang, M., et al. (2022). Design of functional hydrogels using smart polymer based on elastin-like polypeptides. *Chem. Eng. J.* 435, 135155. doi:10.1016/j.cej.2022.135155
- Hannaford, B., Jaax, K., and Klute, G. (2001). Bio-inspired actuation and sensing. *Aut. Robots* 11 (3), 267–272. doi:10.1023/A:1012495108404
- Huang, W., Rollett, A., and Kaplan, D. L. (2015). Silk-elastin-like protein biomaterials for the controlled delivery of therapeutics. *Expert Opin. Drug Deliv.* 12 (5), 779–791. doi:10.1517/17425247.2015.989830
- Huang, W. M., Yang, B., Zhao, Y., and Ding, Z. (2010). Thermo-moisture responsive polyurethane shape-memory polymer and composites: a review. *J. Mater. Chem.* 20 (17), 3367–3381. doi:10.1039/B922943D
- Ilami, M., Bagheri, H., Ahmed, R., Skowronek, E. O., and Marvi, H. (2021). Materials, actuators, and sensors for soft bioinspired robots. *Adv. Mater.* 33 (19), 2003139. doi:10.1002/adma.202003139
- Indik, Z., Abrams, W. R., Kucich, U., Gibson, C. W., Mecham, R. P., and Rosenbloom, J. (1990). Production of recombinant human tropoelastin: characterization and demonstration of immunologic and chemotactic activity. *Archives Biochem. Biophysics* 280 (1), 80–86. doi:10.1016/0003-9861(90)90521-Y
- Indik, Z., Yeh, H., Ornstein-Goldstein, N., Sheppard, P., Anderson, N., Rosenbloom, J. C., et al. (1987). Alternative splicing of human elastin mRNA indicated by sequence analysis of cloned genomic and complementary DNA. *Proc. Natl. Acad. Sci.* 84 (16), 5680–5684. doi:10.1073/pnas.84.16.5680
- Kamada, R., Miyazaki, H., Janairo, J. I. B., Chuman, Y., and Sakaguchi, K. (2023). Bilayer hydrogel composed of elastin-mimetic polypeptides as a bio-actuator with bidirectional and reversible bending behaviors. *Molecules* 28 (13), 5274. doi:10.3390/molecules28135274
- Kim, B., and Chilkoti, A. (2008). Allosteric actuation of inverse phase transition of a stimulus-responsive fusion polypeptide by ligand binding. *J. Am. Chem. Soc.* 130 (52), 17867–17873. doi:10.1021/ja0805907
- Kim, S., Laschi, C., and Trimmer, B. (2013). Soft robotics: a bioinspired evolution in robotics. *Trends Biotechnol.* 31 (5), 287–294. doi:10.1016/j.tibtech.2013.03.002
- Lao, U. L., Sun, M., Matsumoto, M., Mulchandani, A., and Chen, W. (2007). Genetic engineering of self-assembled protein hydrogel based on elastin-like sequences with metal binding functionality. *Biomacromolecules* 8 (12), 3736–3739. doi:10.1021/bm700662n
- Le, D. H. T., Hanamura, R., Pham, D.-H., Kato, M., Tirrell, D. A., Okubo, T., et al. (2013). Self-assembly of elastin-mimetic double hydrophobic polypeptides. *Biomacromolecules* 14 (4), 1028–1034. doi:10.1021/bm301887m
- Le, D. H. T., Tsutsui, Y., Sugawara-Narutaki, A., Yukawa, H., Baba, Y., and Ohtsuki, C. (2017). Double-hydrophobic elastin-like polypeptides with added functional motifs: self-assembly and cytocompatibility. *J. Biomed. Mater. Res. Part A* 105 (9), 2475–2484. doi:10.1002/jbm.a.36105
- Lee, J. S., Kang, M. J., Lee, J. H., and Lim, D. W. (2022a). Injectable hydrogels of stimuli-responsive elastin and calmodulin-based triblock copolypeptides for controlled drug release. *Biomacromolecules* 23 (5), 2051–2063. doi:10.1021/acs.biomac.2c00053
- Lee, K., Noh, Y., Bae, Y., Kang, S., and Cha, C. (2022b). Tunable physicochemical and drug release properties of *in situ* forming thermoresponsive elastin-like polypeptide hydrogels. *Biomacromolecules* 23 (12), 5193–5201. doi:10.1021/acs.biomac.2c01001
- Lee, S., Kim, J.-S., Chu, H. S., Kim, G.-W., Won, J.-I., and Jang, J.-H. (2011). Electrospun nanofibrous scaffolds for controlled release of adeno-associated viral vectors. *Acta Biomater.* 7 (11), 3868–3876. doi:10.1016/j.actbio.2011.06.035
- Lendlein, A. (2018). Fabrication of reprogrammable shape-memory polymer actuators for robotics. *Sci. Robotics* 3 (18), eaa9090. doi:10.1126/scirobotics.aa9090
- Li, M., Pal, A., Aghakhani, A., Pena-Francesch, A., and Sitti, M. (2022). Soft actuators for real-world applications. *Nat. Rev. Mater.* 7 (3), 235–249. doi:10.1038/s41578-021-00389-7
- Lima, L. F., Sousa, M. G. D. C., Rodrigues, G. R., de Oliveira, K. B. S., Pereira, A. M., da Costa, A., et al. (2022). Elastin-like polypeptides in development of nanomaterials for application in the medical field. *Front. Nanotechnol.* 4, 874790. doi:10.3389/fnano.2022.874790
- Liu, J., Jiang, L., He, S., Zhang, J., and Shao, W. (2022). Recent progress in PNIPAM-based multi-responsive actuators: a mini-review. *Chem. Eng. J.* 433, 133496. doi:10.1016/j.cej.2021.133496
- Lo, Y. C., Chiang, M. Y., Chen, W. L., and Chen, S. Y. (2017). "Elastin-like polypeptide-based hydrogel actuator for cardiac tissue engineering", in: 2017 IEEE 17th International Conference on Nanotechnology (IEEE-NANO), 701–704.
- López Barreiro, D., Minten, I. J., Thies, J. C., and Sagt, C. M. J. (2023). Structure–property relationships of elastin-like polypeptides: a review of experimental and computational studies. *ACS Biomaterials Sci. Eng.* 9 (7), 3796–3809. doi:10.1021/acsbomaterials.1c00145
- Lu, X., Guo, S., Tong, X., Xia, H., and Zhao, Y. (2017). Tunable photocontrolled motions using stored strain energy in malleable azobenzene liquid crystalline polymer actuators. *Adv. Mater.* 29 (28), 1606467. doi:10.1002/adma.201606467
- MacEwan, S. R., and Chilkoti, A. (2010). Elastin-like polypeptides: biomedical applications of tunable biopolymers. *Peptide Sci.* 94 (1), 60–77. doi:10.1002/bip.21327
- Mahimwalla, Z., Yager, K. G., Mamiya, J.-i., Shishido, A., Priimagi, A., and Barrett, C. J. (2012). Azobenzene photomechanics: prospects and potential applications. *Polym. Bull.* 69 (8), 967–1006. doi:10.1007/s00289-012-0792-0
- Maksimkin, A. V., Dayyoub, T., Telyshev, D. V., and Gerasimenko, A. Y. (2022). Electroactive polymer-based composites for artificial muscle-like actuators: a review. *Nanomaterials* 12 (13), 2272. doi:10.3390/nano12132272
- Martin, S. L., Vrhovski, B., and Weiss, A. S. (1995). Total synthesis and expression in *Escherichia coli* of a gene encoding human tropoelastin. *Gene* 154 (2), 159–166. doi:10.1016/0378-1119(94)00848-M
- Martino, M., Coviello, A., and Tamburro, A. M. (2000). Synthesis and structural characterization of poly(LGGVG), an elastin-like polypeptide. *Int. J. Biol. Macromol.* 27 (1), 59–64. doi:10.1016/S0141-8130(99)00118-X
- McDaniel, J. R., MacKay, J. A., Quiroz, F. G., and Chilkoti, A. (2010). Recursive directional ligation by plasmid reconstruction allows rapid and seamless cloning of oligomeric genes. *Biomacromolecules* 11 (4), 944–952. doi:10.1021/bm901387t
- McDaniel, J. R., Weitzhandler, I., Prevost, S., Vargo, K. B., Appavou, M.-S., Hammer, D. A., et al. (2014). Noncanonical self-assembly of highly asymmetric genetically encoded polypeptide amphiphiles into cylindrical micelles. *Nano Lett.* 14 (11), 6590–6598. doi:10.1021/nl503221p
- Menon, A. V., Madras, G., and Bose, S. (2019). The journey of self-healing and shape memory polyurethanes from bench to translational research. *Polym. Chem.* 10 (32), 4370–4388. doi:10.1039/C9PY00854C
- Meyer, D. E., and Chilkoti, A. (1999). Purification of recombinant proteins by fusion with thermally-responsive polypeptides. *Nat. Biotechnol.* 17 (11), 1112–1115. doi:10.1038/15100
- Meyer, D. E., and Chilkoti, A. (2002). Genetically encoded synthesis of protein-based polymers with precisely specified molecular weight and sequence by recursive directional ligation: examples from the elastin-like polypeptide system. *Biomacromolecules* 3 (2), 357–367. doi:10.1021/bm015630n
- Natsume, K., Nakamura, J., Sato, K., Ohtsuki, C., and Sugawara-Narutaki, A. (2023). Biological properties of self-assembled nanofibers of elastin-like block polypeptides for tissue-engineered vascular grafts: platelet inhibition, endothelial cell activation and smooth muscle cell maintenance. *Regen. Biomater.* 10, rbac111. doi:10.1093/rb/rbac111
- Neuhaus, R., Zahiri, N., Petrs, J., Tahouni, Y., Siegert, J., Kolaric, I., et al. (2020). Integrating ionic electroactive polymer actuators and sensors into adaptive building skins – potentials and limitations. *Front. Built Environ.* 6, 95. doi:10.3389/fbuil.2020.00095
- Novelli, G. L., Vargas, G. G., and Andrade, R. M. (2023). Dielectric elastomer actuators as artificial muscles for wearable robots. *J. Intelligent Material Syst. Struct.* 34 (9), 1007–1025. doi:10.1177/1045389x221128567
- Olvera Bernal, R. A., Olekhovich, R. O., and Uspenskaya, M. V. (2023). Chitosan/PVA nanofibers as potential material for the development of soft actuators. *Polymers* 15 (9), 2037. doi:10.3390/polym15092037
- Ozsvar, J., Yang, C., Cain, S. A., Baldock, C., Tarakanova, A., and Weiss, A. S. (2021). Tropoelastin and elastin assembly. *Front. Bioeng. Biotechnol.* 9, 643110. doi:10.3389/fbioe.2021.643110
- Prashanna, A., Taylor, P. A., Qin, J., Kiick, K. L., and Jayaraman, A. (2019). Effect of peptide sequence on the LCST-like transition of elastin-like peptides and elastin-like peptide–collagen-like peptide conjugates: simulations and experiments. *Biomacromolecules* 20 (3), 1178–1189. doi:10.1021/acs.biomac.8b01503

- Putzu, M., Causa, F., Nele, V., de Torre, I. G., Rodriguez-Cabello, J. C., and Netti, P. A. (2016). Elastin-like-recombinamers multilayered nanofibrous scaffolds for cardiovascular applications. *Biofabrication* 8 (4), 045009. doi:10.1088/1758-5090/8/4/045009
- Ratna, D., and Karger-Kocsis, J. (2008). Recent advances in shape memory polymers and composites: a review. *J. Mater. Sci.* 43 (1), 254–269. doi:10.1007/s10853-007-2176-7
- Rodriguez-Cabello, J. C., Gonzalez De Torre, I., González-Pérez, M., González-Pérez, F., and Montequi, I. (2021). Fibrous scaffolds from elastin-based materials. *Front. Bioeng. Biotechnol.* 9, 652384. doi:10.3389/fbioe.2021.652384
- Roy, D., Brooks, W. L. A., and Sumerlin, B. S. (2013). New directions in thermoresponsive polymers. *Chem. Soc. Rev.* 42 (17), 7214–7243. doi:10.1039/C3CS35499G
- Saha, S., Banskota, S., Roberts, S., Kirmani, N., and Chilkoti, A. (2020). Engineering the architecture of elastin-like polypeptides: from unimers to hierarchical self-assembly. *Adv. Ther.* 3 (3), 1900164. doi:10.1002/adtp.201900164
- Scalet, G. (2020). Two-way and multiple-way shape memory polymers for soft robotics: an overview. *Actuators* 9 (1), 10. doi:10.3390/act9010010
- Shen, Z., Chen, F., Zhu, X., Yong, K.-T., and Gu, G. (2020). Stimuli-responsive functional materials for soft robotics. *J. Mater. Chem. B* 8 (39), 8972–8991. doi:10.1039/D0TB01585G
- Shu, T., Hu, L., Shen, Q., Jiang, L., Zhang, Q., and Serpe, M. J. (2020). Stimuli-responsive polymer-based systems for diagnostic applications. *J. Mater. Chem. B* 8 (32), 7042–7061. doi:10.1039/D0TB00570C
- Tarakanova, A., Yeo, G. C., Baldock, C., Weiss, A. S., and Buehler, M. J. (2019). Tropoelastin is a flexible molecule that retains its canonical shape. *Macromol. Biosci.* 19 (3), 1800250. doi:10.1002/mabi.201800250
- Tokudome, Y., Kuniwaki, H., Suzuki, K., Carboni, D., Poologundarampillai, G., and Takahashi, M. (2016). Thermoresponsive wrinkles on hydrogels for soft actuators. *Adv. Mater. Interfaces* 3 (12), 1500802. doi:10.1002/admi.201500802
- Trabbic-Carlson, K., Setton, L. A., and Chilkoti, A. (2003). Swelling and mechanical behaviors of chemically cross-linked hydrogels of elastin-like polypeptides. *Biomacromolecules* 4 (3), 572–580. doi:10.1021/bm025671z
- Urry, D. W. (1988). Entropic elastic processes in protein mechanisms. I. Elastic structure due to an inverse temperature transition and elasticity due to internal chain dynamics. *J. Protein Chem.* 7 (1), 1–34. doi:10.1007/BF01025411
- Urry, D. W., Haynes, B., Zhang, H., Harris, R. D., and Prasad, K. U. (1988). Mechanochemical coupling in synthetic polypeptides by modulation of an inverse temperature transition. *Proc. Natl. Acad. Sci.* 85(10), 3407–3411. doi:10.1073/pnas.85.10.3407
- Valiaev, A., Abu-Lail, N. I., Lim, D. W., Chilkoti, A., and Zauscher, S. (2007). Microcantilever sensing and actuation with end-grafted stimulus-responsive elastin-like polypeptides. *Langmuir* 23 (1), 339–344. doi:10.1021/la0616698
- Varanko, A. K., Su, J. C., and Chilkoti, A. (2020). Elastin-like polypeptides for biomedical applications. *Annu. Rev. Biomed. Eng.* 22 (1), 343–369. doi:10.1146/annurev-bioeng-092419-061127
- Wang, E., Desai, M. S., and Lee, S.-W. (2013). Light-controlled graphene-elastin composite hydrogel actuators. *Nano Lett.* 13 (6), 2826–2830. doi:10.1021/nl401088b
- Wang, H., Cai, L., Paul, A., Enejder, A., and Heilshorn, S. C. (2014). Hybrid elastin-like polypeptide–polyethylene glycol (ELP-PEG) hydrogels with improved transparency and independent control of matrix mechanics and cell ligand density. *Biomacromolecules* 15 (9), 3421–3428. doi:10.1021/bm500969d
- Wang, Y., Huang, W., Wang, Y., Mu, X., Ling, S., Yu, H., et al. (2020). Stimuli-responsive composite biopolymer actuators with selective spatial deformation behavior. *Proc. Natl. Acad. Sci.* 117(25), 14602–14608. doi:10.1073/pnas.2002996117
- Wei, M., Gao, Y., Li, X., and Serpe, M. J. (2017). Stimuli-responsive polymers and their applications. *Polym. Chem.* 8 (1), 127–143. doi:10.1039/C6PY01585A
- Wise, S. G., Mithieux, S. M., and Weiss, A. S. (2009). “Engineered tropoelastin and elastin-based biomaterials,” in *Advances in protein chemistry and structural biology*. Editor A. McPherson (Academic Press), 1–24.
- Wu, W. J., Vrhovski, B., and Weiss, A. S. (1999). Glycosaminoglycans mediate the coacervation of human tropoelastin through dominant charge interactions involving lysine side chains. *J. Biol. Chem.* 274 (31), 21719–21724. doi:10.1074/jbc.274.31.21719
- Xia, Y., He, Y., Zhang, F., Liu, Y., and Leng, J. (2021). A review of shape memory polymers and composites: mechanisms, materials, and applications. *Adv. Mater.* 33 (6), 2000713. doi:10.1002/adma.202000713
- Zarrintaj, P., Ahmadi, Z., Reza Saeb, M., and Mozafari, M. (2018). Poloxamer-based stimuli-responsive biomaterials. *Mater. Today Proc.* 5 (3), 15516–15523. doi:10.1016/j.matpr.2018.04.158
- Zarrintaj, P., Ramsey, J. D., Samadi, A., Atoufi, Z., Yazdi, M. K., Ganjali, M. R., et al. (2020). Poloxamer: a versatile tri-block copolymer for biomedical applications. *Acta Biomater.* 110, 37–67. doi:10.1016/j.actbio.2020.04.028
- Zhang, H., Niu, C., Zhang, Y., Wang, X., and Yang, B. (2020a). A mechanically strong polyvinyl alcohol/poly(2-(N,N'-dimethyl amino) ethyl methacrylate)-poly (acrylic acid) hydrogel with pH-responsiveness. *Colloid Polym. Sci.* 298 (6), 619–628. doi:10.1007/s00396-020-04652-1
- Zhang, Y., Desai, M. S., Wang, T., and Lee, S.-W. (2020b). Elastin-based thermoresponsive shape-memory hydrogels. *Biomacromolecules* 21 (3), 1149–1156. doi:10.1021/acs.biomac.9b01541
- Zhang, Y., Xie, S., Zhang, D., Ren, B., Liu, Y., Tang, L., et al. (2019). Thermo-responsive and shape-adaptive hydrogel actuators from fundamentals to applications. *Eng. Sci.* 6, 1–11. doi:10.30919/es8d788
- Zhang, Y.-N., Avery, R. K., Vallmajo-Martin, Q., Assmann, A., Vegh, A., Memic, A., et al. (2015). A highly elastic and rapidly crosslinkable elastin-like polypeptide-based hydrogel for biomedical applications. *Adv. Funct. Mater.* 25 (30), 4814–4826. doi:10.1002/adfm.201501489
- Zhu, D., Wang, H., Trinh, P., Heilshorn, S. C., and Yang, F. (2017). Elastin-like protein-hyaluronic acid (ELP-HA) hydrogels with decoupled mechanical and biochemical cues for cartilage regeneration. *Biomaterials* 127, 132–140. doi:10.1016/j.biomaterials.2017.02.010



OPEN ACCESS

EDITED BY

Milana C. Vasudev,
University of Massachusetts Dartmouth,
United States

REVIEWED BY

Guoxu Zhao,
Hainan University, China
Arunkumar Palaniappan,
Vellore Institute of Technology (VIT), India

*CORRESPONDENCE

Isabelle Texier,
✉ isabelle.texier-nogues@cea.fr

RECEIVED 14 September 2023

ACCEPTED 02 January 2024

PUBLISHED 21 February 2024

CITATION

Sacchi M, Sauter-Starace F, Mailley P and
Texier I (2024), Resorbable conductive
materials for optimally interfacing medical
devices with the living.
Front. Bioeng. Biotechnol. 12:1294238.
doi: 10.3389/fbioe.2024.1294238

COPYRIGHT

© 2024 Sacchi, Sauter-Starace, Mailley and
Texier. This is an open-access article distributed
under the terms of the [Creative Commons
Attribution License \(CC BY\)](#). The use,
distribution or reproduction in other forums is
permitted, provided the original author(s) and
the copyright owner(s) are credited and that the
original publication in this journal is cited, in
accordance with accepted academic practice.
No use, distribution or reproduction is
permitted which does not comply with these
terms.

Resorbable conductive materials for optimally interfacing medical devices with the living

Marta Sacchi ^{1,2}, Fabien Sauter-Starace ¹, Pascal Mailley¹
and Isabelle Texier^{1*}

¹Université Grenoble Alpes, CEA, LETI-DTIS (Département des Technologies pour l'Innovation en Santé), Grenoble, France, ²Université Paris-Saclay, CEA, JACOB-SEPIA, Fontenay-aux-Roses, France

Implantable and wearable bioelectronic systems are arising growing interest in the medical field. Linking the microelectronic (electronic conductivity) and biological (ionic conductivity) worlds, the biocompatible conductive materials at the electrode/tissue interface are key components in these systems. We herein focus more particularly on resorbable bioelectronic systems, which can safely degrade in the biological environment once they have completed their purpose, namely, stimulating or sensing biological activity in the tissues. Resorbable conductive materials are also explored in the fields of tissue engineering and 3D cell culture. After a short description of polymer-based substrates and scaffolds, and resorbable electrical conductors, we review how they can be combined to design resorbable conductive materials. Although these materials are still emerging, various medical and biomedical applications are already taking shape that can profoundly modify post-operative and wound healing follow-up. Future challenges and perspectives in the field are proposed.

KEYWORDS

conductive, resorbable, biopolymer, conducting polymers, bioelectronics, implanted sensors, wearable sensors, tissue engineering

1 Introduction

The current landscape of electronic systems in the medical field is diverse, encompassing wearable and implantable devices tailored to various applications, such as drug delivery, occasional or continuous monitoring, or stimulation. These systems primarily rely on traditional materials like metals, semiconductors, and plastics and conventional processes such as patterning and lithography from the realm of microelectronics. In recent years, much effort has been dedicated to conferring these systems with mechanical properties more suitable for *in vivo* use, for instance, with the employment of thinned structures, and the development of processes compatible with flexible and stretchable substrates such as elastomers (Palma et al., 2022; Veletić et al., 2022). However, the large majority of presently used medical bioelectronic systems display a fundamental difference with living tissues: they are not resorbable, meaning they are not composed of materials that progressively dissolve in the body or onto the skin, without inducing toxicity or immunogenicity. Long-term implants are required for a set of medical applications that are presently addressed (e.g., cardiac and neural implants such as deep brain stimulation implants for Parkinson's disease or vagus nerve stimulation devices), or for which it would be highly desirable to prolong the device lifetime (e.g., continuous glucose monitoring sensors, drug delivery pumps, etc.). However, innovative applications

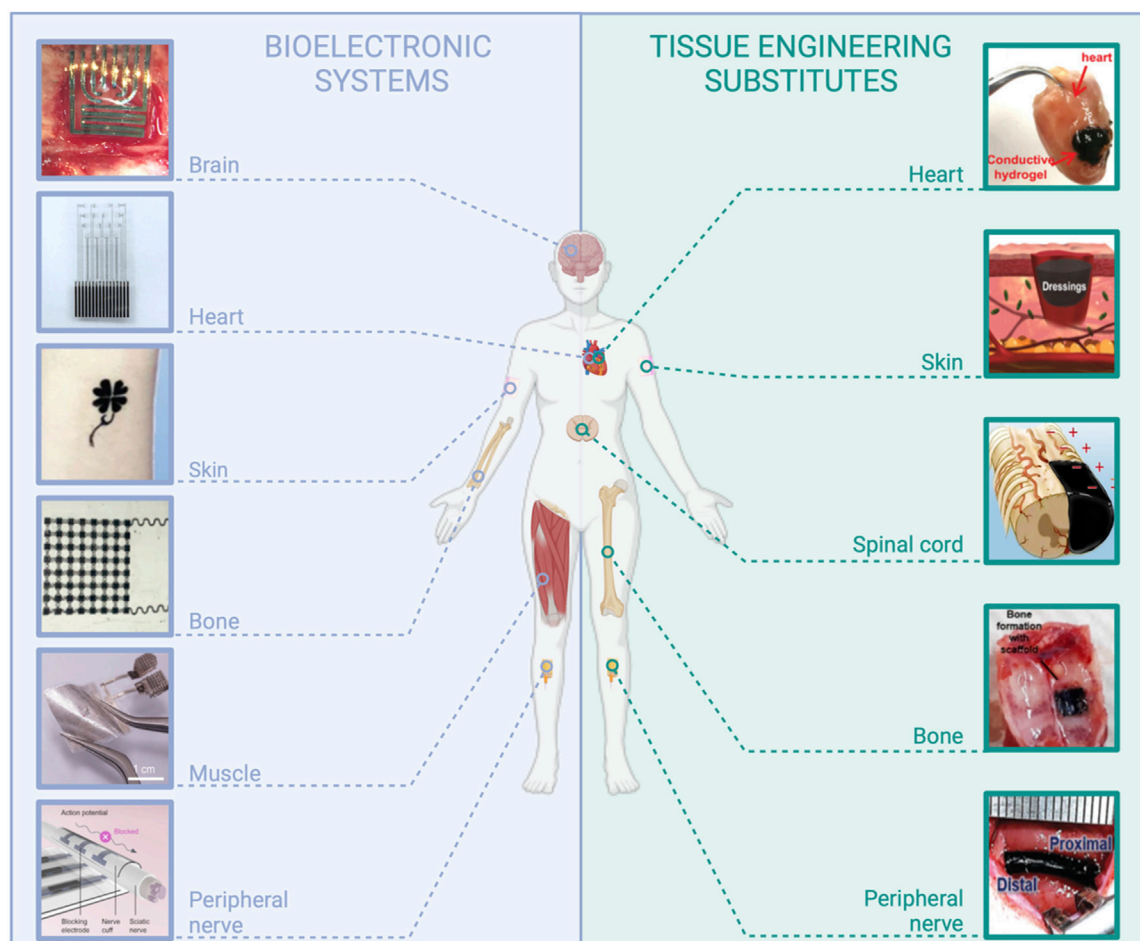


FIGURE 1

Examples of applications in the field of medical devices requiring the use of resorbable conductive materials. *Bioelectronic systems*: brain: reproduced with permission, Copyright 2019, John Wiley and Sons (Xu K. et al., 2019). Heart: adapted with permission, Copyright 2023, the Authors, published by *Science Advances* (Chen et al., 2023). Skin: reproduced with permission, Copyright 2019, John Wiley and Sons (Wang Q. et al., 2019). Bone: adapted with permission, Copyright 2021, the Authors, published by *PNAS* (Yao et al., 2021). Muscle: adapted with permission from Huang et al. (2022), Copyright 2022, the American Chemical Society. Peripheral nerve: Copyright 2022, the Authors, published by *Science Advances* (Lee et al., 2022). *Tissue engineering substitutes*: Heart: adapted from Xu Y. et al. (2019), Copyright 2019, John Wiley and Sons. Skin: adapted with permission from Huang et al. (2018), Copyright 2018, the American Chemical Society. Spinal cord: adapted from Chen et al. (2022), Copyright 2022, Springer Nature. Bone: reproduced from eSilva et al. (2021), Copyright 2021, Springer Nature. Peripheral nerve: reproduced with permission, Copyright 2020, John Wiley and Sons (Park et al., 2020), created with BioRender.com.

could emerge with the advent of resorbable, wearable, or implanted medical bioelectronic systems (Figure 1). Resorbable bioelectronics can be used for the design of microelectrode arrays for transient neuromodulation (brain, spinal cord, and peripheral nerve), on-skin sensors, and heart, skin, muscle, or bone stimulation to promote healing. More prospectively, resorbable sensors can be dedicated to post-surgical follow-up to alert on infection risks or ensure the success of a graft (tissue anastomosis). Resorbable conductive materials are also intensively sought for tissue engineering, in particular in the case of electro-responsive organs such as the heart, nerves, or skin, and for demanding *in vitro* applications, particularly in the field of 3D cell culture models (Guo et al., 2018; Park et al., 2022b; Tringides et al., 2022).

It is noteworthy that material resorbability in the body or onto the skin is more demanding than biodegradability, which may also encompass degradation in the natural environment under a more general definition. In the body, biodegradable materials

degrade in smaller fragments that can eventually diffuse from their implantation site but not necessarily be eliminated. Contrarily, resorbable materials are totally eliminated from the body. These are materials that degrade into safe, smaller components when exposed to physiologically relevant conditions like biological fluids and enzymes. These resulting components and by-products are subsequently removed from the body via either metabolic processes or excretion (Eglin et al., 2008; Grosjean et al., 2023). Material resorbability can occur through different mechanisms, i.e., chemical and enzymatic degradations. The main chemical degradation processes occur through the hydrolysis of the polymer backbone bonds. Notably, the kinetics of degradation of commonly used synthetic polyesters such as poly(lactic acid) (PLA), poly(lactic-co-glycolic acid) (PLGA), and poly(hydroxyalkanoates) (PHA) can be controlled by their molecular composition, polymer molecular weight, and crystallinity (Bano et al., 2018). Natural polymers such as

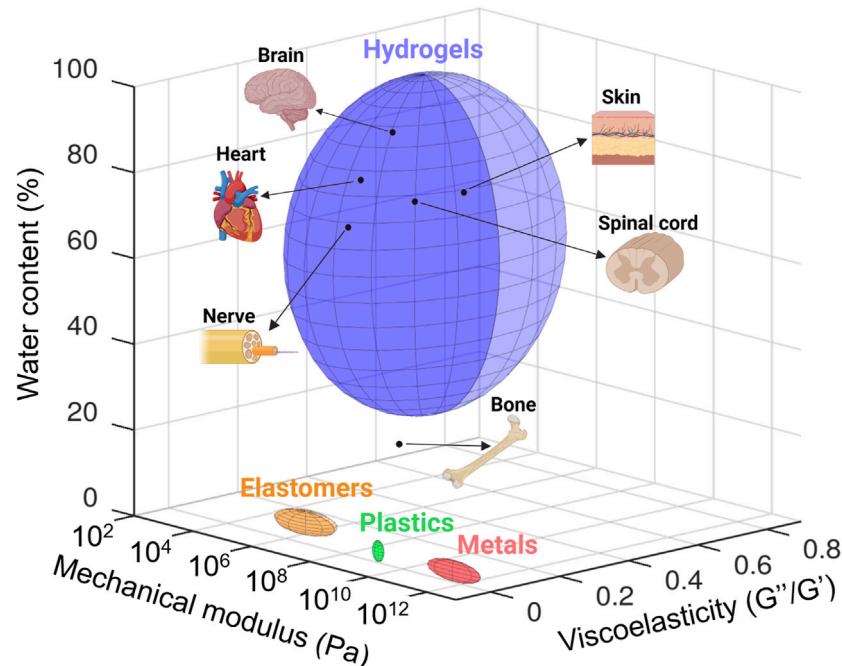


FIGURE 2

Quantification and comparison of the mechanical modulus (Pascal, Pa), viscoelasticity (loss modulus/storage modulus, G''/G'), and water content (percentage of weight) of tissues with those of materials classically employed in bioelectronic devices and tissue engineering (i.e., metals, plastic, elastomers, and hydrogels). Data taken from literature. Mechanical modulus: brain (Hall et al., 2021), heart (Jacot et al., 2010), spinal cord (Karimi et al., 2017), nerve (Rosso et al., 2019), skin (Kalra et al., 2016), bone (Morgan et al., 2018), and materials classically employed in bioelectronic devices and tissue engineering (Tringides et al., 2022). Viscoelasticity: adapted from Tringides et al. (2022). Water content: bone (Surowiec et al., 2022), nerve (Anand et al., 1988), spinal cord (Mbori et al., 2016), skin (Téllez-Soto et al., 2021), heart (Eitel et al., 2011), and brain (Gottschalk et al., 2021). Created with Octave (software version 8.2.0) and adapted on BioRender.com.

collagen, gelatin, and hyaluronic acid are primarily degraded by proteolytic and glycolytic enzymes.

In addition to biocompatibility, materials employed in designing medical devices must fulfill additional requirements due to their intimate interaction with tissues. Indeed, these tissues can display a wide range of mechanical properties. First, bones, tendons, and nerves can be considered very hard and poorly stretchable tissues, with mechanical stiffness quantified by Young's modulus in the decreasing order of 12 GPa (Keller et al., 1990), 550 MPa (O'Brien et al., 2010), and 580 kPa (Borschel et al., 2003), respectively. They exhibit high elastic moduli, similar to those of plastic materials (Figure 2). The skin is both relatively tough and stretchable (0.5–1 MPa elastic modulus) (Li et al., 2012), whereas very soft tissues like the brain display very high viscoelastic properties (elastic modulus G' below 10 kPa, elastic-to-viscous moduli ratio $G''/G' > 0.5$) (Hall et al., 2021; Tringides et al., 2022). In any case, tissue mechanical properties are quite different from those of rigid metal, plastics, or elastomers, classically employed in electronic devices (Figure 2) (Sunwoo et al., 2021). Such a mechanical mismatch between these materials and tissues at the intimate cellular level can be responsible for undesired effects, ranging from progressive material encapsulation by tissues, therefore inhibiting the correct functioning of the device, to acute inflammatory reaction and pain (Rivnay et al., 2017; Sunwoo et al., 2020). Another remarkable difference between tissues and materials such as metals, semiconductors, and elastomers presently used in bioelectronics

consists in their morphological structure. While tissues display a macroporous/microporous structure, most of these synthetic materials are shaped as solid bulk or thin continuous layers without either no or poor porosity. Very importantly, many tissues are intimately exposed to biological fluids like interstitial fluid and blood, even sometimes with shear flow as in the cardiac and circulatory systems, and many of them, in particular soft tissues, are continuously bathed in these fluids making them an integral part of the tissue itself (Figure 2). By comparison, metals, semiconductors, and synthetic elastomers do not comprise water. For tissue engineering applications, material water content is an important hallmark to allow the necessary perfusion of nutrients, oxygen, and biological cues. In these perspectives, hydrogels—3D cross-linked polymer networks that can absorb large quantities of water—are interesting to explore. Their mechanical properties can be tuned across a wide range of Young's modulus and viscoelasticity to design scaffolds with mechanical properties similar to those of the different types of tissues, from bone to brain (Figure 2) (Yuk et al., 2022). However, they are not intrinsically electronic conductors (though they can be ionic conductors), and consequently, they cannot be used as such to design electrically conductive materials for medical applications that require moderate to high electronic conductivity (10^3 – 10^5 S cm^{-1}). Therefore, for all the above reasons, it is clear that beyond resorbability, bioelectronics and tissue engineering applications can advantageously benefit from the use of innovative conductive materials that better display the fundamental characteristics of tissues, i.e., hydrogel-based materials.

Passive (i.e., non-conductive) resorbable polymer-based medical devices have been extensively developed for the short-term or prolonged delivery of active ingredients. These drug-delivery implants are mainly based on synthetic polyesters like PLA, PLGA, poly(caprolactone) (PCL), and PHA that are sometimes also referred to as “bioplastics” (Bano et al., 2018) or on resorbable biopolymer-based hydrogels. Though bioplastics and biopolymer-based hydrogels are both resorbable, these materials differ markedly by their mechanical and swelling properties (“tough” and quite hydrophobic materials for bioplastics and “soft” and wet materials for hydrogels). Resorbable synthetic polyesters, such as PLA, PLGA, and PHA, are interesting because they can act as insulating supports or passivation layers in bioelectronic systems, taking advantage of their rather hydrophobic properties. First resorbable elastomers have also been recently reported (Turner et al., 2022). Hydrogels, from their side, are by definition highly hydrophilic materials and not suitable to act as insulating substrates in the design of bioelectronic systems, but they can be combined with conductive moieties to obtain suitable interfaces (for instance, electrodes) with the tissues or for the development of 3D cell cultures or organoids (Caliari et al., 2016; Kozłowski et al., 2021). Silk fibroin is a resorbable natural polymer combining the interesting features of both bioplastics (i.e., mechanical properties) and hydrogels (i.e., porous biopolymer scaffold).

Concerning electrical conductors, the interest in conducting polymers such as poly(pyrrole) (PPy), poly(aniline) (PANI), and poly(3,4-ethylenedioxythiophene) (PEDOT) to optimize system/tissue bioelectronic interface was underlined several times due to both their ionic and electronic conductivity (Chen et al., 2021; Han et al., 2022). Indeed, Sansinena et al. (1997) and Kim et al. (2000) first pointed out the interest in such conductive materials, used in conjunction with hydrogels, for the design of artificial muscles exhibiting interesting actuation capabilities. However, other conductive materials of high interest are largely employed in bioelectronics and tissue engineering applications, especially when it is necessary to achieve high material conductivities. There exist a few biocompatible and resorbable metals such as molybdenum, tungsten, and iron. Two-dimensional (2D) transition-metal chalcogenides (e.g., MoS₂ sheets) and carbon-based structures and fillers like carbon nanotubes (CNTs) and graphene derivatives are also commonly employed materials.

In this review, we will describe how resorbable substrates and scaffolds such as elastomers, synthetic polyesters, and biopolymer-based hydrogels can be combined with a variety of electrical conductors like metals, micro- and macro-structured fillers, and conducting polymers, to lead to resorbable conductive materials with a wide range of mechanical properties. Some reviews have already discussed related subjects, such as conductive hydrogels (Rogers et al., 2020; Xu et al., 2020; Chen et al., 2021; Xu et al., 2021; Gao et al., 2022; Zhu et al., 2023a), conductive materials for neural interfaces (Fattahi et al., 2014), and conductive materials for tissue engineering (Min et al., 2018; Mostafavi et al., 2020; Rogers et al., 2020; Zhao et al., 2022b; Gao et al., 2022). However, we herein focus specifically on conductive materials that exhibit resorbability, a topic that has received comparatively less attention, especially for bioelectronic systems. As discussed earlier, the resorbability of conductive materials holds significant relevance for both the

fields of bioelectronic devices and tissue engineering. It is worth noting that there is a noticeable gap in the existing literature concerning a comprehensive work that effectively merges the domains of soft bioelectronic systems that interact with living tissues and tissue engineering. This review aims to bridge the gap between these two distinct yet interconnected fields, which both rely on similar polymer and electrical components, as well as process methodologies, especially when it comes to resorbable conductive materials. Thus, we aim to provide readers with a review and thorough analysis of various approaches within the context of bioresorbable materials, allowing for an in-depth exploration of specific challenges and opportunities, encompassing both bioelectronics and tissue engineering applications. Special emphasis will also be placed on resorbable hydrogel-based materials. As highlighted earlier, these materials exhibit exceptional properties for replicating the characteristics of living tissues, making them a natural choice for tissue engineering applications. Furthermore, our extensive literature review has unveiled that the utilization of resorbable hydrogels represents a smart and emerging approach to the design of resorbable bioelectronic devices. While this review encompasses resorbable conductive materials and their applications in a broader sense, we will particularly emphasize the role of hydrogel-based systems in this context. Note that although these are closely related domains, we will not review here electronic textiles and refer the reader to other publications in that field (Kim et al., 2019; Alhashmi Alamer et al., 2022; Gong et al., 2022; Zhang et al., 2022; Wei et al., 2023).

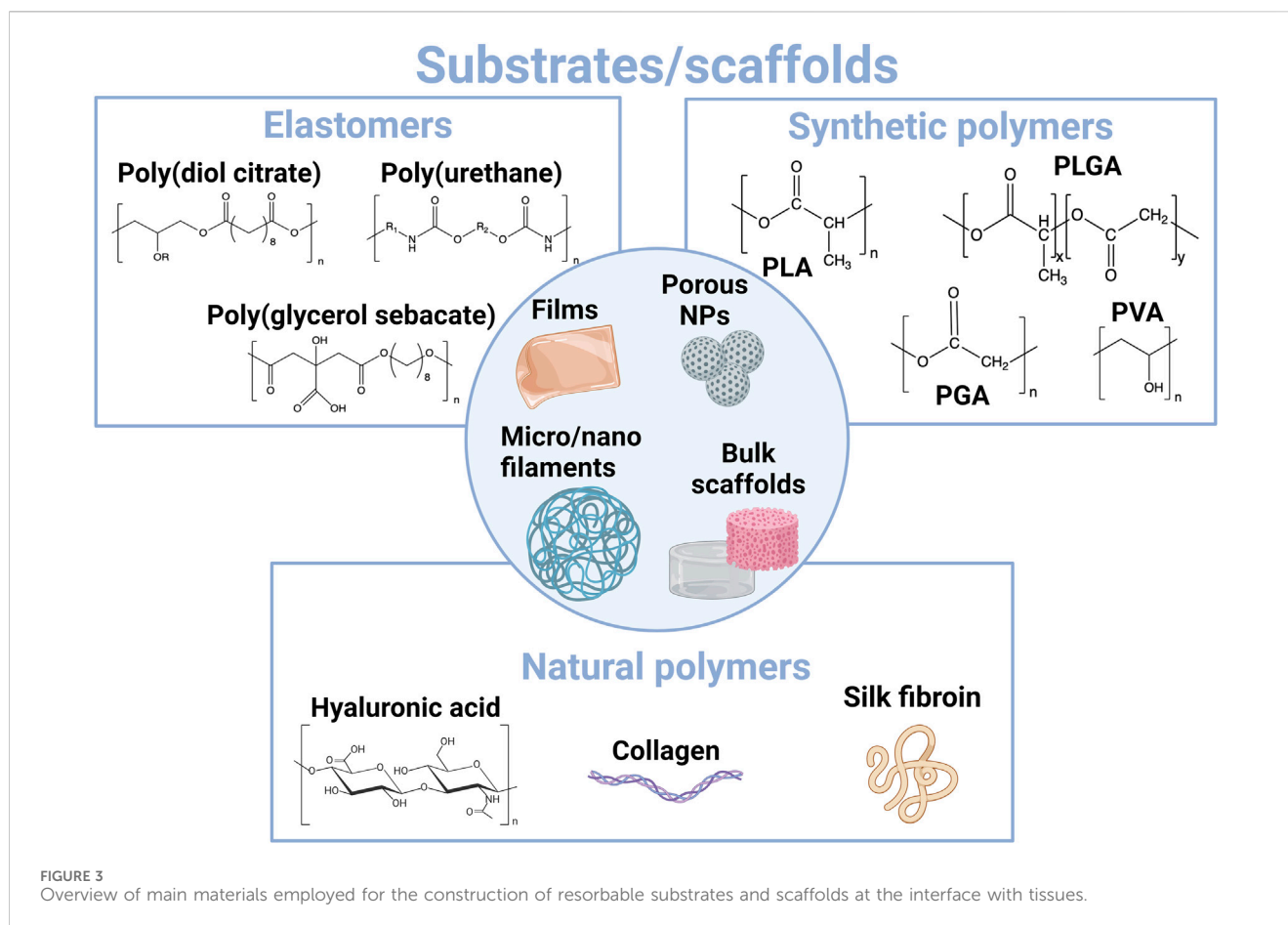
Following the examination of various resorbable substrates and scaffolds, we will review the selection of electrical conductors that present resorbability. Subsequently, we will describe the different processes that can be used to combine them into resorbable conductive materials. These processes can impact the resorbability, conductivity, and mechanical properties of the resultant resorbable devices. These innovative resorbable conductive materials have broad applications, such as the development of novel transient bioelectronic systems for monitoring and stimulation, which will not require retrieval surgery after they have served their purpose. Additionally, they hold promise for on-skin electronic applications, 3D cell culture, and tissue engineering, particularly in the context of electro-sensitive organs like the heart, nerves, brain, and skin. They are therefore expected to address emerging applications in the biomedical field.

2 Selecting components for the design of resorbable conductive hydrogels

Resorbable conductive materials rely on the combination of a 2D substrate or a 3D scaffold and an electrical conductor. In this section, we will give a short overview of these materials.

2.1 Substrates and scaffolds

The different resorbable materials that can be employed as 2D substrates or 3D scaffolds (Figure 3) do not display similar mechanical properties (Young's modulus and viscoelasticity), the same hydrophobic/hydrophilic properties, or degradation kinetics



and mechanisms (Figure 2) (Tringides et al., 2022). Since it is desirable to select a material whose mechanical properties match as much as possible those of the tissue that it is in contact with to limit discomfort and inflammation, the different types of substrates and scaffolds are used for different applications. Classical substrates for the design of wearable or implantable bioelectronic systems are mainly based on elastomers, such as silicone rubber or poly(urethane)-based films. These materials exhibit high chemical stability and can withstand very large strain rates. Therefore, they are particularly well-suited for seamlessly integrating with tissue movements, such as stretching, bending, and torsion, in particular for their application in skin electronics. They are also good candidates for applications involving tubing or highly flexible structures, such as cuff electrodes. However, the design of resorbable elastomers is still an emerging field (Turner et al., 2022). Therefore, bioplastics such as resorbable polyesters have driven much attention, especially considering that some of them, such as PLGA, PLA, and PHAs, are already approved implant materials by regulatory agencies (the Food and Drug Administration and European Medical Agency) (Nair et al., 2007; Ulery et al., 2011; Bano, 2018; Lu et al., 2023a). Elastomers and bioplastics are mainly employed as 2D thin-film substrates that are assembled with electrical conductors to design multilayer electronic systems. When aiming to create more viscoelastic 3D scaffolds, for instance, for 3D cell culture or tissue engineering applications, biopolymer-based hydrogels are more appropriate. From its

natural origin, silk can display both hydrogel resorbability and eventual swellability and bioplastic-like mechanical properties. It is therefore a particularly relevant polymer to use as a resorbable substrate and packaging material in bioelectronics.

2.1.1 Resorbable elastomers

Recent advancements in the design, synthesis, and medical uses of resorbable elastomers, mainly polyurethanes (PUs), poly(glycerol sebacate), and poly(diols citrate) (Figure 3), have been recently reviewed (Turner et al., 2022). Polyurethanes are a large class of copolymers where at least two organic monomers react to create a carbamate bond. Typically, PUs are produced by the reaction between a diisocyanate and polyol. A judicious choice of reactants makes it possible to confer degradability to the polymer, for instance, by selecting degradable monomers comprising an ester bond (Christenson et al., 2007). PUs are interesting in medical applications for their biocompatibility, the versatility of their chemical structure, and their high stretchability. The addition of poly(urethane) cross-links in an already resorbable bioplastic material can also confer it with elastomeric properties while maintaining its resorbability (Sharma et al., 2018). For instance, Sharma et al. designed a resorbable elastomeric stent based on a network of poly(glycolide-co-caprolactone) chains cross-linked with short polyurethane segments. The material, initially resorbable and stretchable, but without any deformation reversibility, displayed elastomeric behavior after PU cross-linking.

Poly(glycerol sebacate) (PGS) elastomers are polyesters obtained by the polycondensation of FDA-approved glycerol and sebacic acid. Due to their high biocompatibility, elastomeric properties, and biodegradability, PGS elastomers constitute materials of choice for medical applications (Rai et al., 2012). They have been used mainly in tissue engineering, in particular for neural and cardiac tissues, and wound healing. More recently, PGS elastomers have been combined with different conductive materials for the design of smart textiles that include pressure, strain, and temperature sensors (Vogt et al., 2021). Poly(diols citrate) elastomers are also polyesters derived from the condensation of citric acid with polyols during thermal treatment, with potential for tissue engineering applications. Poly(octamethylene maleate (anhydride)) (POMaC) has been combined with PGS to package resorbable strain and pressure sensors made of PLA and magnesium (Boutry et al., 2018). The resorbable device was intended to follow up tendon repair and self-degrade after its service to avoid second retrieval surgery.

Most of the resorbable elastomers described above are not yet commercial, which has limited their use in resorbable medical devices to proof-of-concept studies until now. However, a variety of chemical structures are possible to tune their mechanical and degradation properties. Depending on the materials, compression moduli, tensile strength, and elongation at break have been reported to range from 0.025 to 400 MPa, 0.2 to 2,500 MPa, and 10% to 2,500%, respectively (Turner et al., 2022). These materials typically degrade in a few weeks in water (Turner et al., 2022), due to the hydrolysis of ester bonds in saline media, accelerated in a basic medium, and by the action of endogenous esterases. Resorbable elastomers can also be combined with other materials such as bioplastics (PLA, PLGA, PCL, etc.) to obtain copolymers with intermediate mechanical or degradation properties. Elastomers do not possess the viscoelastic properties of soft tissues (Figure 2). However, they are particularly interesting in interfacing with highly stretchable tissues, such as skin, and are extensively used in the field of wearable bioelectronic systems and “skin electronics” (e-skin) (Park et al., 2022a; Gong et al., 2022; Liu et al., 2023a). Their mechanical toughness makes them also interesting when in contact with moderately “hard” tissues, like the tendons and heart. Therefore, it can be foreseen that resorbable elastomers will attract more and more interest in the coming years.

2.1.2 Synthetic polyesters and other polymers

Thanks to their biocompatibility and well-controlled structure-tunable degradability, synthetic aliphatic polyesters have been extensively developed in medical devices since the 1970s. In particular, they have been used as surgical sutures, drug delivery systems, and tissue-engineering scaffolds. Most employed materials include PLA, poly(glycolic acid) (PGA), PLGA, PCL, and PHA (Figure 3). Because these materials generally display thermoplastic properties and can also serve as alternatives to petro-sourced polymers in other applications such as packaging, they have also been described as “bioplastics” (Bano et al., 2018; Jiang et al., 2022).

PLA is obtained by the poly(condensation) of lactic acid, which can interestingly be obtained by the bacterial fermentation of carbohydrates or synthetically. The L-lactide isomer is naturally produced and leads to PLLA (poly(L-lactide)). PLLA is quite a hydrophobic and slow-degrading crystalline polymer, with a glass transition temperature of 60°C–65°C and melting temperature of

175°C (Nair et al., 2007). It displays a relatively high tensile strength (0.01–5 GPa) (Eglin et al., 2008; Ulery et al., 2011) and a high modulus, with resorption kinetics up to 5 years (Ulery et al., 2011), making it suitable for use in surgical sutures. To increase its kinetics of resorbability, the two isomers, D and L, can be combined to obtain amorphous PLA with less mechanical strength and a lifetime of 12–16 months (Nair et al., 2007). Lactic acid can also be combined with glycolic acid to obtain PLGA. PLGA polymers are extensively used in medical applications since they can be processed with a wide range of different shapes: micro-structured films (Abu Ammar et al., 2021), porous scaffolds (Pan et al., 2012), microspheres and nanoparticles (Lu et al., 2023a), and microfibers (Chor et al., 2020). They can be used for drug delivery and tissue engineering applications or as surgical sutures or substrates for bioelectronics. Indeed, by modulating not only the L/G monomer ratio but also the polymer molecular mass and ending groups, it is possible to fine-tune the thermal, mechanical, and degradation properties of PLGA to make them match with the targeted application (Bano et al., 2018; Lu et al., 2023a). Contrary to PLA and PGA, PLGA are amorphous polymers when the L/G ratio is between 1/3 and 3, with fast kinetics of hydrolysis degradation up to 1–2 months for the 1/1 copolymer (Ulery et al., 2011). PGA is less hydrophobic and resistant against hydrolysis than PLA, but still crystalline and with a high melting temperature (>200°C), as well as displaying very high tensile strength (0.3–0.9 GPa) (Eglin et al., 2008; Ulery et al., 2011), which has made it a relevant material for surgical sutures and tissue engineering.

Poly(caprolactone) (PCL) is a hydrophobic semi-crystalline polymer that is interesting for its low glass transition (–54°C) and melting (approximately 60°C) temperatures, and its high elongation (300%–4,700%) and tensile strength (20–40 MPa) at break (Eglin et al., 2008; Ulery et al., 2011). It displays a very long degradation time (2–4 years). Because of its high permeability, it is mainly used in drug delivery systems and tissue engineering (Bano et al., 2018). PCL is also extensively used in combination with PLLA, PLA, and PLGA.

Poly(hydroxyalkanoates) (PHAs) are a family of polyesters produced by bacterial fermentation or algal bioproduction and presenting a very wide variety of structures and properties. To date, PHAs used in the biomedical field are mainly poly(3-hydroxybutyrate) (PHB) and poly(3-hydroxybutyrate-co-3-hydroxyvalerate) (PHBV) (Singh et al., 2019; Tebaldi et al., 2019; Ansari et al., 2021). Their biocompatibility, non-immunogenicity, and non-carcinogenic properties have been regularly pointed out. Their mechanical properties can be tuned to match those of very soft (skin) to very hard (bone) tissues. Their kinetics of degradation can be tuned from weeks to several years, for short- or long-term drug delivery or implant use. Present biomedical applications of PHA include resorbable surgical sutures (muscle and skin regeneration) (Piarali et al., 2020), cardiovascular stents, bone and cartilage implants, or nerve repair conduits. In addition to tissue engineering applications, their use as drug delivery systems has also been explored (Koller, 2018; Singh et al., 2019; Tebaldi et al., 2019; Piarali et al., 2020; Ansari et al., 2021).

Bioplastics have been extensively used in resorbable bioelectronic applications, mainly as substrate films, eventually conformable and stretchable, but they can also be processed as fibers. For instance, electrospun PLA or PCL fibers coated with

poly(aniline) or gold nanoparticles, eventually assembled in mats, have been used in cardiac tissue engineering (Fleischer et al., 2014; Wang et al., 2017a) and PCL fibers embedded with graphene and carbon nanotubes for nerve reconstruction (Sun et al., 2021). If bioplastics present tunable thermal and mechanical properties, as well as kinetics of resorbability, they remain rather hydrophobic materials. They can be combined with more hydrophilic polymer segments such as poly(ethylene glycol) (PEG), poly(vinyl alcohol) (PVA), and polyvinylpyrrolidone (PVP) to create copolymers. PEG, PVA, and PVP are synthetic polymers that can form after chain cross-linking hydrogels, i.e. 3D cross-linked polymer networks that can encapsulate large quantities of water. Because of their important swelling in aqueous buffers and biological fluids, hydrogels constitute ionic conductive materials when wet (Chen et al., 2021). As such, hydrogels also constitute materials of choice to mimic the tissue extracellular matrix (ECM). PEG, PVA, and PVP polymers are resorbable in the sense that they can be excreted through urine when their molecular mass is not too high (Yamaoka et al., 1994; Jensen et al., 2016; Kurakula et al., 2020). However, pure cross-linked PEG networks could present limited resorbability and potential safety concerns (Ulery et al., 2011). PVP and PVA are highly soluble in water and, therefore, are rather used as formulation aids but not often as scaffolds by themselves. If not cross-linked, they dissolve very quickly in water.

2.1.3 Natural polymers

Natural polymers comprise mainly polysaccharides and protein-derived macromolecules.

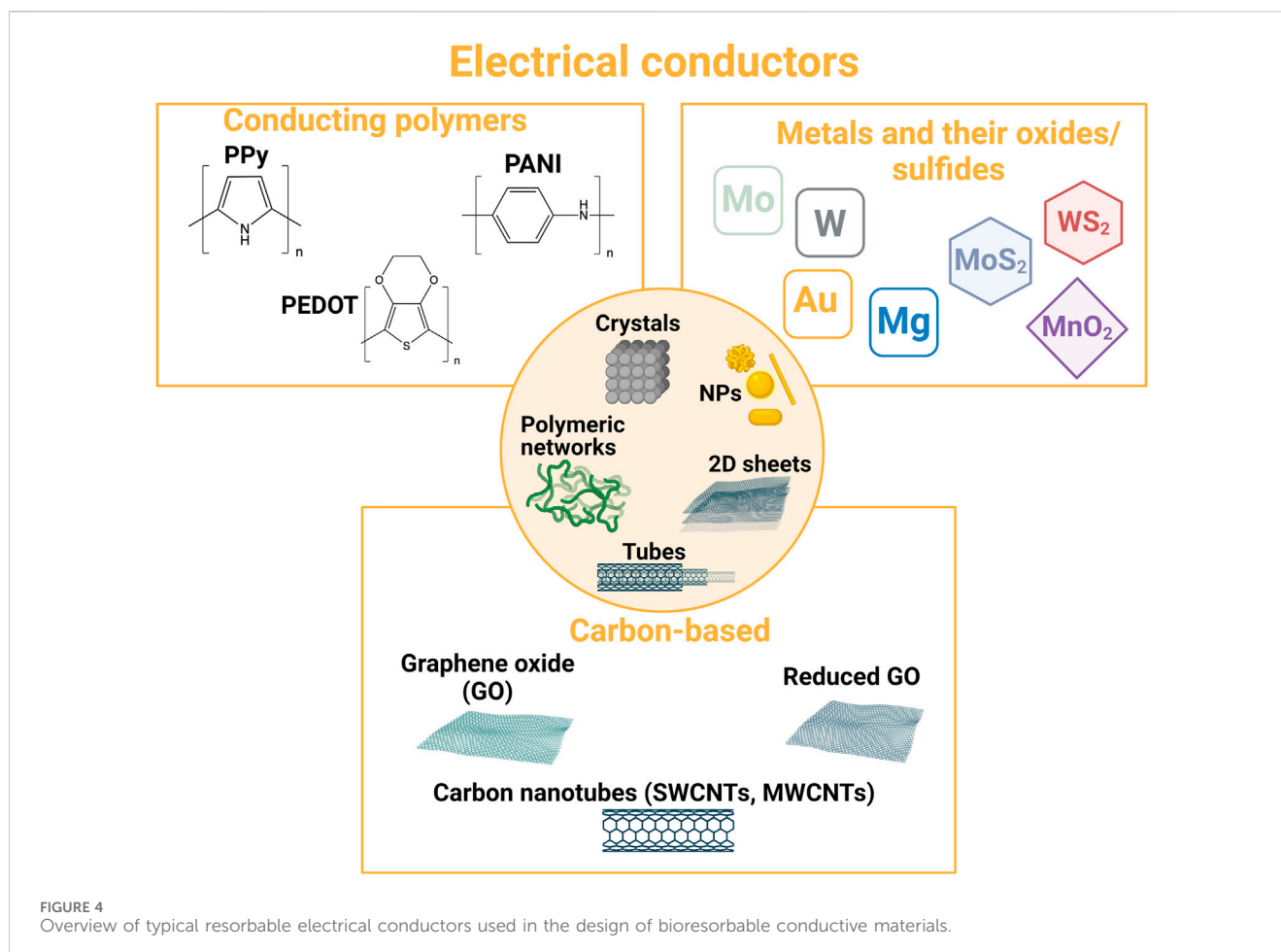
Polysaccharides have aroused large interest due to their high availability, biocompatibility, variety of structures, and chemical and biological properties that they offer (Yang et al., 2022). In particular, hyaluronic acid (HA) is a highly relevant material for bioelectronics because it is an endogenous glycosaminoglycan of the extracellular matrix (ECM), which is widely available today as it is being produced by controlled bacterial fermentation, is easily processable (high water solubility and functional groups amenable to chemical modification on the polymer backbone), and is already being used in numerous biomedical applications (Knopf-Marques et al., 2016; Kobayashi et al., 2020; Vasvani et al., 2020). HA contributes to maintaining homeostasis and promotes cell migration, adhesion, and differentiation and as such has long been used in drug delivery systems and tissue engineering, in particular when in contact with the brain tissue (Miyata et al., 2017). HA is fully resorbable, with a degradation rate of a few hours to days (according to the body location) when not cross-linked. Other polysaccharides of interest for medical applications are chitosan which presents mucoadhesive properties (Dash et al., 2011), celluloses (Aghazadeh et al., 2022), and alginate (Zhang et al., 2023). Though they display high biocompatibility and are degradable, only a few of their derivatives, such as oxidized cellulose and oxidized alginate, appear resorbable. Nevertheless, a few alginate-based materials will be described below since they were largely used to develop and illustrate innovative concepts, particularly in the field of dynamic hydrogels (Tringides et al., 2021; Tringides et al., 2023).

Another class of natural polymers is protein-derived macromolecules, such as collagen and its gelatin derivative, fibrin, elastin, elastin-like polypeptides, and silk fibroin. Similar

to HA, collagen, fibrin, and elastin are endogenous components of the ECM. This confers to these materials mechanical properties that are very close to that of native tissues and a high biocompatibility although they can also elicit an immune response (Ulery et al., 2011). However, their supply can be limited by their extraction from animal sources and their cost (Wang et al., 2023). Mainly, silk has been explored for the design of resorbable bioelectronic systems, while collagen and gelatin have been used to design conductive hydrogels for tissue engineering.

Silk is a natural material produced by a variety of arthropods; the one extracted from the cocoons of *Bombyx mori* has been used for centuries and is still the most exploited due to its extraction by simple processes (Ullah et al., 2019). After processing, the major components, silk sericin and silk fibroin, are obtained. Fibroin, a structural protein composed of 18 amino acids, is constituted of crystalline β -sheets that self-assemble through intramolecular and intermolecular interactions (such as H-bonds, van der Waals, and hydrophobic interactions) and of hydrophilic and amorphous random coil domains. Playing with processing conditions that can tune the rearrangement and the ratio of the crystalline and amorphous domains, silk fibroin can be processed as nanofibers, microfibers (that can be converted to yarns and textiles), films, aerogels/cryogels, and hydrogels (Wang et al., 2019a). Its protein nature confers the material with high biocompatibility and programmable degradability and opens the possibility to further genetically engineer the protein (e.g., insert elastin-like sequences to improve elasticity for instance) to match the desired properties (Wang et al., 2021). The proteolytic degradation of silk fibroin films by enzymes such as chymotrypsin, actinase, and carboxylase can be accelerated by reducing the protein β -sheet content through the presence of chaotropic agents or the drying process (Cao et al., 2009; Chatterjee et al., 2019; Ullah et al., 2019). Because of its high biocompatibility and processability, the absence of adverse immune reaction, its resorbability, and outstanding mechanical toughness, silk fibroin has been employed for centuries in biomedical applications, for instance, as surgical sutures, besides its use in the textile industry.

Silk films were identified as early as the late 2000s as resorbable substrates of high interest for the design of soft electronics, particularly in the group of Rogers (Kim et al., 2009; Kim et al., 2010; Hwang et al., 2012; Tao et al., 2014). Transient electrode microarrays were designed by transfer printing very thin silicon patterns onto a casted 5- to 15- μ m-thick silk fibroin film (Kim et al., 2009; Kim et al., 2010; Hwang et al., 2012). The very soft material showed high conformability to adapt to brain morphology and resorbability in water of approximately 1 h. Silk was also combined with resorbable magnesium [Mg (conductive) and MgO (insulating)] materials to develop a resorbable implanted system for the on-demand delivery of antibiotics to treat infected surgical wounds (Tao et al., 2014). The high Young's modulus (5–12 GPa) and low stretchability (20%) of silk fibroin films were modulated by Chen et al. (2018a) in order to obtain stretchable films suitable for on-skin electronics. The authors studied the plasticization of a fibroin film through the addition of CaCl₂ and ambient hydration, guided by molecular dynamics simulations of the rearrangement of β -sheets and coil domains into the film structure. After patterned vacuum deposition of gold, electrodes were obtained onto a wrinkled highly stretchable



(>400%) film (Young's modulus 0.1–2 MPa), and the device was tested for skin interfacial impedance measurement.

Silk fibroin can also be used to design resorbable conductive inks. Graphene derivatives and silk fibroin are particularly interesting to combine thanks to hydrogen bonds that can be reversibly created between the two materials (Wang et al., 2021). For instance, Dorishetty et al. (2022) studied the formulation, microstructure, and biocompatibility of a set of extrusion printable silk/graphene inks with different rGO content. An increase in the rGO concentration was shown to decrease the obtained material pore size while increasing its mechanical resistance. A PEDOT-based conductive printable ink was also developed by the addition of photosensitive sericin in an aqueous dispersion of PEDOT:PSS (Pal et al., 2016) (Figure 5). Silk sericin was modified with photosensitive methacrylate groups and mixed with PEDOT:PSS conductive ink. The photosensitive conductive resin was then spin-coated onto the fibroin substrate and UV-exposed through a photomask to create micropatterns after development in water.

The above examples demonstrate the high versatility and processability of silk that make it a real asset in the design of resorbable conductive materials. Similar to bioplastics, silk displays programmable structure-related degradability and mechanical properties and can moreover form optically transparent films for optoelectronic applications. As a natural

polymer, silk is also a highly biocompatible and sustainable material, processable in water, and amenable to chemical modifications that can improve its interaction with conductive materials or tissue adhesion.

We have highlighted in this section the wide range of substrates/scaffolds that can be used to design resorbable materials. In the next section, we will focus on the electrical conductors.

2.2 Electrical conductors

Different conductive components can be employed to design resorbable materials for healthcare applications (Figure 4). Metals and semiconductors are the electrical conductors that are usually employed in microelectronics. Therefore, when resorbable, they have been used to design resorbable bioelectronic systems dedicated to wearable or *in vivo* sensing or stimulation. To address tissue engineering applications and design 3D medical devices, such materials are employed in micro- or nanoparticle forms. Other micro- and nanostructures can also be used, and transition-metal dichalcogenides and carbon-based fillers (carbon nanotubes and graphene derivatives) are very popular in the field, either for the design of bioelectronic systems or tissue engineering. Conducting polymers are also very relevant materials for the bioelectronic system/tissue interface, either for the design of

wearable bioelectronic systems or tissue engineering. Their strengths are their mixed ionic/electronic behavior and their polymeric nature, making them both a structuring and conductive material.

2.2.1 Metals and semiconductors

Classically employed materials for designing conductive patterns in microelectronics are semiconductors or metals. Several are biocompatible (platinum, gold, titanium nitride, silicon, etc.), while some are resorbable (molybdenum, magnesium, tungsten, iron, silicon, germanium, and zinc/zinc oxide) (Chatterjee et al., 2019). Their resorbability is mainly accounted for by the formation of metal hydroxides or oxides that are dissolvable in biofluids. The kinetics of bioresorption of resorbable metals can vary over different orders of magnitude, from 1.7 $\mu\text{m}/\text{day}$ at pH 7 at 37°C for Mg to 7 nm/day for Mo (Chatterjee et al., 2019). Silicon hydrolysis depends not only on pH, temperature, and ionic concentration but also on its crystalline form (Hwang et al., 2012). Although these materials are inherently hard in bulk, they can be deposited on a flexible substrate in thin layers, of the order of a hundred nanometers, or can be thinned after deposit to obtain flexible bioelectronic systems. Metals and semiconductors can also be shaped into nanostructures such as nanotubes or nanowires to increase the contact surface with tissues (Duan et al., 2012; Robinson et al., 2012). Combining resorbable polymer substrates and metals, different research groups have started developing resorbable electronic systems since the late 2000s. For instance, the group of Rogers has extensively developed the electronic on-silk concept (Kim et al., 2009; Kim et al., 2010; Hwang et al., 2012; Tao et al., 2014). Huang et al. (2014a) developed a fully printed circuit board using poly(ethylene oxide) and carboxymethyl cellulose as substrate materials combined with magnesium stacks and a paste comprising tungsten microparticles for electrical connections. Still, resorbable polyester substrates such as PLGA films are presently the most employed.

The high interest of semiconductors and metals is their high intrinsic conductivity. However, it could be complicated to combine them in bulk with highly porous and hydrophilic materials such as hydrogels. Choi et al. (2020) described the possibility of combining hydrogels with a liquid metal, an eutectic alloy of 75% gallium and 25% indium (mass ratio). Though the biocompatibility of liquid metal Galinstan, an eutectic mixture of 68% Ga, 22% In, and 10% Sn (mass ratio), has been assessed (Foremny et al., 2021), the use of such materials still remains questionable from the biocompatibility and resorbability points of view. Another possibility to combine metals and other conductive materials to resorbable scaffolds is their use as micro- or nanostructures.

2.2.2 Conductive nanostructures

A large variety of inorganic conductive micro- and nanostructures are available to design conductive materials (Figure 4). Micro- and nanostructures include semiconductor or metallic flakes, nanowires or nanorods, 2D materials like transition metal dichalcogenides (MoS_2 and WS_2), Xenes (e.g., black phosphorous), MXenes (2D carbides or nitrides), transition metal oxides (e.g., MnO_2 and MoO_3), and carbon-based structures, such as carbon nanotubes and graphene-based materials. The increased surface/volume ratio facilitates and fastens the material resorption in the body, when possible. We will shortly focus

below on the few structures that have been highlighted in literature and for which more solid resorption data exist. Numerous other conductive micro- and nanomaterials are presently under development and could be acknowledged in the near future as suitable for the design of resorbable bioelectronics (Choi et al., 2019).

Concerning metallic nanostructures, because of biocompatibility issues, copper and silver are ruled out for most biomedical applications (Han et al., 2022). The *in vivo* safety of platinum nanoparticles (Pt NPs) has also been questioned (Czubacka et al., 2019; Gutiérrez de la Rosa et al., 2022). As a highly stable metal in biological fluids, Pt NPs require a very long time for dissolution-based resorption but can possibly be eliminated by urinary excretion. Because of their high biocompatibility and processability, gold nanoparticles, nanocages, nanorods, and nanowires are extensively studied in tissue engineering applications (Yadid et al., 2019), especially cardiac engineering (Saghebasl et al., 2022). However, they are not bioresorbable, even if very recently, small gold-polymer nanostructures (90 nm size, 4.5% w/w gold) were found to be excretable (Cassano et al., 2019), 4–22 nm-diameter gold nanostructures were also found to be degraded and metabolized by cells by similar pathways than gold ions, but into biopersistent products (Balfourier et al., 2020).

Two-dimensional transition-metal dichalcogenides, such as molybdenum disulfide (MoS_2) sheets, are very attractive thanks to their 2D electrical conductivity and optical transparency in the visible range that can be used advantageously in optoelectronic systems (Choi et al., 2019). The resorbability of MoS_2 -isolated crystals and large-area polycrystalline films in representative fluids and cranial environments was studied (Chen et al., 2018b). The polycrystalline MoS_2 monolayer (grain size ~ 200 nm) dissolved in approximately 2 months in PBS solution at 37°C, and the CVD-grown monolayer inserted in implantable device prototypes was dissolved completely in 1 month. Such implantable bioelectronic systems can be used to monitor pressure, strain, and temperature (Chen et al., 2018b), as well as serve as an image sensor array when implanted in the eye, thanks to their photoabsorption and photocurrent generation performances (Choi et al., 2017).

Pristine graphene is also a 2D material of high interest for bioelectronic applications (Choi et al., 2019). Because of the thickness of individual layers (a few angstroms), graphene can be soft and flexible, yet strain-resistant and optically transparent. Based on a hexagonal honeycomb lattice of carbon atoms, graphene is also biocompatible and can be functionalized easily for better interactions with tissues or other materials though its impact on the immune system is being questioned (Ban G et al., 2023). Endogenous peroxidases such as human myeloperoxidase can degrade graphene in the form of a single or a few layers, in tens of hours to days (Ma et al., 2020). However, pristine graphene is quite hydrophobic and hence poorly compatible with hydrogels (Chen et al., 2021). Graphene oxide (GO), more hydrophilic and dispersible in water, displays poor conductivity because of the damaged conductive network due to the oxidation of the graphene structure. Therefore, reduced graphene oxide (rGO), for which the graphene structure has been partially restored, constitutes a good compromise between conductivity and limited hydrophobicity and is preferred for biomedical applications (Chen et al., 2021). The kinetics of degradation of GO and rGO

is related to the oxygen atom content of the structures, and therefore they resorb in the body with faster kinetics than pristine graphene (Ma et al., 2020).

Carbon nanotubes (CNTs) also constitute a hexagonal lattice of carbon atoms rolled up into a tube of 0.5–2 nm diameter for single-walled carbon nanotubes (SWCNTs), with several SWCNTs in a tube-in-tube structure for multi-walled carbon nanotubes (MWCNTs). Like graphene, their carbon atoms can be oxidized and functionalized to confer additional functionalities and hydrophilicity. For instance, Liu et al. (2011) studied *in vitro* the influence of carbon nanotube surface chemistry (carboxylic acids, amines, and alcohols) on neuron network organization, offering cells a high variety of adhesion orientation and sites. They have been particularly explored in wearable sensor applications (Gandhi et al., 2020; Palumbo et al., 2022) and nerve constructs for tissue engineering (Salehi et al., 2018; Manousiouthakis et al., 2022). Though resorbable, thanks to their degradation by peroxidases (Ma et al., 2020), their biocompatibility is questionable (Mishra et al., 2018). It seems to mostly depend on their synthesis and purification process, as well as their aspect ratio.

2.2.3 Conducting polymers

Electronic conducting polymers (CPs) such as poly(pyrrole) (PPy), polyaniline (PANI), poly(thiophene) (PTh), and poly(3,4-ethylenedioxythiophene) (PEDOT) are a class of polymers that possess π -conjugated structures, enabling electron delocalization along their backbone (Guo et al., 2020). Given the aromaticity of the polymer structure, the overlapping of π -orbitals results in a conductive pathway obtained by freely moving delocalized π -electrons (Nezakati et al., 2018). In their pristine state, CPs behave as semiconductor materials exhibiting weak conductivity compared to classical semiconductors. When oxidized (0.25–0.33 charge per monomeric unit) through electrochemical treatments or oxidation/reduction chemical reactions, they gain high electronic conductivity. This (electro)-oxidation process is accompanied by the introduction in the CP films of counter anions that maintain their electroneutrality. Such an ion exchange property is generally referred to as a doping process correlatively to inorganic semiconductors, the counter anions being referred to as the dopant species (Namsheer et al., 2021). As such, conducting polymers are a category of organic materials characterized by distinctive electrical and electrochemical performances. They combine the advantages of a wide range of electrical conductivity (10^{-5} – 10^5 S cm⁻¹) like carbon- or metal-based electrical conductors and of structure tunability, flexibility, and relatively low cost, like polymers. They also feature both ionic (such as tissues) and electronic (such as bioelectronic systems) conductivities, making them ideal interface materials for bioelectronic applications (Fattahi et al., 2014; Onorato et al., 2019; Gao et al., 2022). CP coatings on metallic electrodes can significantly enhance the electrical properties at the interface of tissues as compared to bare electrodes, especially decreasing electrical impedance and increasing charge transfer capacity (Ludwig et al., 2006; Richardson-Burns et al., 2007; Khodagholy et al., 2015). For instance, conducting polymer microstructures (microcups) were obtained by the electrochemical deposition of conducting polymers (PEDOT, PPy) onto the surface of PLLA/PLGA sacrificial microspheres (Antensteiner et al., 2017a; Khorrami

et al., 2017). These microstructures deposited on the surface of a metallic electrode enhanced the surface roughness of the CP films by over 90% through the control of both deposition time and applied electrical voltage. The impedance of PPy-modified electrodes was found to decrease by up to 88% in comparison to bare electrodes (Antensteiner et al., 2017b). These neural electrodes improved the cellular response of neurons during chronic stimulation and recording (Antensteiner et al., 2017a; Khorrami et al., 2017). Thanks to these unique combined properties, as well as their ease of preparation and biocompatibility, conducting polymers have attracted significant attention for a wide range of biomedical applications such as the development of (bio)-sensors, actuators, drug delivery systems, and tissue engineering scaffolds. Due to their availability and physiologically relevant electrical conductivity upon intrinsic or external doping, PPy, PANI, PEDOT, and their derivatives, are the most widely used CPs for bio-interfacing applications.

Poly(pyrrole) (PPy) is a heterocyclic polymer that can be easily synthesized in different solvents (such as water) and polymerized via chemical or electrochemical routes of pyrrole oxidation (Mao et al., 2018). Due to its high biocompatibility, ease of preparation, and good conductivity in physiological conditions, it has been widely used at the interface between bioelectronic systems and cells or tissues, for both recording and stimulation purposes (Liu et al., 2023b). Notably, PPy is a suitable substrate in the modulation of different cellular activities (such as cell attachment and proliferation) and possesses excellent biocompatibility *in vivo* (Huang et al., 2014b). Furthermore, it can be easily chemically modified to allow the conjugation of bioactive molecules such as proteins and enzymes (e.g., glucose oxidase and antibodies), short peptides with specific “recognition sequences” (providing binding sites for cells), nucleic acids, DNA/RNA, or growth factors (which allow the immobilization of cytokines). These bioactive molecules can act as PPy dopants, improving material conductivity and/or further promoting material–tissue integration. Nevertheless, additional polymer modifications are required to overcome issues with water solubility, mechanical rigidity, and poor processability, which significantly limits its use as a standalone material. In addition, PPy is very sensitive to over-oxidation in the presence of radical oxygen species present in biological media or generated by local inflammatory processes (Palmisano et al., 1995). Despite its considerable biocompatibility, at its pristine state, PPy is also poorly degradable. Bioerodible forms of PPy can be prepared via electrochemical polymerization of beta-substituted pyrrole monomers containing hydrolyzable side groups (Zelikin et al., 2002) or by PPy integration in biodegradable polymers, such as PLA or PCL (Boutry et al., 2012).

Polyaniline (PANI) is a phenylene-based polymer offering several advantages in biomedical applications, such as high thermal and environmental stability, high conductivity values (10^1 – 10^2 S cm⁻¹), and inexpensive and easy synthesis processes (Solazzo et al., 2019). It can be synthesized via electrochemical processes, or chemical oxidation of aniline monomer, typically in the presence of ammonium persulfate as the oxidizing agent. Fine control over synthesis conditions, such as pH, the presence of acids, and the choice of solvents and oxidizing levels, greatly influence the physical and electrical properties of the obtained PANI polymers that can be under different forms

(i.e., leucoemeraldine, emeraldine, and pernigraniline) that differ by the oxidation level of the backbone (Tran et al., 2022). PANI generally offers several advantages for biomedical applications, such as high thermal and environmental stability, antibacterial properties, inexpensive and easy synthesis processes, and excellent charge transport due to the doping/de-doping process (Beygisangchin et al., 2021). Another major advantage of PANI is its good solubility in a few selected organic solvents, as well as in water, thereby largely improving material processability. Nevertheless, the biocompatibility of both pristine PANI and its derivatives is still controversial. Several studies have reported high *in vitro* cytotoxicity and chronic inflammation episodes after cell/tissue contact (Wang et al., 1999; Borriello et al., 2011; Zhang et al., 2019), despite a plethora of studies having reported good *in vitro* and *in vivo* compatibility of PANI oligomers (pentamers and tetramers) when employed in subcutaneous films or biomimetic sensors for short-term use (Humpolicek et al., 2012; Guo et al., 2018; Pyarasani et al., 2019). Furthermore, similar to the other conducting polymers, PANI used as a standalone material is also non-degradable. As well as for PPy applications, in recent years, numerous studies have focused on combining PANI with other biodegradable synthetic or natural polymers to develop blends or composite systems (Rai et al., 2022). Despite this, *in vivo* studies assessing the resorbability of PANI-based materials or their long-term presence in the body (eventually in degraded form) have not been extensively carried out.

Poly(3,4-ethylenedioxythiophene) (PEDOT), a thiophene derivative of the less stable and less biocompatible pristine poly(thiophene), is one of the most widely studied CPs in bioelectronics and tissue engineering applications due to its improved chemical and environmental stability and biocompatibility compared to PPy and PANI (Tropp et al., 2021). PEDOT is generally synthesized in the presence of a dopant, typically polystyrene sulfonate (PSS), which plays the role of the counter anion of the positively charged PEDOT (more conductive than the pristine form) and improves polymer solubility and conductivity (Gueye et al., 2020). Although poly(styrene sulfonate) (PSS) is the most widely studied PEDOT dopant to design soft flexible conductive materials for bioelectronics, PSS lacks biocompatibility and degradability (Kayser et al., 2019). Several biomolecules have therefore been investigated to obtain resorbable PEDOT:biomolecule inks to be used for the design of transient implantable electronic devices (Boehler et al., 2019; Leprince et al., 2023a). PEDOT is generally obtained via three polymerization routes: i) oxidative chemical polymerization of EDOT-based monomers using various oxidants, yielding a suspension of PEDOT (or PEDOT:dopant) particles (ink) (Nie et al., 2021; Leprince et al., 2023a), ii) electrochemical polymerization of an EDOT-based monomer onto a conductive substrate in a three-electrode setup yielding a PEDOT coating or a film, and iii) using transition-metal-mediated coupling (Nie et al., 2021). When not electrochemically synthesized onto a substrate or as a self-standing film, PEDOT can be formulated to be further coated, casted, or printed by different processes (spin-coating, dip-coating, spray coating, screen printing, inkjet printing, doctor blading, roll-to-roll printing, etc.). The relative ease of PEDOT (or PEDOT:dopant) processing and the possibility to design it as resorbable using biomolecule-based dopants have led to the widespread use of PEDOT in the development of modified electrodes for tissue interface (Wang et al., 2019b) and tissue engineering applications (Bhat et al., 2021).

Despite CPs promising bioelectrical characteristics and ease of processability, the same intrinsic structure enabling conductivity is also characterized by strong bond dissociation energies, imparting the materials with excessive rigidity and poor degradability, limiting their application as biointerfaces with tissues (Liu et al., 2023b). CPs' conjugated backbones are indeed hardly cleavable in physiological conditions, unless for small molecular mass, resulting in a poor to null degradation and metabolization in the body. Furthermore, several classical dopants, such as PSS for PEDOT, are not cleavable in the physiological condition as well, further hindering CPs' *in vivo* employability. Replacing PSS by potentially (bio)degradable molecules, such as alginate (Puiggali-Jou et al., 2020; Yang et al., 2020), heparin (Xu et al., 2019b), or hyaluronic acid (Guo et al., 2018; Leprince et al., 2023a) is a widely known strategy to increase PEDOT:dopant biocompatibility and degradability, preserving the inherent conductivity of the polymer (Guo et al., 2013). Interestingly, such biopolymer-based dopants can also be used to design the conductive substrate/scaffold part of the conductive material. If resorbable and associated with CP oligomers, resorbable conductive hydrogels can be obtained with high interest in bioelectronics and tissue engineering. A second reported strategy is the integration of cleavable chemical motifs in the CPs' backbone, which allows their partial or complete degradation into smaller products (monomer or oligomer fragments) that can be processed through different physiological mechanisms, such as phagocytosis, metabolization, bioabsorption, or excretion (Feig et al., 2018). Disintegrable organic semiconductors can also be obtained by utilizing degradable or reversible dynamic covalent linkages, for instance, based on Schiff base chemistry, within each conducting polymer repeat unit (Tropp et al., 2021). The use of hydrolyzable linkages within a CP monomer leads to a degradable conducting polymer backbone that affords the design of high-performance transient and biocompatible semiconductors (Lei et al., 2017). In conclusion, extensive and rigorous studies on the mid- and long-term use of CP-based materials in transient implantable devices are still required to solve the pending questions of device biocompatibility and electroconductive stability over time. However, such materials display high structural versatility and offer large possibilities and interest in bioelectronic applications, especially on-skin electronics and tissue engineering.

Only a limited number of electrical conductors inherently exhibit full bioresorbability such as resorbable metals, semiconductors, and MoS₂ sheets. However, the functionalization of others (such as graphene, carbon nanotubes, and their derivatives) through the application of organic coatings or the combination of conductive oligomers with bioresorbable polymers has paved the way for enhancing these materials' biocompatibility and resorbability. Consequently, strategies that amalgamate structuring scaffolds with electrical conductors play a pivotal role in achieving resorbable conductive materials.

3 Combining structuring scaffolds and electrical conductors

Based on the large variety of existing chemical structures for both resorbable substrates/scaffolds and electrical conductors, there exist different possibilities to combine them to obtain conductive

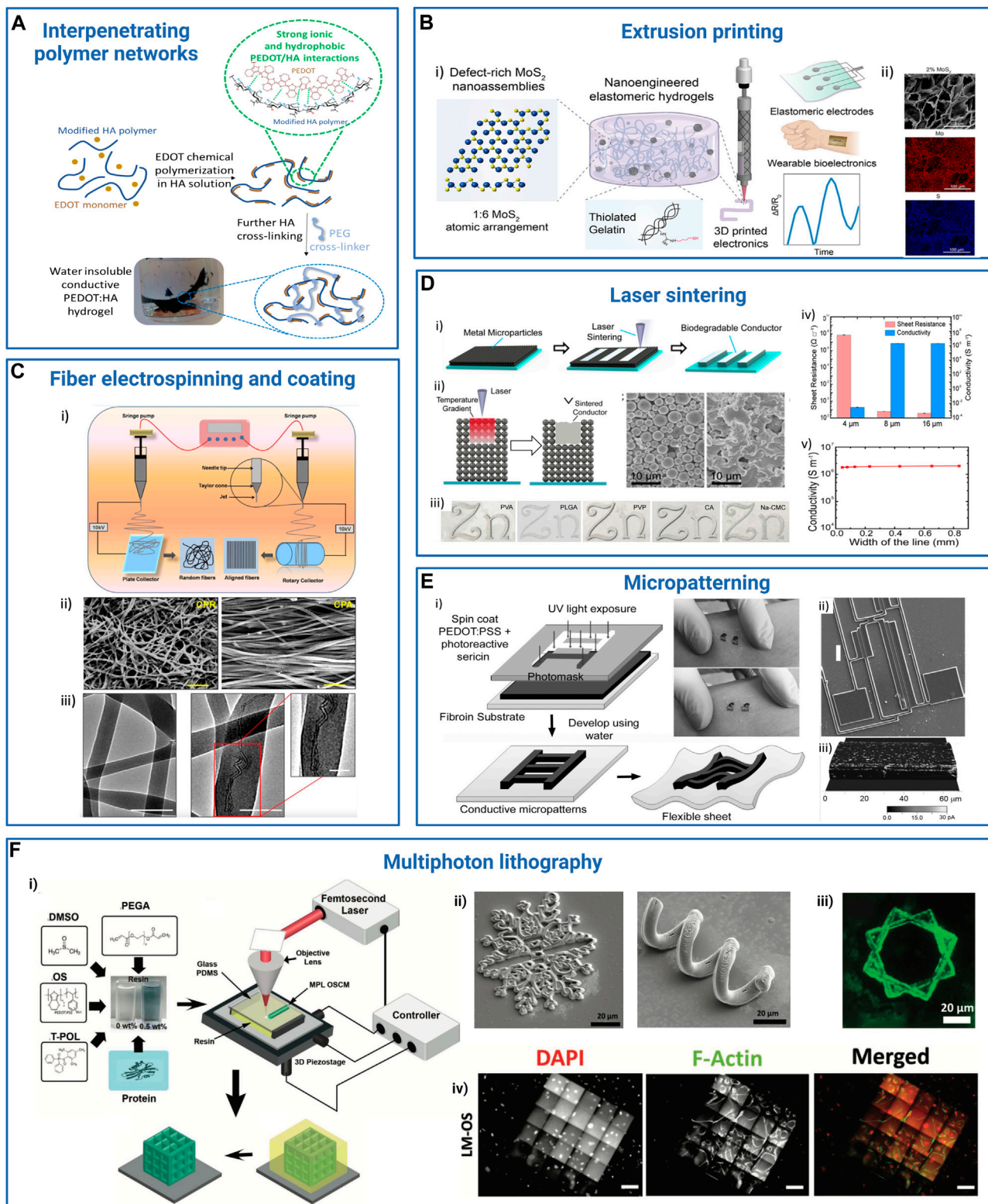


FIGURE 5

Examples of processes and strategies used to obtain resorbable conductive materials for their application in bioelectronics. **(A)** *Interpenetrating networks of scaffolding and conducting polymers*: conducting polymer PEDOT is chemically synthesized in a solution of modified hyaluronic acid (HA) polymer. The PEDOT:HA ink can be further photo-cross-linked to achieve non-water soluble resorbable conductive hydrogels (Leprince et al., 2023b). Adapted with permission from Leprince et al. (2023a), Copyright 2023, Elsevier, and Leprince et al. (2023b), Copyright 2023, the Royal Society of Chemistry. **(B)** *Extrusion printing*: (i) a bioprintable conductive ink is obtained by mixing thiolated gelatin and defect-rich MoS₂ nano-assemblies. This ink can be further extrusion-printed as a stand-alone material to design wearable sensors. (ii) Scanning electron microscopy (SEM) and energy-dispersive (Continued)

FIGURE 5 (Continued)

X-ray spectroscopy (EDS) images of a transverse cross-section of the hydrogel: gelatin scaffold (top), molybdenum (Mo, middle), and sulfur (S, bottom). Scale bar: 100 μm . Reprinted with permission from Deo et al. (2022), Copyright 2022, the American Chemical Society. (C) *Fiber electrospinning and coating*: electrospun PCL-collagen fibers coaxially reinforced with MWCNTs. i) Electrospinning parameters were modulated to deposit random or parallel fibers. ii) SEM images of the random (CPR, left) and aligned (CPA, right) MWCNT-reinforced fiber scaffolds. Scale bar: 1 μm . iii) TEM images of scaffolds without (left) and with (right) MWCNT fibers. Scale bar: 200 nm, inset: 100 nm. Adapted with permission from Ghosh et al. (2020), Copyright 2020, the American Chemical Society. (D) *Laser sintering*: laser sintering process to integrate zinc or iron microparticle inks into hydrogels (i). The microparticle ink (black) was spin-coated onto the hydrogel substrate (blue), and the device was washed in the appropriate solvent after laser sintering to reveal the pattern. ii) Scheme illustrating the sintering process. Scale bar: 10 μm . iii) Examples of Zn patterns obtained on different polymer substrates [PVA, PLGA, PVP, cellulose acetate (CA), and sodium carboxymethyl cellulose (Na-CMC)]. iv and v) Resistance and conductivity of Zn line patterns with different thicknesses (iv) and widths (v) onto PVA substrate. Adapted with permission from Feng et al. (2019), Copyright 2019, the American Chemical Society. (E) *Photolithography micro-patterning*: i) scheme depicting the microfabrication of silk sericin/PEDOT:PSS patterns onto a silk fibroin substrate. ii) SEM image of a complex resorbable device (ii, scale bar: 100 μm). iii) Conductive AFM image of a 50- μm -thick ink line deposited on a glass surface. Reproduced with permission, Copyright 2015, John Wiley and Sons (Pal et al., 2016). (F) *Multiphoton lithography*: i) schematics illustrating the composition of the organic semiconductor (OS) resin, featuring PEDOT:PSS, photoinitiator (3-(trimethoxysilyl)propyl methacrylate), dimethyl sulfoxide (DMSO), laminin, glucose oxidase, and the experimental setup for multiphoton lithography, resulting in the formation of 3D OS composite microstructures (OSCM) upon resin removal (depicted in yellow). ii) SEM images showcasing diverse conductive and bioactive complex microstructures. Scale bar: 20 μm . iii) Fluorescent microscopy images depicting laminin-incorporated OS (LM-OS) microstructures in green. Scale bar: 20 μm . iv) Epifluorescence microscopy images showing endothelial cells on LM-OS microstructures after 48 h of culture, stained with DAPI (red, indicating cell nuclei) and phalloidin (green, representing F-actin). Scale bar: 100 μm . Reproduced with permission, Copyright 2022, John Wiley and Sons (Dadras-Toussi et al., 2022). Created with BioRender.com.

materials for their use in bioelectronics or tissue engineering. We propose below an insight into the most popular processes encountered in the bibliography. Some of them are illustrated in Figure 5.

3.1 Blending structuring scaffolds/substrates and electrical conductors

Blending is the easiest way to combine synthetic or natural polymer-based substrates/scaffolds with electrical conductors such as metallic or semiconducting nanoparticles, nanorods or nanowires, carbon-based conductive fillers, and conducting polymers. We provide below general examples of blended resorbable conductive materials, preceding a brief section concerning polymer cross-linking that can be used to ensure material infusibility in tissues in contact with biological fluids and place specific emphasis on conducting polymer/hydrogel interpenetrated polymer networks.

3.1.1 Blended resorbable conductive materials

Blending has been used to design several parts of resorbable bioelectronic systems.

Biodegradable conductive pastes were developed by blending tungsten micro-/nanoparticles with natural waxes (issued from bee, soy, myrtle, or candelilla) (Won et al., 2018; Kim et al., 2023a). These hydrophobic pastes, which degrade within days to weeks, can be used to interconnect different electronic components of resorbable bioelectronic systems (Won et al., 2018; Choi et al., 2021).

Resorbable PVA films filled with iron nanoparticles and MWCNT were used to design biodegradable tactile sensors (Karmakar et al., 2022). Wang et al. (2019c) designed a resorbable strain sensor based on a dynamic network of PVA, borate, and GO particles partially reduced during dopamine oxidative self-polymerization. The PVA-PDA-rGO material displayed self-healing features, and the rGO filler acted both as a mechanical stiffener and electrically conductive particles. rGO was also combined with PCL, PU, PEG, gelatin methacrylate (GelMA),

collagen, and chitosan for cardiac (Saghebasl et al., 2022) or neural (Manousiouthakis et al., 2022) tissue engineering. Tringides et al. (2021) blended alginate hydrogels with both graphene flakes and carbon nanotubes prior to gelation and freeze drying to obtain macroporous materials. They thoroughly studied the impact of the two types of materials on the structure and conductivity of the obtained conductive hydrogels. They showed that graphene flakes were integrated into the walls of the porous materials, whereas CNT acted as interconnects through the pores, to achieve conductivities as high as 35 S m^{-1} . The conductive alginate hydrogel (100 μm thick) could then be encapsulated between two thin layers (15 μm) of a resorbable viscoelastic elastomer in which openings could be performed with a CO_2 laser and to design a resorbable electrode array for the heart or brain electrical recording or stimulation.

In tissue engineering applications, blending conductive fillers or conducting polymers into resorbable hydrogels is the usual method to obtain conductive ECM-like scaffolds. For instance, AuNPs have been integrated with different polymer-based scaffolds (alginate, chitosan, PCL/gelatin, etc.) and shown to improve the mechanical and electrical properties of the matrices and tissue regeneration from stem cells. PEDOT:PSS was mixed with collagen and (3-glycidoxypentyl)trimethoxysilane as a cross-linker to design 3D conductive scaffolds that can be used to measure impedance and monitor cell growth (Inal et al., 2017). In nerve tissue reconstruction, 2D graphene materials have often been combined with carbon nanotubes as polyester or hydrogel fillers (Gupta et al., 2019; Sun et al., 2021; Huang et al., 2023). The objective is to optimize the material conductivity by ensuring the percolation of the conductive domains, while minimizing the impact of these additives on the scaffold biocompatibility and/or mechanical properties.

Nano- and microparticles and 2D materials are interesting to blend with a polymer matrix to obtain resorbable devices for different reasons. Their size and dimensionality make them soft and suitable to be combined with flexible substrates to match the curvilinear shape of the human body and fasten and ease their resorption. In addition to their electrical properties, they can also confer the materials with additional functional properties, such as optical transparency, when at low concentration or present as a thin

layer. The increased surface-to-volume ratio can also increase electric signal sensitivity to the adsorption of molecules or biomolecules. Therefore, the use of such materials is a real asset to design resorbable optoelectronic systems and sensors or biosensors. However, we have to consider that the presence of fillers generally modifies the material's toughness and stretchability (most of the time, the material becomes harder), which can impact its interaction with tissues.

It is also noteworthy that it is necessary to achieve high payloads of electrical conductors within the polymer matrix to ensure high material conductivity, especially when dry materials, i.e., elastomer- or bioplastic-based substrates are concerned. Indeed, in that case, the electrical conductors have to percolate into the by-nature insulating matrix to ensure material conductivity. In this perspective, the blending strategy is particularly interesting to combine electrical conductors and hydrogels. The ionic conductivity of hydrogels and their porous structure potentially facilitating the percolation of electronic conductors, could offer advantages to achieve conductive materials with moderate electrical conductivities.

When synthetic or natural polymers are used as substrates/scaffolds, it is sometimes required that the polymer chains are cross-linked so that the material is resorbable in the mid to long term but remains infusible when in contact with biological fluids during its use. This is particularly true for hydrophilic polymer networks that are hydrogels. Polymer cross-linking strategies will be detailed in the following sections.

3.1.2 Polymer cross-linking

Cross-linking by physical bonds like H-bonding and hydrophobic interactions, or chemical bonds, in particular covalent bonds, can be achieved through thermal, mechanical, or chemical treatments. A variety of functional groups natively present on synthetic or natural polymers can be exploited for chemical cross-linking, such as alcohols (-OH), thiols (-SH), carboxylic acids (-COOH), and amines (-NH₂). Other chemical functions (such as alkenes, alkynes, acrylates, methacrylates, azides, hydrazides, hydroxyamines, etc.) can be introduced, notably to further use click chemistry-based cross-linking strategies that can be performed in water and limit the formation of potentially toxic by-products (Hu et al., 2019; Chiulan et al., 2021; Battigelli et al., 2022; Mueller et al., 2022). Popular chemical cross-linking reactions include Michael additions, Diels-Alder reactions, azide-alkyne cycloadditions, thiol-ene photo-reaction, or photo-initiated methacrylate polymerization. By the modulation of the nature of the polymer, polymer and cross-linker concentrations, and eventually the number of chemical groups per polymer chain (degree of substitution), the crosslink density and hence the porosity and the mechanical and swelling properties of obtained materials can be fine-tuned.

More recently, the limitations of purely elastic polymer networks (i.e., cross-linked with static covalent bonds) were underlined, especially in the field of tissue engineering (Chaudhuri et al., 2015; Chaudhuri et al., 2016; Yang et al., 2016; Morgan et al., 2022). Dynamic polymeric networks, especially hydrogels, were described that can offer self-healing behavior, and dynamicity and stress relaxation properties that exist in tissues (Elosegui-Artola, 2021). Dynamic hydrogels are also intensively explored in

the field of wearable bioelectronic systems as outstanding reversible adhesives to interface electronics and skin. Hydrogel/tissue interface interactions can rely on electrostatic or hydrophobic interactions, topological adhesion, and irreversible or reversible (i.e., dynamic) covalent bonding (Cong et al., 2022). In particular, bioinspired approaches such as those based on catechol chemistry (mussel-inspired) allow the establishment of stable and high-strength adhesive interfaces using easy polymer modification by functional moieties such as catechol, dopamine, or tannic acid (Zhang et al., 2020). The conductive version of these adhesive hydrogels is of greatest interest as ideal electrode interfaces between electronic systems and tissues. Other typical dynamic linkages are boronic esters, disulfide bonds, and hydrazine and oxime bonds (Zhu et al., 2023b; Grosjean et al., 2023). In particular, hydrogels obtained by mixing fast equilibrium hydrazide cross-links ($K_{eq} \approx 10^3\text{--}10^4 \text{ L mol}^{-1}$) and slow equilibrium oxime cross-links ($K_{eq} \approx 10^6\text{--}10^8 \text{ L mol}^{-1}$) have aroused high interest in tissue engineering (Morgan et al., 2022). They can be easily obtained by mixing an aldehyde or a methyl-ketone-modified polysaccharide with a mixture of bis(hydrazine) and bis(oxamine) cross-linkers, whose ratio can be tuned to obtain a series of hydrogels with a range of elastic and viscoelastic properties (Su et al., 2010; Koivusalo et al., 2019; Baker et al., 2021; Morgan et al., 2022).

Taking advantage of the polymeric structure of both conducting polymers such as PANI, PPy, and PEDOT and hydrogels, the above-described crosslinking strategies can be pushed further to interpenetrate the two polymeric networks (Rogers et al., 2020; Xu et al., 2020; Chen et al., 2021; Xu et al., 2021; Gao et al., 2022; Zhu et al., 2023a).

3.1.3 Interpenetrated networks of conducting polymers and hydrogels

Conducting polymer hydrogels have garnered particular interest because it is possible to uniquely play with the polymer nature of both the CP and hydrogel scaffold to end with original molecular designs where the two networks are interpenetrated. Integrating CPs within the hydrogel matrix allows the generation of conductive hydrogels that combine the tissue-biomimetic characteristics of hydrogels, such as soft mechanical properties and high swelling ratio, minimizing mismatch at the interface with biological tissues, with the peculiar conductivity of CPs (Liu et al., 2023b).

CP/hydrogel interpenetrated networks (IPNs) can be obtained by different strategies (Xu et al., 2020; Liu et al., 2023b). In a one-step strategy, the conductive monomer and the scaffold precursors are mixed, then the *in situ* redox polymerization of the conductive monomer (for instance, EDOT) is conducted simultaneously to the reticulation/gelation of the polymer matrix. For instance, a PEDOT: alginate hydrogel to support the 3D culture of brown adipose-derived stem cells was obtained by mixing in one pot EDOT, alginate, ammonium persulfate (as EDOT oxidant), and adipic acid dihydrazide (as alginate cross-linker) (Yang et al., 2020). However, the one-step strategy requires that the scaffold precursors and the conductive monomer react simultaneously, or with orthogonal chemistries. In a two-step strategy, the conductive monomer is mixed within the already cross-linked scaffold and then oxidized chemically or electrochemically to obtain the conducting polymer intertwined within the scaffold matrix. EDOT was chemically polymerized in the presence of a chitosan/gelatin

cross-linked scaffold for neural tissue engineering (Wang et al., 2017b). Despite that relatively high conductivity was obtained (0.17 S/cm), the authors first swelled the hydrogel for 3 h in ammonium persulfate buffer, before immersing it in an EDOT/hexane solution to perform EDOT polymerization, probably in order to avoid EDOT polymerization that only occurs at the hydrogel interface. Alternatively, scaffold precursors are dispersed in a conducting polymer dispersion (for instance, a PEDOT:PSS ink), and then polymerized or reticulated. A conductive PEDOT:PSS/silk fibroin/tannic acid adhesive hydrogel that could serve as a skin/electrode interface was developed, where the PEDOT:PSS ink was mixed with silk fibroin before polymer cross-linking using Ca^{2+} and tannic acid (Luo et al., 2020). Interestingly, Ca^{2+} can form complexes with PSS, establishing strong interactions between the fibroin and PEDOT:PSS networks. This results in highly stretchable (≈ 300 – 400% , up to $32,000\%$ for specific formulations) and adhesive materials, with a conductivity of 3 S/cm.

PSS can also be replaced by another biopolymer-based resorbable dopant, whose cross-linking can lead to the hydrogel scaffold, avoiding dilution of the PEDOT conducting moiety into the material. Our group developed a specific biodegradable hyaluronic-based dopant of PEDOT in order to achieve a PEDOT:HA ink with good conductivity (1.6 ± 0.2 S/cm) in comparison to similar PEDOT:biomolecule inks described in the literature (below 0.1 S/cm) (Leprince et al., 2023a). The introduction of both sulfonic acid and aromatic aminophenylboronic groups on the HA polymer backbone to mimic the PSS structure was shown to enhance ink conductivity above the additive effect, by providing, at the same time, charge carrier mobility and intra-/inter-chain charge transport through PEDOT/aminophenylboronic π -stacking interactions (Figure 5). The HA dopant was further functionalized to introduce alkene moieties that could photo-crosslink with a PEG-bis(thiol) linker to obtain a resorbable PEDOT:HA conductive ink. This ink was inkjetted on a flexible PLGA substrate in order to design a bioelectronic system that could resorb within 2 months in physiological conditions (Leprince et al., 2023b).

IPN conductive hydrogels are characterized by good biocompatibility, easy processing, and high processability (Zhu et al., 2023a). Contrary to a blend of carbon/metallic particles that are island-type distributed into the polymer matrix, the CP chains can come into contact with each other, forming a 3D interconnected conducting network, for electron transporting with relatively low resistance (Yao et al., 2017; Onorato et al., 2019). As a consequence, electronic conductivity in bulk electronically conductive hydrogels not only depends on the intrinsic CP electronic conductivity but also, and more particularly, on the inter-chain connectivity of the CPs and therefore on their spatial arrangement and concentration in the 3D matrix (Li et al., 2017; Xu et al., 2018). Still, limitations of such materials can come from the poor degradability of CPs, unless they are used in their oligomer form. However, the tunability of conductive hydrogel structures and properties make them a real asset in the field of bioelectronics.

The resorbable conductive materials obtained by the blending of scaffolds/substrates and electrical conductors are generally used without significant modification in tissue engineering applications. For these applications, they are applied onto the wound/skin, or implanted into the tissue through surgical

intervention or injection. However, resorbable conductive materials can also be shaped into fibers. Another possibility is to combine them with specific patterns of the electrical conductor onto the resorbable 2D substrate to obtain wearable or implanted bioelectronic systems.

3.2 Fabricating composite resorbable conductive micro- and nanofibers

Two main strategies have been described to obtain nano- or microfibers of resorbable conductive material (Wei et al., 2023).

The first strategy uses the blending of the polymeric scaffold, selected for its spinning ability (e.g., PLGA, PLLA, PCL, silk, HA, etc.), and the electrical conductor (e.g., CNTs, graphene derivatives, PEDOT:PSS, PANI, PPy, Au nanoparticles, etc.). The blend can then be processed using microfluidics, extrusion printing, wet spinning, or electrospinning to obtain conductive nano- or microfibers, whose diameter (from a few hundreds of nanometers to a few hundreds of micrometers) highly depends on the production method and processing parameters. For instance, Wang et al. (2017) blended PLA and PANI before electrospinning to yield nanofibrous sheets, suitable for cardiomyocyte culture. The thin material sheets could also be rolled up or folded to obtain different shapes. While microfluidics can be used to design core/shell structured fibers, it is worth noting that such a strategy generally results in fibers that consist of the homogeneous blend of the electrical conductor and polymeric scaffold.

On the contrary, the second strategy consists of first fabricating polymer nano- or microfibers using similar techniques as those quoted before (microfluidics, extrusion printing, wet spinning, and electrospinning, with the two last being the more generally used) and subsequently coating them with the conductive material. This strategy results in polymer-based fibers coated with an electrical conductor layer and is largely used for biomedical applications. It should, however, be carefully handled to avoid the issues of delamination or poor adhesion of the conductive layer onto the fiber substrate and is particularly critical whenever the fibers are foreseen to withstand important elongation (Wei et al., 2023). To overcome these issues, the fibers can be coated with the electrical conductor under stretching, or their surface can be nano- or microstructured or functionalized with chemical groups like silanes or dopamine to promote the adhesion of the electrical conductor layer. For instance, electrospun PLLA fibers were coated with carboxylic- and dopamine-modified MWCNTs, rGO, or a mixture of both (Ramamy et al., 2022). Poly(dopamine) improved not only the adhesion of the conductive materials but also the hydrophilicity and biocompatibility of the fiber-based scaffolds. Zou et al. (2016) prepared an aligned conductive fibrous scaffold of electrospun PLLA fibers that were coated by a PPy layer co-doped with poly(glutamic acid)/dodecyl benzenesulfonic acid by chemical oxidation. Weak polar van der Waals forces between PPy coating and PLLA fibers ensured the coating's mechanical adhesion. Interestingly, Jiang et al. (2019) used the opposite configuration, with the sheathing of PEDOT:PSS wires by silk fibroin in order to design resorbable (within a few weeks), insulated and flexible, connectors for fully organic bioelectronic systems dedicated to ascorbic acid sensing. "Pure" PPy or PEDOT nanotubes

(70–175 nm diameter) could also be obtained by the electrochemical deposition of the conducting polymers onto the surface of PLLA/PLGA sacrificial electrospun fibers deposited on the electrode surface of a microelectrode array (Abidian et al., 2008; Abidian et al., 2009; Abidian et al., 2010). Eventually, the fibers could be aligned if the PLLA/PLGA fibers were so templated (Khorrami et al., 2018). The obtained microelectrode arrays were used for chronic neural recording. The PEDOT nanotubes were also filled with dexamethasone, an anti-inflammatory drug, and released the drug upon electrical stimulation (Abidian et al., 2006). These nanotubes that displayed a large electroactive surface were also implemented as mechanical actuators driven by the oxidoreductive incorporation of ions and water in their structures (Eslamian et al., 2021).

Electrospinning is largely employed to fabricate nano- or microfibers dedicated to medical applications. Interestingly, the electrospun fibers can be collected as fiber mats with a fiber anisotropic distribution, typically to design dressings or wearable bioelectronic systems, or alternatively as aligned fibers, particularly interesting for the oriented growth of neural cells or cardiomyocytes. For instance, Ghosh et al. (2020) electrospun a blend of PCL, collagen, and MWCNTs on a rotating mandrel (Figure 5). The alignment of the conductive fibers could be tuned according to the applied voltage and mandrel rotating speed. Random or parallel fibers could be obtained to study the effect of fiber alignment on nerve regeneration. Interestingly, the MWCNTs showed an end-to-end connection insuring electrical conductivity and a coaxial alignment within the PCL-collagen fiber. Zhao et al. (2022a) designed rGO-functionalized electrospun silk patches for post-infarction repair and observed that the anisotropic arrangement of fibers was beneficial to tissue repair in comparison to a random arrangement or the absence of fibers.

If conductive fibers are mainly used in tissue engineering applications, wearable or implanted bioelectronic systems result from the 2D patterning of conductive materials.

3.3 Patterning conductive materials onto 2D substrates

The classic microfabrication processes used in “hard” and “soft” microelectronics (i.e., lithography, etching, printing, etc.) can be used to produce resorbable bioelectronic systems. The major advantages of these microfabrication technologies are their well-proven and established processes, the collective production of a large number of devices, and the possibility to define micrometric and even nanometric scale patterns or roughness.

3.3.1 Usual microelectronic system fabrication techniques

Classic microfabrication techniques are used for working with a “hard” (typically silicon, silicon oxide) or “soft” (polymer or bioplastic sheet) substrate. During the fabrication process, the soft substrate is most of the time attached to a more rigid one, like glass or silicon. To pattern metals or semiconductor tracks/electrodes and insulation layers, the traditional approach involves a series of sequential steps, such as deposition (evaporation or sputtering), and the application of photoresists through methods

like spray coating or spin coating to delineate the areas to be etched or protected. Subsequently, a selective etching process is employed, which can be either wet (involving acids or bases) or dry, using free radicals from various gases (SF_6 , CF_4 , etc.). These potentially harsh techniques must be adapted to align with the materials used in the construction of resorbable devices while also meeting the peculiar requirements of bioelectronics, such as device flexibility and stretchability.

Kurland et al. (2013) have developed a “silk protein lithography” technique, for which fibroin and sericin proteins are modified by methacrylate groups to obtain photosensitive resists amenable to lithography patterning. The authors blended PEDOT:PSS dispersion with photosensitive sericin in order to obtain a printable PEDOT-based conductive ink. This ink was then spin-coated onto a 50- μm -thick UV-cross-linked fibroin-methacrylate substrate. Subsequently, the coated substrate was exposed to UV light through a mask and developed in water, resulting in devices featuring water-insoluble conductive patterns made of PEDOT:PSS/sericin on the fibroin substrates with a resolution as low as 1 μm (Pal et al., 2016). The conductive tracks could withstand bending without alteration of their resistivity or charge storage capacity.

To step toward device flexibility necessary for bioelectronics, the first strategy consists of building the functional stack on a sacrificial layer, resulting in a thin chip upon transfer or etching. When applied in the context of resorbable bioelectronics, it is necessary to reduce the thickness of resorbable semiconductive and metallic layers to the greatest possible extent and to subsequently transfer or encapsulate them within thin, flexible, and elastomeric resorbable substrates. For instance, Choi et al. (2021) designed a bioresorbable cardiac pacemaker where a tungsten-coated magnesium (W/Mg) (700 nm thick/50 μm) coil antenna and a radiofrequency PIN diode based on a very thin doped silicon nano-membrane (320 nm) were encapsulated into a 50- μm -thick PLGA substrate. Another critical bioelectronic system specification concerns stretchability. If there exists a large choice of materials to design resorbable stretchable substrates such as resorbable synthetic and natural polymers, as described above, this requirement is much more difficult to meet for conductive tracks. To better address the need for stretchability, i.e., elastic limit in elongation, a common approach is to employ zig-zag or serpentine patterns for conductive tracks, where the resulting increase in track length is compensated by an increase in the track cross-sectional area to mitigate the impedance impact. For instance, Held et al. (2022) designed serpentine tracks on resorbable PGS films and compared the device properties with its non-resorbable Ecoflex (silicone) counterpart. The PGS film patterned with serpentine tracks could withstand 130%–350% elongation at the break without any decrease of track conductivity, similar to the non-resorbable bioelectronic system, and be applied for the design of biodegradable (approximately 60% degradation in 3 months) wearable or implanted strain sensors or electronic circuit boards.

Resorbable carbon conductive fillers can also be introduced in bioelectronic systems through the use of microelectronic techniques. Carbon-based structures such as boron-doped diamond (Hébert et al., 2014) or carbon nanotubes (Keefer et al., 2008) are good candidates to boost the effective contact surface of electrodes. Their surface chemistry can also be tuned to improve cell or protein adhesion. Technically, the growth of an oriented or wild forest of carbon nanotubes directly on the electrode array structure requires

substrates compatible with high-temperature processes (in the range of 600°C) such as ceramic, quartz, or silicon as performed by [Sauter-Starace et al. \(2011\)](#) on silicon shanks. To circumvent the substrate temperature limit before degradation, carbon nanotubes may be grown at a very high temperature on a mineral substrate and then transferred onto the polymeric flexible film of interest ([Roy et al., 2017](#)). The use of graphene-based materials is interesting to obtain transparent electrodes for optical stimulation and characterization. For example, [Williams et al.](#) developed, for simultaneous electrophysiology and optical imaging, arrays of transparent neuronal microelectrodes from ultraviolet to infrared wavelengths and displaying a high signal-to-noise ratio ([Park et al., 2014a](#)). To achieve this goal, the authors grew graphene flakes on copper blocks and transferred them onto a flexible substrate using a PMMA sheet as the carrier; the copper blocks were then etched using ferric chloride solution, and any remaining residues were removed with a 1:10 HF solution. Afterward, the PMMA sheet carrier was dissolved in acetone, and the graphene layer was patterned to establish a junction with the metal pads and the edge of the transparent part of the design.

Laser sintering processes have been developed to pattern resorbable metals on elastomeric or bioplastic substrates. A layer of metal microparticles or a metallic foil was initially deposited on the substrate. Subsequently, a laser beam was applied to the targeted patterns, causing the metal to melt and penetrate into the first layer of the film. [Rahimi et al. \(2018\)](#) achieved direct integration of Zn conductive patterns onto a stretchable, resorbable, photo-cross-linked acrylamide-based elastomer. In another study, a Zn foil was deposited on a $\approx 250\text{-}\mu\text{m}$ -thick polymer film subjected to laser cutting. The laser ablation process enabled the metal to penetrate the substrate to a depth of approximately 50 μm . After encapsulation by a second polymer film, the device was used for wireless thermotherapy on the skin. [Feng et al. \(2019\)](#) demonstrated the feasibility of this approach using Mo, Zn, and Fe, creating a set of different transient wearable bioelectronic systems featuring conductive patterns deposited on degradable substrates (composed of cellulose acetate, CMC, PVA, PVP, and polyvinyl acetate) for optical image display and temperature sensing ([Figure 5](#)).

Microelectronic patterns are intrinsically made of a stacking of layers on a 2D substrate. However, recent strategies have led to the transition from 2D to 3D bioelectronic systems. For instance, [Dadras-Toussi et al. \(2022\)](#) developed a 3D multiphoton lithography method to obtain 3D patterns on a polymer substrate using a photosensitive resin based on poly(ethylene glycol diacrylate), PEDOT:PSS, and 3-(trimethoxysilyl)propyl methacrylate as the photoinitiator ([Figure 5](#)). [Liu et al.](#) introduced the concept of three-dimensional macroporous nano-electronic networks, which they called “syringeable electronics” ([Liu et al., 2013](#); [Liu et al., 2015](#)). The concept relied on a 2D mesh network of passivated polymer fibers, some of which were coated by conductive nanowires and nanotubes to define electrical connects and contacts of the device. The thinness of the conductive layer and the flexibility of the mesh made it possible to flex it in a 3D conformation and deform it into a syringe restriction for tissue injection. If system resorbability was not targeted (and hence studied) in these publications, the concept could be applied in the future to the

minimally invasive injection into the tissues of resorbable medical devices such as sensors. [Rogers et al.](#) developed an alternative strategy to obtain 3D electronic systems from 2D layer stacks ([Park et al., 2021](#)). The 3D electrode frameworks were created by encapsulating star-shaped patterned chromium/gold (10/200 nm) thin electrodes into a flexible polyimide substrate of the same shape, which was finally attached to a 30% elongated PDMS elastomeric substrate only at specific locations. When the PDMS substrate relaxed, the encapsulated metal electrodes flexed to create a 3D framework, suitable for the encapsulation of a cortical spheroid ([Park et al., 2021](#)). Such 3D advanced strategies are still under development and not yet implemented with resorbable metals to the extent of our knowledge. However, they have already paved the way for innovative designs of transient bioelectronics.

3.3.2 Flexible electronics techniques

Another family of microfabrication processes is that used in the field of flexible electronics. These include spin coating, dip coating, coating through metering rods, spray coating, screen printing, inkjet printing, doctor-blading, and stamping, among others. For instance, PEDOT:PSS conductive materials can be processed by these different techniques by tuning the conductive formulation to display different physicochemical properties (surface tension, viscosity, wettability) playing on the pH, concentration, and ionic strength, and the addition of surfactants, viscosity enhancers, or co-solvents, in the dispersion ([Glasser et al., 2019](#)). Poorly viscous dispersions (referred to as “inks”) will preferentially be inkjet-printed, while very viscous ones (referred to as “pastes”) will rather be screen printed. [Park et al. \(2014b, 2017\)](#) developed a stamping method to create conducting polymer patterns on the surface of a gold substrate. Agarose hydrogel stamps with desired patterned posts were fabricated from PDMS mold templates. The stamps were then impregnated for approximately 20 min within a CP monomer (EDOT and pyrrole) and dopant (PSS) solution. The impregnated stamps were then applied onto a gold-coated surface and a voltage was applied between the gold electrode and the hydrogel to polymerize the CP film at the post location. The same stamp could be used several times. The thickness of the CP film was controlled by the application time of the stamp and the applied voltage. Interestingly, each post could be further functionalized by specific biomolecules (avidin and laminin peptide sequence) to create specific cell biorecognition patterns. Extrusion printing is also a very popular technique, mostly concerning hydrogel-based formulations. For tissue engineering applications in particular, the development of bioinks combining hydrogels (conductive or not) with cells has appeared as a very active research field during the last decade. In this case, the printability of the material is the key to obtaining printed structures with satisfactory pattern resolution while preserving cell viability ([Gillispie et al., 2020](#)). The use of self-healable and dynamic hydrogels is particularly interesting to achieve this goal ([Morgan et al., 2022](#)).

Conductive inks and pastes can be developed with different electrical conductors such as gold nanoparticles, carbon nanotubes, graphene derivatives, or MoS₂ sheets dispersed in polymer solutions or hydrogels. [Deo et al. \(2022\)](#) developed a conductive and 3D printable ink combining thiolated gelatin and defect-rich 2D MoS₂

nanomaterials (Figure 5). Scanning electron microscopy (SEM) and energy-dispersive X-ray spectroscopy (EDS) evidenced the porous structure of the gelatin scaffold loaded with a homogeneous dispersion of molybdenum in the matrix. Interestingly, MoS₂ ensured material conductivity and acted as covalent cross-links for the hydrogel, ensuring its printability and stability. The material displayed sensitivity to strain, and potentially to pH and biological interactions. As such, it is foreseen to be of high interest for wearable electronics, and for the development of conformable implanted sensors that would necessitate minimal intervention, thanks to the injectability of the materials. Kim et al. (2023b) developed a thermoplastic tungsten-based conductive paste (7 10⁵ S cm⁻¹) composed of a mixture of beeswax (as resorbable matrix), tungsten nanoparticles (as electrical conductor, 500 nm–10 μm size), and glycofulol (as formulation aid). The paste can be filled at moderate temperature (approximately 70°C) into molds and screen-printed, and remains stable at body and room temperatures; it gets degraded in PBS buffer in approximately 80 days. To design resorbable bioelectronic systems, both the substrate and conductive ink patterns should be resorbable. Wang et al. (2019d) designed wearable devices based uniquely on graphene and silk. They combined calcium-plasticized fibroin with graphene (Ca/fibroin/graphene) to directly write or print conductive patterns onto a Ca²⁺/silk stretchable film. Interestingly, the Ca/fibroin/graphene ink displayed self-healing properties that facilitated printing.

Following deposition of the conductive material (ink or paste) onto the substrate, it is often necessary to post-process the material so that the conductive patterns cannot be subsequently washed out or be rapidly dissolved in biological fluids. This post-treatment should, however, not compromise the material functionality, biocompatibility, or resorbability. Depending on the materials, post-processing can include chemistry, light, or heat treatment. Thermal and UV cross-linking are particularly interesting due to their ease of implementation.

This section has evidenced the wide range of processes that can be used to combine scaffolds/substrates and electrical conductors to obtain resorbable conductive materials with a variety of chemical structures, morphologies, properties, and shapes. The next section is dedicated to the description of the applications of such materials in the biomedical field.

4 Applications in the biomedical field

Various applications of resorbable conductive materials are emerging and are foreseen to expand in the near future; they require different specifications and shall comply with different regulations. After a short section dedicated to material biocompatibility requirements, we will review the different domains of applications of resorbable conductive materials.

4.1 Biocompatibility and other requirements

Wearable devices require sufficient biocompatibility to avoid skin irritation and intradermal sensitization (biocompatibility standard ISO 10993-Part 10: Tests for skin sensitization),

whereas implantable devices and tissue substitutes may require the full list of biocompatibility tests required by ISO 10993-1, depending on the contact duration and their invasiveness, in particular ISO 10993-6 (Part 6: Tests for local effects after implantation). In the case of biodegradable materials, the identification and safety of degradation products are also of paramount importance. To this aim, the investigator shall refer to ISO 10993-13 and ISO 10993-15, dedicated to the degradation of products from polymer-based medical devices and metal alloys, respectively. Then, according to the risk analysis, the investigator shall evaluate the tolerable intake (TI) based on the maximum amount of substances below the threshold of adverse effects [the no-observed-adverse-effect-limit (NOAEL)] and modifying factors according to ISO 10993-17. Other material requirements, such as mechanical and conductive properties, also strongly depend on the targeted application. Tissue engineering and 3D cell culture applications demand high biocompatibility because of the intimate contact between materials and cells and require suitable mechanical properties (for instance, soft but stable dynamic hydrogels), but do not require high conductivity (Xu et al., 2021; Gao et al., 2022). On the contrary, a highly conductive material like metal should be used to fabricate the electrical tracks of a resorbable bioelectronic system.

4.2 Medical devices for sensing and recording

4.2.1 Wearable bioelectronic systems

In these applications, resorbable conductive materials are essentially obtained by 2D patterning processes on a flexible, sometimes stretchable, substrate (typically an elastomer or polyester film). Wearable bioelectronic systems are mainly dedicated to sensing, display, and stimulation. Electrical stimulation for wound healing will be specifically addressed in the tissue engineering section since the conductive materials employed can serve both as stimulation electrodes and tissue substitutes.

Most of the described resorbable wearable systems concern physical sensing (strain, temperature) and display. For instance, Wang et al. (2019d) designed a Ca/fibroin/graphene ink whose resistivity was sensitive to strain, temperature, and humidity and that could be printed onto Ca²⁺/silk stretchable films to design wearable devices. The bioelectronic systems were applied onto the skin as sensing tattoos (Figure 6A). A hydrogel dynamic network composed of PVA, borate, and GO particles partially reduced by dopamine oxidative self-polymerization was applied on the skin as a strain-sensing material (Wang et al., 2019c). Held et al. (2022) designed Galinstan serpentine tracks (approximately 2 mm thick) entrapped between two layers of resorbable PGS/PGS-acrylate or gelatin films. Galinstan is a liquid metal, an eutectic mixture of 68% Ga, 22% In, and 10% Sn (mass%), whose biocompatibility has been assessed (Foremny et al., 2021). The high elongation at a break that can withstand the films was used to design strain sensors to monitor elbow bending (Figure 6B). Feng et al. (2019) developed resorbable, temperature-sensitive, and optically transparent Zn electrodes patterned onto PVA films for temperature sensing or wearable heaters. Using the same

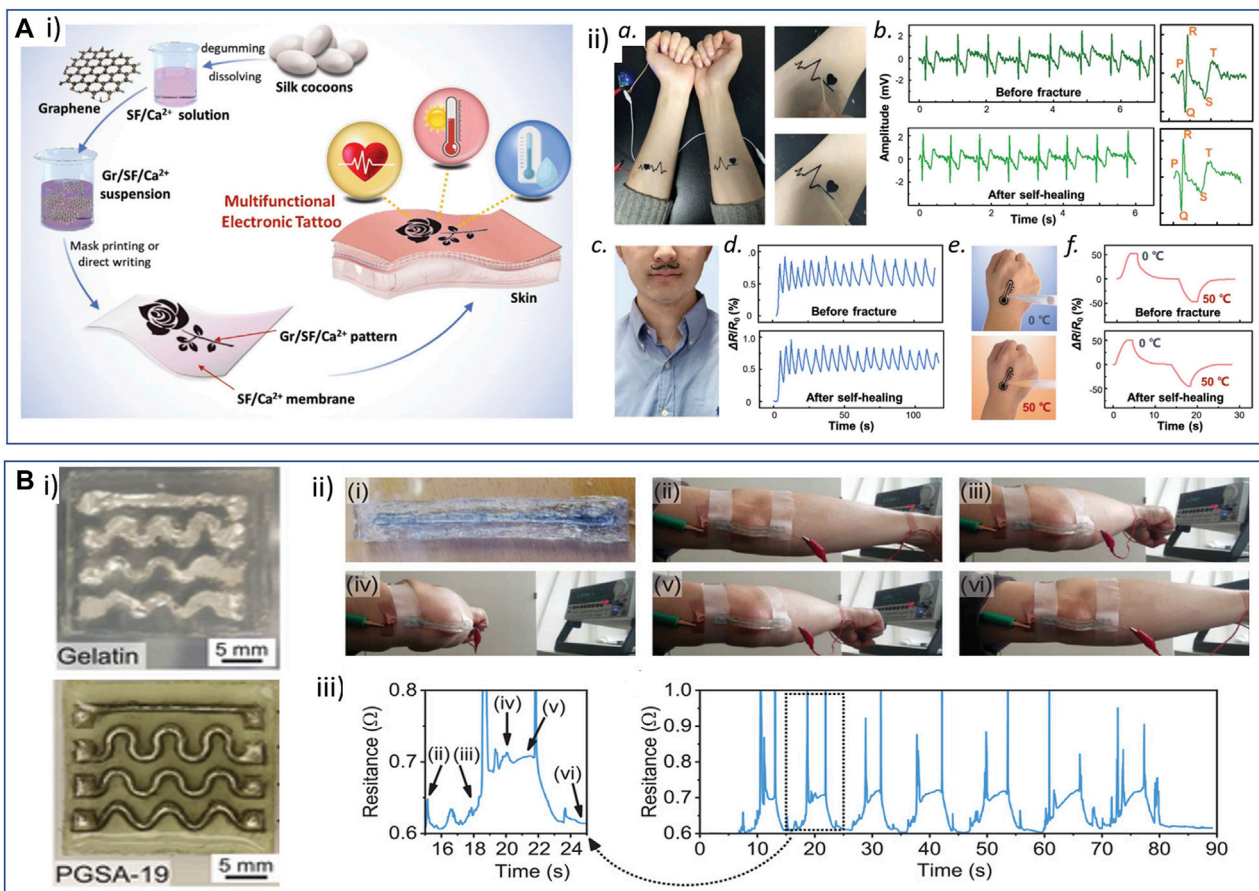


FIGURE 6

Examples of resorbable wearable sensors. **(A)** Wearable resorbable tattoo sensors based on silk and graphene materials: i) silk fibroin (SF) was extracted from *B. mori* cocoons and mixed with Ca²⁺ and graphene aqueous suspension to obtain a conductive ink that could be used to directly write or mask-print conductive patterns onto a SF/Ca²⁺ cross-linked membrane. ii) The resistivity of the obtained devices was sensitive to strain, humidity, and temperature, which makes them useful in designing an electrocardiogram (ECG) recording device (a,b), or respiration (c,d) and temperature (e,f) sensors. Interestingly, the materials presented self-healing properties that made it possible to continue signal recording with conductive pattern fracture and healing. Reproduced with permission, Copyright 2019, John Wiley and Sons, (Wang Q. et al., 2019). **(B)** Strain sensors based on Galistan metal liquid tracks embedded in gelatin or PGSa-19 films: (i) the gelatin-based sensor was then applied on a volunteer subject to monitor elbow bending. (ii) The device withstood important bending without rupture. (iii) The motion could be monitored by recording the resistivity of the conductive track. Reproduced with permission, Copyright 2022, John Wiley and Sons (Held et al., 2022).

materials but different patterns obtained by laser sintering, they designed a partially resorbable device for near-field communication and display.

Electrochemical-based sensors hold great potential for sensing and biosensing, and if processed as resorbable, can be used as transient devices deposited onto the skin or injected into the dermis. Liang et al. (2014) obtained a 70-μm-thick graphene/silk conductive composite film using the vacuum filtration of a graphene oxide and silk fibers suspension, followed by the chemical reduction of GO. Platinum nanospheres were then grown onto the film by cyclic voltammetry electrodeposition in order to obtain an H₂O₂ sensor or a glucose biosensor after immobilization of glucose oxidase (GOx) on Pt nanoparticles. Though no resorbability study was reported, the employed sensing materials could be resorbable and serve to design a transient wearable bioelectronic system. Kurland et al. (2013) developed a PEDOT:PSS/sericin ink loaded with glucose oxidase enzyme that they printed onto a UV-cross-linked fibroin-methacrylate substrate in order to obtain highly sensitive and

selective glucose electrochemical sensors that could withstand 30° bending and be resorbed in approximately 4 weeks. Devices comprising PEDOT- or PANI-based inks loaded with enzymes and printed on different substrates for the analysis of a few metabolites (glucose, lactate, and cholesterol) extracted from sweat (Bilbao et al., 2023) hold great promises. The use of micro- or nanostructured patterns (nanotubes and microcups) of conducting polymers combined with GOx or laminin cell adhesion peptide could further enhance the sensitivity of the sensors in comparison to plain films by increasing the sensing surface (Yang et al., 2014). 3D-printed patterns of a conductive resin could further enhance the recognition sensitivity of the conductive hydrogel. Dadras-Toussi et al. (2022) developed a photosensitive resin comprising poly(ethylene glycol diacrylate), PEDOT:PSS, a photosensitizer, and GOx or laminin cell adhesion peptide (Figure 5). 3D multiphoton lithography was used to obtain self-standing 3D patterns of cell-adhesion conductive materials or GOx-coated patterned microelectrodes that exhibited high

sensitivity and specificity. These electrically conductive resins therefore appeared appealing for the design of biosensors and sensing in organ-on-chip devices.

However, the development of resorbable sensors is still limited by several barriers that are yet to be overcome. A main limitation is the poor conductivity of some materials, especially conducting polymers when combined with resorbable hydrogels. CPs' conductivity can potentially be improved by combining them with other conductive fillers such as carbon nanotubes or graphene derivatives although it could stiffen the materials and decrease their flexibility and stretchability. When designing ion-selective electrodes, another important limitation is the present use of non-safe and non-degradable materials in the design of the sensing part (Cánovas et al., 2019). Therefore, the design of fully resorbable electrochemical-based wearable sensors still largely remains an unmet challenge.

Although a few examples of resorbable wearable sensors have been described in the literature, the fact that the devices are laid onto the skin and can be easily removed after use limits their applications. However, the development of wearable resorbable devices can appear as the first step and proof-of-concept toward the development of resorbable implanted bioelectronic systems and presents high environmental interest in reducing electronics waste (Feng et al., 2019).

4.2.2 Implanted microelectrode arrays and bioelectronic systems

The field of cardiac or neural tissue recording or stimulation is a good example to describe the evolution of materials and processes used through the last 25 years, with the objective to progress toward softer, more conformable, and flexible bioelectronic systems intended for use in the heart, brain, spinal cord, peripheral nerve, muscle, and skin (Tringides et al., 2021). Ultimately, it has now turned its attention toward device resorbability, particularly for specific applications such as short- to medium-term monitoring for epilepsy seizure (Yu et al., 2016; Xu et al., 2019a), neural stimulation for temporary pain relief (Lee et al., 2022), or intracranial pressure monitoring (Shin et al., 2019).

The first electrode arrays cleared by the FDA were the renowned Utah array (Rousche et al., 1998). These arrays comprised a hundred silicon cones, each covered by an insulator (silicon dioxide and/or parylene), except for their apex. These devices sparked considerable interest as they offered the possibility of concurrent neural recordings from up to a hundred channels, thus initiating the development of implantable devices for brain-computer interfaces (Hochberg et al., 2006). However, the risks of damaging blood vessels and triggering microhemorrhages, along with inflammatory response and the eventual formation of glial scar, remain very high (Kozai et al., 2015). In response to this challenge, Neuralink has developed a specialized sewing machine capable of gently introducing flexible polyimide shanks into the cortex while avoiding blood vessels, with the assistance of medical imaging. Owing to the substantial difference between Young's modulus of polyimide and the stiffness of the brain tissue, the thickness of the shank was decreased to attain a targeted range of 1 μm (Lycke et al., 2023). However, for insertion into the brain tissue, as the thinned structure was no longer stiff enough to prevent buckling, the authors utilized a 75- μm tungsten wire affixed to the shank via a biodegradable PEG adhesive.

Alternately, to reduce the mechanical mismatch with the brain tissue, using softer materials that closely resemble it, such as hydrogels, is a viable approach. A transient microarray for the recording of electrophysiological signals from the cortex was designed by the group of Rogers (Yu et al., 2016). It involved the utilization of thin silicon tracks transferred onto a PLGA film and coated with a SiO_2 dielectric layer (Yu et al., 2016). More recently, the same research group introduced a bioresorbable device designed for the transient electrostimulation of the sciatic nerve to act as an electronic pain blocker (Figure 7A) (Lee et al., 2022). In this bioelectronic system, fast-resorbable magnesium was used to design tracks in contact with the external connector (kilo-hertz frequency alternating current pulses sent during treatment), whereas slowly degrading Mo was used to make contact with the nerve. Thin strips of Mo were put in contact with Mg strips using a conductive resorbable carbon wax (C-wax) in a woven electrode pattern. The primary objective of this design was to ensure that the rapid resorption of the 50- μm -thick Mg patterns after the electrostimulation treatment (approximately 10 days in phosphate buffer, 2 months when implanted in rodents) did not impose any constraints on the nerve. The nerves were in contact with 700-nm-thick Mo electrodes that were resorbed over a longer time scale (approximately 2 months in phosphate buffer). Note that different substrate materials were also tested and selected for the fabrication of the system to achieve suitable kinetics of bioresorption. Conducting polymers were shown to improve the bioelectronic interface between metals (gold and platinum) and neural tissues, especially by decreasing the electrical impedance and increasing the charge transfer capacity (Ludwig et al., 2006; Richardson-Burns et al., 2007; Khodagholy et al., 2015). CP nanotubes (70–175 nm diameter) (Abidian et al., 2008; Abidian et al., 2009; Abidian et al., 2010) and microstructures (Antenstainer et al., 2017a; Khorrami et al., 2017) advantageously enhanced the surface roughness of the CP films and improved the cellular response of neurons for chronic stimulation and recording. Our group recently developed a resorbable PEDOT:HA ink that can be inkjet-printed and UV-cross-linked on molybdenum tracks patterned onto a flexible PLGA substrate, to serve as a transient recording device of visual stimuli (Leprince et al., 2023b). The conductivity of the tracks and signal recording was maintained for approximately 4 months of implantation on rat cortex, correlated with the system resorption *in vivo*.

Other microelectrode arrays have been designed for various applications, for instance, interacting with bones. Yao et al. (2021) described a bioresorbable and self-powered implant to stimulate and monitor the resorption of bone fracture. The device was composed of two parts: a self-powering generator with micro-pyramid-shaped PLGA structures between two Mg conductive islands and an interdigitated electrode dressing for bone electrical stimulation and healing monitoring (Figure 7B). It can be foreseen that transient electrochemical sensors (for instance, monitoring pH, lactate, and inflammation) can be of high interest in assessing infection risks during the few months following prosthesis implantation (Dai et al., 2023). A thermoresponsive and injectable self-supporting conductive hydrogel made of collagen and polypyrrole was described to detect glucose by amperometry (Ravichandran et al., 2018). The key issue of connectivity was however not addressed or described, and the demonstration of

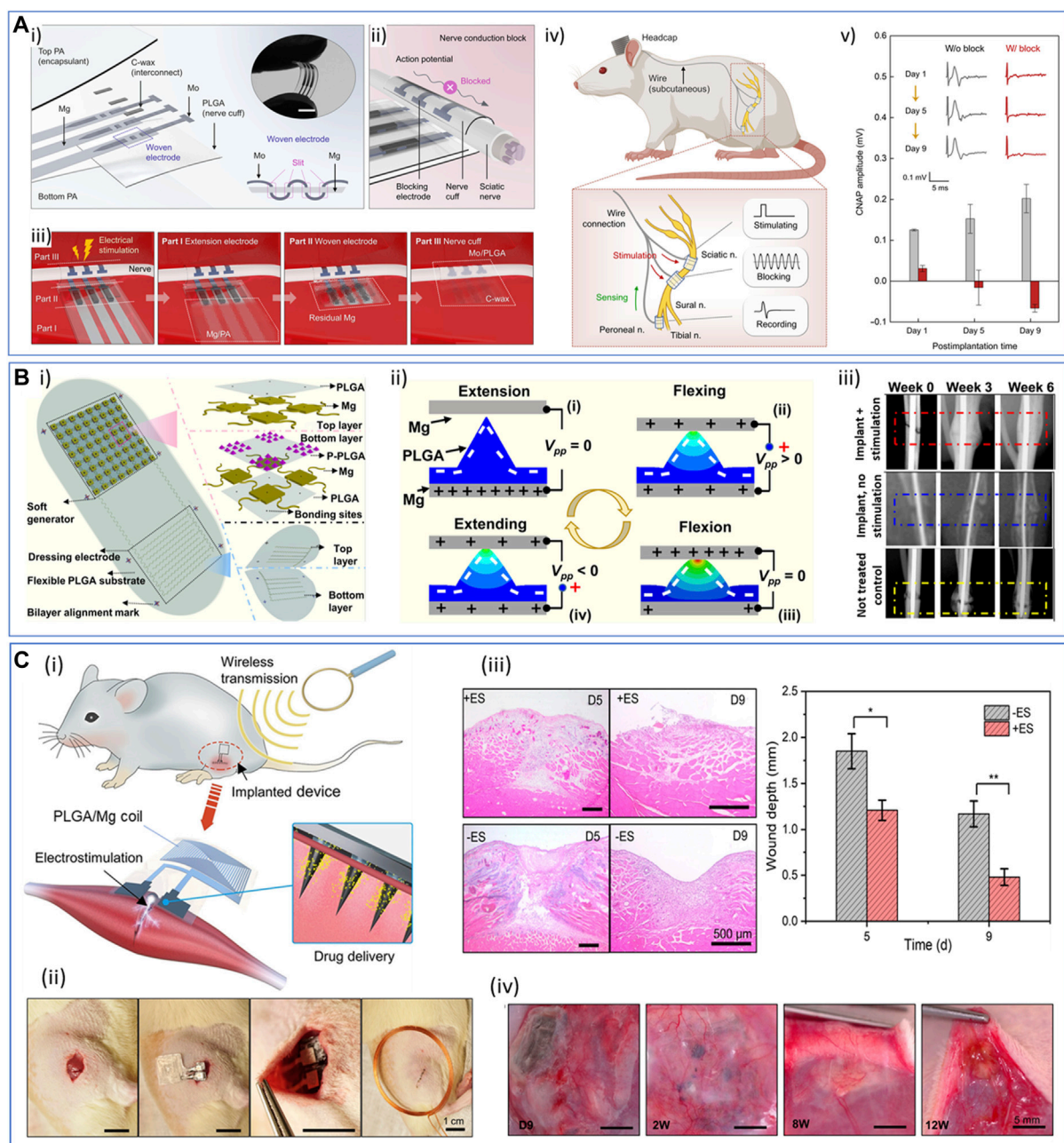


FIGURE 7

Examples of resorbable implanted medical devices. **(A)** Bioresorbable nerve cuff as a stimulator to electronically block pain. i) Schematic representation of the device, showing the Mg/Mo woven electrode structure connected through C-wax. ii) Schematic of the process of the nerve conduction block in the cuff-geometry device. iii) Illustration of the functioning and progressive bioresorption of the device through various stages of its lifetime. iv) Illustration of the *in vivo* implantation: a subcutaneous pathway for the placement of nerve cuffs and wire interconnects (top) and cuffs wrapping around nerves for stimulation, blockage, and recording (bottom). v) Representative compound nerve action potential (CNAP) measurements at days 1, 5, and 9 after implantation, without (w/o) or with electrical stimulation of the pain-blocking device. Copyright 2022, the Authors, published by *Science Advances* (Lee et al., 2022). **(B)** Self-powered implant to stimulate and monitor the resorption of bone fracture. i) Representative scheme of the device, showing the two parts: the self-powering generator (top) and the interdigitated electrode dressing for electrical stimulation (bottom). ii) Triboelectric working principle of the self-powering generator part. iii) X-ray photographs of bone fracture healing (right tibia) with time in rodents, when treated with an active device (i.e., implantation of the fully active device, top row), when treated with the inactive device (i.e., implantation of the device for which the self-powering unit has been disconnected from the interdigitated electrode pattern, middle row), when not treated (no device implantation, bottom row). Reproduced with permission, Copyright 2021, the Authors, published by *PNAS* (Yao et al., 2021). **(C)** Resorbable microneedle-based device for in-depth and wireless electrotherapy and drug delivery into injured muscle tissue. i) The device is composed of a drug-loaded PLGA microneedle array assembled with a PLGA sheet comprising magnesium coils acting as an antenna for wireless power transmission. ii) Invasive surgical procedure for the implantation of the device in rat muscle injury models. Scale bar: 1 cm. iii) Muscle healing assessment with (+ES) or without (-ES) electrostimulation at days 5 (D5) and 9 (D9) after treatment: representative H&E staining section images (scale bar: 500 μ m) and statistical analysis of muscle injury depth. iv) Photographs of microneedle-based devices implanted in rats at different times after therapy (9 days, 2 weeks, 8 weeks, and 12 weeks). Scale bar: 5 mm. Adapted with permission from Huang et al. (2022), Copyright 2022, the American Chemical Society.

functionality was made in a piece of meat, evidencing the long pathway to human applications.

Microneedle (MN)-based devices to measure or stimulate in a minimally invasive way through the skin have emerged in the last 10 years (Huang et al., 2022; GhavamiNejad et al., 2023). If the benefit of microneedles essentially relies on their skin-anchoring function, which minimizes potential artifacts due to body movements, they still remain invasive systems for microneedle heights above 80 μm , which makes us consider them as implanted devices. If the anchoring function and improvement of measure quality and reliability can counterbalance the regulatory issue due to the invasiveness of such systems, they should expand rapidly for minimally invasive transdermal sensing in the coming years. Microneedles have so far been made mainly from non-resorbable materials, and intended to be removed at the end of their use. For instance, GhavamiNejad et al. (2023) designed an MN patch for glucose sensing based on a blend of hyaluronic acid, dopamine, PEDOT:PSS, Pt nanoparticles, and glucose oxidase. They associated this MN patch as the working electrode with two other patches made of polycarbonate, coated with a Pt layer (counter-electrode) and Ag/AgCl (reference electrode) for glucose transdermal sensing. In the future, the use of long-term (1–2 months) fully resorbable materials can be a real asset to improve the safety of such devices, as well as their disposal after use. In this perspective, Huang et al. (2022) very recently described a resorbable implantable electronic system composed of a drug-loaded PLGA microneedle array (25 MN of 900 μm height) coated by a tungsten layer (1 μm thick), assembled through a conductive paste (mixture of W nanoparticles and candelilla wax) with a PLGA sheet comprising square-shaped magnesium coils (41 μm thick) acting as the antenna for wireless power transmission (Figure 7C). This device was used for the in-depth electrostimulation conjugated to the delivery of anti-inflammatory drugs (aspirin or ibuprofen) into injured muscle tissue. While the Mg coils resorbed in approximately 8 weeks, the degradation of the PLGA material was slower, within 12 weeks. However, the bioelectronic system was not implanted onto the skin surface but directly onto the muscle tissue using an invasive surgery procedure. The microneedle structuration of the device was therefore used for its tissue-anchoring function but not to reduce the invasiveness of the implantation.

4.3 Tissue engineering

Tissue engineering has emerged as a promising therapeutic approach, aiming to replace damaged tissue with a functional one that is generally grown within a biologically functional scaffold. Notably, efforts have been focused on constructing biomaterials-based scaffolds that resemble the extracellular matrix to promote cellular regrowth, differentiation, and tissue regeneration. However, designing scaffolds that achieve optimal cellular responses and integration with the host tissue remains a challenge. Recently, there has been growing interest in incorporating both electroconductive and bioresorbable properties into biomaterials used for tissue engineering. Electroconductive materials can mimic the natural electrical microenvironment of living tissues, facilitating accurate cell responses and tissue

development. Meanwhile, bioresorbable materials gradually degrade and are absorbed by the body, reducing the need for invasive procedures and potential complications associated with permanent implants. Therefore, the combination of electroconductive and bioresorbable properties in tissue engineering scaffolds holds promise for tissue regeneration and functional organ restoration. The following section will primarily focus on exploring the latest advancements in electroconductive scaffolds for understanding the fundamental mechanisms underlying *in vitro* cellular monitoring and stimulation in the presence of electroconductive elements. Subsequently, the latest advancements in electroconductive and biodegradable materials in tissue engineering will be treated, with a particular focus on the functional restoration of four of the major electroactive tissues: the heart, nervous system, skin, and bones.

4.3.1 Engineered *in vitro* culture systems for cellular monitoring and stimulation

Nowadays, advanced *in vitro* culture systems have emerged as valuable tools for studying the intricate structure and functionality of human tissues, bridging the gap between *in vitro* and *in vivo* investigations. These systems enable the recreation of physiologically relevant microenvironments, in particular the 3D native extracellular matrix (ECM) that serves as a dynamic scaffold that supports cell adhesion, migration, and differentiation. This capability is crucial to accurately recapitulate complex pathophysiological phenomena and support various applications, such as tissue engineering, regenerative medicine, and drug discovery. In this context, the integration of physiologically relevant electroconductivity into 3D *in vitro* cell culture models adds a new dimension to their capabilities, as several tissues, such as the heart, nerves, skin, and brain, are known to display electrical properties (Xu et al., 2021). By incorporating conductive materials into hydrogel matrices, it becomes possible to develop scaffolds that not only support cell growth but also provide electrical stimulation to mimic the natural electrical cues found in living tissues. This unique combination of physicochemical support and electrical conductivity promotes cell proliferation, differentiation, and tissue regeneration, making electroconductive hydrogels a promising tool for the development of functional, biomimetic tissue constructs (Min et al., 2018).

Electroconductive hydrogels play a significant role in the monitoring of cell growth *in vitro*. These hydrogels offer the unique capability of integrating electrical monitoring within the 3D culture systems. The electrical properties of the culture, such as impedance, capacitance, and electrical resistance, can be measured and monitored, which can provide insights into cellular behaviors such as proliferation, viability, and metabolism (De León et al., 2020). The electrical monitoring of cell growth in electroconductive hydrogels allows for real-time and non-invasive assessment of cell behavior. Changes in electrical signals can reflect alterations in cell morphology, cell adhesion, and cellular responses to environmental cues. These electrical cues can serve as indicators of cell growth, functionality, and response to external stimuli (Khan et al., 2019). In particular, impedance measurements at the cell–material interface offer non-invasive and real-time monitoring of cellular behavior and allow to correlate and quantify cell viability over time. Inal et al. (2017) developed a conducting polymer scaffold, made of

macroporous PEDOT:PSS integrated with collagen and dodecylbenzenesulfonic acid (DBSA) for the growth and monitoring of MDCK-II cells in a 3D system via electrochemical impedance spectroscopy. The presence of collagen provides cells with a biologically supportive, biomimetic environment to grow. On the other hand, the intimate contact of cells with the electroactive material allows a highly efficient signal transduction at the electrode interface, providing valuable, quantitative insights into MDCK-II growth and migration when compared to the bare collagen scaffold condition (Inal et al., 2017). Furthermore, the possibility to create seamless interfaces between cells and tissues and electronics is gaining significant interests in the contexts where intimate and long-lasting contact is required for monitoring complex *in vitro* systems. Ferlauto et al. (2018) developed a soft electroconductive interface through the selective electrodeposition of a hybrid material made from alginate and PEDOT:PSS onto platinum microelectrodes within a planar microelectrode array (MEA). The integration resulted in a substantial reduction of both mechanical and electrical mismatch at the tissue/electrode interface. Notably, it significantly reduced the electrical noise during recording when iPSC-derived neurospheres were encapsulated within these hydrogels, in contrast to using bare alginate hydrogels. Additionally, it provided a soft, supportive microenvironment for the long-term growth of organoids.

In addition to cell and tissue monitoring, the possibility to electrically stimulate cells *in vitro* (via endogenous or exogenous routes) has been shown to deeply influence cell behavior and stem cell differentiation, offering a potential strategy for generating tissue-specific cell types in regenerative medicine and tissue engineering applications (Chen et al., 2019). In a seminal study, a biohybrid hydrogel composed of collagen, alginate, and PEDOT:PSS was shown to induce *in vitro* maturation and beating properties of hiPSCs-derived cardiomyocytes, upon external electrical stimulations (Figure 8A) (Roshanbifar et al., 2018). Similarly, the *in vitro* electrical stimulation of neural stem cells (NSCs) embedded in a collagen-based network containing PPy showed NSC proliferation and differentiation into astrocytes, provoking NSC transcriptome alternation, such as genes involved in cell proliferation and synaptic remodeling (Xu et al., 2022).

The molecular mechanisms underlying electrically induce cell growth and differentiation involves intricate cellular signaling pathways and gene expression regulation (Thrivikraman et al., 2018; Chen et al., 2019; Katoh, 2022). Electrical stimulation triggers the activation of specific ion channels and transporters on the cell membrane, leading to changes in intracellular ion concentrations, particularly calcium ions. These changes initiate downstream signaling cascades, such as activation of protein kinases, phosphorylation of transcription factors, and modulation of gene expression. This ultimately regulates cell growth and differentiation by influencing cell cycle progression, proliferation, and the activation of lineage-specific genes. Additionally, electrical stimulation can modulate the activity of growth factors and cytokines, further contributing to cell growth and differentiation processes. It is however worth noting that the specific molecular mechanisms underlying electrically induced cell growth and differentiation are still partially unclear and can greatly vary depending on the cell type and on the specific characteristics of the conductive material in contact with cells.

It is also evident that cellular differentiation in such systems relies on the combination of mechanical and electrical stimulations through a concert of biochemical and mechanobiological pathways (Bielfeldt et al., 2022). The possibility to independently investigate the two stimuli might give further insight into the biological processes underpinning cell type formation and help develop a more accurate platform for regenerative medicine applications. In a recent study, Tringides et al. (2023) developed a porous conductive scaffold by incorporating carbon nanomaterials (CNTs and carbon flakes) into an alginate hydrogel matrix with tunable mechanical and electrical properties in the range of the typical neural tissue values (Figure 8B). By varying the degree of matrix viscoelasticity and CNT content, the authors could study and characterize the ability of encapsulated neural progenitor cells to grow and differentiate under different electrical and mechanical environments. Notably, it was found that the more viscoelastic and conductive scaffolds produced denser neurite networks and differentiated into astrocytes and myelinating oligodendrocytes. These findings were consistent with previous studies examining the influence of matrix viscoelasticity and conductivity associated with carbon nanotubes (CNTs) on the maturation of neural cells (Chaudhuri et al., 2015; Chen et al., 2019; Samanta et al., 2022). Importantly, this study provides novel insights into the individual contributions of each stimulus, shedding light on their independent effects.

Interestingly, the dynamic rearrangement of the internal matrix nanostructure, as a result of the continuous cell–environment interaction, was shown to further alter the endogenous conductivity of the system. This phenomenon was particularly evident upon cell encapsulation in dynamic hydrogel networks. In an electroconductive PEDOT:PSS/peptide-PEG hydrogel, the assembly of peptide-PEG and negatively charged PEDOT:PSS nanostructure resulted in a dynamic non-covalent network, prone to structural rearrangements under cellular action, such as growth and maturation (Figure 8C) (Xu et al., 2018). Despite that the underlying biological and chemical mechanisms remained undetermined, the increase in conductivity after 5 days of mesenchymal stromal cell culture was associated with a simultaneous marked change in the matrix network structure, with the presence of nanofiber bundles around the cells.

In conclusion, the exploration of the underlying biological processes governing cellular differentiation and phenotypic expression in the presence of electroconductive elements is crucial for advancing regenerative medicine applications. Further investigation of these intricate mechanisms offers an opportunity to develop refined and precise platforms that can accurately replicate the complex cellular environments found *in vivo*. By unraveling the intricacies of cell–biomaterial interactions at a fundamental level, new insights can be gained into cellular fate determination, lineage commitment, and the modulation of cellular functions, thereby enhancing *in vitro* modeling capabilities and driving the development of innovative therapeutic approaches for tissue engineering applications.

4.3.2 Cardiac tissue engineering

Cardiovascular diseases, such as myocardial infarction, occur with imparted electrical activity and alteration of the heart's mechanical function, which causes severe damage to the heart tissue, such as the loss of cardiomyocytes (CMs). The infarcted

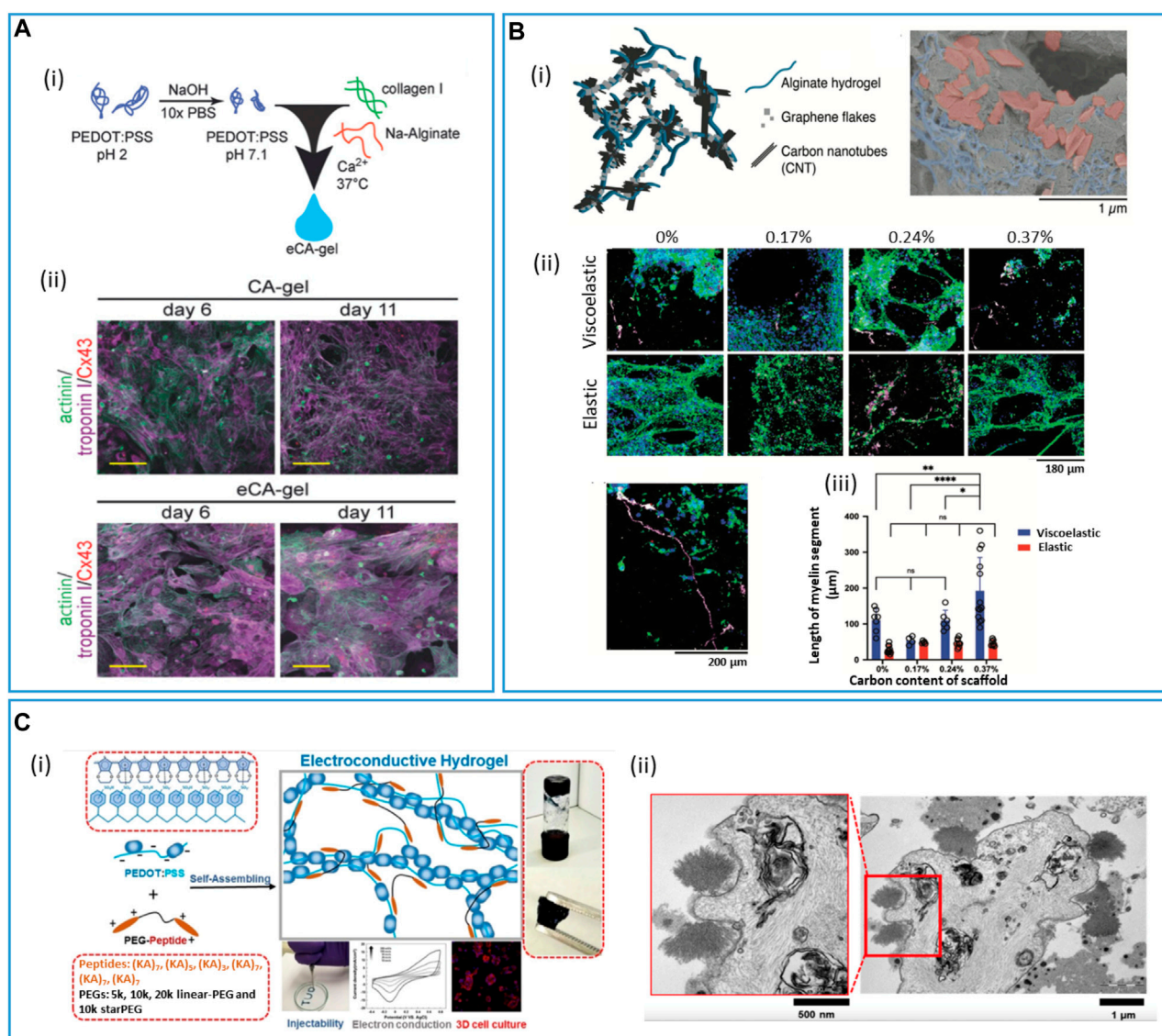


FIGURE 8

Cell-conductive material interactions in advanced hydrogels and scaffolds for *in vitro* 3D culture models. **(A)** Biohybrid hydrogel composed of collagen, alginate, and PEDOT:PSS for *in vitro* hiPSCs-derived cardiomyocyte maturation. (i) Schematic of the conductive biohybrid hydrogel formation (eCA-gel). (ii) Maturation of hiPSC-derived cardiomyocytes in the non-conductive hydrogel control (CA-gel) and electroconductive hydrogels (eCA-gel). Confocal images projection of tissue constructs stained for cardiomyocyte-specific markers troponin I, sarcomeric- α -actin, and connexin 43. Scale bars: 25 μm . Adapted with permission, Copyright 2018, John Wiley and Sons (Roshanbinfar et al., 2018). **(B)** Porous, conductive scaffold made of alginate and carbon nanomaterials (CNTs and carbon flakes) for the electromechanical differentiation of neural progenitor cells (NPCs). (i) Schematic of the porous scaffold and scanning electron microscopy (SEM) images of the internal structure, showing the entrapment of carbon flakes (red) and CNT (blue) into alginate (gray). Scale bar: 1 μm . (ii) 3D reconstruction of NPC micrographs in scaffolds of different mechanical properties (viscoelastic and elastic) and carbon content (%) after 6 weeks in culture. Staining for oligodendrocyte markers TuJ1 (green), myelin basic protein (MBP, magenta), and NPC (red). Scale bars: 180 μm . (iii) Quantification of the length of myelin for different carbon contents (%) and mechanical properties (viscoelastic, elastic) of the scaffolds. Adapted with permission, Copyright 2022, John Wiley and Sons (Tringides et al., 2023). **(C)** Characteristics of PEDOT:PSS/peptide-PEG conductive dynamic hydrogels. (i) Self-assembling and representative hydrogel formation through reversible and non-covalent interactions. (ii) Transmission electron microscopy (TEM) images of MSCs encapsulated in the PEDOT:PSS/peptide-PEG hydrogel showing the formation of nanofiber bundles around cells. Scale bars: 500 nm (left) and 1 μm (right). Adapted with permission from Xu et al. (2018), Copyright 2018, the American Chemical Society.

myocardial tissue triggers a pro-fibrotic response, which is responsible for the stiffening of the tissue and loss of contractility. Compared to other tissues, the cardiac regenerative capacity is really limited. In this context, cardiac tissue engineering aims at assembling tissue patches, adhesives, or injectable materials, which can intrinsically integrate with the cardiac tissue. Notably, apart from being biocompatible and biodegradable, those scaffolds

should match the mechanical and electrical behavior of the myocardium ECM in order to mimic and transduce the heartbeat. Moreover, as the heart has a low inherent regenerative capacity, it is crucial that these systems allow for the maturation and differentiation of implanted cells into conductive and contractile CMs. The conductivity range of native myocardium, which can be used as reference values for designing electroconductive hydrogels

for cardiac repair, varies from $5 \times 10^{-5} \text{ S cm}^{-1}$ (transversally) to 0.0016 S cm^{-1} (longitudinally) (Gao et al., 2022).

The main strategy used in cardiac tissue engineering consists of the addition of carbon nanotubes, gold nanoparticles, and graphene and its derivatives, or conducting polymers such as PPy, PANI, and PEDOT, to hydrogels. The electrically conductive properties of the materials incorporated in ECM-mimic hydrogels have been shown to improve *in vivo* cardiac function and electrical impulse propagation in the absence of external stimulation (Morsink et al., 2022). On the other side, it is widely accepted that the inclusion of nano- or microstructured materials, regardless of their conductivity, also changes the stiffness and topography of the scaffold, influencing the maturation and irritability of the heart tissue. It has been argued that the incorporation of intrinsic conductive materials results in the formation of tight connections between cell membranes and the scaffold, forming a hybrid conductive network that, in turn, facilitates signal propagation and excitability of heart cells. Furthermore, the presence of nano- or microelectrical conductors has been shown to promote cell attachment and the expression of cardiac-specific markers (e.g., sarcomeric alpha-actin striations and connexin 43 (cx-43)) (Morsink et al., 2022). Lee et al. (2019) have characterized the effects of the addition of CNTs, GO, and rGO in gelatin methacrylate (GelMA) hydrogels on cardiomyocytes' function and behavior, underlying the importance of directing cardiac tissue regeneration through mechanical and electrical cues of carbon derivatives. GelMA-CNT and GelMA-rGO scaffolds resembled typical stiffness values of the heart, featured electrophysiological properties, and displayed electrical conductivity. Surprisingly, the different types of carbon functionalization direct different types of *in vitro* tissue maturation. While GelMA-CNT hydrogels led to ventricular-like tissue, GelMA-GO hydrogels guided to atrial-like tissue. This is likely the result of the integrin-mediated differentiation of the CMs, which was stimulated differently by using different carbon nanoparticles and thus different gel topography.

Injectable electroconductive hydrogels can be deployed into the infarct site and surrounding area to promote myocardial tissue function restoration, providing an effective and minimally invasive method. Once injected into the myocardium, the hydrogel undergoes fast *in situ* polymerization, not only acting as a structural support for the damaged tissue but also bridging the electrical mismatch between healthy and damaged CMs, promoting cardiac resynchronization (Gao et al., 2022). Liang et al. (2018) developed a series of electroconductive hydrogels by combining PPy with gelatin and PEGDA via a two-step Michael addition reaction. The injectable material was directly painted into the infarcted area in a myocardial infarction rat model, and *in situ* polymerization occurred in less than 10 s, avoiding any adverse hydrogel leakage and creating a seamless interface between the hydrogel and the tissue. Four weeks post-implantation, the PPy-containing hydrogels were mostly degraded, likely due to enzymatic and hydrolysis degradation, and the cardiac tissue presented a remarkably improved electrophysiological signal restoration and reconstruction. Injectable hydrogels could also load cells, drugs, and biomolecules into the tissues, further boosting myocardial restoration and cardiac function. Bao et al. (2017) developed an injectable PEGDA-melamine/hyaluronan-thiol

(HA-SH)/GO hydrogel, where GO interacted with the melamine core through π - π conjugation, and this was loaded with adipose-derived stem cells. The flowable behavior of the hydrogel allowed the safe injection of the cells into the myocardial infarction area in rats, by mitigating the injection-associated shear stress. *In vivo* results have shown a remarkable improvement in heart function, characterized by an increase in ejection fraction and reduction of the infarcted area together with enhanced angiogenesis (Bao et al., 2017).

Among other electrically conductive nanoparticles, AuNPs are widely employed for cardiac tissue engineering due to the ease of producing particles with different sizes, shapes, and surface properties, allowing for tunable electrical and mechanical properties. Saravanan et al. (2018) incorporated graphene oxide gold nanosheets (GO-Au) into degradable chitosan polymer. *In vitro*, the scaffold exhibited Go-Au concentration-dependent degradation properties, supported cell attachment and maturation, displayed no cytotoxicity, and increased electrical conductivity and signal propagation. When tested *in vivo*, in a rat model of myocardial infarction, the cardiac patch showed improved heartbeat, contractility, conductivity, and restoration of the ventricular function. However, despite low levels of inflammation, contrary to the *in vitro* tests, after 5 weeks post-implantation, the patch was still present in the heart, suggesting the need for more elaborative studies on the long-term fate of this class of implanted scaffolds and their long-term effects on cardiac function (Saravanan et al., 2018). In general, to be clinically relevant, cardiac patches should withstand the continuous, dynamic-stress environment of the heart and should hold great tissue adhesion, enabling tissue restoration while providing mechanical and electrical support to the infarction site. As such, conductive dynamically bonded hydrogels, featuring self-healing behaviors, are the desired materials to mimic the ability of native cardiac tissue to regenerate through the continuous formation of new chemical bonds (Rogers et al., 2020). To further enhance hydrogel wet-adhesion to tissues, conductive dopamine-based materials have been widely employed due to their notable gluing properties. To this end, Jing et al. (2017) developed electroconductive chitosan-based hydrogels functionalized with GO and featuring dynamic, self-healing, and self-adhesive behavior, by the incorporation of poly(dopamine). *In vitro* cell culture results showed enhanced viability and proliferation of human stem cell-derived fibroblasts and CMs in the conductive chitosan-dopamine/GO hydrogels, as well as faster, spontaneous, and physiologically relevant beating rate when compared to the non-conductive control.

Interestingly, Wu et al. (2020) developed a combined approach therapy, by synthesizing two types of biodegradable and bio-conductive hydrogels for the co-administration of a self-adhesive conductive hydrogel patch and injectable and self-healable hydrogel to the infarcted myocardium (Figure 9A). The dynamic, injectable hydrogel, obtained via Schiff-base hydrazone bonds between oxidized HA and hydrazide-functionalized HA, was first injected at the infarcted area in order to provide mechanical support and promote angiogenesis. Subsequently, the self-adhesive hydrogel patch, obtained by combining gelatin-dopamine and dopamine-modified PPy upon Fe^{3+} trigger, was painted and rapidly bound to the outermost layer of the beating myocardium in order to provide

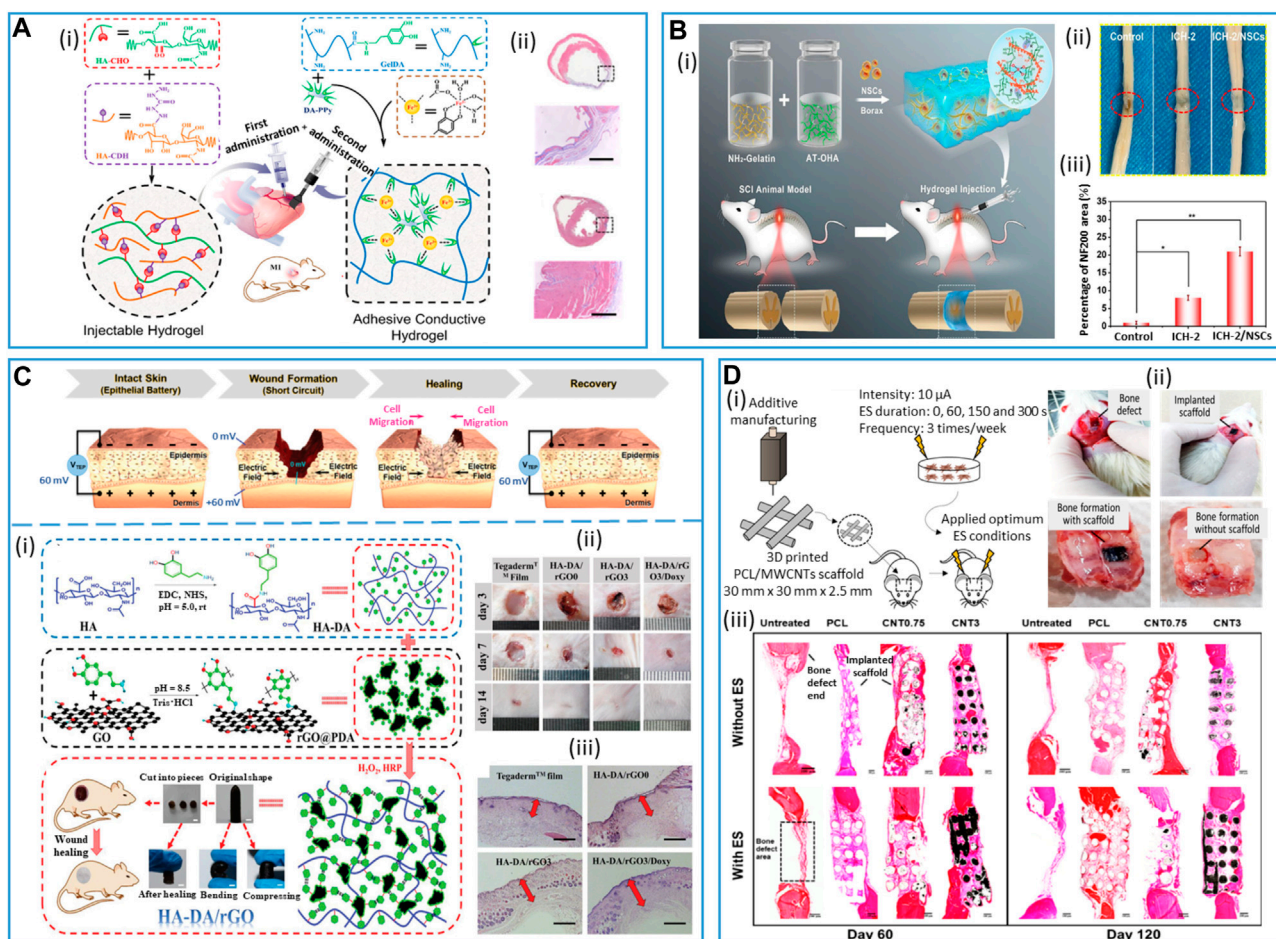


FIGURE 9

Conductive hydrogels for tissue engineering applications. **(A)** Co-administration of an injectable hydrogel (HA-CHO/HA-CDH) and an adhesive conductive hydrogel patch (Gel-DA/DA-PPy) to treat myocardial infarction. (i) Schematic depicting the synthesis and co-administration of the two hydrogels. (ii) Masson's trichrome-stained sections showing infarct size and related fibrotic tissue (blue stained infarct scar) of the myocardium for the untreated group (top) and the hydrogels co-administration group (bottom). Scale bars: 1 mm. Adapted with permission from Wu et al. (2020), Copyright 2020, the American Chemical Society. **(B)** Injectables, conductive, self-healing hydrogel (ICH) scaffold for spinal cord injury repair. (i) Schematic illustration of the hydrogel, based on amino-modified gelatin (NH₂-gelatin) and aniline tetramer-grafted oxidized hyaluronic acid (AT-OHA), loaded with exogenous neural stem cells (NSCs) and its administration in a rat model of total spinal cord injury (SCI). (ii) Total spinal cord resection samples 6 weeks after implantation of ICH, NSCs-loaded ICH (ICH-NSCs), and without any treatment (control group). (iii) Semi-quantitative analysis of the proportion of neurofilament 200 (NF200)-positive regions in rats by immunofluorescence staining. Adapted with permission from Liu H. et al. (2023), Copyright 2023, the American Chemical Society. **(C)** Conductive hydrogels for skin repair and wound dressing. (Top) Trans-epithelial potential and electric field at the wound site before and after the healing process. Reproduced with permission, Copyright 2020, John Wiley and Sons (Korupalli et al., 2021). (Bottom) (i) Diagrammatic sketch of soft hemostatic antioxidant conductive HA-DA/rGO@polydopamine (PDA) hydrogel preparation, macroscopic characteristics, and implantation at the wound site. Scale bar: 5 mm. (ii) Pictures of wounds at days 3, 7, and 14 post-implantation. (iii) Granulation tissue (red arrows) thickness for the different groups on day 14 post-implantation. Scale bar: 500 μ m. TegadermTM film: commercial film dressing (control); HA-DA/rGO0: HA-DA hydrogel in the absence of rGO; HA-DA/rGO3: HA-DA hydrogel cross-linked with rGO@PDA; HA-DA/rGO3/Doxy: doxycycline-loaded HA-DA/rGO@PDA hydrogel. Adapted with permission, Copyright 2019, John Wiley and Sons (Liang et al., 2019). **(D)** In vivo study of conductive 3D-printed PCL/MWCNTs scaffolds for bone tissue engineering. (i) Schematic illustration of the experimental setup: synthesis of the conductive scaffolds and their implantation with electrical stimulation (ES) treatment. (ii) Bone defect formation in the animal model and bone tissue formation with and without conductive scaffold after 60 days. (iii) Cross-section histological images of bone tissue formation at the bone defect for all groups (PCL, PCL/MWCNTs 0.75% wt and PCL/MWCNTs 3% wt) after 60 and 120 days, with and without electrical stimulation (ES). Adapted from eSilva et al. (2021), Copyright 2022, Springer Nature.

high hydrogel-tissue integration and homogenous electrical conductivity. These combined hydrogel/patch approaches featured good biodegradability of both materials upon *in vivo* implantation and a more pronounced improvement of the conductive functions, in terms of electrophysiological, histological, and antigenic outcomes when compared to single-mode systems (cardiac patch or injectable hydrogel) (Wu et al., 2020).

4.3.3 Nerve tissue engineering

Nerves' regrowth upon injury can be slow and often results in incomplete functional recovery as a consequence of the limited nervous tissue regenerative capacity. Endogenous and external electrical stimulations have been shown to promote nerve growth, enhance axonal regeneration, and guide the direction of nerve growth. Similar to cardiac tissue, recent studies have shown that conductive hydrogels can be used as electrical stimulators and

greatly promote neural cell proliferation, elongation, orientation, and neuronal differentiation, making these scaffolds promising for tissue repair (Rogers et al., 2020; Gao et al., 2022). Notably, conductive hydrogels employed as structural and electrical “functional bridges” at the lesion site could stimulate new neurogenesis and subsequent functional neural network formation. Such hydrogels are also the most suitable candidates for delivering stem cells, retaining and protecting cells after injection at the target tissue, and even directing the differentiation of neural stem cells by fine-tuning the modulus and conductivity of hydrogels. Notably, electrical stimulation in the presence of neural stem cells (NSCs) has been demonstrated to enhance their differentiation toward a neuron-like phenotype, as evidenced by a general increase in TuJ1 expression and the development of longer neurites, promoting neuronal differentiation over astrocyte differentiation (lower GFAP levels of expression) (Zhu et al., 2019; Sordini et al., 2021).

Spinal cord injury is a serious and disabling health issue that causes loss of motor functioning and sensing. It causes neural necrosis and axonal disruption with a low to null regenerative capacity. Implantation of injectable conductive hydrogels can restore the spinal cord by providing physiologically relevant electrical signal pathways (estimated to be $8\text{--}100\text{ S cm}^{-1}$ for the spinal cord). The promotion of specific cell proliferation and differentiation at the injured site has been shown to be a promising clinical treatment. Liu et al. (2023) developed injectable, biodegradable, and self-healing hydrogel scaffolds based on aniline tetramer grafted onto oxidized hyaluronic acid and amino-modified gelatin, eventually loaded with NSCs (Figure 9B). The resulting hydrogels displayed electroconductive (134 S cm^{-1}) and mechanical ($G' = 446\text{ Pa}$) properties that matched the natural spinal cord values. When injected into the back skin tissue of Sprague–Dawley rats, it showed good compatibility and complete degradation after 16 days (aniline tetramer is generally metabolized in physiological environments). Furthermore, when injected in a rat model of total spinal cord resection, the loaded NSCs differentiated into neurons and further grew into new nerve axons. The self-healing properties, together with the good conductivity of the hydrogel scaffold promoted endogenous neurogenesis, by providing continuous tissue electro-activity, which finally led to nerve regeneration and locomotor function recovery. Notably, the controlled degradation rate of the hydrogel allowed the complete axon integration within the tissue, without hindering their prior growth and connection (Liu H. et al., 2023). Similarly, Luo et al. (2022) developed an ECM-mimic hydrogel composed of borax-functionalized oxidized chondroitin sulfate, PPy, and gelatin, featuring injectable, self-healing properties (Schiff-base and borate-diol ester dynamic bonds), as well as physiologically relevant electrical (50 S cm^{-1} conductivity) and mechanical ($G' = 930\text{ Pa}$) properties. The injection of such hydrogels into the injury site to fill the lesion cavity promoted endogenous neural stem cells' neurogenesis and induced myelinated axon regeneration into the lesion site, thereby achieving significant locomotor function restoration in rats with spinal cord injury. Hydrogel degradation occurred within 21 days post-implantation (into rat subcutaneous tissue) with no histological damage to major organs (kidney, heart, liver, and spleen) (Luo et al., 2022). Furthermore, external electrical stimulation was proven to

enhance recovery of nerve injuries. Zhang et al. (2021) developed a wireless method for spinal cord regeneration by developing magneto-metric Fe_3O_4 Ba TiO_3 NP loaded with biodegradable ECM-like HA/collagen hydrogels and used an external magnetic field to induce electrical stimulation. Transplantation of this scaffold with wireless stimulation in the rat hemi-section spinal cord injury model showed the promotion of neural regeneration and paved the way for non-invasive remote control electrical devices for soft tissue stimulation. Contrary to the central nervous system, the peripheral nervous system has a good regenerative capacity after injury. Nevertheless, the complete restoration of nerve defects remains a big clinical challenge due to the side effects related to the use of autologous grafts as the golden standard, such as donor shortages, rejection, and infection risks. In the framework of tissue engineering, nerve guidance conduits (NGCs) are promising alternatives to nerve auto-grafting (Vijayavenkataraman, 2020). NGCs are generally tubular polymeric scaffolds that act as functional bridges between the injured nerve endings, providing structural and trophic support for the axon reconstruction along the conduit. As such, the requirements for an ideal NGC include suitable mechanical properties and structural support for promoting the longitudinal alignment of the new axons, high porosity, biocompatibility, and electrical conductivity. In this regard, an NGC made of PEDOT NPs incorporated in a tetrapeptide-modified chitin hydrogel was developed (Huang et al., 2021). The incorporation of PEDOT NPs, together with the highly porous structure of the hydrogel film, significantly promoted sciatic nerve regeneration after 20 weeks, featuring gastrocnemius muscle restoration and thickness of myelinated axon, similar to the auto-graft control groups. Despite the promising results, data on the conductive hydrogel degradation rates were reported only for *in vitro* experiments. Park et al. (2020) developed conductive NGCs by polymerizing *in situ* a GelMA/GO composite hydrogel using an annulus mold and further chemically reducing it to the r(GO/GelMA) form under mild conditions. The obtained material featured suitable mechanical stability (57 kPa Young's modulus), permeability, flexibility, and electrical conductivity (90 S cm^{-1}) for nerve restoration. *In vitro*, the hydrogel at its reduced form r(GO/GelMA) displayed remarkable neurogenesis capacity compared to the non-reduced form and pristine GelMA hydrogel, likely due to the electroactive interaction of rGO within the hydrogel. *In vivo* studies with a 10-mm peripheral defect model showed that the r(GO/GelMA) material significantly promotes neural regrowth, myelination, and functional regeneration of muscle and nerve tissues within 8 weeks post-implantation, without significant toxicity to other major organs. Nevertheless, at week 8, the r(GO/GelMA) hydrogel was only partially degraded at the implantation site (Pyarasani et al., 2019). Despite encouraging *in vitro* data on the degradation kinetics of hydrogel, future long-term investigations on material degradation and its systemic toxicity are necessary.

4.3.4 Wound dressing and skin repair

Similar to the myocardium and nerves, the skin also exhibits sensitivity to electrical signals, characterized by a conductivity ranging from 2.6 to $1 \times 10^{-7}\text{ S cm}^{-1}$. In intact skin, the epithelial tissue transports ions to the epidermis to form a transdermal potential ($\sim 10\text{--}60\text{ mV}$). When a wound occurs, the homeostatic

balance of the transdermal potential is disrupted, resulting in a potential decrease at the wound site and the formation of positive currents flowing toward the wound center. As a result, the formation of these endogenous electric fields promotes cellular recruitment and proliferation at the wound site, following the electrical gradient (electrotaxis), until complete wound healing is achieved, and the initial transdermal potential is restored (Shaner et al., 2023).

Therefore, to enhance such a regenerative capacity of the skin and accelerate the healing process, conductive hydrogel dressings can be employed. Such materials applied at the wound site should possess multifunctional properties. Notably, conductive dressings should exhibit adhesiveness to secure the dressing, possess antibacterial properties to prevent infections, scavenge radicals to minimize oxidative stress, and have sufficient conductivity and good mechanical properties to support cell migration, proliferation, and tissue regeneration. In this context, a series of soft hemostatic antioxidant conductive hydrogels based on HA-graft-dopamine and rGO have been developed (Liang et al., 2019) (Figure 9C). *In vivo*, the injected hydrogels showed high tissue adhesive properties, viscoelasticity, conductivity, and hemostatic ability. The hydrogel dressing showed substantial tissue repair after 7 days of treatment in a mouse full-thickness skin defect repair model, accelerating epidermal remodeling and promoting neovascularization at the lesion site. Furthermore, *in vitro* drug release studies in physiological conditions and zone of inhibition tests of antibiotics-loaded hydrogels showed a promising sustained drug release capacity of these hydrogels (Liang et al., 2019).

Apart from the re-establishment of the skin's endogenous electrical field through conductive dressing, the application of an external electrical field can also improve wound healing. Lei et al. (2021) developed an adaptive conductive hydrogel by incorporating tannic acid and human-like collagen into a polyvinyl alcohol and borax hydrogel dynamic cross-linking network. The dynamicity of the bonds imparted the hydrogel with self-healing and self-adaptive behavior at the wound site, which facilitated cell-to-cell signaling, promoted hemostatic repair, and maintained hydrogel structural and functional capacity. Furthermore, such adaptive behavior allowed endogenous and external current conduction, promoting electrostimulation in wound tissue. The combination of electrostimulation and hydrogel greatly promoted L929 cell migration and proliferation and *in vivo* wound healing, with subcutaneous tissue (blood vessels and pores) reconstruction. *In vivo* degradability tests showed gradual and complete hydrolytic degradation of the hydrogel in accordance with wound repair, avoiding any possible secondary damage due to adhesive peeling (Lei et al., 2021). Interestingly, the incorporation of additional characteristics into these electroconductive hydrogels could impart them with superior regenerative capabilities for a broad range of tissue engineering applications. In this context, Li et al. (2020) developed biomechanically active conductive hydrogels that could promote wound healing through the combination of biomechanical and biochemical functions. By combining quaternized chitosan, poly(dopamine)-coated reduction graphene oxide and poly(N-isopropylacrylamide), a series of multifunctional, injectable hydrogels have been developed. While the biochemical characteristics provided the hydrogels with self-healing, antioxidant, and adhesive properties, as well as good conductivity, the self-

contraction ability of the poly(N-isopropylacrylamide) in response to temperature changes played a crucial role in wound closure, leading to a significant improvement in tissue restoration in an *in vivo* full-thickness skin defect (Li et al., 2020).

4.3.5 Bone tissue engineering

Bone has a naturally good regenerative capacity to recover small bone defects; however, larger fractures generally require external intervention to restore the damaged tissue (Schemitsch, 2017). In this context, bone tissue engineering demands the creation of biocompatible, osteogenic scaffolds, which can sustain the dynamic nature and irregular structure of the microenvironment of the bone. These scaffolds should allow bone tissue remodeling and regeneration, providing physicochemical properties for osteoblast attachment, strong mechanical properties, and scaffold mineralization. Bone tissue engineering undergoes a process initiated by the migration and recruitment of bone cells, subsequently followed by proliferation, differentiation, and matrix formation (calcium deposition) (Mostafavi et al., 2020). Electrical stimuli play a key role in a broad spectrum of biological processes involved in bone regeneration, such as angiogenesis, cell division, and signaling. In this context, conductive hydrogels have been shown to effectively stimulate and sustain the effect of endogenous electric fields in bone tissue repair (Arambula-Maldonado et al., 2022).

In order to increase scaffold elastic modulus, roughness, and conductivity, the main strategy consists of the development of functional hybrid hydrogel/fiber composites. Notably, the combination of fibrous PANI in a graphene-containing hydrogel demonstrated that the inclusion of conducting fibers yielded materials that better supported human osteoblast-like cell adhesion, proliferation, and morphology when compared to hydrogel alone (Khorshidi et al., 2018). However, considerations on the *in vivo* biological toxicity of PANI, especially in the form of fiber, must be taken into account. On the other hand, the introduction of GO to porous hydrogel matrices was shown to significantly improve the efficiency of the mineralization process through electrostatic interactions, which sustained crystal growth and apatite deposition. In another study, β -cyclodextrin (β -CD)-functionalized rGO was used as a conductive component and mixed with GelMA/acryloyl- β -cyclodextrin (Ac-CD)-based photo-cross-linked hydrogel (Li et al., 2022). Such a hydrogel was shown to accelerate the *in vivo* defect repair in a rat skull defect model by promoting collagen deposition and mineralization. *In vitro* degradation tests confirmed the ability of the hydrogels to provide adequate mechanical and structural support in the early stages and to subsequently undergo gradual degradation, providing a good foundation for *in vivo* bone repair (Li et al., 2022).

Recently, conductive scaffolds were also obtained through the incorporation of multi-walled carbon nanotubes (MWCNTs) in a biodegradable PCL hydrogel and cut to fit the bone defect in rat skull models (eSilva et al., 2021) (Figure 9D). Upon exogenous electrical stimulation over a period of 120 days, thicker bone tissue reformation was observed, along with angiogenesis and mineralization. In particular, the combination of conductive hydrogel and electrostimulation was shown to play an important role in bone remodeling, inducing osteoclast formation and functioning.

5 Challenges and perspectives

As shown in this review, the field of resorbable conductive materials applied to biomedical applications is emerging and already fast expanding, giving rise to a growing interest in the community of advanced medical devices and tissue engineering. This is shown by the large number of publications in the domain reported in this review, and their novelty (>75% in the last 5 years, >95% since 2013). The field of resorbable bioelectronic systems is relatively young compared to chronic implantable devices such as pacemakers, deep brain stimulators, neural stimulators, or cochlear implants. However, there exist already several proofs of concept at the *in vitro* and preclinical (mainly in rodents) stages. The fact that implanted systems may be designed as resorbable is expected to extend their use to non-chronic pathologies requiring transient therapy and/or monitoring. Tissue engineering applications are quite novel in general, and the use of conductive materials will help address important applications (for instance tissue healing and heart and nerve reconstruction) that are still at the proof-of-concept stage. Therefore, it can be foreseen that the requirement for resorbable conductive materials that can optimally interface with tissues or act as tissue substitutes will quickly expand in the coming decades.

Another striking point that appears through this overview is the variety of employed polymer substrates/scaffolds, electrical conductors, and processes, which can be used to obtain resorbable conductive materials. This is largely accounted for by not only the large range of addressed biomedical applications but also the wide panoply of available components (scaffolds and electrical conductors) that allow choosing different strategies to design and fabricate resorbable bioelectronic systems, implants, or tissue substitutes. The variety of proposed approaches in the domain is interesting in order to meet the different challenges yet to be addressed.

Technical challenges concern the fabrication processes, stretchability and conformability of the devices, as well as material conductivity. In addition, communication of the implanted device with the external world has to be addressed in terms of electric and power connectivity, as well as for eventual information transfer. Concerning the fabrication process, the adhesion between different device layers, or at the interface between metals and polymers, for instance, can still be an issue, with poor adhesion or delamination being a source of low electrical contact (and hence low device performance) and/or premature degradation. For certain applications, such as spinal cord stimulation or recording, the stretchability of the device is key. The more stretchable it is, the better it can withstand large displacements and torsions in the spine during movements. In this perspective of high stretchability/conformability to tissues, conducting polymer-based materials, thanks to their mechanical and structural properties, appear very interesting in designing electrical tracks or contact electrodes. However, their electrical conductivity is still several orders of magnitude below the ones of resorbable metals. Therefore, innovative chemical designs are still intensively sought to achieve conductive materials presenting simultaneously features of high conductivity, stretchability, and biocompatibility.

Another challenge concerns the identification of relevant medical applications that will boost scientific and technical developments, in particular in the field of resorbable implanted bioelectronic systems. For instance, if the resorbable pacemaker prototype proposed by the group of Rogers (Choi et al., 2021) is a remarkable technical achievement,

doubt can exist concerning its medical relevance. However, relevant applications of resorbable implanted bioelectronic systems are foreseen in the fields of i) minimally invasive transient monitoring (wearable devices and microneedle-based devices), ii) post-surgery transient monitoring and drug delivery [e.g., for the prevention/detection of infections, the follow-up of orthopedic surgery (bone fracture and prosthesis implantation), and the assessment of flaps resection and anastomosis], and iii) electrical stimulation for the healing of the skin or internal tissue wounds, or for muscular recovery and reinforcement. At the present time, the reported studies mainly appear to be supported by technical research groups rather than by medical teams. The technical signs of progress and first preclinical proofs of concept of devices, implants, and tissue substitutes based on resorbable conductive materials will hopefully pique clinicians' interest and will lead to the emergence of new applications of these materials.

Concerning the clinical translation challenge, in addition to the identification of relevant medical applications that are already emerging, the main task remains the demonstration of the full resorbability of devices or full integration of tissue substitutes, without any acute or long-term side effects, and the safety of the employed materials. The scaffolds/substrates and electrical conductors that have been described in Section 2 of this review have been reported as "biocompatible" and "resorbable," but it has to be reminded that material safety has to be evaluated according to its dose, its precise preparation process, its location of implantation into the body and its residence time, its metabolism pathway, its degradation products, and possible migration away from its site of implantation. Some of the described materials are highly questionable, such as CNTs (Mishra et al., 2018) and ZnO or Zn (that will oxidize in zinc oxide during its degradation process) (Xia et al., 2008; Jin et al., 2021). In presently reported studies, the resorbability of the materials is mainly assessed qualitatively by photographs or/and indirectly by the measurement of physical parameters such as impedance for an electrical contact, or a quality factor for an antenna. Safety evaluations involve the immunostaining and histology of tissue sections that come into contact with the devices or tissue substitutes. If such preliminary results, which already represent a huge amount of work, can be satisfactory in the first stage of the development of a resorbable material or device, further investigations will be required to enable the translation to the clinic. They include i) the evaluation of the dissolution rate of the material and the comparison of the employed dose with the toxicity intake limits given in meta-analysis databases such as <https://pubchem.ncbi.nlm.nih.gov/>; ii) the study of the metabolism pathways and identification of the degradation products of the conductive material; iii) the assessment of the biodistribution and the clearance of the material components and degradation products with time in the different organs; and iv) the study of potential side effects in the short and long terms. Another consideration to take into account is that the degradation rate of the material should be aligned as best as possible to its targeted use to minimize risks.

In conclusion, resorbable conductive materials already appear to have a bright future in biomedical applications and serve different purposes in the design of tissue substitutes and optimized interfaces between tissues and medical devices. This already very active research field should expand in the coming years, with intensive work to improve the performances of the materials to simultaneously present features of high conductivity, stretchability/conformability, and

biocompatibility and to assess their safe use. These are the necessary conditions for their adoption into the clinics.

Author contributions

MS: conceptualization, visualization, writing—original draft, and writing—review and editing. FS-S: conceptualization, writing—original draft, and writing—review and editing. PM: writing—review and editing and conceptualization. IT: conceptualization, visualization, writing—original draft, and writing—review and editing.

Funding

The authors that declare financial support was received for the research, authorship, and/or publication of this article. This work was supported by the CEA internal funding “Organoids on chip” focus program (PhD grant for MS). LETI-DTIS was supported by the French National Research Agency in the framework of the

STRETCH project (ANR- 8-CE19-0018-01), the LabEx Arcane (grant ANR-17-EURE-0003) and Glyco@Alps (ANR-15-IDEX-02) programs.

Conflict of interest

The authors declare that the research was conducted in the absence of any commercial or financial relationships that could be construed as a potential conflict of interest.

Publisher's note

All claims expressed in this article are solely those of the authors and do not necessarily represent those of their affiliated organizations, or those of the publisher, the editors, and the reviewers. Any product that may be evaluated in this article, or claim that may be made by its manufacturer, is not guaranteed or endorsed by the publisher.

References

- Abidian, M. R., Corey, J. M., Kipke, D. R., and Martin, D. C. (2010). Conducting-polymer nanotubes improve electrical properties, mechanical adhesion, neural attachment, and neurite outgrowth of neural electrodes. *Small* 6 (3), 421–429. doi:10.1002/sml.200901868
- Abidian, M. R., Kim, D.-H., and Martin, D. C. (2006). Conducting-polymer nanotubes for controlled drug release. *Adv. Mater.* 18 (4), 405–409. doi:10.1002/adma.200501726
- Abidian, M. R., Ludwig, K. A., Marzullo, T. C., Martin, D. C., and Kipke, D. R. (2009). Interfacing conducting polymer nanotubes with the central nervous system: chronic neural recording using poly(3,4-ethylenedioxythiophene) nanotubes. *Adv. Mater.* 21 (37), 3764–3770. doi:10.1002/adma.200900887
- Abidian, M. R., and Martin, D. C. (2008). Experimental and theoretical characterization of implantable neural microelectrodes modified with conducting polymer nanotubes. *Biomaterials* 29 (9), 1273–1283. doi:10.1016/j.biomaterials.2007.11.022
- Abu Ammar, A., Abdel-Haq, M., Abd-Rbo, K., and Kasem, H. (2021). Developing novel poly(lactic-Co-glycolic acid) (PLGA) films with enhanced adhesion capacity by biomimetic mushroom-shaped microstructures. *Biotribology* 27, 100184. doi:10.1016/j.biotri.2021.100184
- Aghazadeh, M. R., Delfanian, S., Aghakhani, P., Homaegohar, S., Alipour, A., and Shahsavari, H. (2022). Recent advances in development of natural cellulosic non-woven scaffolds for tissue engineering. *Polymers* 14 (8), 1531. doi:10.3390/polym14081531
- Alhashmi Alamer, F., and Almalki, G. A. (2022). Fabrication of conductive fabrics based on SWCNTs, MWCNTs and graphene and their applications: a review. *Polymers* 14 (24), 5376. doi:10.3390/polym14245376
- Anand, P., Llewellyn, J. G., Thomas, P. K., Gillon, K. R. W., Lisk, R., and Bloom, S. R. (1988). Water content, vasoactive intestinal polypeptide and substance P in intact and crushed sciatic nerves of normal and streptozotocin-diabetic rats. *J. Neurological Sci.* 83 (2), 167–177. doi:10.1016/0022-510X(88)90066-4
- Ansari, S., Sami, N., Yasin, D., Ahmad, N., and Fatma, T. (2021). Biomedical applications of environmental friendly poly-hydroxyalkanoates. *Int. J. Biol. Macromol.* 183, 549–563. doi:10.1016/j.jbiomac.2021.04.171
- Antensteiner, M., and Abidian, M. R. (2017b). “Tunable nanostructured conducting polymers for neural interface applications,” in Proceedings of the 39th Annual International Conference of the IEEE Engineering in Medicine and Biology Society (EMBC), Jeju Island, South Korea, July 11–15, 2017, 1881–1884.
- Antensteiner, M., Khorrami, M., Fallahianbijan, F., Borhan, A., and Abidian, M. R. (2017a). Conducting polymer microcircuits for organic bioelectronics and drug delivery applications. *Adv. Mater.* 29 (39), 1702576. doi:10.1002/adma.201702576
- Arambula-Maldonado, R., and Mequanint, K. (2022). Carbon-based electrically conductive materials for bone repair and regeneration. *Mater. Adv.* 3 (13), 5186–5206. doi:10.1039/d2ma00001f
- Baker, A. E. G., Cui, H., Ballios, B. G., Ing, S., Yan, P., Wolfer, J., et al. (2021). Stable oxime-crosslinked hyaluronan-based hydrogel as a biomimetic vitreous substitute. *Biomaterials* 271, 120750. doi:10.1016/j.biomaterials.2021.120750
- Balfourier, A., Luciani, N., Wang, G., Lelong, G., Ersen, O., Khelifa, A., et al. (2020). Unexpected intracellular biodegradation and recrystallization of gold nanoparticles. *Proc. Natl. Acad. Sci.* 117 (1), 103–113. doi:10.1073/pnas.1911734116
- Ban, G., Hou, Y., Shen, Z., Jia, J., Chai, L., and Ma, C. (2023). Potential biomedical limitations of graphene nanomaterials. *Int. J. Nanomedicine* 18, 1695–1708. doi:10.2147/IJN.S402954
- Bano, K., Pandey, R., and Roohi, J. (2018). New advancements of bioplastics in medical applications. *Int. J. Pharm. Sci. Res.* 9 (2), 402–416. doi:10.13040/IJPSR.0975-8232.9(2).402-16
- Bao, R., Tan, B., Liang, S., Zhang, N., Wang, W., and Liu, W. (2017). A π - π conjugation-containing soft and conductive injectable polymer hydrogel highly efficiently rebuilds cardiac function after myocardial infarction. *Biomaterials* 122, 63–71. doi:10.1016/j.biomaterials.2017.01.012
- Bashir, S., Hina, M., Iqbal, J., Rajpar, A. H., Mujtaba, M. A., Alghamdi, N. A., et al. (2020). Fundamental concepts of hydrogels: synthesis, properties, and their applications. *Polymers* 12 (11), 2702. doi:10.3390/polym12112702
- Battigelli, A., Almeida, B., and Shukla, A. (2022). Recent advances in bioorthogonal click chemistry for biomedical applications. *Bioconjugate Chem.* 33 (2), 263–271. doi:10.1021/acs.bioconjchem.1c00564
- Beygisangchin, M., Abdul Rashid, S., Shafie, S., Sadrolhosseini, A. R., and Lim, H. N. (2021). Preparations, properties, and applications of polyaniline and polyaniline thin films—a review. *Polymers* 13 (12), 2003. doi:10.3390/polym13122003
- Bhat, M. A., Rather, R. A., and Shalla, A. H. (2021). PEDOT and PEDOT:PSS conducting polymeric hydrogels: a report on their emerging applications. *Synth. Met.* 273, 116709. doi:10.1016/j.synthmet.2021.116709
- Bielfeldt, M., Rebl, H., Peters, K., Sridharan, K., Staehle, S., and Nebe, J. B. (2022). Sensing of physical factors by cells: electric field, mechanical forces, physical plasma and light—importance for tissue regeneration. *Biomed. Mater. Devices* 1, 146–161. doi:10.1007/s44174-022-00028-x
- Bilbao, E., Garate, O., Rodríguez Campos, T., Roberti, M., Mass, M., Lozano, A., et al. (2023). Electrochemical sweat sensors. *Chemosensors* 11 (4), 244. doi:10.3390/chemosensors11040244
- Boehler, C., Agraw, Z., and Asplund, M. (2019). Applications of PEDOT in bioelectronic medicine. *Bioelectron. Med.* 2 (2), 89–99. doi:10.2217/bem-2019-0014
- Borriello, A., Guarino, V., Schiavo, L., Alvarez-Perez, M. A., and Ambrosio, L. (2011). Optimizing PANi doped electroactive substrates as patches for the regeneration of cardiac muscle. *J. Mater. Sci. Mater. Med.* 22 (4), 1053–1062. doi:10.1007/s10856-011-4259-x
- Borschel, G. H., Kia, K. F., Kuzon, W. M., and Dennis, R. G. (2003). Mechanical properties of acellular peripheral nerve. *J. Surg. Res.* 114 (2), 133–139. doi:10.1016/S0022-4804(03)00255-5
- Boutry, C. M., Kaizawa, Y., Schroeder, B. C., Chortos, A., Legrand, A., Wang, Z., et al. (2018). A stretchable and biodegradable strain and pressure sensor for orthopaedic application. *Nat. Electron.* 1 (5), 314–321. doi:10.1038/s41928-018-0071-7

- Boutry, C. M., Müller, M., and Hierold, C. (2012). Junctions between metals and blends of conducting and biodegradable polymers (PLLA-PPy and PCL-PPy). *Mater. Sci. Eng. C* 32 (6), 1610–1620. doi:10.1016/j.msec.2012.04.051
- Calìari, S. R., and Burdick, J. A. (2016). A practical guide to hydrogels for cell culture. *Nat. Methods* 13 (5), 405–414. doi:10.1038/nmeth.3839
- Cánovas, R., Padrell Sánchez, S., Parrilla, M., Cuartero, M., and Crespo, G. A. (2019). Cytotoxicity study of ionophore-based membranes: toward on-body and *in vivo* ion sensing. *ACS Sensors* 4 (9), 2524–2535. doi:10.1021/acssensors.9b01322
- Cao, Y., and Wang, B. (2009). Biodegradation of silk biomaterials. *Int. J. Mol. Sci.* 10 (4), 1514–1524. doi:10.3390/ijms10041514
- Cassano, D., Summa, M., Poció-Martínez, S., Mapanao, A.-K., Catelani, T., Bertorelli, R., et al. (2019). Biodegradable ultrasmall-in-nano gold architectures: mid-period *in vivo* distribution and excretion assessment. *Part. Part. Syst. Charact.* 36 (2), 1800464. doi:10.1002/ppsc.201800464
- Chatterjee, S., Saxena, N., Padmanabhan, D., Jayachandra, M., and Pandya, H. J. (2019). Futuristic medical implants using bioresorbable materials and devices. *Biosens. Bioelectron.* 142, 111489. doi:10.1016/j.bios.2019.111489
- Chaudhuri, O., Gu, L., Darnell, M., Klumpers, D., Bencherif, S. A., Weaver, J. C., et al. (2015). Substrate stress relaxation regulates cell spreading. *Nat. Commun.* 6 (1), 6365. doi:10.1038/ncomms7365
- Chaudhuri, O., Gu, L., Klumpers, D., Darnell, M., Bencherif, S. A., Weaver, J. C., et al. (2016). Hydrogels with tunable stress relaxation regulate stem cell fate and activity. *Nat. Mater.* 15 (3), 326–334. doi:10.1038/nmat4489
- Chen, C., Bai, X., Ding, Y., and Lee, I.-S. (2019). Electrical stimulation as a novel tool for regulating cell behavior in tissue engineering. *Biomaterials Res.* 23 (1), 25. doi:10.1186/s40824-019-0176-8
- Chen, G., Matsuhisa, N., Liu, Z., Qi, D., Cai, P., Jiang, Y., et al. (2018a). Plasticizing silk protein for on-skin stretchable electrodes. *Adv. Mater.* 30 (21), 1800129. doi:10.1002/adma.201800129
- Chen, L., Wang, W., Lin, Z., Lu, Y., Chen, H., Li, B., et al. (2022). Conducting molybdenum sulfide/graphene oxide/polyvinyl alcohol nanocomposite hydrogel for repairing spinal cord injury. *J. Nanobiotechnology* 20 (1), 210. doi:10.1186/s12951-022-01396-8
- Chen, X., Park, Y. J., Kang, M., Kang, S.-K., Koo, J., Shinde, S. M., et al. (2018b). CVD-grown monolayer MoS₂ in bioabsorbable electronics and biosensors. *Nat. Commun.* 9 (1), 1690. doi:10.1038/s41467-018-03956-9
- Chen, Z., Chen, Y., Hedenqvist, M. S., Chen, C., Cai, C., Li, H., et al. (2021). Multifunctional conductive hydrogels and their applications as smart wearable devices. *J. Mater. Chem. B* 9 (11), 2561–2583. doi:10.1039/d0tb02929g
- Chen, Z., Lin, Z., Obaid, S. N., Rytkin, E., George, S. A., Bach, C., et al. (2023). Soft, bioresorbable, transparent microelectrode arrays for multimodal spatiotemporal mapping and modulation of cardiac physiology. *Sci. Adv.* 9 (27), eadi0757. doi:10.1126/sciadv.adi0757
- Chiulan, I., Heggset, E. B., Voicu, Ș. I., and Chinga-Carrasco, G. (2021). Photopolymerization of bio-based polymers in a biomedical engineering perspective. *Biomacromolecules* 22 (5), 1795–1814. doi:10.1021/acs.biomac.0c01745
- Choi, C., Choi, M. K., Liu, S., Kim, M., Park, O. K., Im, C., et al. (2017). Human eye-inspired soft optoelectronic device using high-density MoS₂-graphene curved image sensor array. *Nat. Commun.* 8 (1), 1664. doi:10.1038/s41467-017-01824-6
- Choi, C., Lee, Y., Cho, K. W., Koo, J. H., and Kim, D.-H. (2019). Wearable and implantable soft bioelectronics using two-dimensional materials. *Accounts Chem. Res.* 52 (1), 73–81. doi:10.1021/acs.accounts.8b00491
- Choi, Y. S., Yin, R. T., Pfenniger, A., Koo, J., Avila, R., Lee, K. B., et al. (2021). Fully implantable and bioresorbable cardiac pacemakers without leads or batteries. *Nat. Biotechnol.* 39 (10), 1228–1238. doi:10.1038/s41587-021-00948-x
- Choi, Y. Y., Ho, D. H., and Cho, J. H. (2020). Self-healable hydrogel-liquid metal composite platform enabled by a 3D printed stamp for a multimodal sensor system. *ACS Appl. Mater. Interfaces* 12 (8), 9824–9832. doi:10.1021/acsami.9b22676
- Chor, A., Gonçalves, R. P., Costa, A. M., Farina, M., Ponche, A., Sirelli, L., et al. (2020). *In vitro* degradation of electrospun poly(lactic-Co-glycolic acid) (PLGA) for oral mucosa regeneration. *Polymers* 12 (8), 1853. doi:10.3390/polym12081853
- Christenson, E. M., Anderson, J. M., and Hiltner, A. (2007). Biodegradation mechanisms of polyurethane elastomers. *Corros. Eng. Sci. Technol.* 42 (4), 312–323. doi:10.1179/174327807x238909
- Cong, Y., and Fu, J. (2022). Hydrogel-tissue interface interactions for implantable flexible bioelectronics. *Langmuir* 38 (38), 11503–11513. doi:10.1021/acs.langmuir.2c01674
- Czubacka, E., and Czerczak, S. (2019). Are platinum nanoparticles safe to human health? *Med. Pr.* 70 (4), 487–495. doi:10.13075/mp.5893.00847
- Dadras-Toussi, O., Khorrami, M., Louis Sam Titus, A. S. C., Majd, S., Mohan, C., and Abidian, M. R. (2022). Multiphoton lithography of organic semiconductor devices for 3D printing of flexible electronic circuits, biosensors, and bioelectronics. *Adv. Mater.* 34 (30), 2200512. doi:10.1002/adma.202200512
- Dai, C., Kong, D., Chen, C., Liu, Y., and Wei, D. (2023). Graphene transistors for *in vitro* detection of health biomarkers. *Adv. Funct. Mater.* 33, 2301948. doi:10.1002/adfm.202301948
- Dash, M., Chiellini, F., Ottenbrite, R. M., and Chiellini, E. (2011). Chitosan—a versatile semi-synthetic polymer in biomedical applications. *Prog. Polym. Sci.* 36 (8), 981–1014. doi:10.1016/j.progpolymsci.2011.02.001
- De León, S. E., Pupovac, A., and McArthur, S. L. (2020). Three-Dimensional (3D) cell culture monitoring: opportunities and challenges for impedance spectroscopy. *Biotechnol. Bioeng.* 117 (4), 1230–1240. doi:10.1002/bit.27270
- Deo, K. A., Jaiswal, M. K., Abasi, S., Lokhande, G., Bhunia, S., Nguyen, T.-U., et al. (2022). Nanoengineered ink for designing 3D printable flexible bioelectronics. *ACS Nano* 16 (6), 8798–8811. doi:10.1021/acsnano.1c09386
- Dorishetty, P., Balu, R., Gelmi, A., Mata, J. P., Quigley, A., Dutta, N. K., et al. (2022). Microporosity engineered printable silk/graphene hydrogels and their cytocompatibility evaluations. *Mater. Today Adv.* 14, 100233. doi:10.1016/j.mtadv.2022.100233
- Duan, X., Gao, R., Xie, P., Cohen-Karni, T., Qing, Q., Choe, H. S., et al. (2012). Intracellular recordings of action potentials by an extracellular nanoscale field-effect transistor. *Nat. Nanotechnol.* 7 (3), 174–179. doi:10.1038/nnano.2011.223
- Eglin, D., and Alini, M. (2008). Degradable polymeric materials for osteosynthesis: tutorial. *Eur. Cells Mat.* 16, 80–91. doi:10.22203/ecm.v016a09
- Eitel, I., and Friedrich, M. G. (2011). T2-weighted cardiovascular magnetic resonance in acute cardiac disease. *J. Cardiovasc. Magnetic Reson.* 13 (1), 13. doi:10.1186/1532-429x-13-13
- Elosegui-Artola, A. (2021). The extracellular matrix viscoelasticity as a regulator of cell and tissue dynamics. *Curr. Opin. Cell Biol.* 72, 10–18. doi:10.1016/j.cob.2021.04.002
- eSilva, E. P., Huang, B., Helaehil, J. V., Nalesso, P. R. L., Bagne, L., de Oliveira, M. A., et al. (2021). *In vivo* study of conductive 3D printed PCL/MWCNTs scaffolds with electrical stimulation for bone tissue engineering. *Bio-Design Manuf.* 4 (2), 190–202. doi:10.1007/s42242-020-00116-1
- Eslamian, M., Mirab, F., Raghunathan, V. K., Majd, S., and Abidian, M. R. (2021). Organic semiconductor nanotubes for electrochemical devices. *Adv. Funct. Mater.* 31 (49), 2105358. doi:10.1002/adfm.202105358
- Fattahi, P., Yang, G., Kim, G., and Abidian, M. R. (2014). A review of organic and inorganic biomaterials for neural interfaces. *Adv. Mater.* 26 (12), 1846–1885. doi:10.1002/adma.201304496
- Feig, V. R., Tran, H., and Bao, Z. (2018). Biodegradable polymeric materials in degradable electronic devices. *ACS Central Sci.* 4 (3), 337–348. doi:10.1021/acscentsci.7b00595
- Feng, S., Cao, S., Tian, Z., Zhu, H., and Kong, D. (2019). Maskless patterning of biodegradable conductors by selective laser sintering of microparticle inks and its application in flexible transient electronics. *ACS Appl. Mater. Interfaces* 11 (49), 45844–45852. doi:10.1021/acsami.9b14431
- Ferlauto, L., D'Angelo, A. N., Vagni, P., Airaghi Leccardi, M. J. I., Mor, F. M., Cuttaz, E. A., et al. (2018). Development and characterization of PEDOT:PSS/alginate soft microelectrodes for application in neuroprosthetics. *Front. Neurosci.* 12, 648. doi:10.3389/fnins.2018.00648
- Fleischer, S., Shevach, M., Feiner, R., and Dvir, T. (2014). Coiled fiber scaffolds embedded with gold nanoparticles improve the performance of engineered cardiac tissues. *Nanoscale* 6 (16), 9410–9414. doi:10.1039/c4nr00300d
- Foremny, K., Nagels, S., Kreienmeyer, M., Doll, T., and Deferme, W. (2021). Biocompatibility testing of liquid metal as an interconnection material for flexible implant technology. *Nanomaterials* 11 (12), 3251. doi:10.3390/nano11123251
- Gandhi, B., and Raghava, N. S. (2020). Fabrication techniques for carbon nanotubes based ECG electrodes: a review. *IETE J. Res.*, 1–20. doi:10.1080/03772063.2020.1768909
- Gao, C., Song, S., Lv, Y., Huang, J., and Zhang, Z. (2022). Recent development of conductive hydrogels for tissue engineering: review and perspective. *Macromol. Biosci.* 22 (8), 2200051. doi:10.1002/mabi.202200051
- GhavamiNejad, P., GhavamiNejad, A., Zheng, H., Dhingra, K., Samarikhajaj, M., and Poudineh, M. (2023). A conductive hydrogel microneedle-based assay integrating PEDOT:PSS and Ag-Pt nanoparticles for real-time, enzyme-less, and electrochemical sensing of glucose. *Adv. Healthc. Mater.* 12 (1), 2202362. doi:10.1002/adhm.202202362
- Ghosh, S., Haldar, S., Gupta, S., Bisht, A., Chauhan, S., Kumar, V., et al. (2020). Anisotropically conductive biodegradable scaffold with coaxially aligned carbon nanotubes for directional regeneration of peripheral nerves. *ACS Appl. Bio Mater.* 3 (9), 5796–5812. doi:10.1021/acsabm.0c00534
- Gillispie, G., Prim, P., Copus, J., Fisher, J., Mikos, A. G., Yoo, J. J., et al. (2020). Assessment methodologies for extrusion-based bioink printability. *Biofabrication* 12 (2), 022003. doi:10.1088/1758-5090/ab6f0d
- Glasser, A., Cloutet, É., Hadzioannou, G., and Kellay, H. (2019). Tuning the rheology of conducting polymer inks for various deposition processes. *Chem. Mater.* 31 (17), 6936–6944. doi:10.1021/acs.chemmater.9b01387

- Gong, Y., Cheng, Y. Z., and Hu, Y. C. (2022). Preparation of polymer conductive hydrogel and its application in flexible wearable electronic devices. *Prog. Chem.* 34 (3), 616–629. doi:10.7536/pc210329
- Gottschalk, A., Scafidi, S., and Toungh, T. (2021). Brain water as a function of age and weight in normal rats. *PLoS ONE* 16 (9), e0249384. doi:10.1371/journal.pone.0249384
- Grosjean, M., Gangolphe, L., and Nottelet, B. (2023). Degradable self-healable networks for use in biomedical applications. *Adv. Funct. Mater.* 33 (13), 2205315. doi:10.1002/adfm.202205315
- Gueye, M. N., Carella, A., Faure-Vincent, J., Demadrille, R., and Simonato, J.-P. (2020). Progress in understanding structure and transport properties of PEDOT-based materials: a critical review. *Prog. Mater. Sci.* 108, 100616. doi:10.1016/j.pmatsci.2019.100616
- Guo, B., Glavas, L., and Albertsson, A.-C. (2013). Biodegradable and electrically conducting polymers for biomedical applications. *Prog. Polym. Sci.* 38 (9), 1263–1286. doi:10.1016/j.progpolymsci.2013.06.003
- Guo, B., and Ma, P. X. (2018). Conducting polymers for tissue engineering. *Biomacromolecules* 19 (6), 1764–1782. doi:10.1021/acs.biomac.8b00276
- Guo, X., and Facchetti, A. (2020). The journey of conducting polymers from discovery to application. *Nat. Mater.* 19 (9), 922–928. doi:10.1038/s41563-020-0778-5
- Gupta, P., Agrawal, A., Murali, K., Varshney, R., Beniwal, S., Manhas, S., et al. (2019). Differential neural cell adhesion and neurite outgrowth on carbon nanotube and graphene reinforced polymeric scaffolds. *Mater. Sci. Eng. C* 97, 539–551. doi:10.1016/j.msec.2018.12.065
- Gutiérrez de la Rosa, S. Y., Muñoz Diaz, R., Villalobos Gutiérrez, P. T., Patakfalvi, R., and Gutiérrez Coronado, Ó. (2022). Functionalized platinum nanoparticles with biomedical applications. *Int. J. Mol. Sci.* 23 (16), 9404. doi:10.3390/ijms23169404
- Hall, C. M., Moenendarbary, E., and Sheridan, G. K. (2021). Mechanobiology of the brain in ageing and Alzheimer's disease. *Eur. J. Neurosci.* 53 (12), 3851–3878. doi:10.1111/ejn.14766
- Han, W. B., Yang, S. M., Rajaram, K., and Hwang, S.-W. (2022). Materials and fabrication strategies for biocompatible and biodegradable conductive polymer composites toward bio-integrated electronic systems. *Adv. Sustain. Syst.* 6 (2), 2100075. doi:10.1002/advsu.202100075
- Hébert, C., Mazellier, J. P., Scorsone, E., Mermoux, M., and Bergonzo, P. (2014). Boosting the electrochemical properties of diamond electrodes using carbon nanotube scaffolds. *Carbon* 71, 27–33. doi:10.1016/j.carbon.2013.12.083
- Held, M., Pichler, A., Chabeda, J., Lam, N., Hindenberg, P., Romero-Nieto, C., et al. (2022). Soft electronic platforms combining elastomeric stretchability and biodegradability. *Adv. Sustain. Syst.* 6 (2), 2100035. doi:10.1002/advsu.202100035
- Hochberg, L. R., Serruya, M. D., Friehe, G. M., Mukand, J. A., Saleh, M., Caplan, A. H., et al. (2006). Neuronal ensemble control of prosthetic devices by a human with tetraplegia. *Nature* 442 (7099), 164–171. doi:10.1038/nature04970
- Hu, W., Wang, Z., Xiao, Y., Zhang, S., and Wang, J. (2019). Advances in crosslinking strategies of biomedical hydrogels. *Biomaterials Sci.* 7 (3), 843–855. doi:10.1039/c8bm01246f
- Huang, L., Yang, X., Deng, L., Ying, D., Lu, A., Zhang, L., et al. (2021). Biocompatible chitin hydrogel incorporated with PEDOT nanoparticles for peripheral nerve repair. *ACS Appl. Mater. Interfaces* 13 (14), 16106–16117. doi:10.1021/acsmi.1c01904
- Huang, W.-J., and Wang, J. (2023). Development of 3D-printed, biodegradable, conductive PGSA composites for nerve tissue regeneration. *Macromol. Biosci.* 23 (3), 2200470. doi:10.1002/mabi.202200470
- Huang, X., Liu, Y., Hwang, S.-W., Kang, S.-K., Patnaik, D., Cortes, J. F., et al. (2014a). Biodegradable materials for multilayer transient printed circuit boards. *Adv. Mater.* 26 (43), 7371–7377. doi:10.1002/adma.201403164
- Huang, X.-W., Wei, J.-J., Zhang, M.-Y., Zhang, X.-L., Yin, X.-F., Lu, C.-H., et al. (2018). Water-based black phosphorus hybrid nanosheets as a moldable platform for wound healing applications. *ACS Appl. Mater. Interfaces* 10 (41), 35495–35502. doi:10.1021/acsmi.8b12523
- Huang, Y., Li, H., Hu, T., Li, J., Yiu, C. K., Zhou, J., et al. (2022). Implantable electronic medicine enabled by bioresorbable microneedles for wireless electrotherapy and drug delivery. *Nano Lett.* 22 (14), 5944–5953. doi:10.1021/acs.nanolett.2c01997
- Huang, Z.-B., Yin, G.-F., Liao, X.-M., and Gu, J.-W. (2014b). Conducting polypyrrole in tissue engineering applications. *Front. Mat. Sci.* 8 (1), 39–45. doi:10.1007/s11706-014-0238-8
- Humpolicek, P., Kasparkova, V., Saha, P., and Stejskal, J. (2012). Biocompatibility of polyaniline. *Synth. Met.* 162 (7), 722–727. doi:10.1016/j.synthmet.2012.02.024
- Hwang, S.-W., Tao, H., Kim, D.-H., Cheng, H., Song, J.-K., Rill, E., et al. (2012). A physically transient form of silicon electronics. *Science* 337 (6102), 1640–1644. doi:10.1126/science.1226325
- Inal, S., Hama, A., Ferro, M., Pitsalidis, C., Ozat, J., Iandolo, D., et al. (2017). Conducting polymer scaffolds for hosting and monitoring 3D cell culture. *Adv. Biosyst.* 1 (6), 1700052. doi:10.1002/adbi.201700052
- Jacot, J. G., Martin, J. C., and Hunt, D. L. (2010). Mechanobiology of cardiomyocyte development. *J. Biomechanics* 43 (1), 93–98. doi:10.1016/j.jbiomech.2009.09.014
- Jensen, B. E. B., Dávila, I., and Zelikin, A. N. (2016). Poly(vinyl alcohol) physical hydrogels: matrix-mediated drug delivery using spontaneously eroding substrate. *J. Phys. Chem. B* 120 (26), 5916–5926. doi:10.1021/acs.jpcc.6b01381
- Jiang, D.-H., Satoh, T., Tung, S. H., and Kuo, C.-C. (2022). Sustainable alternatives to nondegradable medical plastics. *ACS Sustain. Chem. Eng.* 10 (15), 4792–4806. doi:10.1021/acssuschemeng.2c00160
- Jiang, Y., Xu, M., and Yadavalli, V. K. (2019). Silk fibroin-sheathed conducting polymer wires as organic connectors for biosensors. *Biosensors* 9 (3), 103. doi:10.3390/bios9030103
- Jin, M., Li, N., Sheng, W., Ji, X., Liang, X., Kong, B., et al. (2021). Toxicity of different zinc oxide nanomaterials and dose-dependent onset and development of Parkinson's disease-like symptoms induced by zinc oxide nanorods. *Environ. Int.* 146, 106179. doi:10.1016/j.envint.2020.106179
- Jing, X., Mi, H.-Y., Napiwocki, B. N., Peng, X.-F., and Turng, L.-S. (2017). Mussel-inspired electroactive chitosan/graphene oxide composite hydrogel with rapid self-healing and recovery behavior for tissue engineering. *Carbon* 125, 557–570. doi:10.1016/j.carbon.2017.09.071
- Kalra, A., Lowe, A., and Al-Jumaily, A. M. (2016). Mechanical behaviour of skin: a review. *J. Mat. Sci. Eng.* 5 (4), 1–7. doi:10.4172/2169-0022.1000254
- Karimi, A., Shojaei, A., and Tehrani, P. (2017). Mechanical properties of the human spinal cord under the compressive loading. *J. Chem. Neuroanat.* 86, 15–18. doi:10.1016/j.jchemneu.2017.07.004
- Karmakar, R. S., Chu, C.-P., Liao, Y.-C., and Lu, Y.-W. (2022). PVA tactile sensors based on Electrical Contact Resistance (ECR) change mechanism for subtle pressure detection. *Sensors Actuators A Phys.* 342, 113613. doi:10.1016/j.sna.2022.113613
- Katoh, K. (2022). Effects of electrical stimulation on the signal transduction-related proteins, c-src and focal adhesion kinase, in fibroblasts. *Life* 12 (4), 531. doi:10.3390/life12040531
- Kayser, L. V., and Lipomi, D. J. (2019). Stretchable conductive polymers and composites based on PEDOT and PEDOT:PSS. *Adv. Mater.* 31 (10), 1806133. doi:10.1002/adma.201806133
- Keefer, E. W., Botterman, B. R., Romero, M. I., Rossi, A. F., and Gross, G. W. (2008). Carbon nanotube coating improves neuronal recordings. *Nat. Nanotechnol.* 3 (7), 434–439. doi:10.1038/nnano.2008.174
- Keller, T. S., Mao, Z., and Spengler, D. M. (1990). Young's modulus, bending strength, and tissue physical properties of human compact bone. *J. Orthop. Res.* 8 (4), 592–603. doi:10.1002/jor.1100080416
- Khan, M. A., Cantù, E., Tonello, S., Serpelloni, M., Lopomo, N. F., and Sardini, E. (2019). A review on biomaterials for 3D conductive scaffolds for stimulating and monitoring cellular activities. *Appl. Sci.* 9 (5), 961. doi:10.3390/app9050961
- Khodagholy, D., Gelineas, J. N., Thesen, T., Doyle, W., Devinsky, O., Malliaras, G. G., et al. (2015). NeuroGrid: recording action potentials from the surface of the brain. *Nat. Neurosci.* 18 (2), 310–315. doi:10.1038/nn.3905
- Khorrami, M., and Abidian, M. R. (2018). “Aligned conducting polymer nanotubes for neural prostheses,” in Proceedings of the 40th Annual International Conference of the IEEE Engineering in Medicine and Biology Society (EMBC), Honolulu, HI, USA, July 18–21, 2018, 6080–6083.
- Khorrami, M., Antensteiner, M., Fallahianbijan, F., Borhan, A., and Abidian, M. R. (2017). “Conducting polymer microcontainers for biomedical applications,” in Proceedings of the 39th Annual International Conference of the IEEE Engineering in Medicine and Biology Society (EMBC), Jeju Island, South Korea, July 11–15, 2017, 1869–1872.
- Khorshidi, S., and Karkhanav, A. (2018). Hydrogel/fiber conductive scaffold for bone tissue engineering. *J. Biomed. Mater. Res. Part A* 106 (3), 718–724. doi:10.1002/jbm.a.36282
- Kim, B. C., Spinks, G., Too, C. O., Wallace, G. G., and Bae, Y. H. (2000). Preparation and characterisation of processable conducting polymer-hydrogel composites. *React. Funct. Polym.* 44 (1), 31–40. doi:10.1016/S1381-5148(99)00074-7
- Kim, D.-H., Kim, Y.-S., Amsden, J., Panilaitis, B., Kaplan, D. L., Omenetto, F. G., et al. (2009). Silicon electronics on silk as a path to bioresorbable, implantable devices. *Appl. Phys. Lett.* 95 (13), 133701. doi:10.1063/1.3238552
- Kim, D.-H., Vivenzi, J., Amsden, J. J., Xiao, J., Vigeland, L., Kim, Y.-S., et al. (2010). Dissolvable films of silk fibroin for ultrathin conformal bio-integrated electronics. *Nat. Mater.* 9 (6), 511–517. doi:10.1038/nmat2745
- Kim, J., Campbell, A. S., de Ávila, B. E.-F., and Wang, J. (2019). Wearable biosensors for healthcare monitoring. *Nat. Biotechnol.* 37 (4), 389–406. doi:10.1038/s41587-019-0045-y
- Kim, K. S., Maeng, W.-Y., Kim, S., Lee, G., Hong, M., Kim, G.-B., et al. (2023a). Isotropic conductive paste for bioresorbable electronics. *Mater. Today Bio* 18, 100541. doi:10.1016/j.mtbio.2023.100541
- Kim, S., Baek, S., Sluyter, R., Konstantinov, K., Kim, J. H., Kim, S., et al. (2023b). Wearable and implantable bioelectronics as eco-friendly and patient-friendly integrated nanoarchitectonics for next-generation smart healthcare technology. *EcoMat* 5, e12356. doi:10.1002/eom2.12356

- Knopf-Marques, H., Pravda, M., Wolfova, L., Velebny, V., Schaaf, P., Vrana, N. E., et al. (2016). Hyaluronic acid and its derivatives in coating and delivery systems: applications in tissue engineering, regenerative medicine and immunomodulation. *Adv. Healthc. Mat.* 5, 2841–2855. doi:10.1002/adhm.201600316
- Kobayashi, T., Chamme, T., and Itano, N. (2020). Hyaluronan: metabolism and function. *Biomolecules* 10 (11), 1525. doi:10.3390/biom10111525
- Koivusalo, L., Kauppi, M., Samanta, S., Parihar, V. S., Ilmarinen, T., Miettinen, S., et al. (2019). Tissue adhesive hyaluronic acid hydrogels for sutureless stem cell delivery and regeneration of corneal epithelium and stroma. *Biomaterials* 225, 119516. doi:10.1016/j.biomaterials.2019.119516
- Koller, M. (2018). Biodegradable and biocompatible polyhydroxy-alkanoates (PHA): auspicious microbial macromolecules for pharmaceutical and therapeutic applications. *Molecules* 23 (2), 362. doi:10.3390/molecules23020362
- Korupalli, C., Li, H., Nguyen, N., Mi, F.-L., Chang, Y., Lin, Y.-J., et al. (2021). Conductive materials for healing wounds: their incorporation in electroactive wound dressings, characterization, and perspectives. *Adv. Healthc. Mater.* 10 (6), 2001384. doi:10.1002/adhm.202001384
- Kozai, T. D. Y., Jaquins-Gerstl, A. S., Vazquez, A. L., Michael, A. C., and Cui, X. T. (2015). Brain tissue responses to neural implants impact signal sensitivity and intervention strategies. *ACS Chem. Neurosci.* 6 (1), 48–67. doi:10.1021/cn500256e
- Kozlowski, M. T., Crook, C. J., and Ku, H. T. (2021). Towards organoid culture without Matrigel. *Commun. Biol.* 4 (1), 1387. doi:10.1038/s42003-021-02910-8
- Kurakula, M., and Rao, G. S. N. K. (2020). Pharmaceutical assessment of polyvinylpyrrolidone (PVP): as excipient from conventional to controlled delivery systems with a spotlight on COVID-19 inhibition. *J. Drug Deliv. Sci. Technol.* 60, 102046. doi:10.1016/j.jddst.2020.102046
- Kurland, N. E., Dey, T., Kundu, S. C., and Yadavalli, V. K. (2013). Precise patterning of silk microstructures using Photolithography. *Adv. Mater.* 25 (43), 6207–6212. doi:10.1002/adma.201302823
- Lee, G., Ray, E., Yoon, H.-J., Genovese, S., Choi, Y. S., Lee, M.-K., et al. (2022). A bioresorbable peripheral nerve stimulator for electronic pain block. *Sci. Adv.* 8 (40), eabp9169. doi:10.1126/sciadv.abp9169
- Lee, J., Manoharan, V., Cheung, L., Lee, S., Cha, B.-H., Newman, P., et al. (2019). Nanoparticle-based hybrid scaffolds for deciphering the role of multimodal cues in cardiac tissue engineering. *ACS Nano* 13 (11), 12525–12539. doi:10.1021/acsnano.9b03050
- Lei, H., and Fan, D. (2021). Conductive, adaptive, multifunctional hydrogel combined with electrical stimulation for deep wound repair. *Chem. Eng. J.* 421, 129578. doi:10.1016/j.cej.2021.129578
- Lei, T., Guan, M., Liu, J., Lin, H.-C., Pfattner, R., Shaw, L., et al. (2017). Biocompatible and totally disintegrable semiconducting polymer for ultrathin and ultralightweight transient electronics. *Proc. Natl. Acad. Sci.* 114 (20), 5107–5112. doi:10.1073/pnas.1701478114
- Leprince, M., Mailley, P., Choinsard, L., Auzély-Velty, R., and Texier, I. (2023a). Design of hyaluronan-based dopant for conductive and resorbable PEDOT ink. *Carbohydr. Polym.* 301, 120345. doi:10.1016/j.carbpol.2022.120345
- Leprince, M., Regal, S., Mailley, P., Sauter-Starace, F., Texier, I., and Auzély-Velty, R. (2023b). A cross-linkable and resorbable PEDOT-based ink using a hyaluronic acid derivative as dopant for flexible bioelectronic devices. *Mater. Adv.* 4 (16), 3636–3644. doi:10.1039/d3ma00170a
- Li, C., Guan, G., Reif, R., Huang, Z., and Wang, R. K. (2012). Determining elastic properties of skin by measuring surface waves from an impulse mechanical stimulus using phase-sensitive optical coherence tomography. *J. R. Soc. Interface* 9 (70), 831–841. doi:10.1098/rsif.2011.0583
- Li, J., Fang, L., Tait, W. R., Sun, L., Zhao, L., and Qian, L. (2017). Preparation of conductive composite hydrogels from carboxymethyl cellulose and polyaniline with a nontoxic crosslinking agent. *RSC Adv.* 7 (86), 54823–54828. doi:10.1039/c7ra10788a
- Li, M., Liang, Y., He, J., Zhang, H., and Guo, B. (2020). Two-pronged strategy of biomechanically active and biochemically multifunctional hydrogel wound dressing to accelerate wound closure and wound healing. *Chem. Mater.* 32 (23), 9937–9953. doi:10.1021/acs.chemmater.0c02823
- Li, Y., He, J., Zhou, J., Li, Z., Liu, L., Hu, S., et al. (2022). A conductive photothermal non-swelling nanocomposite hydrogel patch accelerating bone defect repair. *Biomaterials Sci.* 10 (5), 1326–1341. doi:10.1039/d1bm01937f
- Liang, B., Fang, L., Hu, Y., Yang, G., Zhu, Q., and Ye, X. (2014). Fabrication and application of flexible graphene silk composite film electrodes decorated with spiky Pt nanospheres. *Nanoscale* 6 (8), 4264–4274. doi:10.1039/c3nr06057h
- Liang, S., Zhang, Y., Wang, H., Xu, Z., Chen, J., Bao, R., et al. (2018). Paintable and rapidly bondable conductive hydrogels as therapeutic cardiac patches. *Adv. Mater.* 30 (23), 1704235. doi:10.1002/adma.201704235
- Liang, Y., Zhao, X., Hu, T., Chen, B., Yin, Z., Ma, P. X., et al. (2019). Adhesive hemostatic conducting injectable composite hydrogels with sustained drug release and photothermal antibacterial activity to promote full-thickness skin regeneration during wound healing. *Small* 15 (12), 1900046. doi:10.1002/smll.201900046
- Liu, C., Kim, J. T., Yang, D. S., Cho, D. H., Yoo, S., Madhupathy, S. R., et al. (2023a). Multifunctional materials strategies for enhanced safety of wireless, skin-interfaced bioelectronic devices. *Adv. Funct. Mater.* 33. doi:10.1002/adfm.202302256
- Liu, D., Huan, C., Wang, Z., Guo, Z., Zhang, X., Torun, H., et al. (2023b). Conductive polymer based hydrogels and their application in wearable sensors: a review. *Mater. Horizons* 10, 2800–2823. doi:10.1039/d3mh00056g
- Liu, H., Feng, Y., Che, S., Guan, L., Yang, X., Zhao, Y., et al. (2023c). An electroconductive hydrogel scaffold with injectability and biodegradability to manipulate neural stem cells for enhancing spinal cord injury repair. *Biomacromolecules* 24 (1), 86–97. doi:10.1021/acs.biomac.2c00920
- Liu, J., Appaia, F., Bibari, O., Marchand, G., Benabid, A.-L., Sauter-Starace, F., et al. (2011). Control of neuronal network organization by chemical surface functionalization of multi-walled carbon nanotube arrays. *Nanotechnology* 22 (19), 195101. doi:10.1088/0957-4484/22/19/195101
- Liu, J., Fu, T.-M., Cheng, Z., Hong, G., Zhou, T., Jin, L., et al. (2015). Syringe-injectable electronics. *Nat. Nanotechnol.* 10 (7), 629–636. doi:10.1038/nnano.2015.115
- Liu, J., Xie, C., Dai, X., Jin, L., Zhou, W., and Lieber, C. M. (2013). Multifunctional three-dimensional macroporous nanoelectronic networks for smart materials. *Proc. Natl. Acad. Sci.* 110 (17), 6694–6699. doi:10.1073/pnas.1305209110
- Lu, Y., Cheng, D., Niu, B., Wang, X., Wu, X., and Wang, A. (2023a). Properties of poly (Lactic-co-Glycolic acid) and progress of poly (Lactic-co-Glycolic acid)-based biodegradable materials in biomedical research. *Pharmaceuticals* 16 (3), 454. doi:10.3390/ph16030454
- Ludwig, K. A., Uram, J. D., Yang, J., Martin, D. C., and Kipke, D. R. (2006). Chronic neural recordings using silicon microelectrode arrays electrochemically deposited with a poly(3,4-ethylenedioxythiophene) (PEDOT) film. *J. Neural Eng.* 3 (1), 59–70. doi:10.1088/1741-2560/3/1/007
- Luo, J., Yang, J., Zheng, X., Ke, X., Chen, Y., Tan, H., et al. (2020). A highly stretchable, real-time self-healable hydrogel adhesive matrix for tissue patches and flexible electronics. *Adv. Healthc. Mater.* 9 (4), 1901423. doi:10.1002/adhm.201901423
- Luo, Y., Fan, L., Liu, C., Wen, H., Wang, S., Guan, P., et al. (2022). An injectable, self-healing, electroconductive extracellular matrix-based hydrogel for enhancing tissue repair after traumatic spinal cord injury. *Bioact. Mater.* 7, 98–111. doi:10.1016/j.bioactmat.2021.05.039
- Lycke, R., Kim, R., Zolotavin, P., Montes, J., Sun, Y., Koszeghy, A., et al. (2023). Low-threshold, high-resolution, chronically stable intracortical microstimulation by ultraflexible electrodes. *Cell Rep.* 42 (6), 112554. doi:10.1016/j.celrep.2023.112554
- Ma, B., Martin, C., Kurapati, R., and Bianco, A. (2020). Degradation-by-design: how chemical functionalization enhances the biodegradability and safety of 2D materials. *Chem. Soc. Rev.* 49 (17), 6224–6247. doi:10.1039/c9cs00822e
- Manousiouthakis, E., Park, J., Hardy, J. G., Lee, J. Y., and Schmidt, C. E. (2022). Towards the translation of electroconductive organic materials for regeneration of neural tissues. *Acta Biomater.* 139, 22–42. doi:10.1016/j.actbio.2021.07.065
- Mao, J., and Zhang, Z. (2018). “Polypyrrole as electrically conductive biomaterials: synthesis, biofunctionalization, potential applications and challenges,” in *Cutting-edge enabling technologies for regenerative medicine*. Editors H. J. Chun, C. H. Park, I. K. Kwon, and G. Khang (Singapore: Springer Singapore), 347–370.
- Mbore, N. J. R., Chuan, X. Y., Feng, Q. X., Alizadeh, M., and Zhan, J. (2016). Evaluation of the combination of methylprednisolone and tranilast after spinal cord injury in rat models. *J. Korean Neurosurg. Soc.* 59 (4), 334–340. doi:10.3340/jkns.2016.59.4.334
- Min, J. H., Patel, M., and Koh, W.-G. (2018). Incorporation of conductive materials into hydrogels for tissue engineering applications. *Polymers* 10 (10), 1078. doi:10.3390/polym10101078
- Mishra, V., Kesharwani, P., and Jain, N. K. (2018). Biomedical applications and toxicological aspects of functionalized carbon nanotubes. *Crit. Reviews™ Ther. Drug Carr. Syst.* 35 (4), 293–330. doi:10.1615/CritRevTherDrugCarrierSyst.2018014419
- Miyata, S., and Kitagawa, H. (2017). Formation and remodeling of the brain extracellular matrix in neural plasticity: roles of chondroitin sulfate and hyaluronan. *Biochim. Biophys. Acta* 1861 (10), 2420–2434. doi:10.1016/j.bbagen.2017.06.010
- Morgan, E. F., Unnikrisnan, G. U., and Hussein, A. I. (2018). Bone mechanical properties in healthy and diseased states. *Annu. Rev. Biomed. Eng.* 20 (1), 119–143. doi:10.1146/annurev-bioeng-062117-121139
- Morgan, F. L. C., Fernández-Pérez, J., Moroni, L., and Baker, M. B. (2022). Tuning hydrogels by mixing dynamic cross-linkers: enabling cell-instructive hydrogels and advanced bioinks. *Adv. Healthc. Mater.* 11 (1), 2101576. doi:10.1002/adhm.202101576
- Morsink, M., Severino, P., Luna-Ceron, E., Hussain, M. A., Sobahi, N., and Shin, S. R. (2022). Effects of electrically conductive nano-biomaterials on regulating cardiomyocyte behavior for cardiac repair and regeneration. *Acta Biomater.* 139, 141–156. doi:10.1016/j.actbio.2021.11.022
- Mostafavi, E., Medina-Cruz, D., Kalantari, K., Taymoori, A., Soltantabar, P., and Webster, T. J. (2020). Electroconductive nanobiomaterials for tissue engineering and regenerative medicine. *Bioelectricity* 2 (2), 120–149. doi:10.1089/bioe.2020.0021
- Mueller, E., Poulin, I., Bodnaryk, W. J., and Hoare, T. (2022). Click chemistry hydrogels for extrusion bioprinting: progress, challenges, and opportunities. *Biomacromolecules* 23 (3), 619–640. doi:10.1021/acs.biomac.1c01105

- Nair, L. S., and Laurencin, C. T. (2007). Biodegradable polymers as biomaterials. *Prog. Polym. Sci.* 32 (8), 762–798. doi:10.1016/j.progpolymsci.2007.05.017
- Namsheer, K., and Rout, C. S. (2021). Conducting polymers: a comprehensive review on recent advances in synthesis, properties and applications. *RSC Adv.* 11 (10), 5659–5697. doi:10.1039/d0ra07800j
- Nezakati, T., Seifalian, A., Tan, A., and Seifalian, A. M. (2018). Conductive polymers: opportunities and challenges in biomedical applications. *Chem. Rev.* 118 (14), 6766–6843. doi:10.1021/acs.chemrev.6b00275
- Nie, S., Li, Z., Yao, Y., and Jin, Y. (2021). Progress in synthesis of conductive polymer poly(3,4-ethylenedioxythiophene). *Front. Chem.* 9, 803509. doi:10.3389/fchem.2021.803509
- O'Brien, T. D., Reeves, N. D., Baltzopoulos, V., Jones, D. A., and Maganaris, C. N. (2010). Mechanical properties of the patellar tendon in adults and children. *J. Biomechanics* 43 (6), 1190–1195. doi:10.1016/j.jbiomech.2009.11.028
- Onorato, J. W., and Luscombe, C. K. (2019). Morphological effects on polymeric mixed ionic/electronic conductors. *Mol. Syst. Des. Eng.* 4 (2), 310–324. doi:10.1039/c8me00093j
- Pal, R. K., Farghaly, A. A., Collinson, M. M., Kundu, S. C., and Yadavalli, V. K. (2016). Photolithographic micropatterning of conducting polymers on flexible silk matrices. *Adv. Mater.* 28 (7), 1406–1412. doi:10.1002/adma.201504736
- Palma, M., Khoshnevis, M., Lion, M., Zenga, C., Kefs, S., Fallegger, F., et al. (2022). Chronic recording of cortical activity underlying vocalization in awake minipigs. *J. Neurosci. Methods* 366, 109427. doi:10.1016/j.jneumeth.2021.109427
- Palmisano, F., Malitesta, C., Centonze, D., and Zamboni, P. G. (1995). Correlation between permselectivity and chemical structure of overoxidized polypyrrole membranes used in electroproduced enzyme biosensors. *Anal. Chem.* 67, 2207–2211. doi:10.1021/ac00109a046
- Palumbo, A., Li, Z., and Yang, E. H. (2022). Trends on carbon nanotube-based flexible and wearable sensors via electrochemical and mechanical stimuli: a review. *IEEE Sensors J.* 22 (21), 20102–20125. doi:10.1109/jsen.2022.3198847
- Pan, Z., and Ding, J. (2012). Poly(lactide-co-glycolide) porous scaffolds for tissue engineering and regenerative medicine. *Interface Focus* 2 (3), 366–377. doi:10.1098/rsfs.2011.0123
- Park, C., Kim, M. S., Kim, H. H., Sunwoo, S. H., Jung, D. J., Choi, M. K., et al. (2022a). Stretchable conductive nanocomposites and their applications in wearable devices. *Appl. Phys. Rev.* 9 (2). doi:10.1063/5.0093261
- Park, D.-W., Schendel, A. A., Mikael, S., Brodnick, S. K., Richner, T. J., Ness, J. P., et al. (2014a). Graphene-based carbon-layered electrode array technology for neural imaging and optogenetic applications. *Nat. Commun.* 5 (1), 5258. doi:10.1038/ncomms5258
- Park, J., Jeon, J., Kim, B., Lee, M. S., Park, S., Lim, J., et al. (2020). Electrically conductive hydrogel nerve guidance conduits for peripheral nerve regeneration. *Adv. Funct. Mater.* 30 (39), 2003759. doi:10.1002/adfm.202003759
- Park, S., Abidian, M. R., and Majd, S. (2017). “Micro-patterned films of bio-functionalized conducting polymers for cellular engineering,” in Proceedings of the 39th Annual International Conference of the IEEE Engineering in Medicine and Biology Society (EMBC), Jeju Island, South Korea, July 11–15, 2017, 1595–1598.
- Park, S., Yang, G., Madduri, N., Abidian, M. R., and Majd, S. (2014b). Hydrogel-mediated direct patterning of conducting polymer films with multiple surface chemistries. *Adv. Mater.* 26 (18), 2782–2787. doi:10.1002/adma.201306093
- Park, Y., Chung, T. S., Lee, G., and Rogers, J. A. (2022b). Materials chemistry of neural interface technologies and recent advances in three-dimensional systems. *Chem. Rev.* 122 (5), 5277–5316. doi:10.1021/acs.chemrev.1c00639
- Park, Y., Franz, C. K., Ryu, H., Luan, H., Cotton, K. Y., Kim, J. U., et al. (2021). Three-dimensional, multifunctional neural interfaces for cortical spheroids and engineered assembloids. *Sci. Adv.* 7 (12), eabf9153. doi:10.1126/sciadv.abf9153
- Piarali, S., Marlinghaus, L., Viebahn, R., Lewis, H., Ryadnov, M. G., Groll, J., et al. (2020). Activated polyhydroxyalkanoate meshes prevent bacterial adhesion and biofilm development in regenerative medicine applications. *Front. Bioeng. Biotechnol.* 8, 442. doi:10.3389/fbioe.2020.00442
- Puiggali-Jou, A., Cazorla, E., Ruano, G., Babeli, I., Ginebra, M.-P., García-Torres, J., et al. (2020). Electroresponsive alginate-based hydrogels for controlled release of hydrophobic drugs. *ACS Biomaterials Sci. Eng.* 6 (11), 6228–6240. doi:10.1021/acsbomaterials.0c01400
- Pyrasani, R. D., Jayaramudu, T., and John, A. (2019). Polyaniline-based conducting hydrogels. *J. Mater. Sci.* 54 (2), 974–996. doi:10.1007/s10853-018-2977-x
- Rahimi, R., Shams Es-haghi, S., Chittiboyina, S., Mutlu, Z., Lelièvre, S. A., Cakmak, M., et al. (2018). Laser-enabled processing of stretchable electronics on a hydrolytically degradable hydrogel. *Adv. Healthc. Mater.* 7 (16), 1800231. doi:10.1002/adhm.201800231
- Rai, R., Roether, J. A., and Boccaccini, A. R. (2022). Polyaniline based polymers in tissue engineering applications: a review. *Prog. Biomed. Eng.* 4 (4), 042004. doi:10.1088/2516-1091/ac93d3
- Rai, R., Tallawi, M., Grigore, A., and Boccaccini, A. R. (2012). Synthesis, properties and biomedical applications of poly(glycerol sebacate) (PGS): a review. *Prog. Polym. Sci.* 37 (8), 1051–1078. doi:10.1016/j.progpolymsci.2012.02.001
- Ramasamy, S. M., Bhaskar, R., Narayanan, K. B., Purohit, S. D., Park, S. S., Manikkavel, A., et al. (2022). Combination of polydopamine and carbon nanomaterials coating enhances the piezoelectric responses and cytocompatibility of biodegradable PLLA nanofiber scaffolds for tissue engineering applications. *Mater. Today Commun.* 33, 104659. doi:10.1016/j.mtcomm.2022.104659
- Ravichandran, R., Martinez, J. G., Jager, E. W. H., Phopase, J., and Turner, A. P. F. (2018). Type I collagen-derived injectable conductive hydrogel scaffolds as glucose sensors. *ACS Appl. Mater. Interfaces* 10 (19), 16244–16249. doi:10.1021/acsami.8b04091
- Richardson-Burns, S. M., Hendricks, J. L., Foster, B., Povlich, L. K., Kim, D.-H., and Martin, D. C. (2007). Polymerization of the conducting polymer poly(3,4-ethylenedioxythiophene) (PEDOT) around living neural cells. *Biomaterials* 28 (8), 1539–1552. doi:10.1016/j.biomaterials.2006.11.026
- Rivnay, J., Wang, H., Fenno, L., Deisseroth, K., and Malliaras, G. G. (2017). Next-generation probes, particles, and proteins for neural interfacing. *Sci. Adv.* 3 (6), e1601649. doi:10.1126/sciadv.1601649
- Robinson, J. T., Jorgolli, M., Shalek, A. K., Yoon, M.-H., Gertner, R. S., and Park, H. (2012). Vertical nanowire electrode arrays as a scalable platform for intracellular interfacing to neuronal circuits. *Nat. Nanotechnol.* 7 (3), 180–184. doi:10.1038/nnano.2011.249
- Rogers, Z. J., Zeevi, M. P., Koppes, R., and Bencherif, S. A. (2020). Electroconductive hydrogels for tissue engineering: current status and future perspectives. *Bioelectricity* 2 (3), 279–292. doi:10.1089/bioe.2020.0025
- Roshanbifar, K., Vogt, L., Greber, B., Diecke, S., Boccaccini, A. R., Scheibel, T., et al. (2018). Electroconductive biohybrid hydrogel for enhanced maturation and beating properties of engineered cardiac tissues. *Adv. Funct. Mater.* 28 (42), 1803951. doi:10.1002/adfm.201803951
- Rosso, G., and Guck, J. (2019). Mechanical changes of peripheral nerve tissue microenvironment and their structural basis during development. *Appl. Bioeng.* 3 (3), 036107. doi:10.1063/1.5108867
- Rousche, P. J., and Normann, R. A. (1998). Chronic recording capability of the Utah Intracortical Electrode Array in cat sensory cortex. *J. Neurosci. Methods* 82 (1), 1–15. doi:10.1016/S0165-0270(98)00031-4
- Roy, S., David-Pur, M., and Hanein, Y. (2017). Carbon nanotube-based ion selective sensors for wearable applications. *ACS Appl. Mater. Interfaces* 9 (40), 35169–35177. doi:10.1021/acsami.7b07346
- Saghebasl, S., Akbarzadeh, A., Gorabi, A. M., Nikzamir, N., SeyedSadjadi, M., and Mostafavi, E. (2022). Biodegradable functional macromolecules as promising scaffolds for cardiac tissue engineering. *Polym. Adv. Technol.* 33 (7), 2044–2068. doi:10.1002/pat.5669
- Salehi, M., Naseri-Nosar, M., Ebrahimi-Barough, S., Nourani, M., Khojasteh, A., Hamidieh, A.-A., et al. (2018). Sciatic nerve regeneration by transplantation of Schwann cells via erythropoietin controlled-releasing polylactic acid/multiwalled carbon nanotubes/gelatin nanofibrils neural guidance conduit. *J. Biomed. Mater. Res. Part B Appl. Biomaterials* 106 (4), 1463–1476. doi:10.1002/jbm.b.33952
- Samanta, S., Ylä-Outinen, L., Rangasami, V. K., Narkilahti, S., and Oommen, O. P. (2022). Bidirectional cell-matrix interaction dictates neuronal network formation in a brain-mimetic 3D scaffold. *Acta Biomater.* 140, 314–323. doi:10.1016/j.actbio.2021.12.010
- Sansíñena, J. M., Olazábal, V., Otero, T. F., Sansíñena, J. M., Polo da Fonseca, C. N., and De Paoli, M. A. (1997). A solid state artificial muscle based on polypyrrole and a solid polymeric electrolyte working in air. *Chem. Commun.*, 2217–2218. doi:10.1039/A705341J
- Saravanan, S., Sareen, N., Abu-El-Rub, E., Ashour, H., Sequiera, G. L., Ammar, H. I., et al. (2018). Graphene oxide-gold nanosheets containing chitosan scaffold improves ventricular contractility and function after implantation into infarcted heart. *Sci. Rep.* 8 (1), 15069. doi:10.1038/s41598-018-33144-0
- Sauter-Starace, F., Torres-Martinez, N., Agache, V., Pudda, C., Dijon, J., Piallat, B., et al. (2011). “Epileptic seizure recordings of a non-human primate using carbon nanotube microelectrodes on implantable silicon shanks,” in 2011 5th International IEEE/EMBS Conference on Neural Engineering, Cancun, Mexico, April 2011.
- Schemitsch, E. H. (2017). Size matters: defining critical in bone defect size. *J. Orthop. Trauma* 31, S20–S22. doi:10.1097/bot.0000000000000978
- Shafique, H., de Vries, J., Strauss, J., Khorrami Jahromi, A., Siavash Moakhar, R., and Mahshid, S. (2023). Advances in the translation of electrochemical hydrogel-based sensors. *Adv. Healthc. Mater.* 12 (1), 2201501. doi:10.1002/adhm.202201501
- Shaner, S., Savellyeva, A., Kvartuh, A., Jedrusik, N., Matter, L., Leal, J., et al. (2023). Bioelectronic microfluidic wound healing: a platform for investigating direct current stimulation of injured cell collectives. *Lab a Chip* 23 (6), 1531–1546. doi:10.1039/d2lc01045c
- Shin, J., Yan, Y., Bai, W., Xue, Y., Gamble, P., Tian, L., et al. (2019). Bioresorbable pressure sensors protected with thermally grown silicon dioxide for the monitoring of chronic diseases and healing processes. *Nat. Biomed. Eng.* 3 (1), 37–46. doi:10.1038/s41511-018-0300-4
- Shou, Y., Teo, X. Y., Wu, K. Z., Bai, B., Kumar, A. R. K., Low, J., et al. (2023). Dynamic stimulations with bioengineered extracellular matrix-mimicking hydrogels

for mechano cell reprogramming and therapy. *Adv. Sci.* 10, 2300670. doi:10.1002/advs.202300670

Singh, A. K., Srivastava, J. K., Chandel, A. K., Sharma, L., Mallick, N., and Singh, S. P. (2019). Biomedical applications of microbially engineered polyhydroxyalkanoates: an insight into recent advances, bottlenecks, and solutions. *Appl. Microbiol. Biotechnol.* 103 (5), 2007–2032. doi:10.1007/s00253-018-09604-y

Solazzo, M., O'Brien, F., Nicolosi, V., and Monaghan, M. (2019). The rationale and emergence of electroconductive biomaterial scaffolds in cardiac tissue engineering. *Apl. Bioeng.* 3 (4), 041501. doi:10.1063/1.5116579

Sordini, L., Garrudo, F. F. F., Rodrigues, C. A. V., Linhardt, R. J., Cabral, J. M. S., Ferreira, F. C., et al. (2021). Effect of electrical stimulation conditions on neural stem cells differentiation on cross-linked PEDOT:PSS films. *Front. Bioeng. Biotechnol.* 9, 591838. doi:10.3389/fbioe.2021.591838

Su, W.-Y., Chen, Y.-C., and Lin, F.-H. (2010). Injectable oxidized hyaluronic acid/adipic acid dihydrazide hydrogel for nucleus pulposus regeneration. *Acta Biomater.* 6 (8), 3044–3055. doi:10.1016/j.actbio.2010.02.037

Sun, Y., Liu, X., George, M. N., Park, S., Gaihr, B., Terzic, A., et al. (2021). Enhanced nerve cell proliferation and differentiation on electrically conductive scaffolds embedded with graphene and carbon nanotubes. *J. Biomed. Mater. Res. Part A* 109 (2), 193–206. doi:10.1002/jbma.37016

Sunwoo, S.-H., Ha, K.-H., Lee, S., Lu, N., and Kim, D.-H. (2021). Wearable and implantable soft bioelectronics: device designs and material strategies. *Annu. Rev. Chem. Biomol. Eng.* 12 (1), 359–391. doi:10.1146/annurev-chembioeng-101420-024336

Sunwoo, S.-H., Han, S. I., Joo, H., Cha, G. D., Kim, D., Choi, S. H., et al. (2020). Advances in soft bioelectronics for brain research and clinical neuroengineering. *Matter* 3 (6), 1923–1947. doi:10.1016/j.matt.2020.10.020

Surowiec, R. K., Allen, M. R., and Wallace, J. M. (2022). Bone hydration: how we can evaluate it, what can it tell us, and is it an effective therapeutic target? *Bone Rep.* 16, 101161. doi:10.1016/j.bonr.2021.101161

Tao, H., Hwang, S.-W., Marelli, B., An, B., Moreau, J. E., Yang, M., et al. (2014). Silk-based resorbable electronic devices for remotely controlled therapy and *in vivo* infection abatement. *Proc. Natl. Acad. Sci.* 111 (49), 17385–17389. doi:10.1073/pnas.1407743111

Tebaldi, M. L., Maia, A. L. C., Poletto, F., de Andrade, F. V., and Soares, D. C. F. (2019). Poly(-3-hydroxybutyrate-co-3-hydroxyvalerate) (PHBV): current advances in synthesis methodologies, antitumor applications and biocompatibility. *J. Drug Deliv. Sci. Technol.* 51, 115–126. doi:10.1016/j.jddst.2019.02.007

Téllez-Soto, C. A., Pereira Silva, M. G., dos Santos, L., de, O., Mendes, T., Singh, P., et al. (2021). *In vivo* determination of dermal water content in chronological skin aging by confocal Raman spectroscopy. *Vib. Spectrosc.* 112, 103196. doi:10.1016/j.vibspec.2020.103196

Thrivikraman, G., Boda, S. K., and Basu, B. (2018). Unraveling the mechanistic effects of electric field stimulation towards directing stem cell fate and function: a tissue engineering perspective. *Biomaterials* 150, 60–86. doi:10.1016/j.biomaterials.2017.10.003

Tran, V. V., Lee, S., Lee, D., and Le, T.-H. (2022). Recent developments and implementations of conductive polymer-based flexible devices in sensing applications. *Polymers* 14 (18), 3730. doi:10.3390/polym14183730

Tringides, C. M., Boulingre, M., Khalil, A., Lungiangwa, T., Jaenisch, R., and Mooney, D. J. (2023). Tunable conductive hydrogel scaffolds for neural cell differentiation. *Adv. Healthc. Mater.* 12 (7), 2202221. doi:10.1002/adhm.202202221

Tringides, C. M., and Mooney, D. J. (2022). Materials for implantable surface electrode arrays: current status and future directions. *Adv. Mater.* 34 (20), 2107207. doi:10.1002/adma.202107207

Tringides, C. M., Vachicouras, N., de Lázaro, I., Wang, H., Trouillet, A., Seo, B. R., et al. (2021). Viscoelastic surface electrode arrays to interface with viscoelastic tissues. *Nat. Nanotechnol.* 16 (9), 1019–1029. doi:10.1038/s41565-021-00926-z

Tropp, J., and Rivnay, J. (2021). Design of biodegradable and biocompatible conjugated polymers for bioelectronics. *J. Mater. Chem. C* 9 (39), 13543–13556. doi:10.1039/d1tc03600a

Turner, B., Ramesh, S., Menegatti, S., and Daniele, M. (2022). Resorbable elastomers for implantable medical devices: highlights and applications. *Polym. Int.* 71 (5), 552–561. doi:10.1002/pi.6349

Ulery, B. D., Nair, L. S., and Laurencin, C. T. (2011). Biomedical applications of biodegradable polymers. *J. Polym. Sci. Part B Polym. Phys.* 49 (12), 832–864. doi:10.1002/polb.22259

Ullah, M. W., Fu, L., Lamboni, L., Shi, Z., and Yang, G. (2019). “Chapter 3 - current trends and biomedical applications of resorbable polymers,” in *Materials for biomedical engineering*. Editors V. Grumezescu and A. M. Grumezescu (Amsterdam, Netherlands: Elsevier), 41–86.

Vasvani, S., Kulkarni, P., and Rawtani, D. (2020). Hyaluronic acid: a review on its biology, aspects of drug delivery, route of administrations and a special emphasis on its approved marketed products and recent clinical studies. *Int. J. Biol. Macromol.* 151, 1012–1029. doi:10.1016/j.ijbiomac.2019.11.066

Veletić, M., Apu, E. H., Simić, M., Bergsland, J., Balasingham, I., Contag, C. H., et al. (2022). Implants with sensing capabilities. *Chem. Rev.* 122 (21), 16329–16363. doi:10.1021/acs.chemrev.2c00005

Vijayavenkataraman, S. (2020). Nerve guide conduits for peripheral nerve injury repair: a review on design, materials and fabrication methods. *Acta Biomater.* 106, 54–69. doi:10.1016/j.actbio.2020.02.003

Vogt, L., Ruther, F., Salehi, S., and Boccaccini, A. R. (2021). Poly(Glycerol sebacate) in biomedical applications—a review of the recent literature. *Adv. Healthc. Mater.* 10 (9), 2002026. doi:10.1002/adhm.202002026

Wang, C., Xia, K., Zhang, Y., and Kaplan, D. L. (2019a). Silk-based advanced materials for soft electronics. *Accounts Chem. Res.* 52 (10), 2916–2927. doi:10.1021/acs.accounts.9b00333

Wang, C., Yokota, T., and Someya, T. (2021). Natural biopolymer-based biocompatible conductors for stretchable bioelectronics. *Chem. Rev.* 121 (4), 2109–2146. doi:10.1021/acs.chemrev.0c00897

Wang, C. H., Dong, Y. Q., Sengothi, K., Tan, K. L., and Kang, E. T. (1999). *In-vivo* tissue response to polyaniline. *Synth. Met.* 102 (1), 1313–1314. doi:10.1016/S0379-6779(98)01006-6

Wang, K., Tian, L., Wang, T., Zhang, Z., Gao, X., Wu, L., et al. (2019b). Electrodeposition of alginate with PEDOT/PSS coated MWCNTs to make an interpenetrating conducting hydrogel for neural interface. *Compos. Interfaces* 26 (1), 27–40. doi:10.1080/09276440.2018.1465766

Wang, L., Wu, Y., Hu, T., Guo, B., and Ma, P. X. (2017a). Electrospun conductive nanofibrous scaffolds for engineering cardiac tissue and 3D bioactuators. *Acta Biomater.* 59, 68–81. doi:10.1016/j.actbio.2017.06.036

Wang, M., Chen, Y., Khan, R., Liu, H., Chen, C., Chen, T., et al. (2019c). A fast self-healing and conductive nanocomposite hydrogel as soft strain sensor. *Colloids Surfaces A Physicochem. Eng. Aspects* 567, 139–149. doi:10.1016/j.colsurfa.2019.01.034

Wang, Q., Ling, S., Liang, X., Wang, H., Lu, H., and Zhang, Y. (2019d). Self-healable multifunctional electronic tattoos based on silk and graphene. *Adv. Funct. Mater.* 29 (16), 1808695. doi:10.1002/adfm.201808695

Wang, S., Sun, C., Guan, S., Li, W., Xu, J., Ge, D., et al. (2017b). Chitosan/gelatin porous scaffolds assembled with conductive poly(3,4-ethylenedioxythiophene) nanoparticles for neural tissue engineering. *J. Mater. Chem. B* 5 (24), 4774–4788. doi:10.1039/c7tb00608j

Wang, Z., Wei, H., Huang, Y., Wei, Y., and Chen, J. (2023). Naturally sourced hydrogels: emerging fundamental materials for next-generation healthcare sensing. *Chem. Soc. Rev.* 52 (9), 2992–3034. doi:10.1039/d2cs00813k

Wei, L., Wang, S., Shan, M., Li, Y., Wang, Y., Wang, F., et al. (2023). Conductive fibers for biomedical applications. *Bioact. Mater.* 22, 343–364. doi:10.1016/j.bioactmat.2022.10.014

Won, S. M., Koo, J., Crawford, K. E., Mickle, A. D., Xue, Y., Min, S., et al. (2018). Natural wax for transient electronics. *Adv. Funct. Mater.* 28 (32), 1801819. doi:10.1002/adfm.201801819

Wu, T., Cui, C., Huang, Y., Liu, Y., Fan, C., Han, X., et al. (2020). Coadministration of an adhesive conductive hydrogel patch and an injectable hydrogel to treat myocardial infarction. *ACS Appl. Mater. Interfaces* 12 (2), 2039–2048. doi:10.1021/acsami.9b17907

Xia, T., Kovochich, M., Liong, M., Mädler, L., Gilbert, B., Shi, H., et al. (2008). Comparison of the mechanism of toxicity of zinc oxide and cerium oxide nanoparticles based on dissolution and oxidative stress properties. *ACS Nano* 2 (10), 2121–2134. doi:10.1021/nn800511k

Xu, J., Tsai, Y.-L., and Hsu, S.-h. (2020). Design strategies of conductive hydrogel for biomedical applications. *Molecules* 25 (22), 5296. doi:10.3390/molecules25225296

Xu, K., Li, S., Dong, S., Zhang, S., Pan, G., Wang, G., et al. (2019a). Bioresorbable electrode array for electrophysiological and pressure signal recording in the brain. *Adv. Healthc. Mater.* 8 (15), 1801649. doi:10.1002/adhm.201801649

Xu, X., Wang, L., Jing, J., Zhan, J., Xu, C., Xie, W., et al. (2022). Conductive collagen-based hydrogel combined with electrical stimulation to promote neural stem cell proliferation and differentiation. *Front. Bioeng. Biotechnol.* 10, 912497. doi:10.3389/fbioe.2022.912497

Xu, Y., Patino Gaillez, M., Rothe, R., Hauser, S., Voigt, D., Pietzsch, J., et al. (2021). Conductive hydrogels with dynamic reversible networks for biomedical applications. *Adv. Healthc. Mater.* 10 (11), 2100012. doi:10.1002/adhm.202100012

Xu, Y., Patsis, P. A., Hauser, S., Voigt, D., Rothe, R., Günther, M., et al. (2019b). Cytocompatible, injectable, and electroconductive soft adhesives with hybrid covalent/noncovalent dynamic network. *Adv. Sci.* 6 (15), 1802077. doi:10.1002/advs.201802077

Xu, Y., Yang, X., Thomas, A. K., Patsis, P. A., Kurth, T., Kräter, M., et al. (2018). Noncovalently assembled electroconductive hydrogel. *ACS Appl. Mater. Interfaces* 10 (17), 14418–14425. doi:10.1021/acsami.8b01029

Yadid, M., Feiner, R., and Dvir, T. (2019). Gold nanoparticle-integrated scaffolds for tissue engineering and regenerative medicine. *Nano Lett.* 19 (4), 2198–2206. doi:10.1021/acs.nanolett.9b00472

- Yamaoka, T., Tabata, Y., and Ikada, Y. (1994). Distribution and tissue uptake of poly(ethylene glycol) with different molecular weights after intravenous administration to mice. *J. Pharm. Sci.* 83 (4), 601–606. doi:10.1002/jps.2600830432
- Yang, B., Yao, F., Ye, L., Hao, T., Zhang, Y., Zhang, L., et al. (2020). A conductive PEDOT/alginate porous scaffold as a platform to modulate the biological behaviors of brown adipose-derived stem cells. *Biomaterials Sci.* 8 (11), 3173–3185. doi:10.1039/c9bm02012h
- Yang, C., DelRio, F. W., Ma, H., Killaars, A. R., Basta, L. P., Kyburz, K. A., et al. (2016). Spatially patterned matrix elasticity directs stem cell fate. *Proc. Natl. Acad. Sci.* 113 (31), E4439–E4445. doi:10.1073/pnas.1609731113
- Yang, G., Kampstra, K. L., and Abidian, M. R. (2014). High performance conducting polymer nanofiber biosensors for detection of biomolecules. *Adv. Mater.* 26 (29), 4954–4960. doi:10.1002/adma.201400753
- Yang, Q., Peng, J., Xiao, H., Xu, X., and Qian, Z. (2022). Polysaccharide hydrogels: functionalization, construction and served as scaffold for tissue engineering. *Carbohydr. Polym.* 278, 118952. doi:10.1016/j.carbpol.2021.118952
- Yao, B., Wang, H., Zhou, Q., Wu, M., Zhang, M., Li, C., et al. (2017). Ultrahigh-conductivity polymer hydrogels with arbitrary structures. *Adv. Mater.* 29 (28), 1700974. doi:10.1002/adma.201700974
- Yao, G., Kang, L., Li, C., Chen, S., Wang, Q., Yang, J., et al. (2021). A self-powered implantable and bioresorbable electrostimulation device for biofeedback bone fracture healing. *Proc. Natl. Acad. Sci.* 118 (28), e2100772118. doi:10.1073/pnas.2100772118
- Yu, K. J., Kuzum, D., Hwang, S.-W., Kim, B. H., Juul, H., Kim, N. H., et al. (2016). Bioresorbable silicon electronics for transient spatiotemporal mapping of electrical activity from the cerebral cortex. *Nat. Mater.* 15 (7), 782–791. doi:10.1038/nmat4624
- Yuk, H., Wu, J., and Zhao, X. (2022). Hydrogel interfaces for merging humans and machines. *Nat. Rev. Mater.* 7 (12), 935–952. doi:10.1038/s41578-022-00483-4
- Zelikin, A. N., Lynn, D. M., Farhadi, J., Martin, I., Shastri, V., and Langer, R. (2002). Erodible conducting polymers for potential biomedical applications. *Angew. Chem. Int. Ed.* 41 (1), 141–144. doi:10.1002/1521-3773(20020104)41:1<141::aid-anie141>3.0.co;2-v
- Zhang, S., Dong, J., Pan, R., Xu, Z., Li, M., and Zang, R. (2023). Structures, properties, and bioengineering applications of alginates and hyaluronic acid. *Polymers* 15 (9), 2149. doi:10.3390/polym15092149
- Zhang, W., Wang, R., Sun, Z., Zhu, X., Zhao, Q., Zhang, T., et al. (2020). Catechol-functionalized hydrogels: biomimetic design, adhesion mechanism, and biomedical applications. *Chem. Soc. Rev.* 49 (2), 433–464. doi:10.1039/c9cs00285e
- Zhang, Y., Chen, S., Xiao, Z., Liu, X., Wu, C., Wu, K., et al. (2021). Magnetoelectric nanoparticles incorporated biomimetic matrix for wireless electrical stimulation and nerve regeneration. *Adv. Healthc. Mater.* 10 (16), 2100695. doi:10.1002/adhm.202100695
- Zhang, Y., Zhou, J., Zhang, Y., Zhang, D., Yong, K. T., and Xiong, J. (2022). Elastic fibers/fabrics for wearables and bioelectronics. *Adv. Sci.* 9 (35), 2203808. doi:10.1002/advs.202203808
- Zhang, Y., Zhou, M., Dou, C., Ma, G., Wang, Y., Feng, N., et al. (2019). Synthesis and biocompatibility assessment of polyaniline nanomaterials. *J. Bioact. Compatible Polym.* 34 (1), 16–24. doi:10.1177/0883911518809110
- Zhao, G., Feng, Y., Xue, L., Cui, M., Zhang, Q., Xu, F., et al. (2022). Anisotropic conductive reduced graphene oxide/silk matrices promote post-infarction myocardial function by restoring electrical integrity. *Acta Biomater.* 139, 190–203. doi:10.1016/j.actbio.2021.03.073
- Zhao, G., Zhou, H., Jin, G., Jin, B., Geng, S., Luo, Z., et al. (2022b). Rational design of electrically conductive biomaterials toward excitable tissues regeneration. *Prog. Polym. Sci.* 131, 101573. doi:10.1016/j.progpolymsci.2022.101573
- Zhu, R., Sun, Z., Li, C., Ramakrishna, S., Chiu, K., and He, L. (2019). Electrical stimulation affects neural stem cell fate and function *in vitro*. *Exp. Neurol.* 319, 112963. doi:10.1016/j.expneurol.2019.112963
- Zhu, T., Ni, Y., Biesold, G. M., Cheng, Y., Ge, M., Li, H., et al. (2023a). Recent advances in conductive hydrogels: classifications, properties, and applications. *Chem. Soc. Rev.* 52 (2), 473–509. doi:10.1039/d2cs00173j
- Zhu, W., Zhang, J., Wei, Z., Zhang, B., and Weng, X. (2023b). Advances and progress in self-healing hydrogel and its application in regenerative medicine. *Materials* 16 (3), 1215. doi:10.3390/ma16031215
- Zou, Y., Qin, J., Huang, Z., Yin, G., Pu, X., and He, D. (2016). Fabrication of aligned conducting PPy-PLLA fiber films and their electrically controlled guidance and orientation for neurites. *ACS Appl. Mater. Interfaces* 8 (20), 12576–12582. doi:10.1021/acsami.6b00957

Glossary

CNT/SWCNT/ MWCNT	carbon nanotube/single-wall CNT/multiwall CNT
β-CD	β-cyclodextrin
CVD	chemical vapor deposition
CMC	carboxymethyl cellulose
CMs	cardiomyocytes
CP	conducting polymer
DNA/RNA	deoxyribonucleic acid/ribonucleic acid
DBSA	dodecylbenzenesulfonic acid
ECG	electrocardiography
ECM	extracellular matrix
EDOT/PEDOT	3,4-ethylenedioxythiophene/ poly(3,4-ethylenedioxythiophene)
GelMA	gelatin methacrylate
GFAP	glial fibrillary acidic protein
GO/rGO	graphene oxide/reduced graphene oxide
GOx	glucose oxidase
HA	hyaluronic acid
iPSC/hiPSC	induced pluripotent stem cells/human induced pluripotent stem cell
MEA	microelectrode array
MN	Microneedle
NP	Nanoparticle
NOAEL	no-observed-adverse-effect limit
NGCs	nerve guidance conduits
NSCs	neuronal stem cells
PANI	poly(aniline)
PBS	Phosphate-buffered saline
PCL	poly(caprolactone)
PDMS	poly(dimethyl-siloxane)
PEG	poly(ethylene glycol)
PGA	poly(glycolic acid)
PGS	Poly(glycerol sebacate)
PHA	poly(hydroxyalkanoates)
PHB/PHBV	poly(3-hydroxybutyrate)/ poly(3-hydroxybutyrate-co-3-hydroxyvalerate)
PLA	poly(lactic acid)
PLLA	poly(L-lactide)
PLGA	poly(lactic-co-glycolic acid)
POMaC	Poly(octamethylene maleate anhydride)
PMMA	poly(methyl methacrylate)
PPy	poly(pyrrole)

PU	pol(urethane)
PSS	poly(styrene sulfonate)
PVA	poly(vinyl alcohol)
PVP	polyvinylpyrrolidone
TI	tolerable intake

Frontiers in Bioengineering and Biotechnology

Accelerates the development of therapies,
devices, and technologies to improve our lives

A multidisciplinary journal that accelerates the
development of biological therapies, devices,
processes and technologies to improve our lives
by bridging the gap between discoveries and their
application.

Discover the latest Research Topics

[See more →](#)

Frontiers

Avenue du Tribunal-Fédéral 34
1005 Lausanne, Switzerland
frontiersin.org

Contact us

+41 (0)21 510 17 00
frontiersin.org/about/contact



Frontiers in
Bioengineering
and Biotechnology

